

**Université de Montréal**

**Molecular mechanisms involved in the induction and  
maintenance of cellular senescence**

par

**Sebastian Igelmann**

Département de biochimie et médecine moléculaire  
Faculté de médecine

Thèse présentée en vue de l'obtention du grade de  
Philosophiæ Doctor (Ph.D.)  
en biochimie et médecine moléculaire

Août 2021



# Université de Montréal

Faculté de médecine

Cette thèse intitulée

## **Molecular mechanisms involved in the induction and maintenance of cellular senescence**

présentée par

**Sebastian Igelmann**

a été évaluée par un jury composé des personnes suivantes :

*Mohan Malleshaiah*

(président-rapporteur)

*Gerardo Ferbeyre*

(directeur de recherche)

*Marc Prentki*

(membre du jury)

*Antonis Koromilas*

(examineur externe)

*Katherine Borden*

(représentant du doyen de la FESP)

## Résumé

---

La sénescence cellulaire est une barrière à la progression tumorale qui est contournée par les cellules cancéreuses. Elle se met en place suivant différents événements tels que l'activation constante d'oncogènes comme H-RAS et correspond à un arrêt stable du cycle cellulaire. Un autre aspect des cellules sénescents est la dégradation spécifique des protéines impliquées dans la régulation du cycle cellulaire, la biogenèse des ribosomes, l'homéostasie mitochondriale et le métabolisme cellulaire.

Dans cette étude, nous voulions identifier quelles sont les contributions de la dégradation des protéines spécifiques à l'homéostasie mitochondriale, au métabolisme cellulaire ainsi qu'à la biogenèse des ribosomes. De plus, nous voulons voir comment la dégradation des protéines impliquées dans ces voies affecte la sénescence cellulaire. Afin de répondre à ces questions, nous avons divisé nos travaux en 2 parties. La première s'est concentrée sur les ribosomes et les altérations de la biogenèse ribosomale dans la sénescence. La deuxième partie s'est focalisée sur la contribution de la dégradation des protéines importantes pour le métabolisme cellulaire et l'homéostasie mitochondriale.

Premièrement, nous avons identifié que la mise en place de la sénescence s'accompagne d'une désynchronisation de la biogenèse des ribosomes. Plus précisément, certains ARNr sont moins transcrits alors que la transcription de certaines protéiques ribosomiques n'est pas altérée. Ceci entraîne un déséquilibre entre la quantité des protéines ribosomiques et celle des ARNr ribosomiques. Il provoque l'accumulation de ribo protéines en dehors des ribosomes. Ces protéines acquièrent en conséquence de nouvelles fonctions. Nous avons identifié RPL29 comme une ribo protéine libre du ribosome. Elle est accumulée dans les cellules sénescents et peut être utilisée comme nouveau biomarqueur afin d'identifier les cellules senescent *in vitro* et *in vivo*. L'identification d'un nouveau biomarqueur de cellules sénescents est cruciale car aucun marqueur spécifique de la sénescence n'est encore disponible.

Par ailleurs, nous avons identifié RPS14 comme une protéine qui peut interagir avec le complexe CDK4-cyclin D1 et ainsi, en inhibant son activité, elle limite la prolifération cellulaire. L'arrêt du cycle cellulaire initié par cette protéine ribosomique hors du ribosome est indépendant de la protéine suppressive p53. Ceci pourrait offrir une opportunité thérapeutique pour le traitement des tumeurs déficientes pour l'expression de p53.

La deuxième partie de ce travail s'est concentrée sur les altérations du métabolisme cellulaire en particulier le métabolisme du NAD et l'homéostasie mitochondriale. Dans un premier temps, nous avons confirmé que la perte d'expression de protéines impliquées dans l'homéostasie mitochondriale favorise la mise en place de la sénescence via l'accumulation de NADH et la stabilisation de p53. De plus, nous avons observé que la diminution des régulateurs de l'homéostasie redox NAD<sup>+</sup> et NADPH est suffisante pour induire l'entrée en sénescence. A l'inverse la normalisation de ce paramètre est à l'origine d'un contournement de la sénescence.

Dans ce cadre, nous avons identifié un nouveau complexe protéique formé par l'enzyme malique, la malate déshydrogénase et la pyruvate carboxylase dont les actions concertées transfèrent l'ion hydrure du NADH vers le NADPH. Nous avons nommé ce complexe HTC pour complexe de transfert d'hydrure. Les réactions métaboliques des protéines de l'HTC permettent la normalisation des niveaux de NAD<sup>+</sup> et de NADPH. L'augmentation des niveaux de NAD<sup>+</sup> et de NADPH a déjà été associé à la tumorigénèse. A travers ces travaux, nous avons constaté que la surexpression des protéines qui forment le complexe HTC coopère avec l'oncogène Ras à la transformation de cellules primaires. Par ailleurs, les enzymes du complexe HTC sont fortement exprimées *in vivo* au niveau des cancers de la prostate d'origine murine ou humaine. De plus, inactivation d'une protéine du complexe HTC déclenche l'entrée en sénescence des cellules tumorales y compris en l'absence de p53.

Nous avons ainsi caractérisé un nouveau complexe multi-enzymatique qui peut reprogrammer le métabolisme et empêcher la mise en place de la sénescence cellulaire. L'inhibition de la formation du complexe HTC pourrait permettre de cibler spécifiquement sa fonction *de novo* tout en limitant de bloquer l'activité physiologique normale des ces enzymes en dehors de ce complexe.

Par l'ensemble de ces travaux, nous avons mis en évidence l'importance des défauts de biogénèse des ribosomes ainsi que des altérations métaboliques dans la mise en place et le maintien de la sénescence. D'une part, l'accumulation de RPS14 en dehors des ribosomes constitue un nouveau mécanisme de régulation du cycle cellulaire. De plus, l'accumulation de RPL29 dans le nucleole constitue un nouveau biomarker de la sénescence. D'autre part, l'identification du complexe HTC a mise en évidence une nouvelle façon de contourner la sénescence et ainsi de contribuer à la transformation de cellules primaires. Ces observations renforcent l'importance de la sénescence cellulaire en tant que mécanisme de suppression tumorale. Ces découvertes créent de nouvelles opportunités thérapeutiques afin de réactiver la sénescence dans les cellules cancéreuses.

**Mots-cléf : Sénescence cellulaire, suppression tumoral, p53, alterations dans la biogenèse des ribosomes, régulation du cycle cellulaire, RPS14, RPL29, métabolisme du NAD, altération dans la transformation cellulaire, cycle métabolique, MDH1, ME1, PC**

## Abstract

---

Cellular senescence is a barrier to tumor progression that is circumvented in cancer cells. Senescence is a stable cell cycle arrest and can be triggered by various oncogenic events, such as constant activation of the oncogene H-RAS. Other critical aspects of senescent cells include a specific degradation of proteins implicated in cell cycle regulation, ribosome biogenesis, mitochondrial homeostasis, and cellular metabolism.

In this study, we wanted to identify the contributions of the specific protein degradation to mitochondrial homeostasis, cellular metabolism, and ribosome biogenesis and how the degradation of proteins implicated in those pathways affects the senescence response. In order to answer our question, we divided our research into two aspects. The first aspect was focused on ribosomes and the alterations in ribosome biogenesis in senescence. The second aspect was the contribution of degradation of proteins implicated in cellular metabolism and mitochondrial homeostasis.

First, we identified that a desynchronization of ribosome biogenesis accompanies senescence, meaning that certain rRNA are less transcribed, whereas specific ribosomal proteins do not decrease their transcription leading to an imbalance in ribosomal protein and ribosomal RNA. This imbalance causes an accumulation of ribosomal free riboproteins. Those accumulated riboproteins acquire novel functions. We identified RPL29 as a ribosomal free riboprotein that accumulated in senescent cells and can be used as a novel biomarker to identify senescent cells *in vitro* and *in vivo*. Identification of novel senescent cell biomarkers is crucial as no specific marker of senescence is available. Furthermore, we identified RPS14 as a protein that can interact with the CDK4-cyclinD1 complex and decrease cell cycle progression. Of utmost importance is that cell cycle repression was even possible in cancer cells devoided of p53 highlighting novel strategies for p53 null cancer treatments.

In the second part, we focused on alterations in cellular metabolism, particularly in light of NAD metabolism and mitochondria homeostasis. We could confirm that the degradation of proteins implicated in mitochondrial homeostasis can induce senescence via the accumulation of NADH and p53 stabilization. Furthermore, we confirmed that the decrease in redox homeostasis regulators, namely NAD<sup>+</sup> and NADPH, can trigger senescence. In the same idea, we showed that the normalization of those redox potentials could bypass the senescence response. Most importantly, we identified a novel protein complex formed by malic enzyme, malate dehydrogenase,

and pyruvate carboxylase. The concerted actions of those three metabolic enzymes can transfer the hydride ion from NADH towards NADPH. Thus, we coined this complex HTC for hydride transfer complex. These metabolic reactions in HTC allow for two things, the normalization of NAD<sup>+</sup> levels and the normalization of NADPH levels. Intriguingly, both NAD<sup>+</sup> and NADPH level increase were previously linked to transformation, and indeed, we were able to show that expression of HTC in combination with oncogenic Ras is sufficient to transform primary cells. Moreover, HTC enzymes are highly expressed *in vivo* in mouse and human prostate cancer models, and their inactivation triggers senescence even in the absence of p53. We provide evidence for a new multi-enzymatic complex, with *de novo* functions that reprogram metabolism and prevent cellular senescence. Inhibition of formation of the HTC complex might allow targeting specifically the *de novo* function of this complex with fewer effects on normal enzyme function.

All in all, we highlighted the contributions of ribosome biogenesis and metabolic alterations in inducing and maintaining the senescence response. Furthermore, RPS14 accumulation allows for a novel cell cycle regulation mechanism, and the accumulation of RPL29 in the nucleolus can be used as a novel biomarker for cellular senescence. Moreover, the expression of HTC demonstrated a novel way of avoiding senescence, thus promoting cellular transformation. Both pathways highlight the importance of cellular senescence as a tumor suppressors mechanism, and these discoveries allow for novel strategies for cancer drug development.

**Keywords:** Cellular senescence, tumor suppression, p53, ribosome-biogenesis alterations, cell cycle regulation, RPS14, RPL29, NAD metabolism, metabolic alterations in transformation, metabolic cycles, MDH1, ME1, PC

## Résumé non scientifique

---

Le cancer est une des principales causes de mortalité au Québec. Ainsi, l'identification de nouveaux mécanismes limitant le développement tumoral est primordial. Les cellules cancéreuses sont notamment caractérisées par une prolifération élevée ainsi qu'une altération du métabolisme : deux traits qui sont requis pour le développement tumoral. Normalement, l'initiation d'un cancer est contrainte par la mise en place de mécanismes de suppression tumorale tels que la sénescence cellulaire. Ce mécanisme correspond à un arrêt stable de la prolifération cellulaire et ces cellules ne peuvent plus se diviser et alors le développement d'un cancer est retardé. La sénescence peut être observée chez l'humain : par exemple dans les grains de beauté ou dans certaines régions de la prostate portant des lésions bénignes (non-cancéreuses). Cependant, certaines cellules sont capables de contourner ces mécanismes anti-tumoraux et échappent ainsi à la sénescence cellulaire.

Dans cette étude, nous avons essayé de mieux appréhender les mécanismes moléculaires qui permettent aux cellules de contourner les points de contrôle anti-tumoraux et ainsi de devenir cancéreuses. Nous nous sommes focalisés sur les altérations métaboliques entre les cellules précancéreuses et les cellules tumorales malignes. Nos travaux ont été initiés par la découverte d'une dérégulation du métabolisme de NAD et de la ribogénèse dans les cellules sénescents.

Premièrement, les ribosomes sont des complexes de la cellule impliqués dans la traduction c'est-à-dire la formation de protéines à partir d'un ARN messager. Les ribosomes se composent de plusieurs molécules différentes telles que des ARN et des protéines ribosomiques. Nous avons montré que la biogénèse ribosomale est désynchronisée dans les cellules sénescents. Effectivement, la production de certains constituants ribosomiques sont altérées ou réduites lors de la sénescence. En conséquence, certains éléments des ribosomes s'accumulent et d'autres ne sont plus suffisamment produits. Dans ce contexte, nous avons observé que certaines protéines ribosomiques sont détournées de leurs fonctions habituelles au sein des ribosomes et participent à la régulation du cycle cellulaire.

Deuxièmement, il est connu que des cellules cancéreuses peuvent changer leur métabolisme et ainsi modifier leur manière d'utiliser les nutriments tels que le sucre et les acides aminés. Également, nous savons que les cellules qui sont sénescents /pré-cancéreuses ont aussi un métabolisme différent vis-à-vis des cellules cancéreuses . Un élément métabolique très important est le



NAD. De nombreuses réactions métaboliques importantes pour le bon fonctionnement de la cellule requièrent le NAD. Il a été observé que les cellules cancéreuses ont une dépendance accrue en ce métabolite. A l'inverse, les niveaux de NAD sont plus faibles dans les cellules sénescences. Nous avons dès lors émis l'hypothèse qu'une modification du métabolisme du NAD des cellules sénescence/pré-cancéreuses à des niveaux similaires aux cellules cancéreuses soit suffisant pour contourner la sénescence et ainsi promouvoir la tumorigénèse.

Dans ce contexte, nous avons identifié l'existence d'un complexe capable de régénérer le NAD ainsi que le NADPH, une autre molécule similaire au NAD également très importante pour les cellules cancéreuses. Au sein des cellules sénescences, les niveaux des trois protéines qui composent ce complexe sont très réduits. En conséquence, ce complexe ne peut se former et ainsi augmenter les niveaux cellulaires de NAD et NADPH. Cependant, suivant notamment la survenue de mutations, l'expression de ces protéines peut être restaurée. Dès lors, le complexe peut se former et accroître les niveaux de NAD et NADPH. Nous avons observé que la protéine p53 réprime l'expression des membres de ce complexe. De manière intéressante, cette protéine est mutée dans environ 50% des cas de cancers chez l'Homme. Nous avons également constaté que l'expression des protéines de ce complexe était fortement augmentée dans les cancers alors qu'elle est à l'inverse réduite au niveau des cellules sénescences des lésions tumorales bénignes prostatiques. Par ailleurs, nous avons montré que l'inhibition de l'assemblage du complexe est suffisante pour réduire la prolifération de cellules cancéreuses.

La description de ce nouveau complexe protéique et son influence marquée sur le métabolisme cellulaire représente une avancée significative dans le domaine du métabolisme du cancer. Jusqu'à présent, ce complexe n'était pas reconnu comme un contributeur important au processus de transformation. En conclusion, nous avons confirmé dans nos études que la sénescence cellulaire constitue une barrière à la transformation cellulaire. Dans ce contexte, nous avons identifié de nouveaux facteurs essentiels au maintien de l'état sénescence et qui réduisent la prolifération de cellules potentiellement cancéreuses. De plus, nous avons caractérisé de nouveaux acteurs qui permettent le contournement des mécanismes de suppression tumorale et favorisent dès lors la formation de cellules cancéreuses. Ainsi, les deux découvertes augmentent la compréhension des mécanismes qui concourent à la génération de cellules cancéreuses par le contournement des mécanismes de contrôle anti-tumoraux. Les recherches futures pourraient permettre l'application clinique de ces observations.

## Non scientific abstract

---

Cancer is one of the leading death causes in Canada. Thus, understanding the cellular mechanisms that prevent the development of cancer is essential. Cancer cells exhibit a high rate of proliferation and altered cellular metabolism: two traits required for cancer development.

Cancer initiation is prevented by mechanisms that suppress tumor development. One of that tumor-suppressive mechanisms is cellular senescence. Cellular senescence is a barrier against cancer development because senescent cells can no longer divide. Therefore, the development of cancer is delayed. The senescence response can be observed in humans, for example, in nevi or some prostate regions with benign (non-cancerous) lesions. Unfortunately, the anti-tumor mechanisms are not flawless, and some cells can escape these control mechanisms. In the present study, we tried to understand better the molecular mechanisms that reinforce tumor suppression and those allowing cells to escape anti-tumor checkpoints and thus become cancerous.

In doing so, we paid particular attention to alterations in the metabolism of pre-cancerous and cancerous cells. Our research was based on the discovery that there are alterations in several metabolic pathways in cellular senescence, namely the pathway of ribosome generation and NAD metabolism.

Firstly, ribosomes are big molecular complexes in cells, and they are essential for the production of proteins. Ribosomes are composed of several different molecules. We have shown that ribosome biogenesis, the process of ribosome generation, is altered in cellular senescence. Hence, we have demonstrated that some molecules accumulate, whereas others are not produced in sufficient quantities. Moreover, we identified that those accumulated proteins could acquire new functions. One of the new functions that we have observed is the cell cycle regulation by these proteins. This discovery adds a new way to inhibit proliferation. New drugs that inhibit proliferation are crucial in the fight against cancer.

In the second part of our research, we focused on cellular metabolism, in particular NAD metabolism. It was known that cancer cells could change their metabolism and alter how they use nutrients such as sugar and amino acids. It was also known that senescent cells have a different metabolism from cancer cells. A vital metabolic element is NAD: a small molecule that can be used in many cellular metabolic reactions. Cancer cells require high levels of NAD. In contrast, NAD levels are reduced in senescent/non-cancerous cells.

Therefore, we hypothesized that senescent cells have to normalize their NAD level. We supposed that senescent cells could reprogram their metabolism so that their NAD levels resemble the level found in cancer cells. If senescent cells could alter their metabolism, this could bypass cellular senescence and thus transform these cells.

As predicted, we have found a complex of three proteins that can associate together and act to regenerate NAD and NADPH. NADPH is a similar molecule to NAD and is also very important for cancer cells. Furthermore, in senescent or non-cancerous cells, this complex is repressed. As a result, the levels of the proteins in the complex are low; hence they cannot associate together to perform their metabolic actions.

However, suppose this repression is removed, for example, by mutations levels of the complex rise. In that case, all three proteins can associate together to perform their metabolic reactions, increasing the levels of NAD and NADPH. The increase in NAD and NADPH can then drive the bypass of senescence and cellular transformation.

In addition, we have shown that one of the repressors of this complex is the protein p53. This protein is mutated in approximately 50% of cancers. In addition to having identified this metabolic complex, we validated that the complex levels are significantly increased in cancers and decreased in senescent lesions of the prostate. Also, we have shown that inhibition of the assembly of the complex is sufficient to reduce the proliferation and reaction of cellular senescence of cancer cells. This result is particularly exciting because it demonstrates that it is possible to reintroduce senescence in cells that had previously escaped the senescence response.

The discovery of this new protein complex and its marked influence on cell metabolism represents a significant advance in the field of cancer metabolism. Up to now, this complex was not recognized as an important contributor to the transformation process.

All in all, we highlighted in our studies cellular senescence as a barrier to cellular transformation. In addition, we identified factors that maintain the senescence response, allow identification of senescent cells and lower the proliferation of potentially cancerous cells. Likewise, we identified factors that can escape anti-tumor checkpoints and trigger cancer development. Both discoveries contribute to the growing understanding of cancer, and future research will allow the clinical application of our findings.

## Kurzfassung

---

Krebs ist eine der häufigsten Todesursachen in der westlichen Welt. Aus diesem Grund ist es von hoher Bedeutung die molekularen Prozesse die eine Zelle entarten, also zum Krebs werden lassen besonders genau zu untersuchen. Im Allgemeinen haben Zellen Mechanismen, die das Entarten verhindern sollen, jedoch sind diese Mechanismen nicht immer fehlerfrei. Ein solcher Mechanismus ist die Zellseneszenz. Dieser Schutzmechanismus kann auf verschiedene Weise, wie zum Beispiel durch das Mutieren eines Onkogenes, aktiviert werden. Die Zellseneszenz ist dadurch charakterisiert, dass sie potentielle Krebszellen an ihrer Zellteilung hindert und es deswegen zu keiner Entstehung eines Karzinoms kommt. Wie bereits angedeutet sind die Mechanismen, welche die Entartung von Zellen stoppen sollen nicht fehlerfrei und die Inaktivität dieser Schutzmechanismen kann zur Entartung - auch maligne Transformation genannt - einer Zelle führen.

In dieser Doktorarbeit haben wir aufgezeigt, welche molekularen Prozesse in der Zelle aktiviert bzw. verändert werden und dann dazu führen, dass der Schutzmechanismus der Zellseneszenz umgangen wird. Im Allgemeinen haben wir zwei Prozesse, die während der malignen Transformation verändert werden, untersucht. Dies ist auf der einen Seite die Veränderung von ribosomer Entwicklung und auf der anderen Seite sind es die Veränderungsprozesse im Zellstoffwechsel. Ribosome sind makromolekulare Komplexe in Zellen, die aus speziellen Proteinen und RNA aufgebaut sind und besonders wichtig für die Zelle sind, da sie die Produktion von Proteinen ermöglichen.

Wir haben aufgezeigt, dass während der Aktivierung von Zellseneszenz die Produktion von Ribosomen ungleichmäßig in der Zelle heruntergefahren wird. Dies führt dazu, dass bestimmte Proteine, die wichtig für die Ribosomen sind sich im Zellkern bzw. im Kernkörperchen ansammeln. Hier seien besonders zwei Proteine zu nennen, RPS14 and RPL29. Wir haben festgestellt, dass diese Ansammlung von RPL29 im Kernkörperchen als Biomarker für die Ermittlung von Zellseneszenz *in vivo* dienen kann. Außerdem haben wir dargestellt, dass die Ansammlung von dem Protein RPS14 dazu führt, dass der Zellzyklus gestoppt wird. Die Entdeckung von RPS14 als Regulator für den Zellzyklus ist insofern wichtig, da dieser Prozess unabhängig von p53, einem Protein welches in über 50 Prozent aller Krebsarten inaktiv ist, stattfinden kann.

Bisher waren zwei Mechanismen zur Zellzyklus Regulierung bekannt. Die Beschreibung von RPS14 im Zellzyklus erlaubt uns einen weiteren Mechanismus hinzuzufügen. Dies ist ein wichtiger Schritt zur Erforschung von neuen Inhibitoren der Zellteilung.

Im zweiten Teil der Arbeit haben wir untersucht inwiefern der Zellstoffwechsel sich während der Zellseneszenz verändert. Wir haben herausgefunden, dass sich das Niveau von wichtigen Co-Faktoren, die den Redoxstatus der Zelle regulieren während der Zellseneszenz verändert. Insbesondere das Molekül NAD<sup>+</sup> zeigte eine starke Verringerung im Niveau. Weiterhin wussten wir, dass das Niveau von NAD<sup>+</sup> und auch das Niveau von NADPH, ein Molekül ähnlich dem NAD, in Krebszellen besonders hoch ist.

Wir haben festgestellt, dass in der Zelle ein Proteinkomplex aus Stoffwechselproteinen entstehen kann, welcher die Level von NAD<sup>+</sup> und NADPH durch die Stoffwechselaktion dieser Proteine wieder normalisiert. Dieser Komplex besteht aus drei Proteinen Malic Enzyme 1, Malate Dehydrogenase 1 und Pyruvate Carboxylase. Besonders hervorzuheben hierbei ist unsere Entdeckung, dass Pyruvate Carboxylase in Krebszellen nicht nur in den Mitochondrien vorhanden ist, sondern auch im Zellplasma. Die Aktivierung dieses Proteinkomplexes ermöglicht Zellen die normalerweise in die Zellseneszenz gehen würden, diesen Schutzmechanismus zu umgehen und dabei bösartig zu entarten. Diese Entdeckung ist besonders interessant, da der Zellstoffwechsel von Krebszellen seit langem untersucht wird, es jedoch bisher noch nicht bekannt war, dass dieser Proteinkomplex in der Lage ist die Zelle bösartig zu transformieren. Wir konnten nachweisen, dass die Proteinlevel von unserem Komplex in Prostatakrebs im Vergleich zu normalem Prostatagewebe erhöht sind. Darüber hinaus waren wir in der Lage zu zeigen, dass die Inaktivierung von einem der Proteine aus dem Komplex dazu führt, dass die Zelle ihren Zellzyklus verlangsamt und weniger aggressiv in einem Kanzerogenitätstest ist. Dies ist selbst dann möglich, wenn die Krebszelle über kein aktives p53 Protein mehr verfügt. Besonders hervorzuheben diese Entdeckung, weil das p53 Protein eines der wichtigsten Proteine ist, welches die Zelle vor einer bösartigen Transformation schützt.

Zusammenfassend ist zu sagen, dass wir zwei neue Mechanismen aufgezeigt haben die Veränderung der Ribosomenproduktion und die Stoffwechselprozesse, die sich während der malignen Transformation von Zellen verändern. In der Zukunft wird unsere Forschung versuchen zu verstehen inwiefern diese neuen Erkenntnisse dazu genutzt werden können neue Moleküle zu entwickeln die speziell die beschriebenen Prozesse nutzen, um den Zellzyklus von Krebszellen zu verlangsamen.

# Contents

---

<b>Résumé</b> .....	i
<b>Abstract</b> .....	iii
<b>Résumé non scientifique</b> .....	v
<b>Non scientific abstract</b> .....	vii
<b>Kurzfassung</b> .....	ix
<b>List of Tables</b> .....	xv
<b>List of Figures</b> .....	xvii
<b>Abbreviations</b> .....	xix
<b>Acknowledgments</b> .....	xxvii
<b>Chapter 1. Introduction</b> .....	1
1.1. The bases of cancer biology .....	1
1.1.1. Cell cycle regulation .....	1
1.1.2. The processus of cellular transformation .....	4
1.2. Activation of oncogenes .....	6
1.3. Loss of tumor suppressor mechanisms .....	8
1.3.1. Limitations of the tumor suppressor and oncogene model .....	10
1.4. Cellular senescence; More than a tumor suppressor mechanism .....	11
1.4.1. Inducers and effectors of cellular senescence .....	12
1.4.2. Aging the price of tumor suppression .....	14
1.4.3. Role of senescence in wound healing and developmental senescence .....	15
1.5. Senescence as a tumor suppressor mechanism .....	17
1.5.1. Markers of cellular senescence .....	18
1.5.2. Molecular consequences of cellular senescence .....	20

1.5.3.	Senescence associated protein degradation .....	24
1.5.4.	Targets of the SAPD and their molecular consequences .....	24
1.5.5.	Ribosome biogenesis defects in senescence.....	25
1.5.6.	Role of mitochondria in cellular senescence .....	27
1.5.7.	Mitochondrial dysfunction and mitophagy in cellular senescence .....	29
1.6.	Metabolic adaptations in senescent and cancerous cells; a requirement for malignant transformation? .....	31
1.6.1.	Metabolism of amino acids and lipids .....	33
1.6.2.	Metabolic alterations resulting in post transitional modification.....	37
1.6.3.	Warburg effect and metabolic requirements for cancerous cells .....	39
1.6.4.	p53 as a regulator of metabolism .....	42
1.7.	Alteration of metabolism in senescent cells.....	43
1.7.1.	Amino acid, lipid, nucleotide metabolism in senescent cells.....	43
1.7.2.	Glucose metabolism in senescent cells .....	47
1.8.	Could alterations in NAD or NAD intermediates be a significant contributor to the aging phenotype and the cellular transformation? The roles of NAD and NADPH metabolism in cancer and senescent cells .....	48
1.9.	General goals of this thesis .....	56
<b>Chapter 2.</b>	<b>Scientific articles .....</b>	<b>59</b>
2.1.	General information .....	59
2.2.	Context for the article 1 .....	59
2.3.	Contribution to the article 1.....	60
2.4.	Senescence-associated ribosome biogenesis defects contributes to cell cycle arrest through the Rb pathway .....	62
2.4.1.	Abstract .....	62
2.4.2.	Introduction .....	62
2.4.3.	Results .....	63
2.4.4.	Discussion .....	69
2.4.5.	Acknowledgments .....	70
2.4.6.	Main figures and supplementary figures .....	70
2.4.7.	References .....	108

2.5.	Context for the article 2 .....	111
2.6.	Contribution to the article 2.....	112
2.7.	A Hydride transfer complex reprograms NAD metabolism and bypasses senescence	115
2.7.1.	Abstract .....	115
2.7.2.	Introduction .....	115
2.7.3.	Results .....	116
2.7.4.	Discussion .....	125
2.7.5.	Main figures and supplementary figures .....	129
2.7.6.	References .....	172
2.8.	Contribution to the article 3.....	179
2.9.	STAT3 and STAT5 activation in solid cancers.....	181
2.9.1.	Abstract .....	181
2.9.2.	Introduction .....	181
2.9.3.	STAT3 and STAT5 in Solid Cancers .....	181
2.9.4.	Mechanisms of Transformation by STAT3/5 Proteins in Solid Cancers .....	185
2.9.5.	Tumor Suppressor Functions and Negative Regulation of STAT3/5 Signaling ...	188
2.9.6.	Concluding Remarks .....	192
2.9.7.	References .....	194
<b>Chapter 3.</b>	<b>Discussion .....</b>	<b>213</b>
3.1.	General.....	213
3.2.	Ribosome biogenesis alterations in senescence .....	214
3.2.1.	RPL29, a new marker of cellular senescence.....	215
3.2.2.	Impact of accumulation of other ribosomal proteins .....	215
3.3.	STAT3 in aging and cancer .....	218
3.3.1.	Are alterations in STAT3 levels oncogenic?.....	220
3.4.	Implication of metabolic changes in senescent cells .....	223
3.4.1.	Implication of PC outside of mitochondria .....	225
3.5.	Different roles of HTC .....	226
3.5.1.	Role of HTC in Cancer .....	227
3.5.2.	Role of HTC in physiological contexts .....	228
3.5.3.	The roles of HTC on aging T-cells.....	231



3.5.4. HTC in the mitochondria .....	231
3.5.5. The core complex HTC .....	232
3.6. Transformation with NAD without loss of p53 or RB .....	233
3.7. Impact of other metabolons or metabolic cycles .....	234
3.8. NAD regulation in senescence, aging, and stem cells .....	235
3.9. Roles of NAD and ribosomes biogenesis alterations on tissue aging .....	236
3.10. Implications of liquid-liquid phase separation in HTC formation and nucleolus ...	238
3.11. Does cellular transformation require cellular senescence bypass .....	239
3.12. Conclusion .....	240
<b>Bibliography</b> .....	<b>243</b>
<b>Chapter A. Appendix</b> .....	<b>285</b>
A.1. Supplementary files from the article "Senescence-associated ribosome biogenesis defects contribute to cell cycle arrest through the Rb pathway" .....	285
A.2. Supplementary files from the article "A Hydride transfer complex reprograms NAD metabolism and bypasses senescence" .....	301
A.3. Article contributions .....	322
A.3.1. Metformin inhibits the senescence-associated secretory phenotype by interfering with IKK/NF-kappa-B activation .....	323
A.3.2. Tumor suppressor activity of the ERK/MAPK pathway by promoting selective protein degradation .....	324
A.3.3. Ribosomal protein RPL22/eL22 regulates the cell cycle by acting as an inhibitor of the CDK4-cyclin D complex .....	326
A.3.4. Circumventing senescence is associated with stem cell properties and metformin sensitivity .....	327

## List of Tables

---

1.1	Classes of cellular senescence .....	13
1.2	Nucleolar proteins with increased degradation in cellular senescence .....	26



## List of Figures

---

1.1	Cell cycle .....	2
1.2	Transformation and evasion of tumor suppressor mechanism.....	5
1.3	Hallmarks of cancer .....	7
1.4	Inducer and marker of cellular senescence .....	17
1.5	STAT3 pathway .....	28
1.6	Overview on metabolism covered in this thesis .....	32
1.7	Glutaminolysis.....	34
1.8	Redox control by proline .....	35
1.9	Pathways of NAD biosynthesis and NAD consumption.....	49
1.10	Pathways that can generate or consume NADPH .....	53
3.1	Pyruvate cycling pathways in insulin secretion .....	230
3.2	Contributions of RPS14, RPL29 and the HTC complex to senescence .....	241



## Abbreviations

---

**$\alpha$ -KG:**  $\alpha$ -ketoglutarate  
 **$\gamma$ -H2A.X:** histone 2a phosphorylated on S139  
**2-HG:** 2-hydroxyglutarate  
**4E-BP1:** eukaryotic translation initiation factor 4E-binding protein 1  
**53BP1:** TP53 binding protein 1  
**5hmC:** 5-Hydroxymethylcytosine  
**ACLY:** ATP citrate synthase/lyase  
**AKT:** ak strain transforming-Protein  
**ALS:** amyotrophic lateral sclerosis  
**ALT:** alanine transaminase  
**ARG1:** arginase 1  
**ATAC-Seq:** assay for transposase-accessible chromatin by sequencing  
**ATAD3A:** ATPase family AAA domain containing 3A protein  
**ATM:** ataxia telangiectasia mutated  
**ATPase:** adenosine triphosphate hydrolysis enzyme  
**ATR:** ataxia telangiectasia and Rad3-related protein  
**BAG3:** BCL2 associated athanogene 3  
**BCL-2 family:** B-cell lymphoma 2 protein family  
**BCL-xL:** B-cell lymphoma-extra large protein  
**BCL2:** B-cell lymphoma 2 protein  
**BPH:** benign prostatic hyperplasia  
**BRCA 1/2:** breast Cancer gene 1/2  
**BubR1:** mitotic spindle checkpoint serine/threonine-protein kinase Bub1  
**c-MYC:** cellular-avian myelocytomatosis viral oncogene homolog  
**C2CD5:** C2 calcium dependent domain containing 5  
**CAF:** cancer associated fibroblasts  
**CALD1:** caldesmon1  
**CAR-T:** chimeric antigen receptors T-cells  
**CD27:** cluster of differentiation 27

**CDK:** cyclin dependant kinase  
**CDK1:** cyclin dependant kinase 1  
**CDK2:** cyclin dependant kinase 2  
**CDK4:** cyclin dependant kinase 4  
**CDK6:** cyclin dependant kinase 6  
**CDKi:** cyclin dependant kinase inhibitors  
**cGAS-STING:** cyclic GMP-AMP Synthase- Stimulator of Interferon Genes  
**CHIP-Seq:** chromatin immunoprecipitation followed by sequencing  
**CIP/KIP:** CDK-interacting protein/kinase inhibitory protein  
**COPD:** chronic obstructive pulmonary disease  
**CPS1:** carbamoyl phosphate synthetase 1  
**CPT1A:** carnitine palmitoyltransferase 1A  
**CR:** caloric restriction  
**CtBP:** C-Terminal Binding Protein  
**CXCL1:** chemokine (C-X-C motif) ligand 1  
**DAMPs:** damage-associated molecular patterns  
**DDA1:** DET1 and DDB1 associated 1  
**DDR:** DNA damage response  
**DDX21:** DExD-box helicase 21  
**DDX51:** DExD-box helicase 51  
**DNA:** deoxyribonucleic acid  
**E-CAD:** epithelial cadherin  
**E2F:** E2 promoter binding factor  
**E2F1:** E2 promoter binding factor 1  
**EBP2:** Epstein-Barr nuclear antigen binding protein 2  
**ECM:** extracellular matrix  
**eIF- $\alpha$ :** eukaryotic initiation factor 2 subunit 1  
**EMT:** epithelial-mesenchymal transition  
**ER:** endoplasmic reticulum  
**ERBB2:** erythroblastic oncogene B or HER2/neu  
**ERK:** extracellular signal-regulated kinase  
**ETC:** electron transport chain  
**FAO:** fatty acid oxidation  
**FAS:** fatty acid synthetase  
**FFA:** free fatty acids

**FH:** fumarate hydratase  
**FHIT:** fragile histidine triad protein  
**FISH:** fluorescence *in situ* hybridization  
**FLNB:** filamin B  
**FOXM1:** Forkhead box protein M1  
**FOXO:** forkhead box proteins subfamily O  
**FTD:** frontotemporal dementia  
**G6PD:** glucose-6-phosphate dehydrogenase  
**GAPDH:** glyceraldehyde 3-phosphate dehydrogenase  
**GLS1:** glutaminase-1  
**GLS2:** glutaminase-2  
**GLUD1:** glutamate dehydrogenase 1  
**GOT1/ASTc:** glutamic-oxaloacetic transaminase1 / aspartate transaminase cytoplasmic  
**GOT2/ASTm:** glutamic-oxaloacetic transaminase2 / aspartate aminotransferase mitochondrial  
**GPDH:** glycerol-3-phosphate dehydrogenase  
**GRIM19:** gene associated with retinoic and interferon-induced mortality 19 protein  
**GSH:** glutathione  
**H-RAS:** Harvey-RAS  
**H3K9me2/3:** Histone 3 di- or tri- methylated on lysine 9  
**HDR:** homology directed repair  
**HIF:** hypoxia-inducible factor  
**HK:** hexokinase  
**HMGB2:** high mobility Group Box 2  
**HSP70:** heat shock protein 70  
**HSP90:** heat shock protein 90  
**HUVEC:** human umbilical vein endothelial cells  
**IDH:** isocitrate dehydrogenase1/2  
**IDRs:** intrinsically disordered regions  
**IL1 $\beta$ :** interleukin 1 $\beta$   
**IL6:** interleukin 6  
**INK:** inhibitor of kinase  
**INK-ATTAC:** INK4A locus regulated apoptosis through targeted activation of caspase  
**Jumonji demethylases:** jumonji domain containing histone lysine demethylases  
**Jun:** jun proto-oncogene- AP-1 transcription factor subunit avian sarcoma virus 17 protein



**KAP1/TRIM28:** tripartite motif-containing 28  
**KAT:** lysine acetyltransferase  
**KDAT:** lysine deacetylases  
**Ku70/XRCC6 and Ku80/XRCC5:** X-ray repair complementing defective repair in Chinese hamster cell member 5 or 6  
**LDHA:** lactate dehydrogenase A  
**LEDGF:** lens epithelium-derived growth factor  
**LKB1:** liver kinase B1  
**llps:** liquid-liquid phase-separation  
**LOTIS:** loss of tumor suppressor-induced senescence  
**MCM2:** minichromosome Maintenance Complex Component 2  
**MCT1:** mono-Carboxylate transporter 1  
**MDH1:** malate dehydrogenase 1  
**MDM2:** mouse double minute 2 homolog  
**ME1:** malic enzyme  
**MMP:** matrix metallo protease  
**morpholinos:** phosphorodiamidate morpholino oligomer  
**MPTP:** mitochondrial permeability transition pore  
**MSH3:** mutS homolog 3  
**MSIS:** metabolic stress-induced senescence  
**NA:** nicotinic acid/ niacin  
**NAAD:** nicotinamide adenine dinucleotide  
**NAD<sup>+</sup>:** nicotinamide adenine dinucleotide  
**NADK:** nicotinamide adenine dinucleotide kinase  
**NADPH:** nicotinamide adenine dinucleotide phosphate + hydrogen  
**NAM:** nicotinamide  
**NAMN:** nicotinamide mononucleotide  
**NAMPT:** nicotinamide phosphoribosyltransferase  
**NAPRT:** nicotinate phosphoribosyltransferase  
**NCL:** nucleolin  
**NF- $\kappa$ -B:** nuclear factor- $\kappa$ -B  
**NF1:** neurofibromin 1  
**NGF:** neuron growth factor  
**NHJE:** non homologous end joining  
**NK:** natural killer

**NMN:** nicotinamide mononucleotide  
**NMNAT:** nicotinamide mononucleotide adenylyltransferase  
**NNT:** nicotinamide nucleotide transhydrogenase  
**NOXA:** phorbol-12-myristate-13-acetate-induced protein 1  
**NQO1:** NAD(P)H quinone dehydrogenase 1  
**NR:** nicotinamide riboside  
**NRK:** nicotinamide riboside kinase  
**NS:** nucleostemin also known as GNL3 (Guanine nucleotide-binding protein-like 3)  
**OAA:** oxaloacetate  
**OIS:** oncogene-induced senescence  
**OTC:** ornithine transcarbamoylase  
**P15<sup>INK4B</sup>:** protein 15 of the INK family transcript b (CDKN2B)  
**P16<sup>INK4A</sup>:** protein 16 of the INK family transcript a (CDKN2A)  
**P18<sup>INK4C</sup>:** protein 18 of the INK family transcript c (CDKN2C)  
**P19<sup>INK4D</sup>:** protein 19 of the INK family transcript d (CDKN2D)  
**p21<sup>cip1-waf1</sup>:** cyclin dependent kinase inhibitor 1A protein (CDKN1A gene)  
**p27<sup>Kip</sup>(CDKN1B):** cyclin dependent kinase inhibitor 1B  
**p57<sup>Kip2</sup> (CDKN1C):** cyclin dependent kinase inhibitor 1C  
**P5C:** pyrroline-5-carboxylate reductase  
**PanIN:** pancreatic intraepithelial neoplasia  
**PARP:** poly (ADP-ribose) polymerase  
**PC:** pyruvate carboxylase  
**PD:** Parkinson's disease  
**PD-1:** programmed cell death protein 1  
**PDAC:** pancreatic ductal adenocarcinoma  
**PDGF-AA:** platelet-derived growth factor AA  
**PDH:** pyruvate dehydrogenase  
**PDK:** pyruvate dehydrogenase kinase  
**PDK1:** pyruvate dehydrogenase kinase 1  
**PFK1:** phosphofructokinase 1  
**PFKFB3:** 6-phosphofructo-2-kinase/fructose-2'6-biphosphatase 3  
**PGM:** phosphoglycerate mutase  
**PH:** Preiss-Handler  
**PHD:** prolyl hydroxylase domain protein  
**PHGDH:** phosphoglycerate dehydrogenase

**PI3K:** phosphoinositide 3-kinases  
**PIN:** prostatic intraepithelial neoplasia  
**PKM1:** pyruvate kinase M1  
**PKM2:** pyruvate kinase M2  
**PLXNA3:** plexin a3  
**PML:** promyelocytic leukemia protein  
**PolI:** RNA polymerase 1  
**PolIII:** RNA polymerase 3  
**PPP:** pentose phosphate pathway  
**pRB:** phosphorylated RB protein  
**PSAT:** phosphoserine aminotransferase1  
**PTEN:** phosphatase and tensin homolog  
**PTM:** post translational modification  
**PUFAs:** polyunsaturated fatty acids  
**PUMA:** p53 upregulated modulator of apoptosis  
**QA:** quinolinic acid  
**RAS:** rat sarcoma viral oncogene homolog  
**RB:** retinoblastoma protein  
**RNPs:** ribonucleoproteins  
**RNR:** ribonucleotide reductase  
**ROS:** reactive oxygen species  
**RPIC:** ribosomal protein inhibiting CDKs  
**RPL:** ribosomal protein large subunit  
**RPL11:** ribosomal protein large subunit 11 also known as uL5  
**RPL29:** ribosomal protein large subunit 29 also known as eL29  
**RPL5:** ribosomal protein large subunit 5 also known as uL18  
**RPs:** ribosomal proteins  
**RPS:** ribosomal protein small subunit  
**RPS14:** ribosomal protein small subunit 14 also known as uS11  
**rRNA:** ribosomal ribonucleic acid  
**RSL1D1:** ribosomal L1 domain-containing protein 1  
**RSV:** Rous sarcoma virus  
**SA- $\beta$ -Gal:** senescence-associated-beta-galactosidase  
**SAH:** S-Adenosyl-L-homocysteine  
**SAHF:** senescence-associated heterochromatin foci

**SAM:** S-Adenosyl methionine  
**SAPD:** senescence-associated protein degradation  
**SASP:** senescence-associated secretory phenotype  
**SCO2:** synthesis of cytochrome c oxidase assembly 2  
**SDH:** succinate dehydrogenase  
**SERPINB:** serine protease inhibitors B  
**SIRT7:** sirtuin 7  
**SMAD:** small mothers against decapentaplegic homolog family  
**SMAD4:** small mothers against decapentaplegic homolog 4  
**SMARCA5:** SWI/SNF-related matrix-associated actin-dependent regulator of chromatin subfamily A member 5  
**src:** sarcoma element  
**STAT3:** signal transducer and activator of transcription 3  
**TCA cycle:** tricarboxylic acid cycle also known as Krebs cycle  
**TERF2IP:** telomeric repeat-binding factor 2-interacting protein 1  
**TET:** ten-eleven translocation methylcytosine dioxygenases  
**TGF $\beta$ :** transforming growth factor beta  
**THF:** tetrahydrofolate  
**TIGAR:** TP53-induced glycolysis and apoptosis regulator  
**TIS:** therapy-induced senescence  
**TLRs:** toll-like receptors  
**TOMM34:** translocase of outer mitochondrial membrane 34  
**TOMM70:** translocase of outer mitochondrial membrane 70  
**TOP2:** DNA topoisomerase II  
**TP53:** tumor protein p53  
**TRAIL:** TNF-related apoptosis-inducing ligand  
**TRF2:** telomeric repeat-binding factor 2  
**uORF:** upstream open reading frames  
**uPAR:** urokinase-type plasminogen activator receptor  
**UPR:** unfold protein response  
**VHL:** von Hippel–Lindau protein



## Acknowledgments

---

A Ph.D. is a long and tedious process, despite the difficult times we sometimes have to face during a Ph.D., it remains a great journey is dotted with extraordinary people who make a Ph.D. an unforgettable experience.

First of all, I want to thank my supervisor Dr. Gerardo Ferbeyre for allowing me to do my Ph.D. in his laboratory. When I sent out e-mails to find a laboratory to do my Bachelor project outside of Germany, not many laboratories were eager to allow me to join them. Thank you for taking the risk of allowing me to do my internship and then my Ph.D. in your laboratory. I really want to thank you for all the great discussions we had over the time of my Ph.D., and I want to especially thank you for your open door and flat hierarchy policy in your laboratory. I want to thank you for allowing me to challenge every scientific suggestion you made, and I think with our discussion, you let me grow as a scientist. Thanks a lot for all the great beer discussions and your scientific enthusiasm. I would not have been able to complete my Ph.D. in the way I did without your support, patience, and understanding.

I also want to thank all the members of the Ferbeyre laboratory I work with during my Ph.D. First of all, I want to mention Xavier, who trained me during my internship as well as during the first year of my Ph.D. Xav, thanks for your patience and devotion to training me because I know I might not have been the easiest student to train. Furthermore, I want to thank my bench neighbor Fred. Fred, you are one of the most enthusiastic scientists I have seen, and your optimism and positive vibes have made many disappointing weekends much more bearable. You have a unique way to motivate people, and I was lucky to have you as my bench partner. I also want to thank the two summer interns I trained during my Ph.D., Mehdi, and Jacob; you both helped my development as a scientist as I learned it is one thing to know a technique; it is a whole different thing to be able to teach it. Thanks, both of you, for your patience and scientific enthusiasm, which allowed me to grow as a scientist. I want to particularly thank Jacob for the many hours you spent in the laboratory to help me finish the Mol cell paper. Without your help, Jacob, many parts of the Mol cell paper would not have been possible.

I also want to thank all the other Ferbeyre lab members for your help, scientific input, and friendship. Vero, Lian, Ana, Marie-Camille, Stéphane, Alexandra, Camille, Benji, Emma, Neylen, Rose, Jordan, Paloma, Olga, Marianna, Mat, Karine, Genevieve, you all helped me to grow as a

scientist and to work with you was a great pleasure. All of you filled my Ph.D. with great memories, and I really want to thank you for this. One of the great things about the Ferbeyre laboratory is the great beer get-togethers where we could discuss science but also just have fun. Thank you all for the great times.

Of course, I want to thank all the support staff in particular Robert, who is in charge of running the autoclave and washing the dishes. Robert, your support was of the utmost help during the time of my Ph.D. Your encouragements and happiness are contagious and allow one to push through even the toughest research days. Thanks a lot.

I also want to thank all the Professors that guided me during my Ph.D. My thesis comity Dr. Mallette and Dr. Bouvier, your input and scientific knowledge was of great help, and I want to thank you for the time and discussions. Furthermore, I want to thank Dr. Roy, Dr. Chartrand, Dr. DesGroseillers, and Dr. Omichinski for the scientific discussions and input during presentations or department retreats. I also want to highlight Dr. Lea Brakier-Gingras, who helped me to integrate into the group and helped with the administrative work for international students when I joined the lab.

I also want to thank the thesis evaluation comity for reading my thesis as well as your great comments.

Finally, I want to thank all the great collaborators who helped me greatly with all the laboratory work. I want particularly mention here the microscopy platform and Monique and Nico. You allowed me to master most microscopy tasks, and without your support, many microscopy images would not have been possible. I want to thank Haythem, Mohammed, Pierre, and Gunjan for your help on protein purification and in vitro protein complex assembly. You all taught me a lot. I want to thank Aurélien for helping me with the electron microscopy and your friendship. It was a pleasure working with you. I want to mention the laboratory of Ivan Topisirovic as well as David and Oro. Ivan, you allowed me to take from you and Oro's time to perform many metabolic experiments. I really appreciate working with you guys. Oro, I want to thank you for your scientific rigor and devotion to the HTC project; this paper would not have been possible without your work and dedication. Even though the lab work is important during a Ph.D., the social and fun component allows for decompression from work. I want in particular thank Sam, Aurélien, Charline, Maxime, Pierre, Lauriane, Ariane, Kate for your friendship. So whether it was the camping weekends or the trip to the ski chalet, or just hanging out together, it was always fun.

Most importantly I want to thank my family for their support and help. Mama, Papa ohne eure Hilfe wäre der PhD so nicht möglich gewesen. Eure Hilfe hat es mir erlaubt mein Abitur zu schaffen sowie auch nach Kanada zu gehen und meinen Doktor hier zu machen. Ihr habt mich durch trotz der 6000km immer unterstützt und ermutigt weiter zu arbeiten. Ich möchte mich auch

bei meinen beiden Brüdern danken für die Hilfe und die Ermunterungen wenn ich mal wieder über das Labor geschimpft habe. Außerdem und das darf hier nicht fehlen Malte an die bessere motivation vor dir meine Arbeit abzuschließen, es kann ja nicht sein das du derjenige wärst der schneller den höheren akademischen Titel hast als ich. Desweiteren möchte ich mich auch bei meine Großeltern insbesondere dir Bernhard bedanken für die Unterstützung die es mir erlaubt hat regelmäßig wieder nach Hause zu kommen auch wenn es immer nur für Ferien war. Einen ganz besonderen Dank möchte ich auch an Dr. Kappenberg richten meinen Chemielehrer der Mittel- und Oberstufe, der mir das wissenschaftliche Arbeiten und Forschung gezeigt hat. Ich frage mich noch manchmal was wäre ich geworden ohne die Chemie AG und Ihren Enthusiasmus uns Chemie und Wissenschaft beizubringen und die doch reichlichen Explosionen von Gummibärchen.

Je voudrais également remercier ma belle-famille ici qui est devenue comme ma deuxième famille. Particulièrement merci à Paul et Paule pour votre support, votre aide, et votre disponibilité. Également je voudrais remercier Hubert, Jeanne et Eloi qui m'ont supporté, chacun à leur manière. J'aimerais aussi mentionner Robert et Marc qui, malgré les nombreuses questions que je pose sur le sirop d'érable, n'ont jamais perdu patience avec l'allemands qui as deux mains gauches. Les fins de semaines à la cabane a ne pas penser à la science sont toujours reposant et une source de force pour la semaine. Un grand merci. Lastly, I want to thank the most important people in my life. Alix, I want to thank you for your patience, your understanding, our discussions, your help, and just everything that allowed me to finish my Ph.D. You are the best partner. Of course, I also want to thank Olivia and Elodie for your patience and understanding that daddy has to work sometimes late or on the weekend.





# Chapter 1

---

## Introduction

### 1.1. The bases of cancer biology

The advances of modern medicine have allowed an increased understanding of the biology of human illnesses. However, there are undoubtedly still significant knowledge gaps to fill. For example, one of the most devastating maladies is undeniably cancer. About 44% of people living in Canada will have a cancer diagnosis in their lifetime, and 1/4 will die of cancer, making cancer the number one cause of death in Canada [1]. The molecular processes at the base of cancer development are started to be understood, and a significant process was made in the last decades in curing cancer. Regardless of those advances, cancer remains one of the most daunting illnesses of humanity. The understandings of the biological processes involved in malignant transformation and cancer initiation are thus of utmost importance.

#### 1.1.1. Cell cycle regulation

The human body is a complex system assembled by the interplay of different tissues and organs, which can be further divided into cells and extracellular spaces. The average human body contains approximately  $3.72 \times 10^{13}$  cells [2]. Most cells have a definite lifespan, and tissues undergo a constant renewing by cell divisions. Cell division is a complex multi-step process orchestrated by cyclin dependant kinases (CDKs) and cyclins [3]. Each cellular division follows the same pattern, which is called the cell cycle, and this can be separated into four major phases: The G1, S, G2, and the M phase [4]. See figure 1.1.

Each phase of the cell cycle is characterized by the expression of a specific cyclin along with a specific CDK and cyclin dependant kinase inhibitors (CDKi) [4]. For this thesis, the G1 phase, as well as the transition from G1 to S phase, are the most relevant phases of the cell cycle and will be discussed in greater detail later. Briefly, the G1 phase is characterized by the expression of cyclin dependant kinase 4 (CDK4) and cyclin dependant kinase 6 (CDK6) with cyclin D1. At the

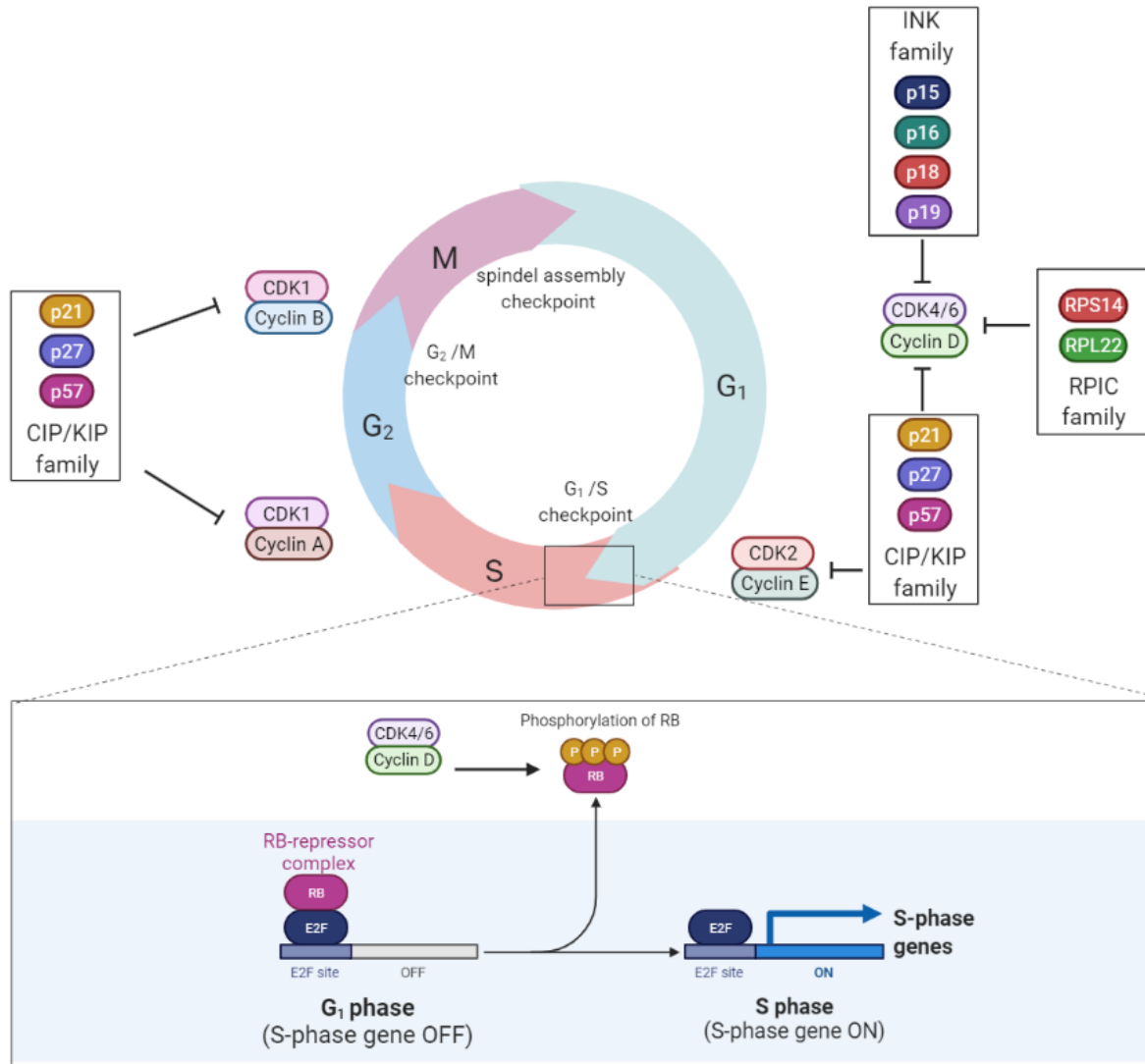


### Figure 1.1. Steps and regulation of cell cycle

The interplay of CDKs and cyclins drives the progression of the cell cycle. Each cyclin's levels vary during the cell cycle and the interaction of cyclins with the corresponding CDK results in kinase activity of the CDK and phosphorylation of CDK targets. The cell cycle starts with the G<sub>1</sub>-Phase. In this phase, cells prepare for subsequent phases. The tumor suppressor RB mediates the transition from G<sub>1</sub> to S. In S phase, DNA and other macromolecules required for division are amplified. During the S phase, levels of cyclin A increase resulting in the transition to the G<sub>2</sub> phase. At the end of G<sub>2</sub> is the G<sub>2</sub>/M checkpoint. This checkpoint verifies that all material is present for cell division. Increased levels of cyclin B bypass this checkpoint and allow progression into Mitosis. M-Phase is the actual division into two cells. Once cell division is completed cell cycle can start again with the G<sub>1</sub> phase. In the lower part, a Zoom in on the G<sub>1</sub>-S checkpoint and the actions of RB are shown. If CDK4 and CDK2 do not phosphorylate RB, the E2F transcription factor is tightly associated and repressed by RB. Once RB gets phosphorylated, E2F is released, resulting in transcription of S Phase genes. Regulation of CDK activity is achieved by CDKi, the inhibitory proteins of the CDKs. In the G<sub>1</sub> phase, all three families of CDKi can stop CDK4 activity. Abbreviations: RB: retinoblastoma protein, RPIC: ribosomal protein inhibiting CDKs, CDK: cyclin dependent kinase, INK: inhibitors of CDK, CIP/KIP: CDK interacting protein/Kinase inhibitory protein. This image is adapted from [5] and adapted from templates with BioRender.

end of the G1 phase, there is a checkpoint, and in order to transit from G1 to S phase, phosphorylation of RB by CDK4/6 releases E2 promoter binding factors (E2Fs) from pocket proteins such as retinoblastoma protein (RB). E2Fs can then induce transcription of cyclin E and other genes involved in S phase. The S phase, or synthesis phase, is the phase when all the genetic information is duplicated, plus the cell amplifies the materials required for the daughter cell. This phase is also crucial for DNA damage repair as homologous repair of the DNA occurs in this phase of the cell cycle. Whether there is a checkpoint at the end of the S phase for transition into the G2 phase is still a matter of debate. However, it has been shown that inhibition of ataxia telangiectasia and Rad3-related protein (ATR) during the S phase results in early Forkhead box protein M1 (FOXO1) increase which in turn leads to early mitosis, under replicated DNA, and DNA damage [6]. Following S phase, there is the G2 phase characterized by the expression of cyclin A and cyclin dependant kinase 1 (CDK1). Finally, at the end of the G2 phase is the G2/M checkpoint. This checkpoint verifies if all DNA replication and synthesis of biomolecules are done, and the cell is ready to process into the actual division phase. Bypass of this checkpoint is achieved by high levels of CDK1 and cyclin B [4]. M phase is the phase of the actual division of the cell into two daughter cells and is initiated by high levels of CDK1 and cyclin B [4]. The antagonists to CDKs are the CDKi which can be divided into three categories. The two classic CDKi, CDK-interacting protein/kinase inhibitory protein (CIP/KIP) family and the inhibitor of kinase (INK) family and a third novel class of ribosomal protein inhibiting CDKs (RPIC) [5]. The CIP family is composed of cyclin dependent kinase inhibitor 1A protein (CDKN1A gene) (p21<sup>cip1-waf1</sup>), cyclin dependent kinase inhibitor 1B (p27<sup>Kip</sup>(CDKN1B)) as well as cyclin dependent kinase inhibitor 1C (p57<sup>Kip2</sup>(CDKN1C)) and is characterized by its binding to the CDK-cyclin complexes, such as cyclin dependant kinase 2 (CDK2)- cyclin E complex or CDK1-cyclin B complex [4]. The INK family includes protein 15 of the INK family transcript b (CDKN2B) (P15<sup>INK4B</sup>), protein 16 of the INK family transcript a (CDKN2A) (P16<sup>INK4A</sup>), protein 18 of the INK family transcript c (CDKN2C) (P18<sup>INK4C</sup>) and protein 19 of the INK family transcript d (CDKN2D) (P19<sup>INK4D</sup>) and this family is characterized by binding to only the CDKs and inhibiting binding of CDK4/6 to cyclin D proteins [4].

The third class of CDKi, ribosomal protein inhibiting CDKs (RPICs)[5], has recently been discovered and will be further described in article 1 of this thesis. Briefly, ribosomal dysfunction on senescent cells results in the accumulation of ribosome-free ribosomal proteins [7, 8]. Furthermore, those ribosomal proteins outside of the ribosome can interact with CDK4 and limit its kinase activity resulting in decreased cell cycle progression [5, 7, 8].

The interplay of CDK cell cycle promoting activity and CDKi cell cycle inhibition is at the base of cancer development as an uncontrolled cell division could result in uncontrolled growth, an alteration in cell homeostasis, and eventual tumor growth [3, 9].

It has been known for several decades now that alterations in the homeostasis of the cell and disturbance of the integrity of the deoxyribonucleic acid (DNA) are at the base of malignant transformation [9, 10]. Alterations in the DNA integrity can result in uncontrolled cell cycle progression and eventually the development of a malignant mass. The human body is constantly exposed to agents that can induce mutations in the DNA as well as factors changing the epigenetic code of the cell.

### **1.1.2. The processus of cellular transformation**

The sources of mutagens can be endogenous such as reactive oxygen species (ROS) [11], genetic predispositions [12], cellular age [13], random errors in DNA replication [14, 15] or external such as oncogenic viruses [16], bacterial pathogens [17], exposure to UV light [18], consumption of toxins (smoking, alcohol, etc.), cytotoxic drugs [9] or epigenetic modifications such as, accumulation of oncometabolites [19–21] or availability of co-factors for epigenetic modifiers such as acetyl-CoA, nicotinamide adenine dinucleotide derivates, *α*-ketogluterate or s-adenosyl methionine (SAM) [21–25].

In recent times, even more factors able to induce cancer were suggested, for example, changes in expression of lncRNA or miRNAs [26, 27] gene fusions by read-through [28], translational read-through events [29]. Interestingly, a recent pan-cancer whole-genome analysis of more than 30.000 cancer patients could not find apparent drivers for cancer initiation in 10% of the samples suggesting that there are new cancer genes yet to be discovered [27]. No matter which factor will be the most important, it is also clear that the body has several mechanisms to detect and repair those genetic mutations or alterations. However, over time the accumulation of mutation in one cell can lead to cellular transformation and cancer development [13].

By now, it is known that cellular transformation is at the base of the development of cancerous cells. Transformation of cells can be seen as a multi-step process in which the cell loses, due to the factors mentioned above, its ability to adequately regulate cell cycle resulting in the uncontrolled division and amplification of the cells [30]. This multi-step process, called cellular transformation, can be divided into different steps that can rarely occur simultaneously but mainly happen over a long time see figure [1.2].

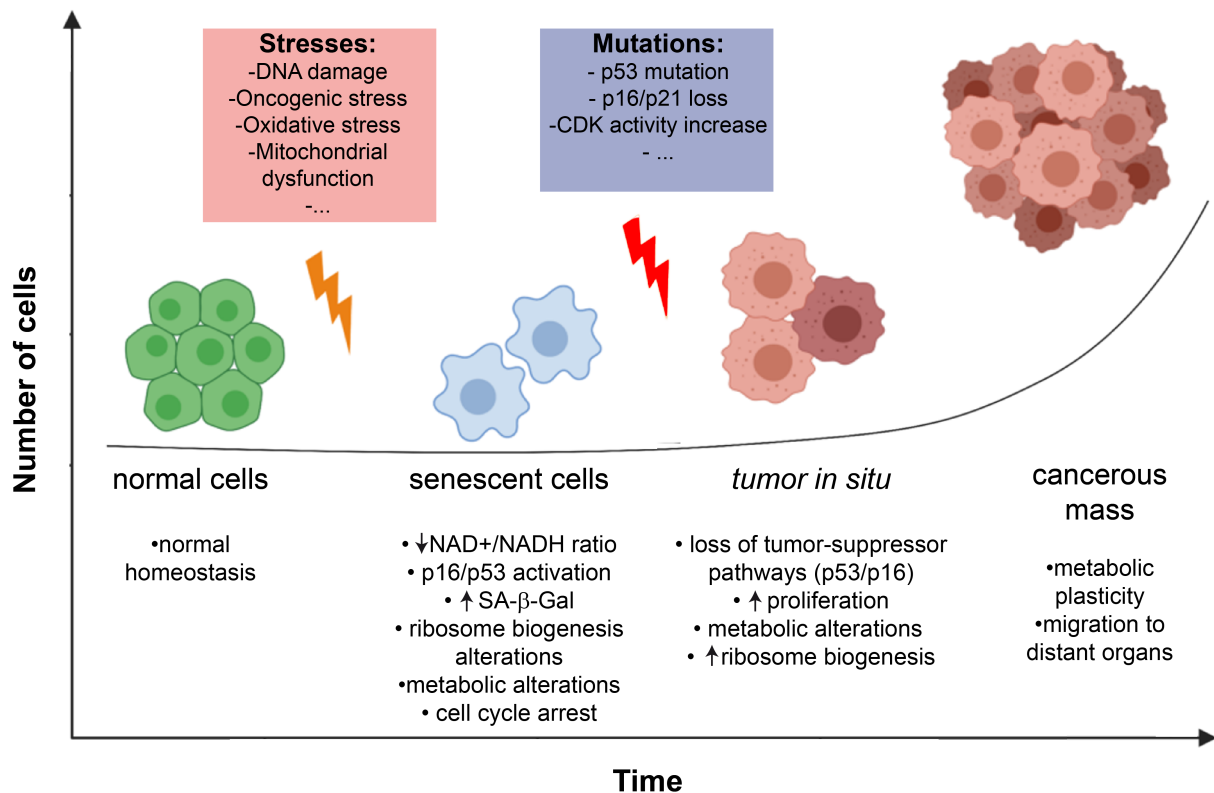


### Figure 1.2. Cellular transformation and bypass of cellular senescence

This cartoon highlights the requirements for bypass of senescence and malignant transformation. Normal cells can induce cellular senescence following the encounter of various potentially oncogenic stresses. Those stresses include but are not limited to activation of oncogenes, loss of tumor suppressors, oxidative stress, DNA damage, etc. The senescence response is mediated by the actions of tumor suppressors such as RB and p53. Other markers of senescence highlighted here are the increased SA $\beta$ -Gal and cell cycle arrest, p16 and p53 activation and accumulation, as well as a decrease in NAD<sup>+</sup>/NADH ratio. In case both tumor suppressors p53 and RB, are inactivated in human cells, malignant transformation can occur. This process takes several months or years, and eventually, further mutations occur, and cells gain proliferate advantage and become a detectable tumor burden. Interestingly, even though some tumor cells have lost p53 and RB tumor suppressors, induction of senescence or senescence-like phenotype is possible. Most often, the inducers of tumor-induced senescence include chemotherapeutic drugs or over-activation of an oncogene. Regardless, the effectors of tumor cell-induced senescence are still to be uncovered. Image generate with BioRender.

In the currently accepted model of cancer development, the clonal model, one cell gains a proliferate advantage and develops into a pre-neoplastic lesion [31, 32]. In pre-neoplastic lesions such as benign prostatic hyperplasia (BPH), pancreatic intraepithelial neoplasia (PanIN) or nevi it was observed that tumor suppressor mechanisms such as cellular senescence are activated and

maintain a non-invasive state [33–37]. We will discuss the effects of cellular senescence later on. Even though tumor suppressor mechanisms such as cellular senescence exist, further mutations in the pre-neoplastic lesion can lead to a bypass of those tumor suppressor mechanisms and the development of non-invasive pre-cancerous lesions, also called *tumor in situ*. Further alterations in the cell can lead to invasive behavior of these cells and invasion into the surrounding tissue, and eventually, those primary cancer cells metastasize into distant organs. Once a cancer cell has acquired the ability to metastasize, treatment of those cancer becomes extremely difficult [38, 39].

As previously mentioned, the accumulation of mutations is the underlying cause of cancer initiation and cellular transformation. Mutations or epigenetic changes can drive cancer formation by the following processes: The constant activation of oncogenes, the loss of tumor suppressor genes, the alteration of metabolism or acquirement of metabolic flexibility, immune cell evasion, resistance to death signals, the capacity of invasion, extensive genomic and epigenetic diversification [10, 22, 30, 40, 41]. See figure [1.3].

All those factors are defined today as the hallmarks of cancer. In total, ten cancer hallmarks have been suggested, and most hallmarks can be found in each cancer. In the following focus will mainly be on tumor suppression mechanisms in cell cycle regulation, metabolic alterations in cancer and tumor suppression, and activation of oncogenes in the regulation of the cell cycle.

## 1.2. Activation of oncogenes

For a cancerous development to occur, a cell has to gain the ability to proliferate faster than the surrounding cells. One way to increase the proliferation of a cell is to amplify the activity of genes responsible for proliferation. The idea of amplifying pro-proliferative genes for cancer development was proposed in 1914 by a German researcher, Theodor Boveri, who saw that cancerous cells had amplification of certain chromosomal parts. He called those parts *Teilungsfördernde Chromosomen* for pro-proliferative chromosomes or onco-chromosomes [42, 43]

It was then in the 1970ies that researchers identified the sarcoma element (*src*) the first oncogene while studying the chicken Rous sarcoma virus (RSV) [44–46]. Shortly after, an endogenous *src* was discovered in avian DNA [47]. Interestingly, endogenous *src* required a activation mutation to transform cells suggesting that endogenous *src* is a proto transformation gene. In order to distinguish between those two possibilities, the following terms were coined: The term oncogenes for genes that without further mutation, such as v-*src* (viral *src*), have transformation ability. As well as the term proto-oncogene for genes that require further mutation for transformation such as cellular *src* (c-*src*) [44]. By now, around 40 oncogenes and proto-oncogenes have been described among others, the rat sarcoma viral oncogene homolog (RAS) family of proto-oncogenes,

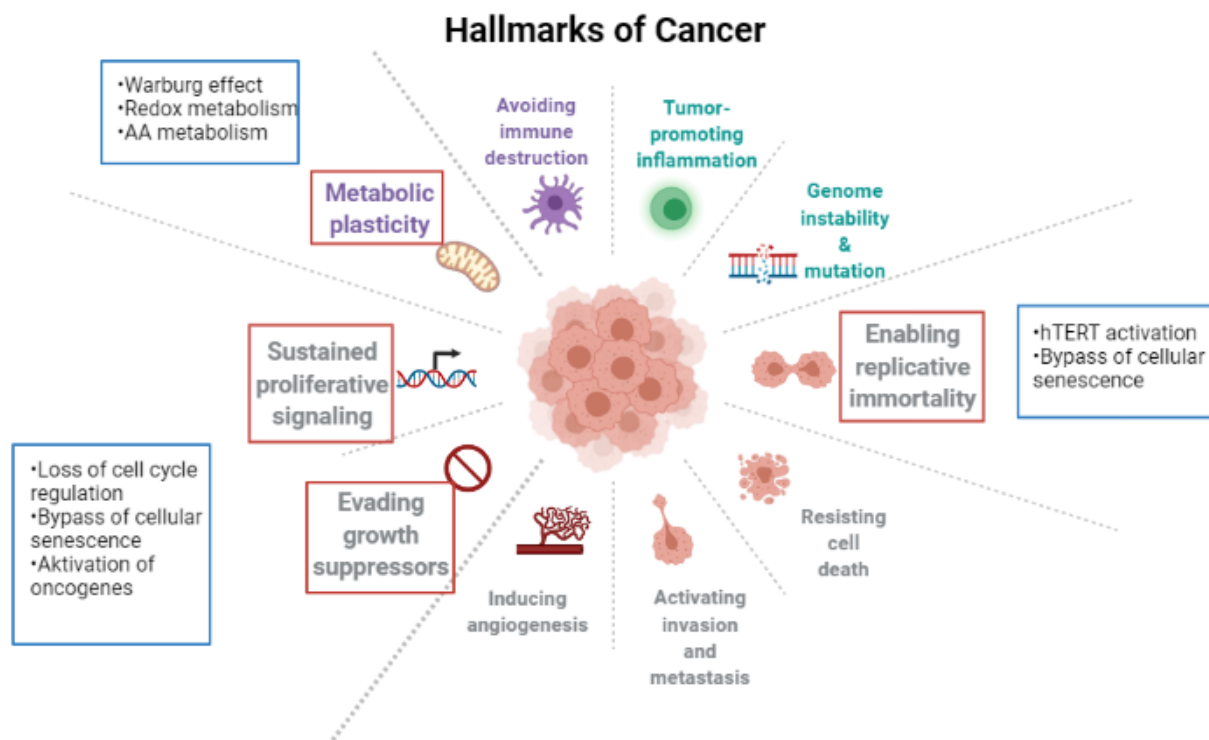


**Figure 1.3. Hallmarks of cancer**

In total, ten hallmarks of cancer have been proposed. The image shows the different hallmarks, and the hallmarks relevant for this thesis have been highlighted (red squares). Those hallmarks include acquiring metabolic flexibility in cancer cells, loss of growth suppressors, sustained proliferative signaling, and replicative immortality. Some key features of each hallmark that will be discussed are shown next to the hallmark (blue squares). Metabolic flexibility is characterized by, the Warburg effect, an alteration in amino acid metabolism, and alterations of REDOX metabolism. In the following, the molecular alterations leading to metabolic flexibility are discussed. Similarly, the sustained proliferation and loss of growth suppression and replicative immortality are mediated by key proteins in cellular senescence such as p16 and p53. Roles of those tumor suppressors and oncogenes in light of metabolic alterations and cell cycle regulation will be discussed further on. Image adapted from [22] and BioRender templates.

the cellular-avian myelocytomatosis viral oncogene homolog (c-MYC) proto-oncogene or the erythroblastic oncogene B or HER2/neu (ERBB2) proto-oncogene [48, 49] and in many cancer types at least one, often several, of those oncogenes will be activated [50].

A big pitfall of the discoveries of oncogenes in the 1980ies was that most of them were extracted and tested in already premalignant cancerous cells. Thus, a big surprise arose when Newbold *et al.* put the newly discovered oncogene Harvey-RAS (H-RAS) into primary hamster fibroblast cells and showed that these cells did not form any tumors in soft agar. Those results suggested



that the activation of the oncogene alone was not sufficient to induce transformation [51]. This discovery was controversial, and it took more than ten years before Serrano *et al.* could demonstrate that expression of H-RAS would not only increase expression of pro-proliferative genes but also would lead to the accumulation of tumor suppressor protein p53 and p16<sup>INK4a</sup> [52]. They characterized this oncogenic feedback mechanism and revealed that the cells are permanently arrested in G1 of the cell cycle, hence opposing the transformation process [37, 53]. Further, it was shown that those cells have similarities with primary cells that have surpassed their replication capacity, a process called cellular senescence [54, 55], thus they called this response to oncogenic activation oncogene-induced senescence (OIS) [37, 52]. Subsequently, it was shown that most oncogenes, at least as a single activation in primary cells, would lead to activation of tumor suppressor mechanisms, hence opposing the transformation process [56]. In the following, the implication of tumor suppressors will be discussed.

### 1.3. Loss of tumor suppressor mechanisms

As previously mentioned, the activation of an oncogene is in most cases accompanied by the activation of tumor suppressors genes and in order to get transformed, potentially cancerous cells have not only to increase the activity of oncogenes but also lose the tumor suppressor genes [57]. The best-known tumor suppressor gene is tumor protein p53 (TP53) and this protein is mutated in about 50% of all cancers [58–60]. In contrast to the activation of oncogenes, where only one of the two copies of the gene needs to be altered, most tumor suppressors are haplo-sufficient, meaning a bi-allelic inactivation is required to abolish the function of those proteins entirely. This model was initially proposed by Knudsen while studying the RB tumor suppressor gene [61, 62]. The Knudsen two-hit model suggests that both copies of the tumor suppressor in the genome, within the same cell, are needed to be inactivated so that tumor suppressor function is lost. With more research on the Knudsen two-hit model it was shown that this model does only apply to few tumor suppressors as it is now known that some tumor suppressors are haploinsufficient; thus, exceptions to this rule exist. For example the tumor suppressor genes TP53, p27<sup>Kip</sup>(CDKN1B) phosphatase and tensin homolog (PTEN), small mothers against decapentaplegic homolog 4 (SMAD4) or neurofibromin 1 (NF1) [58, 63–68]. For instance, p53 is working as a tetramer, and it is hypothesized that one allele of p53 is not sufficient to achieve high enough p53 WT levels to prevent cellular transformation [68]. In an old model, tumor suppressors can be classified into three groups gatekeepers, caretakers, and landscapers [69, 70] although it seems that more and more tumor suppressors can adhere to two or all three groups [71, 72].

Landscapers are tumor suppressors that regulate extracellular matrix proteins, cellular surface markers, cellular adhesion molecules, and growth factors. For example, proteins that maintain epithelial polarization such as epithelial cadherin (E-CAD) or  $\beta$ 1-integrins have been shown, at least in some cancer models, to reduce cancer initiation and metastasis burden [41, 73]. In addition, tumor suppressors such as PTEN, SMAD4 or cluster of differentiation 27 (CD27) were shown to positively modulate the immune response so that neoplastic lesions could be cleared more efficiently [74, 75].

Caretakers tumor suppressors are all the proteins that maintain genomic integrity by repairing damaged DNA either by non homologous end joining (NHJE) or homology directed repair (HDR). Examples of caretakers are, breast Cancer gene 1/2 (BRCA 1/2) or X-ray repair complementing defective repair in Chinese hamster cell member 5 or 6 (Ku70/XRCC6 and Ku80/XRCC5). Another category of caretakers tumor suppressors are proteins that mediate the DNA damage response (DDR) such as ataxia telangiectasia mutated (ATM), ATR or mutS homolog 3 (MSH3). Following a strong activation of the DDR caretaker tumor suppressors are often activators of gatekeepers.

Gatekeepers are proteins that directly regulate the cell cycle, differentiation, as well as cell death, and some members of this group are p53, P16 <sup>*INK4A*</sup>, p21 <sup>*cip1-waf1*</sup>, and RB. For instance, high levels of DNA-damage in cells result in ATM activation that will phosphorylate p53 on S15 hence stabilizing p53 [76]. Depending on the level of damage and the duration of the signal, p53 will induce apoptosis, permanent cell cycle arrest, or transient cell cycle arrest [77]. In addition, it is known that p53 will induce p53 upregulated modulator of apoptosis (PUMA) and phorbol-12-myristate-13-acetate-induced protein 1 (NOXA) to induce apoptosis and p21 for the arrest of the cell cycle [78]. Even though many post-translational modifications of p53 are known, the exact modifications on p53 that achieve tumor suppression and whether apoptosis or cellular senescence promoting proteins are induced are still under investigation [79].

Another group of gatekeepers are tumor suppressors that regulate metabolism and in case of dysfunction would result in pro tumorigenic metabolism. This group is composed among others of von Hippel–Lindau protein (VHL) [72], liver kinase B1 (LKB1) [80], fumarate hydratase (FH) [81], TP53-induced glycolysis and apoptosis regulator (TIGAR) [82], succinate dehydrogenase (SDH) [83], isocitrate dehydrogenase1/2 (IDH) [21, 84], and fragile histidine triad protein (FHIT) [72]. Mutations that slow the reaction speed of FH or SDH enzymes result in the accumulation of fumarate or succinate and those metabolites are structurally similar to  $\alpha$ -ketoglutarate ( $\alpha$ -KG) but can not be metabolized in  $\alpha$ -ketoglutarate dependent reactions. High level of succinate or fumarate result in inhibition of  $\alpha$ -KG obligate reactions of ten-eleven translocation methylcytosine dioxygenases (TET) or jumonji domain containing histone lysine demethylases (Jumonji demethylases)

resulting in altered DNA and histone methylation state [80] as well as in inhibition of prolyl hydroxylase domain protein (PHD) which target hypoxia-inducible factor (HIF) for degradation via the E3 ligase VHL [85, 86]. High HIF levels result in increased glycolysis, a Warburg-like effect, and lactate secretion which can inhibit immune cell clearance [87] as well as increased *de novo* angiogenesis [88].

Loss of function of the tumor suppressor IDH has similar effects as mutations in the IDH gene result in the production of 2-hydroxyglutarate (2-HG) which is chemically similar to  $\alpha$ -KG [84, 89]. It was shown that mutations of IDH1 in residue 132 from arginine to histidine (R132H) result in the production of 2-HG. Similarly, mutation of arginine residue R172 in IDH2 into histidine or other amino acids results in the production of 2-HG. By looking chemically at 2-HG and  $\alpha$ -KG, one can appreciate that the only difference between both molecules is the carbonyl group instead of a hydroxyl group at the fourth carbon. Because of the chemical similarity of both 2-HG and  $\alpha$ -KG accumulation of 2-HG results in binding of 2-HG in the active site of  $\alpha$ -KG obligate reactions such as TET enzymes or Jumonji demethylases family enzymes. Inhibition of  $\alpha$ -KG obligate reactions results in alterations of DNA and Histone methylation marks such as 5hmC or H3K9 [89]. Alterations in the methylation mark result in aberrant gene transcription, and low levels of methylated DNA are associated with high differentiated cells such as stem cells or highly aggressive cancers.

In summary, tumor suppressor genes will regulate pathways involving cell division inhibition, induction of apoptosis, DNA damage repair response, metabolism, inhibition of metastasis, and induction of immune response [72].

### 1.3.1. Limitations of the tumor suppressor and oncogene model

As concluding remarks for the last section, it should be stated that the model of oncogenes and tumor suppressor genes is a try to explain a far more complex biological phenomenon [72]. Although the classic oncogenes will mostly promote cancer, there are cellular contexts in which oncogenes would rather be classified as tumor suppressors. Some examples of this would be signal transducer and activator of transcription 3 (STAT3) [90], programmed cell death protein 1 (PD-1) [91], mouse double minute 2 homolog (MDM2) [92] extracellular signal-regulated kinase (ERK) [93, 94] and many others. The roles of STAT3 (in the review article) and ERK as tumor suppressors will be discussed later on.

Similar to the oncogenes, there are tumor suppressor genes that in certain contexts might rather act as oncogenes, such as p21 [95] or p27 [96], as their accumulation in the cytosol was shown to be a driver for cancer promotion. Other examples would be E-CAD [97] or RAD51 [98]. Part of

these phenomena can also be explained by the loss of cofactor in interaction partner hence the loss of initial protein function or change in localization [99].

On top of the limitation to the oncogene and tumor suppressor gene model, a recent analysis of 30.000 tumors samples has shown that 10% of all those cancers do not have a known driver mutation calling for further research [50].

## 1.4. Cellular senescence; More than a tumor suppressor mechanism

One of the aforementioned mechanisms of tumor suppression is the permanent cell cycle arrest or cellular senescence [37, 53]. However, cellular senescence has not been discovered as a tumor suppressor mechanism *per se*, but rather as a mechanism of cellular aging in cell culture. Hayflick and colleagues in the 1960ies showed that primary fibroblasts could not proliferate indefinitely in culture, as such, they might have an internal clock that stops their proliferation after a distinct amount of cell divisions [54, 55]. However, it was only in the late 1980ies that the molecular mechanism behind this aging clock was discovered as Blackburn and colleges showed the role of telomeres and telomerase [100–102]. Like most human cells, human fibroblasts do not express telomerase, an enzyme required to maintain the telomere structure at the end of the chromosomes. So during the division process, the end of the chromosomes can not be replicated due to the end-replication problem. The end-replication problem describes the inability of DNA replication at the end of the lagging strand at the edges of the chromosomes. After several rounds of division, the telomere structure, which avoids fusion of different chromosomes together, becomes so short that the chromosomes can fuse together, activate the DDR and induce cellular senescence. This state, in which primary cells stop due to erosion of is telomeres, is called replicative senescence or Hayflick limit [103].

In 1997, researchers could demonstrate that cellular senescence was not only a mechanism of aging but also a tumor suppressor mechanism. They activated the oncogene H-RAS in primary fibroblasts and observed that those cells displayed several features cellular senescence [52]. In general cellular senescence is seen today as a double edge sword. On the one hand, cellular senescence and the stop of proliferation helps to avoid cancer development; however, on the other hand, accumulation of those same senescent cells leads to aging and aging phenotypes [53, 104]. Understanding the benefits and risks of senescent cells will be discussed in the following parts.

### **1.4.1. Inducers and effectors of cellular senescence**

Cellular senescence, as a tumor suppressor mechanism, was first identified in primary cells upon activation of oncogenes such as H-RAS, but research over the last years identified numerous inducers of senescence, which can be classified into seven categories. OIS, loss of tumor suppressor-induced senescence (LOTIS), activation of tumor suppressors, therapy-induced senescence (TIS), metabolic stress-induced senescence (MSIS), replicative senescence, and programmed senescence. Some of those inducers of senescence mentioned above are now also used as biomarkers to identify senescent cells *in vivo* or *in vitro*. For an overview of inducers, see table [\[1.1\]](#).

**Table 1.1. Different stresses can induce cellular senescence.**

Cellular senescence can be classified into different groups based on the inducer of the senescence response. This list shows some examples of senescence inducers. The consequence of all inducers of senescence is cell cycle arrest. Nevertheless, each inducer of senescence can have specific markers of senescence.

Abbreviations: OIS: oncogene-induced senescence, LOTIS: Loss of tumor suppressor- induced senescence, TIS: Therapy-induced senescence, MSIS: Metabolic stress-induced senescence H-RAS: Harvey rat sarcoma viral oncogene homolog, B-RAF: Rapidly accelerated fibrosarcoma family protein and murine sarcoma viral oncogene homolog B, c-MYC: Cellular avian myelocytomatosis viral oncogene homolog, AKT: Ak strain transforming protein, STAT5: Signal transducer and activator of transcription 5 PTEN: Phosphatase and tensin homolog, NF1: Neurofibromin 1, CDK: cyclin-dependent kinase, PARP: poly (ADP-ribose) polymerase, HDAC: Histone deacetylase

Class	Examples of senescence inducer
OIS	constant activation of H-RAS [52], B-RAF [105], c-MYC [106], AKT [107], STAT5 [108], leukemogenic fusion proteins [109]
LOTIS	the loss of PTEN can activate AKT [110], loss of NF1 can activate RAS [111]
TIS	classic chemotherapy agents Doxorubicin [112], Camptothecin, Aurora kinase A inhibitors or Bleomycin [113], target approaches with CDK inhibitors [114], PARP inhibitors [115]
Activation of tumor suppressors	high expression of p16 or p21 [116], reactivation of p53 in tumors [117], expression of PML [118], expression of SOCS1 [119]
Programmed senescence	developmental senescence [120, 121] , tissue healing [122]
Replicative senescence	telomere shortening [103, 123]
MSIS	mitochondrial dysfunction [124], interference with mitochondrial respiratory chain [125], inhibitors of HDACs resulting in altered protein acetylation [126], inhibition of sirtuins [127], nucleolar stress [128], ribosome biogenesis alterations [7], chronic inflammation [129, 130]

An example of a senescence inducer that can be used as a biomarker would be the accumulation of the tumor suppressor p16 [131]. Unfortunately, the accumulation of p16 is not specific only to senescent cells; hence other biomarkers are required to identify senescent cells [132]. One obvious marker of senescent cells is the cell cycle stop in G1 which can be seen by the absence of E2F target gene expression or the low level of phosphorylated RB protein (pRB). However, low levels of phosphorylated RB is again an unspecific senescence marker because non-senescent cells which are in G<sub>0</sub> or postmitotic cells *in vivo* display low levels of pRB, too. The lack of a specific biomarker is a big challenge in the identification of senescent cells. Most senescence markers used today are somehow related to the molecular consequences of senescence. In the following, those molecular consequences of the induction of cellular senescence will be discussed. One of the molecular consequences of the accumulation of senescent cells suggested for a long time was premature aging. It was hypothesized that senescent cells accumulate to maintain tissue integrity as only some senescent cells are cleared by the organism [104]. For example, massive apoptosis, another tumor-suppressive mechanism, can damage tissue integrity because apoptotic cells are cleared from the tissue. In contrast to this, senescent cells can stay in the body examples would be nevi or BPH and maintain tissue integrity [33, 133]. It remains to be shown how some senescent cells do get cleared by the immune system, whereas other cells stay to maintain tissue integrity. Based on those observations, it was suggested that premature aging would be the price for tumor suppression. [53, 134].

#### **1.4.2. Aging the price of tumor suppression**

As mentioned previously, the primary mechanism that defines replicative senescence is telomere shorting, and for a long time, it was suggested that the accumulation of senescent cells could be a pro-aging mechanism. However, it was only in 2011 when Baker *et al.* could establish the role of senescent cells in aging [135]. They engineered a mouse model where the p16 promoter controlled an inactive FKBP-Casp8 fusion protein. Several stresses can activate p16, and only one of them is the induction of senescence [136]. FKBP-Casp8 fusion protein-positive cells, senescent cells, along cells that endogenously express high levels of p16 are killed by apoptosis upon the administration of AP20187, a synthetic drug that induces dimerization of FKBP leading to activation of Caspase 8. This model is known as the INK4A locus regulated apoptosis through targeted activation of caspase (INK-ATTAC) model for INK for the p16 promoter and the ATTAC for apoptosis through targeted activation of caspase. Next, they crossed their model with a mouse strain having a hypomorphism of the mitotic spindle checkpoint serine/threonine-protein kinase Bub1 (BubR1) gene resulting in chromosomal aberrations leading to a premature aging phenotype [135] [137]. Using their final genetic model INK-ATTAC with BubR1 mutation, they showed that

in mice where p16 positive cells were cleared, the onset of age-related diseases, such as cataracts and sarcopenia, was significantly delayed compared to control mice (mice where p16<sup>+/+</sup> senescent cells were not eliminated) [135].

In 2016, the same group proved that the accumulation of senescent cells is not only relevant for the aging phenotype in accelerated aging models but in normal aging, too. Their results showed that mice where p16 positive cells were removed, starting at the age of 1 year, had a lower incidence of spontaneous tumor formation, increased spontaneous movement and exploratory behavior, and better cardiac age [138]. Up to now, several similar model have been developed and they have been used to show implications of senescent cells *in vivo* in numerous age-related diseases such as, adipose atrophy [138], atherosclerosis [139], age related bone loss [140], neurodegeneration [141], cardiomyocyte hypertrophy [138], glomerulo-sclerosis [142], idiopathic pulmonary fibrosis [143], osteoarthritis [144], renopathy [145].

Following the proof of concept that eliminating senescent cells can alleviate aging phenotypes, searches for senolytic drugs that specifically kill senescent cells were started. Subsequently, several senolytics have been proposed on rational design. For instance, it is known that senescence cells have higher resistance to apoptosis [146] due to higher expression of B-cell lymphoma 2 protein (BCL2) and B-cell lymphoma-extra large protein (BCL-xL) [147]. One of the earliest senolytics were ABT263 [148] and ABT737 [147, 149] both inhibitors of the B-cell lymphoma 2 protein family (BCL-2 family). Other drugs or natural products have been shown to have senolytic capacity depending on the cell type and the strength of the senescence [150]. Up to now, over 100 drugs have been suggested for senolytic activity [151].

Despite the positive effect of senescent cell clearance on aging, it has been pointed out that removing senescent cells can also have detrimental effects. For example, after acute injury to the liver or after massive blood loss, there are increased numbers of senescent cells; and removal of those senescent cells resulted in the premature death of the animals [152–154]. Moreover, positive roles of senescence and senescent cells have been shown in wound healing, developmental senescence, and of course, the aforementioned tumor suppressor activity; hence constant elimination of senescent cells might impair these beneficial effects [155].

### **1.4.3. Role of senescence in wound healing and developmental senescence**

In the last part, the detrimental effects of senescent cells were discussed, although the positive effects are present, too. For example, it has been shown that the presence of senescent cells can limit fibrosis in skin or liver [156, 157], lung [158] and heart [159]. Fibrosis is one of the biggest health problems in the aging population and no efficient treatment to reverse fibrosis is available;



however other researchers have suggested that senescent cell removal limits fibrosis [160]. Regardless of the effects of senescent cells on fibrosis, extreme caution should be taken for senolysis experiments, and further research will determine the contribution of senescence to fibrosis.

Another positive factor of senescent cells is increased wound healing. It was demonstrated that the presence of senescence cells increases the speed of wound healing through the secretion of senescence-associated secretory phenotype (SASP) factors such as the protein platelet-derived growth factor AA (PDGF-AA) [122].

A further interesting aspect of senescence is the presence of senescent cells in developing structures in embryos [120, 121]. Interestingly, this senescence does not have an inflammatory SASP but is dependent on p21. Furthermore, developmental senescence is not mediated by increased DDR or p16-p53 but the axis transforming growth factor beta ( $TGF\beta$ ) /small mothers against decapentaplegic homolog family (SMAD)- and forkhead box proteins subfamily O (FOXO) and phosphoinositide 3-kinases (PI3K) seems to be relevant for this senescence [161]. Further research confirmed that not only is senescence present in the developing mouse embryo, but also it occurs in other model organisms. Model organism with developmental senescence include, the axolotl [162], see also the article in annex 2, the zebrafish [162, 163], the naked rat mole [164] or the chicken [164].

We demonstrated in the axolotl that the pronephros, a structure that is converted into the mesonephros during development, displays features of senescence [162]. Furthermore, we were able to show that the olfactory nerve fascicles in the nasal pit area, corresponding to the olfactory epithelium, contain senescence-associated-beta-galactosidase (SA- $\beta$ -Gal) positive cells during embryonic development. Furthermore, we observe those senescent cells only in distinct stages of development, suggesting that the senescent cells are cleared later in development [162] highlighting the importance of cellular senescence in development.

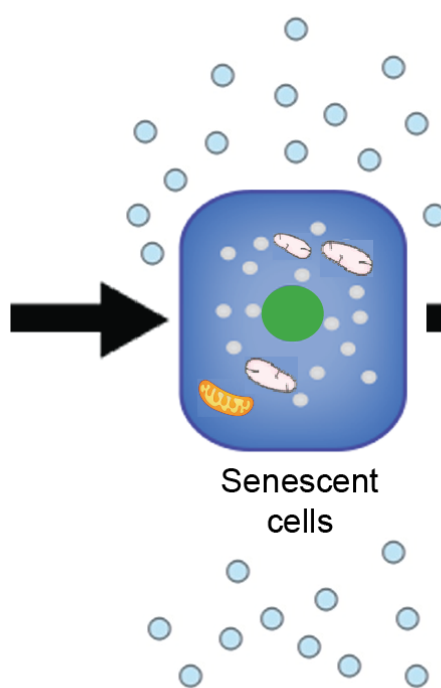
In summary, senescence is a variable program that can be induced by various triggers and leads to many biological consequences that can be beneficial, such as tumor suppression, wound healing, and development, or detrimental such as premature aging and chronic inflammation. As heterogeneous as the biological consequences of senescence are, so are the markers of senescence. There are no unique senescence markers; therefore, the combination of several biomarkers should be used to identify a senescent cell.

## 1.5. Senescence as a tumor suppressor mechanism

In the last part, some of the positive and negative roles of cellular senescence on a more global level of the organism were discussed. The next section, it will be focused on the molecular consequences of senescent cells. It is to be noted that most of the molecular alterations discussed could also be used as biomarkers for cellular senescence. See figure [1.4].

### Inducer of senescence

- Tumor suppressor reactivation (p53, PML)
- Oncogene activation (HRAS, AKT)
- Oncogene inactivation (MYC)
- Telomere dysfunction
- Mitochondrial dysfunction
- DNA damage
- Oxidative Stress
- Cytotoxic drugs
- Cell culture stress
- Tumor suppressor inactivation (RB)
- Nucleolar stress (CX-5461)
- Metabolic alterations (Acetylation changes)



### Characteristics of senescent cells

- Cell cycle arrest (p16/p21 increase)
- Enlarged morphology
- Chromatin remodelling (SAHF)
- Endoplasmic reticulum stress
- SA-  $\beta$ -galactosidase
- Autophagy
- DNA damage response ( $\gamma$ -H2A.X 53BP-1 foci)
- Tumor suppressor activation (increased p53 level)
- PML foci
- Secreted factors (SASP)
- Protein degradation (SAPD)
- Ribosome biogenesis defects (RSL1D1 loss)
- NADH accumulation
- Altered mitochondrial structure
- Altered lipid and AA metabolism

**Figure 1.4. Inducer and marker of cellular senescence**

Cellular senescence is a complex tumor suppressor mechanism. Here some of the known inducer of cellular senescence and their molecular consequences are highlighted. It is to be noted that depending on the inducer of the senescence not all characteristics of a senescent cell are present, hence a combination of senescent markers should be used to identify senescent cells. Senescent cell shows dysfunctional mitochondria, big round nucleolus (green), secretion of small soluble factors(SASP). Image adapted from [165] with information from [5, 104, 124, 128, 166]

### 1.5.1. Markers of cellular senescence

One of the earliest molecular markers of senescence discovered is the senescence-associated-beta-galactosidase (SA- $\beta$ -Gal) test. This test takes advantage of the increased lysosomal mass and consequently higher activity of the enzyme  $\beta$ -galactosidase even at suboptimal pH (between pH 5 to 6.5 depending on the cell type). The galactosidase can catalyze an artificial sugar, X-Gal, into a blue-colored product; hence senescent cells will be colored faster than cells that do not have the increased lysosomal galactosidase activity [167].

Another known marker of senescence cells is the senescence-associated secretory phenotype (SASP) [129, 168, 169]. Although the proteins secreted depend on the cell type, most senescent cells show increased secretion of pro-inflammatory cytokines, chemokines as well as matrix metallo protease (MMP) and exosomes [170, 171]. Even though not true for all senescent cells, the SASP most commonly includes interleukin 6 (IL6), IL8, chemokine (C-X-C motif) ligand 1 (CXCL1), interleukin 1 $\beta$  (IL1 $\beta$ ), and TGF $\beta$  [172, 173]. It is suggested that the increased secretory phenotype has three major consequences.

First, it signals to the surrounding cells that there is a problem [170] and the presence of senescent cells can induce senescence in the surrounding cells. This effect is called paracrine senescence [174]. The second effect of the secretory phenotype of senescent cells is to attract immune cells in order to become cleared [117, 171]. It is still a matter of debate which immune cells are the most efficient to clear senescent cells. However, evidence suggests that NK [117, 175], macrophages [176], as well as neutrophils [177], and T lymphocytes and other components of the immune system can play major roles in senescent cell elimination [178, 179]. Interestingly, it is yet unknown why some senescent cells accumulate with age whereas others get cleared within days [178, 180].

The third consequence of the increased inflammation is in relationship to the previous ones. In case the SASP remains at high levels, and the cells do not get cleared, the tissue can enter a highly inflammatory state which can contribute to cancer development [181], faster cancer progression [182] and Inflammaging [183]. The term Inflammaging denotes a concept of chronic inflammatory tissue state resulting in premature aging of the tissue [184]. Interestingly, a chronic state of inflammation, for example, chronic pancreatitis, can overcome senescence leading to transformation [185]. These results highlight the double edge sword of the SASP, which can provide tumor suppression but also promote tumor progression. Nonetheless, the formal proof that the senescent cell is reentering the cell cycle following chronic inflammation has yet to be done with lineage tracing experiments.

On top of all those classic senescence biomarkers shown in figure 4 recently, whole-genome sequencing, single-cell sequencing, and proteomics have identified other senescent biomarkers [172].

In this report, the authors identified 13 core senescence markers that are transcriptionally regulated in senescence. In order to obtain their core signature, the authors combined five different senescent inducers in five different cell lines and analyzed their expression data. Core genes identified in this study include some genes that were previously linked to senescence, such as PATZ1 (inducer of senescence via p53), CCND1 (regulator of CDK4/6 activity), and p21 but also novel senescent markers such as C2 calcium dependent domain containing 5 (C2CD5) DET1 and DDB1 associated 1 (DDA1) plexin a3 (PLXNA3). The reason for the altered expression for the last three is yet to be uncovered, and sequencing data from other groups did not confirm those markers [186]. These discrepancies between senescence markers can be possibly attributed to different aspects. First, different cell lines can alter the senescence response, but also, the stress that induces the senescence stress and time of analysis can influence the expression of senescent markers [172, 186]. Moreover, these studies only focused on the expression data, and changes in expression are not always reflected in protein level. Interestingly, even single-cell sequencing data from one cell line revealed up to 6 different subtypes of senescent cells, highlighting again, the heterogeneity of the senescence response [187, 188]. Another study revealed changes in the proteome of senescent cells [173]. In this study, the authors focused on secreted protein and could confirm the heterogeneity of senescence marker based on cell type and senescent inducer. One interesting protein family increased in protein level through several cellular senescent cell models is the family of serine protease inhibitors B (SERPINB). SerpinB proteins are serine/cysteine protease inhibitors [173], and it was previously shown that increase of SerpinB in senescence would enforce the senescence response as well as modulate mitochondria homeostasis [189]. Alterations in mitochondria are going to be discussed later on. Another interesting protein increased in senescent cells was the urokinase-type plasminogen activator receptor (uPAR). In this study, the authors used the increased presence of this protein at the surface of senescent cells to engineer senolytic CAR-T cells targeting this protein [190].

These results highlight that even though senescent makers are heterogeneous and dependent on the cell types, identifying more senescent markers will better characterize those different senescent sub-types and help to elucidate other senescent cell functions. The lack of validated senescence markers is particularly important for senescence research *in vivo* as most of the above-mentioned biomarkers were identified *in vitro* and only a few had been validated *in vivo* [131]. Identifying new senescence biomarkers *in vivo* is a crucial aspect of further research.

All in all, senescence can be induced by various stress, and a combination of biomarkers can identify senescent cells. Despite the lack of a unique biomarker, the accumulation of senescent cells *in vivo*, was still shown to be a significant driver of aging phenotypes [191]. In the next section, the discussion will be about the consequences of senescent cells in the body.

## 1.5.2. Molecular consequences of cellular senescence

One of the earliest observations in senescent cells was that senescent cells display a flattened large shaped morphology at least *in vitro* [55]. The exact role for the increase in size is not known; however, for the molecular consequences of the flattened morphology, it was suggested that lipid composition via altered mTOR activity in senescent cells changes cellular morphology [192–194]. Furthermore, sphingolipids, a class of aliphatic amino alcohols that include sphingosine, accumulate in senescent cells [195–197]. Moreover, cardiolipin, a lipid in the inner mitochondrial membrane, is increased [198]. In addition, the altered lipid state can result in the exposure of mitochondrial membrane lipids, for instance, cardiolipin. Cardiolipin are recognized as bacteria lipids, by toll-like receptors (TLRs) resulting in an inflammatory response [199]. In fact, several other components of the mitochondria are considered to be damage-associated molecular patterns (DAMPs) and the inflammatory response following exposure to material from the inner par of mitochondrial is thought to be a major driver of the aging response [184, 200].

Furthermore, the stiffness of senescent cells is altered as well as membrane resistance to osmotic stress [201, 202]. One senescence model which was used to identify these roles is progeria. Progeria is a premature aging phenotype from a genetic mutation in the Lamin A gene. For instance, in fibroblasts from progeria patients, it was shown that a constitutively active RhoA resulted in increased F-actin stress fibers and stiffness followed by induction of micronuclei and cytoskeleton reorganization. In addition, inhibition of RhoA in those fibroblasts resulted in alleviation of aforementioned phenotypes [203]. Moreover, accumulation of senescent epithelial cells seems to contribute to loss of epithelial function (less barrier protection, difficulty of fluid balance, and reduction of clearance of particulate in pulmonary epithelium), resulting in induction of pulmonary fibrosis along with induction of pro-inflammatory state resulting in chronic obstructive pulmonary disease (COPD). Another instance of reduced barrier resistance in senescence cells would be endothelial senescence, where it was shown that a monolayer with senescent cells would have fewer junction proteins and a down-regulation of occludin and claudin-5, resulting in higher permeability of the endothelial cells [204].

Interestingly, it is not only the cell membrane that is altered but also the mitochondrial membrane and the nuclear envelope [205–207]. Regarding the nuclear envelope, it was shown that senescence induction results in Lamin B loss and instability of the nuclear envelope [208–210]. Furthermore, it was demonstrated that small fragments of DNA and Histones could escape through the weakened nuclear envelope resulting in cytosolic DNA and chromatin fragments. As a consequence, the DNA molecule sensing pathway cyclic GMP-AMP Synthase- Stimulator of Interferon Genes (cGAS-STING) is activated [211]. Following cGAS-STING activation nuclear factor- $\kappa$ -B

(NF- $\kappa$ -B), a significant mediator of the SASP is activated, resulting in increased SASP secretion; consequently, the senescence program is enforced [212].

Not only can DNA escape the nuclear envelope, but also the DNA remaining in the nucleus is subject to profound changes upon the induction of cellular senescence [213]. As a result, the chromatin landscape of senescent cells is heavily altered; thus, areas of strongly condensed chromatin with repressive transcriptional marks, such as Histone 3 di- or tri- methylated on lysine 9 (H3K9me2/3) occur. Those repressive areas can be seen as bright spots with the DNA stain DAPI and are also called senescence-associated heterochromatin foci (SAHF) [214, 215]. Other markers of heterochromatin, such as macro H2A, display a specific pattern in senescence cells, too [216].

Another important player of heterochromatin regulation in cellular senescence is high mobility Group Box 2 (HMGB2) [217]. Chromatin immunoprecipitation followed by sequencing (CHIP-Seq) analyses revealed that HMGB2 preferentially binds to SASP gene loci, for example, IL6 or IL8 in senescent cells, to prevent the addition of repressive histone marks; correspondingly, the SASP genes continue to be highly expressed [218]. Once again, the increased amount of cytokines is thought to be responsible for enforcing the senescence response.

Moreover, assay for transposase-accessible chromatin by sequencing (ATAC-Seq) analyses of senescent human umbilical vein endothelial cells (HUVEC) cells revealed that there are more than 2000 changes in chromatin accessibility in senescent cells when compared to non-senescent HUVEC cells. Interestingly, genes that were close to areas with increased accessibility to chromatin significantly correlated with an increase in expression in cellular senescence, suggesting that the alteration of the chromatin landscape is a significant mediator of alterations of gene expression in the senescence response [219].

Another consequence of the loss of nuclear organization is that a lot of senescent cells display constant areas of DNA damage measurable by, for example, TP53 binding protein 1 (53BP1) or histone 2a phosphorylated on S139 ( $\gamma$ -H2A.X) foci [123, 220–222], although the reason for this constant DNA damage is not yet fully understood for all senescent types. Obviously, in replicative senescence, the shortening of the telomeres results in chromosome fusion and activation of the DNA repair machinery [123]. In contrast to this OIS and MSIS have normal telomere lengths, nevertheless display constant DDR [125, 220]. One hypothesis is hyper replication stress. After the activation of the RAS oncogene, there is a phase of hyperproliferation, and it was suggested that this hyper replication would lead to prematurely terminated DNA replication forks resulting in DNA double-strand breaks [221, 222].

Another hypothesis to explain the constant DDR would be the increased amount of ROS produced by dysfunctional mitochondria, another characteristic of most senescent cells, which could

result in oxidation of the DNA, although it seems unlikely that a reactive molecule will travel from the mitochondria into the nucleus to damage the DNA [223].

Other studies suggested that proteins of the shelterin complex such as TRF2 and TRF2BP1 are decreased, resulting in a DDR at the telomeres without telomere shortening [93, 165]. Moreover, it was shown that shelterin dysfunction could induce endothelial cell senescence as well as COPD in a mouse model and was confirmed by observation of shelterin dysfunction in human COPD patient samples [224–226]. DDR in the shelterin complex is persistent as no DNA repair can occur in the telomeric regions [227]. Another possible explanation of the constant DDR could be the lack of an S phase. The S phase is the phase of the cell cycle in which HR usually occurs, and the lack of S phase could result in insufficient expression of DNA synthesis or DNA repair proteins. It was also suggested that metabolic changes could result in less nucleotide or nucleosides synthesis required for DNA repair [228].

All in all, it is yet to be determined which of the aforementioned effects are more important drivers of the constant DDR in senescent cells. However, this is likely going to depend on the stress and the cell type. Notwithstanding this, it is important to notice that the persistent DDR reinforces the senescent response.

Another type of nuclear foci which is increased in senescent cells is the p53 regulated tumor suppressor protein promyelocytic leukemia protein (PML). Expression of isoform 4 of PML itself can result in induction of senescence, but also it was observed that most senescent cells display an increased amount of PML nuclear foci [118, 229]. Roles of PML nuclear foci include the modification and sequestering of proteins away from their effectors. For instance, it was shown that sumoylation, a post translational modification (PTM) which can occur in PML bodies, is altered upon induction of senescence [229, 230]. Interestingly, the E2F proteins can accumulate in PML bodies; consequently, S phase genes can no longer be induced. Accordingly, the senescence response is enforced [133].

Apart from all the nuclear modifications, the cytosol of senescent cells is considerably different from proliferating cells, too [231]. Senescent cells display higher lysosomal content [232], higher amount of autophagy [233], as well as altered cytoskeletal structure [231]. It is still unclear how much of these effects are the drivers of senescence response or whether they are just bystander effects of the senescence induction. Especially the increased lysosomal content and increased autophagy can be observed in other cellular contexts which are not related to senescent cells, like starved cells or pancreatic tumor cells [124, 234, 235].

One major protein in regulating autophagy is mTOR, and its roles in senescence bring to light one of the most puzzling aspect of senescent cells [231]. Senescent cells display high level of

phosphorylated eukaryotic initiation factor 2 subunit 1 (eIF- $\alpha$ ) [236, 237], a protein which reduces cap-dependent translation. It was hypothesized that in senescent cells, the high levels of phosphorylated eIF- $\alpha$  is driven by unfold protein response (UPR) and would allow for increased tolerance against ROS [237]. High levels of autophagy as observed in senescent cells results in low mTORC1 activity. Surprisingly, mTORC1 activity, as well as global translation level, for example, measured but S35 incorporation, are not affected or even increased in senescent cells [238, 239]. It was suggested that compartmentalization occurs, resulting in local foci of highly active translation activity. In contrast, other areas display high levels of autophagy and barely detectable activity of translation [239].

Interestingly, inhibition of mTOR by rapamycin delayed the onset of senescence, underlying once again that high mTORC1 activity helps to maintain cellular senescence [240]. One of several hypotheses here would be that high mTOR activity would increase phosphorylation of S6 kinase and eukaryotic translation initiation factor 4E-binding protein 1 (4E-BP1) causing increased translation. High translation rates have been linked to cell exhaustion triggering premature aging [241]. Likewise, it was suggested that rapamycin could inhibit the production of the SASP, can stimulate mitophagy, and alter the immune response, thus reducing senescent cell burden [242].

Moreover, it was shown that particular mRNA with upstream open reading frames (uORF) get translated preferentially in stressed cells, highlighting once more the importance of further understanding of cap dependent and independent translation in senescent cells [243].

Other aspects of translation in senescence are the alterations in the ribosomes, as it was suggested that ribosomes in senescent cells might be different than in normal cells. For example, a recent study suggested that ribosomes from senescent cells are less prone to read through than proliferating cells [29], although ribosome biogenesis is decreased in cellular senescence [7]. The roles of ribosomes and ribosome biogenesis in senescence are part of the first article of this thesis and will be discussed later on.

In summary, the induction of senescence seems to be a double edge sword. On the one hand, various alterations in nuclear and cytoplasmic homeostasis allow for cell cycle arrest and tumor suppression; however, persistent accumulation of senescent cells and, particularly, the increase in SASP, seems to allow for tumor promotion. Many of these observed molecular changes in senescent cells are generally considered tumor-suppressive, although promoting cancer growth in specific contexts. In light of the absence of a specific senescence biomarker, it is of utmost importance to identify other specific senescence makers in order to properly evaluate the contribution of senescence in tumor suppression or tumor promotion. It is quite possible that the state that is characterized today as cellular senescence is, in reality, two or three different cells states. A good marker for those different kinds of senescence cells would allow to properly identify cells that are



detrimental to tumor suppression and cells that are beneficial to tumor suppression. Accordingly, it was discussed that there are deep senescent cells (will always be senescent and do not promote tumor growth) and reversible senescent cells (can promote tumor growth) [104, 244, 245]. We have suggested that degradation of specific proteins in senescence can distinguish between those different types of senescent cells. Cells that display high patterns of protein degradation seem to be in the group of deeply senescent cells were as cell that do not display senescence-associated protein degradation seem to be in the group of tumor promoting senescent cells [165].

### **1.5.3. Senescence associated protein degradation**

Interestingly, it was shown that not only transcription and translation in senescence are different but also protein stability [93, 165, 246].

In 2013 we have shown that constant activation of the ERK leads to a degradation of specific proteins such as STAT3, c-MYC, ribosomal L1 domain-containing protein 1 (RSL1D1), tripartite motif-containing 28 (KAP1/TRIM28), translocase of outer mitochondrial membrane 34 (TOMM34), translocase of outer mitochondrial membrane 70 (TOMM70), DExD-box helicase 21 (DDX21) and heat shock protein 70 (HSP70) [93]. It was hypothesized that the hyperphosphorylation of these proteins caused their degradation. In this report, we were able to show that more than 1000 proteins have increased degradation upon induction of senescence, and this was called senescence-associated protein degradation (SAPD). The proteins identified span across all cellular functions; however, most notably, it was a degradation of cell cycle regulator proteins, cell membrane, motility proteins, ribosome biogenesis factors, mitochondrial functions proteins, as well as regulators of proteotoxic stress [246]. It was further suggested that the specific degradation of those proteins could enforce the senescence response. In fact, the sole degradation of one target of the SAPD could induce cellular senescence [93].

### **1.5.4. Targets of the SAPD and their molecular consequences**

The degradation of some of the SAPD could also explain some of the alterations observed in senescent cells. For example, c-MYC, minichromosome Maintenance Complex Component 2 (MCM2), and jun proto-oncogene- AP-1 transcription factor subunit avian sarcoma virus 17 protein (Jun) were shown to be important for cell cycle progression from G1 to S phase, suggesting that the decrease of those proteins enforces the cell cycle arrest and the senescence response [247–249]. Degradation of those proteins could be markers of deep senescent cells.

Another example would be the degradation of protein of the cytoskeleton such as, caldesmon1 (CALD1), Cortactin and filamin B (FLNB) which could explain the enlarged flattened morphology of senescent cells [165]. Furthermore, we identified components of the shelterin complex of telomeres, as well as DNA integrity proteins to be degraded in senescence, namely DNA topoisomerase II (TOP2), telomeric repeat-binding factor 2-interacting protein 1 (TERF2IP) and telomeric repeat-binding factor 2 (TRF2) [93]. Thus, the decrease of the shelterin complex could result in persistent DNA damage at the telomeres, and telomere dysfunction-induced DNA damage foci are irreparable; hence they can contribute to enforcing the cell cycle arrest [250–253].

### **1.5.5. Ribosome biogenesis defects in senescence**

Interestingly, the discovery of SAPD could not only start explaining some of the alterations in senescent cells but also reveal new molecular aspects of senescent cells. One of those is the alteration in ribosome biogenesis in cellular senescence [165].

Ribosome biogenesis is the process that generates new ribosomes, and this procedure requires high amounts of energy and the concerted actions of more than 200 proteins and RNAs [254]. The assembly of a ribosome is a multi-step process within the nucleolus and the cytoplasm. Ribosome biogenesis starts with the transcription of 35S precursor ribosomal ribonucleic acid (rRNA)(containing 5.8S, 25S in the ribosome and 5' ETS, ITS1, ITS2, 3' ETS excluded from ribosome) by RNA polymerase 1 (PolI) in the nucleolus and transcription of 5S rRNA by RNA polymerase 3 (PolIII) in the nucleus. The rRNA components are co-transcriptionally and post-transcriptionally subjected to a series of modifications such as pseudouridylation, 2'-O-methylation, RNA cleavage, interaction, and assembly with ribosomal proteins to finally give rise to the small 40S pre-subunit and the large 60S pre-subunit [254]. Those two subunits are then exported independently into the cytosol, finally processed to give rise to the 40S subunit-containing, the 18S rRNA with 33 small subunit ribosomal proteins called ribosomal protein small subunit (RPS) and the 60S large subunit containing the 5S, 5.8S, and 25S rRNA as well as 42 to 47 ribosomal proteins of the large subunit, called ribosomal protein large subunit (RPL) [255]. It is to be noted that a new nomenclature of RPS and RPL was recently suggested. Therefore, in the following, both the RPS and RPL nomenclature, as well as the new nomenclature based on the conservation between bacterial(b) eubacterial (e) archaeal(a) and universal (u) as being present in all domains [256], will be used.

The assembly of the pre-ribosomal particle with the modifying proteins, as well as the ribosomal proteins and the snoRNAs is a 2.2 to 6 MDa multi enzymatic ribonucleoproteins (RNPs), called SSU and LSU processosome [257, 258]. The exact composition of those processosomes

varies over time of maturation and is started to be understood for yeast but far from uncovered for human ribosome generation [259–261].

Notably, for cellular senescence, it is known that targets of the SAPD are inside the processosomes, and those proteins are, namely DDX21 and DExD-box helicase 51 (DDX51), RNA helicases which are essential for the processing of the 3' end of the 28S rRNA as well as for processing snoRNAs [262, 263]. Another component is the protein RSL1D1 which is important for nucleolar localization of nucleostemin as well as rRNA processing [264]. Moreover, RSL1D1 was shown to be an essential regulator of replicative senescence [265]. Further nucleolar factors with increased degradation during senescence are listed in the table below.

**Table 1.2. Nucleolar proteins with increased degradation in cellular senescence**

Nucleolar Protein	Function
NOL6	Processing of the 18S rRNA [266]
NOC2L	Processing of the 18S, 28S and 5.8S rRNAs [267]
NCL	Polymerase I transcription; rRNA processing; ribosome assembly and transport [268]
RPLP1	Translational elongation; overexpression bypasses replicative senescence [269]
NOLC1	Important for Polymerase 1 activity and nucleolar assembly [270]
NPM1	Nucleolar protein important for processing of the 32S pre-rRNA to the mature 28S rRNA [271, 272] and interact with MDM2 to regulate p53 [273]

After the discovery of the SAPD in oncogene-induced senescence (OIS) the question remained whether ribosomal defects could induce senescence? Would it be possible that senescence induction by ribosome biogenesis defects can reinforce the senescence response, or is the abundance of ribosomal biogenesis factors targeted for degradation a pure coincidence? Furthermore, we were wondering what would be the consequences of altered ribosome biogenesis in senescent cells? All those questions and the abundance of ribosomal biogenesis factors targeted for degradation in senescent cells strongly supported the idea of ribosome biogenesis defects in senescence. In article 1, we further uncovered the role of ribosome biogenesis in senescence [7].

### 1.5.6. Role of mitochondria in cellular senescence

As mentioned previously, SAPD targets could be found throughout all cellular processes, and mitochondrial homeostasis was no exception. We have identified TOMM70, TOMM34, BCL2 associated athanogene 3 (BAG3), HSP70, heat shock protein 90 (HSP90) as well as STAT3 being degraded specifically in senescent cells, and their degradation could explain some of the mitochondrial dysfunctions observed in senescent cells [93].

The roles of TOMM70, TOMM34, BAG3, HSP70 and HSP90 can be summarized as important for protein import into mitochondria. BAG3, can interact with HSP70 via its adenosine triphosphate hydrolysis enzyme (ATPase) domain and decrease of BAG3 results in alteration of HSP70 chaperon activity resulting in accumulation of misfolded proteins as well as mitochondrial dysfunction [274, 275]. HSP70 and HSP90 are cytosolic chaperons and among other roles, they can bind newly synthesized proteins and bring them close to the TOMM/TIM mitochondrial import complex [276]. Decreases of HSP70 and HSP90 have been shown in aged tissue and exogenous expression to result in delayed onset of senescence as well as improves cognitive health in mice [277]. A decrease of TOMM70 or TOMM34 results in a reduction of mitochondrial protein import followed by mitochondrial dysfunction [278, 279], a characteristic of senescent cells [125, 199]. For instance, in a amyotrophic lateral sclerosis (ALS) mouse model, a neurodegenerative disease which can be delayed by senolysis [280], it was shown that decreased protein import into the mitochondria was one of the critical drivers of the illness [281].

We extensively reviewed the roles of STAT3 in general and in mitochondria for tumor suppression in article 3 of this thesis [90]. Briefly, STAT3 was identified as a regulator of JAK-STAT signaling to induce transcription of pro-survival genes, cytokines, and chemokines, see figure [1.5]. To activate STAT3 signaling, a chemokine, such as, Il6 binds its receptor activating JAK 2, which phosphorylates STAT3, inducing its dimerization and nuclear translocation. Among the canonical roles of STAT3 it was found that STAT3 has other versatile roles for example regulation autophagy [286, 287], energy metabolism [284, 288], the endoplasmic reticulum (ER) [289], ROS metabolism [290] and mitochondrial homeostasis [283, 285, 291]. The mitochondrial functions of STAT3 are the most relevant for this thesis and will be the focus here.

It was shown that mitochondrial-targeted STAT3 was able to regulate mitochondrial electron transport and oxidative phosphorylation [292] as well as, in combination with oncogenic ras, STAT3 was able to sustain anchorage-independent growth in MEF cells [293]. Furthermore, deletion of total STAT3 in hematopoietic cells resulted in rapid aging phenotype with increased ROS production and mitochondrial dysfunction [294]. Similarly, it was shown in the cerebellum of

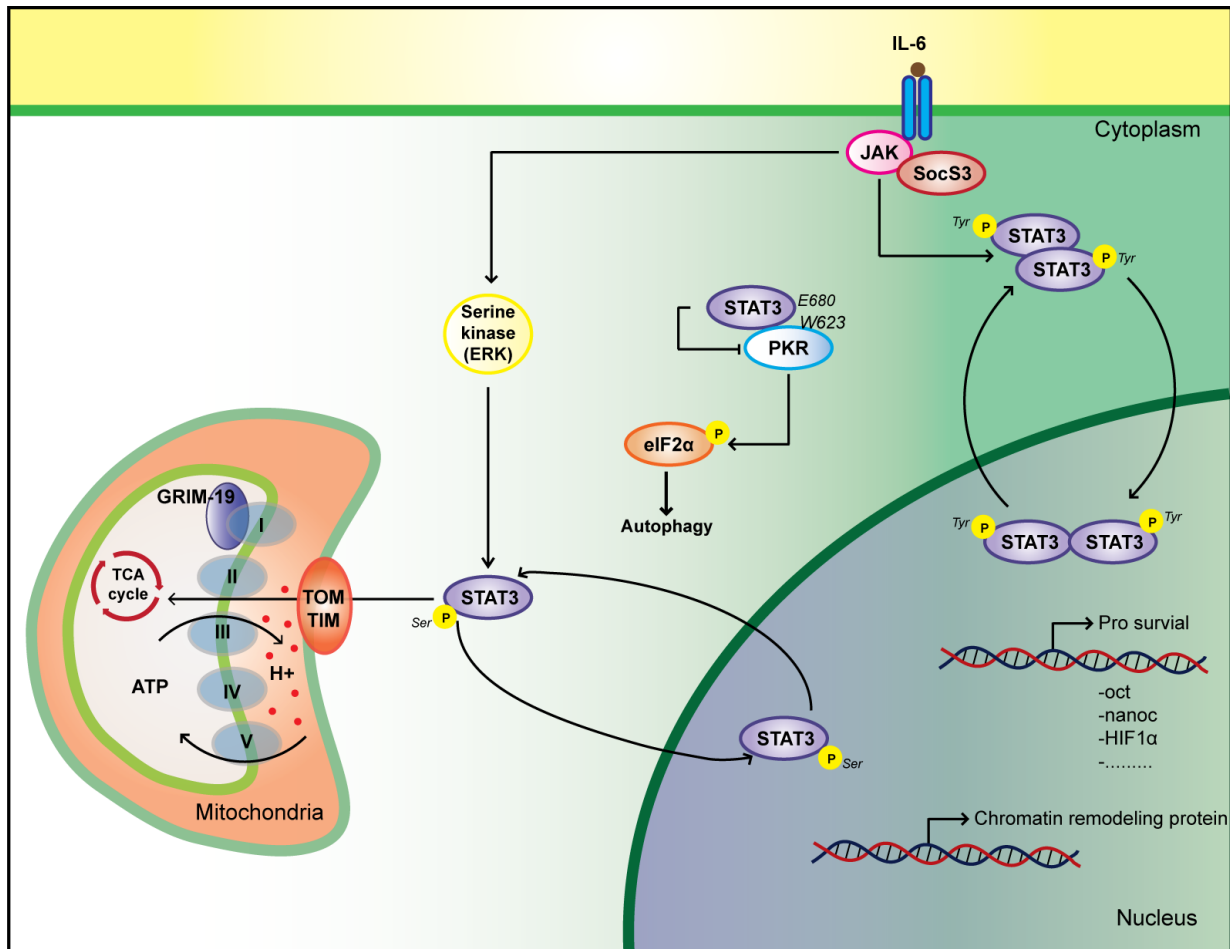


**Figure 1.5. The different roles of STAT3 in the cell**

The canonical activation of STAT3 requires phosphorylation of STAT3 by JAK. Following phosphorylation on Y705, STAT3 dimerizes and can enter the nucleus to activate pro-survival and inflammatory genes. Among classic STAT3 genes are HIF, IL6, NF- $\kappa$ -B, SOCS3, NANOC. STAT3 activity can be boosted by further phosphorylation on S727. Non-canonical roles of STAT3 include interaction PKR and regulation of autophagy. Moreover, STAT3 can be imported into the mitochondria and regulate the activity of the ETC as well as mitochondrial gene transcription. It was suggested that phosphorylation on S727 without Y705 would allow STAT3 import into the mitochondria. Mitochondrial STAT3 was shown to regulate  $Ca^{2+}$  and the opening of the mitochondrial permeability transition pore (MPTP). Further roles of STAT3 are regulation of expression of chromatin modifiers. Image adapted from [282] further information was extracted from [283–285] Abbreviations: STAT3: Signal transducer and activator of transcription, JAK: Janus kinase, SOCS3: Suppressor of cytokine signaling 3, TOM: translocase of outer mitochondrial membrane, TIM: translocase of inner mitochondrial membrane, GRIM19: Gene associated with retinoic and interferon-induced mortality 19 protein; suggested to be important for STAT3 mitochondrial import, TCA cycle: Tricarboxylic acid cycle, PKR: Protein kinase r, ETC: Electron transport chain.

aged rats that STAT3 levels decrease with aging; likewise, a decrease of STAT3 results in alterations in mitochondrial ultrastructure [283, 295]. Moreover, targeting STAT3 in breast cancer cells can lead to senescence-like phenotype [296]. Likewise, cysteines in the DNA binding domain of STAT3 can be S-gluthionylated or oxidized, leading to decreased transcriptional STA3 activity. As mentioned above, reduced STAT3 functions can induce senescence.

On top of this, STAT3 was shown to regulate metabolism, and deletion of STAT3 lead to reduced glutathione synthesis [297] coupled with an alteration in glycolysis [284]. Concordantly, STAT3 can regulate pyruvate metabolism via interaction of acetylated STAT3 with pyruvate dehydrogenase complex E1 resulting in increased conversion of pyruvate to acetyl CoA [298]. Also, mitochondrial STAT3 was shown to regulate transcription of mitochondrial encoded genes, for instance, mt-ND1 and mt-ND4 [299, 300]. Moreover, deletion of total STAT3 or Mito-STAT3 had detrimental effects on cardiac function after ischemia and reperfusion injury; likewise, a decrease of STAT3 level can be found in several age-related cardiac pathologies [301, 302]. On the other hand, higher STAT3 levels resulted in later mitochondrial permeability transition pore (MPTP) opening, less cell death, less ROS and faster recovery of the animals [301].

It was suggested that STAT3 could regulate calcium metabolism as well as MPTP opening; hence, STAT3 is an essential regulator of cell death and senescence. Moreover, it was shown that mitochondrial STAT3 could regulate mitochondrial supercomplex formation [303], although it is still a matter of debate which complex would benefit most of mitochondrial STAT3 [285].

Given the link between senescence removal resulting in increased health-span, it seems tempting to suggest that loss of STAT3 can be a marker for aging. Recovery of STAT3 levels could be used as a tissue rejuvenation marker after senescent cell removal. Finally, it seems that STAT3 could be a significant regulator of mitochondrial homeostasis in senescent cells, and in article 2, we have uncovered more roles of STAT3 in senescent cells. The observation that STAT3 seems to regulate mitochondrial homeostasis might help to explain why senescent cells have dysfunctional mitochondria. Dysfunctional mitochondria were one of the earliest markers of senescent cells, but the molecular details of the roles of mitochondrial dysfunction in senescence need further clarification [304]. In the following, some of the roles of mitochondrial dysfunction in senescence will be discussed.

### **1.5.7. Mitochondrial dysfunction and mitophagy in cellular senescence**

Firstly concerning premature aging, it was identified that accumulated mutations in the mitochondrial genome lead to a premature aging phenotype *in vitro* as well as *in vivo* [305–307]. Shortly after that, it was identified that senescence induction is accompanied by a global increase

in ROS [308]. In a more mechanistic detailed way, Passos *et al.* showed that in replicative senescent cells, cells have higher levels of ROS and altered  $\text{Ca}^{2+}$  homeostasis, a marker of mitochondrial dysfunction. They further identified that mild uncoupling, a way to delay mitochondrial dysfunction, delayed the onset of replicative senescence [309]. Shortly thereafter, it was confirmed that mitochondrial dysfunction is not only observed in replicative senescence but also in OIS [125] and TIS [310]. Furthermore, it was shown in replicative senescence and OIS, that the fusion and fission proteins, Drp1 and Fis1, are decreased [311] resulting in ultrastructure alterations of the mitochondria [199].

The mechanistic question of whether physiological mitochondrial dysfunction in senescence, was a consequence or a sole driver of senescence is still under debate. However, in certain contexts, an increased amount of ROS is required to maintain the senescence response [312]. One problem of the role of mitochondrial dysfunction as a sole driver to induce senescence is that mitochondria affect various pathways, thus making it difficult to pinpoint which are the driving effect of senescence induction. It was shown that alterations in mitochondrial metabolic pathways as the TCA cycle [313], one-carbon metabolism [314], nucleotide biosynthesis [228] or the electron transport chain (ETC) [125] can induce senescence.

In an attempt to prove that senescence is solely dependent on mitochondria, Passos *et al.* engineered a model in which they expressed the mitophagy inducer Parkin to remove most of the mitochondria from the cell. They then induced senescence and could show that some phenotypes of the senescence, including the SASP and the DDR, were decreased; however, the cell cycle arrest remained [315]. These results highlighted that dysfunctional mitochondria do play a role in some senescence phenotypes, but the removal of dysfunctional mitochondria from cells does not reverse all aging phenotypes [304, 316]. Interestingly, further connections between mitochondrial removal and senescence can be drawn. It was shown that loss of mitophagy was able and sufficient to drive senescence [104, 317] and alterations in mitophagy are recognized as drivers of cellular and organism aging [184].

All in all, the senescence response as a tumor suppressor mechanism is a complex phenotype with various characteristics and markers, and further work will elucidate the positive and negative implications of cellular senescence in aging and tumor suppression. The diversity of phenotypes and molecular alterations in senescent cells allow for the speculation that cellular senescence is not a homogeneous state but rather a heterogeneous program that is activated in response to cellular stress. Many contradictions towards the benefits or detrimental effects of senescence have been shown, highlighting the urgent need to define the senescence cell state and its biological consequences. It remains an open question how senescent, as a response to stress, was selected by evolution, and answering this question might elucidate the contribution of senescence towards aging

and cancer. Nevertheless, the molecular consequences of the induction of cellular senescence drive aging phenotype because removing those senescent cells alleviates age-related diseases. In light of senescence's tumor-promoting or tumor-suppressive roles, heterogeneity of senescence inducer and molecular consequences most likely hide several different senescent programs. It remains an open question whether senescence induced in cancer cells by chemotherapy agents (TIS) is truly cell senescence or rather an intermediate state towards reemergence of the tumor. Furthermore, how senescent cells get eliminated within days and other senescent cells accumulate in the body remains an open question. Is it possible that the short appearance of senescence cells allows for tumor suppression, whereas the persistent accumulation of senescence can drive tumor formation? Finally, a crucial question that remains unanswered is whether each cancer requires cellular senescence bypass. Lineage tracing experiments *in vivo* could elucidate this burning question; however, the lack of a specific marker of senescence is the limiting factor.

Regardless of the contribution of cellular senescence towards tumor suppression and tumor-promoting, it remains that the pathways studied in senescence research are highly altered in human cancer; thus, identifications of differences between cancerous cells and senescent cells allow a better understanding of cancer initiation and cancer promotion processes.

## **1.6. Metabolic adaptations in senescent and cancerous cells; a requirement for malignant transformation?**

In the last part, the role of mitochondria was discussed, and a lot of metabolic reactions occur in the mitochondria. Because senescent cells have dysfunctional mitochondria and the occurrence of metabolic reactions in the mitochondria, it seems likely that senescent cells will also display a distinct metabolic phenotype. Therefore, at the beginning of the text, general aspects of metabolism will be discussed, followed by an analysis of metabolic alterations in senescent and cancerous cells. During the transformation process, a potentially cancerous cell has to rewire its metabolism to sustain the high division rate of cancer cells. As mentioned before, metabolic rewiring is one of the hallmarks of cancerous cells, see [1.3]. Moreover, metabolic flexibility and metabolic adaptation highlight the complexity of cancer metabolism and the interplay of metabolic reactions. An overview of metabolic reactions described later on can be seen in figure [1.6]. An important aspect highlighted by this overview is the interplay of metabolic reactions. In the following, several biosynthesis pathways will be described in a linear fashion; however, metabolism is not linear but rather circular or adaptive. The reaction speed and the direction of flow of metabolites are highly dynamic and dependent on the availability of substrates, products, and cofactors.



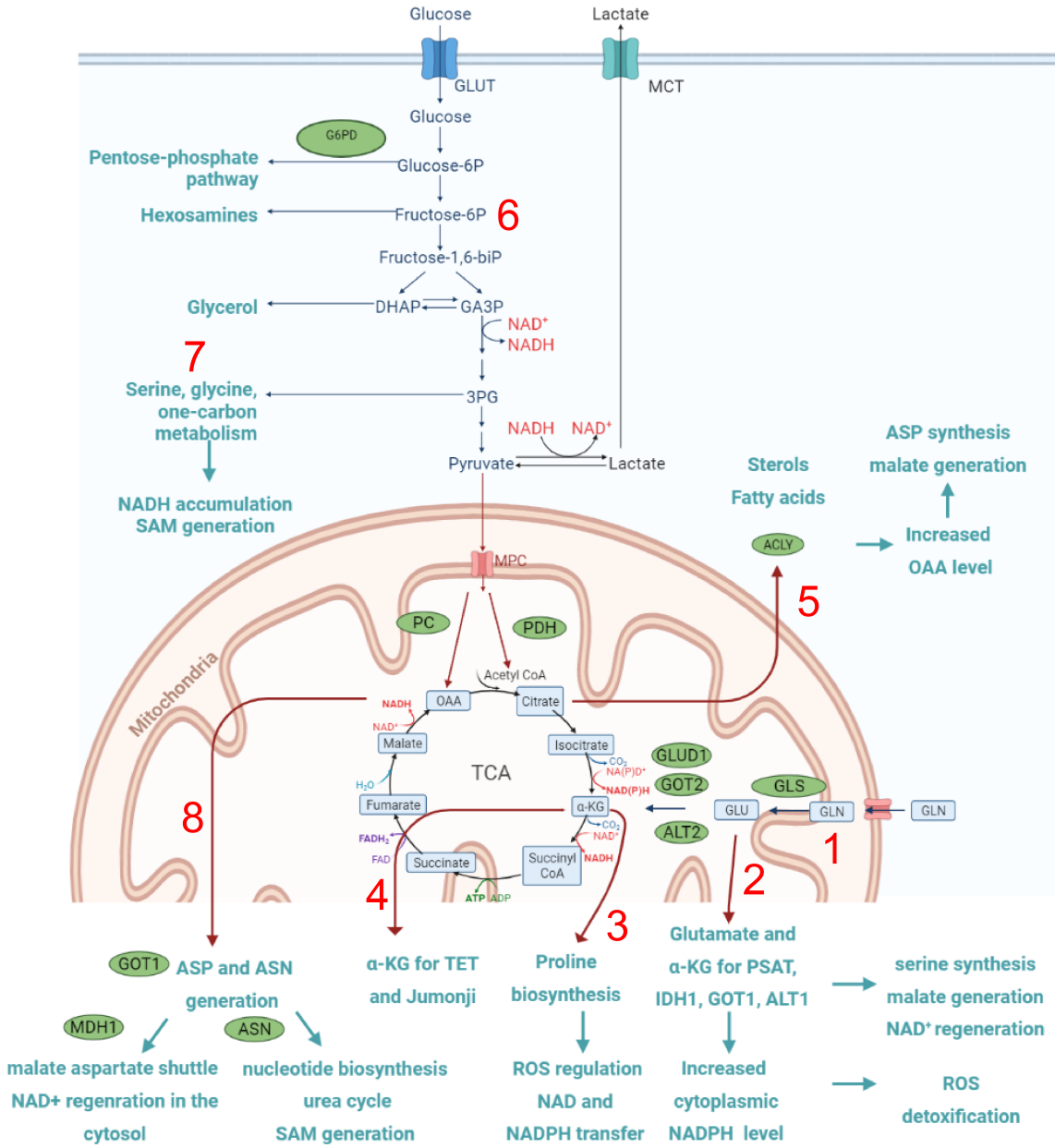


**Figure 1.6. Overview on metabolism covered in this thesis**

The metabolism in cells is highly connected. This overview highlights key parts of the metabolic processes that will be covered here. The overview includes Glycolysis, Shunts of glycolysis, TCA cycle, anaplerosis reaction, citrate metabolism, reduction potential metabolites (NAD, NADH, NADPH, and NADP). Proteins are shown in green; metabolites are shown in blue; metabolic pathways and consequences of metabolism are shown in cyan; NAD reactions are shown in red. Numbers indicate different metabolic pathways discussed later on and should help to orientate the reader. Figure generated using BioRender.

### 1.6.1. Metabolism of amino acids and lipids

One metabolic pathway that is highly altered in cancerous cells is the catabolism of glutamine. It has been known for quite some time now that a lot of cancerous cells have high rates of glutamine uptake as well as glutaminolysis, the degradation of glutamine into  $\alpha$ -ketoglutarate, to fuel tricarboxylic acid cycle also known as Krebs cycle (TCA cycle) as well as the synthesis of other amino acids [318]. Glutamine can be used in nucleotide biosynthesis, asparagine synthesis, glucosamine synthesis as well as NAD<sup>+</sup> biosynthesis; nevertheless, the majority of the glutamine pool up to 90% is used in glutaminolysis [319].

Glutaminolysis, (see figure [1.7] for illustration of glutaminolysis and figure [1.6 numbers 1-4] to integrate glutaminolysis in the global metabolism map), start with the degradation of glutamine into glutamate by glutaminase-1 (GLS1) or glutaminase-2 (GLS2) and in this process, ammonia is released. Although high amounts of ammonia release are toxic for the cells, recent reports have suggested that ammonia is important to maintain pH levels, especially in cells with high lactate secretion such as senescent cells or cancer cells [320]. The produced glutamate can be used in several other metabolic routes as it can be further converted into  $\alpha$ -KG and fuel the TCA cycle or used for proline, arginine, or serine metabolic pathways [321].

Conversion of glutamine into proline requires pyrroline-5-carboxylate reductase (P5C) synthase, and high levels of proline synthesis were shown to be a way to regulate the NAD/NADH ratio as well as the NADPH and ROS metabolism [323]. Furthermore, it was shown that increased proline catabolism is a negative prognostic marker of many solid tumors, as most proline used in catabolism is from the extracellular matrix (ECM). Increased ECM degradation results in remodeling of the ECM into a pro-metastatic environment [324, 325]. It seems contradictory that one side tumor growth would require synthesis as well as degradation of proline, although an interesting model was suggested in which the regulation of NAD and NADPH regulation was at the center of proline synthesis/degradation [326–328]. In this model, proline synthesis (see figure [1.8]) would be used to transfer mitochondrial NAD<sup>+</sup> towards cytosolic NADP<sup>+</sup> while generating NADH in the mitochondria. This could be a way to increase cytosolic NADP<sup>+</sup> levels to fuel the pentose phosphate pathway (PPP) as NADP<sup>+</sup> levels seem rate-limiting to the PPP [328]. An interesting aspect of this proline cycle is the reversibility of the cycle. Suppose NADH becomes accumulated in the mitochondria; proline export instead of P5C export allows the cycle to continue resulting still in NADPH generation in the cytosol. This cycle is a great example of metabolic flexibility amplified in cancer cells. In this model, proline would work similarly to the malate-aspartate shuttle or the glycerol-3-phosphate shuttle.

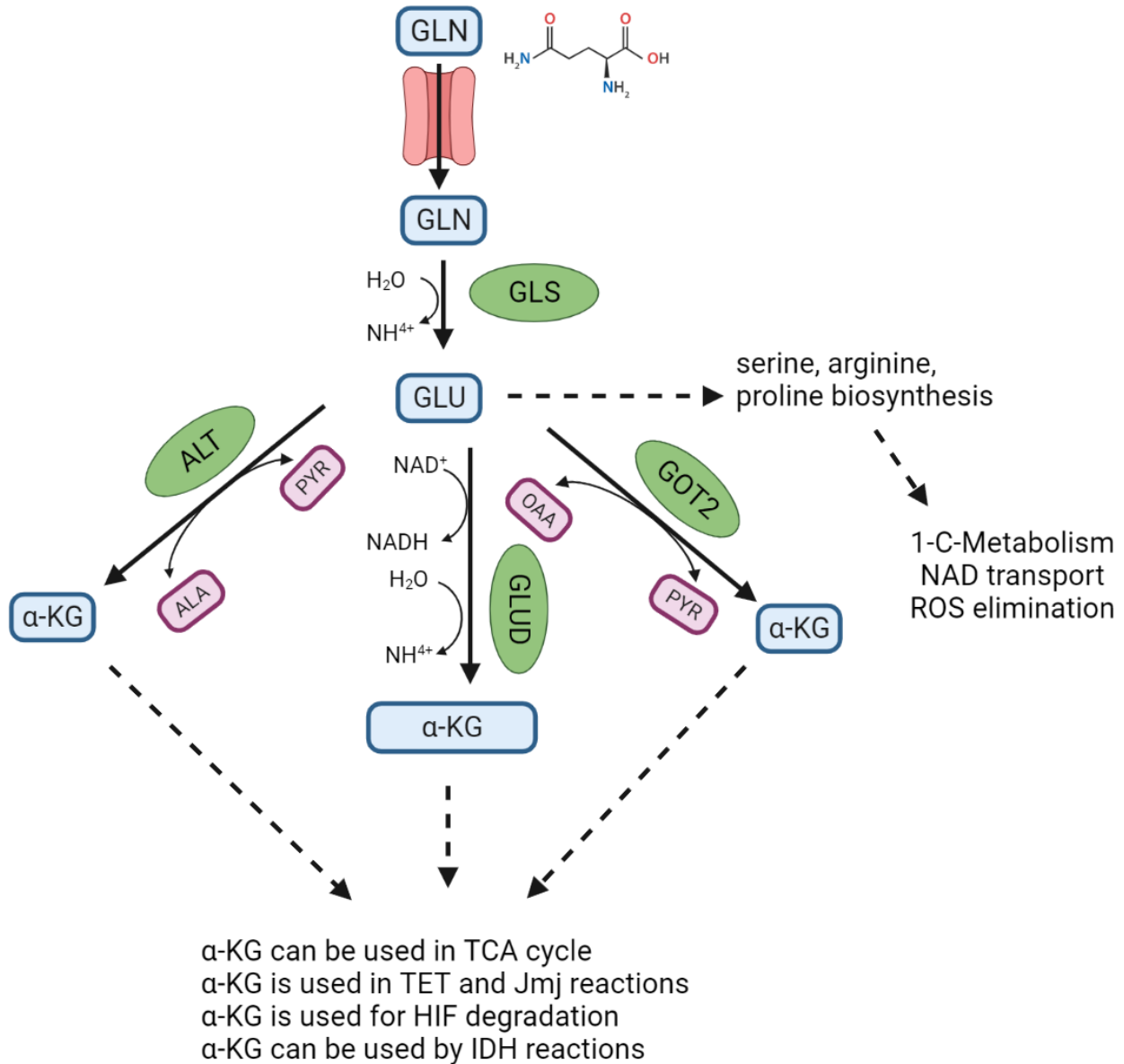


**Figure 1.7. Implications and consequences of glutaminolysis**

Glutamine metabolism is a major contributor to  $\alpha$ -KG levels in the cell. Several metabolic reactions allow the conversion of glutamine into  $\alpha$ -KG. Importantly, glutaminolysis generates other biomolecules. Schematics show metabolites in blue, enzymes in green, and cofactors in red. Branch points into other metabolic reactions and consequences of glutaminolysis are indicated. Abbreviations: GLN: Glutamine, GLU: Glutamate,  $\alpha$ -KG:  $\alpha$ -ketoglutarate, ALA: Alanine, PYR: Pyruvate, OAA: oxaloacetate, GLS: Glutaminase ALT: Alanine transaminase, GOT2: glutamic-oxaloacetic transaminase 2, 1C-Metabolism: One- carbon metabolism, TCA: tricarboxylic acid cycle, TET: ten-eleven translocation methylcytosine dioxygenases, Jmj: Jumonji demethylases, HIF: Hypoxia-induced factor, IDH: Isocitrate dehydrogenase. Figure generated using BioRender.

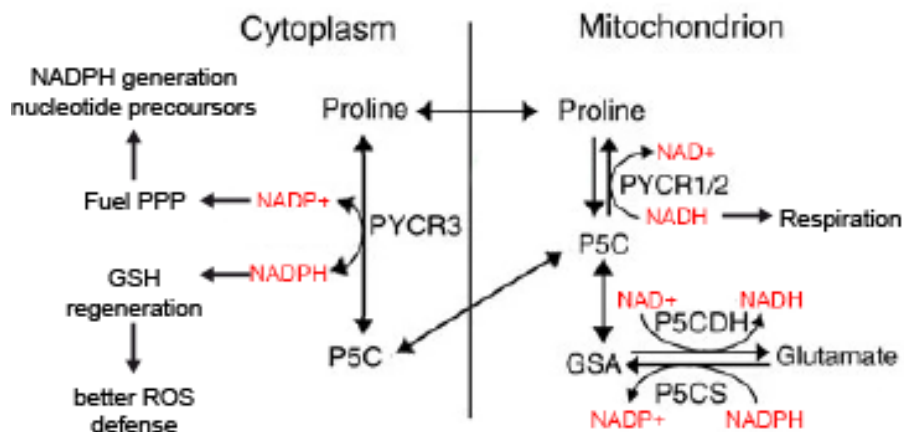


**Figure 1.8. Redox control by proline**

In this metabolic cycle, the synthesis of proline or the import of proline from the ECM can drive redox control. P5C generated from glutamate is exported out of the mitochondria and converted into proline. Thereby generating NADP<sup>+</sup> for the PPP. Proline can enter the mitochondria and be converted to P5C, thereby generating NADH, and the cycle could start again. Interestingly this cycle can also function to generate NAD<sup>+</sup> in the mitochondria and NADPH in the cytosol, as all those metabolic reactions are reversible. This cycle highlights the flexibility in redox control. Images adapted with information from [322]

Also, a high synthesis rate of arginine, a semi-essential amino acid, is important as a NO source for immune cells but in solid tissues rarely limiting. Increased synthesis of arginine was shown in some malignancies; thus, the negative and positive contributions of arginine are tissue type and situation-dependent [329]. Although maintaining a high level of arginine and proline is important, the most important contribution of glutamine to cancerous cells is the conversion into  $\alpha$ -KG.

Two different groups of enzymes can achieve the conversion of glutamate towards  $\alpha$ -KG. First, there is the group of transaminases, including glutamic-oxaloacetic transaminase 1 / aspartate transaminase cytoplasmic (GOT1/ASTc), glutamic-oxaloacetic transaminase 2 / aspartate aminotransferase mitochondrial (GOT2/ASTm), phosphoserine aminotransferase 1 (PSAT), and alanine transaminase (ALT) in which the  $\alpha$ -KG/glutamate pair function as a co-factor and deliver the energy for the reaction. The others enzyme requires energetic cofactors such as NADH or NADPH and is a dehydrogenase, glutamate dehydrogenase 1 (GLUD1). The relevance and contribution of each enzyme towards  $\alpha$ -ketoglutarate generation is cell type-specific and a matter of debate [321].

Importantly, high levels of  $\alpha$ -KG can influence the methylation status of the cells as  $\alpha$ -KG, as mentioned before, is a mandatory cofactor of TET and Jumonji demethylases [330] (see figure [1.6 number 4] for integration in the global map of metabolism). Interestingly,  $\alpha$ -KG was identified as a tumor-suppressive metabolite in pancreatic ductal adenocarcinoma (PDAC) cell and induced by

p53. Furthermore,  $\alpha$ -KG was shown to maintain the differentiated methylation state of cells, and exogenous supply of  $\alpha$ -KG reduced tumor fitness [331]. Furthermore, in this report it was shown that levels of 5-Hydroxymethylcytosine (5hmC), the product of the TET family of enzymes, does decrease along the transition of PanIN towards more advanced PanIN into PDAC [331].

Unfortunately, this report did not show how  $\alpha$ -KG dependent reactions are specifically targeted to maintain tumor-suppressive methylation state, leaving the possibility that other effects than methylation by  $\alpha$ -KG dependent enzymes is at the core of the tumor-suppressive action. For example,  $\alpha$ -KG can fuel the TCA and can decrease NADPH levels via the reverse IDH reaction resulting in higher oxidative stress, driving cells over the tolerable ROS levels resulting in cells death [332]. Moreover, high  $\alpha$ -KG level decreases transaminase activity, and a decrease of GOT2/ASTm activity was shown to be able to induce senescence in PDAC cells [333]. The results highlight that  $\alpha$ -KG might be a tumor-suppressive metabolite, but the molecular mechanism of how tumor suppression by  $\alpha$ -KG is achieved remains to be determined.

Anaplerosis of the TCA cycle by glutamine seems to be the most important driver of glutaminolysis. Anaplerosis can be achieved in several ways, but most importantly by the glutaminolysis or by pyruvate carboxylase (PC) activity. The high growth rate of cancerous cells requires higher anaplerosis as TCA intermediates such as malate, oxaloacetate, citrate,  $\alpha$ -ketoglutarate are removed from the TCA cycle and used in other metabolic reactions, called cataplerosis. Interestingly, cancer cells which have a high level of glutaminolysis are almost insensitive to PC inhibition, and *vice versa* [334, 335]. However, inhibition of glutaminolysis in glutamine dependent cells resulted in increased PC dependent anaplerosis [336]. Finally, inhibition of both PC and GLS resulted in massive apoptosis of those cells. The mechanisms determining to either increase pyruvate carboxylase-driven-anaplerosis or glutaminolysis-driven-anaplerosis are still under investigation [334, 336–338].

Interestingly, although considered a non-essential amino acid, glutamine withdrawal in several cancerous cells leads to cell death and was considered an interesting avenue of cancer treatment for a long time. Unfortunately, *in vivo* the metabolic flexibility of cancer cells is high, and once glutamine was withdrawn, the cancer cells found other nutriment sources. For instance, in PDAC reducing cellular glutamine levels due to glutamine transporter inhibition resulted in increased autophagy and glutamine uptake via the autophagy [339].

Surprisingly, not all cancer cells use the  $\alpha$ -ketoglutarate generated by glutaminolysis to replenish the TCA cycle in a forward way (see overview [1.6 number 5] for integration in the global map of metabolism). It was shown that reductive carboxylation, the reaction of  $\alpha$ -ketoglutarate to isocitrate is increased in hypoxic tumor regions [340], in VHL deficient pseudo hypoxic tumors [341], or rare tumors with mutations in the ETC [342]. It was longtime suggested that this reaction

is increased due to high citrate demand for lipid biosynthesis in fast-dividing cells, but it is also a possible way to generate NAD<sup>+</sup> [343, 344].

Lipid biosynthesis in cancer cells is an important factor, and alterations in lipid metabolism were observed in most cancers, including PDAC, hepatocellular carcinoma, lung cancer. The roles for lipid metabolism in cancer were reviewed in several articles [345–347]. Important for this thesis is the role of citrate generation as well as the fact that increased fatty acid biosynthesis requires the generation of high amounts of NADPH as each generation of palmitate from acetyl-CoA by fatty acid synthetase (FAS) requires 14 molecules of NADPH. The roles of NADPH will be discussed later on.

As mentioned before, reductive carboxylation is a way to generate citrate for fatty acid biosynthesis, but also, allows for generation of NAD<sup>+</sup> and NADPH. The generation of NADPH by reductive carboxylation is a net-zero reaction; actually, the hydride ion is transferred from the mitochondria to the cytosol as reverse IDH2 reaction converts NADPH into NADP, and IDH1 converts NADP into NADPH in the cytosol. The generation of NAD<sup>+</sup>, however, seems to be also a relevant part of reductive carboxylation in cells as it was shown that citrate is rarely limited in cancer cells [348]. In fact, most cancer cells do have low citrate levels, as high citrate levels would activate gluconeogenesis and inhibit glycolysis. As cancer cells are highly relying on glycolysis, it seems unlikely that high citrate would be the reason for reductive carboxylation. Furthermore, high citrate levels were shown in senescent cells [313, 331], cell state opposite of the highly proliferative state of tumor cells. Furthermore, the generation of NAD<sup>+</sup> by reductive carboxylation is important and highlighted by the fact the cells with dysfunctional complex I, main enzyme to accept electron of NADH to generate NAD<sup>+</sup>, or mutations in the ETC display higher levels of reductive carboxylation [342, 343]. In fact, citrate can also be used to generate more NAD<sup>+</sup> as citrate exported to the cytosol can be converted into acetyl-CoA and oxaloacetate by ATP citrate synthase/lyase (ACLY), and the oxaloacetate can be used in the MDH 1 reaction to form Malate and NAD<sup>+</sup>. The contribution of NAD in cancer metabolism is increasingly complex as there are most metabolic reactions require NAD(H), FAD(H), or NADP(H) as cofactors, and alterations in those ratios influence post-translational modifications of enzymes such as acetylation or PolyADP-ribosylation, also known as parylation.

### **1.6.2. Metabolic alterations resulting in post transitional modification**

The activity of many metabolic enzymes is regulated by posttranslational modifications, including phosphorylation, sumoylation, methylation, acetylation, thiolation, and parylation. In the following, the focus is going to be on acetylation and parylation as those modifications are most relevant further on; nonetheless, all PTMs are highly relevant, and their impact on cancer is reviewed

here [349–351]. Concerning parylation, this modification is indirectly regulated by metabolism as the modification requires NAD<sup>+</sup>. The parylation occurs mainly in DNA repair mechanisms, especially in single-strand DNA repair. However, other roles of parylation, for example, in inflammation regulation [352], regulation of the mitotic spindle [353], RNA polymerase activity [354], metabolic regulation [355], gene transcription and much more [356], have been shown. Parylation is carried out by poly (ADP-ribose) polymerase (PARP) family enzymes, mostly by PARP1, as this enzyme is the most abundant of the PARP family [357]. Importantly, high PARP activity was shown to be able to reduce NAD<sup>+</sup> levels significantly, and in case of high levels of DNA damage, the reduction of NAD<sup>+</sup> can induce metabolic stress, reduced ATP levels followed by apoptosis [355, 358]. Interestingly, high PARP activity was associated with longevity and reduced senescence cell burden but also higher tumor incidence highlighting the double role of parylation [359, 360].

Regarding the metabolic alterations, it is to be noted that acetylation can occur either enzymatically, by lysine acetyltransferase (KAT) or spontaneously [361]. The spontaneous additions of acetyl groups to lysines are mostly present in the mitochondria due to the higher pH and the increased availability of acetyl-CoA, the donor of the acetyl group. Importantly, deacetylases can remove the acetylation of proteins, and there are two classes, the class of NAD dependent sirtuins and lysine deacetylases (KDAT). KDAT is a class of deacetylases that require Zn<sup>2+</sup> and can be mainly found in the cytosol and the nucleus. Their activity seems to be basal and not particularly regulated in cancer or under metabolic stresses [362, 363]. In contrast to this is the NAD-dependent sirtuin family. Sirtuins can be found in all compartments of the cell, and deregulation of sirtuins was found in several malignancies, either as a tumor suppressor or as a tumor promoter [364, 365]. Importantly, Sirt enzymes are NAD<sup>+</sup> dependent, and low NAD<sup>+</sup> availability was shown to increase global acetylation [361]. For example, the transcription factor STAT3 was shown to be acetylated in several residues, and this acetylation would alter transcriptional targets as well as increase transcriptional activity of STAT3 [366]. Similar effects have been observed for the E2 promoter binding factor 1 (E2F1) S phase promoting transcription factor [366]. In these cases, the acetylation would be protumorigenic, and reduced Sirt activity would be tumor-promoting [366]. In contrast to this, the tumor suppressor p53 was also shown to be acetylated, and increased acetylation on p53 on lysine residues in the c-terminal domain (K321, K373, K381, K382) would result in loss of MDM2-p53 interaction, thus in the stabilization of p53 and a tumor-suppressive role of the acetylation and tumor-promoting role of higher Sirt activity [366, 367]. Acetylation was not only shown to be important for transcriptional regulation but also important for metabolic enzymes in tumor-promoting as well as tumor-suppressive roles [368]. First, it has to be mentioned that glycolysis, see figure [1.6], requires NAD<sup>+</sup> in the glyceraldehyde 3-phosphate dehydrogenase (GAPDH)

reaction, thus competing for the NAD<sup>+</sup> with cytosolic sirtuins. The higher the Sirt activity, the less NAD<sup>+</sup> is available for glycolysis. Moreover, acetylation of PKM2, the enzyme that catalyzes the last step of glycolysis, PEP to pyruvate, was shown, and this acetylation led to reduced reaction speed of the glycolysis resulting in accumulation of glycolytic intermediates and increased tumor growth [369], most likely via increased PPP activity. This report links the acetylation, whether it is due to lack of sirtuin activity or increased acetyl-CoA level towards glycolytic regulation. In the following, the roles of glycolysis in cancer metabolism will be discussed.

### **1.6.3. Warburg effect and metabolic requirements for cancerous cells**

Metabolic requirements of cells which proliferate and resting cells are obviously different, but differential usage of metabolites can be observed even in different tissues. One of the earliest observations in metabolism was done by Otto Warburg. He stipulated that metabolism in growing embryos should be different than in tumor cells [370]. He took advantage of rat carcinoma, which he continually propagated by transplantation. He took a tissue section and transferred it into an anaerobic glucose solution, and by doing so, he could observe that the cancerous tissue would produce up to 8 times more lactate than the control tissue, a contracting frog leg. Compared to the embryo in anaerobic conditions, he could observe a similar glycolytic rate of the tumor tissue versus the embryonic tissue; however, the tissue did behave differently in aerobic conditions. Once he placed both the carcinoma or the embryonic tissue into oxygen, it became obvious that respiration in the embryo was sufficient to abolish lactate secretion, whereas lactate secretion did not stop in the cancerous tissue. More importantly, when using human benign tumors versus human malignant tumors, he could demonstrate that cancerous tissue maintained lactate secretion even in the presence of sufficient oxygen, whereas the benign tumor ceased the lactate secretion. Thus, Warburg concluded, that benign tissues in oxygen do increase respiration proportionally to the glycolytic rate, whereas malignant tissue maintains lactate secretion even in the presence of oxygen [370].

Today, the phenomenon of increased glucose uptake, and increased lactate secretion in the presence of oxygen, is known as the Warburg effect, and the increased glucose uptake of tumors is used in the clinic to diagnose several cancers [371] (see also figure [1.6 number 6] for an overview of glycolysis). Nonetheless, it has to be mentioned that the knowledge of metabolic requirements of cancerous cells have evolved since Otto Warburg's initial discoveries though it remains to be fully elucidated why cancer cells increase glucose uptake [372]. Therefore, in the following, some of the suggested hypotheses to explain the increased glucose uptake and lactate secretion in cancer cells will be discussed.



Over the past years, researchers have emitted several hypotheses to try to explain the benefits of a cancer cell to increase glucose uptake and lactate secretion while sufficient oxygen is present. Starting in the 1950's researchers thought, even though not supported by Warburg's initial observations, that the increased glucose consumption, while oxygen is present, was due to mitochondrial dysfunction, thus an incapacity to respire. Warburg had shown in his initial observations that the tumors did respire normally, but they do not increase respiration to the same extent then they increase lactate secretion [370]. Furthermore, analysis of tumor samples with evolved measurements for respiration activity showed that all tumors do have detectable respiration [372]. Starting from the 2010's new interest into the Warburg effect emerged, and the initial idea why cancer cells increased glucose uptake would be due to increased carbon usage [373]. This hypothesis seems contraindicative as the cell would lose carbon by secreting lactate, so it seems unlikely as some cancer cells increased secretion of lactate even more than relative corresponding glucose uptake [372]. This would result in a net loss of carbon, thus rendering this idea highly unlikely to be the reason for the increased glucose uptake. A possibility here would be that the secreted lactate is taken by other surrounding cells, and no carbon would be lost [374]. Moreover, those surrounding cells could metabolize the lactate into other metabolites and re-secrete them so that the cancer cells can take them up [374]. In fact, it was shown in some cancer cells that cancer associated fibroblasts (CAF) could take up lactate [375] and exosomes secreted by CAF would contain metabolites for the cancer cells, mainly glutamine and lipids [376].

Another aspect that is discussed is that the Warburg effect is just a bystander effect of oncogene activation or loss of tumor suppressors. In fact, many metabolic genes such as hexokinase (HK)1 to 4, pyruvate kinase M1 (PKM1), pyruvate kinase M2 (PKM2), lactate dehydrogenase A (LDHA), pyruvate dehydrogenase kinase 1 (PDK1) glucose transporters and phosphofructokinase 1 (PFK1) have transcriptional activation binding sites for the oncogenes MYC, RAS or HIF in their promoters resulting in an increased expression of those proteins upon oncogene activation [377]. Furthermore, loss of tumor suppressor p53 has been shown to increase glycolysis by regulating TIGAR [82], phosphoglycerate mutase (PGM) [378] as well as glucose transporter [379]. Activation of TIGAR, an enzyme with 2,6-fructosebisphosphatase activity, decreases the positive allosteric ligands of PFK1, suppressing glycolysis and favoring NADPH production by the PPP [82]. The bystander hypothesis might be true for some cancer, but it seems unlikely that such a ubiquitous observed phenomenon would not provide benefits for cancer cells.

One of the benefits for cancer cells of increased lactate production is avoidance of immunosurveillance, because it was shown that high levels of lactate decrease the immune infiltration of tumors by T-cells [380], macrophages [381], and natural killer (NK) cells [382]. The acid environment generated by high lactate levels would result in lower T-cell proliferation and expression

of exhausting markers such as PD-1, thus lower T-cell activity [383, 384]. Further ideas include that maintaining a high flow of glycolysis and lactate secretion will help to maintain a high pool of glycolysis intermediates; so consequently, those intermediates can be used in shunts of the glycolysis such as the PPP and the serine biosynthesis [373]. This hypothesis seems at least partially validated, although several studies showed that the speed of glycolysis is not increased in cancer cells but rather reduced. For instance, PKM2, the enzyme that catalyzes the last step of glycolysis from PEP to pyruvate, showed increased expression in cancer. PKM2 is normally expressed in the embryo and functions as a dimer or tetramer. PKM2 as a dimer has a lower reaction speed than PKM 1, resulting in an accumulation of intermediates upstream of the PKM reaction. In line with this it was shown that high expression of PKM 2 in lung cancer allows accumulation of glycolytic intermediates and shunting into PPP for increased ROS detoxification [385]. In contrast to this, the germline knockout of PKM2 in mice resulted in spontaneous hepatocarcinoma formation [386]. This study demonstrated that the loss of PKM2 results in changes in metabolite levels and gene expression previously linked to the development of liver cancer [386]. These conflicting results highlight the complex relationship of metabolic alterations in cancer and indicate that it is not PKM2 itself that drives the alterations in glycolysis but other factors. The exact role of PKM2 in cancer initiation needs to be determined, but both observations can be put into agreement if one considers that loss of PKM2 most likely results in highly increased ROS stress which could be the driver of the transformation process in the liver. Likewise, high PKM2 expression can dampen high ROS levels towards a sustainable level allowing cancerous cells to grow. Regardless of the exact mechanism and role of PKM2, the idea of increased biomolecule disponibility seems an interesting point to explore.

Another hypothesis that was considered to be at the bottom of the Warburg effect is the increased reaction speed of ATP production in glycolysis versus mitochondrial respiration [373]. However, a recent study suggests that ATP does not become limiting in cancer cells but rather NAD<sup>+</sup> [387]. In light of the last two ideas, one could suggest combining these hypotheses into the following; the most important part of the Warburg effect would be the regeneration of NAD<sup>+</sup> and intermediates in a speedy manner.

Finally, great progress on understanding the Warburg effect was achieved in the last two decades but the molecular details on the Warburg effect, even though discovered almost 100 years ago, remains to be completely elucidated [372]. It seems obvious that several of the suggested hypothesis above could also interact together, rendering this task even more complex. Nonetheless, several studies point to the NAD<sup>+</sup>/NADH ratio as one of the major drivers of the Warburg effect. As the Warburg effect has shown to be tumor-promoting effects is to be expected that tumor suppressors such as p53 are opposing the effects of the Warburg effect. In the following, it will

be discussed how p53 can regulate metabolism and oppose the Warburg effect. Furthermore, the implication of NAD<sup>+</sup>/NADH as a tumor-promoting agent will be discussed.

#### 1.6.4. p53 as a regulator of metabolism

Above its role in apoptosis and cellular senescence, as previously mentioned, p53 can regulate glycolysis, and in the following, it will be discussed in more detail how p53 can regulate metabolism. An overview of p53 targets in metabolism are described here [60]

First indications that p53 has further roles than regulation of apoptosis and genome integrity were shown when Jones *et al.* demonstrated that p53 could repress mTOR activity [388, 389]. The repression of mTOR by p53 resulted in a decrease in protein synthesis and in an increase in autophagy [390]. Moreover, direct regulation on glycolysis by p53 was shown when the TIGAR protein was identified [82]. Similarly, it was suggested that loss of p53 could upregulate expression of PGM, resulting in increased glycolysis [391]. In the same idea, it was shown that p53 could regulate mitochondrial respiration via activation of expression of synthesis of cytochrome c oxidase assembly 2 (SCO2) which is a major regulator of cytochrome c oxidase complex resulting in increased respiration [392].

p53 is not only able to regulate glucose metabolism, but p53 was shown to be able to regulate fatty acid biosynthesis, beta-oxidation, amino acid catabolism, and cholesterol biosynthesis [60, 393, 394]. It is quite well understood how positive transcriptional regulation of metabolic enzymes by p53 can be achieved. First, it was shown that p53 could bind to its promoter response element, helping to recruit subunits of the mediator complex and components of the general transcription machinery, followed by helping to assemble the preinitiation complex of transcription [395]. In contrast to this, repression of transcription by p53 is not achieved by p53 direct binding to DNA but rather through the DREAM complex of transcriptional regulation [396–398]. The DREAM complex is composed of a core part, p130/p107, E2F4/E2F5, MuvB, RBBP4, and DP1-3, as well as some accessory subunits which help to determine the specific location of transcriptional regulation [398, 399]. Regardless of those discoveries, it is still a matter of debate which are the exact proteins in the DREAM complex to repress metabolic enzymes by p53 [396]. Consequently, a general model is not yet established, and repression by p53 has to be tested one by one on each metabolic gene to confirm regulation by p53.

Concerning this thesis, it is important to mention that p53 was found to be able to repress PC [400]. PC, as mentioned, is an important enzyme for anaplerosis of the TCA cycle but also was shown to be upregulated in several cancer types, including lung [401], mammary [402], and gallbladder cancer [403]. In contrast to the p53 repression PC expression can be increased by

AKT-PI3K pathway, HIF1 $\alpha$  or c-MYC [337]. Increased pyruvate carboxylase activity can generate oxaloacetate (OAA) for *de novo* fatty acid synthesis pathway as well as a precursor for non-essential amino acid biosynthesis. Interestingly, PC activity was also shown to be important in light of ROS regulation via malic enzyme (ME1). In fact, it was shown that knockdown of PC in cancer cells reduced NADPH levels and increased the amount of ROS [404]. Intriguingly, ME1 was also shown to be repressed by p53 [405] highlighting a double attack point of p53 to increase ROS and decrease NADPH level.

Other relevant metabolic genes repressed by p53 include, carbamoyl phosphate synthetase 1 (CPS1) [406], arginase 1 (ARG1) [406], ornithine transcarbamoylase (OTC) [406], phosphoglycerate dehydrogenase (PHGDH) [393], mono-Carboxylate transporter 1 (MCT1) [407], and 6-phosphofructo-2-kinase/fructose-2'6-biphosphatase 3 (PFKFB3) [408]. The consequences of repression by p53 in light to cancer and senescent cell metabolism will be discussed in the following paragraphs. In the context of cellular senescence where p53 is activated, the metabolic effects of activated p53 can be seen.

## 1.7. Alteration of metabolism in senescent cells

In light of the two major topics of this thesis, cellular senescence and metabolism, this section combines both. As described above, p53 is central in mediating the senescence response; likewise, p53 affects the cell's metabolic state, leading to metabolic alterations in senescent cells. Various metabolic adjustments have been described in cellular senescence; however, it has yet to be shown whether metabolic alterations alone are sufficient to induce senescence or are bystander consequences of the senescence response.

### 1.7.1. Amino acid, lipid, nucleotide metabolism in senescent cells

First of all, it was to be noted that metabolic changes in senescent cells are highly dependent on the cell type along with the inducer of senescence. Since the senescent models in this thesis are OIS, MDIS, and replicative senescence, the focus will be mainly those senescent inducers and the metabolic consequences in fibroblasts and epithelial cells.

Some of the changes observed in senescent cells are the increase in lipid content, an increase in lipid membranous organelles as well as changes in the lipid composition of the membrane [197]. It comes as no surprise that those changes are based on alteration of the lipid synthesis and alteration in fatty acid oxidation (FAO) activity. Indeed Quijano *et al.* [409] could show that OIS cells have a decline of lipid synthesis and an increase in FAO mediated by increased activity of

carnitine palmitoyltransferase 1A (CPT1A), the key rate-limiting enzyme responsible for the oxidation of free fatty acids (FFA). Furthermore, it was also shown that a decreased activity of fatty acid synthetase (FAS) in senescent cells contributes to the alterations in lipid biosynthesis [410]. In line with this observation, it was previously mentioned that there is a p53 dependent repression of FASN in cells [411]. Moreover, the levels of nicotinamide adenine dinucleotide phosphate + hydrogen (NADPH) the cofactor for fatty acid biosynthesis are reduced in senescent cells, probably due to high ROS levels as well as a reduction in PPP activity [412]. Likewise, changes were observed in cholesterol oxidase, ceramide, and sphingosine metabolism, although the latter is increased in senescent cells [413–415]. Another lipid class that was shown to accumulate is the class of Oxylipins [416]. Oxylipins are generated by the oxygenation of polyunsaturated fatty acids and are closely related to Prostaglandins, likewise increased in senescent cells [417, 418]. In the article, the authors could show that increased production of prostaglandins induces senescence. Moreover, the release of dihom-15d-PGJ2, a prostaglandin derivate, was increased during senolysis and part of the SASP [416]. Interestingly, Dihomo-15d-PGJ2 release can be used as a marker of senolysis efficiency.

Of note, in several publicly available RNA sequencing analyses of senescent cells, it was shown that alteration in lipid biosynthesis is a highly altered category calling for further research in this area [104, 150, 172, 419]. All in all, lipid metabolism is altered in senescent cells, and further research will underline the relevance of lipids in the senescence field thus it remains context dependent if lipid biosynthesis is increased or decreased. Most likely certain aspects of lipid biosynthesis such as polyunsaturated fatty acids (PUFAs) generation seems to increase in senescence, whereas other lipid biosynthesis pathways will be down regulated.

A branch point of lipid metabolism and other metabolic reactions is citrate. See figure [1.6 number 4]. Indeed citrate, which is generated as the first step of the TCA cycle cycle in the mitochondria, has to be exported into the cytosol for fatty acid biosynthesis. As ACLY the enzyme that supplies acetyl-CoA, the precursor of fatty acid biosynthesis, is a cytosolic enzyme only. Intriguingly, citrate levels increase in replicative senescence and OIS [313, 420]; however, the export of citrate to the cytosol as well as ACLY activity seems to be reduced. Those results suggest a mitochondrial citrate accumulation. The question remains why citrate levels would accumulate in the mitochondria in senescent cells. Of note, knockdown of ACLY induces a p53 dependent senescence [421]. Thus, apart from reduced fatty acid biosynthesis, the reduction in cytosolic acetyl CoA levels results in alteration in acetylation of cytosolic and nuclear proteins as acetyl CoA is the substrate for acetylation reactions. Acetylation of proteins has various implications in cell homeostasis, and the consequences of acetylation were discussed before.

Another metabolic pathway that is affected in senescent cells is nucleotide biosynthesis. As already mentioned, one characteristic of senescent cells is cell cycle arrest; accordingly, cells that do not proliferate can reduce dNTP production. Indeed, it has been demonstrated that p53 can repress ribonucleotide reductase (RNR), the enzyme responsible for the conversion of nucleotides into deoxyribonucleotides, followed by a decrease in dNTP levels of senescent cells. Hence, it was suggested that dNTP decrease could be one major trigger to induce cellular senescence [422, 423]. Indeed, knockdown of RNR can result in senescent cells; however, supplementation of senescent cells with dNTP was not sufficient or only partially sufficient to bypass the senescence response [423]. Thus, these results question the idea that the lack of dNTPs is responsible for the senescent response. Likewise, it is not only the levels of dNTPs that decrease in senescent cells but also the whole synthesis of purines and pyrimidines. Although senescent cells maintain high demands of nucleotides for mRNA synthesis, because it was shown that the global mRNA pool does not decrease in senescent cells, flux analysis revealed that most intermediates in pyrimidine, as well as purine synthesis pathway, are decreased in senescent cells [424]. Intriguingly, this was also true in p53 deficient cells [425]. Nucleotide biosynthesis is a multi-step process involving aspartate, glutamine, glycine, and methyl group donor tetrahydrofolate (THF) [424, 426] and aforementioned tracing revealed a decreased amount of aspartate in senescent cells. Fascinatingly, aspartate levels were shown to be rate-limiting for the induction of purine and pyrimidine synthesis in cells with dysfunctional mitochondria [427–429] as well as in hypoxia [430]. Likewise, aspartate is not only important as a precursor of nucleotide biosynthesis but also a branchpoint for amino acid metabolism. First, aspartate can be a cofactor for glutaminolysis enzyme GOT1 and 2, and decreases in aspartate level could result in decreased glutamine assimilation [321].

Glutamine, as mentioned before, is an important amino acid for anaplerosis of the TCA cycle via the generation of  $\alpha$ -KG and is an important source of nitrogen for the cell [321]. Likewise, it was shown that glutaminolysis provides cofactors for serine biosynthesis via the PSAT reaction (see metabolic overview [1.6 numbers 2 and 7]). Indeed, it was demonstrated that serine levels decrease in senescent cells [431]. In line with alterations in serine levels as a determinant for tumor progression or cell cycle arrest, it was shown that more aggressive pancreatic ductal adenocarcinoma (PDAC) have higher serine levels. Mechanistically it was demonstrated that pancreatic cancer cells secrete a lot of neuron growth factor (NGF) to recruit peripheral axons that can release serine, thus increasing serine levels in the pancreas resulting in more aggressive cancer [432].

Roles of serine have been shown in nucleotide biosynthesis, S-Adenosyl methionine (SAM) production, cysteine, and glycine production, all via the one-carbon metabolism [433]. Likewise, serine is important for the generation of sphingolipids. Interestingly, it was shown that decreased serine biosynthesis affects cell proliferation via NADH accumulation, and NADH accumulation

would slow serine biosynthesis[433, 434]. The codependent regulation of synthesis via the redox state could be well at play in senescent cells as NADH levels have been shown to increase in these cells [127].

A surprising alteration in senescent cells metabolism is the increase of glutaminolysis. It was shown that p53 could activate GLS2, which results in increased glutaminolysis in senescent cells, and inhibition of glutaminolysis leads to a senolytic effect [320, 435, 436]. It seems contra-inductive that senescent and highly aggressive tumor cells have the same metabolic alteration in increased glutaminolysis. Nonetheless, one explanation might be that in both cases, the increased glutaminolysis is mediated by the high levels of ROS in those cells. Indeed, it was shown that glutaminolysis could significantly contribute to cytosolic NADPH level via the isocitrate dehydrogenase reactions. Regardless, the exact role of glutaminolysis in senescent cells and its contribution to the tumor-suppressive environment has still to be uncovered, especially in light of a recent report that showed that induction of senescence via p53 reactivation resulted in decreased glutaminolysis and increased glycolysis in KRAS driven PDAC mouse tumors [331].

In the same line, aspartate generated via glutaminolysis could regulate the urea cycle and ammonia detoxification, a byproduct of amino acid break down, and alteration in urea cycle activity could explain the lower anabolism of amino acids and consequently accumulation of specific amino acids in senescence cells. Of note, CPS1 a rate-limiting enzyme in the urea cycle can be repressed by p53, contributing to the accumulation of specific amino acids [437].

An example of an accumulated amino acid in senescent cells is cysteine. Analysis from human plasma, young versus old persons, has shown an accumulation of cysteine and cystine, the dimeric oxidized form of cysteine, in the aged group [438]. Of note, high intracellular cystine level could be the result of the increased level of ROS or might explain the resistance of senescent cells to ferroptosis [439]; however, other groups have suggested altered iron metabolism as the critical contributor to senescent cell ferroptosis resistance [440].

The increased ROS level and resistance ferroptosis have implications on the metabolism of other amino acids such as glutathione, a small three amino acid peptide composed of glutamate, cysteine, and glycine [441]. Glutathione is the obligate cofactor for many enzymes that reduce oxidized proteins or oxidized lipids [441]. Although no consensus of whether glutathione synthesis is increased or decreased in senescent cells, it was shown that the oxidized form of glutathione GSSG is increased, at least in the acute phase of the senescence induction, in several senescent cell models highlighting the roles of ROS in the senescence response [415, 420, 431]. Furthermore, removal of gamma-glutamyl transferase activity, the enzyme responsible for GSH production, led to induction of cellular senescence in primary cells as well as in cancer cells [442, 443]. The increased levels of GSSG can be reduced by glutathione reductase back to GSH while NADPH

is oxidized to NADP, leading to decreased NADPH level in senescent cells [431, 444]. Reduced NADPH levels have various biological implications, as mentioned before including, alteration in fatty acid biosynthesis, PPP, isocitrate, and malate metabolism. The roles of NADPH will be further discussed later on.

Further amino acids alterations in senescent cells include an accumulation of alanine in senescent cells, although the molecular contribution is not yet known [420]. In contrast to this, accumulation of branched-chain amino acids, leucine valine, and isoleucine were shown to be able to induce a senescence response via the mTOR and p21 induction [445]. In light of cellular senescence as an aging mechanism, it was shown that treatment with several amino acids in worms, yeast, or mice could alter the lifespan [446]. For example, supplementation with serine in worms and yeast showed increased lifespan [447, 448]. Moreover, as mentioned before, serine plasma levels are decreased in aged human and mouse plasma [449, 450]. Roles of supplementation of other amino acids can be found here [446].

Going back to aspartate and amino acid metabolism in senescence, researchers showed that the levels of aspartate and asparagine are important for the regulation of mTOR activity [451, 452]. In senescent cells, the role of mTOR is complicated, as mentioned before, and local foci of high mTOR activity [239] could require local accumulation of aspartate or asparagine, although formal proof of how this would be achieved in senescent cells is not yet done.

Finally, aspartate is also important for the malate aspartate shuttle (see figure [1.6 number 8]). The malate aspartate shuttle is one of the main shuttles in cells, which can transport reducing equivalence from the mitochondria to the cytosol and *vice versa*. Interestingly, both malate, as well as, aspartate levels are decreased in senescent cells [420, 431, 446] raising the question of how reducing equivalents are transported into the mitochondria in senescent cells. These results suggest profound changes in reducing equivalents such as NAD, NADH, and NADPH in senescent cells. A major contributor to NAD<sup>+</sup> and NADH levels is glycolysis because NAD<sup>+</sup> is an obligate cofactor for the GAPDH ratio in glycolysis.

### **1.7.2. Glucose metabolism in senescent cells**

In senescent cells as well as in aged model organisms such as the mouse and fruit fly, it was demonstrated that glucose consumption is increased [453, 454]. Furthermore, it was shown that this increase of glucose was a compensatory mechanism due to a decrease of mitochondrial ATP production in senescent cells [125, 454, 455]. The increase of mitochondrial dysfunction in senescent cells leads to a reduction of ATP production by the respiratory transport chain and a mitochondrial accumulation of NADH [127]. The decrease of ATP production triggers a compensatory glycolysis increase to maintain viability. Of note, the first senolytic cocktail was a combination



of 2-Deoxy-d-glucose, glucose which can not be metabolized, and an autophagy inhibitor. The combination of those two would result in killing therapy-induced senescent cells [455].

The increased glycolysis of senescent cells has two major effects. First, it was shown that increased glycolysis resulted in reduced branching of the glycolysis into the PPP in senescent cells, and this explained the aforementioned decreases of precursor for nucleotide biosynthesis as well as total NADPH level decrease in senescent cells. The decrease of NADPH levels has profound importance, as mentioned above, for glutathione metabolism, nucleotide biosynthesis, and ROS detoxification. Of note, it was shown that glucose-6-phosphate dehydrogenase (G6PD) the rate-limiting enzyme of PPP is reduced in senescent cells via p53 repression and expression of G6PD could extend lifespan in mice [456], although forced expression can also help to transform immortalized cells [457].

The second effect of the increased glucose consumption of senescent cells is the accumulation of cytosolic NADH due to the GAPDH reaction where glyceraldehyde three phosphate is converted into D-glycerate 1,3-bisphosphate and NAD into NADH. Consequently, senescent cells have been shown to increase LDH reaction to maintain lower NADH levels because the LDH reaction converts pyruvate into lactate, concurrently oxidizing NADH into NAD<sup>+</sup>.

It is important to notice that in normal and cancerous cells, most of the NADH generated in glycolysis can be transferred into the mitochondria via the malate aspartate shuttle and then be oxidized into NAD<sup>+</sup> by complex I. As mentioned above, the senescent cells have a dysfunctional complex I; consequently, the reaction rate of complex I is decreased, resulting in a cytosolic and mitochondrial accumulation of NADH. The roles of NADH in senescent will be primarily described in the second article of this thesis.

## **1.8. Could alterations in NAD or NAD intermediates be a significant contributor to the aging phenotype and the cellular transformation? The roles of NAD and NADPH metabolism in cancer and senescent cells**

In the previous section, it was mentioned several times that one of the consequences of the alteration in metabolism is an increase of NADH or a decrease of NADPH and that those changes in the redox pair are at the bottom of senescence and cancer initiation. In the following section, the roles of NAD and NADP metabolism and their role in cancer and senescence will be discussed. One question that remains to be answered and is a center piece of the second article is whether

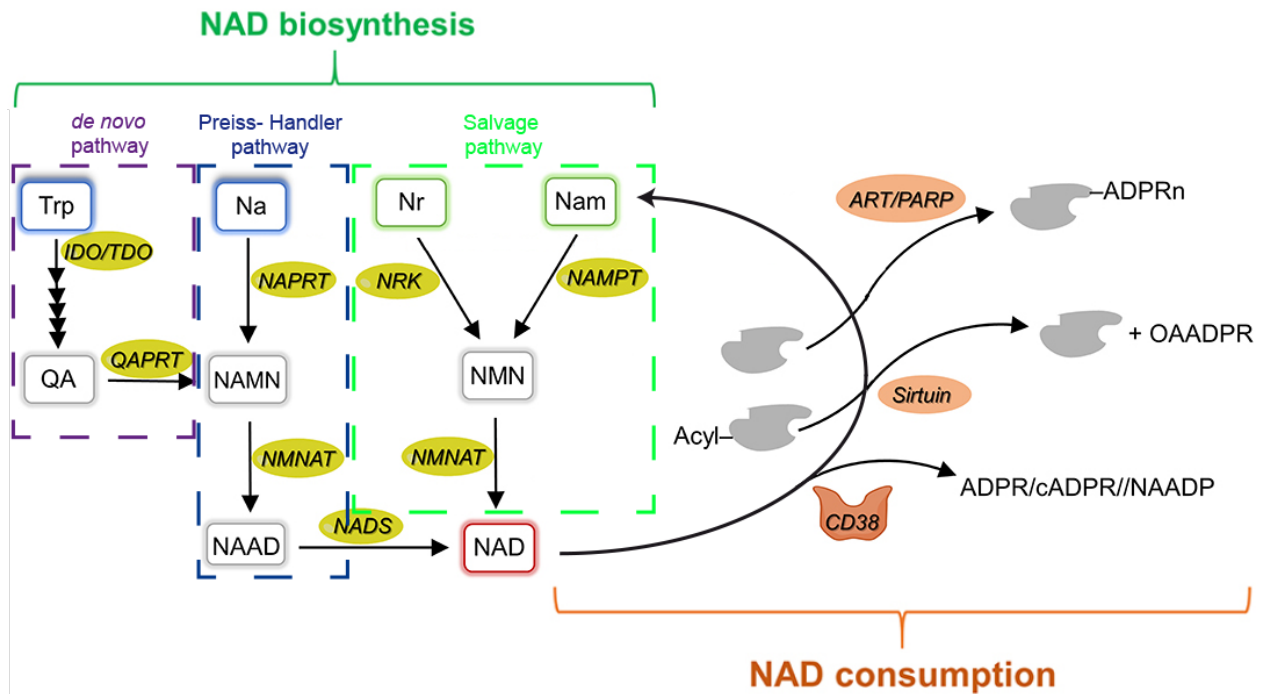


**Figure 1.9. Pathways of NAD biosynthesis and NAD consumption**

NAD levels in the cells are regulated by NAD synthesis (shown in green) and NAD consumption (shown in orange). Three major pathways allow for NAD synthesis, and this is the *de novo* pathway via tryptophan (Trp), the Preiss-Handler pathway via Niacin (NA), or the salvage pathway via nicotinamide riboside (NR) and nicotinamide (NAM). NAD can be consumed by CD38 NAase, sirtuins and parp. Figure adapted from [460]. Abbreviations: IDO/TDO: Tryptophan 2,3-dioxygenase, QA: Quinolinic acid, QAPRT: Quinolinate phosphoribosyltransferase, NAPRT: Nicotinate phosphoribosyltransferase, NMNAT: Nicotinamide/nicotinic acid mononucleotide adenylyltransferase 1, NADS: NAD synthetase, NAMPT: Nicotinamide phosphoribosyltransferase, NRK: Nicotinamide Riboside Kinase NMN: Nicotinamide mononucleotide, NAAD: Nicotinic acid adenine dinucleotide, NAD: nicotinamide adenine dinucleotide.

NAD alterations can be the sole driver of senescence and tumor promotion. In the following, some evidence for this hypothesis will be presented.

The accumulation of NADH in senescent cells is not the only change in nicotinamide nucleotide level in senescent cells. It was shown that not only the ratio change but also the total levels of NAD decrease in old model organisms [458, 459]. The decrease of total NAD level could be due to higher NAD degradation by NADases (CD38, CD157, and SARM1), Sirtuins, and PARP or lower synthesis NAD. Other factors that can alter the NAD pools are enzymes that convert NAD into NADP. For an overview of NAD consuming and NAD producing pathways, see figure [1.9]

The profound changes in NAD homeostasis in aged cells and senescence triggered a series of experiments that showed that NAD alteration could indeed be the source of some aging phenotypes

[458, 461, 462]. It was demonstrated *in vivo* in accelerated aging model [463], physiological aging model [464, 465] as well as age-related disease models such as obesity, Duchenne muscular dystrophy model, or Atm mutant mice (ataxia telangiectasia model) that NAD level decrease in aging [458].

For the hypothesis that decreased NAD levels in aging are due to lack of synthesis, it was shown that supplementation of the precursor of NAD, NR, can extend the lifespan of human cells in culture as well *in vivo* in *C. elegans* [466]. Moreover, NAD supplementation conferred resistance to develop Parkinson's-like symptoms in a fly disease model [467]. Furthermore, it was shown in mice that supplementation with NR or nicotinamide mononucleotide (NMN) could delay age-related diseases such as loss of muscle mass [468], cognitive decline [462, 469], diabetes, and others [458]. Moreover, treatment with NMN, a precursor in the salvage pathway, was shown to reduce age-associated diabetes in postmenopausal women [470].

In mammals, the synthesis of NAD can be achieved through 3 pathways. The salvage pathway(1), the Preiss-Handler (PH) or the *de-novo* pathway(3) see green part of figure [1.9]. In the salvage pathway, nicotinamide (NAM) or nicotinamide riboside (NR) is converted into NMN by nicotinamide phosphoribosyltransferase (NAMPT) and nicotinamide riboside kinase (NRK) enzymes followed by conversion of NMN into NAD by nicotinamide mononucleotide adenylyltransferase (NMNAT). In the PH pathway nicotinic acid/ niacin (NA) is converted by nicotinate phosphoribosyltransferase (NAPRT) into NAMN followed by conversion into nicotinamide adeninedinucleotide (NAAD) and nicotinamide adenine dinucleotide (NAD<sup>+</sup>). The third way to generate NAD is the *de novo* pathway where tryptophan is converted in several steps into quinalinic acid (QA) and then into nicotinamide mononucleotide (NAMN). It was longtime suggested that the major contributor of NAD pools in mammalian cells would be the salvage pathway, but recent reports have shown implications of the *de novo* pathway and PH pathway, especially in cancer cells [471]. Intriguingly, researchers developed a model based on the tumor's tissue origin, which NAD pathway would contribute most to NAD generation. In cases where high NAPRT was found in the tissue, the resulting cancer was highly dependent on PH pathway and showed frequent amplification of the NAPRT gene [472].

Further studies on the metabolism of NAD and the requirements of NAD for cancer proliferation revealed that NAD synthesis pathways and uses for NAD<sup>+</sup> do increase in most cancer cells [24, 461, 473, 474]. Notably, it was shown that inhibition of NAD<sup>+</sup> regeneration by complex I inhibitor or inhibition of NAD salvage by NAMPT inhibition resulted in a decreased growth rate. However, shortly after initiation of treatment, the growth regained, and widespread metabolic rewiring to regain high NAD<sup>+</sup> levels were observed, highlighting once more the importance of

NAD<sup>+</sup> in cancer growth [25, 475]. It remains to be seen whether an increase in NAD<sup>+</sup> is sufficient to transform cells, although it was shown that insufficient NAD<sup>+</sup> supply would be the major contributor to growth reduction in cancer cells [387].

Interestingly, NAD metabolism was not only important in cancer cells it was also shown that high NAD<sup>+</sup> levels are required to maintain stemness in hematopoietic stem cells [476]. Further studies have revealed that an increase in NAD<sup>+</sup> is required for proper Yamanaka factors (OSKM) function in reprogramming cells into iPSC cells as well as maintaining the stemness of embryonic stem cells [461, 477]. These results particularly highlight the relevance of NAD metabolism in aging and youth, although they also warrant a warning in the use of NAD supplements as higher NAD<sup>+</sup> levels can drive cancer progression and also induction of cancer stem-like cells [461, 477]. Moreover, the role of NAD in maintaining youth is also reflected in the fact that in replicative senescent cells, a state opposed to stemness, NAD<sup>+</sup> level decreases.

In replicative senescent cells, it seems to be particularly the activity of the salvage pathway and especially the rate-limiting enzyme NAMPT that decreased with age. Those results highlight the fact that NAD levels can decrease due to lack of NAD synthesis in aging cells [415, 478]. Moreover, it was revealed that also the *de novo* and the PH pathway were altered as intermediates of those pathways, especially NAMN, were increased whereas NAAD was decreased in senescent cells [415].

It was not only the synthesis that was responsible for NAD decrease in aging but also that inhibition of PARPs delayed the onset of replicative senescence. Inhibition of PARP results in an increase of NAD<sup>+</sup> because the PARP enzyme family uses NAD<sup>+</sup> as a substrate to add polymers of adenosine diphosphate ribose to proteins [479]. As parylation is a major PTM on proteins involved in DDR, it was suggested that the activity of PARP could be increased in senescent cells following depletion of the NAD pool [460]. Similarly, it was shown that PARP inhibition in senescent cells could lead to senolysis, raising the question of whether increased PARP activity is a driver of senescence or just a bystander effect [115]. In contrast to this, PARP inhibition was also shown to induce senescence via accumulated DNA damage, highlighting the duality of PARP in senescence [480].

Other NAD-consuming enzymes are sirtuins. Sirtuins use NAD<sup>+</sup> as a cofactor to remove acetyl groups from proteins. It was shown that the activity of several sirtuins is decreased in senescent cells resulting in higher levels of acetylated proteins. However, the consequences of higher protein acetylation are still unclear and probably dependent on each protein individually. Nevertheless, it was shown that overexpression of SIRT3 and SIRT5 could decrease acetylation and delay the onset of replicative senescence, although the exact target that was deacetylated to delay the senescence response remains unclear [127].

In contrast, it was demonstrated that increased acetylation of Histones results in the onset of senescence. Even though the exact mechanism remains to be elucidated, it was suggested that the higher levels of acetylation of Histones led to a hyper-transcription state followed by exhaustion of the cell [126]. Finally, the most interesting report on NAD consuming proteins and senescence was recently published, showing that inhibition of CD38, a NAD hydrolase, delays the onset of senescence in mice. In their report, the authors could show that it was the higher expression of CD38 in aged mice, which would result in degradation of extracellular NAD, which would, in turn, result in the onset of senescence in the surrounding tissue [481].

Apart from decreased synthesis and increased NAD consumption, it was also suggested that increased oxidative stress and mitochondrial dysfunction can be a significant driver of the conversion of NAD into NADP, so that the increased NADP could be used in ROS detoxification [474, 475]. For example, the enzyme nicotinamide adenine dinucleotide kinase (NADK) which is an AKT regulated protein kinase which was shown to be present in the mitochondria and the cytosol. Both isoforms were shown to be an imported contributor to NADP levels in PDAC, breast, and lung cancer [482]. Interestingly, mitochondrial NADK can directly phosphorylate NADH to generate NADPH in the context of high oxidative stress [483]. Another protein that converts NADH into NADPH is the mitochondrial membrane-bound enzyme nicotinamide nucleotide transhydrogenase (NNT). This protein uses the proton motive force generated by the electron transport chain to transfer the hydride ion from NADH to NADPH. It was shown that an increase in NNT activity plays a central role in the metabolic reprogramming of cancer cells. Likewise, knockdown of NNT reduced NADPH production in mitochondria as well as glutamine catabolism [484, 485]. Moreover, it was suggested that about 40% of the mitochondrial NADPH pool is generated by NNT, highlighting the relevance of this enzyme again [486]. As this enzyme requires a high proton gradient to be functional, it was proposed that in senescent cells with dysfunctional mitochondria, the activity of NNT is decreased. Factually, expression of NNT delayed the onset of stem cell senescence, and inhibition of NNT led to induction of premature senescence [487, 488]. Interestingly, NNT can not only work in the production of NADPH but, in a pathological context, can generate ATP and NADH [489]. Finally, NNT seems to be required for reductive carboxylation in some cancer cells, and the inhibition resulted in a loss of reductive carboxylation [485, 490, 491]. These results highlight once again the importance of generation NADPH in cancer metabolism. Apart from NNT, important sources of NADPH are the oxidative branch of the PPP, IDH reactions, and malic enzymes. For an overview of NADPH producing and NADPH consuming pathways, see figure [1.10].

In general, it can be summarized that in cancer, the levels or activities of enzymes to produce NADPH are increased and are associated with negative prognoses, although in some contexts,

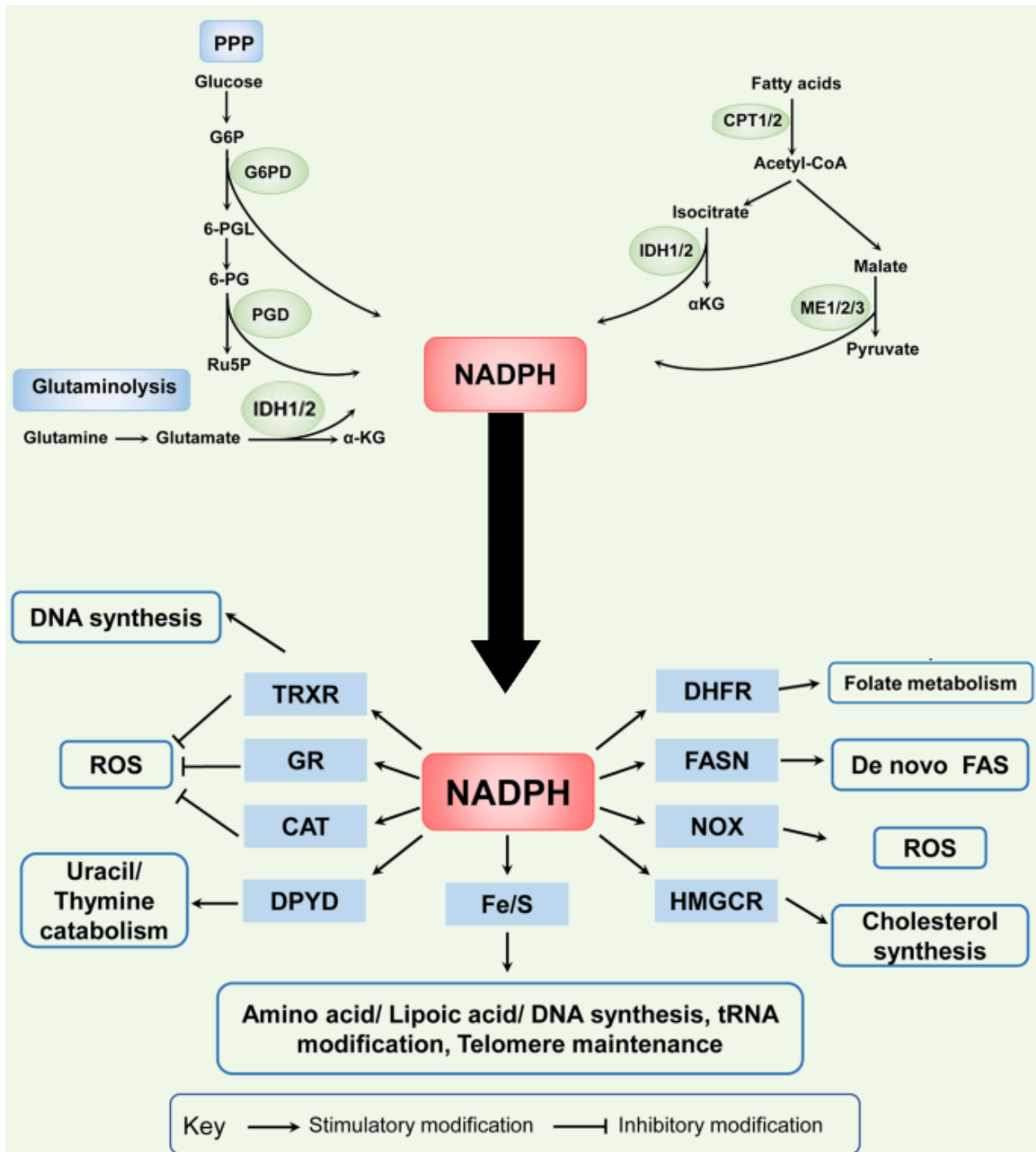


**Figure 1.10. Pathways that can generate or consume NADPH**

The pathways generating NADPH are various in the cell. Here the main generating pathways are highlighted, PPP, IDH reactions, ME reactions. Also, the pathways that are going to transform the NADPH back to NADP<sup>+</sup> are highlighted. Most importantly, ROS, DNA synthesis, FAS, and folate metabolism. Figure adapted from [490].

tumor-suppressive roles of NADPH increase have been shown [82, 490]. Even though all three, PPP, IDH, and ME reactions, have implications in the level of NADPH, it seems that the oxidative branch of the PPP stands out. A well-designed CRISPR study by Chen *et al.* showed that even though all three can compensate for the loss of one NADPH producing pathway to maintain proliferation, the PPP was the only one able to maintain proper folate/one-carbon metabolism [492].

An important aspect of malate metabolism is converting malate into pyruvate, which can be archived by malic enzyme 1 in the cytosol or malic enzyme 2 in the mitochondria. As mentioned before, ME1 and ME2 are repressed in a p53 dependent manner in senescence [405]. Importantly, in this reaction, the NADPH is generated from NADP positioning the malic enzymes in the center of NADPH generation. Notably, the source of malate for malic enzyme can come from MDH1 or MDH2, highlighting the interaction of NAD and NADP metabolic pathways via the aspartate malate shuttle, see overview [1.6] about metabolic reactions.

All in all, NAD and redox homeostasis seem to be important players in the senescence response. First of all, it seems that total levels of NAD decrease in senescence, although the actual trigger for the decrease can be multifactorial. Moreover, the increase in ROS and decrease of the PPP activity combined can trigger a decrease of NADPH levels in senescent cells. Subsequently, rewiring of fatty acid biosynthesis and redox homeostasis in senescent cells can be observed. Finally, NADH accumulation due to higher glycolysis rate and reduced complex I activity seems to be a major trigger of senescence response as a high NADH level can stabilize p53 and trigger a senescence response [493–495]. Mechanistically those studies showed that NADH could bind NAD(P)H quinone dehydrogenase 1 (NQO1) and C-Terminal Binding Protein (CtBP). Upon increase of NADH, the interaction of NADH with NQO1 and CtBP increases and leads to conformational change resulting in interaction with p53. NQO1-p53 interaction protects p53 from binding to MDM2 and leads to stabilization of p53. For CtBP, it was shown that interaction with NADH results in dimerization of CtBP and loss of interaction with MDH2. The loss of MDM2-CtBP interaction results in lower E3 ligase activity of MDM2 towards p53, resulting in increased p53 level [495]. Those results allow for an interesting link between metabolic stress and p53 regulation. If NADH accumulates, like in cells with dysfunctional mitochondria, NADH level can increase stabilize p53 and p53 could then induce cell cycle arrest or maybe even cellular senescence. In case the stress and NADH levels decrease, stabilization factors of p53 are lost, and p53 levels decrease again. This is an interesting fine-tune mechanism based on the metabolic situation of cells. It remains to be seen whether the suggested action of NADH stabilization can induce cellular senescence.

Other metabolism alterations reported in senescent cells include increased pyruvate import into the mitochondria as a compensatory mechanism for low ATP levels. In a landmark paper by Kaplon *et al.*, they could show that in BRAF-induced senescence, the pyruvate dehydrogenase kinase (PDK) enzymes have reduced activity resulting in increased activity of pyruvate dehydrogenase (PDH) and, in turn, higher pyruvate entry into the mitochondria. The increase of pyruvate in the mitochondria has, as a consequence, increased redox stress, and this could be a fed forward loop to maintain the senescence state. Intriguingly, Kaplon *et al.* could observe high levels of pyruvate entry into the mitochondria in OIS, but levels of later TCA intermediates were relatively lower than control cells suggesting that the TCA cycle is interrupted in senescent cells. Indeed the level of succinate seems to accumulate in senescence cells, which is in line with the fact that complex II of the respiratory chain is decreased in senescent cells. Following succinate, levels of fumarate and malate have also been shown to decrease in senescent cells.

All in all, the metabolic changes in senescent cells are various and affect all aspects of metabolism. One major aspect observed in senescent cells is that cofactor of many metabolic reactions, levels of acetyl CoA,  $\alpha$ -KG, NAD or NADP are altered in senescence, and those alterations could well be at the bottom of the senescence response. In light of senescence, it seems established that NAD levels do decrease with age. Moreover, it seems established that NAD increase can allow for increased lifespan; however, the molecular pathways and consequences involved are still unknown. Furthermore, in light of cellular senescence as a tumor suppressor mechanism, it is still unknown whether NAD supplementation does abolish tumor-suppressive effects of cellular senescence. Furthermore, few human trials have looked at the effects of NAD supplementation on human aging, and none of the available studies has looked for a potential increase in cancer incidence. The importance of NAD in cancer metabolism as highlighted here should, however, call for a proper analysis of cancer increase in humans with NAD supplements.

Further important aspects include the metabolic alterations in senescent cells, and it remains to be seen whether the increased glycolysis, increased glutaminolysis, and the altered levels of amino acids and lipids can be tumor-suppressive markers of senescent cells; or are those alterations rather a sign that senescent cells are on the verge towards transformation. It remains an interesting question that p53 can regulate the metabolism of senescent cells; however, it remains to be uncovered whether p53 mediated repression and induction is the prominent way to regulate metabolism in senescent cells. It is quite possible that other proteins that regulate senescence, such as p21 or 16, contribute to the metabolic regulation in senescent cells. In line with this, it was shown that E2F7 could be present in the DREAM complex to repress specific subtypes of genes [399]. Interestingly, E2F7 mediated repression was suggested to be a major regulator for gene repression in senescent cells [496].



## 1.9. General goals of this thesis

Cellular senescence is a strong tumor suppressor mechanism mediated by the actions of p53 and RB. However, despite the tumor suppressors' mechanisms, cancerous cells arise. The main goal of this research was to understand in a more molecular detailed way how the senescence response can be reinforced and the triggers that allow the bypass of the senescence response. Our research was driven by the observation that specific protein degradation is taken place in senescent cells. We called this phenotype senescence-associated protein degradation (SAPD). Using GO term analysis to identify the pathways mainly affected by protein degradation, we identified ribosome biogenesis and mitochondrial homeostasis as two GO terms highly targeted by the SAPD. Furthermore, we identified key proteins of each pathway STAT3 for regulating mitochondrial homeostasis and RSL1D1 and DDX21 for ribosome biogenesis as targets of SAPD. As both mitochondrial homeostasis and ribosome biogenesis are huge pathways, we separated our research into two aspects. First, we focused on ribosome biogenesis, and second, we looked at mitochondrial homeostasis in senescent cells. The key research questions for the ribosome biogenesis part were.

- Do alterations in levels or activity of ribosome biogenesis factors like RSL1D1 or DDX21 result in senescence, and if senescence occurs: what are the molecular consequences of this senescence?
- A second question was whether it would be possible to determine whether ribosome biogenesis defect-induced senescence is mediated by p53 or RB or both?
- Furthermore, we were intrigued by the big nucleolus of senescence cells, and we wanted to know whether this big nucleolus can be a marker of senescent cells?
- Moreover, we were wondering whether ribosome biogenesis and the alterations therein could be used as biomarkers of cellular senescence
- Finally, in light of cellular senescence as a tumor suppressor mechanism, we wanted to know whether ribosome biogenesis defects can enforce oncogene-induced senescence (OIS) or whether normalization of ribosome biogenesis in senescent cells would allow for a senescence bypass?

For the second part, the mitochondrial homeostasis part, our key research questions were

- Can loss of STAT3 induce senescence? If yes, what are the functions of STAT3 that are required to avoid senescence?
- A second question was if STAT3 induced mitochondrial dysfunction does altered mitochondrial homeostasis alter the metabolism of senescent cells? If yes, what are those alterations?

- Moreover, if STAT3 induces senescence, is this senescence maintained by p53 or RB functions, and how?
- Furthermore, can degradation of STAT3 and mitochondrial dysfunction be used as a marker for deep senescent cells?
- Finally, do alterations in metabolism in senescent cells prime senescent cells for transformation, or are those alterations tumor-suppressive?

Finally, in a more global way, our research goal was to validate the SAPD and the implication of protein degradation in senescence. Furthermore, we tried to establish novel characteristics of senescence cells. In particular, we wanted to identify factors that reinforce the senescence response as well as factors that allow for a bypass of the senescence response.



# Chapter 2

---

## Scientific articles

### 2.1. General information

In the following section contains the published articles. Due to the structure of the thesis, the text might be small and I here provided links for the online version of the articles. Moreover, the main text is followed by main figures and supplementary figures. Further information such as supplementary methods and reporting summary are in the Annexes.

- [Senescence-associated ribosome biogenesis defects contributes to cell cycle arrest through the Rb pathway](#)
- [A hydride transfer complex reprograms NAD metabolism and bypasses senescence](#)
- [STAT3 and STAT5 Activation in Solid Cancers](#)

Furthermore, I was forced to reduce the quality of the images in both articles to obtain a reasonable size file. Moreover, it is to be also noted that I did not convert all supplementary tables into PDF. Supplementary tables of the NCB article can be found here:

[Senescence-associated ribosome biogenesis defects contributes to cell cycle arrest through the Rb pathway](#).

For the Molecular cell article, we provided all raw data on Mendeley Data that can be found here: [A hydride transfer complex reprograms NAD metabolism and bypasses senescence](#)

### 2.2. Context for the article 1

The first article of this thesis is based on the observation that senescent cells have a specific protein degradation which helps to maintain the senescence response [93]. We have identified that several proteins implicated in key aspects of senescence, such as cell cycle regulation proteins, mitochondria homeostasis proteins, as well as proteins important for ribosome biogenesis, are degraded upon OIS.

In this article, we wanted to know on a more molecular basis which are the consequences of the degradation of ribosome biogenesis factors on the senescence response. Before this article, it was observed that senescent cells display a single big nucleolus, although the molecular biology behind this was not uncovered. Moreover, it was hypothesized that ribosome biogenesis would be reduced in senescent cells as it requires much energy to generate new ribosomes, and since those cells do not divide, it would be logical that ribosome biogenesis is decreased. We were not only able to provide proof and a timeline for alterations in the ribosome, but we could also pinpoint specific processing steps that are altered in ribosome biogenesis upon induction of senescence.



We were able to show that degradation of targets of the SAPD, namely degradation of RSL1D1, DDX21, Epstein-Barr nuclear antigen binding protein 2 (EBP2) and nucleostemin also known as GNL3 (Guanine nucleotide-binding protein-like 3) (NS) was sufficient to induce senescence, and this senescence was more dependent on the RB suppressor pathway than on p53 as the oncoprotein E7 did whereas E6 did not bypass this senescence response. Moreover, we could demonstrate that the deregulation of ribosome biogenesis results in a fraction of ribosomal-free ribosomal proteins. Those ribosomal free proteins can be used as senescence markers, such RPL29, or those proteins can acquire novel functions. In this article, we were able to show that RPS14 can inhibit CDK4, and this interaction helps to maintain the senescence response and reduces tumor cell growth. The identification of the ribosomal free fraction in senescent cells and their functions opened a new field of research and already led to a new concept of ribosomal free proteins in cell cycle regulation [5]. We could identify that RPS14 can behave as an INK type CDKi, a CIP type CDKi, or there could be a novel function which would be inhibitions of the function of cyclins.

Moreover, the identification of RPL29 as a senescence marker *in vitro* and *in vivo* adds to the growing amount of markers to detect senescent cells. Proper identification of senescent cells is crucial for future research for several aspects. A good senescence marker could be used to evaluate extent of tissue aging but also be a marker for the efficiency of a senolytic treatment [7].

### **2.3. Contribution to the article 1**

My contributions to the article are the following: I performed all the immunofluorescences. The immunofluorescences led to Figures 1a, 1g,h, 2 all panel, 4j, 7a, S2 all panel, S3K, S6j-n, S7 all panels. I performed bioinformatics analysis of data from LC-MS/MS, leading to Figure 4B. I quantified all SA- $\beta$ -gal staining leading to Figure 4i, 6j, S3h, S4a, S5a and i, S6g. I helped to generate Figures of IHC, Figure 3 all panel. I also did one complete replicate to confirm RPS14 senescence and the bypass by shRB. I participated in the writing.

# Senescence-associated ribosome biogenesis defects contributes to cell cycle arrest through the Rb pathway

Frédéric Lessard<sup>1</sup>, Sebastian Igelmann<sup>1</sup>, Christian Trahan<sup>2</sup>, Geneviève Huot<sup>1</sup>, Emmanuelle Saint-Germain<sup>1</sup>, Lian Mignacca<sup>1</sup>, Neylen Del Toro<sup>1</sup>, Stéphane Lopes-Paciencia<sup>1</sup>, Benjamin Le Calvé<sup>5</sup>, Marinieve Montero<sup>1</sup>, Xavier Deschênes-Simard<sup>4</sup>, Marina Bury<sup>6</sup>, Olga Moiseeva<sup>7</sup>, Marie-Camille Rowell<sup>1</sup>, Cornelia E. Zorca<sup>1</sup>, Daniel Zenklusen <sup>1</sup>, Léa Brakier-Gingras<sup>1</sup>, Véronique Bourdeau<sup>1</sup>, Marlene Oeffinger<sup>1,2,3</sup> and Gerardo Ferbeyre <sup>1\*</sup>

**Cellular senescence is a tumour suppressor programme characterized by a stable cell cycle arrest. Here we report that cellular senescence triggered by a variety of stimuli leads to diminished ribosome biogenesis and the accumulation of both rRNA precursors and ribosomal proteins. These defects were associated with reduced expression of several ribosome biogenesis factors, the knockdown of which was also sufficient to induce senescence. Genetic analysis revealed that Rb but not p53 was required for the senescence response to altered ribosome biogenesis. Mechanistically, the ribosomal protein S14 (RPS14 or uS11) accumulates in the soluble non-ribosomal fraction of senescent cells, where it binds and inhibits CDK4 (cyclin-dependent kinase 4). Overexpression of RPS14 is sufficient to inhibit Rb phosphorylation, inducing cell cycle arrest and senescence. Here we describe a mechanism for maintaining the senescent cell cycle arrest that may be relevant for cancer therapy, as well as biomarkers to identify senescent cells.**

## **2.4. Senescence-associated ribosome biogenesis defects contributes to cell cycle arrest through the Rb pathway**

### **2.4.1. Abstract**

Cellular senescence is a tumor suppressor program characterized by a stable cell cycle arrest. Here we report that cellular senescence triggered by various stimuli leads to diminished ribosome biogenesis and the accumulation of both rRNA precursors and ribosomal proteins. These defects were associated with reduced expression of several ribosome biogenesis factors, the knockdown of which was also sufficient to induce senescence. Genetic analysis revealed that Rb but not p53 was required for the senescence response to altered ribosome biogenesis. Mechanistically, the ribosomal protein S14 (RPS14 or uS11) accumulates in the soluble non-ribosomal fraction of senescent cells, where it binds and inhibits CDK4 (cyclin-dependent kinase). Overexpression of RPS14 is sufficient to inhibit Rb phosphorylation, inducing cell cycle arrest and senescence. Here we describe a mechanism for maintaining the senescent cell cycle arrest that may be relevant for cancer therapy, as well as biomarkers to identify senescent cells.

### **2.4.2. Introduction**

Cellular senescence opposes neoplastic transformation by preventing the proliferation of cells that have experienced oncogenic stimuli<sup>1</sup>. Senescence is efficient as a tumor suppressor mechanism as long as it prevents cell cycle progression. Some benign lesions contain senescent cells that remain out of the cell cycle<sup>2,3</sup>. Senescent cells also stimulate their own clearance by the immune system, thereby strengthening the defenses against tumorigenesis<sup>4,5</sup>. However, the process is not infallible and lesions containing senescent cells can progress into malignant cancers<sup>6,7</sup>. To escape from senescence, cells need to increase protein biosynthesis and more importantly the machinery to do so. Indeed, ribosome biogenesis is upregulated in cancer cells<sup>8,9</sup>. Senescent cells exhibit reduced ribosome biogenesis and this has been explained by a delay in ribosomal RNA (rRNA) processing eventually leading to the accumulation of the ribosomal proteins L5 (uL18) and L11 (uL5) that form a complex with the 5S rRNA and disable the E3 ligase MDM2 (or HDM2), thus activating p53<sup>10</sup>. Conversely, drugs that reduce ribosome biogenesis can trigger senescence and are considered very promising anticancer therapeutics<sup>11-13</sup>.

Cellular senescence can be induced in cells in the absence of p53<sup>14</sup> through a pathway that involves several members of the cyclin-dependent kinase inhibitor (CKI) family, such as p16INK4a (p16) and p15INK4b (or CDKN2B), and the retinoblastoma (RB1 or RB) tumor suppressor<sup>15,16</sup>. RB controls cell cycle progression by repressing E2F activity, and in senescent cells, by promoting

the formation of heterochromatin at E2F target promoters<sup>3,17</sup>. In proliferating cells or cells that escape from senescence, RB is inhibited by cyclin-dependent kinases such as CDK2, 4 and 6<sup>18</sup>. Genetic inactivation of CDK4 leads to p53-independent senescence<sup>18</sup> and CDK4 inhibitors can reactivate a latent senescence program in cancer cells<sup>19,20</sup>. Here, we show a mechanism that targets the CDK4/6 kinases in senescent cells. We demonstrate that oncogenic signals interfere with rRNA biogenesis via the degradation of multiple ribosome biogenesis factors leading to a p53-independent but RB-dependent senescence response. Senescent cells accumulated both rRNA precursors and ribosomal proteins in the nucleus and nucleolus. Moreover, we found that the ribosomal protein S14 (uS11) binds and inactivates the cyclin-dependent kinase CDK4, thereby acting as a CKI and linking ribosome biogenesis to cell cycle control. Since p53 is inactivated in most human cancers, this work provides a rationale to target ribosome biogenesis and restore senescence in human tumors in a p53-independent manner.

### 2.4.3. Results

#### **Deficient ribosome biogenesis and accumulation of rRNA precursors in senescent cells**

Non-dividing cells as well as senescent cells have a limited demand for ribosomes and hence ribosome biogenesis. Paradoxically, induction of senescence by oncogenic *ras* or by telomere shortening (replicative senescence) in normal human fibroblasts induces nucleolar clustering into a single prominent nucleolus (Fig. 1a), reminiscent of big and abundant nucleoli of aggressive cancer cells<sup>9</sup>. To determine the relationship between decreased ribosome biogenesis and the senescence program, we first used the model of oncogene-induced senescence (OIS). Shortly after the introduction of oncogenic *ras*, there is an increase in both rRNA synthesis and cell proliferation (days 2-6, Supplementary Fig. 1a). However, when cells became senescent (days 8-20 after Ras expression, PML expression or telomere shortening), rRNA synthesis was dramatically reduced as measured using a three hours pulse of <sup>3</sup>H-uridine (Fig. 1b and Supplementary Fig. 1a-d). We conclude that the synthesis of rRNA is largely reduced in senescent cells irrespective of the stress that triggered the process.

Next, we used probes complementary to the Internal Transcribed Spacers ITS1 and ITS2 (Fig. 1c) to characterize pre-rRNA processing intermediates in senescent cells. We loaded the gels normalized against the amount of mature 28S rRNA as was done for pulse labeling in Figure 1b. While we observed a general decrease in rRNA synthesis in *ras*-senescent cells and old (replicative senescent) cells by pulse labeling (Fig. 1b and Supplementary Fig. 1a), we did not detect a similar decrease in rRNA precursors at steady state by northern blotting. The primary rRNA precursor, 47S, accumulated in senescent cells, while the levels of the small subunit intermediates 21S and 18S-E decreased (Fig. 1d). Consequently, senescent cells had increased



47S/21S (Fig. 1e) and 47S/18S-E (Fig. 1f) ratios. This finding is striking given the observed decrease in rRNA synthesis as shown by pulse labeling (Figure 1b), and is consistent with previous work showing that disabling the small nucleolar RNAs U3 and U8 leads to the accumulation of the 47S rRNA precursor, G1/S cell cycle arrest and nucleolar fusion which are characteristics of cellular senescence<sup>21</sup>. Additionally, we assessed the accumulation of rRNA precursors in senescent cells using single-cell analysis and RNA-FISH with a probe that detects non-processed rRNA intermediates (Fig. 1c). We found a prominent accumulation of these precursors in the nucleolus of *ras*-senescent cells, old cells, and PML-senescent cells, but not in cells arrested by confluence or serum starvation (Fig. 1g-h and Supplementary Fig. 2). We thus conclude that senescence involves a reduction in both rRNA synthesis and processing.

### **Accumulation of ribosomal protein RPL29: a biomarker for cellular senescence**

It has been reported that some ribosomal proteins (i.e. ribosomal protein L29: RPL29 or eL29) accumulate in nucleoli following defects in ribosome biogenesis<sup>22</sup>. Consistently, we found an accumulation of RPL29 in the nucleoli of *ras*-senescent cells, PML-senescent cells and old cells (Fig. 2a-b), but not in cells arrested by serum starvation or confluence (Fig. 2b). A prominent nucleolus that accumulates RPL29 was also characteristic of the senescence response to camptothecin (therapy-induced senescence) (Fig. 2c) and  $\beta$ -interferon (Fig. 2d).

The consistent accumulation of markers of altered ribosome biogenesis in senescent cells suggested that they could be used as senescence biomarkers *in vivo*. Towards this goal, we first studied nevi which are senescent benign lesions<sup>2</sup>. In agreement with our observations from cells in culture, p16INK4a positive nevi also accumulated RPL29 in their cell nucleus, while little staining was observed in the cell nucleus of normal skin or in basal cell carcinoma lesions, where most of the staining was cytoplasmic (Fig. 3a-b). Upon magnification, prominent nucleoli positive for RPL29 were observed in nevi cells (Fig. 3c). Similarly, p16INK4a positive benign prostatic hyperplasia lesions accumulated RPL29 in the cell nucleus, while this biomarker was absent in nuclei of normal prostate epithelial cells or prostate adenocarcinoma cells (Fig. 3d-f).

### **Cellular senescence involves reduced levels of ribosome biogenesis factors**

To investigate the mechanism leading to decreased ribosome biogenesis and ribosomal protein accumulation in senescent cells, we studied the levels of several ribosome biogenesis factors previously found as candidate targets for proteasome dependent senescence-associated protein degradation (SAPD) in *ras*-induced senescence (Supplementary Fig. 3a)<sup>1,23</sup>. We found that the more unstable ribosome biogenesis factors Ribosomal L1 Domain Containing 1 (RSL1D1)<sup>24</sup>, nucleostemin (NS or GNL3)<sup>24,25</sup>, DExD-Box Helicase 21 (DDX21)<sup>25</sup> and EBNA1 Binding Protein 2

(EBP2 or EBNA1BP2)<sup>25</sup> were downregulated at the protein level in *ras*-senescent, PML-senescent and old cells (Fig. 4a). However, the mRNAs encoding these proteins were not reduced in senescent cells (Supplementary Fig. 3b-d). RSL1D1, was previously linked to senescence<sup>23,26</sup> and NS is known to be required for the processing of the 32S rRNA precursor<sup>25</sup>. Notably, we found that many nucleolar proteins interact with RSL1D1, as assessed by mass spectrometry after immunoprecipitation of a triple flag version of this protein in HEK-293 cells (Fig. 4b and Supplementary Table 1). Moreover, we found RSL1D1 to interact specifically with NS, DDX21 and EBP2 (Fig. 4c), all of which are downregulated in senescent cells.

Next, we characterized the effects of directly decreasing the ribosome biogenesis factors RSL1D1, NS, DDX21 or EBP2 using shRNAs (Fig. 4d-g and Supplementary Fig. 3e). Depletion of these factors induced a proliferation arrest (Fig. 4h), a decrease in the proliferation markers KI67 and CENPA (Supplementary Fig. 3f-g), and an increase in senescence-associated  $\beta$ -galactosidase staining (SA- $\beta$ -Gal) (Fig. 4i and Supplementary Fig. 3h). Immunoblots of cell extracts from these senescent cells showed signs of activation of both the p53 and the RB pathways as assessed by measuring both total and Ser15 phosphorylated p53 levels (Fig. 4d-g). Additionally, we observed a reduction in E2F target genes such as MCM6 and CENPA, (Fig. 4d-g and Supplementary Fig. 3g), and an accumulation of p21 (Supplementary Fig. 3i). In contrast, p16INK4a was not consistently increased by shRNAs that depleted ribosome biogenesis factors (Supplementary Fig. 3j). Moreover, knockdown of RSL1D1, NS, DDX21 and EBP2 led to accumulation of RPL29 in the nucleolus (Fig. 4j and Supplementary Fig. 3k). We thus conclude that decreasing ribosome biogenesis factors is sufficient to trigger cellular senescence.

### **Ribosome biogenesis defects engage the retinoblastoma tumor suppressor pathway**

To investigate the signalling pathways linking reduced ribosome biogenesis to cellular senescence, we prepared IMR90 cells expressing a combination of papillomavirus oncoproteins E6 and E7, E6 alone or E7 alone. The E6 oncoprotein is known to block p53 functions, whereas E7 deactivates the RB pathway<sup>27</sup>. In our model, E6 and E7 combined or E7 alone efficiently prevented senescence after knockdown of RSL1D1, while E6 had only a partial effect (Fig. 5a and Supplementary Fig. 4a-e). These results suggest that defects in ribosome biogenesis mainly engage the RB pathway in human cells. To validate this conclusion, we used mutants of E7 that differ in their ability to block RB functions<sup>28</sup>. The E7 mutant  $\Delta$ 79-83, which binds and inhibits RB, rescued cells from senescence after knockdown of RSL1D1, while mutants E7  $\Delta$ 6-10 and E7  $\Delta$ 21-24 that do not bind RB were not efficient at inhibiting senescence after knockdown of RSL1D1 (Supplementary Fig. 4f-j). Furthermore, the kinases CDK4 and CDK6, which are able to phosphorylate and inactivate RB,<sup>29</sup> were also capable of preventing senescence after

knockdown of RSL1D1 (Fig. 5b-c and Supplementary Fig. 5a-h). Expression of intact CDK4, but not of a catalytically inactive mutant, i.e. CDK4(K35M), efficiently bypassed senescence, preventing the downregulation of KI67 expression, as well as rescuing RB phosphorylation and the expression of E2F targets such as CENPA and MCM6 after knockdown of RSL1D1 (Fig. 5b-c and Supplementary Fig. 5i-l). CDK4 expression also increased the levels of the mitotic marker H3-pS10 and reduced the levels of the CKI p21 (Fig. 5c and Supplementary Fig. 5m). Although expression of CDK4/6 kinases inhibited the senescence response to RSL1D1 depletion, shRNAs against p16INK4a or p21 did not have a similar effect (Supplementary Fig. 6a-e), suggesting that additional mechanisms control senescence in these cells at the level of CDK4.

### **RPS14 connects ribosome biogenesis defects to the retinoblastoma pathway**

Altered ribosome biogenesis has been linked to p53 activation, and in mouse cells to p53-dependent senescence<sup>30,31</sup>. Defective ribosome biogenesis allows some ribosomal proteins to accumulate in the nucleoplasm and activate p53 by inhibiting MDM2<sup>30,31</sup>. This mechanism explains p53 activation in cells where ribosome biogenesis factors are depleted and likely contributes to p53 activation during OIS. However, our results show that ribosome biogenesis defects in human cells can regulate senescence in a p53-independent but in an RB-dependent manner. We reasoned that some ribosomal proteins might activate the RB pathway perhaps acting as CKIs similarly to p21 or p16INK4a. Since we found that the catalytic activity of CDK4 was required to prevent senescence after RSL1D1 depletion (Fig. 5b-c and Supplementary Fig. 5i-m), we used a catalytically inactive CDK4(K35M) as a bait to examine whether any ribosomal protein can bind CDK4 in senescent cells. The rationale for using an inactive CDK4 allele is driven by the fact that active CDK4 inhibits senescence and induces cell proliferation. Therefore, any ribosomal protein acting as a CDK inhibitor may cease to do so by getting incorporated into ribosomes in growing cells. We immunoprecipitated flag-tagged CDK4(K35M) from cells that were forced into senescence by depletion of RSL1D1 and identified its partners by mass spectrometry. The CDK4 partners CCND1, CCND3, CDKN1A, CDKN1B, CDKN2B and CDKN2C were found in the immunoprecipitates together with the ribosomal protein RPS14 (Supplementary Table 2). We confirmed that endogenous CDK4 and RPS14 interact in PC3 prostate cancer cells and in H1299 (or NCI-H1299) lung cancer cells (Fig. 5d and Supplementary Fig. 6f). GST-pull down assays with purified proteins revealed that RPS14 binds to either CDK4 or cyclin D1 alone or to the complex of CDK4 with cyclin D1 (Fig. 5e). The interaction data suggests that RPS14 can act both like p16INK4a, an inhibitor of the INK family that binds CDK4, and like p21, a CIP family member, which binds to CDK-cyclin complexes (model bottom Fig. 5e). We next mapped the region of RPS14 that binds CDK4 and cyclin D1 by co-immunoprecipitation in HEK-293 cells. We found that binding to both CDK4 and

cyclin D1 maps to the N-terminal globular core domain (residues 2-88) of RPS14 (Figure 5f-h), excluding the C-terminal extension that engages in multiple contacts with rRNA via salt bridges between the basic residues of the protein and the phosphate groups of the rRNA<sup>32</sup>.

Expression of RPS14 in normal human fibroblasts using retroviral gene transfer induced proliferation arrest (Fig. 6a-b) and several senescence biomarkers, including: an accumulation of flat cells positive for SA- $\beta$ -Gal, a reduction in RB phosphorylation, a decrease in E2F target gene expression, a reduction in the levels of the mitotic marker H3-pS10, and an accumulation of PML bodies (Supplementary Fig. 6g-n). However, DNA damage foci were only moderately induced by RPS14, similar to p16INK4a expression (Supplementary Fig 6j, l, m). Serine 15 phosphorylated p53, total p53 or p21 levels were not found strongly increased in cells that expressed high levels of RPS14 (Supplementary Fig. 6h-i). Moreover, in p53 wild-type U2OS osteosarcoma cells, stable expression of RPS14 reduced cell proliferation (Fig. 6c-d). However, RPS14 expression also reduced cell proliferation in p53 null PC3 (Fig. 6e-f) and H1299 cells (Fig. 6g-h). Taken together, these results suggest that RPS14 has the capacity to trigger p53-independent cellular senescence by inhibiting CDK4 kinases and preventing RB phosphorylation. Of note, the senescence phenotype triggered by RPS14 expression is very similar to that of p16INK4a<sup>33</sup>, in agreement with our findings that RPS14, like p16INK4a, inhibits CDK4.

### **RPS14 is a CDK4 inhibitor**

Since RPS14 was recovered from the CDK4 immunoprecipitate in senescent cells, we hypothesized that it acted as a CDK inhibitor to trigger senescence via the RB tumor suppressor pathway. Consistent with this model, RPS14-induced growth arrest and senescence was prevented by shRNAs against RB (Fig. 6i-m). The activation of RB by RPS14 was assessed by measuring the levels of E2F target genes MCM6, CENPA and FANCD2 (Fig. 6k-l). RPS14 expression did not lead to p53 accumulation or to its phosphorylation on serine 15 (Fig. 6k), although we did observe moderate induction of the p53 targets p21 and GADD45A (Fig. 6m). Moreover, as in the cases of p16INK4a- and p21-induced senescence<sup>34</sup>, expression of RPS14 did not strongly increase the expression of IL6 or IL8 (Fig. 6m and Supplementary Fig. 6i).

Next, we investigated whether RPS14 colocalized with CDK4/cyclin D1 complexes as expected for a CKI. In normal growing cells endogenous RPS14 is mostly cytosolic, likely in association with ribosomes. However, in cells where RPS14 is overexpressed, we found a significant fraction of this protein in the nucleus colocalizing with cyclin D1 (Fig. 7a). More importantly, the endogenous RPS14 signal in the nucleus was stronger in most of the senescent cell nuclei (over 90%), independent of the stimuli triggering senescence, while control cells only displayed a moderate signal (at most in ~30% of the cells) (Supplementary Fig. 7a-d). Hyperresolution images

of RPS14 in senescent cells revealed a fine punctate nuclear pattern (Supplementary Fig. 7e-g). In addition, RPS14 was present in the soluble non-ribosomal fraction of *ras*-senescent cells (Fig. 7b). These results suggest that a non-ribosomal fraction of the highly abundant RPS14 accumulates in the nucleus of senescent cells, where it can bind and interfere with the functions of the CDK4/cyclin D1 complexes.

Depletion of RPS14 using RNAi is toxic to both normal cells and to a variety of tumor cells (Supplementary Fig. 8a-h). However, RPS14 was previously identified as a haploinsufficient tumor suppressor in the 5q- syndrome, a myeloproliferative disease with defects in erythroid differentiation<sup>35</sup>. Cells from these patients have high levels of phosphorylated RB that can be reduced upon restoring RPS14 expression using retroviral gene transfer (Fig. 7c). Of note, the level of expression of exogenous RPS14 is similar to that found in the non-ribosomal fraction of *ras*-senescent cells and considerably less than the endogenous level. Moreover, adding back RPS14 in 5q- syndrome cells reduced their proliferation (Fig. 7d), as expected for a CKI. These results suggest that a defect in the RB pathway underlies the 5q- syndrome, and that CDK4/6 inhibitors should restore its functionality in patients.

To investigate whether RPS14 can directly inhibit CDK4, we performed an *in vitro* kinase assay using purified proteins. As expected, CDK4/cyclin D1 phosphorylates the RB fragment 773-928 (Fig. 7e). RPS14 inhibited the kinase activity of the CDK4/cyclin D1 complex in a concentration dependent manner, similar to the CDK4 inhibitor palbociclib (Fig. 7e). In contrast, RPS14 did not inhibit CDK1/cyclin B1 complexes (Fig. 7f), indicating that it acts as a specific CDK4/cyclin D1 inhibitor.

The discovery of a pathway linking reduced ribosome biogenesis to senescence in a p53-independent manner is very important for novel anticancer therapies. In agreement with our findings, use of an RNA polymerase I inhibitor, CX-5461, has been shown to trigger senescence and autophagy in tumor cells lacking p53<sup>11</sup>, and cell death in tumor cells that preserve p53<sup>12</sup>, with limited toxicity to normal cells<sup>11,12</sup>. We found that shortly after treatment of IMR90 cells with CX-5461, the nuclear/cytoplasmic ratio of both RPL29 and RPS14 increased (Fig. 8a), indicating that a sudden decrease in rRNA synthesis alters the localization of these proteins. In parallel with this change in localization, we found both a reduction in RB phosphorylation and in the level of the E2F target gene MCM6 (Fig. 8b), suggesting that in these conditions RPS14 could activate the RB pathway and inhibit cell cycle progression as measured by decreased levels of the mitotic marker H3-pS10 (Fig. 8b). In p53 wild type cells, such as IMR90, CX-5461 also activates p53 (Fig. 8b). However, in p53 mutant tumor cells, this compound was reported to induce a senescence response<sup>11</sup> that can now be explained by the pathway reported above.

#### 2.4.4. Discussion

Senescent cells are defined by their inability to proliferate and at the same time synthesize and secrete a large amount of proteins<sup>36,37</sup>. Hence, the observed reduction in ribosome biogenesis in these cells does not limit their ability to make proteins. More exactly, reduced ribosome biogenesis contributes to senescence by triggering checkpoint mechanisms that prevent cell cycle progression. First, some ribosomal proteins that cannot be incorporated into ribosomes inhibit MDM2 and activate the p53 pathway<sup>30,31,38,39</sup>. Second, RPS14 accumulates in the nucleus and activates RB by inhibiting the CDK4/cyclin D1 complex (Fig. 8c). Finally, a reduced capacity for ribosome biogenesis would prevent the growth of any senescent cell that manages to disable the mechanisms of cell cycle arrest.

The identification of RPS14 as a CDK4 inhibitor suggests a tumor suppressor role for this ribosomal protein. Since RPS14 is required for protein biosynthesis, tumors would rely on subtle mechanisms to avoid RPS14-dependent tumor suppression. Indeed, analysis of microarray data available through OncoPrint shows a reduction in RPS14 expression in breast, leukemia, lung and prostate cancers as well as in melanoma (Supplementary Fig. 8i-m). Conversely, non-neoplastic nevi, which are benign tumors containing senescent cells, accumulate high levels of RPS14 (Supplementary Fig. 8m). In addition, in testicular cancer, where RPS14 is upregulated, CDK4 is also upregulated, and RB is downregulated, consistent with the role we propose here for RPS14 in the RB pathway (Supplementary Fig. 8n). It has been reported that RPS14 also binds MDM2 and contributes to p53 activation upon ribosomal stress<sup>40</sup>. However, we found that RPS14 blocks cell proliferation in PC3 prostate cancer cells and H1299 lung cancer cells where the p53 gene is either absent or mutated (Fig. 6e-h). In addition, knockdown of RB in normal human fibroblasts rescued both the cell cycle arrest and senescence induced by overexpression of RPS14 (Fig. 6i-m). Although in our conditions most of the activity of RPS14 passes through the RB pathway, its MDM2 inhibitory activity could certainly contribute to tumor suppression in other contexts (Fig. 8c).

The discovery of a pathway linking reduced ribosome biogenesis to senescence in a p53-independent manner is very important for the development of anticancer therapies, since the p53 pathway is often disabled in cancer cells. The therapeutic potential of reducing ribosome biogenesis has been shown using an RNA polymerase I inhibitor that triggers senescence in tumor cells while causing very limited toxicity to normal cells<sup>11,12</sup>. We anticipate that targeting rRNA processing will be either equally, or even more, effective. Indeed, a sudden decrease in ribosome biogenesis can lead to a massive accumulation of ribosomal proteins selectively in tumor cells, which are already engaged in a highly active ribosome biogenesis program. Our work thus provides a rationale for a potent and selective anticancer therapy.

### **2.4.5. Acknowledgments**

We thank, Drs. Darren P. Baker (Biogen Idec), Denise A. Galloway (Fred Hutchinson Cancer Center), Nabeel Bardeesy (MGH), Scott Lowe (MSK), Andrew Koff (MSK), Tom Moss (U. Laval), Ivan Topisirovic, Pascal Chartrand (U. Montréal), Volker Blank (McGill University) and Bob Weinberg (MIT) for comments and/or reagents. Éric Bonneil and the IRIC Proteomics Core Facility for proteomic analysis. We thank Julie Hinsinger, Mirela Birlea and the IRIC Histology Core Facility for immunohistochemistry. F.L. is supported by FRQS (Fonds de Recherche du Québec-Santé) and CRS (Cancer Research Society) (C.V.) (D.L.) (R.L.) and G.F. is supported by FRQS. Work was funded by grants from the CIHR (Canadian Institute of Health and Research: CIHR MOP11151) to G.F., (Canadian Institutes of Health Research: CIHR MOP106628) to M.O. and the CCSRI (Canadian Cancer Society Research Institute: 704223) to G.F.

### **2.4.6. Main figures and supplementary figures**

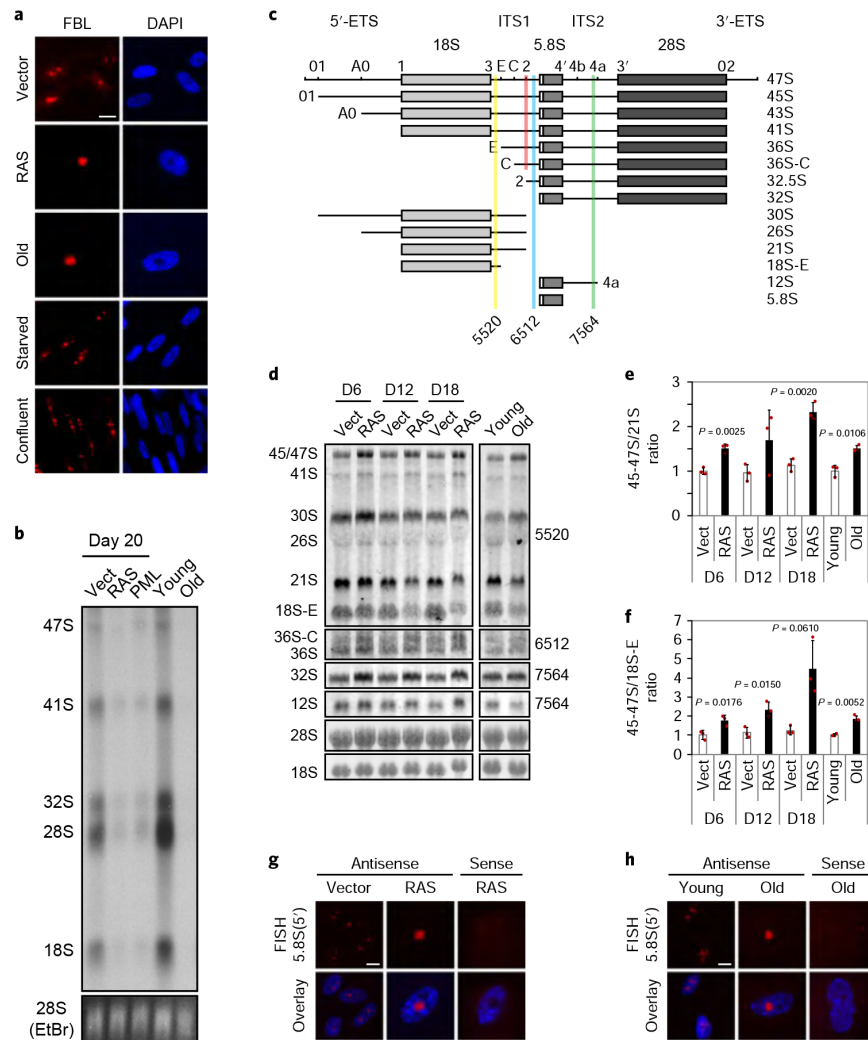


**Fig. 1 | Senescence involves diminished ribosome biogenesis.** **a**, Indirect immunofluorescence (IF) with a specific anti-fibrillarin (FBL) antibody showing the nucleolus. The nucleus was counterstained with DAPI. Images represent IMR90 cells expressing an empty control vector or H-RASV12 (RAS) at day 12 post-infection, IMR90 cells at replicative senescence (old) (passage 40), serum starved for 6 days or confluent arrested for 4 days (1 out of 3 independent experiments with similar results). Scale bar, 20  $\mu$ m. **b**, Autoradiography for de novo rRNA synthesis after a three-hour pulse labelling with [<sup>3</sup>H]-uridine. Total RNA was extracted after the pulse from IMR90 cells at day 20 post-infection with H-RASV12 (RAS), PML-IV (PML) or an empty control vector (Vect), or young (passage 24) and old (passage 38) IMR90 cells and compared to total 28S rRNA detected with ethidium bromide (EtBr) under UV light (1 out of 3 independent experiments with similar results). **c**, Schematic representation of the human 47S rRNA and different rRNA processing intermediates. The regions used for northern probes (yellow, position 5520; blue, position 6512; green, position 7564) and FISH (red) are indicated. **d**, Northern blots with total RNA extracted from IMR90 cells at day 6, day 12 and day 18 post-infection with H-RASV12 (RAS) or an empty control vector (Vect), or young (passage 24) and old (passage 40) IMR90 cells (1 out of 3 independent experiments with similar results). Precursor rRNAs detected with the probes described in **c** are indicated (right). **e, f**, Ratios of 45-47S/21S (**e**) and 45-47S/18S-E (**f**) rRNA levels quantified from experiments as in **d**. All signals were normalized to total 28S rRNA detected with ethidium bromide (EtBr) staining. Error bars are mean  $\pm$  s.d.,  $n=3$  independent experiments.  $P$  value as indicated, two-sided Student's  $t$ -test. **g, h**, Fluorescence in situ hybridization (FISH) with an antisense or sense probe overlapping the 5.8S(5') rRNA processing site 2 as shown in **c**. The nucleus was counterstained with DAPI. Images represent IMR90 cells expressing H-RASV12 (RAS) or an empty control vector at day 20 post-infection (**g**) or young (passage 25) and old (passage 43) IMR90 cells (**h**) (1 out of 2 independent experiments with similar results). Scale bars (**g, h**), 10  $\mu$ m. See also Supplementary Figs. 1 and 2.



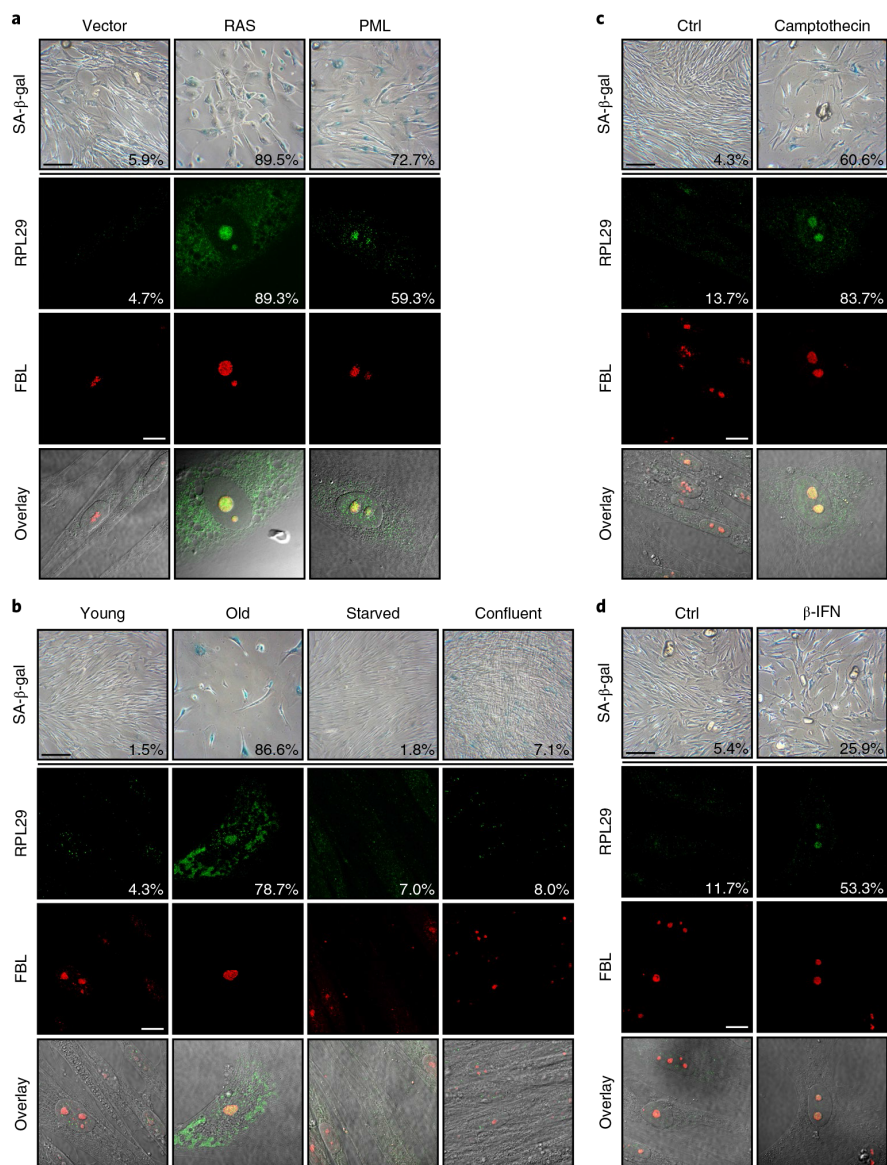


**Fig. 2 | Accumulation of RPL29 as a senescence biomarker.** SA-β-gal and IF (indirect immunofluorescence) for RPL29 and fibrillar (FBL) nucleolar colocalization in IMR90 cells with the indicated treatment of cells. SA-β-gal data were quantified from >5 independent cell counts up to a total of at least 150 cells and are presented as the mean percentage of positive cells. IF data were quantified from 100 cell counts in triplicates and are presented as the mean percentage of cells with nucleolar localization of RPL29. Scale bars: SA-β-gal, 200 μm; IF, 20 μm. **a**, Comparison of IMR90 cells expressing H-RASV12 (RAS), PML-IV (PML) or an empty control vector and fixed at day 12 post-infection (1 out of 3 independent experiments with similar results). **b**, Comparison of young (passage 23), old (passage 40), serum starved for 6 days and confluent arrested for 4 days IMR90 cells (1 out of 3 independent experiments with similar results). **c**, Comparison of IMR90 cells treated for 3 days with DMSO (ctrl) or camptothecin in DMSO (final concentration in medium of 35 nM) (1 out of 3 independent experiments with similar results). **d**, Comparison of IMR90 cells treated every 2–3 days with vehicle (ctrl) or β-IFN (final concentration in the medium of 1,000 U ml<sup>-1</sup>) for 14 days (1 out of 2 independent experiments with similar results).

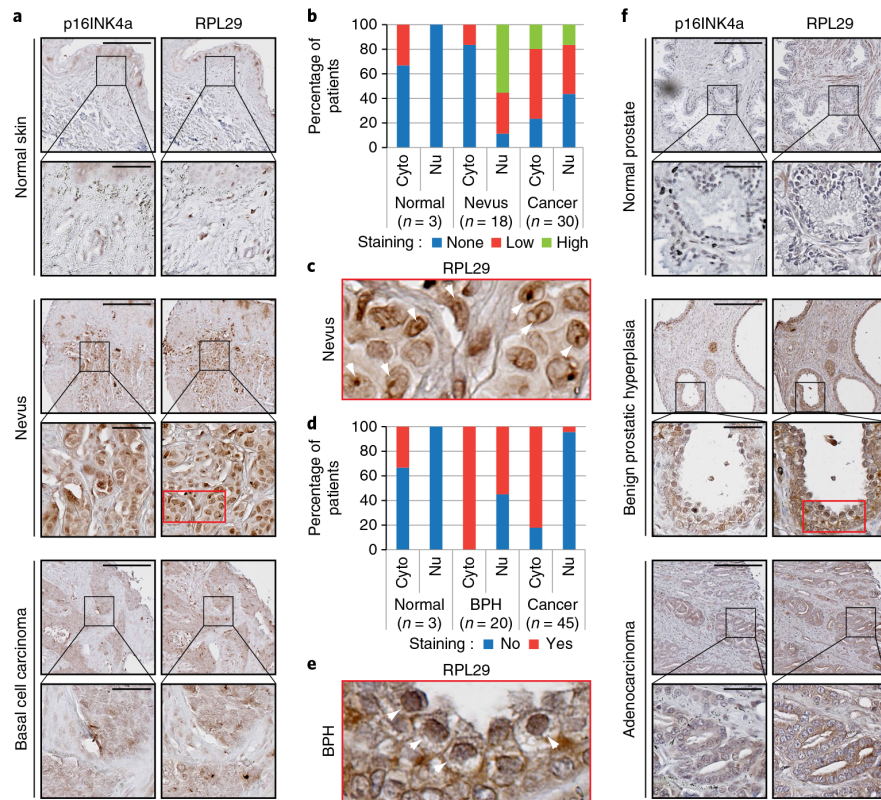


**Fig. 3 | Nuclear RPL29, a biomarker of decreased ribosome biogenesis and senescent cells in vivo.** **a**, p16INK4a and RPL29 immunostaining in samples from patients with nevus (middle), normal skin controls (top), or basal cell carcinoma (bottom). Images represent data from 18, 3 and 30 samples, respectively. **b**, Percentage of patient samples immunostained as in **a** showing no RPL29 staining, or with either a cytoplasmic (Cyto) or nuclear (Nu) RPL29 staining using two different degrees of intensity (low and high). **c**, Enlargement of the red rectangle from nevus (**a**) showing nucleolar staining for RPL29. **d-f**, Percentages of patient samples (in **f**) showing no staining, or with either a cytoplasmic (Cyto) or nuclear (Nu) RPL29 staining (**d**). Enlargement of the red rectangle in BPH (benign prostatic hyperplasia) from **f** showing nuclear staining for RPL29 (**e**). p16INK4a and RPL29 immunostaining (**f**) in samples from patients with BPH (middle), normal prostatic controls (top) or prostate adenocarcinoma (bottom). Images represent data from 20, 3 and 45 samples, respectively. Scale bars (**a,f**): 250  $\mu\text{m}$  (low magnification) and 50  $\mu\text{m}$  (high magnification).

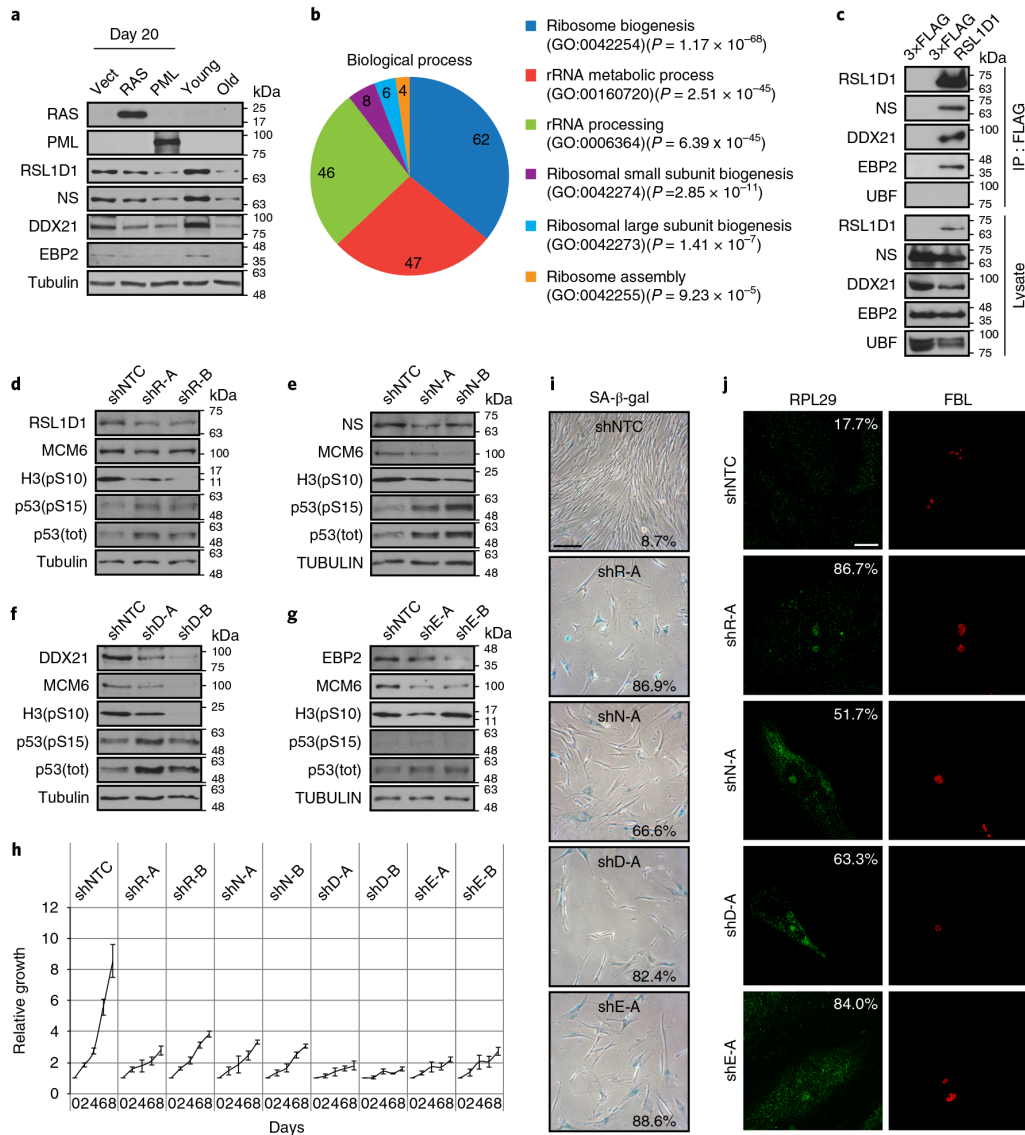


**Fig. 4 | Reduction of ribosome biogenesis factors RSL1D1, nucleostemin, EBP2 or DDX21 triggers senescence.** **a**, Immunoblots for the indicated proteins in IMR90 cells at day 20 post-infection with H-RASV12 (RAS), PML-IV (PML) or an empty control vector (Vect) or young (passage 24) and old (passage 38) IMR90 cells. NS, nucleostemin. Tubulin was used as a loading control. **b**, Gene ontology (GO) terms found after FatiGO single-enrichment analysis with the Babelomics 4.3 platform performed on the proteins that were identified by liquid chromatography-tandem mass spectrometry (LC-MS/MS) after immunoprecipitation of 3xFLAG or 3xFLAG-RSL1D1 transiently transfected in HEK-293 cells. **c**, Interactions between RSL1D1 and several ribosome biogenesis factors. HEK-293 cells were transiently transfected with 3xFLAG or 3xFLAG-RSL1D1 vectors and immunoprecipitated with an anti-FLAG antibody. Lysates and immunoprecipitates were immunoblotted for the indicated proteins. **d-g**, Immunoblots for the indicated proteins in IMR90 cells expressing the indicated shRNA expression vectors at day 14 post-infection. shNTC, non-targeting shRNA; shR-A or shR-B, shRNAs against RSL1D1; shN-A or shN-B, shRNAs against nucleostemin; shD-A or shD-B, shRNAs against DDX21; shE-A or shE-B, shRNAs against EBP2; H3(pS10), histone H3 phosphorylated on serine 10; p53(pS15), p53 phosphorylated on serine 15; p53(tot), total p53; NS, nucleostemin. Tubulin was used as a loading control. **h**, Growth curves started with cells as in **d-g**. Data are presented as means normalized to day 0 of each condition and error bars indicate s.e.m.,  $n = 3$  independent experiments. **i**, SA-β-gal of IMR90 cells expressing the indicated shRNA expression vectors as in **d-g** and fixed at day 14 post-infection. Data were quantified from >5 independent cell counts up to a total of at least 150 cells and are presented as the mean percentage of positive cells (1 out of 3 independent experiments with similar results). Scale bar, 200 μm. **j**, RPL29 and FBL nucleolar localization in IMR90 cells expressing the indicated shRNA expression vectors as in **d-g** and fixed at day 7 post-infection. Data were quantified from 100 cell counts in triplicates and are presented as the mean percentage of positives cells for nucleolar localization of RPL29 (1 out of 3 independent experiments with similar results). Scale bar, 20 μm. See also Supplementary Fig. 3. Blots in **a, c, d, e, f, g** are representative of 3 independent experiments with similar results. Unprocessed blots can be found in Supplementary Fig. 9.

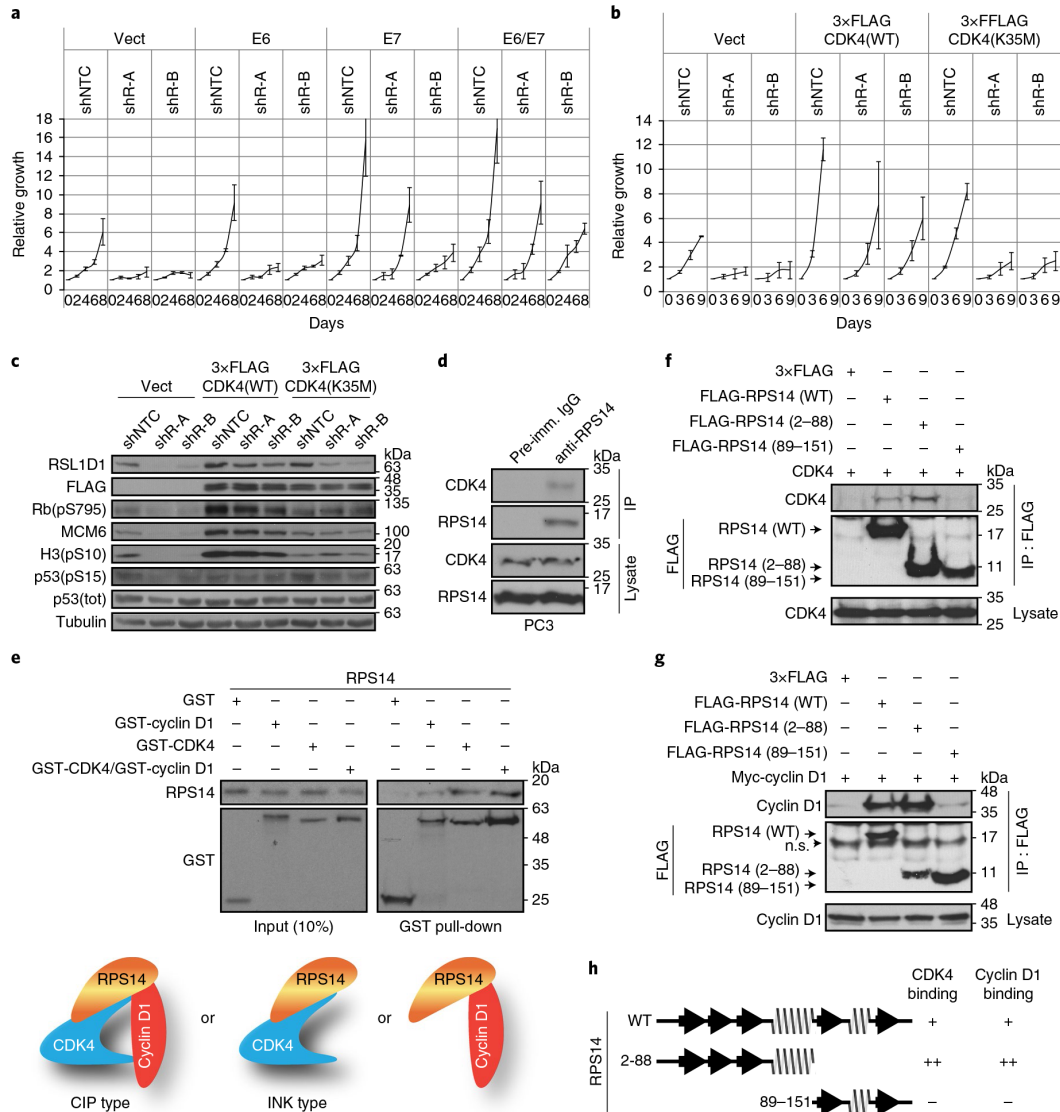


**Fig. 5 | E7 and CDK4, but not E6, bypass RSL1D1 knockdown-induced senescence. a**, Growth curves of IMR90 cells expressing the indicated shRNA expression vectors in combination with the expression of the viral oncoproteins E6 alone, E7 alone, E6/E7 together or an empty control vector (Vect). Data are presented as mean normalized to day 0 of each condition and error bars indicate s.e.m.,  $n = 3$  independent experiments. shNTC, non-targeting shRNA; shR-A or shR-B, shRNAs against RSL1D1. **b**, Growth curves of IMR90 cells expressing the indicated shRNA expression vectors as in **a** in combination with the expression of 3xFLAG-CDK4(WT), 3xFLAG-CDK4(K35M) or an empty control vector (Vect). Data are presented as mean normalized to day 0 of each condition and error bars indicate s.e.m.,  $n = 3$  independent experiments. **c**, Immunoblots for the indicated proteins for cells as in **b** collected 20 days post-infection. Rb(pS795), Rb phosphorylated on serine 795; H3(pS10), histone H3 phosphorylated on serine 10; p53(pS15), p53 phosphorylated on serine 15; p53(tot), total p53. Tubulin was used as a loading control. **d**, Immunoprecipitation with pre-immune serum (Pre-imm. IgG) or with anti-RPS14 antibody in PC3 cells. Lysates and immunoprecipitates were immunoblotted for the indicated proteins. **e**, Top: in vitro GST pull-down of recombinant GST, GST-cyclin D1, GST-CDK4 or GST-CDK4/GST-cyclin D1 and recombinant RPS14-Myc-FLAG using glutathione beads. Lysate and pull-down were immunoblotted for the indicated proteins. Bottom: schematic model showing interactions between RPS14 and cyclin D1, CDK4 or CDK4/cyclin D1. **f**, HEK-293 cells were transfected with vectors expressing CDK4 and 3x FLAG or FLAG-tagged RPS14 wild type (FLAG-RPS14(WT)), FLAG-RPS14(2-88) or FLAG-RPS14(89-151) and immunoprecipitated with an anti-FLAG antibody. Lysates and immunoprecipitates were immunoblotted for indicated proteins. **g**, HEK-293 cells were transfected with a vector expressing Myc-cyclin D1 and vectors expressing 3x FLAG or FLAG-RPS14(WT), FLAG-RPS14(2-88) or FLAG-RPS14(89-151) and immunoprecipitated with an anti-FLAG antibody. Lysates and immunoprecipitates were immunoblotted for indicated proteins (n.s., not specific). **h**, Schematic showing RPS14 regions and their interaction with CDK4 and/or cyclin D1. See also Supplementary Figs. 4, 5 and 6. Blots in **d-g** are representative of 3 independent experiments with similar results, whereas **c** is representative of 2 independent experiments with similar results. Unprocessed blots can be found in Supplementary Fig. 9.

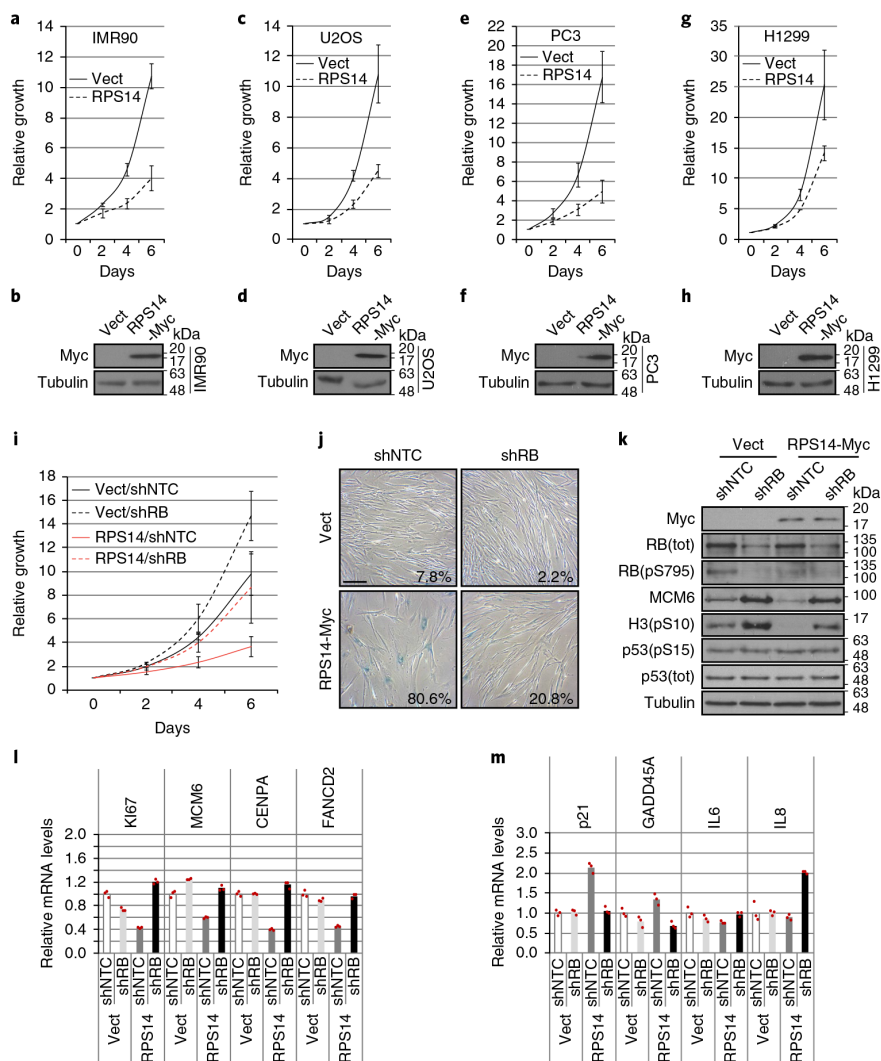


**Fig. 6 | RPS14 regulates the retinoblastoma pathway and senescence.** **a–h**, Growth curves (**a,c,e,g**) of IMR90 cells (**a**), U2OS cells (**c**), PC3 cells (**e**) or H1299 cells (**g**) expressing RPS14-Myc or an empty control vector (Vect). Data are presented as mean normalized to day 0 of each condition and error bars indicate s.e.m.,  $n=3$  independent experiments. Immunoblots for the indicated proteins (**b,d,f,h**) at day 7 post-infection with an empty control vector (Vect) or a vector expressing RPS14-Myc in IMR90 cells (**b**), U2OS cells (**d**), PC3 cells (**f**) or H1299 cells (**h**) (1 out of 3 independent experiments with similar results). Tubulin was used as a loading control. **i**, Growth curves of IMR90 cells expressing a control shRNA (shNTC) or a shRNA against Rb (shRB) in combination with the expression of RPS14-Myc or an empty control vector (Vect). Data are presented as mean normalized to day 0 of each condition and error bars indicate s.e.m.,  $n=3$  independent experiments. **j**, SA-β-gal of IMR90 cells as in **i** at day 18 post-infection. Data were quantified from >5 independent cell counts up to a total of at least 150 cells and are presented as the mean percentage of positive cells (1 out of 2 independent experiments with similar results). Scale bar, 200 μm. **k**, Immunoblots for the indicated proteins for cells as in **i** at day 16 post-infection (1 out of 2 independent experiments with similar results). Rb(tot), total Rb; Rb(pS795), Rb phosphorylated on serine 795; H3(pS10), histone H3 phosphorylated on serine 10; p53(pS15), p53 phosphorylated on serine 15; p53(tot), total p53. **l,m**, q-PCR for the indicated genes performed on reverse-transcribed total RNA extracted from cells as in **i** at day 16 post-infection. Data are normalized over TBP and HMBS and presented as mean relative to vector infected cells (1 out of 2 independent experiments with similar results). See also Supplementary Fig. 6. Unprocessed blots can be found in Supplementary Fig. 9.

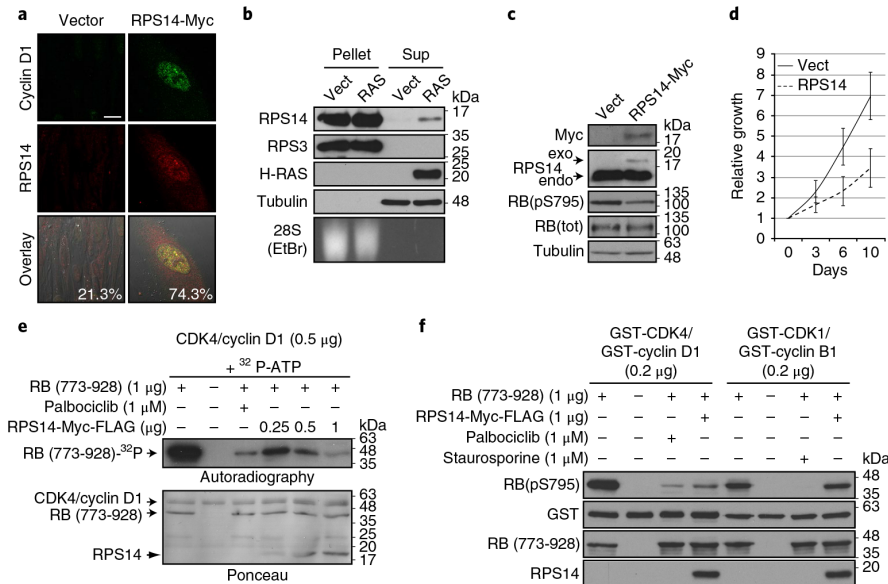


**Fig. 7 | RPS14 regulates senescence by inhibiting CDK4.** **a**, RPS14 and cyclin D1 nuclear colocalization in IMR90 cells expressing RPS14-MYC or an empty control vector and fixed at day 14 post-infection, as revealed by indirect immunofluorescence with specific anti-RPS14 and anti-cyclin D1 antibodies followed by confocal microscopy. Data were quantified from 100 cell counts in triplicate and are presented as the mean percentage of positive cells for colocalization (1 out of 3 independent experiments with similar results). Scale bar, 20  $\mu$ m. **b**, Immunoblots for the indicated proteins and 28S rRNA detected with ethidium bromide (EtBr) following ribosome purification by sedimentation of extracts from IMR90 cells at day 7 post-infection with H-RASV12 (RAS) or an empty control vector (Vect). Pellet, ribosomes; Sup, supernatant. **c**, Immunoblots for the indicated proteins in MUTZ-8 cells expressing RPS14-Myc or an empty control vector (Vect) at day 8 post-infection. Rb(tot), total Rb; Rb(pS795), Rb phosphorylated on serine 795; exo, size for exogenous RPS14; endo, size for endogenous RPS14. **d**, Growth curves for cells as in **c**. Data are presented as mean normalized to day 0 of each condition and error bars indicate s.e.m.,  $n = 3$  independent experiments. **e**, In vitro kinase assay containing  $^{32}$ P-ATP, GST-CDK4/GST-cyclin D1, with or without GST-Rb (773-928), palbociclib and RPS14-Myc-FLAG. In the assay conditions, the RPS14 IC<sub>50</sub>  $\pm$  s.d. = 0.421  $\pm$  0.088  $\mu$ M. **f**, Immunoblots for the indicated proteins after an in vitro kinase assay containing ATP, GST-CDK4/GST-cyclin D1 or GST-CDK1/GST-cyclin B1, with or without GST-Rb (773-928), palbociclib, staurosporine and RPS14-Myc-FLAG. Rb(pS795), Rb phosphorylated on serine 795. See also Supplementary Figs. 7 and 8. Blots in **b, c, e, f** are representative of 3 independent experiments with similar results. Unprocessed blots can be found in Supplementary Fig. 9.

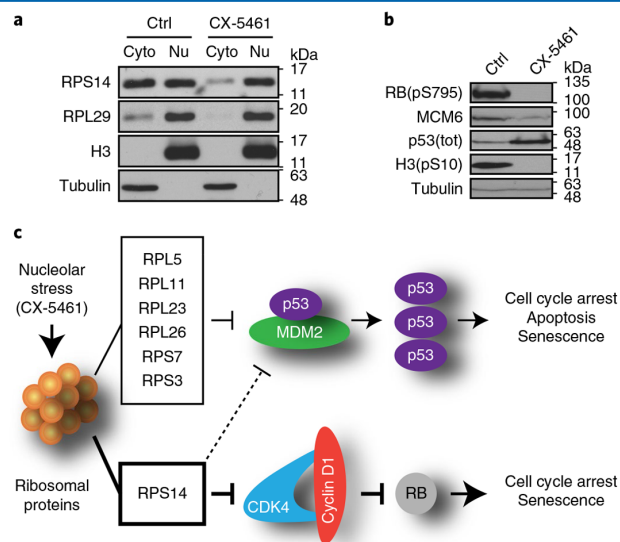


**Fig. 8 | Tumour suppression by the RPS14-mediated checkpoint.**

**a**, Immunoblots for the indicated proteins after cellular fractionation of IMR90 cells treated with dimethylformamide (ctrl) or CX-5461 in dimethylformamide (final concentration in medium of 2  $\mu$ M) for 24 hours. Cyto, cytoplasm; Nu, nuclear extracts. **b**, Immunoblots for the indicated proteins on total cellular extracts of IMR90 cells treated as in **a**. Rb(pS795), Rb phosphorylated on serine 795; p53(tot), total p53; H3(pS10), histone H3 phosphorylated on serine 10. **c**, Model showing how nucleolar stress and ribosome biogenesis defects can lead to activation of p53 and Rb tumour suppressor pathways. Blots in **a, b** are representative of 3 independent experiments with similar results. Unprocessed blots can be found in Supplementary Fig. 9.

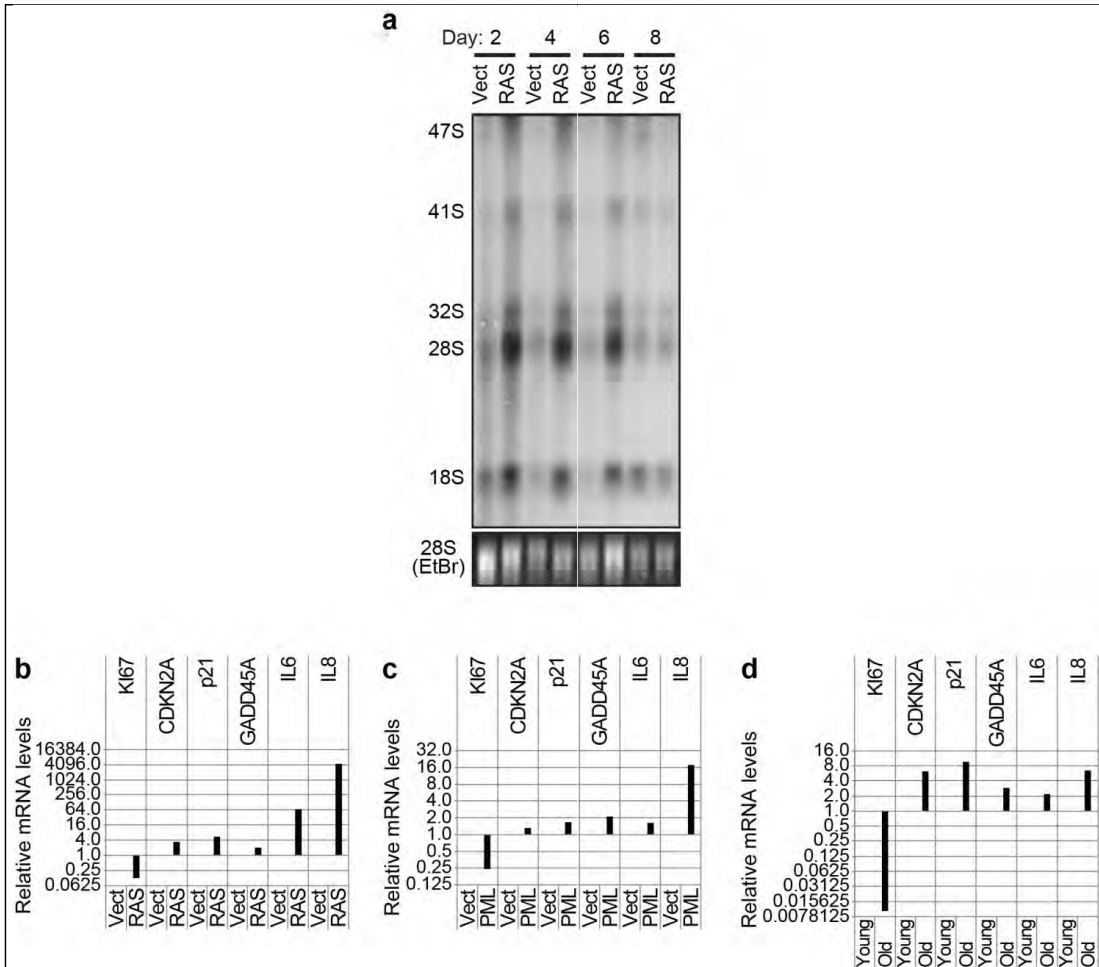
In the format provided by the authors and unedited.

## Senescence-associated ribosome biogenesis defects contributes to cell cycle arrest through the Rb pathway

Frédéric Lessard<sup>1</sup>, Sebastian Igelmann<sup>1</sup>, Christian Trahan<sup>2</sup>, Geneviève Huot<sup>1</sup>, Emmanuelle Saint-Germain<sup>1</sup>, Lian Mignacca<sup>1</sup>, Neylen Del Toro<sup>1</sup>, Stéphane Lopes-Paciencia<sup>1</sup>, Benjamin Le Calvé<sup>5</sup>, Marinieve Montero<sup>1</sup>, Xavier Deschênes-Simard<sup>4</sup>, Marina Bury<sup>6</sup>, Olga Moiseeva<sup>7</sup>, Marie-Camille Rowell<sup>1</sup>, Cornelia E. Zorca<sup>1</sup>, Daniel Zenklusen<sup>1</sup>, Léa Brakier-Gingras<sup>1</sup>, Véronique Bourdeau<sup>1</sup>, Marlene Oeffinger<sup>1,2,3</sup> and Gerardo Ferbeyre<sup>1\*</sup>

<sup>1</sup>Department of Biochemistry and Molecular Medicine, Université de Montréal, Montreal, Quebec, Canada. <sup>2</sup>Institut de Recherches Cliniques de Montréal, Montreal, Quebec, Canada. <sup>3</sup>Faculty of Medicine, Division of Experimental Medicine, McGill University, Montreal, Quebec, Canada. <sup>4</sup>Faculty of Medicine, Department of Medicine, McGill University, Montreal, Quebec, Canada. <sup>5</sup>URBC-NARILIS, University of Namur, Namur, Belgium. <sup>6</sup>Lady Davis Institute for Medical Research, McGill University, Montreal, Quebec, Canada. <sup>7</sup>Generium 601125 Vladimirskaia obl, Petushinsky, Russia. \*e-mail: [g.ferbeyre@umontreal.ca](mailto:g.ferbeyre@umontreal.ca)

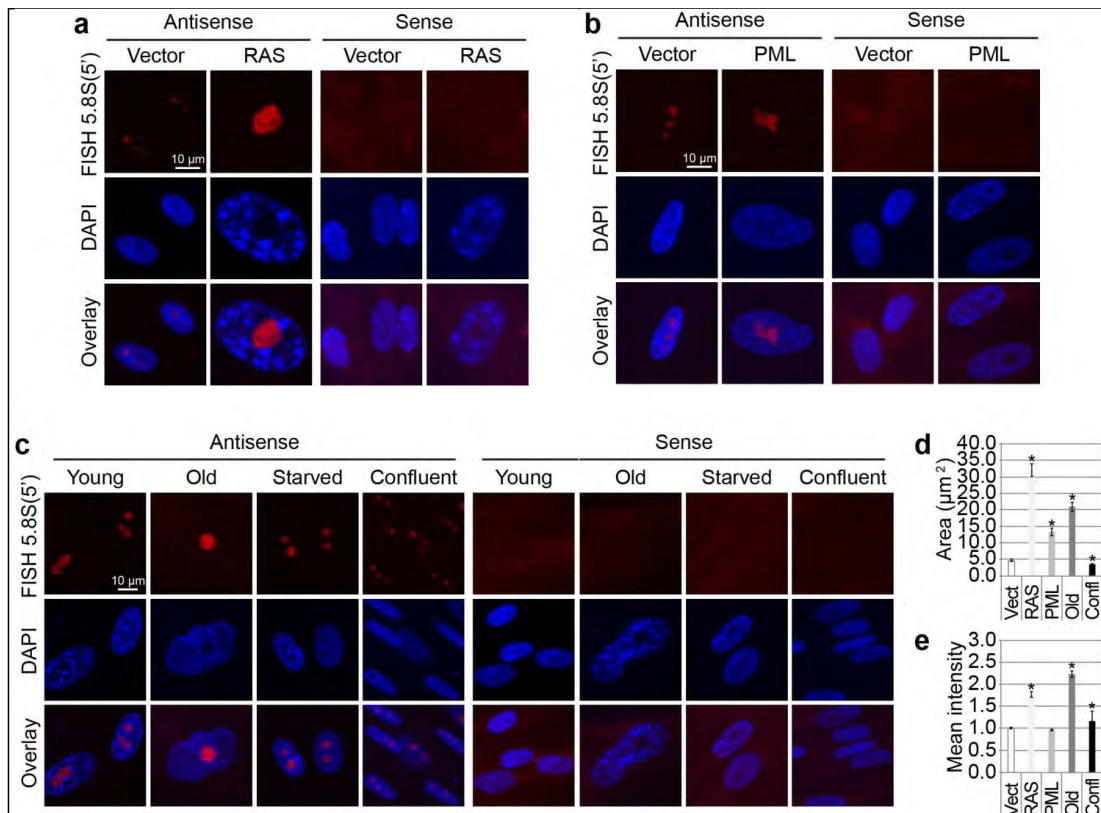




Supplementary Figure 1

Ribosome biogenesis defects in senescent cells induced by oncogenic *ras*, short telomeres or the tumor suppressor PML

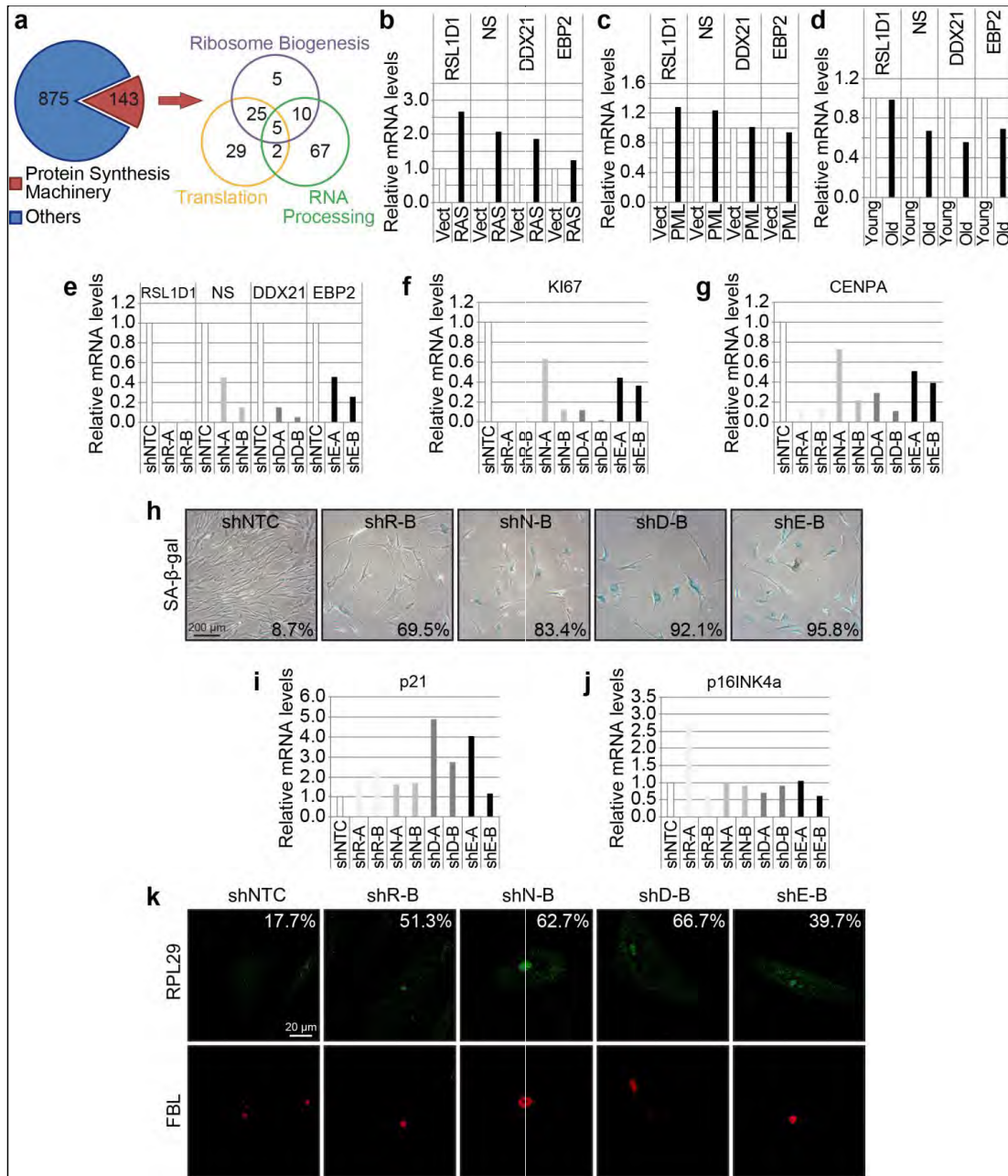
(a) Autoradiography for *de novo* rRNA synthesis after a three hours pulse labeling with [3H]-uridine. Total RNA was extracted after the pulse from IMR90 cells expressing H-RASV12 (RAS) or an empty control vector (Vect) at day 2, 4, 6 and 8 post-infection and compared to total 28S rRNA detected with ethidium bromide (EtBr) under UV light, (1 out of 3 independent experiments with similar results). (b-d) QPCR for senescence biomarkers. Total RNA was extracted from (b-c) IMR90 cells at day 20 post-infection expressing (b) H-RASV12 (RAS), (c) PML-IV (PML) or an empty control vector (Vect) and from (d) uninfected young (passage 24) and old (passage 38) IMR90 cells. RNA was reverse transcribed and analyzed by qPCR for the indicated genes. Data were normalized over TBP and HMBS and presented as mean relative to vector-infected cells or young cells, (1 out of 3 independent experiments with similar results).



Supplementary Figure 2

Nucleolar accumulation of ribosomal RNA precursors in senescent cells

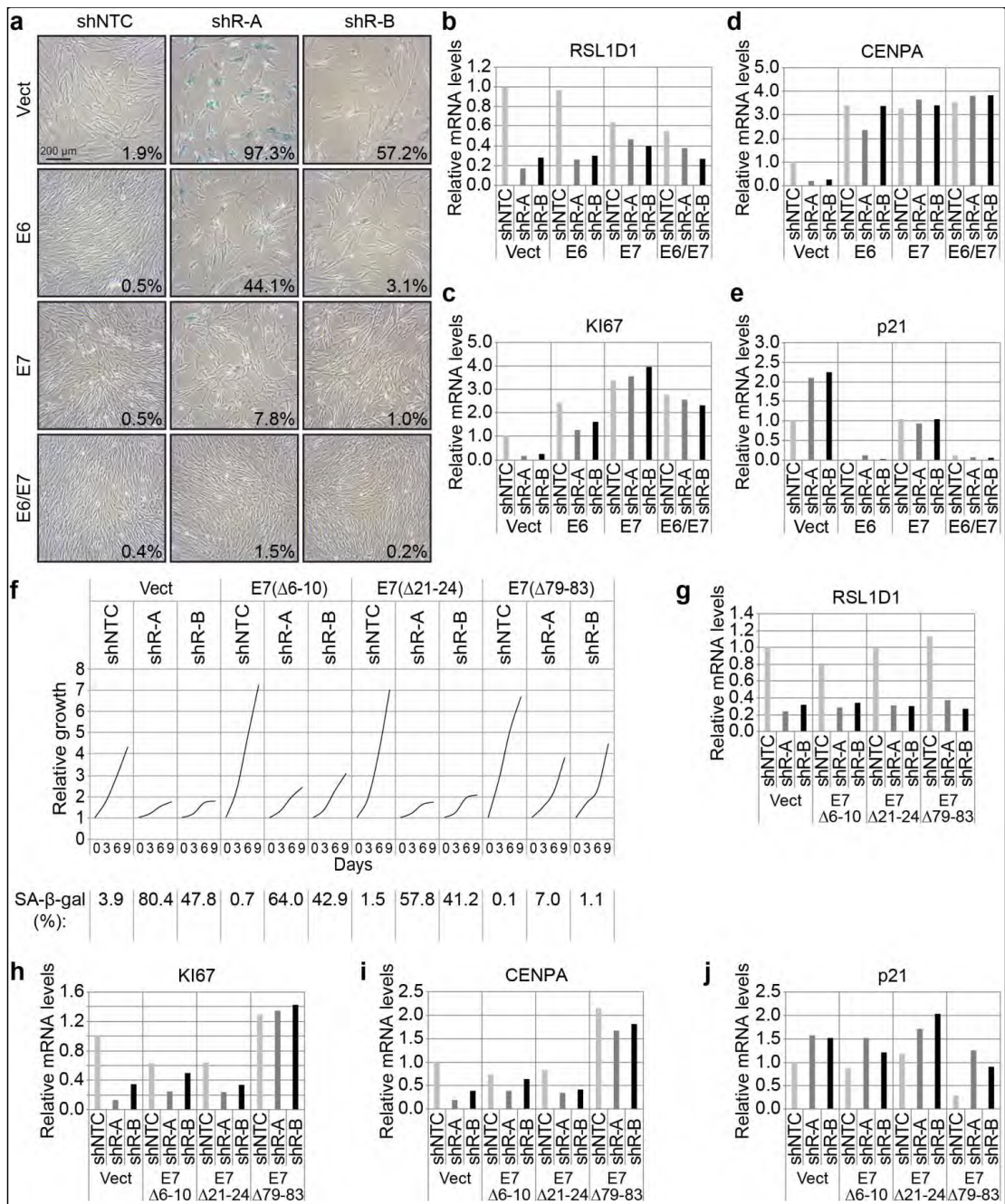
(a-c) Fluorescence *in situ* hybridization with an antisense or sense probe overlapping the 5.8S(5') rRNA processing site 2 as shown in Figure 1c and counterstained with DAPI of (a-b) IMR90 cells at day 20 post-infection expressing (a) H-RASV12 (RAS), (b) PML-IV (PML) or an empty control vector and of (c) uninfected young (passage 25), old (passage 43) cells or confluent (Confl) arrested for 4 days and arrested by serum starvation for 6 days (Starved), (1 out of 2 independent experiments with similar results). (d-e) Quantification of (d) nucleolar mean area ( $\mu\text{m}^2$ ) relative to vector infected cells and (e) nucleolar fluorescence mean intensity relative to vector-infected cells after FISH for cells marked as in (a-c). Number of nucleoli analyzed per condition: Vector (Vect) (n = 174), RAS (n = 100), PML (n = 117), Old (n = 93) and Confluent (Confl) (n = 166). Error bars indicate SEM. \* = p<0.05, using Mann-Whitney U test.



### Supplementary Figure 3

#### Depletion of nucleolar proteins leads to senescence in IMR90 cells

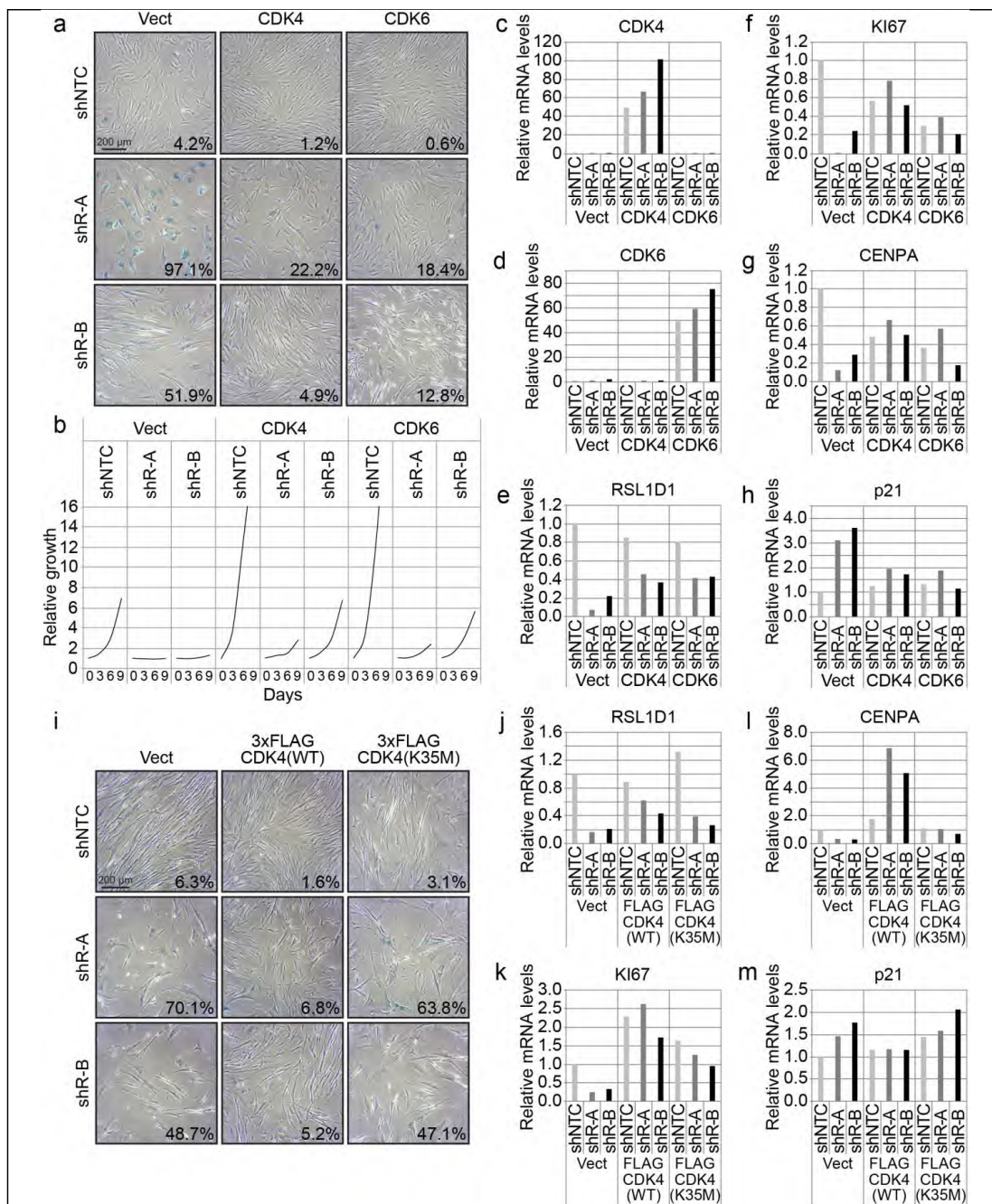
(a) Proteomic analysis of RAS-senescent IMR90 cells treated with MG132 (10  $\mu$ M, 18 hours) or vehicle. 1018 proteins were enriched in MG132-treated cells compared to control. Proteins associated to protein synthesis machinery and the indicated subcategories were retrieved using the Babelomics 4.3 platform. (b-d) QPCR for the indicated genes performed with total RNA extracted from (b-c) cells at day 20 post-infection expressing (b) H-RASV12 (RAS), (c) PML-IV (PML) or an empty control vector (Vect) and from (d) uninfected young (passage 24) and old (passage 38) IMR90 cells. Data were normalized over TBP and HMBS and presented as means relative to vector-infected cells or young cells, (n = 1). (e-g) QPCR for the indicated genes performed with total RNA extracted from cells expressing shNTC (non-targeting shRNA); shR-A or -B (shRNAs against RSL1D1); shN-A or -B, (shRNAs against nucleostemin); shD-A or -B, (shRNAs against DDX21); shE-A or -B, (shRNAs against EBP2) at day 14 post-infection. Data were normalized over TBP and HMBS and presented as mean relative to shNTC infected cells, (1 out of 2 independent experiments with similar results). (h) SA- $\beta$ -gal of cells expressing the indicated shRNA expression vectors and fixed at day 14 post-infection. Data were quantified from >5-independent cell counts up to a total of at least 150 cells and are presented as the mean percentage of positive cells, (1 out of 3 independent experiments with similar results). (i-j) QPCR for p21 and p16INK4a performed with total RNA extracted from cells as in (e-g). Data were normalized over TBP and HMBS and presented as means relative to shNTC infected cells, (1 out of 2 independent experiments with similar results). (k) Indirect immunofluorescence with specific anti-fibrillarin (FBL) and anti-RPL29 antibodies followed by confocal microscopy of cells as in (h) and fixed at day 7 post-infection. Data were quantified from 100 cell counts in triplicate and are presented as the mean percentage of positives cells for nucleolar localization of RPL29, (1 out of 3 independent experiments with similar results).



#### Supplementary Figure 4

##### RSL1D1 knockdown-induced senescence requires the RB pathway

(a) SA- $\beta$ -gal of IMR90 cells expressing the indicated shRNA expression vectors in combination with the expression of E6 alone, E7 alone, E6/E7 together or an empty control vector (Vect) at day 20 post-infection. Data were quantified from >5-independent cell counts up to a total of at least 150 cells and are presented as the mean percentage of positive cells, (1 out of 2 independent experiments with similar results). shNTC: non-targeting shRNA; shR-A or -B: shRNAs against RSL1D1. (b-e) QPCR for the indicated genes performed with total RNA extracted from cells as in (a) at day 20 post-infection. Data were normalized over TBP and HMBS and presented as mean relative to vector/shNTC infected cells, (n = 1). (f) Growth curves of IMR90 cells expressing the indicated shRNA expression vectors in combination with the expression of E7( $\Delta$ 6-10), E7( $\Delta$ 21-24), E7( $\Delta$ 79-83) or an empty control vector (Vect). Data are presented as mean normalized to day 0 of each condition. (1 out of 2 independent experiments with similar results). The percent of SA- $\beta$ -gal positive cells for each condition at day 20 post-infection is indicated at the bottom of each growth curve. Data were quantified from >5-independent cell counts up to a total of at least 150 cells and are presented as the mean percentage of positive cells, (1 out of 2 independent experiments with similar results). shNTC: non-targeting shRNA; shR-A or -B: shRNAs against RSL1D1. (g-j) QPCR for the indicated genes performed on reverse transcribed total RNA extracted from cells as in (f) at day 20 post-infection. Data were normalized over TBP and HMBS and presented as mean relative to vector/shNTC infected cells, (n = 1).

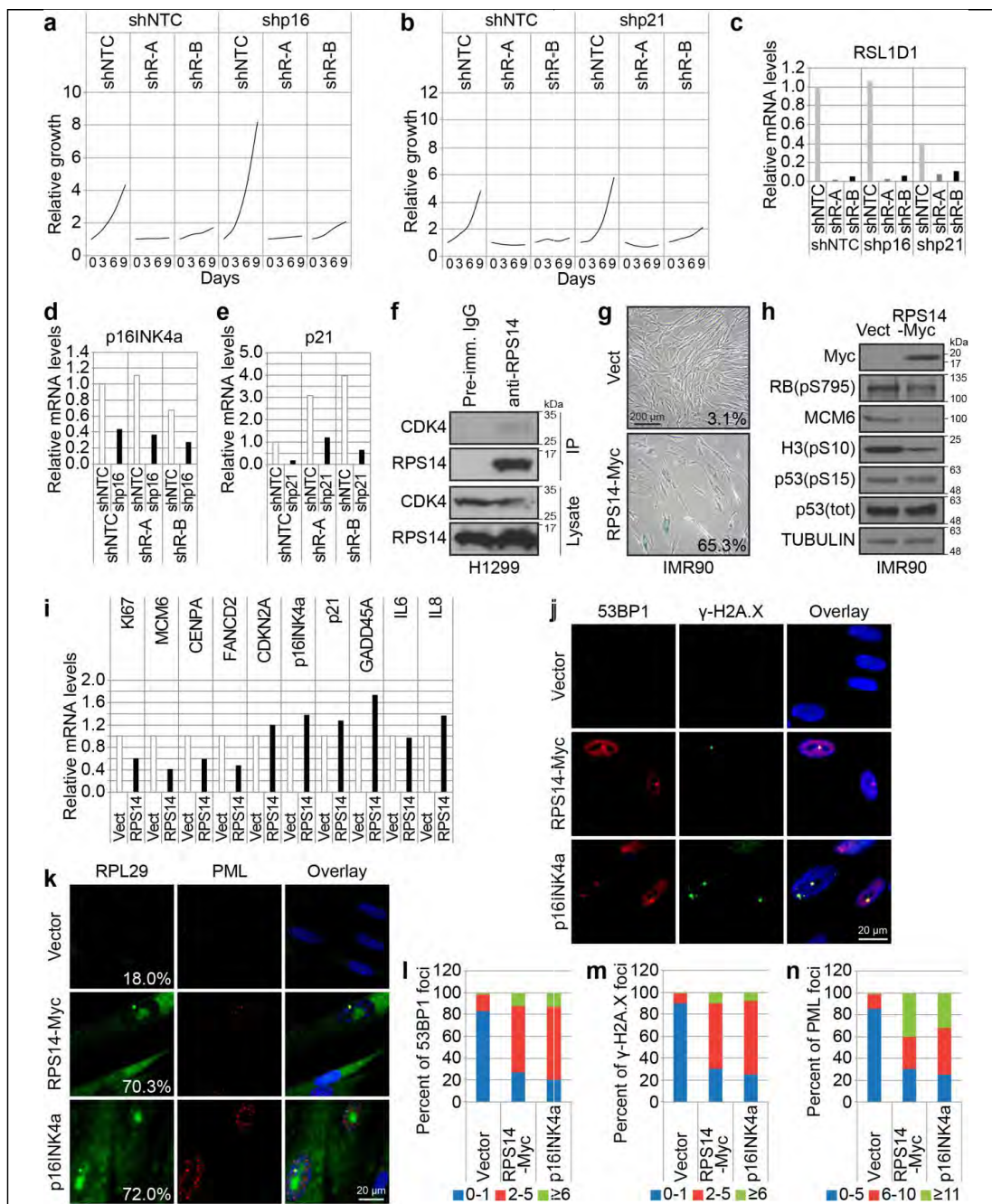


**Supplementary Figure 5**

**CDK4 and CDK6 bypass RSL1D1 knockdown-induced senescence**

(a) SA- $\beta$ -gal of IMR90 cells expressing the indicated shRNA expression vectors in combination with the expression of CDK4 (1 out of 3 independent experiments with similar results), CDK6 (n = 1) or a control vector (Vect) at day 20 post-infection. Data were quantified from >5-independent cell counts up to a total of at least 150 cells and are presented as the mean percentage of positive cells. shNTC: non-targeting shRNA; shR-A or -B: shRNAs against RSL1D1. (b) Growth curves of IMR90 cells as in (a). Data are presented as means normalized to day 0 of each condition. (1 out of 3 independent experiments with similar results for CDK4) and (1 out of 2 independent experiments with similar results for CDK6). (c-h) QPCR for the indicated genes performed on reverse transcribed total RNA extracted from cells as in (a) at day 20 post-infection. Data were normalized over TBP and HMBS and presented as means relative to vector/shNTC infected cells, (1 out of 2 independent experiments with similar results). (i) SA- $\beta$ -gal of IMR90 cells expressing the indicated shRNA expression vectors in combination with the expression of 3xFLAG-CDK4(WT), 3xFLAG-CDK4(K35M) or an empty control vector (Vect) at day 20 post-infection. Data were quantified from >5-independent cell counts up to a total of at least 150 cells and are presented as the mean percentage of positive cells, (1 out of 2 independent experiments with similar results). shNTC: non-targeting shRNA; shR-A or -B: shRNAs against RSL1D1. (j-m) QPCR for the indicated genes performed on reverse transcribed total RNA extracted from cells as in (i). Data were normalized over TBP and HMBS and presented as mean relative to vector/shNTC infected cells, (1 out of 2 independent experiments with similar results).

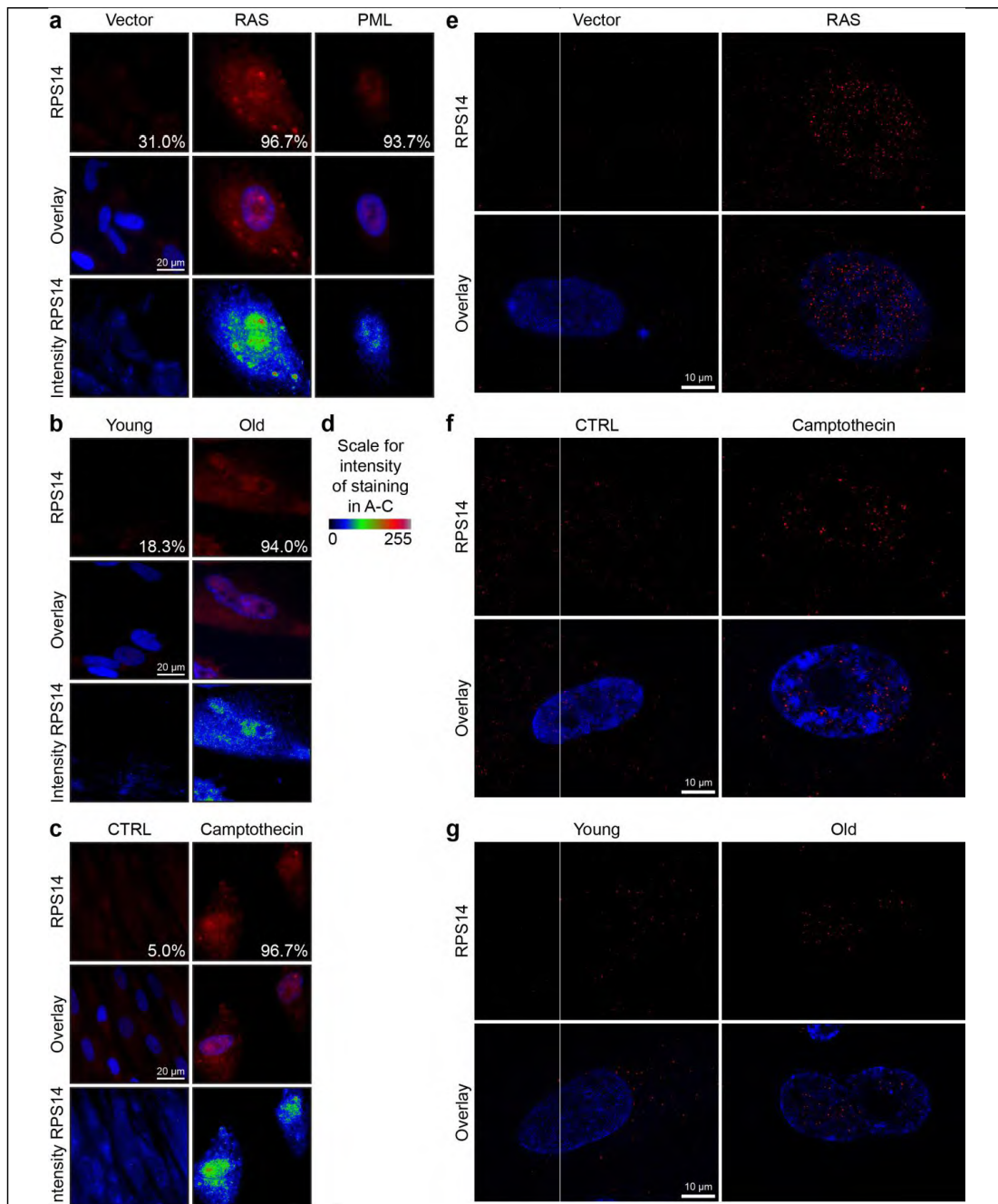




## Supplementary Figure 6

### RSL1D1 knockdown-induced senescence is not affected by CDK4 inhibitors p16INK4a and p21

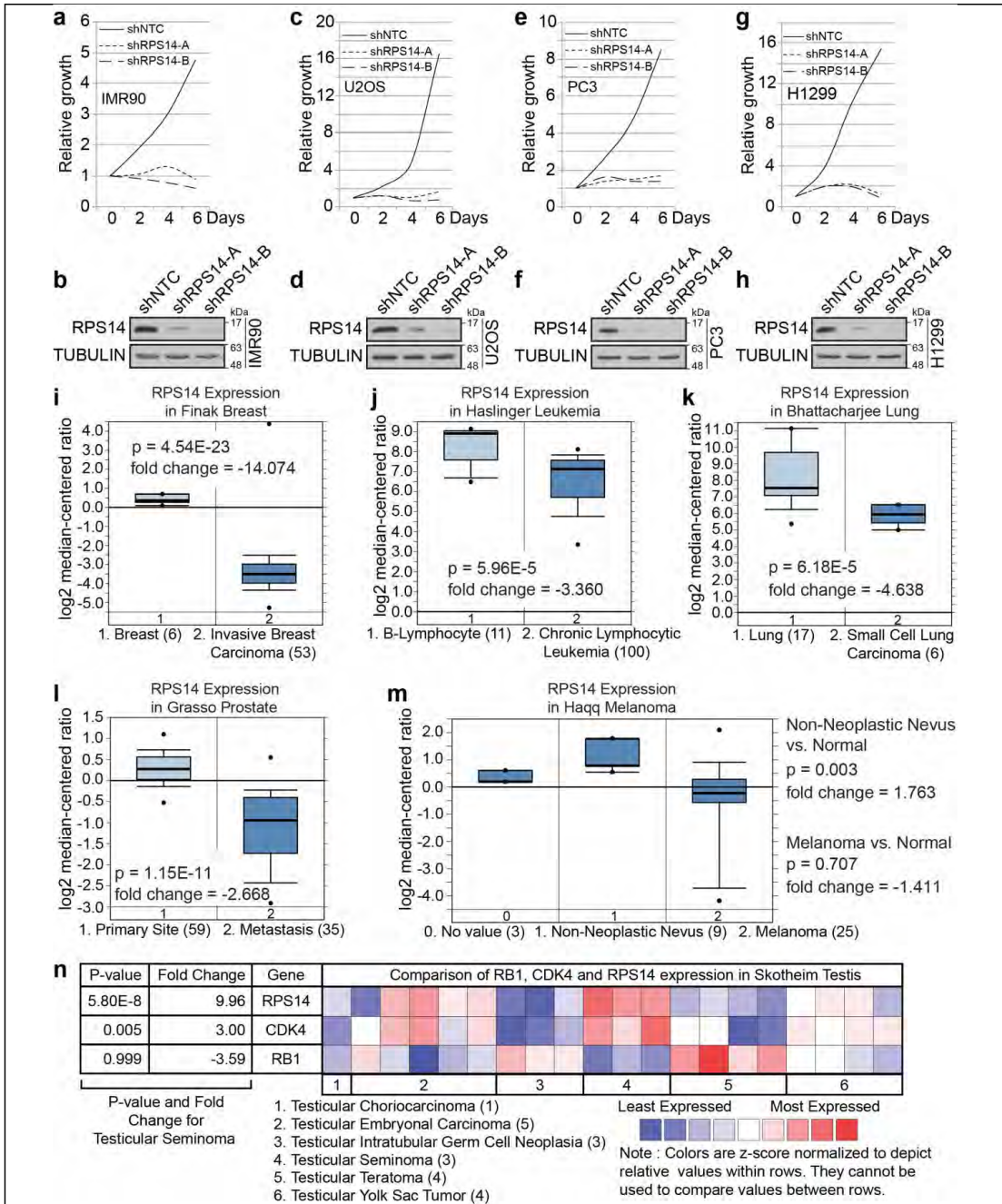
(a-b) Growth curves of IMR90 cells expressing combinations of the indicated shRNAs. Data are presented as means normalized to day 0 of each condition. (1 out of 2 independent experiments with similar results). shNTC: non-targeting shRNA; shp16: shRNA against p16INK4a (CDKN2A); shp21: shRNA against p21 (CDKN1A); shR-A or -B: shRNAs against RSL1D1. (c-e) QPCR for the indicated genes performed on total RNA extracted from cells, as in (a-b), at day 20 post-infection. Data were normalized over TBP and HMBS and presented as means relative to shNTC/shNTC infected cells, (1 out of 2 independent experiments with similar results). (f) Immunoprecipitation with pre-immune serum or with RPS14 antibody in H1299 cells. Lysates and immunoprecipitates were immunoblotted for the indicated proteins (1 out of 3 independent experiments with similar results). (g) SA- $\beta$ -gal of IMR90 cells expressing RPS14-Myc or an empty control vector (Vect) at day 12 post-infection. Data were quantified from >5-independent cell counts up to a total of at least 150 cells and are presented as the mean percentage of positive cells, (1 out of 3 independent experiments with similar results). (h) Immunoblots for the indicated proteins for cells as in (g) at day 7 post-infection, (1 out of 3 independent experiments with similar results). Western blot panels for Myc and tubulin are the same as in Figure 6b. (i) QPCR for the indicated genes performed on total RNA extracted from cells as in (g) and at day 9 post-infection. Data are normalized over TBP and HMBS and presented as mean relative to vector infected cells, (1 out of 2 independent experiments with similar results). (j-k) Indirect immunofluorescence (IF) with specific anti-53BP1, anti- $\gamma$ H2A.X, anti-RPL29 and anti-PML antibodies as indicated and nuclear counterstaining with DAPI. Images represent IMR90 cells expressing RPS14-Myc, p16INK4a or an empty control vector at day 14 post-infection, (1 out of 3 independent experiments with similar results). (k) IF data were quantified from 100 cell counts in triplicate and are presented as the mean percentage of cells with positive nucleolar localization of RPL29. (l-n) IF foci data in cells as in (j-k) were quantified from 100 cell counts in triplicate and are presented as the mean. (l-m) Quantification of the percentage of cells with 0-1, 2-5 or more than 5 foci of 53BP1 and  $\gamma$ H2A.X per cell. (n) Quantification of the percentage of cells with 0-5, 6-10 or more than 10 foci of PML per cell. Unprocessed blots can be found in Supplementary Figure 9.



**Supplementary Figure 7**

**Nuclear accumulation of RPS14 in senescence**

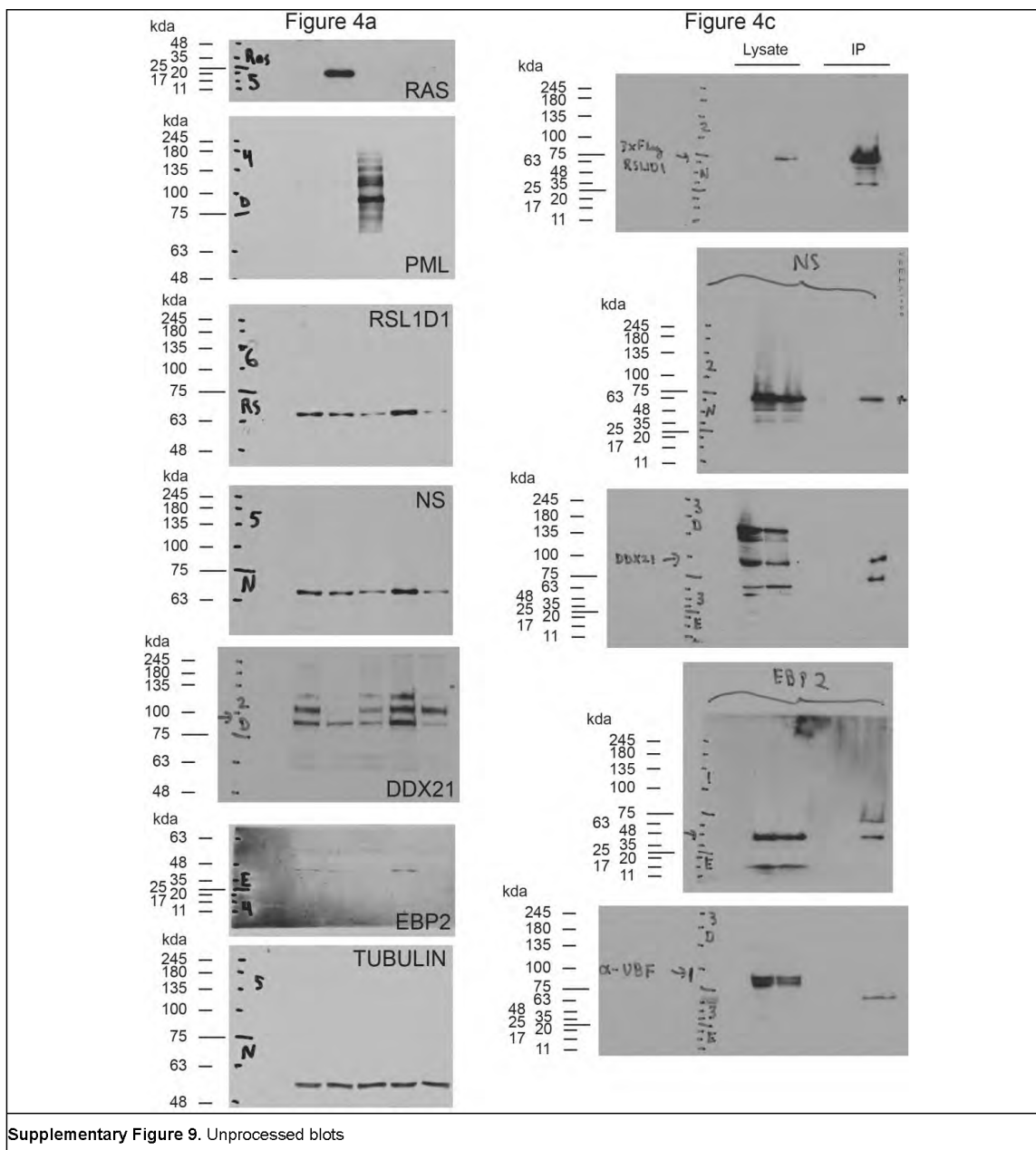
**(a-c)** Indirect immunofluorescence (IF) with specific anti-RPS14 antibody and nuclear counterstaining with DAPI. Images from **(a)** IMR90 cells expressing H-RASV12 (RAS) (1 out of 3 independent experiments with similar results), PML-IV (PML) (1 out of 2 independent experiments with similar results) or an empty control vector at day 12 post-infection, **(b)** young (passage 25) and old (passage 43) IMR90 cells (1 out of 2 independent experiments with similar results) and **(c)** IMR90 cells treated with DMSO (CTRL) or camptothecin in DMSO (final concentration in medium of 35 nM) for 3 days (1 out of 2 independent experiments with similar results). Data in RPS14 panel were quantified from 100 cell counts in triplicate and are presented as the mean percentage of cells with RPS14 nuclear staining. **(d)** Scale for intensity of staining by indirect IF with specific anti-RPS14 as in (a-c). **(e-g)** Hyperresolution structure illumination microscopy of immunofluorescence staining using a specific anti-RPS14 antibody and counterstaining with DAPI. **(e)** Comparison of IMR90 cells expressing H-RASV12 (RAS) or an empty control vector and fixed at day 12 post-infection. CTRL: 2 cells out of 15 showed nuclear staining; RAS: 5 cells out of 6 showed nuclear staining. **(f)** Comparison of IMR90 cells treated with DMSO (CTRL) or camptothecin in DMSO (final concentration in medium of 35 nM) for 3 days. DMSO: 2 cells out of 24 showed nuclear staining; Camptothecin: 4 cells out of 5 showed nuclear staining. **(g)** Comparison of young (passage 25) or old (passage 43) IMR90 cells. Young: 1 cell out of 10 showed nuclear staining; Old: 4 cells out of 4 showed nuclear staining.



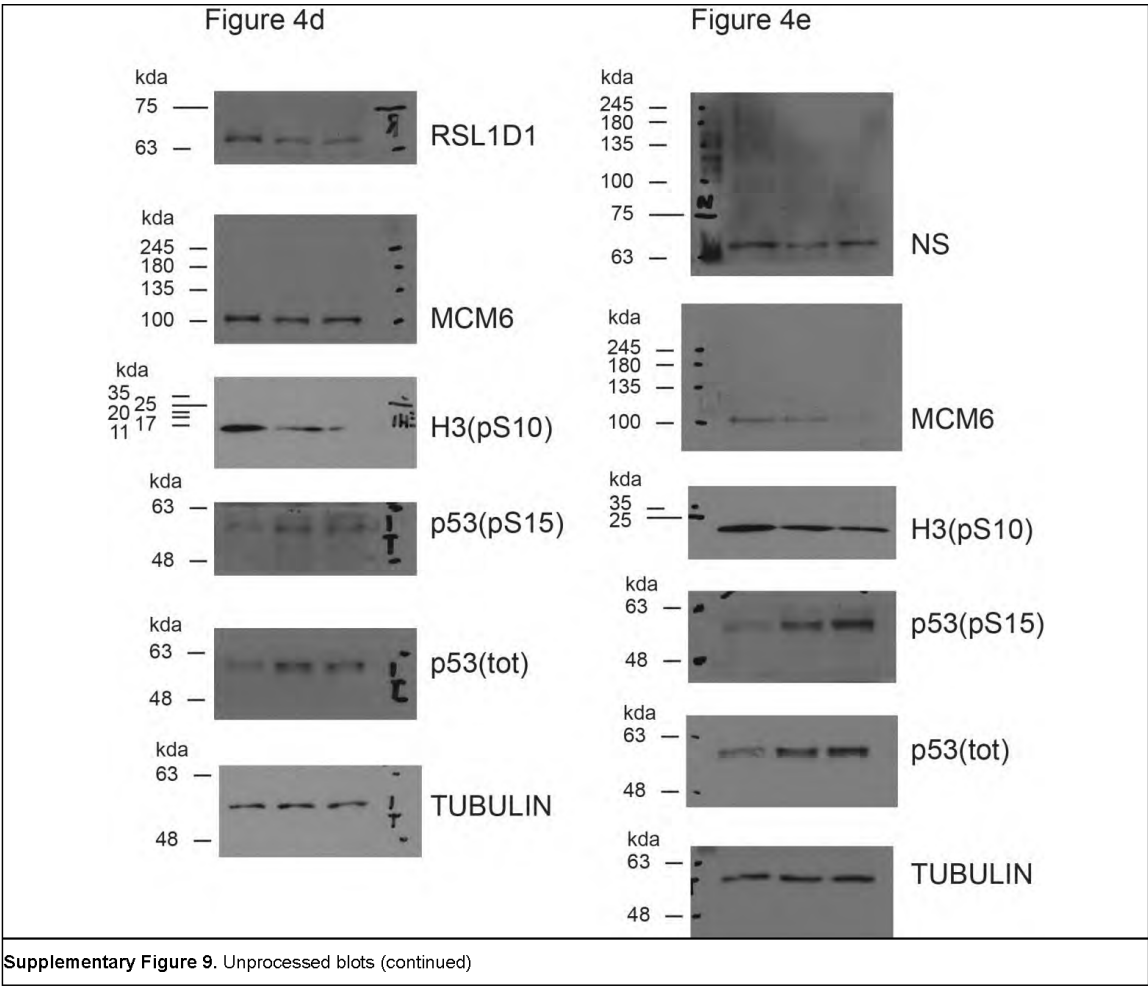
### Supplementary Figure 8

**Cells do not tolerate a significant depletion of RPS14 but RPS14 mRNA levels are downregulated in different types of cancer and increased in nevi**

(a, c, e and g) Growth curves of (a) IMR90 cells, (c) U2OS cells, (e) PC3 cells or (g) H1299 cells expressing a control shRNA (shNTC) and two shRNA against RPS14 (shRPS14-A and -B). Data are presented as means normalized to day 0 of each condition. (1 out of 2 independent experiments with similar results). (b, d, f and h) Immunoblots for the indicated proteins at day 5 post-infection with a control shRNA (shNTC) and two shRNA against RPS14 (shRPS14-A and -B) in (b) IMR90 cells, (d) U2OS cells, (f) PC3 cells or (h) H1299 cells, (1 out of 2 independent experiments with similar results). (i-m) Studies showing the decrease of RPS14 transcript levels using the Oncomine database selected with the following settings: threshold P-value:  $10^{-4}$ ; fold change: 2; gene rank top 10%. Each box plot shows median RPS14 expression, boxes are upper and lower 25% percentiles, whiskers are upper and lower 10% percentiles, minima and maxima are shown by dots. (For precision see Oncomine database). (i) RPS14 expression in Finak Breast. Comparison of Breast (n = 6) and Invasive Breast Carcinoma (n = 53). (j) RPS14 expression in Haslinger Leukemia. Comparison of B-Lymphocyte (n = 11) and Chronic Lymphocytic Leukemia (n = 100). (k) RPS14 expression in Bhattacharjee Lung. Comparison of Lung (n = 17) and Small Cell Lung Carcinoma (n = 6). (l) RPS14 expression in Grasso Prostate. Comparison of Primary Site (n = 59) and Metastasis (n = 35). (m) RPS14 expression in Haqq Melanoma. Comparison of Normal tissue (n = 3), Non-Neoplastic Nevus (n = 9) and Melanoma (n = 25). (n) Summary of studies comparing levels of RPS14, CDK4 and RB1 (RB) transcripts in Skotheim Testis cancers, using the Oncomine database with the following settings: threshold P-value:  $10^{-4}$ ; fold change: 2; gene rank top 10%. Red color indicated an increase in the tumor whereas blue color indicated a decrease and n for each tumor type is indicated between parentheses. (For precision see Oncomine database). Unprocessed blots can be found in Supplementary Figure 9.



Supplementary Figure 9. Unprocessed blots





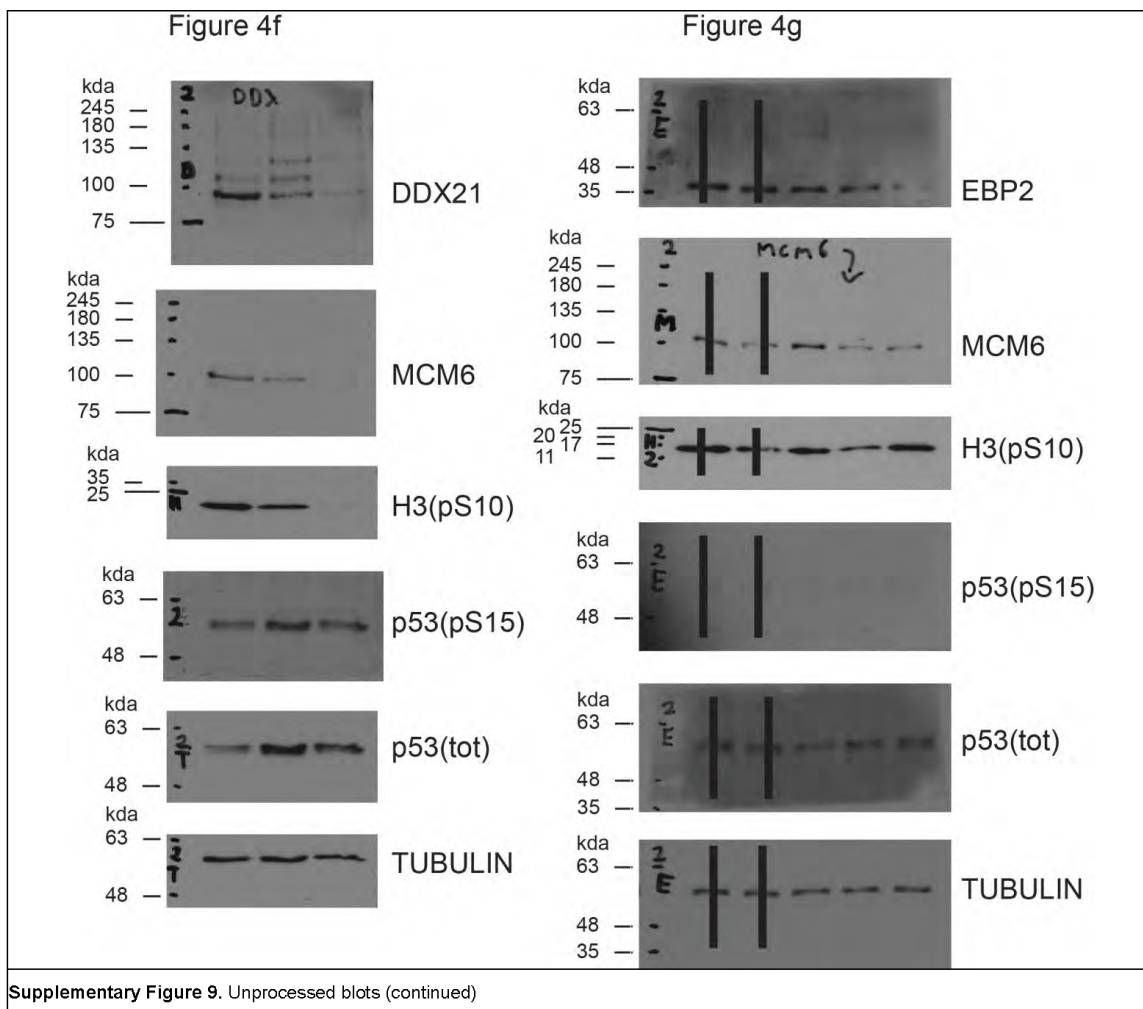
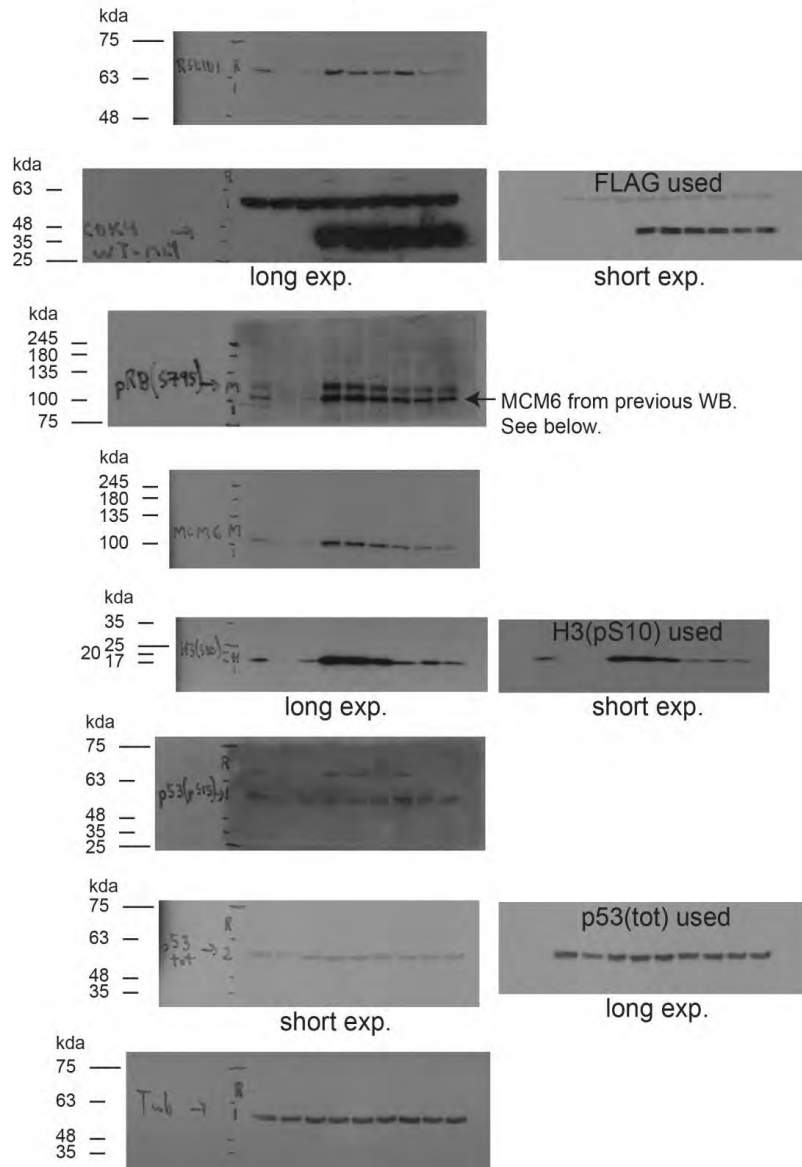


Figure 5c



Supplementary Figure 9. Unprocessed blots (continued)

Figure 5d

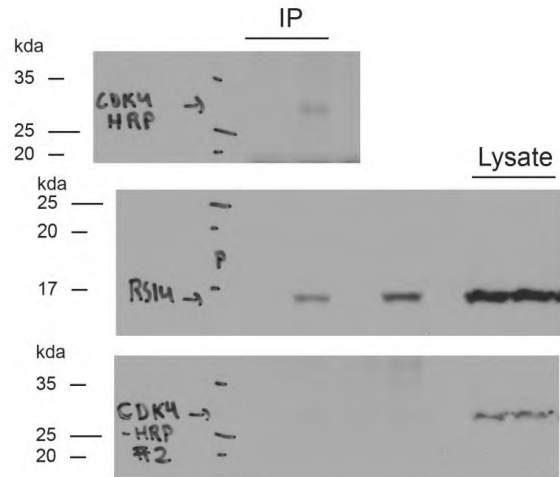
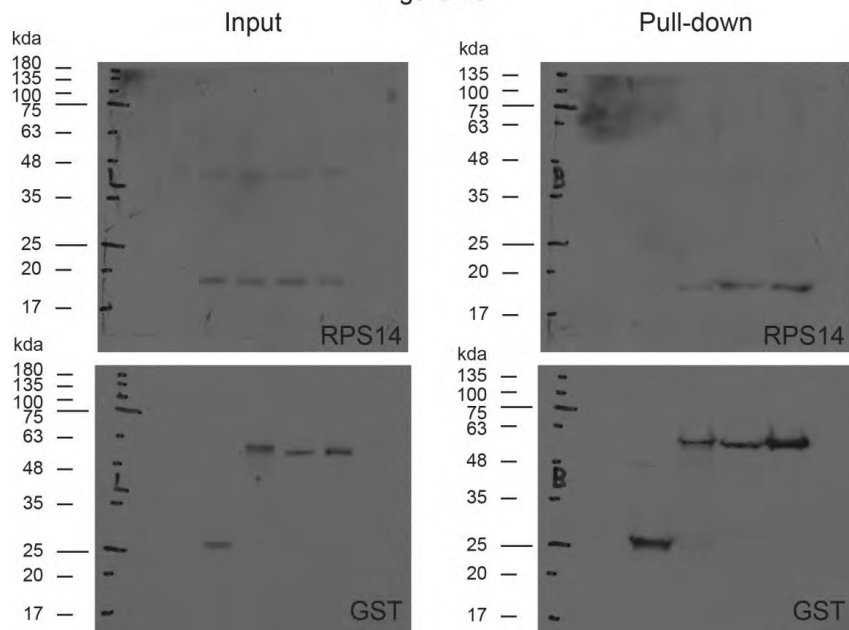


Figure 5e



Supplementary Figure 9. Unprocessed blots (continued)

Figure 5f

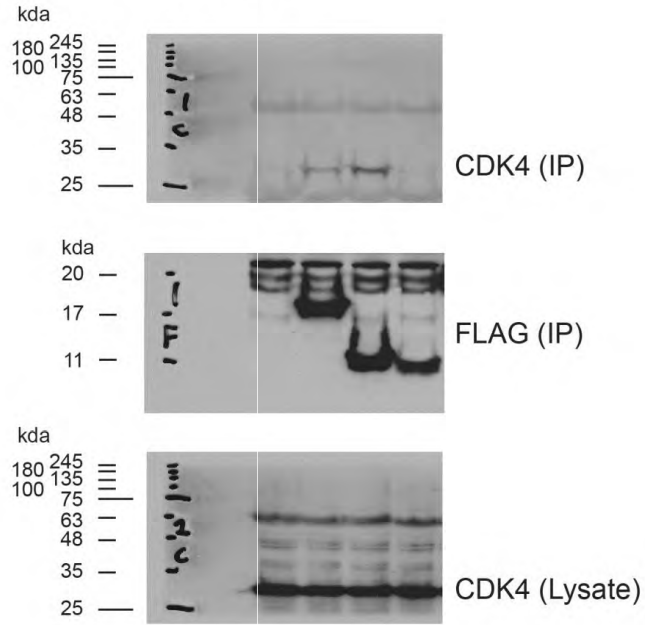
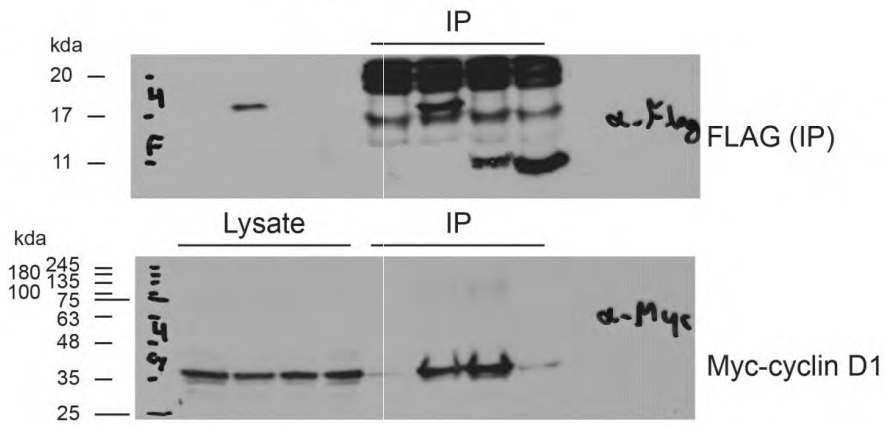
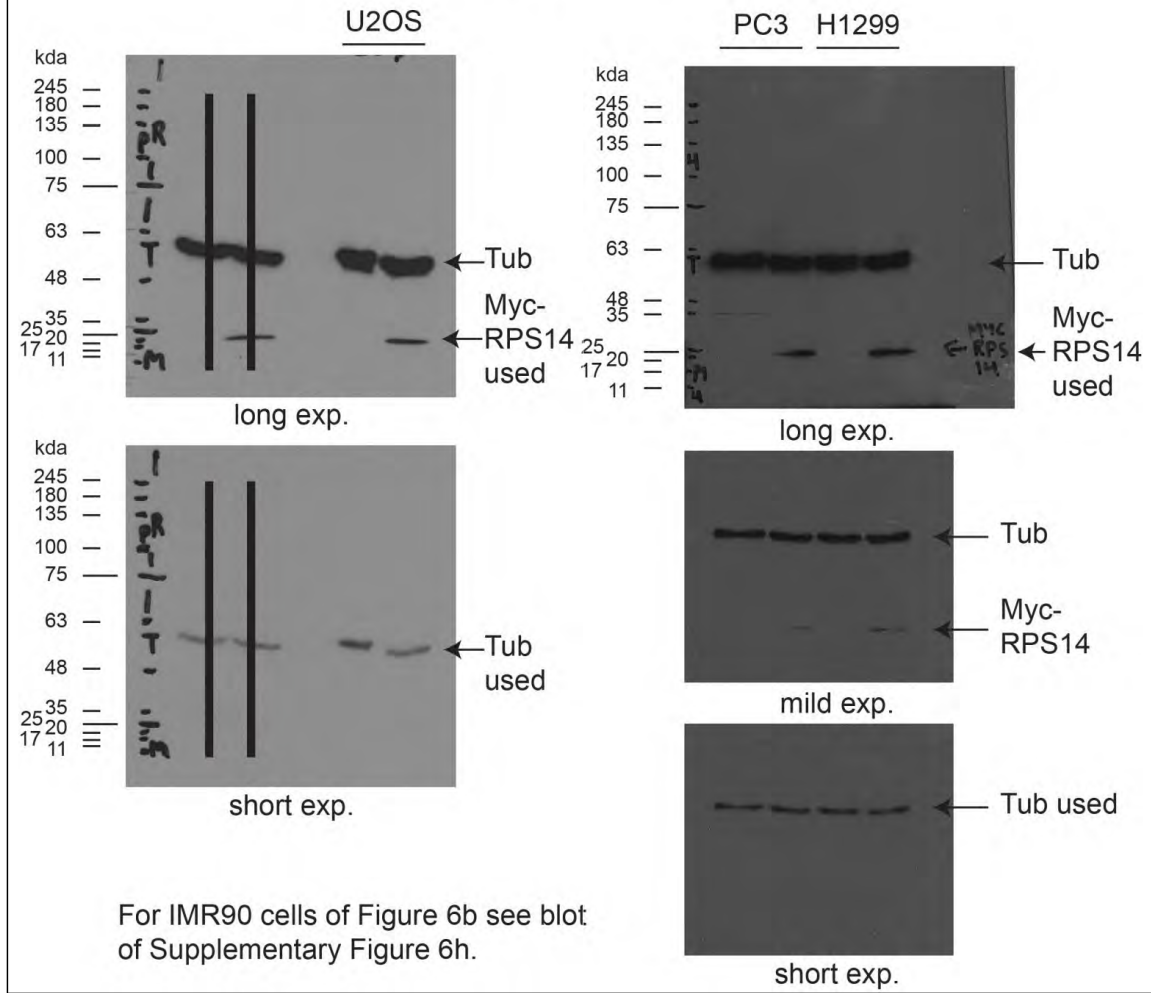


Figure 5g



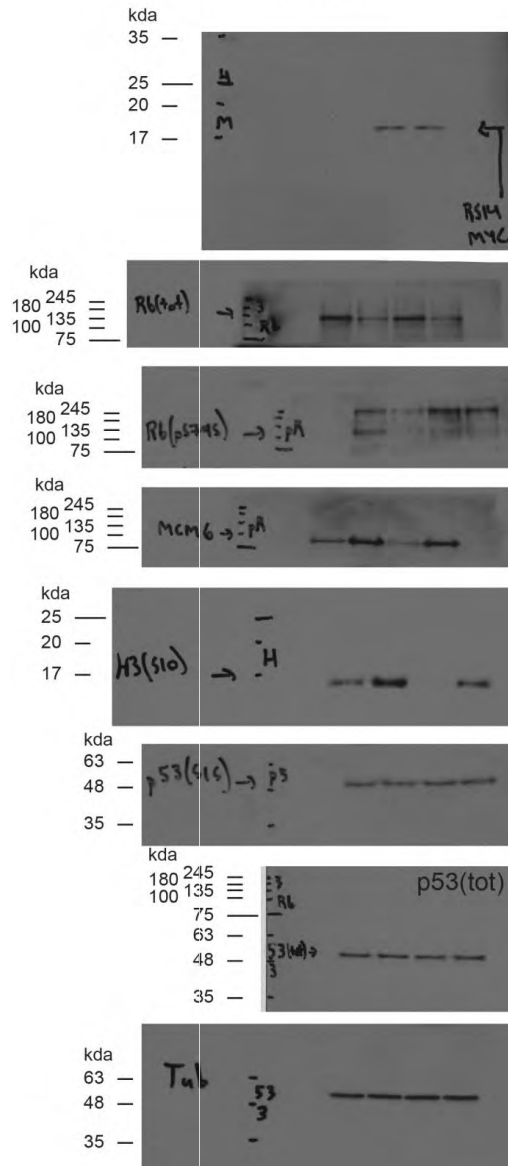
Supplementary Figure 9. Unprocessed blots (continued)

Figure 6b,d,f,h

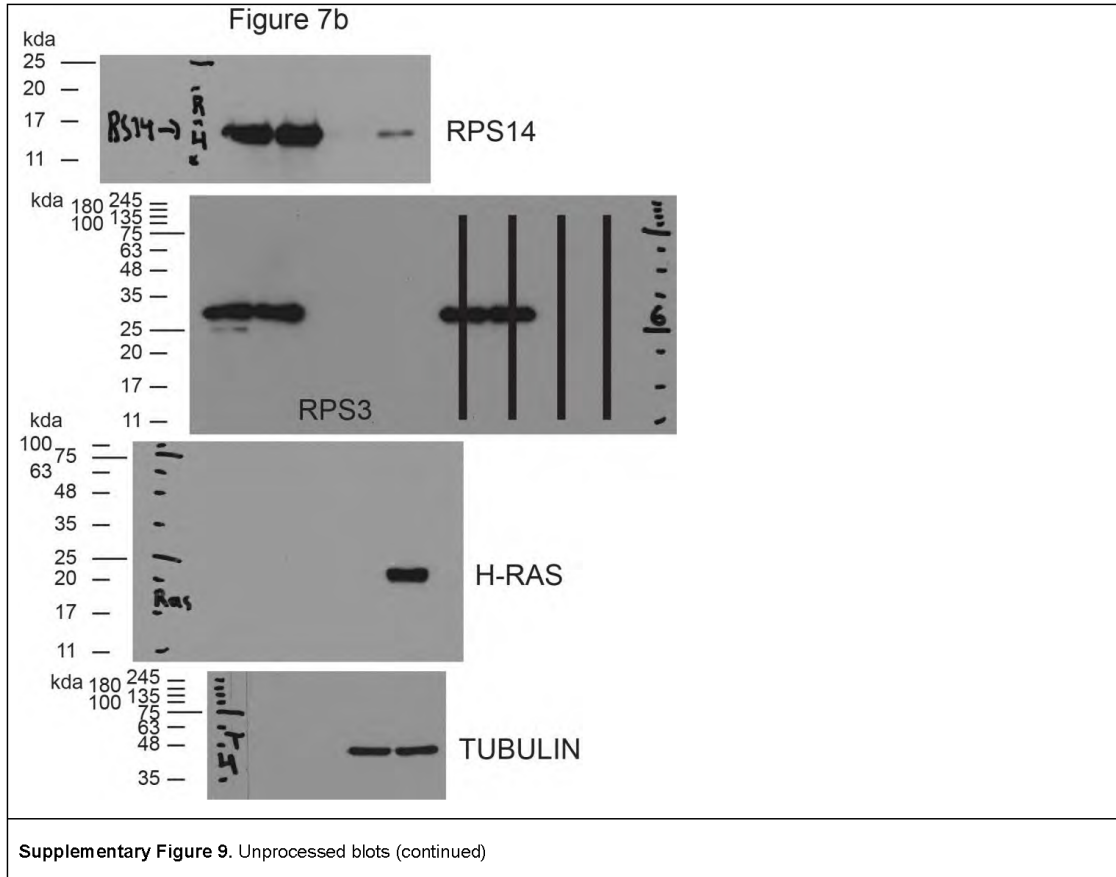


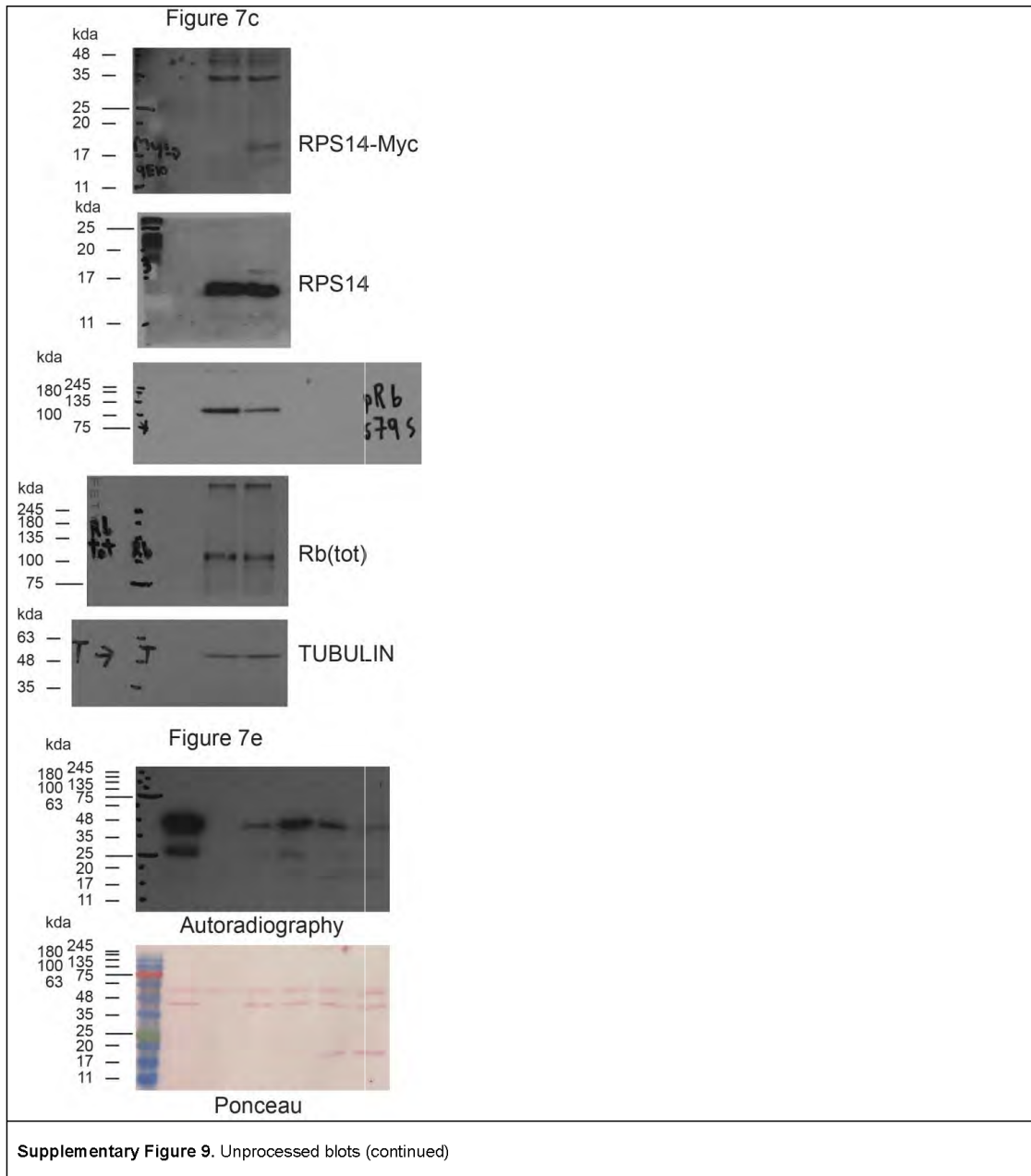
Supplementary Figure 9. Unprocessed blots (continued)

Figure 6k

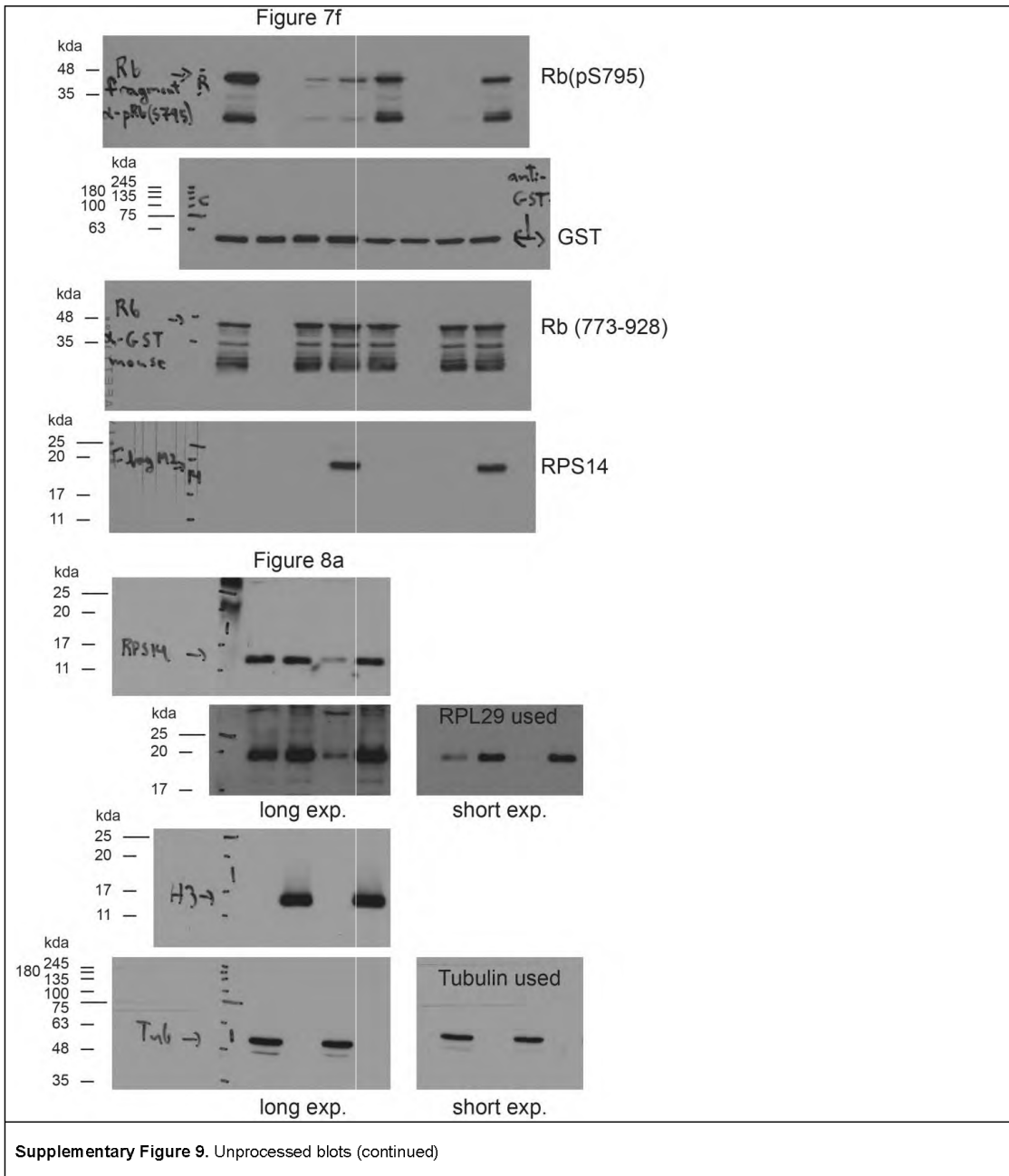


Supplementary Figure 9. Unprocessed blots (continued)



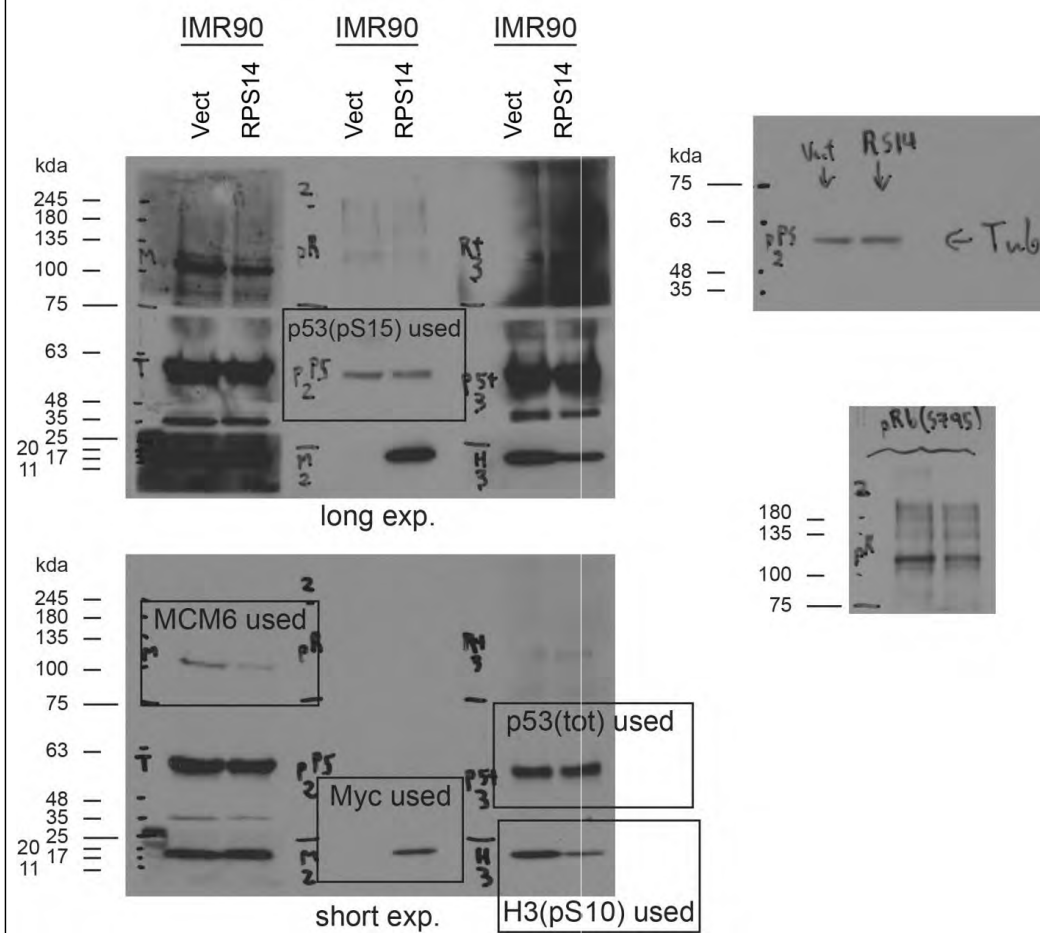






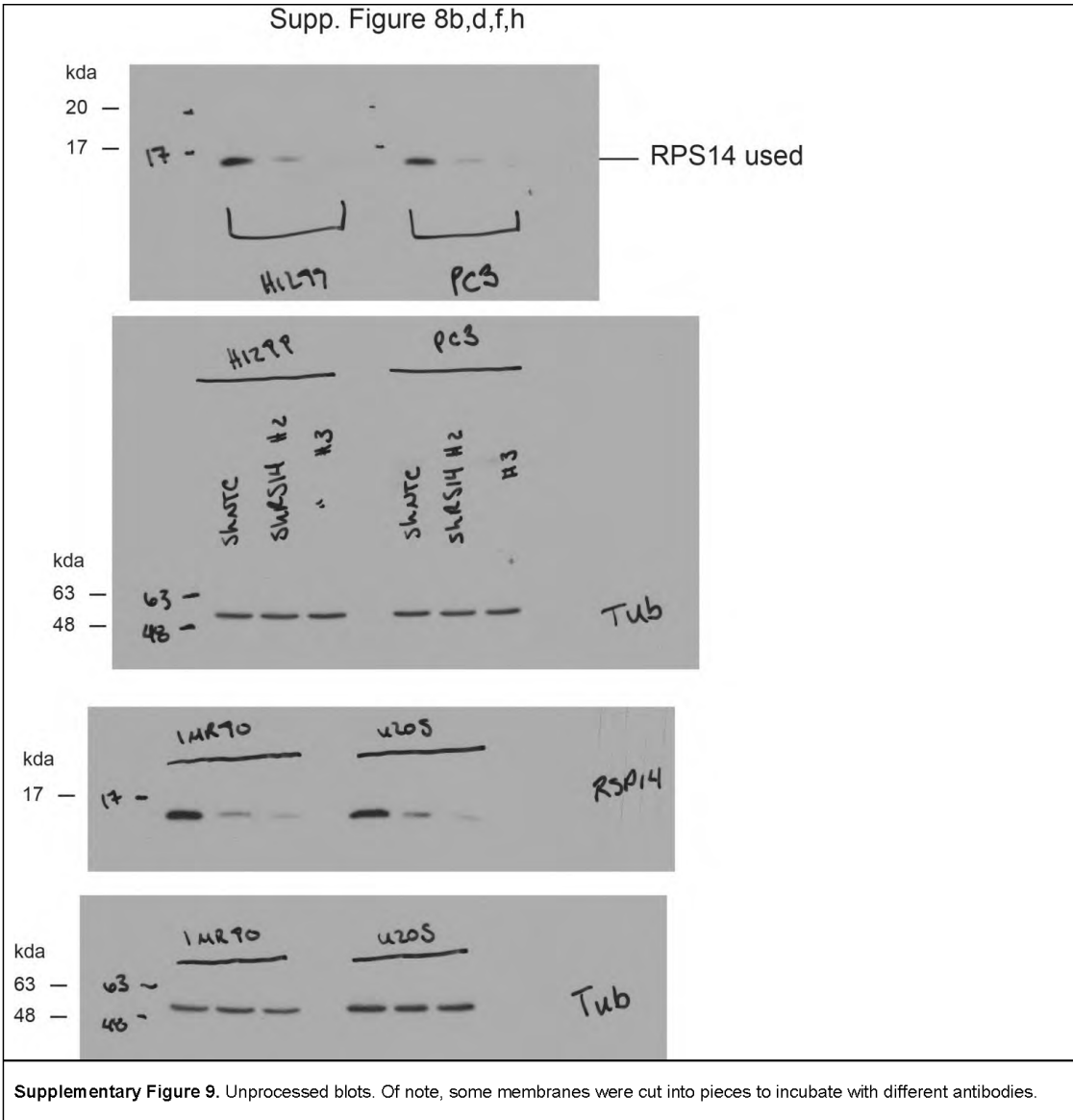


Supp. Figure 6h



Supplementary Figure 9. Unprocessed blots (continued)

Supp. Figure 8b,d,f,h



Supplementary Figure 9. Unprocessed blots. Of note, some membranes were cut into pieces to incubate with different antibodies.

## 2.4.7. References

1. Deschenes-Simard, X., Lessard, F., Gaumont-Leclerc, M.F., Bardeesy, N. & Ferbeyre, G. Cellular senescence and protein degradation: Breaking down cancer. *Cell cycle (Georgetown, Tex)* **13**, 1840-1858 (2014).
2. Michaloglou, C. *et al.* BRAFE600-associated senescence-like cell cycle arrest of human naevi. *Nature* **436**, 720-724 (2005).
3. Vernier, M. *et al.* Regulation of E2Fs and senescence by PML nuclear bodies. *Genes Dev* **25**, 41-50 (2011).
4. Kang, T.W. *et al.* Senescence surveillance of pre-malignant hepatocytes limits liver cancer development. *Nature* **479**, 547-551 (2011).
5. Xue, W. *et al.* Senescence and tumour clearance is triggered by p53 restoration in murine liver carcinomas. *Nature* **445**, 656-660 (2007).
6. Chen, Z. *et al.* Crucial role of p53-dependent cellular senescence in suppression of Pten-deficient tumorigenesis. *Nature* **436**, 725-730 (2005).
7. Guerra, C. *et al.* Pancreatitis-induced inflammation contributes to pancreatic cancer by inhibiting oncogene-induced senescence. *Cancer Cell* **19**, 728-739 (2011).
8. Stumpf, C.R. & Ruggero, D. The cancerous translation apparatus. *Curr Opin Genet Dev* **21**, 474-483 (2011).
9. Bhat, M. *et al.* Targeting the translation machinery in cancer. *Nat Rev Drug Discov* **14**, 261-278 (2015).
10. Nishimura, K. *et al.* Perturbation of Ribosome Biogenesis Drives Cells into Senescence through 5S RNP-Mediated p53 Activation. *Cell reports* **10**, 1310-1323 (2015).
11. Drygin, D. *et al.* Targeting RNA polymerase I with an oral small molecule CX-5461 inhibits ribosomal RNA synthesis and solid tumor growth. *Cancer Res* **71**, 1418-1430 (2011).
12. Bywater, M.J. *et al.* Inhibition of RNA polymerase I as a therapeutic strategy to promote cancer-specific activation of p53. *Cancer Cell* **22**, 51-65 (2012).
13. Devlin, J.R. *et al.* Combination Therapy Targeting Ribosome Biogenesis and mRNA Translation Synergistically Extends Survival in MYC-Driven Lymphoma. *Cancer Discov* **6**, 59-70 (2016).
14. Serrano, M., Lin, A.W., McCurrach, M.E., Beach, D. & Lowe, S.W. Oncogenic ras provokes premature cell senescence associated with accumulation of p53 and p16INK4a. *Cell* **88**, 593-602 (1997).

15. Ohtani, N. *et al.* Opposing effects of Ets and Id proteins on p16INK4a expression during cellular senescence. *Nature* **409**, 1067-1070 (2001).
16. Takahashi, A. *et al.* Mitogenic signalling and the p16INK4a-Rb pathway cooperate to enforce irreversible cellular senescence. *Nat Cell Biol* **8**, 1291-1297 (2006).
17. Chicas, A. *et al.* Dissecting the unique role of the retinoblastoma tumor suppressor during cellular senescence. *Cancer Cell* **17**, 376-387 (2010).
18. Zou, X. *et al.* Cdk4 disruption renders primary mouse cells resistant to oncogenic transformation, leading to Arf/p53-independent senescence. *Genes Dev* **16**, 2923-2934 (2002).
19. Acevedo, M. *et al.* A CDK4/6-Dependent Epigenetic Mechanism Protects Cancer Cells from PML-induced Senescence. *Cancer Res* **76**, 3252-3264 (2016).
20. Goel, S. *et al.* Overcoming Therapeutic Resistance in HER2-Positive Breast Cancers with CDK4/6 Inhibitors. *Cancer Cell* **29**, 255-269 (2016).
21. Langhendries, J.L., Nicolas, E., Doumont, G., Goldman, S. & Lafontaine, D.L. The human box C/D snoRNAs U3 and U8 are required for pre-rRNA processing and tumorigenesis. *Oncotarget* **7**, 59519-59534 (2016).
22. Wild, T. *et al.* A protein inventory of human ribosome biogenesis reveals an essential function of exportin 5 in 60S subunit export. *PLoS Biol* **8**, e1000522 (2010).
23. Deschenes-Simard, X. *et al.* Tumor suppressor activity of the ERK/MAPK pathway by promoting selective protein degradation. *Genes Dev* **27**, 900-915 (2013).
24. Meng, L., Yasumoto, H. & Tsai, R.Y. Multiple controls regulate nucleostemin partitioning between nucleolus and nucleoplasm. *J Cell Sci* **119**, 5124-5136 (2006).
25. Romanova, L. *et al.* Critical role of nucleostemin in pre-rRNA processing. *J Biol Chem* **284**, 4968-4977 (2009).
26. Ma, L. *et al.* CSIG inhibits PTEN translation in replicative senescence. *Mol Cell Biol* **28**, 6290-6301 (2008).
27. Mallette, F.A., Goumard, S., Gaumont-Leclerc, M.F., Moiseeva, O. & Ferbeyre, G. Human fibroblasts require the Rb family of tumor suppressors, but not p53, for PML-induced senescence. *Oncogene* **23**, 91-99 (2004).
28. Helt, A.M. & Galloway, D.A. Destabilization of the retinoblastoma tumor suppressor by human papillomavirus type 16 E7 is not sufficient to overcome cell cycle arrest in human keratinocytes. *J Virol* **75**, 6737-6747 (2001).
29. Malumbres, M. & Barbacid, M. Cell cycle, CDKs and cancer: a changing paradigm. *Nat Rev Cancer* **9**, 153-166 (2009).

30. Donati, G., Peddigari, S., Mercer, C.A. & Thomas, G. 5S ribosomal RNA is an essential component of a nascent ribosomal precursor complex that regulates the Hdm2-p53 checkpoint. *Cell reports* **4**, 87-98 (2013).
31. Sloan, K.E., Bohnsack, M.T. & Watkins, N.J. The 5S RNP couples p53 homeostasis to ribosome biogenesis and nucleolar stress. *Cell reports* **5**, 237-247 (2013).
32. Rabl, J., Leibundgut, M., Ataide, S.F., Haag, A. & Ban, N. Crystal structure of the eukaryotic 40S ribosomal subunit in complex with initiation factor 1. *Science* **331**, 730-736 (2011).
33. Rodier, F. *et al.* Persistent DNA damage signalling triggers senescence-associated inflammatory cytokine secretion. *Nat Cell Biol* **11**, 973-979 (2009).
34. Coppe, J.P. *et al.* Tumor suppressor and aging biomarker p16(INK4a) induces cellular senescence without the associated inflammatory secretory phenotype. *J Biol Chem* **286**, 36396-36403 (2011).
35. Ebert, B.L. *et al.* Identification of RPS14 as a 5q- syndrome gene by RNA interference screen. *Nature* **451**, 335-339 (2008).
36. Dorr, J.R. *et al.* Synthetic lethal metabolic targeting of cellular senescence in cancer therapy. *Nature* **501**, 421-425 (2013).
37. Coppe, J.P. *et al.* Senescence-associated secretory phenotypes reveal cell-nonautonomous functions of oncogenic RAS and the p53 tumor suppressor. *PLoS Biol* **6**, 2853-2868 (2008).
38. Horn, H.F. & Vousden, K.H. Cooperation between the ribosomal proteins L5 and L11 in the p53 pathway. *Oncogene* **27**, 5774-5784 (2008).
39. Marechal, V., Elenbaas, B., Piette, J., Nicolas, J.C. & Levine, A.J. The ribosomal L5 protein is associated with mdm-2 and mdm-2-p53 complexes. *Mol Cell Biol* **14**, 7414-7420 (1994).
40. Zhou, X., Hao, Q., Liao, J., Zhang, Q. & Lu, H. Ribosomal protein S14 unties the MDM2-p53 loop upon ribosomal stress. *Oncogene* **32**, 388-396 (2013).

## 2.5. Context for the article 2

The second article is based again on the observation that in senescence, there is a specific protein degradation [93]. In this article, we wanted to focus on the role of mitochondrial dysfunction and senescence. We had shown that mitochondria import proteins TOMM70 and TOMM34 are targets of the SAPD. Furthermore, STAT3 was identified as being degraded in OIS. We wanted to know the individual contributions of all those proteins towards the senescence response. We could show that removal of STAT3 can induce senescence mediated by an increase in NADH level and a p53 stabilization.

Furthermore, we could identify a complex of three proteins ME1, MDH1, and PC, repressed by p53 in senescent cells that allows if p53 is removed, the regeneration of NAD<sup>+</sup> and the bypass of the senescence response. The concerted actions of MDH1, ME1, and PC allow not only for NAD<sup>+</sup> regeneration but also for NADPH generation. The net reaction of this complex is  $ATP + NADH + NADP^+ = ADP + P_i + H^+ + NAD^+ + NADPH$ .

Moreover, we provided some evidence that PC, a mitochondrial enzyme, can localize outside of mitochondria in the cancerous cells. The relocation of PC is particularly important, as it allows the formation of the aforementioned complex with ME1 MDH1 and PC, and we demonstrated that formation of the complex is required to bypass the senescence response. We could highlight that levels of ME1 MDH1 and PC do increase in human and mouse prostate cancer compared to normal tissue.

Interestingly, we showed that the expression of ME1, MDH1, and PC combined with oncogenic RAS allows bypassing the senescence response while maintaining functional p53. This result allows an interesting suggestion that senescence bypass of oncogene-induced senescence (OIS) can be achieved by NAD<sup>+</sup> and NADPH generation and oncogenic Ras.

The results that NAD<sup>+</sup> and NADPH generation can participate in malignant transformation are particularly important in light of recent suggestions that NAD regeneration would be an efficient and safe anti-aging therapy. However, our results question whether NAD supplementation is safe and suggest increasing cancer incidence instead. Future research will tell the importance of NAD and NADPH in maintaining tumor suppression via cellular senescence and cellular transformation [497].



## 2.6. Contribution to the article 2

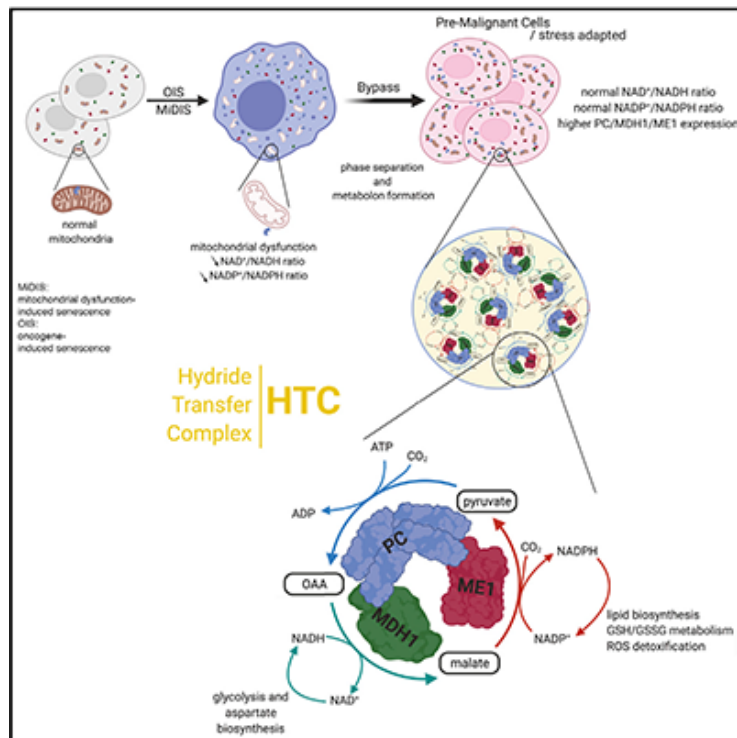
My contributions to this article are the following: I performed most of the experiments present in the article alone or in collaboration with an expert in that particular technique. In detail, I performed all the immunofluorescence, SA- $\beta$ -Gal, DCFDA/MitoSox analysis, NAD<sup>+</sup>/NADH analysis, and the Western Blots.

The following experiments were performed in collaboration. Metabolomics analyses were performed by Oro Uchenunu and me. Endogenous immunoprecipitations of HTC were done with the technical help of Frédéric Lessard. Mapping and immunoprecipitation of HTC complex in 293T cells were performed by summer students Mehdi Benfidil and Jacob Bouchard under my guidance. Experiments leading to HTC roles in PC-3 cells were done by Jacob Bouchard during his summer internship under my guidance. Biophysical characterization of the HTC complex was done by me with help from Haytham Wahba and Jim Omichinski. Roles of hypoxia in HTC formation were performed by me with technical help from Jordan Quenneville. Immunohistochemistry was done by Ana Fernandez-Ruiz and me. Experiments with STAT3 in the mitochondria were done by Jacob Bouchard, Ana Fernandez-Ruiz, and me. Mouse knockout samples for *Stat3* and *Pten* were provided by Jan Pencik, Lukas Kenner, and Richard Moriggl, and analyses were performed by the molecular pathology platform at CRCHUM and me. Experiments leading to senescence bypass by HTC expression in OIS were done by me with technical help from Véronique Bourdeau.

The Seahorse respiration experiments were done by David Papadopoli. Mitochondrial ultrastructure after STAT3 knockdown and immunogold staining were done by Aurélien Fouillen and Katia Julissa Ponce. The allograft experiments were performed by Marie-Camille Rowell and Stéphane Lopes-Paciencia. qPCR were done by Véronique Bourdeau, Lian Mignacca, and Geneviève Huot. Frédéric Lessard, Lian Mignacca and Geneviève Huot provided help with cell culture and valuable technical help. Several replicates to confirm experiments were performed by Frédéric Lessard, Lian Mignacca, Geneviève Huot and Véronique Bourdeau. Gerardo Ferbeyre and me, we wrote the initial draft and all authors provided input for final version of the paper.

# A hydride transfer complex reprograms NAD metabolism and bypasses senescence

## Graphical abstract



## Authors

Sebastian Igelmann, Frédéric Lessard, Oro Uchenunu, ..., James G. Omichinski, Ivan Topisirovic, Gerardo Ferbeyre

## Correspondence

ivan.topisirovic@mcgill.ca (I.T.),  
g.ferbeyre@umontreal.ca (G.F.)

## In brief

Igelmann et al. identified a hydride transfer complex (HTC) that drives metabolic reprogramming to overcome senescence and induces tumorigenesis. HTC consists of pyruvate carboxylase, malate dehydrogenase 1 and malic enzyme 1 and catalyzes a metabolic cycle whose net effect is to supply NAD<sup>+</sup> and NADPH, which are key cofactors for many essential metabolic reactions.

## Highlights

- PC, MDH1, and ME1 form a hydride transfer complex (HTC) in the cytoplasm
- HTC transfers reducing equivalents from NADH to NADP<sup>+</sup>
- HTC promotes tumor formation by bypassing senescence
- HTC confers fitness to cells under hypoxia or mitochondrial dysfunction





Article

## A hydride transfer complex reprograms NAD metabolism and bypasses senescence

Sebastian Igelmann<sup>1, 18</sup>, Frédéric Lessard<sup>18, 19</sup>, Oro Uchenunu<sup>2, 3, 19</sup>, Jacob Bouchard<sup>18, 19</sup>, Ana Fernandez-Ruiz<sup>1, 19</sup>, Marie-Camille Rowell<sup>1</sup>, Stéphane Lopes-Paciencia<sup>1</sup>, David Papadopolu<sup>2, 6</sup>, Aurélien Fouillen<sup>4, 18</sup>, Katia Julissa Ponce<sup>4</sup>, Geneviève Huot<sup>18</sup>, Lian Mignacca<sup>18</sup>, Mehdi Benfdil<sup>18</sup>, Paloma Kalegari<sup>1, 18</sup>, Haytham M. Wahba<sup>12, 18</sup>, Jan Pencik<sup>7, 14, 15</sup>, Nhung Vuong<sup>1</sup>, Jordan Quenneville<sup>9</sup>, Jordan Guillon<sup>1</sup>, Véronique Bourdeau<sup>18</sup>, Laura Hulea<sup>10</sup>, Etienne Gagnon<sup>9, 13</sup>, Lukas Kanner<sup>7, 8, 16, 17</sup>, Richard Moriggl<sup>11</sup>, Antonio Nanci<sup>4</sup>, Michael N. Pollak<sup>2</sup>, James G. Omichinski<sup>18</sup>, Ivan Topisirovic<sup>2, 3, 5, 6</sup> , Gerardo Ferbeyre<sup>1, 18, 20</sup>  

<sup>1</sup> CRCHUM, 900 Saint-Denis St, Montréal, QC H2X 0A9, Canada

<sup>2</sup> Lady Davis Institute for Medical Research, Jewish General Hospital, Montréal, QC H3T1E2, Canada

<sup>3</sup> Department of Experimental Medicine, McGill University, Montreal, QC H4A3T2, Canada

<sup>4</sup> Faculté de médecine dentaire, Université de Montréal, Montréal, QC H3C 3J7, Canada

<sup>5</sup> Department of Biochemistry, McGill University, Montreal, QC H4A 3T2, Canada

<sup>6</sup> Gerald Bronfman Department of Oncology, McGill University, Montreal, QC H4A3T2, Canada

<sup>7</sup> Department of Pathology, Medical University of Vienna, Vienna, Austria

<sup>8</sup> Unit of Laboratory Animal Pathology, University of Veterinary Medicine Vienna, Vienna, Austria

<sup>9</sup> Institut de recherche en immunologie et en oncologie (IRIC), Université de Montréal, Montréal, QC H3C 3J7, Canada

<sup>10</sup> Maisonneuve-Rosemont Hospital Research Centre, Montréal, QC H1T 2M4, Canada, Département de Médecine, Université de Montréal, Montréal, QC H3C 3J7, Canada

<sup>11</sup> Institute of Animal Breeding and Genetics, University of Veterinary Medicine Vienna, 1210 Vienna, Austria

<sup>12</sup> Department of Biochemistry, Faculty of Pharmacy, Beni-Suef University, Beni-Suef 62521, Egypt

<sup>13</sup> Département de Microbiologie, Infectiologie et Immunologie, Université de Montréal, Montréal, QC H3C 3J7, Canada

<sup>14</sup> Molecular and Cell Biology Laboratory, The Salk Institute for Biological Studies, La Jolla, CA 92037, USA

<sup>15</sup> Center for Biomarker Research in Medicine, 8010 Graz, Austria

<sup>16</sup> Christian Doppler Laboratory for Applied Metabolomics, Vienna, Austria

<sup>17</sup> CBmed GmbH - Center for Biomarker Research in Medicine, Graz, Styria, Austria

<sup>18</sup> Département de Biochimie et Médecine Moléculaire, Université de Montréal, Montréal, QC H3C 3J7, Canada

Received 14 December 2020, Revised 25 June 2021, Accepted 20 August 2021, Available online 21 September 2021.

## 2.7. A Hydride transfer complex reprograms NAD metabolism and bypasses senescence

### 2.7.1. Abstract

Metabolic rewiring and redox balance play pivotal roles in cancer. Cellular senescence is a barrier for tumorigenesis circumvented in cancer cells by poorly understood mechanisms. We report a multi-enzymatic complex that reprograms NAD metabolism by transferring reducing equivalents from NADH to NADP<sup>+</sup>. This hydride transfer complex (HTC) is assembled by malate dehydrogenase-1, malic enzyme-1 and cytosolic pyruvate carboxylase. HTC is found in phase-separated bodies in the cytosol of cancer or hypoxic cells and can be assembled in vitro with pure proteins. They are repressed in senescent cells but induced by p53 inactivation. HTC enzymes are highly expressed in mouse and human prostate cancer models and their inactivation triggers senescence. Exogenous expression of HTC is sufficient to bypass senescence, rescue cells from complex I inhibitors and cooperate with oncogenic RAS to transform primary cells. We provide evidence for a new multi-enzymatic complex that reprograms metabolism and overcomes cellular senescence.

### 2.7.2. Introduction

Senescence is a broadly acting tumor suppressor mechanism where cells bearing oncogenic mutations cannot expand due to a chronic state of mitochondrial dysfunction, oxidative stress, DNA damage and activation of tumor suppressors (Wiley and Campisi, 2016). Dysfunctional mitochondria are a hallmark of senescent cells in response to short telomeres (Passos et al., 2007) or oncogenes (Moiseeva et al., 2009). Mitochondrial dysfunction-associated senescence is characterized by decreased NAD<sup>+</sup> (Nicotinamide Adenine Dinucleotide)/NADH (Wiley et al., 2016), increased reactive oxygen species (ROS) and less ATP as compared to non-senescent cells (Moiseeva et al., 2009; Passos et al., 2007). This entices increases in glycolysis to maintain viability (Dorr et al., 2013). Since inhibition of senescence often precedes transformation (Deschenes-Simard et al., 2019; Moiseeva et al., 2020; Yu et al., 2018), it is important to understand how cancer cells overcome the barriers to cell proliferation that characterize senescence, including mitochondrial dysfunction.

The origin of mitochondrial dysfunction in senescent cells is not well understood. During oncogene-induced senescence (OIS), several proteins are targeted for degradation affecting a variety of processes required for cell proliferation (Deschenes-Simard et al., 2013; Deschenes-Simard et al., 2014). One of these proteins is Signal transducer and activator of transcription 3 (STAT3)

(Vallania et al., 2009), which regulates transcription in the nucleus (Kidder et al., 2008) and electron transport and oxidative phosphorylation in mitochondria (Wegrzyn et al., 2009). The mitochondrial functions of STAT3 are required for cellular transformation by oncogenic RAS protein (Gough et al., 2009). Deletion of *STAT3* in hematopoietic stem cells leads to mitochondrial dysfunction, overproduction of ROS and premature aging of blood cells (Mantel et al., 2012). Collectively, these studies suggest that the mitochondrial functions of STAT3 may be required to prevent senescence.

To discover cellular pathways that compensate for mitochondrial dysfunction and allow tumor cells to circumvent senescence, we used several models of cellular senescence. We found that senescence induced by STAT3 depletion required a decrease in the NAD<sup>+</sup>/NADH ratio that was maintained by the actions of the p53 and Retinoblastoma protein (RB) tumor suppressors. p53 and RB repress an enzyme complex that catalyzes a metabolic cycle that transfers the hydride anion (H<sup>-</sup>) from NADH to NADP<sup>+</sup>, thus regenerating NAD<sup>+</sup> and supplying NADPH. This hydride transfer complex (HTC) is formed by malic enzyme 1 (ME1), malate dehydrogenase 1 (MDH1) and pyruvate carboxylase (PC) and can be assembled *in vitro* with pure proteins. We also biophysically characterized HTC as well as its ability to compensate for mitochondrial dysfunction and promote tumorigenesis. Strikingly, inhibiting HTC leads to tumor cell senescence even in the absence of p53, revealing the therapeutic potential of targeting this novel metabolon.

### 2.7.3. Results

#### Depletion of STAT3 induces senescence, mitochondrial dysfunction and a low NAD<sup>+</sup>/NADH ratio

Senescence induced by either oncogenes or short telomeres is accompanied by downregulation of STAT3 (Deschenes-Simard et al., 2013). Since STAT3 is required for mitochondrial functions (Gough et al., 2009; Wegrzyn et al., 2009) we sought to investigate whether disabling STAT3 leads to senescence via mitochondrial dysfunction. We depleted STAT3 from normal human fibroblasts using shRNAs and observed a strong decline in proliferation accompanied by increased senescence-associated- $\beta$ -galactosidase (SA- $\beta$ -Gal) activity and several senescence biomarkers (Figure S1A-H) in line with previous work showing induction of senescence after STAT3 inactivation in some cancer cells (Tkach et al., 2012).

Given the links between STAT3 and mitochondria, (Gough et al., 2009; Wegrzyn et al., 2009) we performed staining for the mitochondria membrane marker TOMM20 (McBride et al., 1996). This revealed that mitochondria in STAT3-depleted cells appear as multiple punctiform structures in contrast to the tubular network of normal human fibroblasts (Figure 1A). Transmission electron

microscopy revealed that mitochondria from STAT3-depleted cells are spherical with disrupted cristae (Figure 1B-C). It was reported that mitochondrial STAT3 regulates mitochondrial gene expression (Macias et al., 2014), and we found that protein levels of mitochondrial-encoded mt-ND1 and mt-ND4 were reduced in cells with low STAT3 levels (Figure 1D). We also found that cells depleted for STAT3 produced higher levels of ROS (Figure 1E-F) and had a dramatically decreased  $\text{NAD}^+/\text{NADH}$  ratio (Figure 1G) which are signs of mitochondrial dysfunction. The decrease in  $\text{NAD}^+/\text{NADH}$  ratio was mainly the result of an increase in NADH since STAT3 depletion did not significantly alter total NAD or  $\text{NAD}^+$  (Figure S1I). In support of mitochondrial dysfunction, we found that both basal and maximal respiration were decreased upon STAT3 depletion (Figure 1H).

To confirm that the lack of STAT3 functions in mitochondria leads to mitochondrial dysfunction, we expressed an shRNA insensitive (i) STAT3 allele with a mitochondrial localization signal in STAT3-depleted cells. This mito-iSTAT3 localized into mitochondria, attenuated senescence and restored the  $\text{NAD}^+/\text{NADH}$  ratio to the level observed in STAT3-non-depleted control cells (Figure S1J-N). We also observed that endogenous STAT3 was reduced in purified mitochondria from cells that undergo OIS (Figure S1O). Furthermore, proximity ligation assay (PLA) revealed that STAT3 interacts with the mitochondrial protein ATAD3A in proliferating cells (Carbognin et al., 2016) whereas in replicative senescent cells or OIS cells interaction of ATAD3A with STAT3 was lost (Figure S1P-U) highlighting the changes of mitochondrial STAT3 levels in response to senescence and aging. By taking advantage of the yeast single subunit complex I NADH dehydrogenase (NDI1) (Birsoy et al., 2014), we next investigated whether mitochondrial complex I inhibition due to STAT3 depletion is the main cause of the observed decrease in the  $\text{NAD}^+/\text{NADH}$  ratio. We found that NDI1 localized to mitochondria, bypassed senescence and partially restored the  $\text{NAD}^+/\text{NADH}$  ratio in STAT3-depleted cells (Figure S2A-F). Together, these data show that mitochondrial STAT3 plays an important role in preventing senescence. The  $\text{NAD}^+/\text{NADH}$  ratio can be restored by pyruvate, which through the action of LDH is converted to lactate while  $\text{NAD}^+$  is regenerated from NADH. Alternatively, pyruvate can be converted to oxaloacetate, which in turn is reduced to malate, thus converting NADH into  $\text{NAD}^+$  (Hanse et al., 2017). Supplementing STAT3-depleted normal human fibroblasts with 2 mM pyruvate rescued cells from growth arrest and senescence while reducing the number of DNA-damage foci and increasing the  $\text{NAD}^+/\text{NADH}$  ratio (Figure S2G-L). We also treated STAT3-depleted cells with duroquinone, a compound that is reduced to durohydroquinone by the cytosolic enzyme NQO1 (NAD(P)H dehydrogenase [quinone]), which uses NADH as an electron donor and therefore regenerates  $\text{NAD}^+$  and decreases the sensitivity to complex I inhibition by biguanides (Gui et al., 2016). We found that this compound increased the  $\text{NAD}^+/\text{NADH}$  ratio without altering the total NAD levels in STAT3-depleted cells, which was paralleled by bypass of senescence (Figure

S2M-S). Next, we used the NADH-oxidase from *Lactobacillus brevis* (LbNOX) to force an increase in the NAD<sup>+</sup>/NADH ratio (Titov et al., 2016). LbNOX expression in the cytosol rescued cells from senescence induced by depletion of STAT3 while increasing the NAD<sup>+</sup>/NADH ratio (Figure S2T-W). It has been shown that cells with dysfunctional mitochondria and low NAD<sup>+</sup>/NADH ratio fail to synthesize sufficient asparagine (Krall et al., 2021) and aspartate (Birsoy et al., 2015; Sullivan et al., 2015) but supplementing STAT3-depleted cells with 20 mM aspartate only moderately rescued the proliferation defects and senescence after STAT3-depletion and it did not normalize the ratio NAD<sup>+</sup>/NADH (Figure S3A-G). Together, these data suggest that a failure to reoxidize NADH is implicated in the induction of cellular senescence.

### **A NAD<sup>+</sup> regeneration metabolic cycle controlled by the p53-RB tumor suppressors**

Depletion of STAT3 leads to the activation of both the p53 and RB tumor suppressor pathways, which are mediators of senescence (Malette et al., 2007). To investigate whether the p53 pathway is required for senescence after STAT3-depletion, we inactivated p53 and p21 with shRNAs. Inactivation of either p53 or p21 prevented the growth arrest and senescence induced by STAT3-depletion (Figure S3H-M). Intriguingly, p53 inactivation also restored the NAD<sup>+</sup>/NADH ratio in STAT3-depleted cells (Figure 1I). Collectively, the results suggest that p53 and/or p21/RB pathway inactivation in STAT3-depleted cells increases the NAD<sup>+</sup>/NADH ratio to sustain the oxidative metabolism of cells that bypass senescence.

To identify NAD<sup>+</sup>-regenerating metabolic pathways repressed by p53 and p21/RB we combined bioinformatics analysis with stable isotope tracing studies. Using CHIP-Atlas, we found that both p53 and RB-binding partner E2F proteins, bind to the promoter region for the NAD<sup>+</sup> regenerating cytosolic enzyme MDH1 (Figure S4A). Moreover, MDH1 expression is reduced in senescent cells induced by STAT3-depletion or telomere-shortening (Figure S4B-C). MDH1 is a cytosolic enzyme that oxidizes NADH and converts oxaloacetate (OAA) into malate (Hanse et al., 2017). To identify the source of OAA for MDH1, we compared glucose metabolism in senescent cells vs. cells that bypassed senescence via p53 knockdown, using <sup>13</sup>C<sub>6</sub>-glucose tracing. Conversion of pyruvate to OAA via Pyruvate Carboxylase (PC) can be estimated from the levels of (m+3) malate, fumarate, and citrate relative to the levels of corresponding (m+2) isotopomers generated in the tricarboxylic acid (TCA) cycle from acetyl-CoA (Figure 1J). Since OAA is hard to measure due to its instability, aspartate (m+3) was used as a surrogate marker (Buescher et al., 2015). We found that the pool of pyruvate converted to (m+3) malate, aspartate, fumarate and citrate is increased in cells that bypass senescence after p53 knockdown (Figure 1K-O). <sup>13</sup>C<sub>6</sub>-glucose may generate (m+3) malate, fumarate and aspartate through multiple rounds of pyruvate oxidation in the TCA cycle, but we discarded this because we failed to detect (m+3) succinate and very little (m+4) citrate

under the conditions (Figure 1O). Hence,  $^{13}\text{C}_6$ -glucose tracing was consistent with PC catalyzed conversion of pyruvate into (m+3) OAA. Labelling cells with  $[3,4-^{13}\text{C}]$ -glucose provides a more direct assessment of PC activity.  $[3,4-^{13}\text{C}]$ -glucose is converted to  $[1-^{13}\text{C}]$ -pyruvate and the latter is converted to m+1 OAA and its derivatives after the PC reaction whereas the labeled carbon is lost in the PDH reaction (Cheng et al., 2011). Bypass of senescence after p53 knockdown increased the pool of m+1 metabolites, while depletion of PC with an shRNA abrogated these effects (Figure 1P-Q). This indicates that p53 loss bolsters PC activity.

Of note, PC is considered a mitochondrial enzyme in mammals, and this implies that pyruvate enters the mitochondria, is converted to OAA by PC and then OAA is either exported to the cytosol as aspartate after transamination or as citrate after conjugation to acetyl-CoA. However, adding aspartate did not rescue the  $\text{NAD}^+/\text{NADH}$  ratio, suggesting that the aspartate pathway is not involved (Figure S3C). In yeast and some *Aspergillus* strains, PC is a cytosolic enzyme (Huet et al., 2000), and mammalian PC can re-localize to the cytosol upon viral infection (Cao et al., 2016) or to the nucleus in 2-cell embryos (Nagaraj et al., 2017). We thus anticipated that a change in cellular localization of PC could supply cytosolic OAA for  $\text{NAD}^+$  regeneration via MDH1. The concerted action of cytosolic PC and MDH1 is positioned to regenerate  $\text{NAD}^+$  in the cytosol to produce (m+3) malate, which is consistent with the m+3 isotopomers that were increased in cells bypassing senescence (Figure 1J-N). In addition, the cytosolic Malic Enzyme (ME1) is expected to convert malate back into pyruvate closing a metabolic cycle that would transfer the hydride ion from NADH to  $\text{NADP}^+$  regenerating  $\text{NAD}^+$  and supplying NADPH (Figure 1J). Notably, like MDH1, the PC and ME1 promoters contain p53 and RB/E2F binding sites (Figure S4A) and levels of the corresponding proteins decreased in models of cellular senescence (Figure S4B-C). These observations are consistent with work showing that p53 and/or E2F bind to the promoters of ME1 (Jiang et al., 2013), PC (Li et al., 2016) and MDH1 (Yuan et al., 2019) regulating their expression.

We next investigated whether bypassing senescence by inhibiting either the p53 or RB pathway can restore expression of MDH1, PC and ME1. We found that both shp53 and shp21 rescued their expression in STAT3-depleted IMR90 cells to levels comparable to control cells (Figure 1R). Collectively, these data suggest that a metabolic cycle catalyzed by MDH1, ME1 and cytosolic PC regenerate  $\text{NAD}^+$  to bypass cellular senescence. Our model predicts that 1) PC localizes to the cytosol in cells that bypass senescence, 2) expression of the enzymes that catalyze the hydride transfer from NADH to  $\text{NADP}^+$  bypasses senescence, and 3) inactivation of these enzymes should lead to a decreased  $\text{NAD}^+/\text{NADH}$  ratio, REDOX stress and growth inhibition.



### **Cytosolic localization of PC and formation of hydride transfer complex (HTC)**

Although PC is more abundant in the mitochondria, we detected full-length PC as well as lower molecular weight forms in the cytosolic fraction of PC-3 prostate cancer cells, which are devoid of STAT3 due to biallelic deletion of the *STAT3* locus (Figure S4D-E). Moreover, we used immunogold staining followed by transmission electron microscopy, which confirmed that a significant proportion of PC localizes to the cytosol in PC-3 cells (Figure 2A). This was further confirmed in IMR90 cells overexpressing PC, where a significant fraction of PC does not colocalize with mitochondria (Figure S4F). Interestingly, overexpression of PC, MDH1 and ME1 in STAT3-depleted IMR90 cells also colocalized in distinctive bodies (Figure 2B) outside mitochondria (Figure S4G). Importantly, we revealed this colocalization pattern with endogenous proteins after inactivation of both STAT3 and p53 in IMR90 cells (Figure 2C-E). Intriguingly, these foci were dissolved by 1,6-hexanediol suggesting that they form via liquid-liquid phase separation (Figure S4H-I). Additional evidence for the colocalization of HTC enzymes in cytosolic foci was obtained using PLA with antibodies against PC and MDH1 or PC and ME1 (Figure 2F-H).

The colocalization of PC, MDH1 and ME1 suggested that they interact to form a hydride transfer complex (HTC) and both PC and ME1 co-immunoprecipitated with FLAG-tagged MDH1 in 293T cells. Also, MDH1 and ME1 co-immunoprecipitated with FLAG-tagged PC, and PC and MDH1 co-immunoprecipitated with HA-tagged ME1 (Figure S5A-C). Importantly, HTC enzymes co-immunoprecipitated in HuH-7 hepatoma cells that endogenously express high levels of the three enzymes (according to the Cancer Cell line Encyclopedia) (Figure 2I) and in PC-3 cells (Figure S5D). PC is a biotinylated enzyme (Xiang and Tong, 2008) and its pulldown with streptavidin from PC-3 cells recovered both MDH1 and ME1 but this was not possible in cells where PC was depleted by a shRNA (Figure S5E). Similar results were obtained in HuH-7 cells (Figure S5F).

### **Biochemical and biophysical characterization of HTC**

To identify the regions required for co-immunoprecipitation of the HTC enzymes we used a series of deletions mutants. In addition to the full-length PC, it was determined that the fragments from positions 430-1178 and 1-956 formed a complex with both MDH1 and ME1. However, amino acids 1-534 of PC failed to do so, indicating that the interacting region comprises residues 534-956 in the pyruvate carboxyltransferase domain (Figure S5G and J). Second, we mapped the regions of MDH1 required to co-immunoprecipitate with PC and ME1. The residues 1-90, 1-141 and 1-192 of MDH1 co-immunoprecipitated with both PC and ME1, but residues 141-334 and 105-334 failed, concluding that the interacting region is within residues 1-90 (Figure S5H and J). Finally, we determined the regions of ME1 required to co-immunoprecipitate PC and MDH1. Full-length ME1 or residues 1-191 immunoprecipitated with both PC and MDH1 but residues 356-562 did

not, which suggests that the interacting region is between residues 1-191 (Figure S5I and J). The minimal interacting regions (PC<sup>430-1178</sup>, MDH1<sup>1-90</sup> and ME1<sup>1-191</sup>) were then confirmed to co-immunoprecipitate (Figure 2J) revealing that the interaction between MDH1 and ME1 requires PC (Figure 2J-K). Together, the data suggest that specific regions of each enzyme mediate HTC formation.

To confirm that HTC occurs endogenously in cells, we used two-dimensional blue native polyacrylamide gel electrophoresis (2D-BN/PAGE) on HuH-7 cell extracts. Proteins were resolved in a Blue Native gel in the first dimension followed by SDS-PAGE in the second dimension. This revealed the presence of MDH1 dimers (Molecular mass 36.4 kDa); monomers, dimers and tetramers of ME1 (Molecular mass 64.1 kDa); and of PC (Molecular mass 129.6 kDa). Importantly, we identified a high molecular weight complex with a mass of ~1 MDa, which contained all three enzymes (Figure 3A-B). To determine whether the HTC enzymes interact directly *in vitro*, we expressed and purified each enzyme from bacteria as well as a fragment of PC from residues 486-1178, because full-length PC form aggregates that affect the identification (Xiang and Tong, 2008).

Size exclusion chromatography with multi-angle light scattering (SEC-MALS) analysis revealed that purified PC forms a tetramer, whereas purified ME1 forms dimers and tetramers while purified MDH1 forms a dimer (Figure S5K-M). Then, mono-avidin was used to perform pulldowns of either PC(486-1178) or full-length PC, which are biotinylated, recovering both MDH1 and ME1 (Figure 3C-D). Next, we characterized the biophysical properties of the HTC. We loaded purified PC(486-1178), MDH1, ME1 alone or a pre-assembled 1:1:1 mixture of the proteins on a Superdex 200 Increase gel filtration column. Whereas the three individual enzymes eluted as described above, the preassembled complex eluted in higher molecular weight fractions, suggesting the formation of a ternary complex (Figure 3E; see arrow). The presence of MDH1 in the complex was identified by measuring NADH absorbance at 340 nm (Figure 3F). Further proof of the formation of HTC was obtained using SEC-MALS analysis of the PC, ME1 and MDH1 mixture. We resolved several complexes of calculated molecular mass of 1MDa, 590 kDa and 471 kDa, which correspond to the molecular mass of either: two tetramers of PC, two tetramers of ME1 and two dimers of MDH1 (1 MDa); or one tetramer of PC, one tetramer of ME1 and one dimer of MDH1 (590 kDa); or one tetramer of PC, one dimer of ME1 and one dimer of MDH1 (471 kDa), respectively (Figure 3G-H).

### HTC enzymes suppress senescence

To investigate whether HTC enzymes bypass the senescence response to STAT3 inactivation, we co-expressed PC, MDH1 and ME1 in IMR90 cells where STAT3 was depleted by shRNA. Strikingly, forced expression of HTC enzymes restored proliferation in cells depleted of STAT3 to the

level observed in cells expressing a control non-targeting shRNA, while significantly reducing the percentage of SA- $\beta$ -Gal positive cells (Figure 4A-B). Expression of HTC enzymes in STAT3-depleted cells reduced the expression of p53, p21, DNA damage response markers and PML bodies while increasing the mitosis marker phospho-H3<sup>Ser10</sup> and MCM6 (Figure 4C and Figure S6A-B). Moreover, expression of HTC enzymes in STAT3-depleted cells restored the NAD<sup>+</sup>/NADH ratio, increased cellular NADPH levels, the ratio of GSH/GSSG and decreased ROS relative to the control (Figures 4D-H and Figures S6C-H). Consistent with these results, the generation of NADPH by ME1 and ME2 was previously linked to ROS detoxification (Jiang et al., 2013). Together, these data suggest that HTC enzymes lead to metabolic reprogramming in STAT3-depleted cells to restore NAD<sup>+</sup> levels, increase NADPH which is paralleled by the suppression of senescent phenotype.

To monitor the effects of HTC enzymes overexpression on senescent cells metabolism, we performed <sup>13</sup>C<sub>6</sub>-glucose tracing. <sup>13</sup>C<sub>6</sub>-glucose flux into (m+3) pyruvate or (m+3) lactate was comparable between the cell lines but HTC enzymes overexpression significantly increased the conversion of pyruvate into OAA via PC as estimated from the (m+3)/(m+2) ratio of malate and aspartate (Figure 4I-K and S6I-J). This interpretation was further validated by the absence of an increase in succinate (m+3) (Figure S6J), ruling out that (m+3) isotopomers are generated by multiple rounds of the TCA cycle from (m+2) acetyl-CoA. In turn, the levels of citrate (m+2) were reduced in cells expressing the HTC enzymes, which is consistent with a decrease in the contribution of pyruvate to acetyl-CoA, as compared to its utilization by PC (Figure S6J). Tracing using 3-<sup>13</sup>C-glucose, confirmed an increase in m+1 metabolites in cells expressing HTC consistent with conversion of pyruvate into m+1 OAA and its derivatives (Figure S6K-L). Collectively, these findings suggest that pyruvate in HTC-overexpressing cells is preferentially converted to OAA via PC, which is subsequently used to replenish the TCA cycle and NAD<sup>+</sup> regeneration via MDH1. Together, these results show that the metabolic program of HTC-overexpressing cells is comparable to that observed in p53-disabled cells.

To determine the contribution of NADPH production by HTC to reduce ROS and bypass senescence we expressed ME1 in STAT3 depleted cells supplemented with malate. ME1/malate did not rescue these cells from senescence but was sufficient to decrease ROS levels (Figure S7A-D). In contrast, duroquinone prevented senescence after STAT3 depletion (Figure S7E), whereby ROS levels remain reduced upon combination of malate and duroquinone (Figure S7F-G). Finally, to determine whether the ability of HTC to form was important for the bypass of senescence we took advantage of the PC residues 1-534 that do not interact with MDH1 or ME1 (Figures 2J-K). This PC fragment failed to bypass senescence in STAT3 depleted cells when combined with ME1 and MDH1 (Figure S7H-J). Together, these results show that HTC enzymes

act in a complex that catalyzes  $\text{NAD}^+$  regeneration and NADPH production to reduce oxidative stress and bypass senescence.

### **HTC enzymes are essential to prevent senescence in transformed cells**

OIS protects normal cells from oncogenic stress (Serrano et al., 1997). In murine embryonic fibroblasts (MEFs) expression of HTC enzymes in combination with oncogenic RAS prevented senescence allowing colony formation despite maintaining an intact p53 pathway (Figure S8A-D). Also, HTC cooperated with RAS to induce tumor formation in mice (Figure 4L-M and S8E-G). Hematoxylin and eosin staining of tumor sections in conjunction with immunohistochemistry using specific antibodies revealed that HTC and RAS-induced tumors are similar to RAS-induced tumors in p53 null MEFs. This included abundant mitotic figures, increased nucleoli, more polynucleated cells and vascularisation (Figure 4P-Q and S8H).

It was reported that MDH1 inactivation decreased the  $\text{NAD}^+/\text{NADH}$  ratio leading to senescence (Lee et al., 2012). To determine whether other HTC enzymes also prevent senescence, we knocked down each HTC enzymes in IMR90 STAT3/p53-depleted cells. We found that reducing the expression of any HTC enzyme decreases the  $\text{NAD}^+/\text{NADH}$  ratio inducing proliferation arrest and senescence (Figure 5A-D). Knockdown of HTC enzymes also induced senescence (Figure 5E-I and S8I-R) and significantly reduced proliferation in a clonogenic assay (Figure 5J) in PC-3 cells. Interestingly, cells using glucose as a carbon and energy source can use the LDH reaction to supply part of the  $\text{NAD}^+$  required for glycolysis. However, many tumor cells use lactate as a carbon source (Faubert et al., 2017; Pertega-Gomes et al., 2014) and cannot use the LDH reaction to regenerate  $\text{NAD}^+$  (Figure 5K). Consistent with this idea, inactivation of HTC enzymes greatly suppressed proliferation of PC-3 cells grown on lactate (Figure 5L). Interestingly, LDH colocalizes with HTC in PC-3 cells grown on lactate (Figure 5M), a situation that facilitates  $\text{NAD}^+$  transfer from HTC to LDH. Together, the results indicate that HTC enzymes prevent senescence and contribute to malignant transformation.

### **HTC enzymes are highly expressed in prostate cancer**

Inactivation of *Stat3* and *Pten* in the prostate leads to tumorigenesis in mice (Pencik et al., 2015). This suggested that elevated expression of HTC enzymes may allow prostate epithelial cells to override senescence caused by STAT3 ablation. Therefore, we measured HTC enzymes in prostate samples from 19-weeks-old wild type (WT), *Stat3*<sup>-/-</sup>, Phosphatase and tensin homolog (*Pten*<sup>-/-</sup>) or *Stat3*<sup>-/-</sup>*Pten*<sup>-/-</sup> mice. Each of the three HTC enzymes was significantly upregulated in the *Stat3*<sup>-/-</sup>*Pten*<sup>-/-</sup> prostate tumors (Figure 6A-G). Interestingly, in *Pten*<sup>-/-</sup> tumors, the expression of the enzymes were also higher but this was mostly confined to Ki67 positive cells, which likely

already bypassed the senescence response to *Pten* abrogation (Figure 6B-C). PLA with PC and ME1 or PC and MDH1 antibodies confirmed colocalization of HTC enzymes in *Stat3<sup>-/-</sup>Pten<sup>-/-</sup>* tumors (Figure 6H-I). We also found high intensity staining for each of the HTC enzymes in more than 60% of human prostate adenocarcinomas, but low staining in normal prostates or prostates with benign prostatic hyperplasia (BPH) (Figure 6J-M). Together, these results suggest that HTC enzymes play a pivotal role in prostate cancer.

### **HTC suppresses both oncogene-induced senescence and replicative senescence in fibroblasts and rescues cells treated with complex I inhibitors**

We previously reported mitochondrial dysfunction (Moiseeva et al., 2009) and STAT3 depletion (Deschenes-Simard et al., 2013) upon OIS. Overexpression of HTC enzymes counteracted RAS-induced senescence in IMR90 cells (Figure S9A-B). Of note, these effects required simultaneous overexpression of all three HTC enzymes (Figure S9A-B). Moreover, deleting the mitochondrial localization signal from PC did not inhibit its ability to bypass OIS in combination with MDH1 and ME1 (Figure S9C-F), nor the capacity to restore a normal NAD<sup>+</sup>/NADH ratio (Figure S9G), which is consistent with an anti-senescence role for cytosolic PC. HTC also bypassed OIS in BJ fibroblasts more efficiently than in IMR90 (Figure S9H-J).

To investigate whether HTC can rescue cells that are already senescent, we induced OIS in MEFs using oncogenic RAS (Figure S10A-D). As expected, RAS-senescent cells are highly sensitive to the senolytic agent ABT-263 (Figure S10E). We infected the senescent cell population and control cells with lentiviral vectors expressing HTC. HTC was able to induce cell proliferation in RAS-senescent cells (Figure S10F). To investigate whether cells that proliferate were senescent and not a minor fraction of non-senescent cells in the population, we treated the cells with ABT-263 after infection. HTC-expressing RAS-cells were more sensitive to ABT-263 than controls as evaluated 24 h after treatment indicating that HTC is not immediately rescuing cells from senescence (Figure S10G). However, after seven days of recovery, RAS cells with HTC escaped from senescence (Figure S10H) while RAS cells with empty vectors remained senescent. Importantly, this escape from senescence was prevented when RAS-senescent cells were treated with ABT-263 (Figure S10H) indicating that HTC acts on senescent cells and not on a subpopulation of non-senescent cells. The expression of RAS and HTC enzymes was confirmed in cell extracts from individual clones that escaped senescence (Figure S10I). We did not succeed to promote proliferation in cultures of RAS-senescent IMR90 after infection with lentiviral vectors expressing HTC, but we did induce proliferation in RAS-senescent BJ human fibroblasts after infection with the same vectors (Figure S10J-N). This result is consistent with results showing that inactivation of

p53 and RB can reverse senescence in BJ but not in other strains of normal fibroblasts (Beausejour et al., 2003).

Although in the context of oncogene expression HTC may favor malignant transformation this complex may play an adaptive role. For example, in normal human fibroblasts, expression of HTC enzymes increased the  $\text{NAD}^+/\text{NADH}$  ratio and delayed replicative senescence (Figure 7A-F). Also, HTC enzymes rescued proliferation inhibition by complex I inhibitor Piericidin A (Figure 7G), suggesting that HTC may contribute to homeostatic adaptation to mitochondrial dysfunction. This may occur during oxygen deprivation. Hypoxia decreases mitochondrial respiration and rewires metabolism to limit excessive ROS production, inhibiting pyruvate entry into mitochondria and increasing glycolysis (Kim et al., 2006). In such contexts, HTC may contribute to metabolic reprogramming by supplying  $\text{NAD}^+$  for glycolysis and NADPH to avoid excessive ROS-mediated toxicity. Consistent with this idea, treatment of normal human fibroblasts with the hypoxia mimetic  $\text{CoCl}_2$  increased the fraction of PC localized to the cytosol where it can cooperate with MDH1 and ME1 in HTC (Figure 7H-I). Furthermore, incubation of IMR90 cells expressing oncogenic RAS in 1 % oxygen led to an increase HTC foci formation together with the induction of several hypoxia-regulated mRNAs compared to IMR90 RAS cells in normoxia (Figure 7J-L). Hypoxia bypasses Ras-induced senescence (Kilic Eren and Tabor, 2014), but depletion of HTC enzymes blocked this effect (Figure 7M-O). These results suggest that HTC may contribute to the senescence bypass observed in cells growing in hypoxic conditions (Parrinello et al., 2003).

#### 2.7.4. Discussion

We demonstrate that NAD metabolism alterations secondary to mitochondrial dysfunction can be compensated by a previously unrecognized metabolic cycle that transfers the hydride ion  $\text{H}^-$  from NADH to NADP, regenerating  $\text{NAD}^+$  and supplying NADPH for anabolism and redox defenses. This metabolic cycle is catalyzed by an enzyme complex formed by MDH1, ME1 and PC dubbed HTC. The net stoichiometry of the HTC cycle is:  $\text{ATP} + \text{NADH} + \text{NADP}^+ = \text{ADP} + \text{P}_i + \text{H}^+ + \text{NAD}^+ + \text{NADPH}$ . Hence, HTC represents a carbon saving strategy to regenerate  $\text{NAD}^+$  and produce NADPH at the expense of ATP. Interestingly, the reactions catalyzed by HTC seem to be confined in localized phase-separated cytosolic structures. Notwithstanding that MDH1, ME1 and PC co-immunoprecipitate from cells, it is likely that other proteins are also present in these structures. These foci may allow for a localized metabolic recycling of pyruvate, OAA and malate without affecting the cellular pool of these metabolites. In addition, the proximity of the active centers for each enzyme in the complex may accelerate metabolic flux by diffusion or the channeling of each substrate (Wheeldon et al., 2016).

Our data demonstrate that HTC plays a role in tumor formation by bypassing or promoting the escape from cellular senescence. Expression of HTC enzymes is sufficient to transform primary mouse fibroblasts in cooperation with oncogenic RAS and is therefore functionally equivalent to a loss of p53. Since HTC enzymes are repressed by p53, our work adds to evidence showing that controlling metabolism is a major tumor suppressor function of p53 (Moon et al., 2019; Morris et al., 2019). Of note, previous work showed that increasing antioxidant capacity by expressing G6PD can transform immortalized but non-tumorigenic fibroblasts (Zhang et al., 2021). HTC provides then two functions for transformation, immortalization dependent on NAD<sup>+</sup> regeneration and antioxidant activity dependent on NADPH generation. These functions are also important for the survival of cells in hypoxia, or for cells growing in lactate that cannot use the LDH reaction to regenerate NAD<sup>+</sup>.

We show that the expression of HTC enzymes and their interaction is increased in samples from prostate cancer patients. PC is also highly expressed in metastatic breast cancer (Shinde et al., 2018), non-small cell lung cancer, glioblastoma, renal carcinoma, and gallbladder cancer (Lao-On et al., 2018). MDH1 is amplified in multiple human cancers (Hanse et al., 2017) and MDH1 but not MDH2 is required for cell proliferation of tumor cell lines (Zhang et al., 2017). Moreover, ME1 expression is associated with poor prognosis in gastric cancer (Lu et al., 2018). Finally, analysis of co-expression of HTC enzymes in OncoPrint revealed positive correlations between HTC enzyme expression in several cancers including small squamous lung cancer and prostate cancer. Our results suggest that targeting HTC could be exploited to develop anti-cancer treatments.

### **Limitations of the Study**

We identified a cytosolic pool of the mitochondrial enzyme PC but the mechanisms responsible for PC relocalization to the cytosol upon p53 inactivation remain unknown. Even though, we were able to show evidence of HTC formation *in vitro*, the efficiency of complex assembly is relatively low. This suggests that the recombinant proteins may lack post-translational modifications that help stabilize the HTC complex. We provide evidence that PC, MDH1 and ME1 are the core of the HTC complex but we could not estimate their precise stoichiometry. Importantly, our data suggest that at least some HTC is contained in complexes larger than 1 MDa suggesting the presence of additional components. While future work is warranted to answer above questions, our present findings enrich the notion that tumor cells hijack specific metabolic pathways that support proliferation and anabolic reactions while conferring protection to oxidative stress.

### **Acknowledgments**

We thank M. Ali, D. Avizonis, M. Birlea, N. Chandel, P. Chartrand, L. Choiniere, N. Cyr, L. G. Dadwhal, P. Dagenais, DesGroseillers, D. Gagné, A. Gosselin, J. Hinsinger, P. Legault, S.W. Lowe, S. Meloche, H. Neubauer, J. Pascal, S. Roy, A. Salvail-Lacoste, N. Stifani, L. Tong, S. Truche, D. TrudeL and M. Vasseur for reagents, comments and/or technical help. Metabolic analysis was performed at The Rosalind and Morris Goodman Cancer Research Centre's Metabolomics Core Facility. Immunohistochemistry was performed at the IRIC's Histology Core Facility or the Molecular Pathology platform of CR-CHUM. We thank the Platform of microscopy of the Biochemistry and Molecular Medicine Department and the electron microscopy platform of the University of Montreal. A detailed list can be found on Mendeley as well as detailed author contributions.

### **Funding:**

Work was supported by grants from CIHR (MOP11151 and PJT-153217) and CCSRI Innovation 706773 to G.F., CIHR MOP130414 to J.G.O., and TFF Oncometabolism Team Grant 239585 to I.T. and M.P. G.F. is supported by the CIBC chair for breast cancer research. S.I. was supported by NSERC CREATE Trainee program and ICM (Institut du cancer de Montréal) Canderel fellowship. F.L. was supported by FRQS (Fonds de Recherche du Québec-Santé). D.P. is supported by a CIHR Postdoctoral Fellowship (MFE-171312). O.U. was supported from FRQS. J.P. was supported by Max Kade fellowship from the Austrian Academy of Sciences. I.T. is supported by FRQS Senior award. L.H. is supported by FRQS Junior 1 award. A.N. is supported by the Canadian Institutes of Health Research grant (CIHR MOP-110972) and is recipient of a Canada Research Chair in Calcified tissues, Biomaterials and Structural Imaging. E.T. acknowledges funding from CIHR (MOP-133726). L.K. was supported by the COMET Competence Center CBmed-Center for Biomarker Research in Medicine (FA791A0906.FFG). The COMET Competence Center CBmed is funded by the Austrian Federal Ministry for Transport, Innovation and Technology (BMVIT); the Austrian Federal Ministry for Digital and Economic Affairs (BMDW); Land Steiermark (Department 12, Business and Innovation); the Styrian Business Promotion Agency (SFG); and the Vienna Business Agency. The COMET program is executed by the FFG. L.K. was in addition funded by the FWF grant P26011 and the Christian Doppler Laboratory for Applied Metabolomics. The financial support by the Austrian Federal Ministry for Transport, Innovation and Technology and the National Foundation for Research, Technology and Development is gratefully acknowledged. R.M. was supported by grants SFB-F4707, SFB-F06107 and EU Transcan-2 consortium ERANET-PLL, all funded via the Austrian Science Funds.



**Authors contributions:**

Conceptualization, S.I. and G.F.; Validation, F.L., J.B., A.F., G.H., H.M.W. and V.B.; Methodology, J.Q., J.G., L.H., A.F., H.M.W. and J.P. ; Formal Analysis, S.I.; Investigation, S.I., F.L., O.U., A.F.R., J.B., M.C.R., S.L.P., J.Q, D.P., A.F., K.J.P., G.H., L.M., M.B., V.B. and L.H. ; Resources, E.G., L.K., R.M., A.N., J.G.O., I.T. and G.F. ; Data curation, S.I., O.U. and G.F.; Writing - Original Draft, S.I. and G.F. Writing - Review & Editing all authors Visualization S.I., M.L., P.K., V.B., Supervision, V.B., A.N., M.N.P, J.G.O., I.T. and G.F. Project Administration, V.B. and G.F. Funding Acquisition E.G., R.M., A.N., M.N.P, J.G.O., I.T. and G.F.

### **2.7.5. Main figures and supplementary figures**

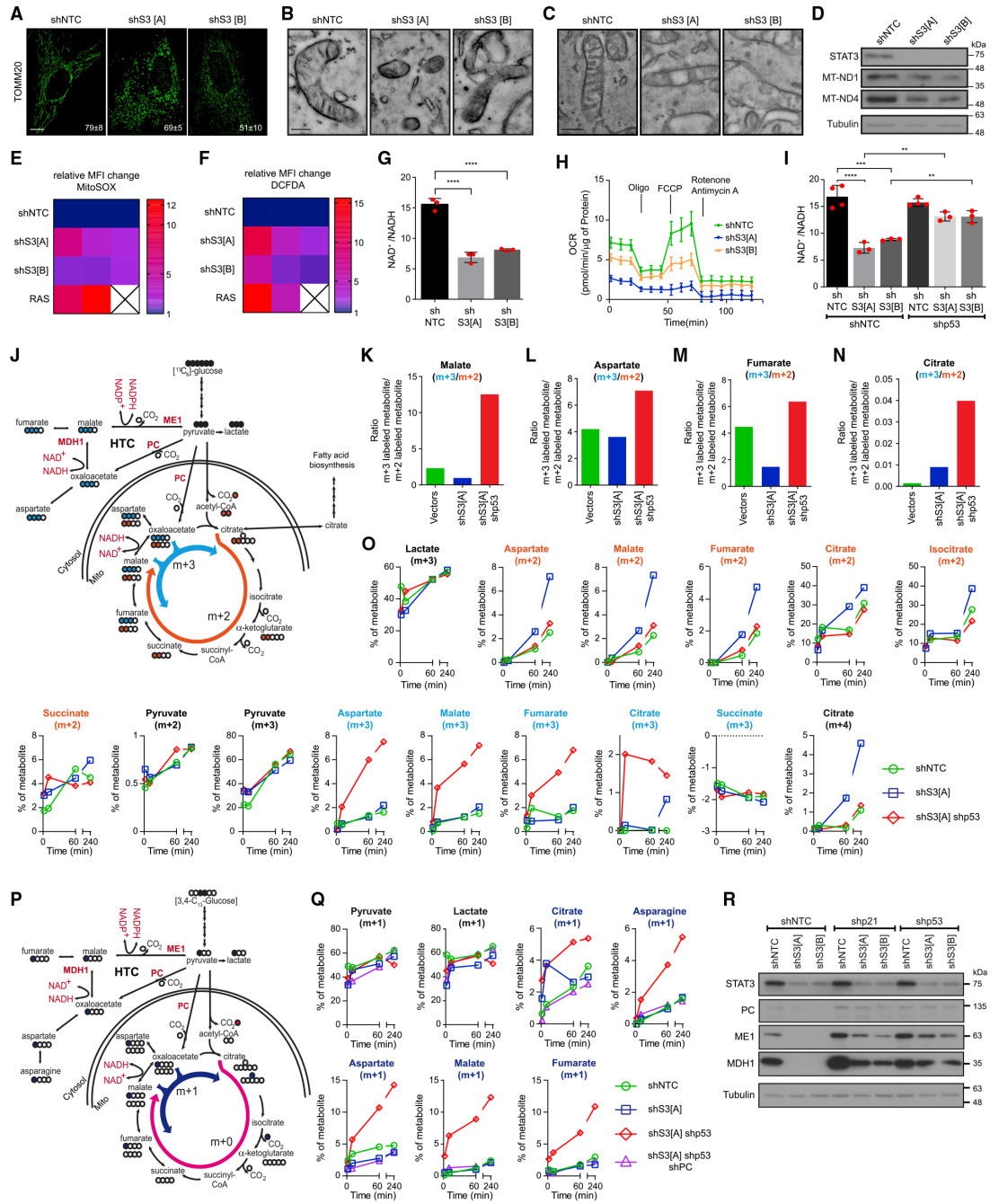


**Figure 1. p53 inactivation reprograms the metabolism of senescent cells with mitochondrial dysfunction**

(A) Immunofluorescence (IF) using anti-TOMM20 antibody in IMR90 cells expressing shRNAs against STAT3 (shS3[A]) and shS3[B] or a control non-targeting shRNA (shNTC). Mean % of staining pattern (tubular or puncta) of cells and standard deviation (SD) is shown in the lower right corner; scale, 10  $\mu$ m.

(legend continued on next page)

(B and C) Scanning transmission electron microscopy (STEM) micrographs (B) and transmission electron microscopy (TEM) (C) of cells as in (A); scale, 250 nm; n = 2.

(D) Western Blot (WB) of indicated proteins in cells as in (A).

(E and F) Heatmap of relative change over control cells in median fluorescent intensity (MFI) for MitoSOX (E) or DCFDA (F) in cells as in (A) and cells expressing oncogenic RAS. Each column represents a biological replicate with a minimum of 10,000 cells, n = 2–3.

(G) NAD<sup>+</sup>/NADH ratio in cells as in (A).

(H) Oxygen consumption rate (OCR) of cells as in (A); n = 4–6, error bars show SEM (standard error of the mean).

(I) Mean NAD<sup>+</sup>/NADH ratio in cells expressing a control shRNA (shNTC) or a shRNA against STAT3 (shS3[A], shS3[B]) in combination with an shRNA against p53 (shp53) or non-target control shRNA (shNTC).

(J) Model of regeneration of NAD<sup>+</sup> by MDH1, ME1 and PC plus schematic of metabolite <sup>13</sup>C labeling patterns after labeling with <sup>13</sup>C<sub>6</sub>-glucose. <sup>13</sup>C are noted by filled circles. Orange cycle is the forward direction of TCA cycle giving (m+2) intermediates (orange-filled circles). Light-blue cycle starts with pyruvate carboxylase (PC) and is characterized by (m+3) intermediates (light-blue-filled circles). HTC, hydride transfer complex; mito, mitochondria.

(K–N) Ratio of (m+3)/(m+2) isotopomers for the indicated metabolites in IMR90 cells expressing a control shRNA (shNTC), a shRNA against STAT3 (shS3[A]) alone or in combination with an shRNA against p53 (shp53). Ratios were calculated 10 min post-labeling.

(O) Amount of indicated labeled intermediates over time measured by GC-MS relative to the total amount of each related metabolite for IMR90 cells as in (K). Data show representative experiment.

(P) Model of PC activity labeling pattern with <sup>13</sup>C-[3,4]-glucose. <sup>13</sup>C-[3,4]-glucose is converted into <sup>13</sup>C-[1]-pyruvate. Each intermediate generated via PDH is not labeled (magenta cycle), while in the PC reaction-labeled carbon is maintained (m+1, dark-blue cycle), filled circles show heavy carbon. HTC, hydride transfer complex; mito, mitochondria.

(Q) Amount of indicated labeled intermediates over time measured by GC-MS relative to the total amount of each related metabolite for IMR90 cells expressing a control shRNA (shNTC), a shRNA against STAT3 (shS3[A]) alone or in combination with an shRNA against p53 (shp53), and/or a shRNA against PC (shPC). Data show representative experiment of n = 2.

(R) WB for the indicated proteins in IMR90 cells expressing a control shRNA (shNTC) or shRNAs against STAT3 (shS3[A] and shS3[B]) together with control shRNA (shNTC) or shRNAs against p53 (shp53) or p21 (shp21).

Experiments other than indicated are from n = 3 biological replicates. (A–D, O, Q–R) show representative images. ANOVA with multiple comparison test (G and I). Mean ± SD for (G and I) with red dots as biological values and mean for (K–N). For (K–O), conditions shNTC and shS3[A] are the same as in [Figures 4J](#) and [4K](#). Related to [Figures S1–S3](#).

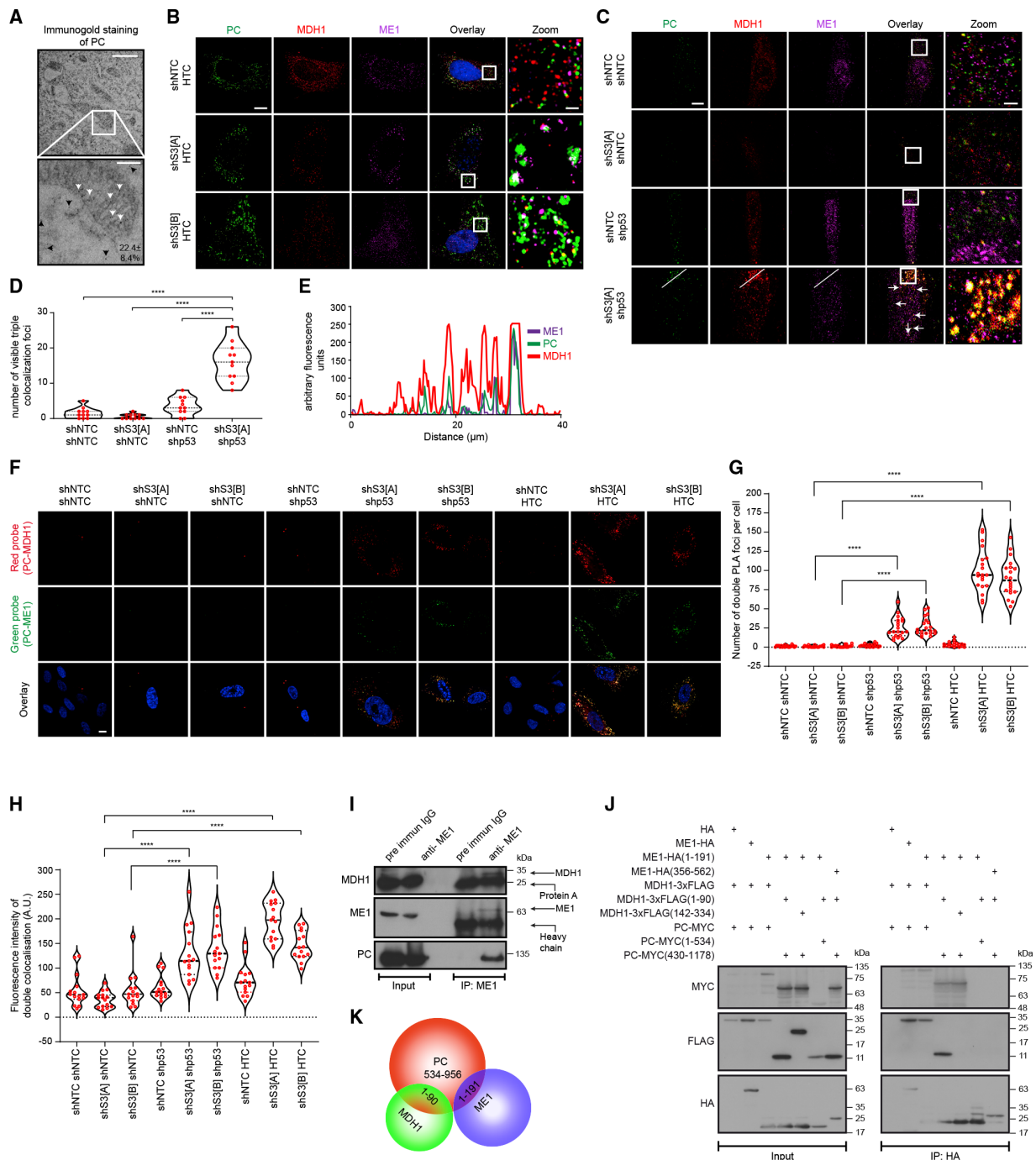


**Figure 2. Colocalization and interactions of the enzymes that catalyze the hydride transfer reactions**

(A) TEM of PC-3 cells stained with anti-PC antibody followed by immunogold labeling. White arrows: mitochondrial PC. Black arrows: cytosolic PC. Scales: top, 800 nm; bottom, 200 nm. Lower corner shows the percentage of cytosolic PC and SD of a count of 18 representative fields.

(B) IF with super-resolution microscope for the indicated enzymes (MDH1, ME1, and PC) expressed in IMR90 cells depleted for STAT3 (shS3[A], shS3[B]) or STAT3 sufficient cells (shNTC). PC (green), MDH1 (red), and ME1 (magenta), triple colocalization in white. DAPI was used to stain the nucleus. Scale, 10  $\mu$ m; zoom scale, 1  $\mu$ m.

(C) Colocalization of endogenous MDH1, ME1, and PC in IMR90 cells expressing shRNAs against STAT3 (shS3[A]) and p53 (shp53) and/or control shRNA (shNTC). Scale, 20  $\mu$ m; zoom scale, 2  $\mu$ m. Triple colocalization in white.

---

(D) Quantification of triple colocalization foci (white foci) per cells as in (C), N=11.

(E) Fluorescence intensity of ME1 (magenta), MDH1 (red), and PC (green) in shS3[A]/shp53-expressing cells. Colocalization was measured across the indicated line in (C) and represented as arbitrary fluorescence units for each enzyme.

(F) Proximity ligation assay with two PLA probes to specifically reveal PC interaction with ME1 or with MDH1. PLA probes used are PLA green (ME1 PC) and PLA red (MDH1 PC) on IMR90 infected with either control shRNA (shNTC) or shRNA against STAT3 (shS3[A], shS3[B]) and shRNA against p53 or control shRNA or HTC enzymes (MDH1, ME1, PC). Scale, 10  $\mu$ m. DAPI was used to stain the nucleus. Colocalization of PLA probe green and red is shown in yellow in overlay, n = 2–3.

(G) Count of PLA foci from cells in (F), N=20.

(H) Fluorescence signal intensity of foci in cells in (F), N=15.

(I) IP of endogenous ME1 from HuH-7 cells followed by WB for all HTC enzymes.

(J) IP with HA beads in 293T cells expressing the indicated variants of PC-MYC, MDH1-3x-FLAG and ME1-HA, or control HA vector. IP was followed by WB against indicated proteins.

(K) Schematic of interaction between regions 1–90 of MDH1 and 1–191 ME1 with 534–956 of PC.

A minimum of 3 biological replicates unless indicated. ANOVA with Tukey (G and H) or Dunnett (D) for multiple comparisons, asterisks represent p values for most important comparisons. Related to [Figures S4](#) and [S5](#).

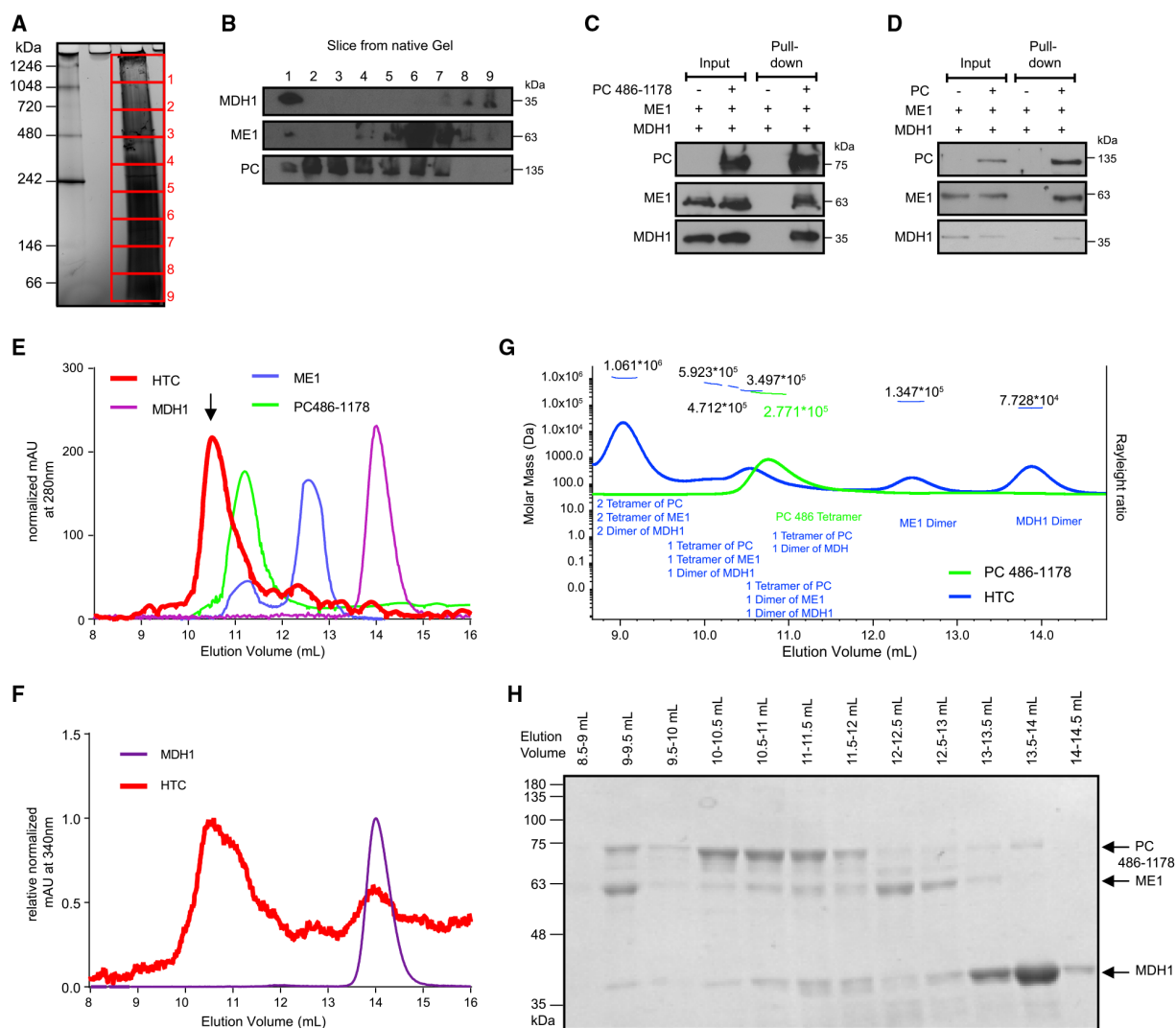
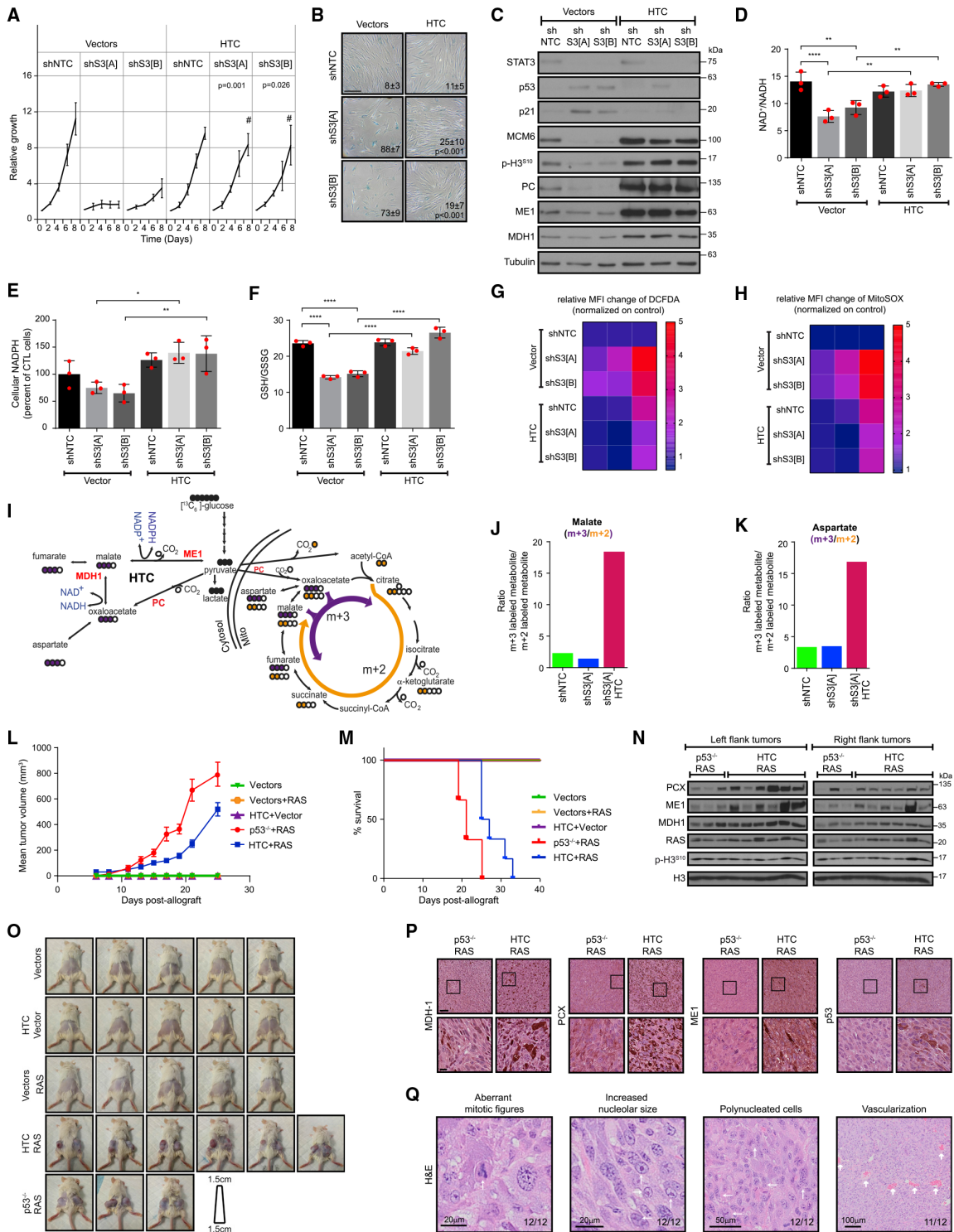


**Figure 3. Biophysical characterization of the hydride transfer complex**

(A and B) Two-dimensional blue native/SDS gel electrophoresis (2D-BN/SDS-PAGE). Coomassie G-250 staining of BN-PAGE (A) with indicated protein sizes corresponding to collected gel slices (red squares) and immunoblots (B) for the indicated proteins performed on gel slices from (A) migrated on SDS-PAGE. (C and D) *In vitro* assembly of the hydride transfer complex (HTC) with purified PC(486-1178) (C) or full-length PC (D). Mono-Avidin pull-down of biotinylated PC after *in vitro* assembly followed by immunoblotting against the indicated proteins. (E) Size-exclusion chromatography (SEC) with either the individual purified proteins or the pre-assembled HTC (fractions 8–12 mL of the assembly) run on a Superdex 200 Increase column. Data show absorbance at 280 nm. Arrow indicates elution peak of assembled complex. (F) Same SEC experiment as in (E) but with the absorbance at 340 nm (NADH absorbance) normalized relative to either MDH1 or the pre-assembled HTC. (G) SEC-MALS (multi-angle light scattering) of purified PC (486-1178) (green) or all fraction of previously assembled HTC (blue). The calculated molecular weight is shown above each peak and possible complexes are indicated below. (H) SDS-PAGE of collected fractions following the SEC-MALS experiment (G) stained with Coomassie Blue to show the purity and assembly of the complexes. For (A–H) representative images of a minimum of 3 replicates. Related to [Figure S5](#).



(legend on next page)



**Figure 4. Expression of the hydride transfer complex enzymes bypasses senescence and promotes transformation**

(A) Relative proliferation of IMR90 expressing shSTAT3 (shS3[A] and shS3[B]) or control shRNA (shNTC) with co-expression of control vectors or the HTC enzymes MDH1, ME1, and PC. # indicates time point used for statistical test.

(B–H) Analysis of cells as in (A).

(B) SA- $\beta$ -Gal staining; percent positive cells  $\pm$  SD is shown in lower corner; scale bar, 250  $\mu$ m.

(C) WB for the indicated proteins.

(D) NAD<sup>+</sup>/NADH ratio.

(E) Total NADPH.

(F) Ratio of GSH/GSSG. Individual levels of NAD, NADH, NADP, GSSG, and GSH can be found in [Figure S6](#).

(G and H) Heat maps of flow cytometry data measuring DCFDA (G) or MitoSOX (H). Data show relative change of median fluorescence intensity (MFI) over control cells. Each column represents a biological replicate with a minimum of 10,000 cells.

(I) Scheme of metabolite <sup>13</sup>C labeling patterns after incubation with <sup>13</sup>C<sub>6</sub>-glucose. Orange cycle is normal direction of tricarboxylic acid (TCA) giving (m+2) intermediates (orange-filled circles). Violet cycle represents the PC pathway giving (m+3) intermediates (violet-filled circles). HTC, hydride transfer complex; mito, mitochondria.

(J and K) Ratio of (m+3)/(m+2) isotopomers for the indicated metabolites from IMR90 cells expressing a control shRNA with control vectors (shNTC), or expressing a shRNA against STAT3 with either control vectors (shS3[A]) or with vectors expressing HTC enzymes (shS3[A]/HTC). Conditions shNTC and shS3[A] are the same as in [Figures 1K–1O](#).

(L) Mean tumor volume from NRG mice after allograft injection of  $1 \times 10^6$  MEFs into both flanks expressing either controls (Vectors), HTC enzymes (HTC), or RAS alone or with HTC overexpression (RAS + HTC). MEFs p53<sup>-/-</sup> overexpressing RAS were used as a positive control (RAS + p53<sup>-/-</sup>), n = 3–6. Data are shown until mice bearing tumors from RAS + p53<sup>-/-</sup> MEFs were all sacrificed.

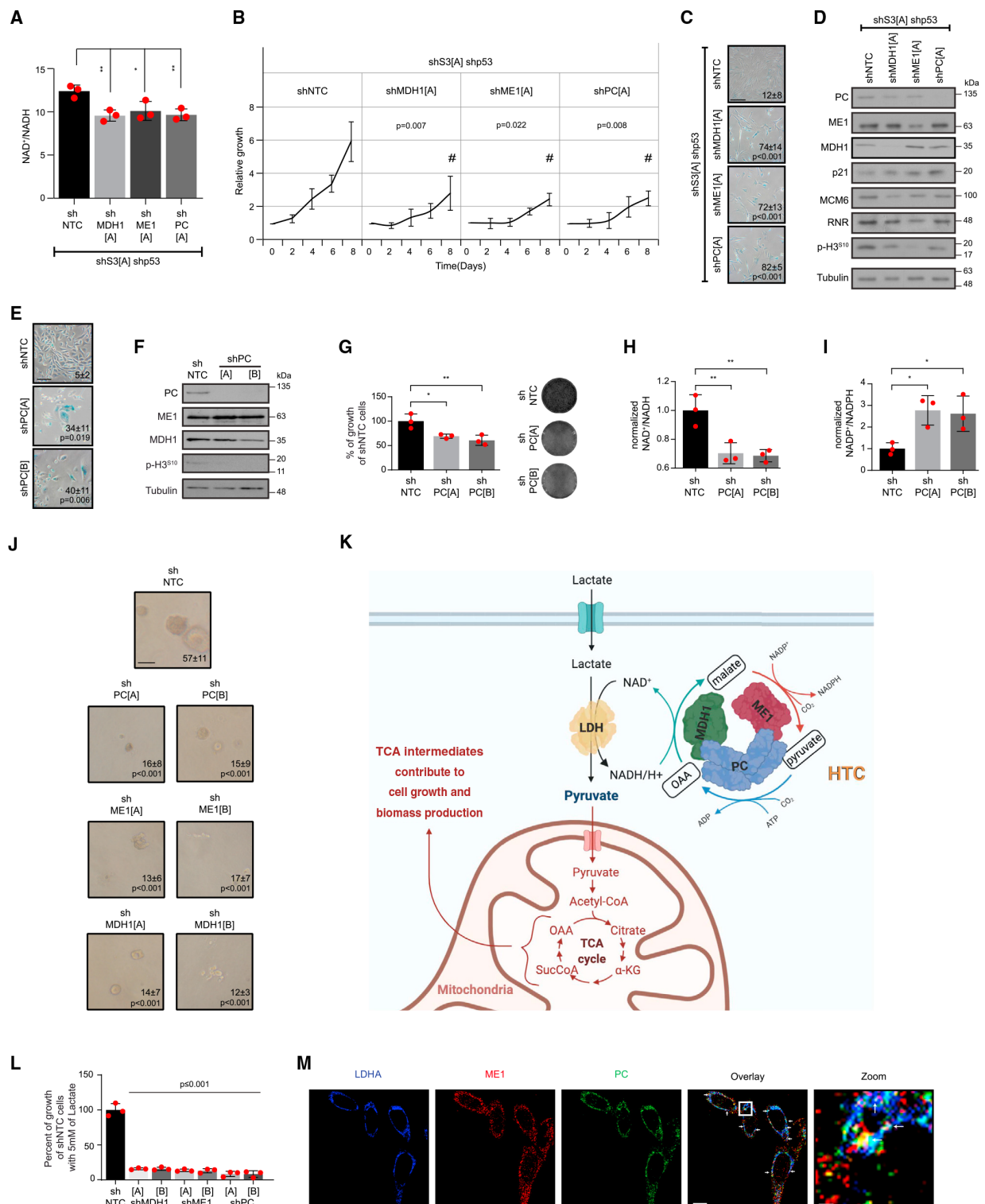
(M) Survival of NRG mice as in (L), n = 3–6.

(N) WB against indicated proteins from tumors shown in (L).

(O) Images of all mice the day of sacrifice after injection of MEFs as in (L).

(P) Immunohistochemistry with indicated antibodies on tumors from (L); scale, 100  $\mu$ m and zoom scale, 20  $\mu$ m.

(Q) Representative H&E images of indicated aberrations in tumors from MEFs expressing RAS and HTC. The numbers represent the frequency of observations. All experiments other than indicated have been repeated a minimum of 3 times. Mean  $\pm$  SD for (A, B, and D–F). Mean  $\pm$  SEM for (L), red dots represent biological value of each replicate (D–F). Two-tailed Student's t test (A) or ANOVA (B and D–F) with Šidák's multiple comparisons test was performed and p value is indicated. Related to [Figures S6–S8](#).



(legend on next page)

---

**Figure 5. Inhibition of the HTC triggers senescence**

(A) Mean NAD<sup>+</sup>/NADH ratio in IMR90 cells expressing shRNAs against STAT3 and p53 (shS3[A] shp53) and either a control shRNA (shNTC) or shRNAs against MDH1 (shMDH1[A]), ME1 (shME1[A]), or PC (shPC[A]).

(B–D) Analysis of cells as in (A).

(B) Relative proliferation, # indicates timepoint used for statistical test.

(C) SA-β-Gal staining; scale, 250 μm, and mean percentage ± SD of SA-β-gal positive cells.

(D) WB of indicated proteins.

(E–I), Inactivation of HTC by shRNAs against PC in PC3 cells. SA-β-Gal staining, scale, 100 μm (E); WB (F); normalized proliferation on shNTC cells with an image of a representative well (G); normalized NAD<sup>+</sup>/NADH ratio (H); and normalized NADP<sup>+</sup>/NADPH ratio (I) of PC-3 cells expressing either a control shRNA (shNTC) or shRNAs against (PC: shPC[A] and shPC[B]). The shNTC control is the same as in [Figures S8L–S8R](#).

(J) Images of clonogenic collagen assays on cells as in (E–I); scale, 200 μm.

(K) Schematic representation of NAD requirements for cells growing on lactate.

(L) PC-3 cells with indicated shRNA were grown on 5 mM Lactate and proliferation was normalized on proliferation of control shNTC cells.

(M) IF of PC-3 cells grown in 5 mM lactate showing triple colocalization indicated in white by white arrows of LDHA (blue), PC (green), and ME1 (red). Scale, 10 μm and zoom scale, 1 μm; representative image from 20 cells analyzed from same biological replicate.

All experiments are of 3 biological replicates. Significance was assessed with ANOVA with Dunnett's test. Related to [Figure S8](#).



---

(H) Proximity ligation assay with green (ME1-PC) and red (MDH1-PC) PLA probes on mouse prostate samples with either WT genotype or double knockout of *Stat3* and *Pten*. In the overlay, the white arrows indicate double colocalization of PLA probes green and PLA probes red; scale, 25  $\mu\text{m}$ .

(I) Quantification of PLA colocalization. 100 cells were counted and amount of double colocalization is shown; two-tailed t test to assess significance is indicated,  $n = 4$  mice.

(J-L) IHC images of prostate tissue microarray with indicated antibodies. Images are serial images (prostate adenocarcinoma  $n = 49$ , normal  $n = 3$ , BPH  $n = 20$ ); scale, 100  $\mu\text{m}$  and zoom scale, 10  $\mu\text{m}$ .

(M) Quantification of (J-L) according to scoring key of levels of ME1, MDH1, and PC from random prostate epithelial regions per sample.

(A-E, H, and J-L) show representative images. Mann-Whitney statistical U test was performed to assess significance for (F-G and M).

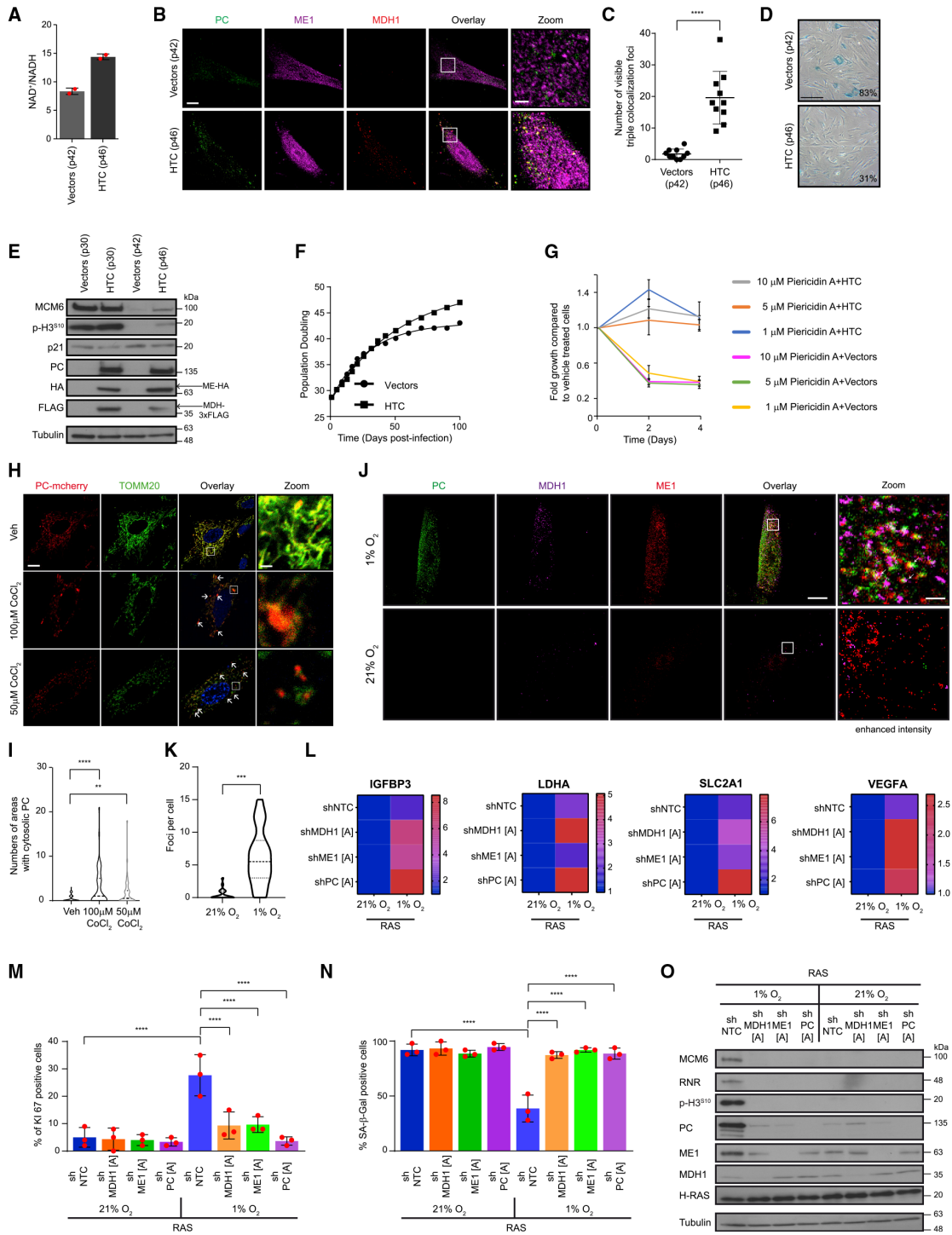


**Figure 7. HTC enzymes extend lifespan of normal cells and prevent the action of mitochondrial poisons**

(A) Mean NAD<sup>+</sup>/NADH ratio in IMR90 cells expressing HTC enzymes (MDH1-3xFLAG, ME1-HA, and PC) or control vectors and grown until replicative senescence for Vector cells (p42). Biological replicate measures are shown in red dots, error bars represent SD.

(legend continued on next page)

- 
- (B) IF of cells as in (A) using antibodies for each HTC enzyme as indicated. Scale, 20  $\mu\text{m}$ ; zoom scale, 2  $\mu\text{m}$ .
- (C) Quantification of foci observed in (B). Number of foci was counted in 10 different cells, and statistics were done using a two-tailed t test.
- (D) SA- $\beta$ -Gal staining on cells as in (A); percent of positive cells is indicated at the bottom right; scale, 250  $\mu\text{m}$ .
- (E) WB for the indicated proteins in early or late passage cells expressing HTC or an empty vector,  $n = 2$  for (A, B, D, and E).
- (F) Population doubling of cells as in (A). A trendline was added with the linear regression function of Graph Pad, image represents one biological replicate.
- (G) Relative fold proliferation of cells expressing HTC enzymes (MDH1, ME1, and PC) or control vectors, treated with indicated concentrations of Piericidin A. Data are normalized to the growth of vehicle-treated cells and show a representative image of  $n = 3$ .
- (H) IF of IMR90 cells expressing PC-cherry treated with indicated amounts of  $\text{CoCl}_2$ . An anti-TOMM20 (green) antibody was used to reveal mitochondria,  $n = 2$ ; scale, 10  $\mu\text{m}$ , zoom, 1  $\mu\text{m}$ .
- (I) Quantification of PC-cherry signal outside of mitochondria from cells as in (H). A minimum of 25 cells were counted per slide. The violin plot represents the amount of PC-cherry signal outside of mitochondria of two independent immunofluorescent slides. A two-tailed t test was performed.
- (J) IF of IMR90 cells expressing RAS cultured in 21% oxygen or 1% oxygen using antibodies for each HTC enzyme as indicated. Scale, 20  $\mu\text{m}$ ; zoom scale, 2  $\mu\text{m}$ .
- (K) Quantification of HTC foci in cells as in (J). Dashed lines represent median and quartiles. A two-tailed t test was performed.
- (L) Heat maps of relative mRNA levels for indicated genes of IMR90 infected with RAS and shRNAs against MDH1, ME1, or PC or control vector (shNTC) followed by either incubation of cells in 21% oxygen or 1% oxygen,  $n = 2-3$ .
- (M and N) Percent of KI67 positive cells (M) and SA- $\beta$ -Gal positive cells (N) in cells as (L). Red dots represent biological value of each replicate. Statistical analysis was done with ANOVA with Dunnett's test.
- (O) WB for the indicated proteins in cells as in (L).

**Molecular Cell, Volume 81**

**Supplemental information**

**A Hydride transfer complex reprograms NAD metabolism and bypass senescence**

Sebastian Igelmann, Frédéric Lessard, Oro Uchenunu, Jacob Bouchard, Ana Fernandez- Ruiz, Marie-Camille Rowell, Stéphane Lopes-Paciencia, David Papadopoli, Aurélien Fouillen, Katia Julissa Ponce, Geneviève Huot, Lian Mignacca, Mehdi Benfdil, Paloma Kalegari, Haytham M. Wahba, Jan Pencik, Nhung Vuong, Jordan Quenneville, Jordan Guillon, Véronique Bourdeau, Laura Hulea, Etienne Gagnon, Lukas Kenner, Richard Moriggl, Antonio Nanci, Michael N. Pollak, James G. Omichinski, Ivan Topisirovic, and Gerardo Ferbeyre



### Supplementary figures legends

#### Supplementary Fig S1. Knockdown of STAT3 induces cellular senescence in human fibroblasts, Related to Fig 1.

**A**, Relative mRNA level of STAT3 in IMR90 cells following knockdown of STAT3 by two independent shRNAs (shS3[A], shS3[B]) or a control non-targeting shRNA (shNTC) represented as mean of biological replicates (red dots) relative to shNTC control cells, error bars indicate SEM.

**B**, Relative proliferation of cells as in (A) (day 0 corresponds to day 10 post-infection) data show the mean of biological replicates and error bars show SD.

**C**, SA- $\beta$ -Gal staining on cells as in (A), three times 50 cells were counted, and the mean % and SD of SA- $\beta$ -Gal positive cells is shown at the bottom-right of each panel, scale= 250  $\mu$ m.

**D**, Immunoblots of indicated proteins in cells as in (A) , p-p53<sup>S15</sup>: p53 phosphorylated on Serine 15, p-RB<sup>S795</sup>: RB phosphorylated on Serine 795, p-H3<sup>S10</sup>: H3 phosphorylated on Serine 10.

**E**, Immunofluorescence of cells as in (A) using anti-PML antibody, BF= bright field, scale = 10  $\mu$ m.

**F**, Quantification of PML bodies from (E) in percent of cells with indicated amount of PML foci, mean percentage and SD is represented.

**G**, Immunofluorescence of cells as in (A) for DNA damage foci using anti  $\gamma$ -H2A.X or anti-53BP1 antibodies, scale = 10  $\mu$ m.

**H**, Quantification of DNA damage foci from (G) represented by percent of cells with indicated amount of DNA damage foci, mean percentage and SD is presented.

**I**, Total NADx (NAD<sup>+</sup> and NADH), NADH and NAD<sup>+</sup> levels in cells as in (A), mean percentage relative to control (CTL) cells and SD is presented and red dots indicated biological replicates.

The values correspond to ratios in Fig. 1G.

**J**, Immunofluorescence with anti-FLAG antibody counterstained with MitoTracker Deep Red and DAPI on cells expressing a shRNA against STAT3 (shS3[A]) and either a control vector (Vector) or a tagged STAT3 variant which is insensitive to the shRNA and is targeted to mitochondria (Mito-iSTAT3-3xFLAG). Scale = 10  $\mu$ m, n = 2.

**K**, Relative proliferation of cells expressing either a control shRNA (shNTC) or a shRNA against STAT3 (shS3[A]) and either a control vector (Vector) or a tagged STAT3 variant insensitive to the shRNA and targeted to mitochondria (Mito-iSTAT3-3xFLAG). Data show the mean of biological replicates and error bars show SD.

**L**, SA- $\beta$ -Gal staining on cells as in (K). Three times 50 cells were counted, and the % and SD of SA- $\beta$ -Gal positive cells is shown at the bottom-right of each panel, scale = 250  $\mu$ m.

**M**, NAD<sup>+</sup>/NADH ratio in cells as in (K). Red dots indicate biological values, and error bars are SD.

**N**, Immunoblots for indicated proteins from cells as in (K), p-H3<sup>S10</sup>: H3 phosphorylated on Serine 10.

**O**, Immunoblot for the indicated proteins on mitochondrial pulldowns (using anti-HA antibodies) from cells with expression of a control vector (Vector) or the tagged Major Outer Membrane Protein 25 fused to GFP (3xHA-GFP-OMP25). Cells were forced into senescence by oncogenic RAS (OIS) and compared to non-senescent cells expressing a control vector, n = 2.

**P and S**, Proximity ligation assay on proliferating young (Y) IMR90, replicative senescence (RS) IMR90, IMR90 cells expressing oncogenic RAS (RAS) or control vector (V) with antibodies against STAT3 and ATAD3A. PLA signal is shown in green and DAPI shows nucleus, scale = 10  $\mu$ m, n = 2.

**Q and T**, Count of PLA foci from cells in (P and S) per condition, black bar indicates mean of 20 counted areas and each circle represents individual counts.

**R and U**, Arbitrary fluorescence units of fluorescence signal intensity in cells of (P and S). In total 50 region of interest (ROI) were analyzed and are represented by colored circles; black bar represents mean.

Experiments other than indicated are from n = 3 biological replicates. Two tailed Student's t-test for (**B, K**) ANOVA with multiple comparison for (**A, C, I, L, M, Q, R, T, U**) and p-value is indicated. For growth curves, a t-test was performed at the last time point indicated by #. (**C-E, G, J, L, N, O, P, S**) show representative images.

**Supplementary Fig S2. Restoration of NAD<sup>+</sup>/NADH ratio bypasses senescence after STAT3-depletion in IMR90 fibroblasts, Related to Fig 1.**

**A**, Immunofluorescence for co-localization of NDI1(yeast complex I)-mCherry with anti-TOMM20 antibody (counterstained with DAPI) of IMR90 cells revealed by super-resolution structured illumination microscopy, scale = 10  $\mu$ m, n = 2.

**B**, Relative proliferation and SA- $\beta$ -Gal of IMR90 cells expressing NDI1-3xFLAG or control vector (Vector) after knockdown of STAT3 by two independent shRNAs (shS3[A], shS3[B]) or a control non-targeting shRNA (shNTC). Data show the mean of biological replicates and error bars show SD. For SA- $\beta$ -Gal staining a minimum of three times 50 cells were counted, the % and SD of SA- $\beta$ -Gal positive cells is shown.

**C**, Immunoblots of the indicated proteins in cells as in (B), p-H3<sup>S10</sup>: phosphorylated H3 on serine 10, p-p53<sup>S15</sup>: phosphorylated p53 on serine 15.

**D-E**, Heat maps of flow cytometry data measuring DCFDA (**D**) or MitoSOX (**E**) on cells as in (B). Data show relative change of median fluorescence intensity (MFI) over control cells. Each column represents a replicate with a minimum of 10,000 cells.

**F**, Mean  $\text{NAD}^+/\text{NADH}$  ratio in cells as in (B), independent biological measures shown in red dots, error bars represent SD.

**G**, Relative proliferation of IMR90 cells with supplementation of 2 mM pyruvate (Pyr) or vehicle (Veh) after knockdown of STAT3 by two independent shRNAs (shS3[A], shS3[B]) or a control shRNA (shNTC), data show the mean of biological replicates and error bars show SD.

**H**, SA- $\beta$ -Gal staining on cells as in (G), three times 50 cells were counted, the mean % and SD of SA- $\beta$ -Gal positive cells is shown in the lower right corner, scale = 250  $\mu\text{m}$ .

**I**, Representative immunoblots for the indicated proteins in cells as in (G), p-H3<sup>S10</sup>: phosphorylated H3 on serine 10.

**J**, Immunofluorescence of cells as in (G), using anti- $\gamma$ -H2A.X and anti-53BP1 antibodies. DNA was counterstained with DAPI, scale = 10  $\mu\text{m}$ .

**K**, Quantification of % of cells and SD according to the amount of foci per cells from (J).

**L**, Mean  $\text{NAD}^+/\text{NADH}$  ratio in cells as in (G), independent biological measures are shown in red dots, error bars represent SD.

**M**, Mean  $\text{NAD}^+/\text{NADH}$  ratio in IMR90 cells supplemented with 5  $\mu\text{M}$  Duroquinone (Duro) or vehicle (Veh) after knockdown of STAT3 by two independent shRNAs (shS3[A], shS3[B]) or expression of a control shRNA (shNTC), independent biological measures are shown in red dots, error bars represent SD.

**N-P**, Normalized values in percent of control (CTL) cells of cellular NADH (**N**),  $\text{NAD}^+$  (**O**) and  $\text{NAD}_x$  (total  $\text{NAD}^+$  and NADH) (**P**) for cells as in (M).

**Q**, Relative proliferation of cells as in (M), data show the mean of biological replicates and error bars show SD.

**R**, SA- $\beta$ -Gal staining on cells as in (M), three times 50 cells were counted, the mean percentage and SD of SA- $\beta$ -Gal positive cells is shown in the lower right corner, scale = 250  $\mu$ m,

**S**, Immunoblots for the indicated proteins in cells as in (M), p-H3<sup>S10</sup>: H3 phosphorylated on Serine 10.

**T**, Relative proliferation of IMR90 fibroblasts expressing either control shRNA(shNTC) or shRNA against STAT3 (shS3[A], shS3[B]) and empty vector (Vector) or cytoplasmic LBNOX-3xFLAG protein (LBNOX), data show the mean of biological replicates and error bars show SD.

**U**, SA- $\beta$ -Gal staining on cells as in (T), three times 50 cells were counted, the mean percentage and SD of SA- $\beta$ -Gal positive cells is shown in the lower right corner, scale = 250  $\mu$ m.

**V**, Immunoblots for the indicated proteins in cells as in (T), p-H3<sup>S10</sup>: H3 phosphorylated on Serine 10.

**W**, Mean NAD<sup>+</sup>/NADH ratio in IMR90 cells as in (T), independent biological measures are shown in red dots, error bars represent SD.

Experiments other than indicated are from n = 3 biological replicates. Two-tailed Student's t-test for (**B**, **G**, **Q**, **T**) or ANOVA with multiple comparison for (**F**, **H**, **L-P**, **R**, **U**, **W**) and p-value is indicated. For growth curve last day of growth curve was used to perform t-test indicated by #. (**A**, **C**, **H-J**, **R**, **S**, **U**, **V**) show representative images. For (**G-L**) the control samples (Veh, shNTC, Veh shS3[A] and Veh shS3[B] are the same as in (Figure S3 B-F).

**Supplementary Fig S3. Effects of aspartate supplementation and p53 inactivation on shSTAT3-induced senescence, Related to Fig 1.**

**A,** Cells depleted for STAT3 had reduced levels of aspartate, nucleotide precursors and nucleotides. Relative amount of indicated metabolites in cells expressing a non-targeting control shRNA (shNTC) or a shRNA against STAT3 (shS3[A]). Media was supplemented with 20 mM aspartate (Asp) or vehicle (Veh) every two days, error bars represent SD and independent biological measures are shown in red dots, n = 5. Supplementing STAT3-depleted cells with 20 mM aspartate rescued the levels of nucleotide precursors and all ribonucleotides except for deoxynucleotides.

**B,** Aspartate only moderately rescued the proliferation defects after STAT3-depletion. Relative proliferation of IMR90 cells expressing two independent shRNAs against STAT3 (shS3[A], shS3[B]) or a control shRNA (shNTC) and treated with either vehicle (Veh) or 20 mM aspartate (Asp), data show the mean of biological replicates and error bars show SD, n = 5.

**C,** Aspartate did not restore the NAD<sup>+</sup>/NADH ratio. Mean NAD<sup>+</sup>/NADH ratio in cells as in (B). Independent biological measures shown in red dots, error bars represent SD.

**D,** SA-β-Gal staining on cells as in (B), a minimum of three times 50 cells were counted and the mean percentage and SD of SA-β-Gal positive cells is shown in the lower right corner, scale = 250 μm.

**E,** Immunofluorescence images of cells as in (B) with anti-γ-H2A.X, anti-53BP1 antibodies and DAPI as a DNA counterstain, scale = 10 μm.

**F,** Quantification of the percentage of cells with indicated number of γ-H2A.X and 53BP1 foci from (E), error bars represent SD.

**G,** Model to explain the effects of aspartate supplementation on nucleotide levels and senescence. Aspartate does not affect the NAD<sup>+</sup>/NADH ratio and NADH can activate p53, which represses ribonucleotide reductase (RNR) and inhibits deoxynucleotide synthesis. Accumulation of NADH

has been shown to prevent the proteasome-dependent degradation of p53 (Asher et al., 2005) and inhibits MDM2 via CtBP (Birts et al., 2020). The resulting p53 activation can then inhibit the synthesis of deoxynucleotides via p21/RB dependent repression of Ribonucleotide Reductase (RNR) expression (Chabes et al., 2004).

**H**, Relative proliferation of IMR90 cells depleted of STAT3 with two shRNAs (shS3[A] and shS3[B]) or control cells expressing a non-targeting shRNA (shNTC) after inactivation of p21 by shRNA (shp21) or p53 (shp53) compared to a control shRNA (shNTC). Data show the mean of biological replicates and error bars show SD.

**I**, Immunoblots of indicated proteins in cells as in (H). p-H3<sup>S10</sup>: phosphorylated H3 on serine 10.

**J**, SA-β-Gal staining on cells as in (H), mean and SD of SA-β-Gal positive cells is shown in the lower right corner from three counts of at least 50 cells, scale = 250 μm.

**K**, Immunofluorescence of cells as in (H) using anti-γ-H2A.X and anti-PML antibodies. DNA was counterstained with DAPI, scale = 10 μm.

**L-M**, Quantification of foci from (K) as percentage of cells with indicated amount of PML bodies and DNA damage foci, n = 2.

Experiments other than indicated are from n = 3 biological replicates. Two-tailed Student's t-test for (A, B, H) and ANOVA for (C, D, J) and p-value is indicated. For growth curve last day of growth curve was used to perform t-test indicated by #. (D, E, I-K) show representative images. For (B-F) the control samples (Veh, shNTC, Veh shS3[A] and Veh shS3[B]) are the same as in (Figure S2 G-L) for 3 replicates .

**Supplementary Fig S4. Malate Dehydrogenase, Malic Enzyme and Pyruvate Carboxylase regulation in senescent and tumor cells, Related to Figs 1 and 2.**

**A**, Representation of genomic regions of MDH1, ME1 and PC using UCSC genome browser with GRCh37/hg19 build. Genes are depicted with blue hatched lines (introns) and full blue rectangles (exons). Different transcriptional variants are shown. Identified p53 ChIP-seq in green comes from 41 ChIP-seq data sets. Sequences were found in at least two independent studies. For positions and binding for other p53 and E2F bindings (light blue), positions were extracted from ChIP-Atlas and from UCSC genome Browser using ENCODE. H3K27Ac Mark (Associated with Regulatory elements; red) was extracted using ENCODE. Promoter regions are indicated in pink as in Gene Cards TSS v4.14 and the EPDnewNC human version. \* denote ChIP signal found in Fibroblasts; ‡ denote ChIP signal found in data sets studying cellular senescence. † denote known gene enhancer regions binding.

**B-C**, Immunoblots of the indicated proteins in different senescence models in IMR90 cells: STAT3-depletion induced senescence (B) with two independent shRNAs against STAT3 (shS3[A] and shS3[B]) versus the control expressing a non-targeting shRNA (shNTC), n = 3, and (C) replicative senescence (RS) versus younger cells passages (Y), n = 3. S4B and S1D come from the same experiment.

**D**, Immunoblots for pyruvate carboxylase (PC), mitochondrial electron transport proteins (OxPhos) and cytochrome c after purification of mitochondria and remaining soluble fraction (cytoplasm/ nuclear proteins) from cell extracts of PC-3 cells, n = 2.

**E**, Immunoblots for PC and Tubulin after infection of PC-3 cells with either a shRNA against PC (shPC[A]) or a non-targeted shRNA (shNTC) to verify that the lower molecular weight protein bands were indeed PC isoforms as they disappeared upon PC knockdown, n = 3.



**F**, Confocal immunofluorescence in IMR90 cells expressing MYC-tagged PC (PC-MYC) showing some PC signal that does not colocalize with mitochondrial TOMM20, scale = 10  $\mu\text{m}$ , zoom scale = 2  $\mu\text{m}$ , n = 3.

**G**, Confocal immunofluorescence against indicated proteins in IMR90 cells expressing shSTAT3 and MDH1, PC and ME1 co-stained with MitoTracker Deep Red. MDH1 (shown in blue), PC (shown in green) and ME1 (shown in red) along with MitoTracker Deep Red (shown in turquoise), double colocalization is shown in yellow (PC, ME1), violet (ME1, MDH1) or orange (PC, MDH1) and triple colocalization (MDH1, ME1, PC) is shown in white. White colocalization areas are outside of mitochondria, scale = 10  $\mu\text{m}$ , zoom scale = 1  $\mu\text{m}$ , n = 2.

**H**, Confocal immunofluorescence against indicated proteins in IMR90 cells expressing shSTAT3 and MDH1, PC and ME1 treated with either 1,6-Hexanediol (Hexanediol) or Vehicle (Veh), scale = 10  $\mu\text{m}$ , n = 2.

**I**, Amount of triple colocalization foci per cells from cells as in (H), Analysis of ten cells from two independent experiments. ANOVA with multiple comparison test was performed and p-value is indicated.

(**B-H**) show representative images of biological replicates.

**Supplementary Fig S5. Interactions between HTC enzymes and their biophysical properties, Related to Figs 2 and 3.**

**A-C**, Immunoprecipitations (IP) of 3xFLAG or MDH1-3xFLAG (**A**), IP of 3xFLAG or PC-3xFLAG (**B**) or IP of HA or ME1-HA (**C**), from extracts of 293T cells expressing the indicated vectors followed by WB against the indicated proteins.

**D**, IP of endogenous ME1 in PC-3 cells followed by WB against PC, MDH1 and ME1. ME1 WB was done with the same antibody used for immunoprecipitation thus showing IgG.

**E-F**, Avidin pull-down followed by WB analysis against indicated proteins in PC-3 cells (E) or HuH-7 cells (F) infected with either control shRNA (shNTC) or an shRNA against pyruvate carboxylase (shPC[A]), n = 2.

**G**, IP of MDH1-3xFLAG from extracts of HEK293T cells expressing also ME1-HA and the indicated variants of MYC-tagged PC followed by immunoblots against the indicated proteins, n = 3.

**H**, IP of MDH1-3xFLAG from extracts of HEK293T cells expressing PC-MYC, ME1-HA and the indicated variants of MDH1 followed by immunoblots against the indicated proteins, n = 3.

**I**, IP of HA alone or the indicated variants of HA-ME1 from extracts of HEK293T cells also expressing MDH1-3xFLAG, PC-MYC and treated with 20  $\mu$ M of MG132 for 6 h followed by immunoblots against the indicated proteins, n = 3.

**J**, Summary of the IP results in (G-I).

**K**, Elution profiles of the indicated proteins after size-exclusion chromatography (SEC) as recorded by measuring absorbance at 280 nm. Results were obtained with the same purification shown in Fig. 3.

**L**, Coomassie Blue staining of indicated purified proteins after SEC as in (K).

**M**, SEC-MALS of indicated purified proteins showing mass determination by MALS (multi-angle light scattering) and  $\Delta$ RI ( $\Delta$  refractive index) of each protein. Results shown for PC 486-1178 represent the same experiment as shown in Figure 3G.

**Supplementary Fig S6. Expression of Hydride Transfer Complex enzymes reestablishes the NAD<sup>+</sup>/NADH ratio and bypasses senescence, Related to Fig 4.**

**A,** Immunofluorescence of STAT3-depleted IMR90 cells with two independent shRNAs (shS3[A] and shS3[B]) or control shRNA (shNTC) and with co-expression of control vectors or the HTC enzymes MDH1, ME1 and PC. DNA damage foci were visualized using anti- $\gamma$ -H2A.X antibody and PML nuclear bodies with anti-PML antibody, scale = 10  $\mu$ m.

**B,** Quantification of PML bodies and  $\gamma$ -H2A.X foci from (A) in percent of cells with indicated amount of foci, mean percentage and SD are represented.

**C,** Relative levels versus control (CTL) of NADP in cells with the same conditions as in (A), showing biological triplicate (red dots), error bars represent SD.

**D-E,** Relative levels versus control (CTL) of NAD (D) and NADH (E) in cells as in (C). Red dots present biological replicates and error bars the SD.

**F-H,** Relative levels of GSSG (F), GSH (G) or total glutathione (H) in cells as in (C).

**I,** Scheme of metabolite <sup>13</sup>C labeling patterns after incubation with <sup>13</sup>C<sub>6</sub>-glucose. Red cycle denotes the forward direction of the TCA cycle yielding (m+2) intermediates (with red-filled circles). Blue cycle represents the Pyruvate Carboxylase (PC) pathway and is characterized by (m+3) intermediates (with blue-filled circles). HTC: hydride transfer complex, Mito: mitochondria.

**J,** Mean amount and SEM of indicated labeled intermediates overtime after incubation with <sup>13</sup>C<sub>6</sub>-glucose from IMR90 cells expressing a control shRNA with control vectors (shNTC/Vectors), cells expressing a shRNA against STAT3 with either control vectors or with vectors expressing HTC enzymes: MDH1, ME1 and PC (shS3[A]/HTC). This experiment was done simultaneously with the one in Fig 1K-O and Fig 4 J-K.

**K**, Model of pyruvate carboxylase activity labeling pattern with  $^{13}\text{C}$ -[3]-glucose.  $^{13}\text{C}$ -[3]-glucose is converted into  $^{13}\text{C}$ -[1]-pyruvate. In the PDH reaction, labeled carbon is lost and each intermediate generated via PDH is not labeled (magenta cycle). In the PC reaction, labeled carbon is maintained and each intermediate is m+1 (green cycle), filled circles show labelled carbon. Heavy carbon is eventually lost in the forward TCA from isocitrate to  $\alpha$ -ketoglutarate.

**L**, Amount of indicated labeled intermediates over time measured by GC-MS relative to the total amount of each related metabolite for IMR90 cells expressing a control shRNA (shNTC), a shRNA against STAT3 (shS3[A]) alone or in combination with expression of HTC (MDH1, ME1 and PC). Data shows one experiment n = 1.

All experiments other than indicates are from three independent biological replicates, and statistical significance was calculated using ANOVA (**C-H**) or Student's t-test (**J**). Values from C-H are from the same experiments then shown in Figure 4 D-F

**Supplementary Fig S7. Roles of NAD<sup>+</sup> and NADPH in cells expressing the Hydride Transfer Complex, Related to Fig 4.**

**A**, Growth curve of IMR90 expressing control vector (V) or ME1 protein (ME1) and control shRNA (shNTC) or shRNA against STAT3 (shS3[A]). Cells were treated every 48h with either vehicle (Veh) or 1 mM dimethylmalate (Malate). Data show mean of three independent experiments with SD for the error bars. shS3[A] + HTC was used as positive control for senescence bypass.

**B**, SA- $\beta$ -Gal staining on cells as in (A), mean and SD of SA- $\beta$ -Gal positive cells is shown in the lower right corner from three counts of at least 50 cells, scale = 250  $\mu\text{m}$ .

shS3[A] + HTC was used as positive control for senescence bypass.

**C-D**, Heat maps of flow cytometry data measuring DCFDA (**C**) or MitoSOX (**D**). Data show relative change of median fluorescence intensity (MFI) over control cells in cells as in (A). Each row represents a replicate with a minimum of 10.000 cells  $n = 4$ . For statistical analysis one-way ANOVA with Dunnett correction was performed for shS3[A] against other conditions. † show relevant significant result  $p \leq 0.01$  for DCFDA and  $p \leq 0.05$  for MitoSOX.

**E**, Growth curve of IMR90 cells expressing control shRNA(shNTC) or shRNA against STAT3(shS3[A], or shS3[B]). Cells were treated every 48h with Vehicle (Veh) or either 5  $\mu$ M Duroquinone (Duro) or 1 mM dimethylmalate (Malate) or both (Duro-Malate). Mean value of SA- $\beta$ -Gal, SD and p-value of relevant t-test are shown below.

**F-G**, Heat maps of flow cytometry data measuring DCFDA (**F**) or MitoSOX (**G**). Data show relative change of median fluorescence intensity (MFI) over control cells in cells as in (E). Each row represents a replicate with a minimum of 10.000 cells  $n = 3$ . For statistical analysis one-way ANOVA with Dunnett correction was performed for shS3[A] against corresponding shRNA with treatment and shS3[B] against corresponding shRNA with treatment. † show relevant significant results.

**H**, WB for the indicated proteins from STAT3-depleted IMR90 cells with shRNAs (shS3[A] and shS3[B]) or control shRNA (shNTC) with co-expression of HTC enzymes MDH1, ME1 and PC(1-534) fragment. Expression of full-length PC with MDH1, ME1 and shS3[A] was used as positive control,  $n = 2$ . p-H3<sup>S10</sup>: phosphorylated H3 on serine 10. RNR is ribonucleotide reductase.

**I**, Relative proliferation of cells as in (H).

**J**, SA- $\beta$ -Gal staining on cells as in (H).

Experiments other than indicated are from  $n = 3$  biological replicates. **B, H, J** representative images. For growth curves last day of growth curve was used to perform t-test indicated by # comparing shRNA+Veh to corresponding shRNA with treatment.

**Supplementary Fig S8. Expression of Hydride Transfer Complex bypasses RAS-induced senescence in MEFs and induces transformation, Related to Figs 4 and 5.**

**A**, Immunoblots of indicated proteins in MEFs expressing a control Vector or RAS and HTC enzymes (MDH1, ME1 and PC) or control vector.

**B**, Colony assay of MEFs as in (A).

**C**, SA- $\beta$ -Gal staining quantification on MEFs as in (A). A minimum of 100 cells were counted per condition in three different petri dishes and mean percentage and SD of positive SA- $\beta$ -Gal staining is shown.

**D**, QPCR for p53 targets in MEF cells expressing RAS and the three HTC enzymes (21 days post-infection, same MEFs used for the injection in NRG mice in Fig. 5O-P and following panels) and treated with vehicle (Veh) control or 300 ng/ml Doxorubicin for 24 h,  $n = 1$ . Data shows mean of technical triplicate and SD show error bars.

**E**, Images of resected tumors obtained in NRG mice the day of sacrifice after injection of MEFs expressing either controls (Vectors), HTC enzymes (HTC), RAS or RAS with HTC enzymes (RAS + HTC),  $p53^{-/-}$  MEFs overexpressing RAS were used as a positive control of tumor formation (RAS +  $p53^{-/-}$ ).

**F-G**, Tumor volume (F) and mass (G) from tumors shown in (E). Mean value on day of sacrifice with SD is shown, individual measures are shown as red dots.

**H**, Number of mitosis per 10 high power fields (10HPF) observed in (Figure 4Q) as an indication of aggressiveness.

**I-R**, Inactivation of HTC in PC3 cells. SA- $\beta$ -Gal staining (**I**, **N**), WB (**J**, **O**), normalized proliferation on shNTC cells with an image of a representative well (**K**, **P**), NAD<sup>+</sup>/NADH ratio normalized over control (shNTC cells), (**L**, **Q**) and NADP<sup>+</sup>/NADPH ratio normalized over control (shNTC cells) (**M**, **R**) of PC-3 cells expressing either a control shRNA (shNTC) or shRNAs against the HTC enzymes (ME1: shME1[A] and shME1[B], MDH1: shMDH1[A] or shMDH1[B]). For SA- $\beta$ -Gal staining, scale = 100  $\mu$ m. SA- $\beta$ -Gal and Immunoblots were done with the same shNTC control.

**Supplementary Fig S9. Expression of Hydride Transfer Complex bypasses RAS-induced senescence in human cells, Related to Fig 4.**

**A**, Relative proliferation and SA- $\beta$ -Gal of IMR90 cells expressing either oncogenic RAS or control Vector and a combination of two or all three HTC enzymes: ME1, MDH1 and PC. Each proliferation data point represents the mean of biological replicates and error bars show SD. # indicates data point used for statistical analysis. For SA- $\beta$ -Gal staining the mean and SD of three different experiments is shown. Minimum of 100 cells were counted per condition.

**B**, Immunoblots against the indicated proteins from cells as in (A), p-H3<sup>S10</sup>: phosphorylated H3 on serine 10.

**C**, Localization of PC (magenta), TOMM20 (red) and MYC tag (green) in control (CTL) cells and cells expressing PC-MYC or PC-MYC without mitochondrial localization signal ( $\Delta$ MitoPC-MYC), scale = 10  $\mu$ m.

**D-E**, Relative proliferation and SA- $\beta$ -Gal of IMR90 cells expressing a control Vector or oncogenic RAS with co-expression of MDH1-3xFLAG, ME1-HA and  $\Delta$ MitoPC-MYC (MYC tagged PC with a deletion of the mitochondrial localization signal) or a control Vector. Each proliferation

data point represents the mean of biological replicates and error bars show the SD. For SA- $\beta$ -Gal staining mean and SD of three different experiment is shown. A minimum of 50 cells were counted per condition.

**F**, Representative immunoblots against the indicated proteins from cells as in (D), p-H3<sup>S10</sup>: phosphorylated H3 on serine 10.

**G**, NAD<sup>+</sup>/NADH ratio of cells as in (D) showing mean of triplicate and red dots show biological replicates, error bars represent SD.

**H**, Representative immunoblots against the indicated proteins from BJ cells infected with oncogenic RAS (R) or control vector (V) and with MDH1-3xFLAG, ME1-HA and PC (HTC) or control vectors (Vectors), p-H3<sup>S10</sup>: phosphorylated H3 on serine 10.

**I**, Relative proliferation of cells as in (H).

**J**, SA- $\beta$ -Gal of cells as in (H).

**A, D, I**, two tailed Student's t test. **E, G and J**, ANOVA with Dunnett.

**Supplementary Fig S10. Hydride Transfer Complex reverses cellular senescence, Related to Fig 4.**

**A**, Schematics on experimental design of senescent MEFs infected with HTC. MEFs were infected with oncogenic RAS or control vector. Cells were then maintained until senescence was established at day 7 post-infection and then the senescent MEFs were either infected with two lentiviral vectors expressing GFP and mCherry (Vectors) generating RAS VV cells or with GFP-T2A-MDH1-P2A-ME1 and mCherry-T2A-PC generating RAS HTC MEF cells. As control MEF cells previously infected with Vector were infected with the same vectors generating MEF V HTC or MEF V VV cells.



**B**, Relative growth of MEF cells infected with either control vector (Vector) shown in green or oncogenic RAS (RAS), shown in blue. Last time point of control MEFs is shown in light green as cells became confluent, p-value is indicated on top of timepoint used for assessment of statistical significance.

**C**, Representative immunoblots against the indicated proteins from MEFs as in (B) at day 7 post-infection with oncogenic RAS.

**D**, SA- $\beta$ -Gal of cells as in (B) at day 7 post-infection. Data shows mean percentage and SD of replicates from a count of a minimum of 50 cells per condition.

**E**, Senolytic treatment of cells as in (B). Data shows mean survival of cells after 24h of 2.5  $\mu$ M ABT-263 treatment.

**F**, Relative growth of cells as MEFs expressing oncogenic RAS and reinfected with either control vectors (Vector) shown in blue or MDH1-P2A-ME1 and PC (HTC) shown in orange.

**G**, Change of cell numbers in percent 24h after senolytic treatment of cells with RAS or control vector that were reinfected at day 8 post RAS infection with control vectors (Vectors) or MDH1-P2A-ME1 and PC (HTC). Data shows mean with SEM and red dots show biological replicate. Data is normalized to number of cells prior to 2.5  $\mu$ M ABT-263 treatment. Significance was assessed using ANOVA with multiple comparisons and the Tukey test. Relevant comparisons are shown.

**H**, Change of cell numbers in percent after senolytic treatment for 24h and 7 Days of recovery. Data show mean of biological triplicates with SEM. Red dots show biological replicates. Data is normalized to the number of cells prior to 2.5  $\mu$ M ABT-263 treatment. Significance was assessed with ANOVA and the Tukey test. Relevant comparisons are shown.

**I**, WB with protein extracts from MEF clones isolated from cells as in (F) after they bypassed senescence.

**J**, Schematics on experimental design of senescent BJ cells infected with HTC. BJ cells were infected with oncogenic RAS or control vector. Cells were then maintained until senescence was established at day 7 post-infection and then the senescent BJ cells were either infected by spin infection with two lentiviral vector expressing GFP and mCherry (Vectors) generating RAS VV cells or BJ cells were infected with GFP-T2A-MDH1-P2A-ME1 and mCherry-T2A-PC generating RAS HTC BJ cells.

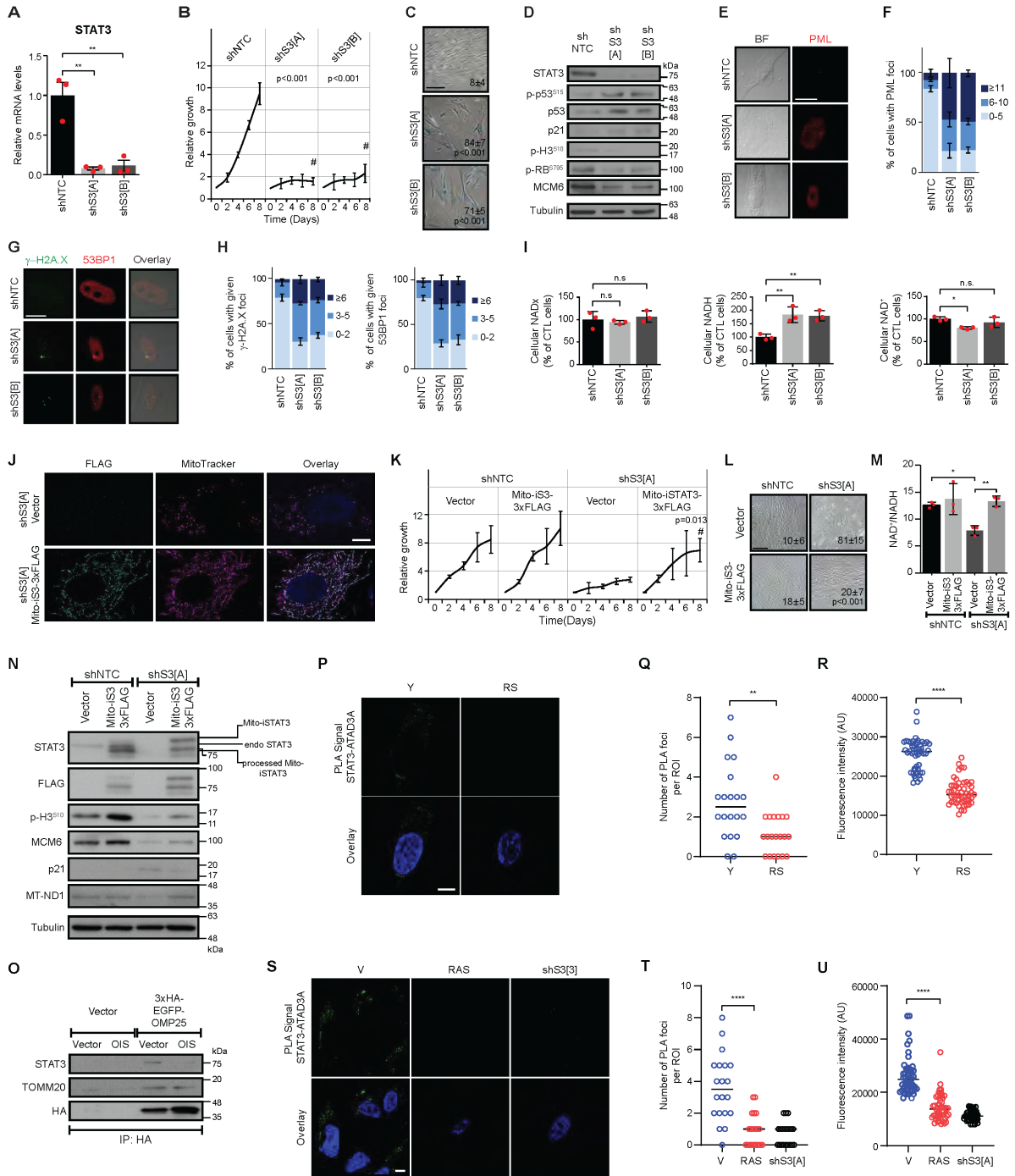
**K**, Representative immunoblots against the indicated proteins from BJ cells infected with oncogenic RAS (RAS) or control vector (Vector) at day 7 post-infection with oncogenic RAS.

**L**, SA- $\beta$ -Gal of cells as in (K) at day 7 post-infection.

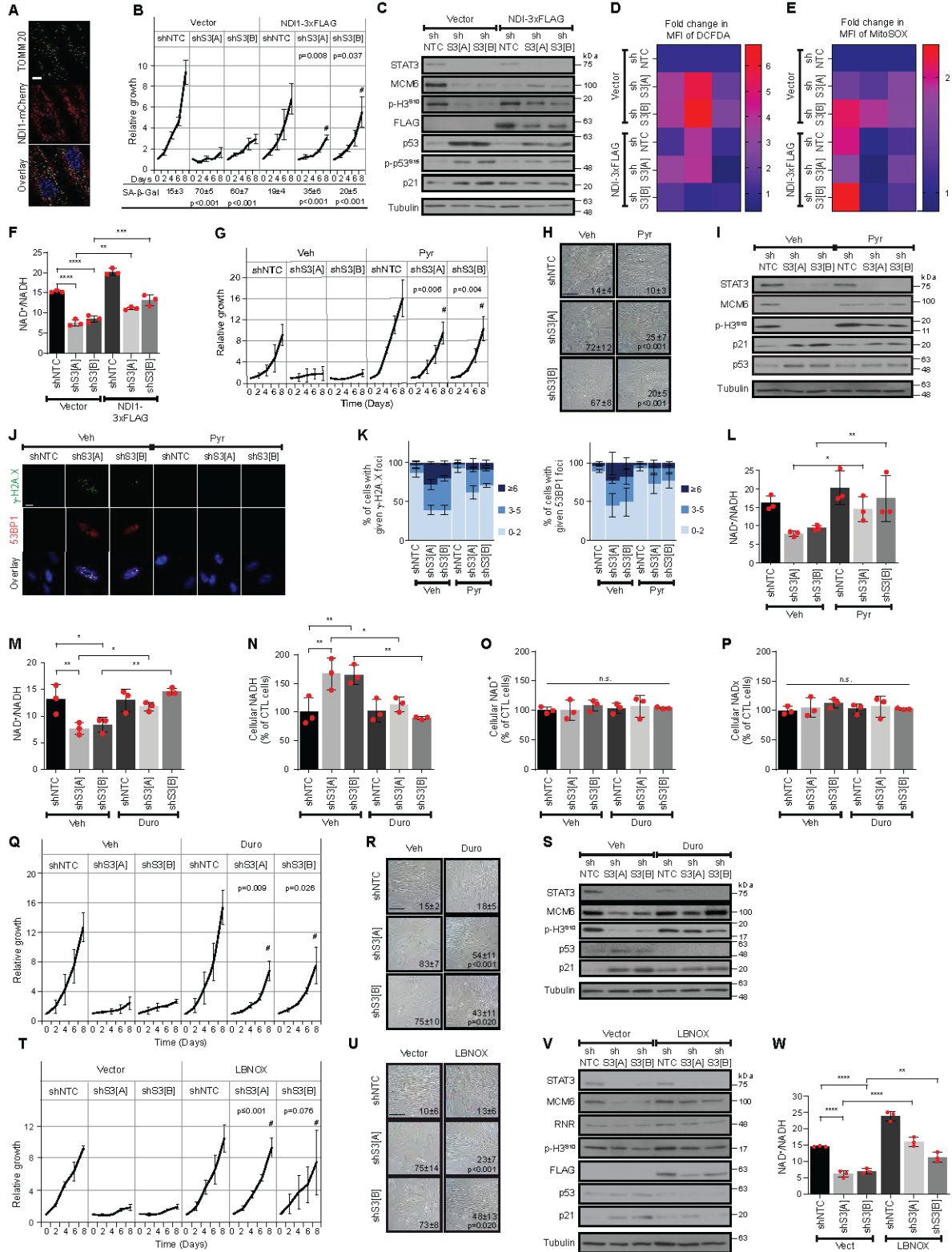
**M**, Relative growth of BJ RAS VV cells (shown in blue) and BJ RAS HTC (shown in red).

**N**, SA- $\beta$ -Gal of cells as in (M) at day 14 post HTC infection.

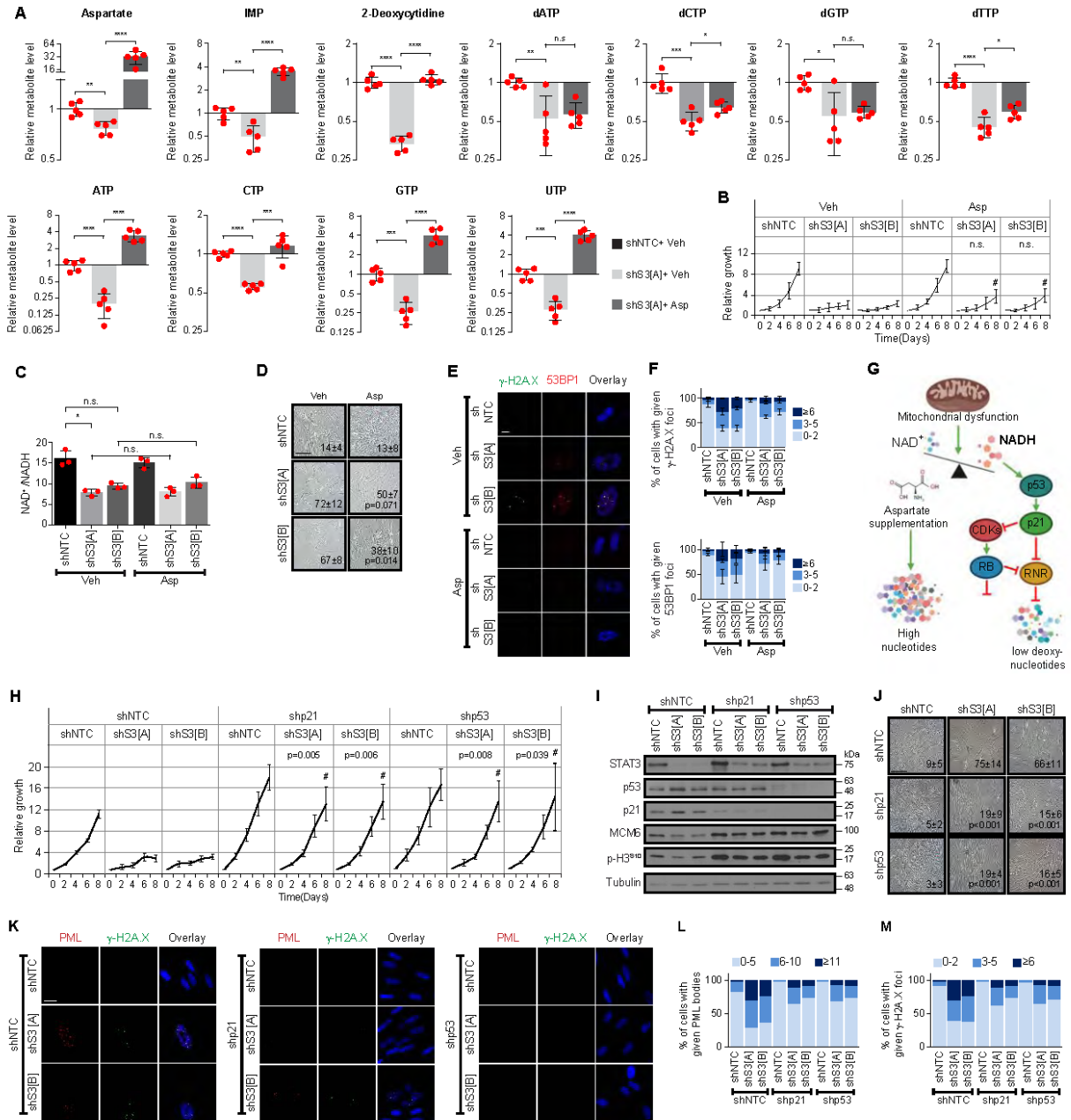
Experiments other than indicated are from  $n = 3$  biological replicates and significance was calculated with a two-tailed Student's t-test.



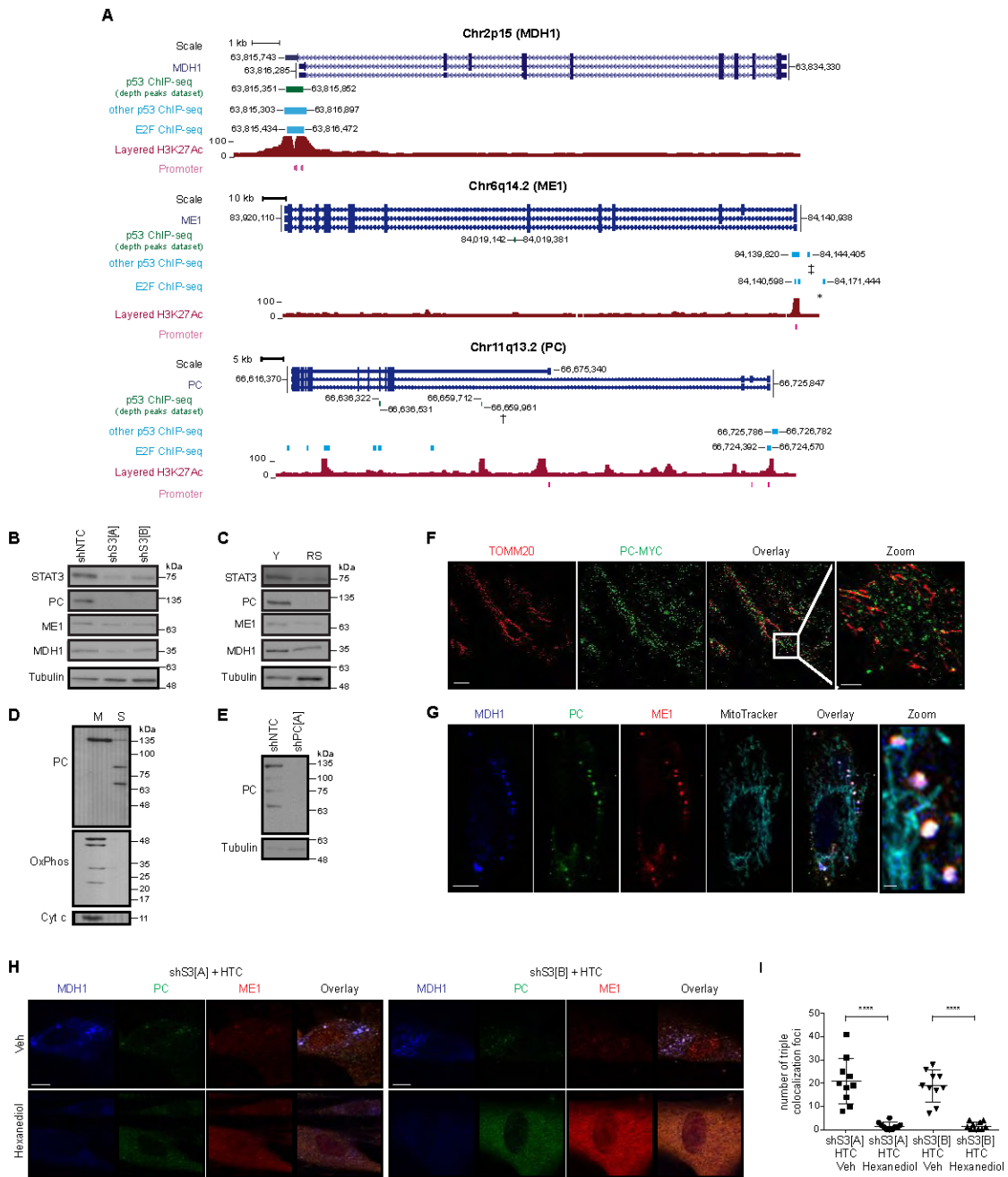
Igelmann et al. Figure S1



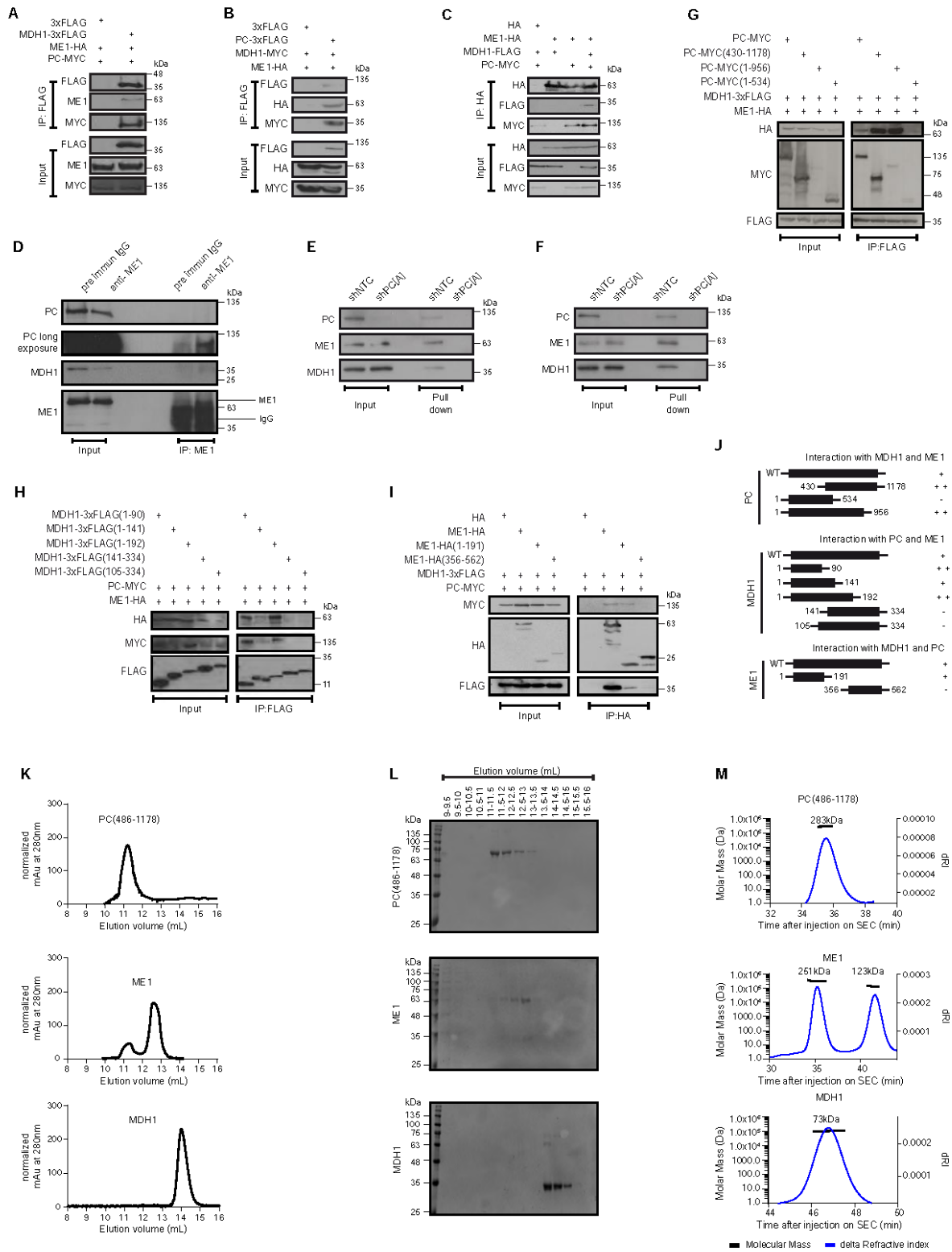
Igelmann et al. Figure S2



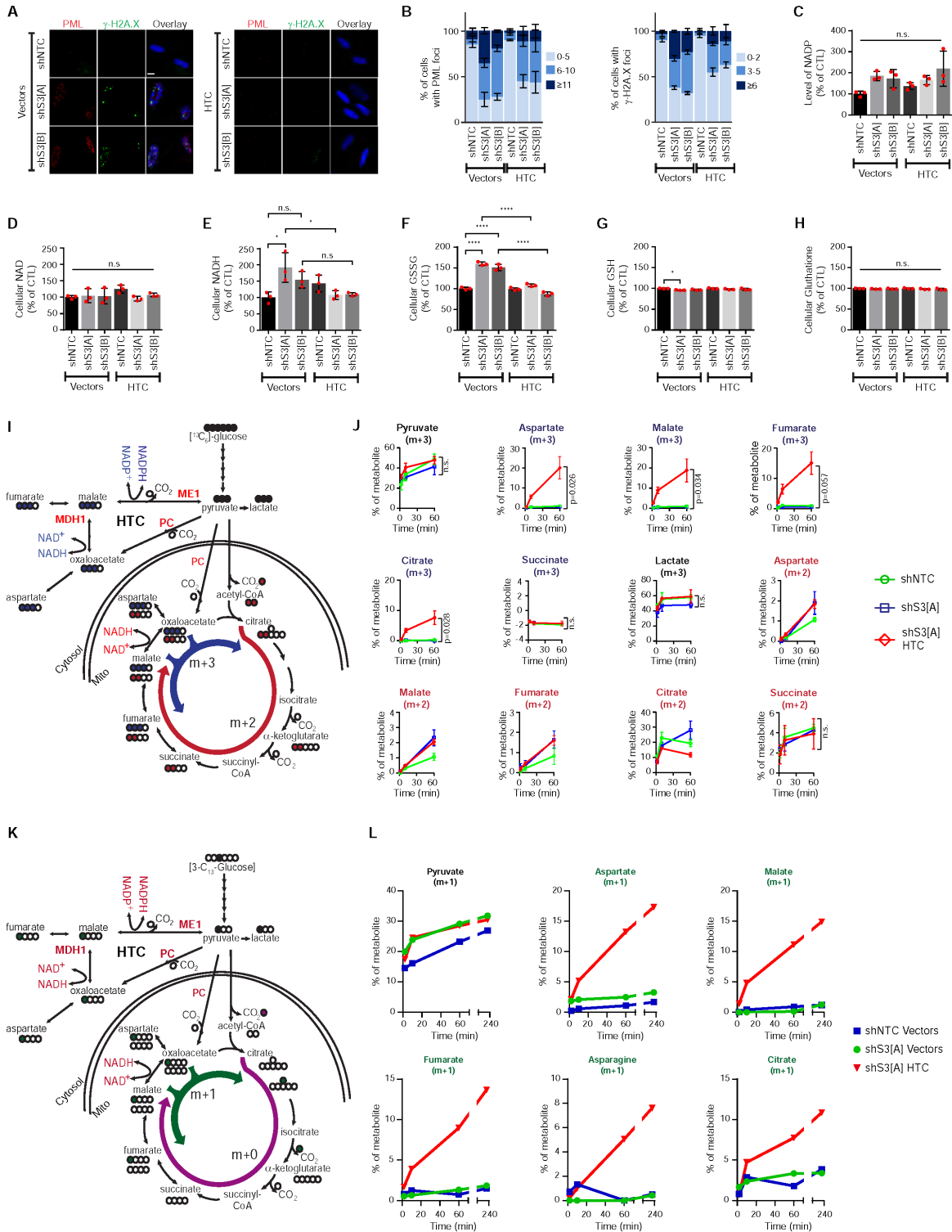
Igelmann et al. Figure S3



Igelmann et al. Figure S4

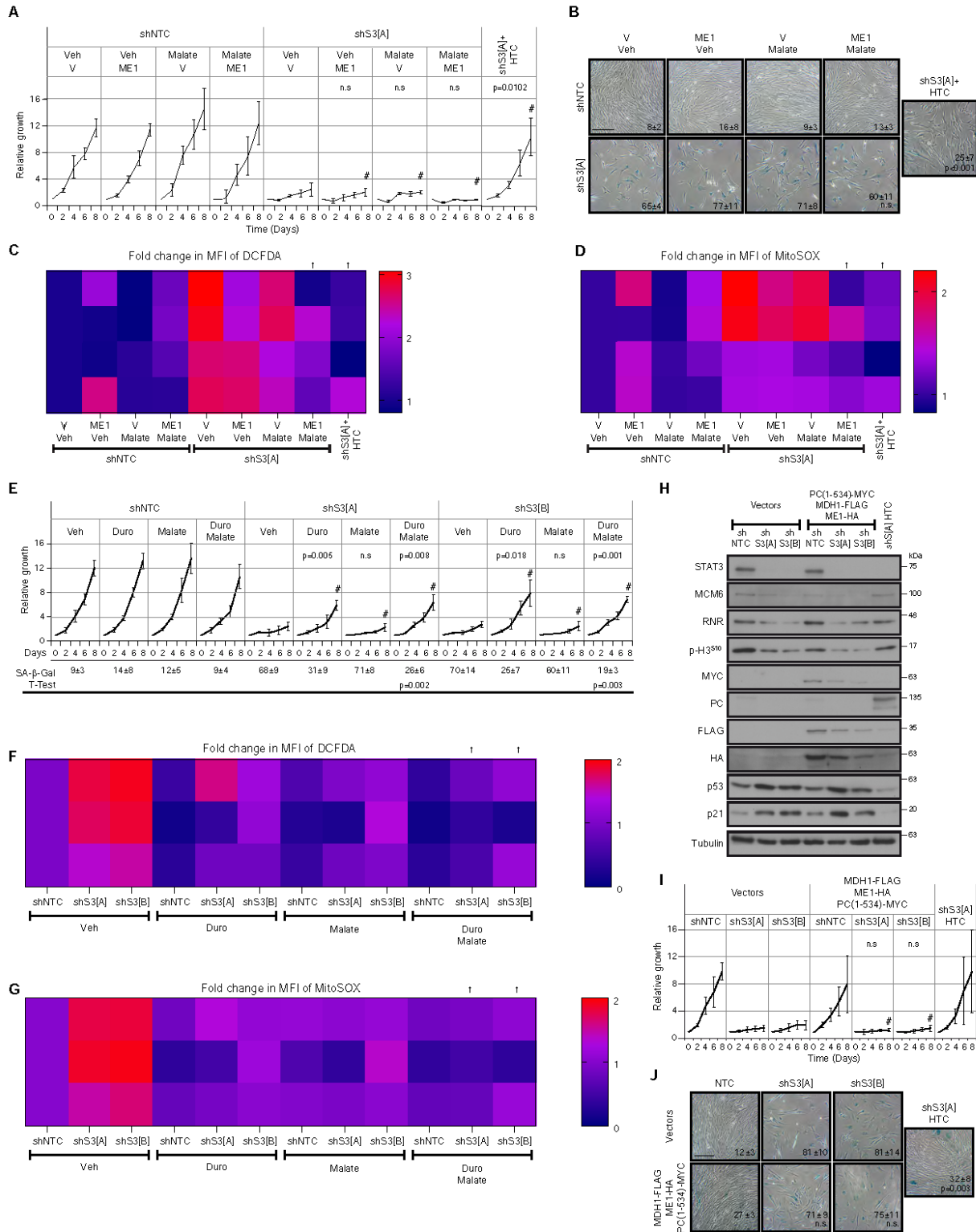


Igelmann et al. Figure S5

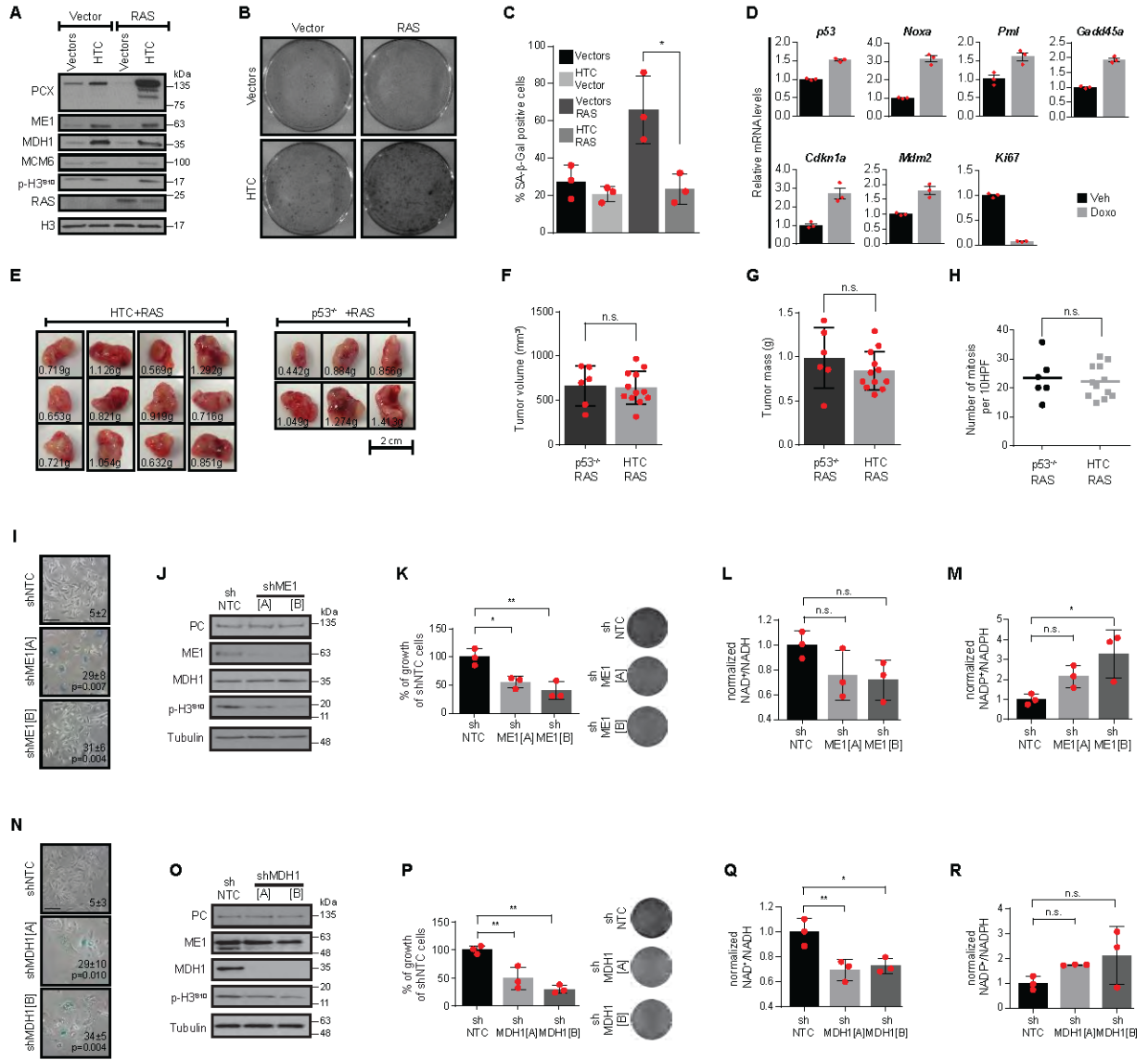


Igelmann et al. Figure S6

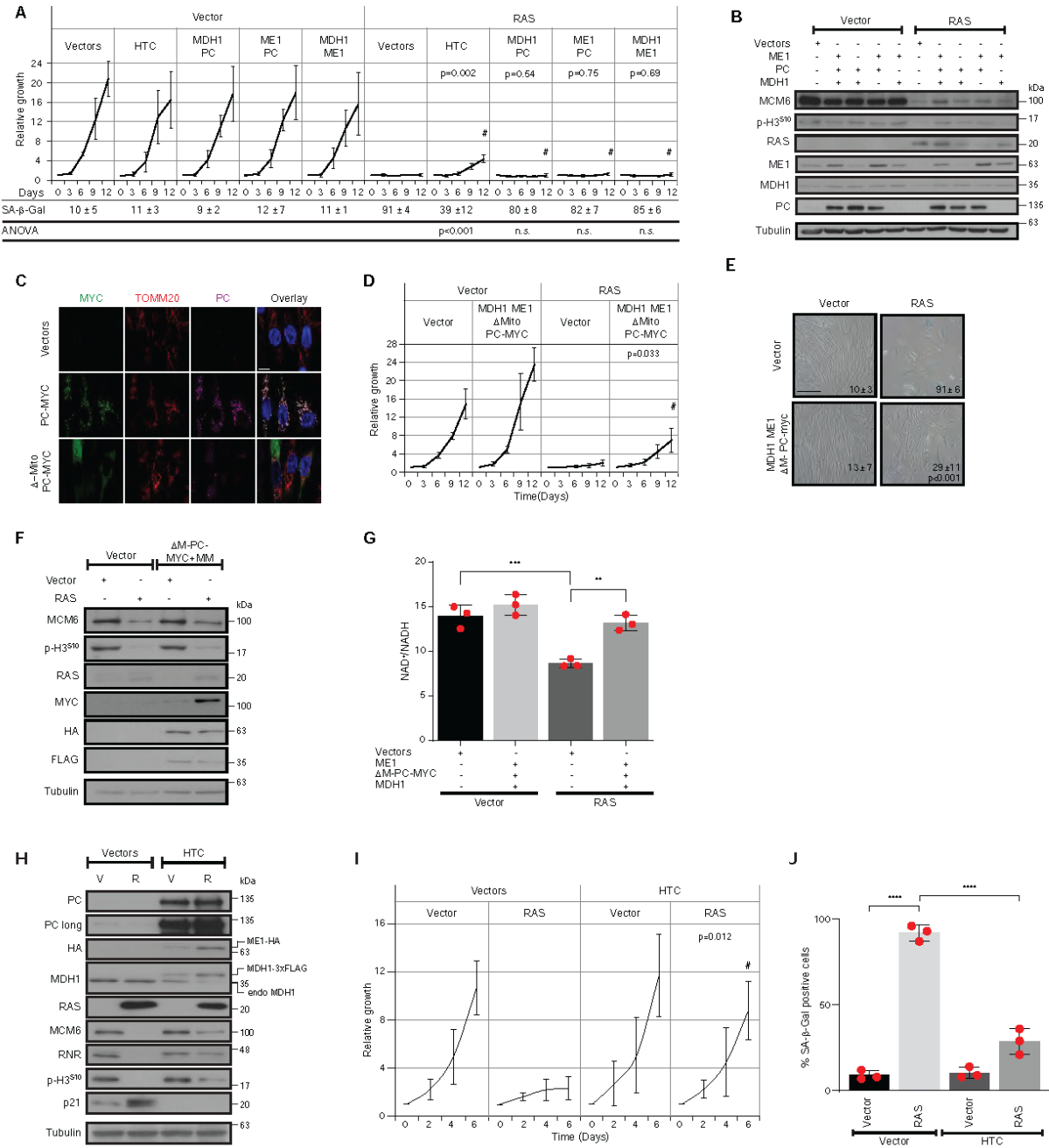




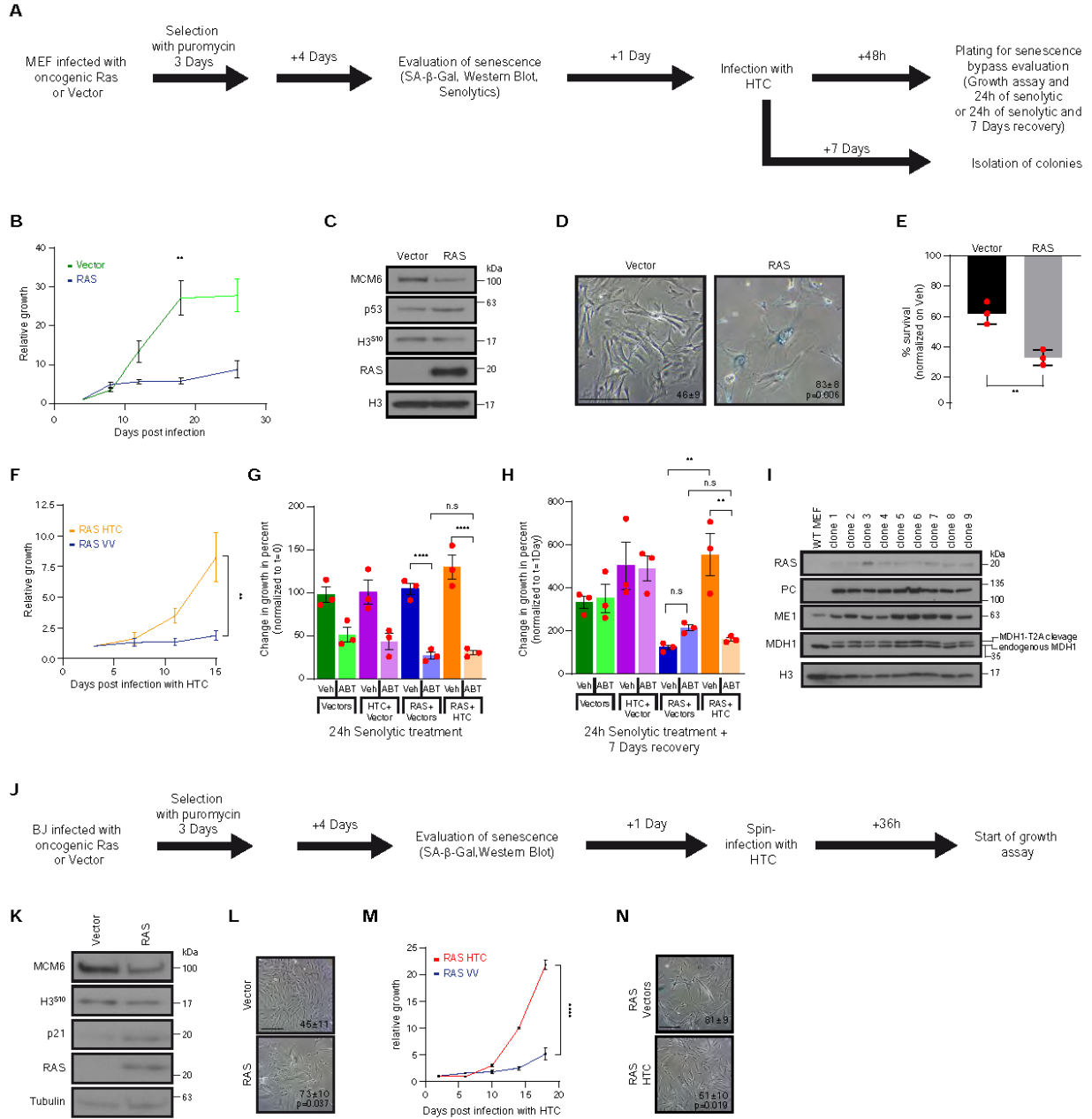
Igelmann et al. Figure S7



Igelmann et al. Figure S8



Igelmann et al. Figure S9



Igelmann et al. Figure S10

## 2.7.6. References

- Asher, G., Tsvetkov, P., Kahana, C., and Shaul, Y. (2005). **A mechanism of ubiquitin-independent proteasomal degradation of the tumor suppressors p53 and p73.** *Genes Dev.* 19, 316-321.
- Audet-Walsh, E., Papadopoli, D.J., Gravel, S.P., Yee, T., Bridon, G., Caron, M., Bourque, G., Giguere, V., and St-Pierre, J. (2016). **The PGC-1 $\alpha$ /ERR $\alpha$  Axis Represses One-Carbon Metabolism and Promotes Sensitivity to Anti-folate Therapy in Breast Cancer.** *Cell Rep.* 14, 920-931.
- Beausejour, C.M., Krtolica, A., Galimi, F., Narita, M., Lowe, S.W., Yaswen, P., and Campisi, J. (2003). **Reversal of human cellular senescence: roles of the p53 and p16 pathways.** *EMBO J.* 22, 4212-4222.
- Birsoy, K., Possemato, R., Lorbeer, F.K., Bayraktar, E.C., Thiru, P., Yucel, B., Wang, T., Chen, W.W., Clish, C.B., and Sabatini, D.M. (2014). **Metabolic determinants of cancer cell sensitivity to glucose limitation and biguanides.** *Nature* 508, 108-112.
- Birsoy, K., Wang, T., Chen, W.W., Freinkman, E., Abu-Remaileh, M., and Sabatini, D.M. (2015). **An Essential Role of the Mitochondrial Electron Transport Chain in Cell Proliferation Is to Enable Aspartate Synthesis.** *Cell* 162, 540-551.
- Birts, C.N., Banerjee, A., Darley, M., Dunlop, C.R., Nelson, S., Nijjar, S.K., Parker, R., West, J., Tavassoli, A., Rose-Zerilli, M.J.J., and Blaydes, J.P. (2020). **p53 is regulated by aerobic glycolysis in cancer cells by the CtBP family of NADH-dependent transcriptional regulators.** *Sci. Signal.* 13, eaau9529.
- Buescher, J.M., Antoniewicz, M.R., Boros, L.G., Burgess, S.C., Brunengraber, H., Clish, C.B., DeBerardinis, R.J., Feron, O., Frezza, C., Ghesquiere, B., et al. (2015). **A roadmap for interpreting (13)C metabolite labeling patterns from cells.** *Curr. Opin. Biotechnol.* 34, 189-201.
- Camacho-Carvajal, M.M., Wollscheid, B., Aebersold, R., Steimle, V., and Schamel, W.W. (2004). **Two-dimensional Blue native/SDS gel electrophoresis of multi-protein complexes from whole cellular lysates: a proteomics approach.** *Mol. Cell. Proteomics* 3, 176-182.
- Cao, Z., Zhou, Y., Zhu, S., Feng, J., Chen, X., Liu, S., Peng, N., Yang, X., Xu, G., and Zhu, Y. (2016). **Pyruvate Carboxylase Activates the RIG-I-like Receptor Mediated Antiviral Immune Response by Targeting the MAVS signalosome.** *Sci. Rep.* 6, 22002.
- Carbognin, E., Betto, R.M., Soriano, M.E., Smith, A.G., and Martello, G. (2016). **Stat3 promotes mitochondrial transcription and oxidative respiration during maintenance and induction of naive pluripotency.** *EMBO J.* 35, 618-634.

Chabes, A.L., Bjorklund, S., and Thelander, L. (2004). **S Phase-specific transcription of the mouse ribonucleotide reductase R2 gene requires both a proximal repressive E2F-binding site and an upstream promoter activating region.** *J. Biol. Chem.* 279, 10796-10807.

Chen, W.W., Freinkman, E., and Sabatini, D.M. (2017). **Rapid immunopurification of mitochondria for metabolite profiling and absolute quantification of matrix metabolites.** *Nat. Protoc.* 12, 2215-2231.

Cheng, T., Sudderth, J., Yang, C., Mullen, A.R., Jin, E.S., Mates, J.M., and DeBerardinis, R.J. (2011). **Pyruvate carboxylase is required for glutamine-independent growth of tumor cells.** *Proc. Natl. Acad. Sci. USA* 108, 8674-8679.

Consortium, E.P.; ENCODE Project Consortium (2012). **An integrated encyclopedia of DNA elements in the human genome.** *Nature* 489, 57-74.

Davis, C.A., Hitz, B.C., Sloan, C.A., Chan, E.T., Davidson, J.M., Gabdank, I., Hilton, J.A., Jain, K., Baymuradov, U.K., Narayanan, A.K., et al. (2018). **The Encyclopedia of DNA elements (ENCODE): data portal update.** *Nucleic Acids Res.* 46 (D1), D794-D801.

Deschenes-Simard, X., Gaumont-Leclerc, M.F., Bourdeau, V., Lessard, F., Moiseeva, O., Forest, V., Igelmann, S., Mallette, F.A., Saba-El-Leil, M.K., Meloche, S., et al. (2013). **Tumor suppressor activity of the ERK/MAPK pathway by promoting selective protein degradation.** *Genes Dev.* 27, 900-915.

Deschenes-Simard, X., Lessard, F., Gaumont-Leclerc, M.F., Bardeesy, N., and Ferbeyre, G. (2014). **Cellular senescence and protein degradation: Breaking down cancer.** *Cell cycle* 13, 1840-1858.

Deschenes-Simard, X., Parisotto, M., Rowell, M.C., Le Calve, B., Igelmann, S., Moineau-Vallee, K., Saint-Germain, E., Kalegari, P., Bourdeau, V., Kottakis, F., et al. (2019). **Circumventing senescence is associated with stem cell properties and metformin sensitivity.** *Aging Cell* 18, e12889.

Dorr, J.R., Yu, Y., Milanovic, M., Beuster, G., Zasada, C., Dabritz, J.H., Lisek, J., Lenze, D., Gerhardt, A., Schleicher, K., et al. (2013). **Synthetic lethal metabolic targeting of cellular senescence in cancer therapy.** *Nature* 501, 421-425.

Faubert, B., Li, K.Y., Cai, L., Hensley, C.T., Kim, J., Zacharias, L.G., Yang, C., Do, Q.N., Doucette, S., Burguete, D., et al. (2017). **Lactate Metabolism in Human Lung Tumors.** *Cell* 171, 358-371.

Ferbeyre, G., de Stanchina, E., Querido, E., Baptiste, N., Prives, C., and Lowe, S.W. (2000). **PML is induced by oncogenic ras and promotes premature senescence.** *Genes Dev.* 14, 2015-2027.

Fishilevich, S., Nudel, R., Rappaport, N., Hadar, R., Plaschkes, I., Iny Stein, T., Rosen, N., Kohn, A., Twik, M., Safran, M., et al. (2017). **GeneHancer: genomewide integration of enhancers and target genes in GeneCards**. Database (Oxford) 2017, bax028.

Fouillen, A., Dos Santos Neves, J., Mary, C., Castonguay, J.D., Moffatt, P., Baron, C., and Nanci, A. (2017). **Interactions of AMTN, ODAM and SCPPPQ1 proteins of a specialized basal lamina that attaches epithelial cells to tooth mineral**. Sci. Rep. 7, 46683.

Ghandi, M., Huang, F.W., Jane-Valbuena, J., Kryukov, G.V., Lo, C.C., McDonald, E.R., 3rd, Barretina, J., Gelfand, E.T., Bielski, C.M., Li, H., et al. (2019). **Next-generation characterization of the Cancer Cell Line Encyclopedia**. Nature 569, 503-508.

Gillies, R.J., Didier, N., and Denton, M. (1986). **Determination of cell number in monolayer cultures**. Anal. Biochem. 159, 109-113.

Gough, D.J., Corlett, A., Schlessinger, K., Wegrzyn, J., Larner, A.C., and Levy, D.E. (2009). **Mitochondrial STAT3 supports Ras-dependent oncogenic transformation**. Science 324, 1713-1716.

Gravel, S.P., Avizonis, D., and St-Pierre, J. (2016). **Metabolomics Analyses of Cancer Cells in Controlled Microenvironments**. Methods Mol. Biol. 1458, 273-290.

Gui, D.Y., Sullivan, L.B., Luengo, A., Hosios, A.M., Bush, L.N., Gitego, N., Davidson, S.M., Freinkman, E., Thomas, C.J., and Vander Heiden, M.G. (2016). **Environment Dictates Dependence on Mitochondrial Complex I for NAD<sup>+</sup> and Aspartate Production and Determines Cancer Cell Sensitivity to Metformin**. Cell Metab. 24, 716-727.

Hanse, E.A., Ruan, C., Kachman, M., Wang, D., Lowman, X.H., and Kelekar, A. (2017). **Cytosolic malate dehydrogenase activity helps support glycolysis in actively proliferating cells and cancer**. Oncogene 36, 3915-3924.

Huet, C., Menendez, J., Gancedo, C., and Francois, J.M. (2000). **Regulation of pyc1 encoding pyruvate carboxylase isozyme I by nitrogen sources in Saccharomyces cerevisiae**. Eur. J. Biochem. 267, 6817-6823.

Jiang, P., Du, W., Mancuso, A., Wellen, K.E., and Yang, X. (2013). **Reciprocal regulation of p53 and malic enzymes modulates metabolism and senescence**. Nature 493, 689-693.

Kidder, B.L., Yang, J., and Palmer, S. (2008). **Stat3 and c-Myc genome-wide promoter occupancy in embryonic stem cells**. PLoS ONE 3, e3932.

Kilic Eren, M., and Tabor, V. (2014). **The role of hypoxia inducible factor-1 alpha in bypassing oncogene-induced senescence**. PLoS ONE 9, e101064.

Kim, J.W., Tchernyshyov, I., Semenza, G.L., and Dang, C.V. (2006). **HIF-1-mediated expression of pyruvate dehydrogenase kinase: a metabolic switch required for cellular adaptation to hypoxia**. Cell Metab. 3, 177-185.

Krall, A.S., Mullen, P.J., Surjono, F., Momcilovic, M., Schmid, E.W., Halbrook, C.J., Thambundit, A., Mittelman, S.D., Lyssiotis, C.A., Shackelford, D.B., et al. (2021). **Asparagine couples mitochondrial respiration to ATF4 activity and tumor growth.** *Cell Metab.* 33, 1013-1026.

Lao-On, U., Attwood, P.V., and Jitrapakdee, S. (2018). **Roles of pyruvate carboxylase in human diseases: from diabetes to cancers and infection.** *J. Mol. Med. (Berl.)* 96, 237-247.

Lee, S.M., Dho, S.H., Ju, S.K., Maeng, J.S., Kim, J.Y., and Kwon, K.S. (2012). **Cytosolic malate dehydrogenase regulates senescence in human fibroblasts.** *Biogerontology* 13, 525-536.

Lessard, F., Igelmann, S., Trahan, C., Huot, G., Saint-Germain, E., Mignacca, L., Del Toro, N., Lopes-Paciencia, S., Le Calve, B., Montero, M., et al. (2018). **Senescence-associated ribosome biogenesis defects contributes to cell cycle arrest through the Rb pathway.** *Nat. Cell Biol.* 20, 789-799.

Li, X., Cheng, K.K.Y., Liu, Z., Yang, J.K., Wang, B., Jiang, X., Zhou, Y., Hallenborg, P., Hoo, R.L.C., Lam, K.S.L., et al. (2016). **The MDM2-p53-pyruvate carboxylase signalling axis couples mitochondrial metabolism to glucose-stimulated insulin secretion in pancreatic b-cells.** *Nat. Commun.* 7, 11740.

Lu, Y.X., Ju, H.Q., Liu, Z.X., Chen, D.L., Wang, Y., Zhao, Q., Wu, Q.N., Zeng, Z.L., Qiu, H.B., Hu, P.S., et al. (2018). **ME1 Regulates NADPH Homeostasis to Promote Gastric Cancer Growth and Metastasis.** *Cancer Res.* 78, 1972-1985.

Macias, E., Rao, D., Carbajal, S., Kiguchi, K., and DiGiovanni, J. (2014). **Stat3 binds to mtDNA and regulates mitochondrial gene expression in keratinocytes.** *J. Invest. Dermatol.* 134, 1971-1980.

Malette, F.A., Gaumont-Leclerc, M.F., and Ferbeyre, G. (2007). **The DNA damage signaling pathway is a critical mediator of oncogene-induced senescence.** *Genes Dev.* 21, 43-48.

Mantel, C., Messina-Graham, S., Moh, A., Cooper, S., Hangoc, G., Fu, X.Y., and Broxmeyer, H.E. (2012). **Mouse hematopoietic cell-targeted STAT3 deletion: stem/progenitor cell defects, mitochondrial dysfunction, ROS overproduction, and a rapid aging-like phenotype.** *Blood* 120, 2589-2599.

Masclé, X.H., Gagnon, C., Wahba, H.M., Lussier-Price, M., Cappadocia, L., Sakaguchi, K., and Omichinski, J.G. (2020). **Acetylation of SUMO1 Alters Interactions with the SIMs of PML and Daxx in a Protein-Specific Manner.** *Structure* 28, 157-168.

McBride, H.M., Goping, I.S., and Shore, G.C. (1996). **The human mitochondrial import receptor, hTom20p, prevents a cryptic matrix targeting sequence from gaining access to the protein translocation machinery.** *J. Cell Biol.* 134, 307-313.



McGuirk, S., Gravel, S.P., Deblois, G., Papadopoli, D.J., Faubert, B., Wegner, A., Hiller, K., Avizonis, D., Akavia, U.D., Jones, R.G., et al. (2013). **PGC-1a supports glutamine metabolism in breast cancer.** *Cancer Metab.*

Moiseeva, O., Bourdeau, V., Roux, A., Deschenes-Simard, X., and Ferbeyre, G. (2009). **Mitochondrial dysfunction contributes to oncogene-induced senescence.** *Mol. Cell. Biol.* 29, 4495-4507.

Moiseeva, O., Bourdeau, V., Vernier, M., Dabauvalle, M.C., and Ferbeyre, G. (2011). **Retinoblastoma-independent regulation of cell proliferation and senescence by the p53-p21 axis in lamin A /C-depleted cells.** *Aging Cell* 10, 789-797.

Moiseeva, O., Guillon, J., and Ferbeyre, G. (2020). **Senescence: A program in the road to cell elimination and cancer.** In *Seminars in cancer biology* (Academic Press).

Moon, S.H., Huang, C.H., Houlihan, S.L., Regunath, K., Freed-Pastor, W.A., Morris, J.P., Tschaharganeh, D.F., Kasthuber, E.R., Barsotti, A.M., Culp-Hill, R., et al. (2019). **p53 Represses the Mevalonate Pathway to Mediate Tumor Suppression.** *Cell* 176, 564-580.

Morris, J.P., 4th, Yashinski, J.J., Koche, R., Chandwani, R., Tian, S., Chen, C.C., Baslan, T., Marinkovic, Z.S., Sanchez-Rivera, F.J., Leach, S.D., et al. (2019).  **$\alpha$ -Ketoglutarate links p53 to cell fate during tumour suppression.** *Nature* 573, 595-599.

Nagaraj, R., Sharpley, M.S., Chi, F., Braas, D., Zhou, Y., Kim, R., Clark, A.T., and Banerjee, U. (2017). **Nuclear Localization of Mitochondrial TCA Cycle Enzymes as a Critical Step in Mammalian Zygotic Genome Activation.** *Cell* 168, 210-223.

Nguyen, T.T., Grimm, S.A., Bushel, P.R., Li, J., Li, Y., Bennett, B.D., Lavender, C.A., Ward, J.M., Fargo, D.C., Anderson, C.W., et al. (2018). **Revealing a human p53 universe.** *Nucleic Acids Res.* 46, 8153-8167.

Oki, S., Ohta, T., Shioi, G., Hatanaka, H., Ogasawara, O., Okuda, Y., Kawaji, H., Nakaki, R., Sese, J., and Meno, C. (2018). **ChIP-Atlas: a data-mining suite powered by full integration of public ChIP-seq data.** *EMBO Rep.* 19, e46255.

Parrinello, S., Samper, E., Krtolica, A., Goldstein, J., Melov, S., and Campisi, J. (2003). **Oxygen sensitivity severely limits the replicative lifespan of murine fibroblasts.** *Nat. Cell Biol.* 5, 741-747.

Passos, J.F., Saretzki, G., Ahmed, S., Nelson, G., Richter, T., Peters, H., Wappler, I., Birket, M.J., Harold, G., Schaeuble, K., et al. (2007). **Mitochondrial dysfunction accounts for the stochastic heterogeneity in telomere- dependent senescence.** *PLoS Biol.* 5, e110.

Pencik, J., Schleder, M., Gruber, W., Unger, C., Walker, S.M., Chalaris, A., Marie, I.J., Hassler, M.R., Javaheri, T., Aksoy, O., et al. (2015). **STAT3 regulated ARF expression suppresses prostate cancer metastasis.** *Nat. Commun.* 6, 7736.

Pertega-Gomes, N., Vizcaino, J.R., Attig, J., Jurmeister, S., Lopes, C., and Baltazar, F. (2014). **A lactate shuttle system between tumour and stromal cells is associated with poor prognosis in prostate cancer.** BMC Cancer 14, 352.

Serrano, M., Lin, A.W., McCurrach, M.E., Beach, D., and Lowe, S.W. (1997). **Oncogenic ras provokes premature cell senescence associated with accumulation of p53 and p16INK4a.** Cell 88, 593-602.

Shinde, A., Wilmanski, T., Chen, H., Teegarden, D., and Wendt, M.K. (2018). **Pyruvate carboxylase supports the pulmonary tropism of metastatic breast cancer.** Breast Cancer Res. 20, 76.

Stelzer, G., Rosen, N., Plaschkes, I., Zimmerman, S., Twik, M., Fishilevich, S., Stein, T.I., Nudel, R., Lieder, I., Mazor, Y., et al. (2016). **The GeneCards Suite: From Gene Data Mining to Disease Genome Sequence Analyses.** Curr Protoc Bioinformatics 54, 1.30.1-1.30.33.

Stewart, S.A., Dykxhoorn, D.M., Palliser, D., Mizuno, H., Yu, E.Y., An, D.S., Sabatini, D.M., Chen, I.S.Y., Hahn, W.C., Sharp, P.A., et al. (2003). **Lentivirus-delivered stable gene silencing by RNAi in primary cells.** RNA 9, 493-501.

Sullivan, L.B., Gui, D.Y., Hosios, A.M., Bush, L.N., Freinkman, E., and Vander Heiden, M.G. (2015). **Supporting Aspartate Biosynthesis Is an Essential Function of Respiration in Proliferating Cells.** Cell 162, 552-563.

Tao, X., Yang, Z., and Tong, L. (2003). **Crystal structures of substrate complexes of malic enzyme and insights into the catalytic mechanism.** Structure 11, 1141-1150.

Titov, D.V., Cracan, V., Goodman, R.P., Peng, J., Grabarek, Z., and Mootha, V.K. (2016). **Complementation of mitochondrial electron transport chain by manipulation of the NAD<sup>+</sup>/NADH ratio.** Science 352, 231-235.

Tkach, M., Coria, L., Rosemblit, C., Rivas, M.A., Proietti, C.J., Diaz Flaque, M.C., Beguelin, W., Frahm, I., Charreau, E.H., Cassataro, J., et al. (2012). **Targeting Stat3 induces senescence in tumor cells and elicits prophylactic and therapeutic immune responses against breast cancer growth mediated by NK cells and CD4<sup>+</sup> T cells.** J. Immunol. 189, 1162-1172.

Vallania, F., Schiavone, D., Dewilde, S., Pupo, E., Garbay, S., Calogero, R., Pontoglio, M., Provero, P., and Poli, V. (2009). **Genome-wide discovery of functional transcription factor binding sites by comparative genomics: the case of Stat3.** Proc. Natl. Acad. Sci. USA 106, 5117-5122.

Voorhoeve, P.M., and Agami, R. (2003). **The tumor-suppressive functions of the human INK4A locus.** Cancer Cell. 4, 311-319.

Wegrzyn, J., Potla, R., Chwae, Y.J., Sepuri, N.B., Zhang, Q., Koeck, T., Derecka, M., Szczepanek, K., Szelag, M., Gornicka, A., et al. (2009). **Function of mitochondrial Stat3 in cellular respiration.** *Science* 323, 793-797.

Wheeldon, I., Minter, S.D., Banta, S., Barton, S.C., Atanassov, P., and Sigman, M. (2016). **Substrate channelling as an approach to cascade reactions.** *Nat. Chem.* 8, 299-309.

Wiley, C.D., and Campisi, J. (2016). **From Ancient Pathways to Aging Cells-Connecting Metabolism and Cellular Senescence.** *Cell Metab.* 23, 1013-1021.

Wiley, C.D., Velarde, M.C., Lecot, P., Liu, S., Sarnoski, E.A., Freund, A., Shirakawa, K., Lim, H.W., Davis, S.S., Ramanathan, A., et al. (2016). **Mitochondrial Dysfunction Induces Senescence with a Distinct Secretory Phenotype.** *Cell Metab.* 23, 303-314.

Xiang, S., and Tong, L. (2008). **Crystal structures of human and Staphylococcus aureus pyruvate carboxylase and molecular insights into the carboxyltransfer reaction.** *Nat. Struct. Mol. Biol.* 15, 295-302.

Yu, Y., Schleich, K., Yue, B., Ji, S., Lohneis, P., Kemper, K., Silvis, M.R., Qutob, N., van Rooijen, E., Werner-Klein, M., et al. (2018). **Targeting the Senescence-Overriding Cooperative Activity of Structurally Unrelated H3K9 Demethylases in Melanoma.** *Cancer Cell.* 33, 322-336.

Yuan, R., Liu, Q., Segeren, H.A., Yuniati, L., Guardavaccaro, D., Lebbink, R.J., Westendorp, B., and de Bruin, A. (2019). **Cyclin F-dependent degradation of E2F7 is critical for DNA repair and G2-phase progression.** *EMBO J.* 38, e101430.

Zhang, B., Tornmalm, J., Widengren, J., Vakifahmetoglu-Norberg, H., and Norberg, E. (2017). **Characterization of the Role of the Malate Dehydrogenases to Lung Tumor Cell Survival.** *J. Cancer* 8, 2088-2096.

Zhang, Y., Xu, Y., Lu, W., Ghergurovich, J.M., Guo, L., Blair, I.A., Rabinowitz, J.D., and Yang, X. (2021). **Upregulation of Antioxidant Capacity and Nucleotide Precursor Availability Suffices for Oncogenic Transformation.** *Cell Metab.* 33, 94-109.

## **2.8. Contribution to the article 3**

This article is a review article we wrote to highlight the different oncogenic and tumorsuppressive roles of STAT3 and STAT5. Each author as an equal contribution in writing and editing the manuscript. All figures presented were done in collaboration.

Review

# STAT3 and STAT5 Activation in Solid Cancers

Sebastian Igelmann <sup>1,2</sup>, Heidi A. Neubauer <sup>3</sup> and Gerardo Ferbeyre <sup>1,2,\*</sup>

<sup>1</sup> Department of Biochemistry and Molecular Medicine, Université de Montréal, C.P. 6128, Succ. Centre-Ville, Montréal, QC H3C 3J7, Canada; sebastian.igelmann@umontreal.ca

<sup>2</sup> CRCHUM, 900 Saint-Denis St, Montréal, QC H2X 0A9, Canada

<sup>3</sup> Institute of Animal Breeding and Genetics, University of Veterinary Medicine Vienna, Vienna 1210, Austria; Heidi.Neubauer@vetmeduni.ac.at

\* Correspondence: g.ferbeyre@umontreal.ca

Received: 1 August 2019; Accepted: 18 September 2019; Published: 25 September 2019



**Abstract:** The Signal Transducer and Activator of Transcription (STAT)3 and 5 proteins are activated by many cytokine receptors to regulate specific gene expression and mitochondrial functions. Their role in cancer is largely context-dependent as they can both act as oncogenes and tumor suppressors. We review here the role of STAT3/5 activation in solid cancers and summarize their association with survival in cancer patients. The molecular mechanisms that underpin the oncogenic activity of STAT3/5 signaling include the regulation of genes that control cell cycle and cell death. However, recent advances also highlight the critical role of STAT3/5 target genes mediating inflammation and stemness. In addition, STAT3 mitochondrial functions are required for transformation. On the other hand, several tumor suppressor pathways act on or are activated by STAT3/5 signaling, including tyrosine phosphatases, the sumo ligase Protein Inhibitor of Activated STAT3 (PIAS3), the E3 ubiquitin ligase TATA Element Modulatory Factor/Androgen Receptor-Coactivator of 160 kDa (TMF/ARA160), the miRNAs miR-124 and miR-1181, the Protein of alternative reading frame 19 (p19ARF)/p53 pathway and the Suppressor of Cytokine Signaling 1 and 3 (SOCS1/3) proteins. Cancer mutations and epigenetic alterations may alter the balance between pro-oncogenic and tumor suppressor activities associated with STAT3/5 signaling, explaining their context-dependent association with tumor progression both in human cancers and animal models.

**Keywords:** solid cancers; cell cycle; apoptosis; inflammation; mitochondria; stemness; tumor suppression

## **2.9. STAT3 and STAT5 activation in solid cancers**

### **2.9.1. Abstract**

The Signal Transducer and Activator of Transcription (STAT)3 and 5 are activated by many cytokine receptors to regulate specific gene expression and mitochondrial functions. Their role in cancer is largely context dependent as they can both act as oncogenes and tumor suppressors. We review here the role of STAT3/5 activation in solid cancers and summarize their association to survival in cancer patients. The molecular mechanisms that underpins the oncogenic activity of STAT3/5 signaling includes the regulation of genes that control cell cycle, cell death, inflammation and stemness. In addition, STAT3 mitochondrial functions are required for transformation. On the other hand, several tumor suppressor pathways act on or are activated by STAT3/5 signaling including the p19ARF/p53 pathway, tyrosine phosphatases, suppressor of cytokine signaling 1 and 3, the sumo ligase PIAS3, the E3 ubiquitin ligase TMF/ARA160 and the miRNAs miR-124 and miR-1181. Cancer mutations and epigenetic alterations may alter the balance between pro-oncogenic and tumor suppressor activities associated to STAT3/5 signaling explaining their context dependent association to tumor progression both in human cancers and animal models.

### **2.9.2. Introduction**

Activation of Signal Transducer and Activator of Transcription (STAT) proteins has been linked to many human cancers. STATs were initially discovered as latent cytosolic transcription factors that are phosphorylated by the Janus Kinase (JAK) family upon stimulation of membrane-associated cytokine and growth factor receptors. Phosphorylation triggers STAT dimerization and translocation to the nucleus to bind specific promoters and regulate transcription [1]. Here, we review the role of STAT family members STAT3 and STAT5 in solid human malignancies, as well as the mechanisms that may explain their association with either worse or better prognosis.

### **2.9.3. STAT3 and STAT5 in Solid Cancers**

The discovery of cancer genes has been propelled by genetic analyses and more recently by next generation DNA sequencing technologies. Combined, these studies have identified 127 significantly mutated cancer genes that cover diverse signaling pathways [2]. Mutations acting as drivers in cancer are positively selected during tumor growth and constitute solid proof of the involvement of a particular gene as a driver in the disease. Mutations in STAT3 and STAT5 have been reported in patients with solid cancers, but unlike hyperactivation of the JAK/STAT pathway, STAT3/5 mutations in cancer are relatively infrequent and occur mostly in hematological malignancies.

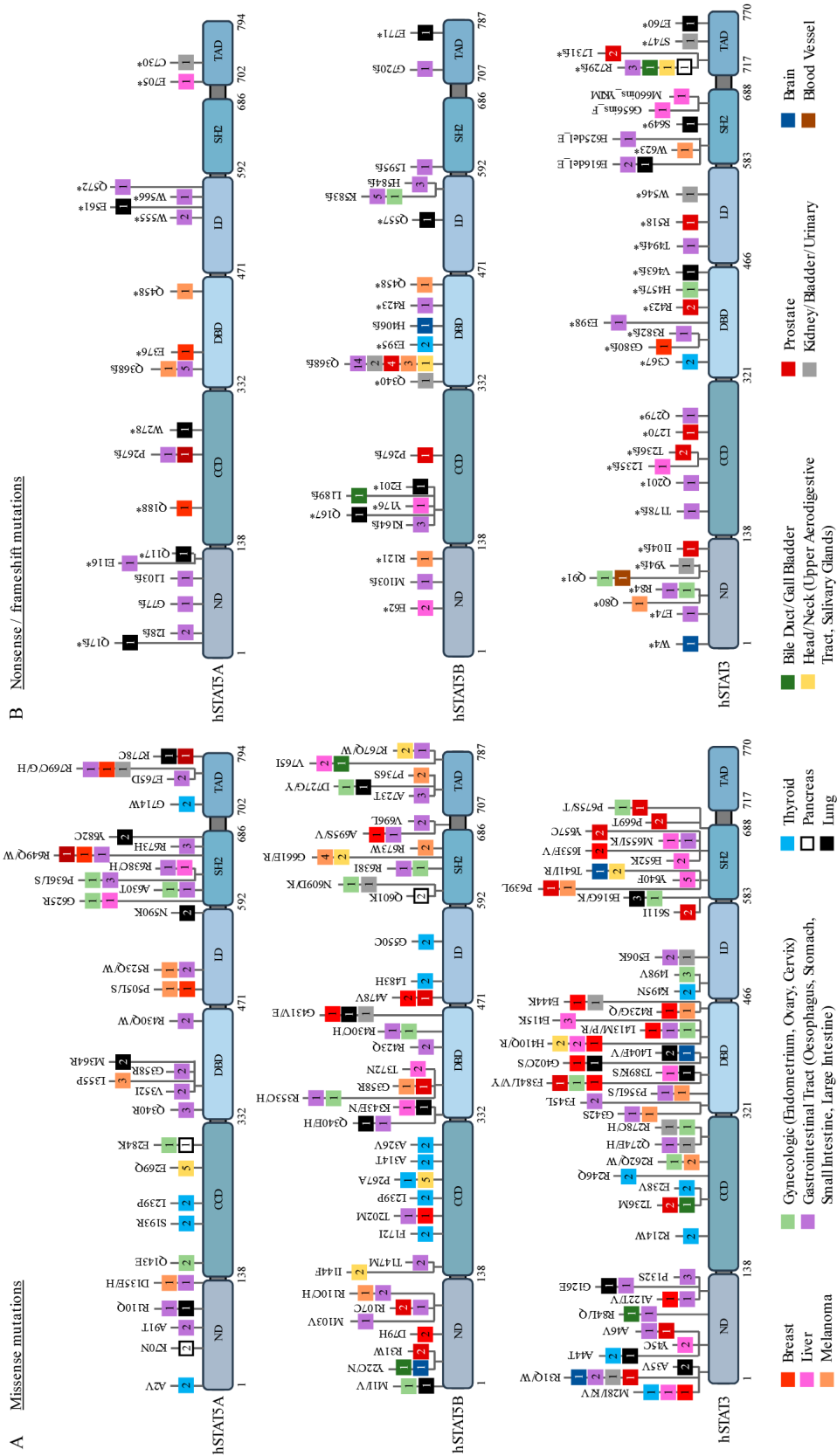


**Figure 1.** Map of somatic mutations detected in human Signal Transducer and Activator of Transcription (STAT)5A, STAT5B and STAT3 in patients with solid cancers. Individual missense mutations found in at least two patients (A), as well as all reported nonsense and frameshift mutations (B), are depicted. Numbers in each box represent the number of cases reported for each mutation. Data were mined from the Catalogue of Somatic Mutations In Cancer (COSMIC) database. ND, N-terminal domain; CCD, Coiled coil domain; DBD, DNA binding domain; SH2, Src homology 2 domain; TAD, Transactivation domain.

An overview of reported STAT3/5 mutations in solid cancers is illustrated in Figure 1, based on data collected from the Catalogue of Somatic Mutations in Cancer (COSMIC) database. Mutations in *STAT3* are more prevalent than mutations in *STAT5A* or *STAT5B* genes. Noticeably, gastrointestinal cancers have the highest rates of STAT3/5 mutations compared with other solid cancers (Figure 1). Missense mutations tend to cluster within the SH2 domain, where gain-of-function mutations were previously characterized [3,4], as well as within the DNA binding domain and to an extent the N-terminal domain (Figure 1A). Interestingly, the *STAT3 Y640F* hotspot gain-of-function mutation reported in various lymphoid malignancies has also been detected in patients with liver cancer (Figure 1A). Nonsense and frameshift mutations are less frequent and more disperse, likely representing loss-of-function events (Figure 1B). Notably, a hotspot frameshift mutation at position Q368 within the DNA binding domain of *STAT5B* has been reported in 24 patients with various types of carcinoma; this frameshift generates a stop codon shortly after the mutation and is therefore likely to be loss-of-function, although characterization of this mutation has not been performed.

As opposed to mutation rates, STAT3/5 activation is very frequent in human cancers, perhaps reflecting increased cytokine signaling or mutations in cytokine receptors or negative regulators. STAT3/5 activation can be detected using antibodies that measure total levels or activation marks in STAT3/5 proteins (e.g. tyrosine phosphorylation). A better assessment of STAT3/5 activation can be obtained by measuring downstream signaling targets (i.e., mRNA levels of STAT3 [5] and STAT5 [6] target genes). A recent metanalysis of 63 different studies concluded that STAT3 overexpression was significantly associated with a worse 3-year overall survival (OS) (OR = 2.06, 95% CI = 1.57 to 2.71,  $p < 0.00001$ ) and 5-year OS (OR = 2.00, 95% CI = 1.53 to 2.63,  $p < 0.00001$ ) in patients with solid tumors [7]. Elevated STAT3 expression was associated with poor prognosis in gastric cancer, lung cancer, gliomas, hepatic cancer, osteosarcoma, prostate cancer and pancreatic cancer. However, high STAT3 expression predicted a better prognosis for breast cancer [7]. This study mixed data of both STAT3 and phospho-STAT3 (p-STAT3) expression limiting its ability to associate pathway activation to prognosis. Here, we summarize the data linking activation of STAT3/5 to overall survival in several major human solid cancers identifying the biomarkers used in each study (Table 1). Taken together, the results clearly show that *STAT3* and *STAT5* are important cancer genes despite their relatively low mutation frequency.

STAT3 activation is clearly a factor linked to bad prognosis in patients with lung cancer, liver cancer, renal cell carcinoma (RCC) and gliomas. In other tumors, the association is not significant. In solid tumors, STAT3 activation is more frequent than STAT5 activation although no explanation for this difference was proposed. In prostate cancer, both STAT3 and STAT5 have been associated



with castration-resistant disease and proposed as therapeutic targets [8,9]. In colon cancer, the association between p-STAT3 and survival varies according to the study, but a high p-STAT3/p-STAT5 ratio indicates bad prognosis [10]. Also in breast cancer, p-STAT5 levels are clearly associated with better prognosis [11]. In liver cancer, STAT5 has ambivalent functions that were recently reviewed by Moriggl and colleagues [12]. Understanding mechanistically how STAT3/5 promote transformation and tumor suppression is important for the eventual design of new treatments. Also, survival data is highly influenced by the response of patients to their treatment and may not always reflect all mechanistic links between STAT3/5 activity and tumor biology. Of note, the effect of any gene is conditioned by the genetic context of gene action. Some genes can clearly exert a tumor suppressor effect in the initial stages of carcinogenesis that is lost when cancer mutations or epigenetic changes inactivate key effectors of these tumor suppressor pathways [13]. Human studies are usually limited to late stage tumors because it is easier to collect samples at that point. Studies in model systems, including primary cells, organoids and mouse models are thus required for a full understanding of how cancer genes work specifically at early stages in tumorigenesis.

**Table 1.** STAT3/5 activity and overall survival in major human solid tumors.

Tumor Type	Biomarker/Type of Study	Overall Survival	Ref
NSCLC	High p-STAT3/Meta-analysis of 9 studies	Log HR 0.67, 95% CI: 0.57–0.77, $p < 0.0001$	[14]
NSCLC	High p-STAT3/Cox regression multivariate analysis	HR 2.45, 95% CI: 1.084–5.556, $p = 0.031$	[15]
Lung cancer	High p-STAT3/Meta-analysis of 13 studies	HR 1.23, 95% CI: 1.04–1.46, $p = 0.02$	[16]
Pancreatic cancer	High p-STAT3/Log-rank test	No association $p > 0.05$	[17]
Liver cancer (HCC)	High p-STAT3/Meta-analysis of 8 studies	HR 1.69, 95% CI: 1.07–2.31, $p < 0.0001$ 3yr HR 1.67, 95% CI: 1.18–2.15, $p < 0.0001$ 5yr	[18]
Breast cancer	High p-STAT3/Meta-analysis of 12 studies	No association $p > 0.05$	[19]
Breast cancer (ER+)	High p-STAT3/Log-rank test	No association $p > 0.05$	[20]
GBM	High p-S727-STAT3/Cox regression multivariate analysis	HR 1.797, 95% CI: 1.028–3.142, $p = 0.040$	[21]
RCC	High p-S727-STAT3/Cox regression multivariate analysis	HR 3.32, 95% CI: 1.26–8.71, $p = 0.014$ 10yr	[22]
Colon cancer	High p-STAT3/p-STAT5 ratio/Cox regression multivariate analysis	HR 4.468, $p = 0.043$ 5yr	[10]
Colon cancer	High p-STAT3/Log-rank test	Worse overall survival, $p < 0.001$	[23]
Colon cancer	High p-STAT3/Cox regression multivariate analysis	HR 1.61, 95% CI: 1.11–2.34, $p = 0.015$	[24]
Breast cancer	Low p-STAT5/Cox regression multivariate analysis	HR 2.49, 95% CI: 1.23–5.05, $p = 0.012$ 5yr	[11]
Prostate cancer	High nuclear STAT5A/B/Cox regression multivariate analysis	HR 1.59, 95% CI: 1.04–2.44, $p = 0.034$	[9]

ER+, estrogen receptor-positive; HCC, hepatocellular carcinoma; GBM, glioblastoma multiforme; NSCLC, non-small-cell lung carcinoma; HR, hazard ratio; RCC, renal cell carcinoma.

## 2.9.4. Mechanisms of Transformation by STAT3/5 Proteins in Solid Cancers

STAT3 and STAT5 promote tumor progression by regulating the expression of cell cycle, survival and pro-inflammatory genes. In addition, they control mitochondrial functions, metabolism and stemness, as discussed below (Figure 2).

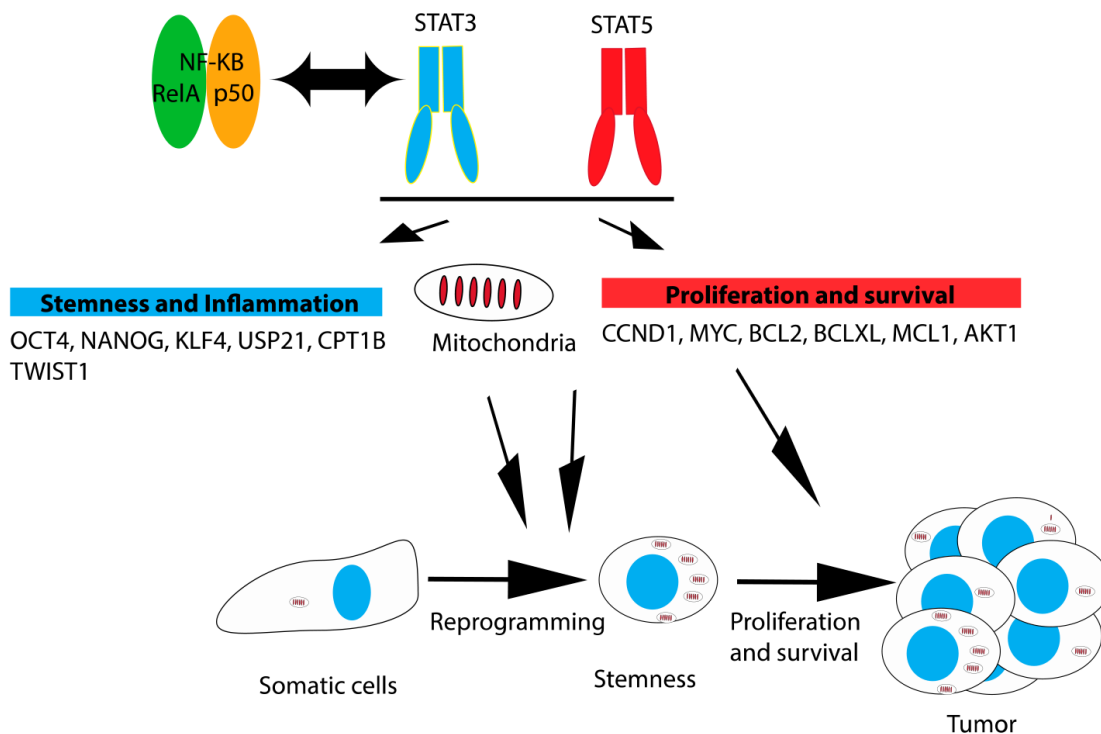


**Figure 2.** Mechanisms of tumorigenic activity of STAT3 and STAT5 signaling in solid tumors.

### Cell Cycle and Apoptosis

As transcription factors, STAT3 and STAT5 regulate many genes required for cell cycle progression and cell survival. A major target of the transcriptional control of the mammalian cell cycle is cyclin D. STAT3 regulates cyclin D in a complex with CD44 and the acetyltransferase p300. The latter acetylates STAT3 promoting its dimerization, nuclear translocation and binding to the cyclin D promoter [25]. Other cell cycle and survival genes regulated by STAT3 include *c-MYC*, *BCL2*, *BCL2L1/BCL-XL*, *MCL1* and *BIRC5/survivin* [26]. Recent studies combined ChIPSeq with whole transcriptome profiling in ABC DLBCL (activated B cell-like diffuse large B cell lymphoma) cell lines and revealed that STAT3 activates genes in the Phosphoinositide 3-Kinase (PI3K)/AKT/Mammalian Target of Rapamycin (mTOR) pathway, the Nuclear Factor Kappa-Light-Chain Enhancer of Activated B-Cells (NF- $\kappa$ -B) pathway and the E2F/G2M cell

cycle regulation pathway, while repressing type I interferon signaling genes [27]. STAT5 also regulates the expression of cell cycle and cell survival genes [13] including *AKT1* [28], which encodes a pro-survival kinase.

### **Inflammation and Innate Immunity**

Although the induction of cell proliferation and cell survival genes by STAT3/5 proteins contribute to their pro-cancer activity, in basal-like breast cancers the major genes associated with STAT3 activation control inflammation and the immune response [29]. Of note, inflammation is initially an adaptive response to pathological insults such as oncogenic stimuli, and it therefore exerts a tumor suppressive function. However, dysregulated inflammation in the long term provides a substrate for tumorigenesis [30]. STAT3 alone or in cooperation with NF- $\kappa$ -B regulates the expression of many pro-inflammatory genes [31-33]. Starved tumor cells activate NF- $\kappa$ -B and STAT3 via endoplasmic reticulum (ER) stress and secrete cytokines that stimulate tumor survival and clonogenic capacity [34]. The coactivation of these two transcription factors amplifies pro-inflammatory gene expression driving cancer-associated inflammation [35]. Of interest, the STAT3- NF- $\kappa$ -B complex can repress the expression of DNA Damage Inducible Transcript 3 (DDIT3), an inhibitor of CCAAT Enhancer Binding Protein Beta (CEBP  $\beta$ ), another pro-inflammatory transcription factor [36].

Pharmacological agents that limit inflammation have been proposed for cancer prevention [37]. The use of metformin, a drug widely used to control diabetes, has been associated with a dramatic reduction in cancer incidence in many tissues [38]. Although the primary site of action of this drug is in mitochondria, a consequence of its effects is a potent reduction in the activation of NF- $\kappa$ -B and STAT3, suggesting that the promising anticancer actions of metformin are related to its ability to curtail pro-inflammatory gene expression [39,40]. In contrast to STAT3, STAT5B inhibits NF- $\kappa$ -B activity in the kidney fibroblast cell line COS by competing with coactivators of transcription [41], while it stimulates NF- $\kappa$ -B in leukemia cells [42]. These results suggest the involvement of different regulatory mechanisms of STAT5 in hematopoietic cancers compared with solid cancers.

### **Mitochondria**

In addition to their canonical roles in inflammation and immunity, STAT3 and STAT5 have been shown to localize to mitochondria. The mitochondrial localization of STAT3 is required for its ability to support malignant transformation in murine embryonic fibroblasts and breast cancer cells [43-46], and mito-STAT3 regulates mitochondrial metabolism and mitochondrial gene expression [45,47-51]. Several reports have suggested that STAT3 can be imported to mitochondria after phosphorylation on S727 [44,45] or upon acetylation [52,53]. Other studies have revealed that STAT3

mitochondrial translocation is mediated by interactions with Heat Shock Protein 22 (HSP22), Gene Associated with Retinoic and Interferon-Induced Mortality 19 (GRIM-19) or Translocase of Outer Mitochondrial Membrane 20 (TOM20) [54-56]. The mRNAs coding for some mitochondrial proteins are translated close to or in physical interaction with the import complex TOM [57,58]. The structural motifs mediating those interactions are located in the 3' and 5' UTRs of the mRNAs [59,60] and it will be interesting to investigate whether the mRNA of STAT3 also possesses RNA localization signals (zip codes) to localize in close proximity to mitochondria.

Whereas the role of mitochondrial STAT3 has been extensively studied, the role of STAT5 in mitochondria is less clear. The import of STAT5 to mitochondria is regulated by cytokines [43]. Once imported into the mitochondria, STAT5 binds the D-loop of mitochondrial DNA, although no increase in transcription of mitochondrial genes was observed [61]. Mito-STAT5 is also able to interact with the Pyruvate Dehydrogenase Complex (PDC) and was shown to regulate metabolism towards glycolysis, as observed in cells treated with cytokines [43,61]. In the same line, STAT3 was also shown to interact with the PDC in mitochondria [53].

### **Reprogramming and Stemness**

The role of STAT3 in stem cell biology was initially recognized due to the requirement for the cytokine LIF to maintain pluripotency in cultures of mouse embryonic stem (ES) cells. STAT3 activation mediates the induction or repression of several genes in mouse ES cells including the pluripotency factors *Oct4*, *Klf4*, *Tfcp2l1* and polycomb proteins [62-64]. Many pluripotency factors, such as Homeobox Protein NANOG, are short-lived proteins. STAT3 controls protein stability by inducing the expression of the deubiquitinase Ubiquitin Specific Peptidase 21 (USP21), stabilizing NANOG in mouse ES cells. Induction of ES cell differentiation promotes the Extracellular Signal-Regulated Kinase (ERK)-dependent phosphorylation of USP21 and its dissociation from NANOG, leading to NANOG degradation [65]. STAT3 also plays a role in the reprogramming of somatic cells into induced pluripotent stem (IPS) cells [66] and it has been suggested that its effects depend on the demethylation of pluripotency factor promoters [67]. STAT3 also activates mitochondrial DNA transcription, promoting oxidative phosphorylation during maintenance and induction of pluripotency [68]. It is thus likely that the ability of STAT3 to stimulate stemness also plays a role in its oncogenic activity.

In many tumors, a subpopulation of cells possess a higher malignant capacity. These so-called tumor-initiating cells are suspected to regenerate the tumor after cancer chemotherapy and express many genes commonly expressed in ES cells [69]. It has been shown that STAT3 is required for the formation of tumor spheres and the viability of the cancer stem cell pool in many different tumors [39,40,70-83]. At least in breast cancer, a critical mechanism stimulated by STAT3 to regulate

stemness involves genes in fatty acid oxidation [78,79] and the ability of STAT3 to adjust the levels of reactive oxygen species (ROS) produced in mitochondria [79]. In colorectal cancer cells, STAT3 forms a complex with the stem cell marker CD44 and the p300 acetyltransferase. Acetylation of STAT3 by this complex allows dimerization, nuclear translocation and binding to the promoters of genes required for stemness such as *c-MYC* and *TWIST1* [84].

The role of STAT5 in promoting cancer stemness does not affect many cell types and is mostly confined to hematopoietic cancers [85]. However, Nevalainen and colleagues reported that STAT5B induces stem cell properties in prostate cancer cells [86] in line with the increase in nuclear STAT5A/B observed in these tumors in correlation with bad prognosis [9]. Furthermore, transgenic mice with increased expression of prolactin in prostate epithelial cells displayed increases in the basal/stem cell compartment in association with activation of STAT5. This enrichment of stem cells was partially reversed by depletion of *Stat5a/b* [87]. The pro-stem cell oncogenic effect of STAT5 in the prostate contrasts with its effects in the mammary gland where STAT5 induces cell differentiation [88]. The ETS transcription factor Elf5 (E74-like factor 5) is a target of the prolactin-STAT5 axis and promotes mammary cell differentiation [89-91], supporting the tumor suppressive role of STAT5 in the mammary gland.

### **2.9.5. Tumor Suppressor Functions and Negative Regulation of STAT3/5 Signaling**

The oncogenic activity of JAK/STAT signaling is controlled by several molecular barriers that limit the activation of this pathway. They include tyrosine phosphatases, E3 SUMO ligases of the PIAS family, E3 ubiquitin ligases and miRNAs. In addition, oncogenic STAT3/5 signaling can activate fail-safe tumor suppressors such as p19ARF, SOCS1 and p53 that trigger apoptosis, ferroptosis and/or senescence in potentially malignant cells (Figure 3). Understanding these different responses to STAT signaling in cancer is important to further distinguish tumors that would benefit from STAT3 or STAT5 inhibitors and those that would not.

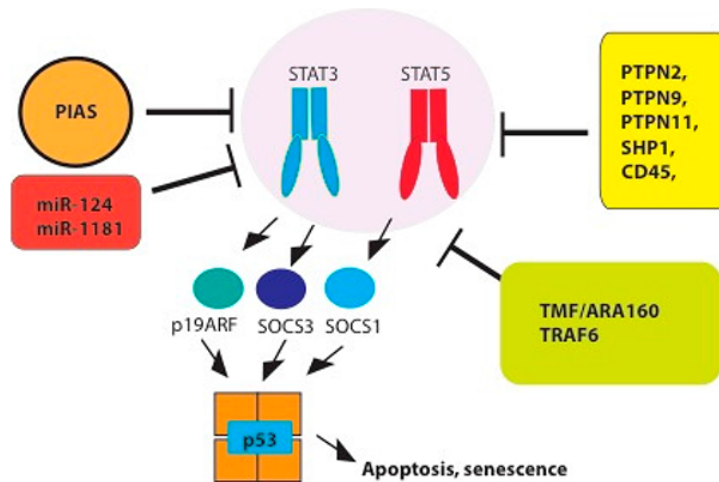


**Figure 3.** Tumor suppressor pathways acting on STAT3/5 activity (Protein Inhibitor of Activated STAT3 PIAS, miRNAs, E3 ligases, phosphatases) or activated by STAT3/5 transcriptional activity (Protein of alternative reading frame 19 (p19ARF) Suppressor of Cytokine Signaling 1 and 3 (SOCS1/3), p53). Abbreviations: (PTPN2 (Tyrosine-protein phosphatase non-receptor type 2), PTPN9/MEG2 (Tyrosine-protein phosphatase non-receptor type 9), PTPN11/SHP2 (Tyrosine-protein phosphatase non-receptor type 11), PTPN6/SHP1 (Tyrosine-protein phosphatase non-receptor type 6) and TNF receptor associated factor 6 (TRAF6)).

## **Tyrosine Phosphatases**

Activation of STAT3 and STAT5 in tumors is often associated with tyrosine phosphorylation, a modification that can be reverted by several protein tyrosine phosphatases such as PTPN2, PTPN9/MEG2, PTPN11/SHP2 [92,93], CD45 [94] and SHP1 [95]. However, little is known about a possible role of these phosphatases in STAT3 activation in solid tumors. In liver cancers, SHP1 is downregulated in cells with mesenchymal features, and restoring its levels both reduced STAT3 phosphorylation and reversed the mesenchymal phenotype of liver cancer cells [95]. SHP1 and SHP2 also target STAT5 [96,97] but the significance of this regulation in solid tumors remains to be investigated.

## **PIAS**

The Protein Inhibitor of Activated STAT3 (PIAS3) inhibits STAT3 transcriptional activity. In gliomas, PIAS3 expression is reduced [98]. Mechanistically, SMAD6 promotes PIAS3 degradation, promoting glioma cell growth and stem cell properties [76]. The PIAS proteins have SUMO E3 ligase activity acting on multiple proteins, and so their effects cannot be solely attributed to STAT3 inhibition [99]. Of interest, PIAS3 can bind NF- $\kappa$ -B promoting its SUMOylation and inhibiting its activity [100,101], potentially targeting the expression of many pro-inflammatory genes required for tumor progression. Also, PIAS3 binds the N-terminus of p53 and prevents the interaction with its negative regulator MDM2, leading to p53 stabilization [102].

## **E3 Ligases**

The Golgi resident and BC-box protein TMF/ARA160 was reported as an E3 ligase that catalyzes STAT3 ubiquitination leading to its proteasome-dependent degradation in myogenic C2C12 cells. The level of TMF/ARA160 was found to be significantly decreased in glioblastoma multiforme tumors, in benign meningioma and in malignant anaplastic meningioma, where STAT3 is known to play an oncogenic role [103]. Like PIAS3, TMF/ARA160 can also bind and ubiquitinate RELA/NF- $\kappa$ -B leading to its proteasome-dependent degradation and a decrease in the expression of inflammatory genes [104]. Furthermore, the ubiquitin ligase TRAF6 binds and ubiquitinates STAT3 inhibiting the expression of STAT3 target genes [105]. During oncogene-induced senescence, STAT3 is degraded by the proteasome but the E3 ligase responsible has not been identified [106]. Recent results revealed that the long non-coding RNA (lncRNA) PVT1 binds STAT3 and protects it from ubiquitin-dependent degradation in gastric cancer [107]. PVT1 is upregulated in multiple cancers predicting poor prognosis for overall survival [108-110].

## **MiRNAs**

The miRNA miR-124 regulates STAT3 signaling by targeting the mRNAs of interleukin-6 receptor (IL6R) [111] and STAT3 [112,113]. Suppression of this miRNA increases STAT3 phosphorylation and induces transformation in immortalized mouse hepatocytes. Of interest, systemic delivery of miR-124 prevented tumor growth in diethylnitrosamine (DEN)-treated mice, and miR-124 levels were found to be reduced in human hepatocellular carcinomas (HCC) [111]. In gliomas, miR-124 is poorly expressed but upregulation of its expression in glioma cancer stem cells inhibited the STAT3 pathway. In this model, STAT3 mediates immunosuppression, which was relieved upon systemic miR-124 delivery [114]. The circular RNA (circRNA) 100782 is upregulated in pancreatic cancer and its knockdown downregulates all miR-124 targets including IL6R and STAT3. This circRNA binds miR-124 suggesting that it may act as a miRNA sponge [115]. Furthermore, the miRNA miR-1181 also targets STAT3 and is downregulated in pancreatic cancer, predicting poorer overall survival. Overexpression of miR-1181 inhibited tumor formation and stem cell properties of pancreatic cancer cells [116].

### **The Suppressor of Cytokine Signaling SOCS**

The members of the SOCS family are major negative feedback regulators of JAK/STAT signaling and their expression is dysregulated in many human cancers [117-119]. These genes provide a barrier for cells with aberrant cytokine activation by inhibiting cytokine signaling [120]. In STAT3 driven cancers, SOCS3 seems to be the most important negative feedback regulator and mouse models of SOCS3 ablation show strong STAT3 activation [119,121-124]. On the other hand, in solid cancers where STAT5 plays a causal role such as liver and prostate cancer, in addition to SOCS3, SOCS1 is frequently inactivated and mouse models of SOCS1 ablation increase both liver and prostate tumorigenesis [125-132]. In addition to their role as JAK/STAT signaling barriers, SOCS1 and SOCS3 can bind p53 and activate tumor suppressor responses such as senescence and ferroptosis when their expression is induced by aberrant STAT5 signaling in primary cells [133-138]. In this way, SOCS1 and SOCS3 also act as fail-safe tumor suppressors in response to aberrant JAK/STAT signaling. So far, the SOCS1-p53-senescence axis has been demonstrated in primary fibroblasts and mammary epithelial cells [133,139-141]. This mechanism may explain the better prognosis of some solid cancers with high p-STAT5 [142-144] and the high frequency of SOCS1 inactivation in STAT5-driven cancers [125-132]. However, it is difficult to obtain evidence of a senescence tumor-suppression response by studying established tumors that have already circumvented this pathway. Senescence is particularly noticeable in premalignant lesions and benign tumors [40,106,145-150], and can be reactivated by cancer chemotherapy [151,152]. For this reason, evidence of STAT5-induced senescence in human cancers is not yet available and should be studied in samples from premalignant tumors or after chemotherapy.



The mechanisms that disable SOCS1 and SOCS3 in human cancers are often epigenetic, mediated either by miRNAs, promoter methylation or protein phosphorylation [127,128,130,131,137,153-162]. The SRC family of kinases (SFK) phosphorylate SOCS1 at Y80, interfering with p53-SOCS1 interactions. SFK inhibitors can reverse this effect and could be used to restore the SOCS1-p53 axis in tumors where these two proteins remain intact [162]. It is also possible to consider treatments that re-express SOCS1/3 in tumors. Indeed, in liver cancer *SOCS3* gene expression can be re-established by drugs that activate the Farnesoid X receptor (FXR) [163,164]. Gene therapy strategies are also under development to re-express SOCS1 or SOCS3 in tumors [165-167].

### **P19ARF-p53 Pathway**

One of the first reports demonstrating that STAT3 can act as a tumor suppressor was shown in glioblastoma multiforme (GBM) [168] where a combination of low PTEN expression and loss of STAT3 in astrocytes increased their tumorigenicity. This observation is in contrast to papers cited above on the requirement for STAT3 to maintain tumor stem cells in GBM [73,75,169]. This could be explained if STAT3 acts early in tumorigenesis as a tumor suppressor but gains oncogenic functions in the context of the cancer genome and epigenome. An interesting mechanism for the tumor suppressor role of STAT3 was recently described in the prostate where STAT3 induces the expression of p19ARF [170]. The latter is a tumor suppressor that activates p53 and inhibits ribosome biogenesis inducing cellular senescence and apoptosis [171-174]. Loss of STAT3 disrupts this STAT3-ARF-p53 axis and permits tumor progression [175]. STAT3 and other STATs can also induce p21 leading to cell cycle arrest or cellular senescence [176,177]. Further evidence for STAT3 as a tumor suppressor has been reported in lung [178], colon [179,180], thyroid [181], liver [182,183], skin [184], neck [185], nasopharynx, rectum [186], salivary gland [187] and breast cancers [188] but the mechanisms remain to be investigated.

### **2.9.6. Concluding Remarks**

Context-dependent activities of STAT3 and STAT5 in solid human cancers justify detailed molecular studies that will clarify the specific molecular mechanisms of action of these two cancer genes. The cancer genome and transcriptome are shaped and selected to favor cancer cell survival and proliferation. Although restoring mutated genes is technologically difficult, reprogramming the transcriptome to restore tumor suppression may be feasible. Drugs acting on STAT3/5 and their regulators may restore the control of cell proliferation in cancer cells.

**Funding:** This research received no external funding.

**Acknowledgments:** We thank Dr. V. Bourdeau for comments. G.F. is supported by the CIBC chair for breast cancer research at the CRCHUM. This work was funded by a grant from the Canadian Institute of Health and Research (CIHR-MOP229774) to G.F. H.A.N. is supported by the Austrian Science Fund (FWF), under the frame of ERA PerMed (I 4218-B). H.A.N. is also generously supported by a private donation from Liechtenstein.

## 2.9.7. References

- (1) Bromberg, J.; Darnell, J.E., Jr. The role of STATs in transcriptional control and their impact on cellular function. *Oncogene* **2000**, *19*, 2468-2473, doi:10.1038/sj.onc.1203476.
- (2) Kandoth, C.; McLellan, M.D.; Vandin, F.; Ye, K.; Niu, B.; Lu, C.; Xie, M.; Zhang, Q.; McMichael, J.F.; Wyczalkowski, M.A.; et al. Mutational landscape and significance across 12 major cancer types. *Nature* **2013**, *502*, 333-339, doi:10.1038/nature12634.
- (3) de Araujo, E.D.; Erdogan, F.; Neubauer, H.A.; Meneksedag-Erol, D.; Manaswiyoungkul, P.; Eram, M.S.; Seo, H.S.; Qadree, A.K.; Israelian, J.; Orlova, A.; et al. Structural and functional consequences of the STAT5B(N642H) driver mutation. *Nat. Commun.* **2019**, *10*, 2517, doi:10.1038/s41467-019-10422-7.
- (4) Koskela, H.L.; Eldfors, S.; Ellonen, P.; van Adrichem, A.J.; Kuusanmaki, H.; Andersson, E.I.; Lagstrom, S.; Clemente, M.J.; Olson, T.; Jalkanen, S.E.; et al. Somatic STAT3 mutations in large granular lymphocytic leukemia. *N. Engl. J. Med.* **2012**, *366*, 1905-1913, doi:10.1056/NEJMoa1114885.
- (5) Carpenter, R.L.; Lo, H.W. STAT3 Target Genes Relevant to Human Cancers. *Cancers (Basel)* **2014**, *6*, 897-925, doi:10.3390/cancers6020897.
- (6) Basham, B.; Sathe, M.; Grein, J.; McClanahan, T.; D'Andrea, A.; Lees, E.; Rascle, A. In vivo identification of novel STAT5 target genes. *Nucleic Acids Res.* **2008**, *36*, 3802-3818, doi:10.1093/nar/gkn271.
- (7) Wu, P.; Wu, D.; Zhao, L.; Huang, L.; Shen, G.; Huang, J.; Chai, Y. Prognostic role of STAT3 in solid tumors: A systematic review and meta-analysis. *Oncotarget* **2016**, *7*, 19863-19883, doi:10.18632/oncotarget.7887.
- (8) Mohanty, S.K.; Yagiz, K.; Pradhan, D.; Luthringer, D.J.; Amin, M.B.; Alkan, S.; Cinar, B. STAT3 and STAT5A are potential therapeutic targets in castration-resistant prostate cancer. *Oncotarget* **2017**, *8*, 85997-86010, doi:10.18632/oncotarget.20844.
- (9) Mirtti, T.; Leiby, B.E.; Abdulghani, J.; Aaltonen, E.; Pavela, M.; Mamtani, A.; Alanen, K.; Egevad, L.; Granfors, T.; Josefsson, A.; et al. Nuclear Stat5a/b predicts early recurrence and prostate cancer-specific death in patients treated by radical prostatectomy. *Hum. Pathol.* **2013**, *44*, 310-319, doi:10.1016/j.humpath.2012.06.001.
- (10) Klupp, F.; Diers, J.; Kahlert, C.; Neumann, L.; Halama, N.; Franz, C.; Schmidt, T.; Laitschka, F.; Warth, A.; Weitz, J.; et al. Expressional STAT3/STAT5 Ratio is an Independent Prognostic Marker in Colon Carcinoma. *Ann. Surg. Oncol.* **2015**, *22*, S1548-S1555, doi:10.1245/s10434-015-4485-4.

- (11) Peck, A.R.; Witkiewicz, A.K.; Liu, C.; Stringer, G.A.; Klimowicz, A.C.; Pequignot, E.; Freydin, B.; Tran, T.H.; Yang, N.; Rosenberg, A.L.; et al. Loss of nuclear localized and tyrosine phosphorylated Stat5 in breast cancer predicts poor clinical outcome and increased risk of antiestrogen therapy failure. *J. Clin. Oncol.* **2011**, *29*, 2448-2458, doi:10.1200/JCO.2010.30.3552.
- (12) Kaltenecker, D.; Themanns, M.; Mueller, K.M.; Spirk, K.; Suske, T.; Merkel, O.; Kenner, L.; Luis, A.; Kozlov, A.; Haybaeck, J.; et al. Hepatic growth hormone-JAK2-STAT5 signalling: Metabolic function, non-alcoholic fatty liver disease and hepatocellular carcinoma progression. *Cytokine* **2018**, doi:10.1016/j.cyto.2018.10.010.
- (13) Ferbeyre, G.; Moriggl, R. The role of Stat5 transcription factors as tumor suppressors or oncogenes. *Biochim. Biophys. Acta* **2011**, *1815*, 104-114, doi:10.1016/j.bbcan.2010.10.004.
- (14) Xu, Y.H.; Lu, S. A meta-analysis of STAT3 and phospho-STAT3 expression and survival of patients with non-small-cell lung cancer. *Eur. J. Surg Oncol.* **2014**, *40*, 311-317, doi:10.1016/j.ejso.2013.11.012.
- (15) Sun, Z.G.; Zhang, M.; Yang, F.; Gao, W.; Wang, Z.; Zhu, L.M. Clinical and prognostic significance of signal transducer and activator of transcription 3 and mucin 1 in patients with non-small cell lung cancer following surgery. *Oncol. Lett.* **2018**, *15*, 4278-4288, doi:10.3892/ol.2018.7858.
- (16) Tong, M.; Wang, J.; Jiang, N.; Pan, H.; Li, D. Correlation between p-STAT3 overexpression and prognosis in lung cancer: A systematic review and meta-analysis. *PLoS ONE* **2017**, *12*, e0182282, doi:10.1371/journal.pone.0182282.
- (17) Koperek, O.; Aumayr, K.; Schindl, M.; Werba, G.; Soleiman, A.; Schoppmann, S.; Sahora, K.; Birner, P. Phosphorylation of STAT3 correlates with HER2 status, but not with survival in pancreatic ductal adenocarcinoma. *APMIS* **2014**, *122*, 476-481, doi:10.1111/apm.12194.
- (18) Liang, C.; Xu, Y.; Ge, H.; Li, G.; Wu, J. Clinicopathological significance and prognostic role of p-STAT3 in patients with hepatocellular carcinoma. *Onco Targets Ther* **2018**, *11*, 1203-1214, doi:10.2147/OTT.S156198.
- (19) Liu, Y.; Huang, J.; Li, W.; Chen, Y.; Liu, X.; Wang, J. Meta-analysis of STAT3 and phospho-STAT3 expression and survival of patients with breast cancer. *Oncotarget* **2018**, *9*, 13060-13067, doi:10.18632/oncotarget.23962.
- (20) Sonnenblick, A.; Salgado, R.; Brohee, S.; Zahavi, T.; Peretz, T.; Van den Eynden, G.; Rouas, G.; Salmon, A.; Francis, P.A.; Di Leo, A.; et al. p-STAT3 in luminal breast cancer: Integrated RNA-protein pooled analysis and results from the BIG 2-98 phase III trial. *Int. J. Oncol.* **2018**, *52*, 424-432, doi:10.3892/ijo.2017.4212.

- (21) Lin, G.S.; Chen, Y.P.; Lin, Z.X.; Wang, X.F.; Zheng, Z.Q.; Chen, L. STAT3 serine 727 phosphorylation influences clinical outcome in glioblastoma. *Int. J. Clin. Exp. Pathol.* **2014**, *7*, 3141-3149.
- (22) Vilardell, J.; Alcaraz, E.; Sarro, E.; Trilla, E.; Cuadros, T.; de Torres, I.; Plana, M.; Ramon, Y.C.S.; Pinna, L.A.; Ruzzene, M.; et al. Under-expression of CK2beta subunit in ccRCC represents a complementary biomarker of p-STAT3 Ser727 that correlates with patient survival. *Oncotarget* **2018**, *9*, 5736-5751, doi:10.18632/oncotarget.23422.
- (23) Kusaba, T.; Nakayama, T.; Yamazumi, K.; Yakata, Y.; Yoshizaki, A.; Inoue, K.; Nagayasu, T.; Sekine, I. Activation of STAT3 is a marker of poor prognosis in human colorectal cancer. *Oncol. Rep.* **2006**, *15*, 1445-1451.
- (24) Morikawa, T.; Baba, Y.; Yamauchi, M.; Kuchiba, A.; Nosho, K.; Shima, K.; Tanaka, N.; Huttenhower, C.; Frank, D.A.; Fuchs, C.S.; et al. STAT3 expression, molecular features, inflammation patterns, and prognosis in a database of 724 colorectal cancers. *Clin. Cancer Res.* **2011**, *17*, 1452-1462, doi:10.1158/1078-0432.CCR-10-2694.
- (25) Lee, J.L.; Wang, M.J.; Chen, J.Y. Acetylation and activation of STAT3 mediated by nuclear translocation of CD44. *J. Cell Biol.* **2009**, *185*, 949-957, doi:10.1083/jcb.200812060.
- (26) Banerjee, K.; Resat, H. Constitutive activation of STAT3 in breast cancer cells: A review. *Int. J. Cancer* **2016**, *138*, 2570-2578, doi:10.1002/ijc.29923.
- (27) Lu, L.; Zhu, F.; Zhang, M.; Li, Y.; Drennan, A.C.; Kimpara, S.; Rumball, I.; Selzer, C.; Cameron, H.; Kellicut, A.; et al. Gene regulation and suppression of type I interferon signaling by STAT3 in diffuse large B cell lymphoma. *Proc. Natl. Acad. Sci. USA* **2018**, *115*, E498-E505, doi:10.1073/pnas.1715118115.
- (28) Creamer, B.A.; Sakamoto, K.; Schmidt, J.W.; Triplett, A.A.; Moriggl, R.; Wagner, K.U. Stat5 promotes survival of mammary epithelial cells through transcriptional activation of a distinct promoter in Akt1. *Mol. Cell. Biol.* **2010**, *30*, 2957-2970, doi:10.1128/MCB.00851-09.
- (29) Tell, R.W.; Horvath, C.M. Bioinformatic analysis reveals a pattern of STAT3-associated gene expression specific to basal-like breast cancers in human tumors. *Proc. Natl. Acad. Sci. USA* **2014**, *111*, 12787-12792, doi:10.1073/pnas.1404881111.
- (30) Karki, R.; Kanneganti, T.D. Diverging inflammasome signals in tumorigenesis and potential targeting. *Nat. Rev. Cancer* **2019**, *19*, 197-214, doi:10.1038/s41568-019-0123-y.
- (31) Martincuks, A.; Andryka, K.; Kuster, A.; Schmitz-Van de Leur, H.; Komorowski, M.; Muller-Newen, G. Nuclear translocation of STAT3 and NF-kappaB are independent of each other but NF-kappaB supports expression and activation of STAT3. *Cell. Signal.* **2017**, *32*, 36-47, doi:10.1016/j.cellsig.2017.01.006.

- (32) Goldstein, I.; Paakinaho, V.; Baek, S.; Sung, M.H.; Hager, G.L. Synergistic gene expression during the acute phase response is characterized by transcription factor assisted loading. *Nat. Commun.* **2017**, *8*, 1849, doi:10.1038/s41467-017-02055-5.
- (33) Grivennikov, S.I.; Karin, M. Dangerous liaisons: STAT3 and NF-kappaB collaboration and crosstalk in cancer. *Cytokine Growth Factor Rev.* **2010**, *21*, 11-19, doi:10.1016/j.cytogfr.2009.11.005.
- (34) Yoon, S.; Woo, S.U.; Kang, J.H.; Kim, K.; Shin, H.J.; Gwak, H.S.; Park, S.; Chwae, Y.J. NF-kappaB and STAT3 cooperatively induce IL6 in starved cancer cells. *Oncogene* **2012**, *31*, 3467-3481, doi:10.1038/onc.2011.517.
- (35) Atsumi, T.; Singh, R.; Sabharwal, L.; Bando, H.; Meng, J.; Arima, Y.; Yamada, M.; Harada, M.; Jiang, J.J.; Kamimura, D.; et al. Inflammation amplifier, a new paradigm in cancer biology. *Cancer Res.* **2014**, *74*, 8-14, doi:10.1158/0008-5472.CAN-13-2322.
- (36) Canino, C.; Luo, Y.; Marcato, P.; Blandino, G.; Pass, H.I.; Cioce, M. A STAT3-NFkB/DDIT3/CEBPbeta axis modulates ALDH1A3 expression in chemoresistant cell subpopulations. *Oncotarget* **2015**, *6*, 12637-12653, doi:10.18632/oncotarget.3703.
- (37) Thi, H.T.H.; Hong, S. Inflammasome as a Therapeutic Target for Cancer Prevention and Treatment. *J. Cancer Prev.* **2017**, *22*, 62-73, doi:10.15430/JCP.2017.22.2.62.
- (38) Pollak, M.N. Investigating metformin for cancer prevention and treatment: The end of the beginning. *Cancer Discov.* **2012**, *2*, 778-790, doi:10.1158/2159-8290.CD-12-0263.
- (39) Hirsch, H.A.; Iliopoulos, D.; Struhl, K. Metformin inhibits the inflammatory response associated with cellular transformation and cancer stem cell growth. *Proc. Natl. Acad. Sci. USA* **2013**, *110*, 972-977, doi:10.1073/pnas.1221055110.
- (40) Deschenes-Simard, X.; Parisotto, M.; Rowell, M.C.; Le Calve, B.; Igelmann, S.; Moineau-Vallee, K.; Saint-Germain, E.; Kalegari, P.; Bourdeau, V.; Kottakis, F.; et al. Circumventing senescence is associated with stem cell properties and metformin sensitivity. *Aging Cell* **2019**, doi:10.1111/acel.12889.
- (41) Luo, G.; Yu-Lee, L. Stat5b inhibits NFkappaB-mediated signaling. *Mol. Endocrinol.* **2000**, *14*, 114-123, doi:10.1210/mend.14.1.0399.
- (42) Kawashima, T.; Murata, K.; Akira, S.; Tonozuka, Y.; Minoshima, Y.; Feng, S.; Kumagai, H.; Tsuruga, H.; Ikeda, Y.; Asano, S.; et al. STAT5 induces macrophage differentiation of M1 leukemia cells through activation of IL-6 production mediated by NF-kappaB p65. *J. Immunol.* **2001**, *167*, 3652-3660.
- (43) Chueh, F.Y.; Leong, K.F.; Yu, C.L. Mitochondrial translocation of signal transducer and activator of transcription 5 (STAT5) in leukemic T cells and cytokine-stimulated cells. *Biochem. Biophys. Res. Commun.* **2010**, *402*, 778-783, doi:10.1016/j.bbrc.2010.10.112.

- (44) Gough, D.J.; Corlett, A.; Schlessinger, K.; Wegrzyn, J.; Larner, A.C.; Levy, D.E. Mitochondrial STAT3 supports Ras-dependent oncogenic transformation. *Science* **2009**, *324*, 1713-1716.
- (45) Wegrzyn, J.; Potla, R.; Chwae, Y.J.; Sepuri, N.B.; Zhang, Q.; Koeck, T.; Derecka, M.; Szczepanek, K.; Szelag, M.; Gornicka, A.; et al. Function of mitochondrial Stat3 in cellular respiration. *Science* **2009**, *323*, 793-797.
- (46) Zhang, Q.; Raje, V.; Yakovlev, V.A.; Yacoub, A.; Szczepanek, K.; Meier, J.; Derecka, M.; Chen, Q.; Hu, Y.; Sisler, J.; et al. Mitochondrial localized Stat3 promotes breast cancer growth via phosphorylation of serine 727. *J. Biol. Chem.* **2013**, *288*, 31280-31288, doi:10.1074/jbc.M113.505057.
- (47) Macias, E.; Rao, D.; Carbajal, S.; Kiguchi, K.; DiGiovanni, J. Stat3 binds to mtDNA and regulates mitochondrial gene expression in keratinocytes. *J. Investig. Dermatol.* **2014**, *134*, 1971-1980, doi:10.1038/jid.2014.68.
- (48) Rincon, M.; Pereira, F.V. A New Perspective: Mitochondrial Stat3 as a Regulator for Lymphocyte Function. *Int. J. Mol. Sci.* **2018**, *19*, doi:10.3390/ijms19061656.
- (49) Avalle, L.; Poli, V. Nucleus, Mitochondrion, or Reticulum? STAT3 a La Carte. *Int. J. Mol. Sci.* **2018**, *19*, doi:10.3390/ijms19092820.
- (50) Luo, D.; Fraga-Lauhirat, M.; Millings, J.; Ho, C.; Villarreal, E.M.; Fletchinger, T.C.; Bonfiglio, J.V.; Mata, L.; Nemesure, M.D.; Bartels, L.E.; et al. Phospho-valproic acid (MDC-1112) suppresses glioblastoma growth in preclinical models through the inhibition of STAT3 phosphorylation. *Carcinogenesis* **2019**, doi:10.1093/carcin/bgz069.
- (51) Sala, D.; Cunningham, T.J.; Stec, M.J.; Etxaniz, U.; Nicoletti, C.; Dall'Agnesse, A.; Puri, P.L.; Dueter, G.; Latella, L.; Sacco, A. The Stat3-Fam3a axis promotes muscle stem cell myogenic lineage progression by inducing mitochondrial respiration. *Nat. Commun.* **2019**, *10*, 1796, doi:10.1038/s41467-019-09746-1.
- (52) Bernier, M.; Paul, R.K.; Martin-Montalvo, A.; Scheibye-Knudsen, M.; Song, S.; He, H.J.; Armour, S.M.; Hubbard, B.P.; Bohr, V.A.; Wang, L.; et al. Negative regulation of STAT3 protein-mediated cellular respiration by SIRT1 protein. *J. Biol. Chem.* **2011**, *286*, 19270-19279, doi:10.1074/jbc.M110.200311.
- (53) Xu, Y.S.; Liang, J.J.; Wang, Y.; Zhao, X.J.; Xu, L.; Xu, Y.Y.; Zou, Q.C.; Zhang, J.M.; Tu, C.E.; Cui, Y.G.; et al. STAT3 Undergoes Acetylation-dependent Mitochondrial Translocation to Regulate Pyruvate Metabolism. *Sci. Rep.* **2016**, *6*, 39517, doi:10.1038/srep39517.
- (54) Boengler, K.; Hilfiker-Kleiner, D.; Heusch, G.; Schulz, R. Inhibition of permeability transition pore opening by mitochondrial STAT3 and its role in myocardial ischemia/reperfusion. *Basic Res. Cardiol.* **2010**, *105*, 771-785, doi:10.1007/s00395-010-0124-1.

- (55) Tammineni, P.; Anugula, C.; Mohammed, F.; Anjaneyulu, M.; Larner, A.C.; Sepuri, N.B. The import of the transcription factor STAT3 into mitochondria depends on GRIM-19, a component of the electron transport chain. *J. Biol. Chem.* **2013**, *288*, 4723-4732, doi:10.1074/jbc.M112.378984.
- (56) Qiu, H.; Lizano, P.; Laure, L.; Sui, X.; Rashed, E.; Park, J.Y.; Hong, C.; Gao, S.; Holle, E.; Morin, D.; et al. H11 kinase/heat shock protein 22 deletion impairs both nuclear and mitochondrial functions of STAT3 and accelerates the transition into heart failure on cardiac overload. *Circulation* **2011**, *124*, 406-415, doi:10.1161/CIRCULATIONAHA.110.013847.
- (57) Gadir, N.; Haim-Vilmovsky, L.; Kraut-Cohen, J.; Gerst, J.E. Localization of mRNAs coding for mitochondrial proteins in the yeast *Saccharomyces cerevisiae*. *RNA* **2011**, *17*, 1551-1565, doi:10.1261/rna.2621111.
- (58) Fox, T.D. Mitochondrial protein synthesis, import, and assembly. *Genetics* **2012**, *192*, 1203-1234, doi:10.1534/genetics.112.141267.
- (59) Zhang, Y.; Chen, Y.; Gucek, M.; Xu, H. The mitochondrial outer membrane protein MDI promotes local protein synthesis and mtDNA replication. *EMBO J.* **2016**, *35*, 1045-1057, doi:10.15252/embj.201592994.
- (60) Hansen, K.G.; Herrmann, J.M. Transport of Proteins into Mitochondria. *Protein J.* **2019**, doi:10.1007/s10930-019-09819-6.
- (61) Richard, A.J.; Hang, H.; Stephens, J.M. Pyruvate dehydrogenase complex (PDC) subunits moonlight as interaction partners of phosphorylated STAT5 in adipocytes and adipose tissue. *J. Biol. Chem.* **2017**, *292*, 19733-19742, doi:10.1074/jbc.M117.811794.
- (62) Kidder, B.L.; Yang, J.; Palmer, S. Stat3 and c-Myc genome-wide promoter occupancy in embryonic stem cells. *PLoS ONE* **2008**, *3*, e3932, doi:10.1371/journal.pone.0003932.
- (63) Hall, J.; Guo, G.; Wray, J.; Eyres, I.; Nichols, J.; Grotewold, L.; Morfopoulou, S.; Humphreys, P.; Mansfield, W.; Walker, R.; et al. Oct4 and LIF/Stat3 additively induce Kruppel factors to sustain embryonic stem cell self-renewal. *Cell Stem Cell* **2009**, *5*, 597-609, doi:10.1016/j.stem.2009.11.003.
- (64) Ye, S.; Li, P.; Tong, C.; Ying, Q.L. Embryonic stem cell self-renewal pathways converge on the transcription factor Tfcp211. *EMBO J.* **2013**, *32*, 2548-2560, doi:10.1038/emboj.2013.175.
- (65) Jin, J.; Liu, J.; Chen, C.; Liu, Z.; Jiang, C.; Chu, H.; Pan, W.; Wang, X.; Zhang, L.; Li, B.; et al. The deubiquitinase USP21 maintains the stemness of mouse embryonic stem cells via stabilization of Nanog. *Nat. Commun.* **2016**, *7*, 13594, doi:10.1038/ncomms13594.



- (66) Yang, J.; van Oosten, A.L.; Theunissen, T.W.; Guo, G.; Silva, J.C.; Smith, A. Stat3 activation is limiting for reprogramming to ground state pluripotency. *Cell Stem Cell* **2010**, *7*, 319-328, doi:10.1016/j.stem.2010.06.022.
- (67) Tang, Y.; Luo, Y.; Jiang, Z.; Ma, Y.; Lin, C.J.; Kim, C.; Carter, M.G.; Amano, T.; Park, J.; Kish, S.; et al. Jak/Stat3 signaling promotes somatic cell reprogramming by epigenetic regulation. *Stem Cells* **2012**, *30*, 2645-2656, doi:10.1002/stem.1225.
- (68) Carbognin, E.; Betto, R.M.; Soriano, M.E.; Smith, A.G.; Martello, G. Stat3 promotes mitochondrial transcription and oxidative respiration during maintenance and induction of naive pluripotency. *EMBO J.* **2016**, *35*, 618-634, doi:10.15252/embj.201592629.
- (69) Ben-Porath, I.; Thomson, M.W.; Carey, V.J.; Ge, R.; Bell, G.W.; Regev, A.; Weinberg, R.A. An embryonic stem cell-like gene expression signature in poorly differentiated aggressive human tumors. *Nat. Genet.* **2008**, *40*, 499-507, doi:10.1038/ng.127.
- (70) Zhou, J.; Wulfkuhle, J.; Zhang, H.; Gu, P.; Yang, Y.; Deng, J.; Margolick, J.B.; Liotta, L.A.; Petricoin, E., 3rd; Zhang, Y. Activation of the PTEN/mTOR/STAT3 pathway in breast cancer stem-like cells is required for viability and maintenance. *Proc. Natl. Acad. Sci. USA* **2007**, *104*, 16158-16163, doi:10.1073/pnas.0702596104.
- (71) Marotta, L.L.; Almendro, V.; Marusyk, A.; Shipitsin, M.; Schemme, J.; Walker, S.R.; Bloushtain-Qimron, N.; Kim, J.J.; Choudhury, S.A.; Maruyama, R.; et al. The JAK2/STAT3 signaling pathway is required for growth of CD44(+)CD24(-) stem cell-like breast cancer cells in human tumors. *J. Clin. Investig.* **2011**, *121*, 2723-2735, doi:10.1172/JCI44745.
- (72) Iliopoulos, D.; Hirsch, H.A.; Struhl, K. An epigenetic switch involving NF-kappaB, Lin28, Let-7 MicroRNA, and IL6 links inflammation to cell transformation. *Cell* **2009**, *139*, 693-706, doi:10.1016/j.cell.2009.10.014.
- (73) Gong, A.H.; Wei, P.; Zhang, S.; Yao, J.; Yuan, Y.; Zhou, A.D.; Lang, F.F.; Heimberger, A.B.; Rao, G.; Huang, S. FoxM1 Drives a Feed-Forward STAT3-Activation Signaling Loop That Promotes the Self-Renewal and Tumorigenicity of Glioblastoma Stem-like Cells. *Cancer Res.* **2015**, *75*, 2337-2348, doi:10.1158/0008-5472.CAN-14-2800.
- (74) Peng, L.; Jiang, D. Resveratrol eliminates cancer stem cells of osteosarcoma by STAT3 pathway inhibition. *PLoS ONE* **2018**, *13*, e0205918, doi:10.1371/journal.pone.0205918.
- (75) Man, J.; Yu, X.; Huang, H.; Zhou, W.; Xiang, C.; Huang, H.; Miele, L.; Liu, Z.; Bebek, G.; Bao, S.; et al. Hypoxic Induction of Vasorin Regulates Notch1 Turnover to Maintain Glioma Stem-like Cells. *Cell Stem Cell* **2018**, *22*, 104-118 e106, doi:10.1016/j.stem.2017.10.005.

- (76) Jiao, J.; Zhang, R.; Li, Z.; Yin, Y.; Fang, X.; Ding, X.; Cai, Y.; Yang, S.; Mu, H.; Zong, D.; et al. Nuclear Smad6 promotes gliomagenesis by negatively regulating PIAS3-mediated STAT3 inhibition. *Nat. Commun.* **2018**, *9*, 2504, doi:10.1038/s41467-018-04936-9.
- (77) He, W.; Wu, J.; Shi, J.; Huo, Y.M.; Dai, W.; Geng, J.; Lu, P.; Yang, M.W.; Fang, Y.; Wang, W.; et al. IL22RA1/STAT3 Signaling Promotes Stemness and Tumorigenicity in Pancreatic Cancer. *Cancer Res.* **2018**, *78*, 3293-3305, doi:10.1158/0008-5472.CAN-17-3131.
- (78) Wang, T.; Fahrman, J.F.; Lee, H.; Li, Y.J.; Tripathi, S.C.; Yue, C.; Zhang, C.; Lifshitz, V.; Song, J.; Yuan, Y.; et al. JAK/STAT3-Regulated Fatty Acid beta-Oxidation Is Critical for Breast Cancer Stem Cell Self-Renewal and Chemoresistance. *Cell Metab.* **2018**, *27*, 136-150, doi:10.1016/j.cmet.2017.11.001.
- (79) Kitajima, S.; Yoshida, A.; Kohno, S.; Li, F.; Suzuki, S.; Nagatani, N.; Nishimoto, Y.; Sasaki, N.; Muranaka, H.; Wan, Y.; et al. The RB-IL-6 axis controls self-renewal and endocrine therapy resistance by fine-tuning mitochondrial activity. *Oncogene* **2017**, *36*, 5145-5157, doi:10.1038/onc.2017.124.
- (80) Chen, M.W.; Yang, S.T.; Chien, M.H.; Hua, K.T.; Wu, C.J.; Hsiao, S.M.; Lin, H.; Hsiao, M.; Su, J.L.; Wei, L.H. The STAT3-miRNA-92-Wnt Signaling Pathway Regulates Spheroid Formation and Malignant Progression in Ovarian Cancer. *Cancer Res.* **2017**, *77*, 1955-1967, doi:10.1158/0008-5472.CAN-16-1115.
- (81) Schroeder, A.; Herrmann, A.; Cherryholmes, G.; Kowolik, C.; Buettner, R.; Pal, S.; Yu, H.; Muller-Newen, G.; Jove, R. Loss of androgen receptor expression promotes a stem-like cell phenotype in prostate cancer through STAT3 signaling. *Cancer Res.* **2014**, *74*, 1227-1237, doi:10.1158/0008-5472.CAN-13-0594.
- (82) Tang, Y.; Kitisin, K.; Jogunoori, W.; Li, C.; Deng, C.X.; Mueller, S.C.; Ransom, H.W.; Rashid, A.; He, A.R.; Mendelson, J.S.; et al. Progenitor/stem cells give rise to liver cancer due to aberrant TGF-beta and IL-6 signaling. *Proc. Natl. Acad. Sci. USA* **2008**, *105*, 2445-2450, doi:10.1073/pnas.0705395105.
- (83) Thiagarajan, P.S.; Zheng, Q.; Bhargava, M.; Mulkearns-Hubert, E.E.; Myers, M.G.; Lathia, J.D.; Reizes, O. STAT3 activation by leptin receptor is essential for TNBC stem cell maintenance. *Endocr Relat Cancer* **2017**, *24*, 415-426, doi:10.1530/ERC-16-0349.
- (84) Su, Y.J.; Lai, H.M.; Chang, Y.W.; Chen, G.Y.; Lee, J.L. Direct reprogramming of stem cell properties in colon cancer cells by CD44. *EMBO J.* **2011**, *30*, 3186-3199, doi:10.1038/emboj.2011.211.
- (85) Schepers, H.; van Gosliga, D.; Wierenga, A.T.; Eggen, B.J.; Schuringa, J.J.; Velting, E. STAT5 is required for long-term maintenance of normal and leukemic human stem/progenitor cells. *Blood* **2007**, *110*, 2880-2888, doi:10.1182/blood-2006-08-039073.

- (86) Talati, P.G.; Gu, L.; Ellsworth, E.M.; Gironde, M.A.; Trerotola, M.; Hoang, D.T.; Leiby, B.; Dagvadorj, A.; McCue, P.A.; Lallas, C.D.; et al. Jak2-Stat5a/b Signaling Induces Epithelial-to-Mesenchymal Transition and Stem-Like Cell Properties in Prostate Cancer. *Am. J. Pathol.* **2015**, *185*, 2505-2522, doi:10.1016/j.ajpath.2015.04.026.
- (87) Boutillon, F.; Pigat, N.; Sala, L.S.; Reyes-Gomez, E.; Moriggl, R.; Guidotti, J.E.; Goffin, V. STAT5a/b Deficiency Delays, but does not Prevent, Prolactin-Driven Prostate Tumorigenesis in Mice. *Cancers (Basel)* **2019**, *11*, doi:10.3390/cancers11070929.
- (88) Liu, X.; Robinson, G.W.; Wagner, K.U.; Garrett, L.; Wynshaw-Boris, A.; Hennighausen, L. Stat5a is mandatory for adult mammary gland development and lactogenesis. *Genes Dev.* **1997**, *11*, 179-186.
- (89) Oakes, S.R.; Naylor, M.J.; Asselin-Labat, M.L.; Blazek, K.D.; Gardiner-Garden, M.; Hilton, H.N.; Kazlauskas, M.; Pritchard, M.A.; Chodosh, L.A.; Pfeffer, P.L.; et al. The ETS transcription factor Elf5 specifies mammary alveolar cell fate. *Genes Dev.* **2008**, *22*, 581-586, doi:10.1101/gad.1614608.
- (90) Metser, G.; Shin, H.Y.; Wang, C.; Yoo, K.H.; Oh, S.; Villarino, A.V.; O'Shea, J.J.; Kang, K.; Hennighausen, L. An autoregulatory enhancer controls mammary-specific STAT5 functions. *Nucleic Acids Res.* **2016**, *44*, 1052-1063, doi:10.1093/nar/gkv999.
- (91) Stute, P.; Sielker, S.; Wood, C.E.; Register, T.C.; Lees, C.J.; Dewi, F.N.; Williams, J.K.; Wagner, J.D.; Stefanelli, U.; Cline, J.M. Life stage differences in mammary gland gene expression profile in non-human primates. *Breast Cancer Res. Treat.* **2012**, *133*, 617-634, doi:10.1007/s10549-011-1811-9.
- (92) Kim, M.; Morales, L.D.; Jang, I.S.; Cho, Y.Y.; Kim, D.J. Protein Tyrosine Phosphatases as Potential Regulators of STAT3 Signaling. *Int. J. Mol. Sci.* **2018**, *19*, doi:10.3390/ijms19092708.
- (93) Huang, Y.; Wang, J.; Cao, F.; Jiang, H.; Li, A.; Li, J.; Qiu, L.; Shen, H.; Chang, W.; Zhou, C.; et al. SHP2 associates with nuclear localization of STAT3: Significance in progression and prognosis of colorectal cancer. *Sci. Rep.* **2017**, *7*, 17597, doi:10.1038/s41598-017-17604-7.
- (94) Kumar, V.; Cheng, P.; Condamine, T.; Mony, S.; Languino, L.R.; McCaffrey, J.C.; Hockstein, N.; Guarino, M.; Masters, G.; Penman, E.; et al. CD45 Phosphatase Inhibits STAT3 Transcription Factor Activity in Myeloid Cells and Promotes Tumor-Associated Macrophage Differentiation. *Immunity* **2016**, *44*, 303-315, doi:10.1016/j.immuni.2016.01.014.

- (95) Fan, L.C.; Shiau, C.W.; Tai, W.T.; Hung, M.H.; Chu, P.Y.; Hsieh, F.S.; Lin, H.; Yu, H.C.; Chen, K.F. SHP-1 is a negative regulator of epithelial-mesenchymal transition in hepatocellular carcinoma. *Oncogene* **2015**, *34*, 5252-5263, doi:10.1038/onc.2014.445.
- (96) Chen, Y.; Wen, R.; Yang, S.; Schuman, J.; Zhang, E.E.; Yi, T.; Feng, G.S.; Wang, D. Identification of Shp-2 as a Stat5A phosphatase. *J. Biol. Chem.* **2003**, *278*, 16520-16527, doi:10.1074/jbc.M210572200.
- (97) Xiao, W.; Ando, T.; Wang, H.Y.; Kawakami, Y.; Kawakami, T. Lyn- and PLC-beta3-dependent regulation of SHP-1 phosphorylation controls Stat5 activity and myelomonocytic leukemia-like disease. *Blood* **2010**, *116*, 6003-6013, doi:10.1182/blood-2010-05-283937.
- (98) Brantley, E.C.; Nabors, L.B.; Gillespie, G.Y.; Choi, Y.H.; Palmer, C.A.; Harrison, K.; Roarty, K.; Benveniste, E.N. Loss of protein inhibitors of activated STAT-3 expression in glioblastoma multiforme tumors: Implications for STAT-3 activation and gene expression. *Clin. Cancer Res.* **2008**, *14*, 4694-4704, doi:10.1158/1078-0432.CCR-08-0618.
- (99) Sundvall, M.; Korhonen, A.; Vaparanta, K.; Anckar, J.; Halkilahti, K.; Salah, Z.; Aqeilan, R.I.; Palvimo, J.J.; Sistonen, L.; Elenius, K. Protein inhibitor of activated STAT3 (PIAS3) protein promotes SUMOylation and nuclear sequestration of the intracellular domain of ErbB4 protein. *J. Biol. Chem.* **2012**, *287*, 23216-23226, doi:10.1074/jbc.M111.335927.
- (100) Jang, H.D.; Yoon, K.; Shin, Y.J.; Kim, J.; Lee, S.Y. PIAS3 suppresses NF-kappaB-mediated transcription by interacting with the p65/RelA subunit. *J. Biol. Chem.* **2004**, *279*, 24873-24880, doi:10.1074/jbc.M313018200.
- (101) Liu, Y.; Bridges, R.; Wortham, A.; Kulesz-Martin, M. NF-kappaB repression by PIAS3 mediated RelA SUMOylation. *PLoS ONE* **2012**, *7*, e37636, doi:10.1371/journal.pone.0037636.
- (102) Zhao, Z.; Wu, L.; Shi, H.; Wu, C. p53 Nterminal binding and stabilisation by PIAS3 inhibits MDM2induced p53 ubiquitination and regulates cell growth. *Mol. Med. Rep.* **2014**, *9*, 1903-1908, doi:10.3892/mmr.2014.1993.
- (103) Perry, E.; Tsruya, R.; Levitsky, P.; Pomp, O.; Taller, M.; Weisberg, S.; Parris, W.; Kulkarni, S.; Malovani, H.; Pawson, T.; et al. TMF/ARA160 is a BC-box-containing protein that mediates the degradation of Stat3. *Oncogene* **2004**, *23*, 8908-8919.
- (104) Abrham, G.; Volpe, M.; Shpungin, S.; Nir, U. TMF/ARA160 downregulates proangiogenic genes and attenuates the progression of PC3 xenografts. *Int. J. Cancer* **2009**, *125*, 43-53, doi:10.1002/ijc.24277.

- (105) Wei, J.; Yuan, Y.; Jin, C.; Chen, H.; Leng, L.; He, F.; Wang, J. The ubiquitin ligase TRAF6 negatively regulates the JAK-STAT signaling pathway by binding to STAT3 and mediating its ubiquitination. *PLoS ONE* **2012**, *7*, e49567, doi:10.1371/journal.pone.0049567.
- (106) Deschenes-Simard, X.; Gaumont-Leclerc, M.F.; Bourdeau, V.; Lessard, F.; Moiseeva, O.; Forest, V.; Igelmann, S.; Mallette, F.A.; Saba-El-Leil, M.K.; Meloche, S.; et al. Tumor suppressor activity of the ERK/MAPK pathway by promoting selective protein degradation. *Genes Dev.* **2013**, *27*, 900-915, doi:10.1101/gad.203984.112.
- (107) Zhao, J.; Du, P.; Cui, P.; Qin, Y.; Hu, C.; Wu, J.; Zhou, Z.; Zhang, W.; Qin, L.; Huang, G. LncRNA PVT1 promotes angiogenesis via activating the STAT3/VEGFA axis in gastric cancer. *Oncogene* **2018**, doi:10.1038/s41388-018-0250-z.
- (108) You, L.; Chang, D.; Du, H.Z.; Zhao, Y.P. Genome-wide screen identifies PVT1 as a regulator of Gemcitabine sensitivity in human pancreatic cancer cells. *Biochem. Biophys. Res. Commun.* **2011**, *407*, 1-6, doi:10.1016/j.bbrc.2011.02.027.
- (109) Xie, Z.; Chen, X.; Li, J.; Guo, Y.; Li, H.; Pan, X.; Jiang, J.; Liu, H.; Wu, B. Salivary HOTAIR and PVT1 as novel biomarkers for early pancreatic cancer. *Oncotarget* **2016**, *7*, 25408-25419, doi:10.18632/oncotarget.8323.
- (110) Pan, X.; Li, B.; Fan, N.; Li, J.; Cai, F.; Zhao, G.; Zheng, G.; Gao, C. Long Noncoding RNA PVT1 as a Potent Predictor of Prognosis in Cancers: A Meta-Analysis. *Clin. Lab.* **2017**, *63*, 1657-1666, doi:10.7754/Clin.Lab.2017.170418.
- (111) Hatziapostolou, M.; Polytarchou, C.; Aggelidou, E.; Drakaki, A.; Poultsides, G.A.; Jaeger, S.A.; Ogata, H.; Karin, M.; Struhl, K.; Hadzopoulou-Cladaras, M.; et al. An HNF4alpha-miRNA inflammatory feedback circuit regulates hepatocellular oncogenesis. *Cell* **2011**, *147*, 1233-1247, doi:10.1016/j.cell.2011.10.043.
- (112) Cai, B.; Li, J.; Wang, J.; Luo, X.; Ai, J.; Liu, Y.; Wang, N.; Liang, H.; Zhang, M.; Chen, N.; et al. microRNA-124 regulates cardiomyocyte differentiation of bone marrow-derived mesenchymal stem cells via targeting STAT3 signaling. *Stem Cells* **2012**, *30*, 1746-1755, doi:10.1002/stem.1154.
- (113) Zhang, J.; Lu, Y.; Yue, X.; Li, H.; Luo, X.; Wang, Y.; Wang, K.; Wan, J. MiR-124 suppresses growth of human colorectal cancer by inhibiting STAT3. *PLoS ONE* **2013**, *8*, e70300, doi:10.1371/journal.pone.0070300.
- (114) Wei, J.; Wang, F.; Kong, L.Y.; Xu, S.; Doucette, T.; Ferguson, S.D.; Yang, Y.; McEnery, K.; Jethwa, K.; Gjyshi, O.; et al. miR-124 inhibits STAT3 signaling to enhance T cell-mediated immune clearance of glioma. *Cancer Res.* **2013**, *73*, 3913-3926, doi:10.1158/0008-5472.CAN-12-4318.

- (115) Chen, G.; Shi, Y.; Zhang, Y.; Sun, J. CircRNA\_100782 regulates pancreatic carcinoma proliferation through the IL6-STAT3 pathway. *Onco Targets Ther.* **2017**, *10*, 5783-5794, doi:10.2147/OTT.S150678.
- (116) Jiang, J.; Li, Z.; Yu, C.; Chen, M.; Tian, S.; Sun, C. MiR-1181 inhibits stem cell-like phenotypes and suppresses SOX2 and STAT3 in human pancreatic cancer. *Cancer Lett.* **2015**, *356*, 962-970, doi:10.1016/j.canlet.2014.11.007.
- (117) Jiang, M.; Zhang, W.W.; Liu, P.; Yu, W.; Liu, T.; Yu, J. Dysregulation of SOCS-Mediated Negative Feedback of Cytokine Signaling in Carcinogenesis and Its Significance in Cancer Treatment. *Front. Immunol.* **2017**, *8*, 70, doi:10.3389/fimmu.2017.00070.
- (118) Ghafouri-Fard, S.; Oskoei, V.K.; Azari, I.; Taheri, M. Suppressor of cytokine signaling (SOCS) genes are downregulated in breast cancer. *World J. Surg. Oncol.* **2018**, *16*, 226, doi:10.1186/s12957-018-1529-9.
- (119) He, B.; You, L.; Uematsu, K.; Zang, K.; Xu, Z.; Lee, A.Y.; Costello, J.F.; McCormick, F.; Jablons, D.M. SOCS-3 is frequently silenced by hypermethylation and suppresses cell growth in human lung cancer. *Proc. Natl. Acad. Sci. USA* **2003**, *100*, 14133-14138, doi:10.1073/pnas.2232790100.
- (120) Inagaki-Ohara, K.; Kondo, T.; Ito, M.; Yoshimura, A. SOCS, inflammation, and cancer. *JAKSTAT* **2013**, *2*, e24053, doi:10.4161/jkst.24053.
- (121) Suzuki, A.; Hanada, T.; Mitsuyama, K.; Yoshida, T.; Kamizono, S.; Hoshino, T.; Kubo, M.; Yamashita, A.; Okabe, M.; Takeda, K.; et al. CIS3/SOCS3/SSI3 plays a negative regulatory role in STAT3 activation and intestinal inflammation. *J. Exp. Med.* **2001**, *193*, 471-481.
- (122) Niwa, Y.; Kanda, H.; Shikauchi, Y.; Saiura, A.; Matsubara, K.; Kitagawa, T.; Yamamoto, J.; Kubo, T.; Yoshikawa, H. Methylation silencing of SOCS-3 promotes cell growth and migration by enhancing JAK/STAT and FAK signalings in human hepatocellular carcinoma. *Oncogene* **2005**, *24*, 6406-6417, doi:10.1038/sj.onc.1208788.
- (123) Rigby, R.J.; Simmons, J.G.; Greenhalgh, C.J.; Alexander, W.S.; Lund, P.K. Suppressor of cytokine signaling 3 (SOCS3) limits damage-induced crypt hyper-proliferation and inflammation-associated tumorigenesis in the colon. *Oncogene* **2007**, *26*, 4833-4841, doi:10.1038/sj.onc.1210286.
- (124) Lesina, M.; Kurkowski, M.U.; Ludes, K.; Rose-John, S.; Treiber, M.; Kloppel, G.; Yoshimura, A.; Reindl, W.; Sipos, B.; Akira, S.; et al. Stat3/Socs3 activation by IL-6 transsignaling promotes progression of pancreatic intraepithelial neoplasia and development of pancreatic cancer. *Cancer Cell* **2011**, *19*, 456-469, doi:10.1016/j.ccr.2011.03.009.

- (125) Gui, Y.; Yeganeh, M.; Ramanathan, S.; Leblanc, C.; Pomerleau, V.; Ferbeyre, G.; Saucier, C.; Ilangumaran, S. SOCS1 controls liver regeneration by regulating HGF signaling in hepatocytes. *J. Hepatol.* **2011**, *55*, 1300-1308, doi:10.1016/j.jhep.2011.03.027.
- (126) Yeganeh, M.; Gui, Y.; Kandhi, R.; Bobbala, D.; Tobelaim, W.S.; Saucier, C.; Yoshimura, A.; Ferbeyre, G.; Ramanathan, S.; Ilangumaran, S. Suppressor of cytokine signaling 1-dependent regulation of the expression and oncogenic functions of p21(CIP1/WAF1) in the liver. *Oncogene* **2016**, *35*, 4200-4211, doi:10.1038/onc.2015.485.
- (127) Yoshikawa, H.; Matsubara, K.; Qian, G.S.; Jackson, P.; Groopman, J.D.; Manning, J.E.; Harris, C.C.; Herman, J.G. SOCS-1, a negative regulator of the JAK/STAT pathway, is silenced by methylation in human hepatocellular carcinoma and shows growth-suppression activity. *Nat. Genet.* **2001**, *28*, 29-35, doi:10.1038/88225.
- (128) Zhao, R.C.; Zhou, J.; He, J.Y.; Wei, Y.G.; Qin, Y.; Li, B. Aberrant promoter methylation of SOCS-1 gene may contribute to the pathogenesis of hepatocellular carcinoma: A meta-analysis. *J. BUON* **2016**, *21*, 142-151.
- (129) Suzuki, M.; Shigematsu, H.; Shivapurkar, N.; Reddy, J.; Miyajima, K.; Takahashi, T.; Gazdar, A.F.; Frenkel, E.P. Methylation of apoptosis related genes in the pathogenesis and prognosis of prostate cancer. *Cancer Lett.* **2006**, *242*, 222-230.
- (130) Kobayashi, N.; Uemura, H.; Nagahama, K.; Okudela, K.; Furuya, M.; Ino, Y.; Ito, Y.; Hirano, H.; Inayama, Y.; Aoki, I.; et al. Identification of miR-30d as a novel prognostic maker of prostate cancer. *Oncotarget* **2012**, *3*, 1455-1471, doi:10.18632/oncotarget.696.
- (131) Chevrier, M.; Bobbala, D.; Villalobos-Hernandez, A.; Khan, M.G.; Ramanathan, S.; Saucier, C.; Ferbeyre, G.; Geha, S.; Ilangumaran, S. Expression of SOCS1 and the downstream targets of its putative tumor suppressor functions in prostate cancer. *BMC Cancer* **2017**, *17*, 157, doi:10.1186/s12885-017-3141-8.
- (132) Villalobos-Hernandez, A.; Bobbala, D.; Kandhi, R.; Khan, M.G.; Mayhue, M.; Dubois, C.M.; Ferbeyre, G.; Saucier, C.; Ramanathan, S.; Ilangumaran, S. SOCS1 inhibits migration and invasion of prostate cancer cells, attenuates tumor growth and modulates the tumor stroma. *Prostate Cancer Prostatic Dis.* **2017**, *20*, 36-47, doi:10.1038/pcan.2016.50.
- (133) Calabrese, V.; Mallette, F.A.; Deschenes-Simard, X.; Ramanathan, S.; Gagnon, J.; Moores, A.; Ilangumaran, S.; Ferbeyre, G. SOCS1 links cytokine signaling to p53 and senescence. *Mol. Cell* **2009**, *36*, 754-767.
- (134) Mallette, F.A.; Calabrese, V.; Ilangumaran, S.; Ferbeyre, G. SOCS1, a novel interaction partner of p53 controlling oncogene-induced senescence. *Aging* **2010**, *2*, 445-452.

- (135) Saint-Germain, E.; Mignacca, L.; Vernier, M.; Bobbala, D.; Ilangumaran, S.; Ferbeyre, G. SOCS1 regulates senescence and ferroptosis by modulating the expression of p53 target genes. *Aging* **2017**, *9*, 2137-2162, doi:10.18632/aging.101306.
- (136) Kong, X.; Feng, D.; Wang, H.; Hong, F.; Bertola, A.; Wang, F.S.; Gao, B. Interleukin-22 induces hepatic stellate cell senescence and restricts liver fibrosis in mice. *Hepatology* **2012**, *56*, 1150-1159, doi:10.1002/hep.25744.
- (137) Bouamar, H.; Jiang, D.; Wang, L.; Lin, A.P.; Ortega, M.; Aguiar, R.C. MicroRNA 155 control of p53 activity is context dependent and mediated by Aicda and Socs1. *Mol. Cell. Biol.* **2015**, *35*, 1329-1340, doi:10.1128/MCB.01446-14.
- (138) Cui, X.; Shan, X.; Qian, J.; Ji, Q.; Wang, L.; Wang, X.; Li, M.; Ding, H.; Liu, Q.; Chen, L.; et al. The suppressor of cytokine signaling SOCS1 promotes apoptosis of intestinal epithelial cells via p53 signaling in Crohn's disease. *Exper. Mol. Pathol.* **2016**, *101*, 1-11, doi:10.1016/j.yexmp.2016.05.011.
- (139) Mallette, F.A.; Gaumont-Leclerc, M.F.; Ferbeyre, G. The DNA damage signaling pathway is a critical mediator of oncogene-induced senescence. *Genes Dev.* **2007**, *21*, 43-48.
- (140) Mallette, F.A.; Gaumont-Leclerc, M.F.; Huot, G.; Ferbeyre, G. Myc Down-regulation as a Mechanism to Activate the Rb Pathway in STAT5A-induced Senescence. *J. Biol. Chem.* **2007**, *282*, 34938-34944.
- (141) Mallette, F.A.; Moiseeva, O.; Calabrese, V.; Mao, B.; Gaumont-Leclerc, M.F.; Ferbeyre, G. Transcriptome analysis and tumor suppressor requirements of STAT5-induced senescence. *Ann. N. Y. Acad. Sci.* **2010**, *1197*, 142-151, doi:10.1111/j.1749-6632.2010.05192.x.
- (142) Barash, I. Stat5 in the mammary gland: Controlling normal development and cancer. *J. Cell. Physiol.* **2006**, *209*, 305-313.
- (143) Nevalainen, M.T.; Xie, J.; Torhorst, J.; Bubendorf, L.; Haas, P.; Kononen, J.; Sauter, G.; Rui, H. Signal transducer and activator of transcription-5 activation and breast cancer prognosis. *J. Clin. Oncol.* **2004**, *22*, 2053-2060.
- (144) Peck, A.R.; Witkiewicz, A.K.; Liu, C.; Klimowicz, A.C.; Stringer, G.A.; Pequignot, E.; Freydin, B.; Yang, N.; Ertel, A.; Tran, T.H.; et al. Low levels of Stat5a protein in breast cancer are associated with tumor progression and unfavorable clinical outcomes. *Breast Cancer Res.* **2012**, *14*, R130, doi:10.1186/bcr3328.
- (145) Castro, P.; Giri, D.; Lamb, D.; Ittmann, M. Cellular senescence in the pathogenesis of benign prostatic hyperplasia. *Prostate* **2003**, *55*, 30-38.
- (146) Gray-Schopfer, V.C.; Cheong, S.C.; Chong, H.; Chow, J.; Moss, T.; Abdel-Malek, Z.A.; Marais, R.; Wynford-Thomas, D.; Bennett, D.C. Cellular senescence in naevi and immortalisation in melanoma: A role for p16? *Br. J. Cancer* **2006**, *95*, 496-505.



- (147) Maldonado, J.L.; Timmerman, L.; Fridlyand, J.; Bastian, B.C. Mechanisms of cell-cycle arrest in Spitz nevi with constitutive activation of the MAP-kinase pathway. *Am. J. Pathol.* **2004**, *164*, 1783-1787, doi:10.1016/S0002-9440(10)63736-4.
- (148) Michaloglou, C.; Vredeveld, L.C.; Mooi, W.J.; Peeper, D.S. BRAF(E600) in benign and malignant human tumours. *Oncogene* **2008**, *27*, 877-895.
- (149) Michaloglou, C.; Vredeveld, L.C.; Soengas, M.S.; Denoyelle, C.; Kuilman, T.; van der Horst, C.M.; Majoor, D.M.; Shay, J.W.; Mooi, W.J.; Peeper, D.S. BRAFE600-associated senescence-like cell cycle arrest of human naevi. *Nature* **2005**, *436*, 720-724.
- (150) Vernier, M.; Bourdeau, V.; Gaumont-Leclerc, M.F.; Moiseeva, O.; Begin, V.; Saad, F.; Mes-Masson, A.M.; Ferbeyre, G. Regulation of E2Fs and senescence by PML nuclear bodies. *Genes Dev.* **2011**, *25*, 41-50, doi:10.1101/gad.1975111.
- (151) Dorr, J.R.; Yu, Y.; Milanovic, M.; Beuster, G.; Zasada, C.; Dabritz, J.H.; Lisec, J.; Lenze, D.; Gerhardt, A.; Schleicher, K.; et al. Synthetic lethal metabolic targeting of cellular senescence in cancer therapy. *Nature* **2013**, *501*, 421-425, doi:10.1038/nature12437.
- (152) Jing, H.; Kase, J.; Dorr, J.R.; Milanovic, M.; Lenze, D.; Grau, M.; Beuster, G.; Ji, S.; Reimann, M.; Lenz, P.; et al. Opposing roles of NF-kappaB in anti-cancer treatment outcome unveiled by cross-species investigations. *Genes Dev.* **2011**, *25*, 2137-2146, doi:10.1101/gad.17620611.
- (153) Zardo, G.; Tiirikainen, M.I.; Hong, C.; Misra, A.; Feuerstein, B.G.; Volik, S.; Collins, C.C.; Lamborn, K.R.; Bollen, A.; Pinkel, D.; et al. Integrated genomic and epigenomic analyses pinpoint biallelic gene inactivation in tumors. *Nat. Genet.* **2002**, *32*, 453-458.
- (154) Liu, T.C.; Lin, S.F.; Chang, J.G.; Yang, M.Y.; Hung, S.Y.; Chang, C.S. Epigenetic alteration of the SOCS1 gene in chronic myeloid leukaemia. *Br. J. Haematol.* **2003**, *123*, 654-661.
- (155) Chim, C.S.; Wong, K.Y.; Loong, F.; Srivastava, G. SOCS1 and SHP1 hypermethylation in mantle cell lymphoma and follicular lymphoma: Implications for epigenetic activation of the Jak/STAT pathway. *Leukemia* **2004**, *18*, 356-358, doi:10.1038/sj.leu.2403216.
- (156) Ekmekci, C.G.; Gutierrez, M.I.; Siraj, A.K.; Ozbek, U.; Bhatia, K. Aberrant methylation of multiple tumor suppressor genes in acute myeloid leukemia. *Am. J. Hematol.* **2004**, *77*, 233-240, doi:10.1002/ajh.20186.
- (157) Sutherland, K.D.; Lindeman, G.J.; Choong, D.Y.; Wittlin, S.; Brentzell, L.; Phillips, W.; Campbell, I.G.; Visvader, J.E. Differential hypermethylation of SOCS genes in ovarian and breast carcinomas. *Oncogene* **2004**, *23*, 7726-7733.
- (158) Hatirnaz, O.; Ure, U.; Ar, C.; Akyerli, C.; Soysal, T.; Ferhanoglu, B.; Ozelik, T.; Ozbek, U. The SOCS-1 gene methylation in chronic myeloid leukemia patients. *Am. J. Hematol.* **2007**, *82*, 729-730, doi:10.1002/ajh.20886.

- (159) Jiang, S.; Zhang, H.W.; Lu, M.H.; He, X.H.; Li, Y.; Gu, H.; Liu, M.F.; Wang, E.D. MicroRNA-155 functions as an OncomiR in breast cancer by targeting the suppressor of cytokine signaling 1 gene. *Cancer Res.* **2010**, *70*, 3119-3127, doi:10.1158/0008-5472.CAN-09-4250.
- (160) Merkel, O.; Hamacher, F.; Griessl, R.; Grabner, L.; Schiefer, A.I.; Prutsch, N.; Baer, C.; Egger, G.; Schleder, M.; Krenn, P.W.; et al. Oncogenic role of miR-155 in anaplastic large cell lymphoma lacking the t(2;5) translocation. *J. Pathol.* **2015**, *236*, 445-456, doi:10.1002/path.4539.
- (161) Zhao, X.D.; Zhang, W.; Liang, H.J.; Ji, W.Y. Overexpression of miR -155 promotes proliferation and invasion of human laryngeal squamous cell carcinoma via targeting SOCS1 and STAT3. *PLoS ONE* **2013**, *8*, e56395, doi:10.1371/journal.pone.0056395.
- (162) Saint-Germain, E.; Mignacca, L.; Huot, G.; Acevedo, M.; Moineau-Vallee, K.; Calabrese, V.; Bourdeau, V.; Rowell, M.C.; Ilangumaran, S.; Lessard, F.; et al. Phosphorylation of SOCS1 inhibits the SOCS1-p53 tumor suppressor axis. *Cancer Res.* **2019**, doi:10.1158/0008-5472.CAN-18-1503.
- (163) Guo, F.; Xu, Z.; Zhang, Y.; Jiang, P.; Huang, G.; Chen, S.; Lyu, X.; Zheng, P.; Zhao, X.; Zeng, Y.; et al. FXR induces SOCS3 and suppresses hepatocellular carcinoma. *Oncotarget* **2015**, *6*, 34606-34616, doi:10.18632/oncotarget.5314.
- (164) Attia, Y.M.; Tawfiq, R.A.; Ali, A.A.; Elmazar, M.M. The FXR Agonist, Obeticholic Acid, Suppresses HCC Proliferation & Metastasis: Role of IL-6/STAT3 Signalling Pathway. *Sci. Rep.* **2017**, *7*, 12502, doi:10.1038/s41598-017-12629-4.
- (165) Sugase, T.; Takahashi, T.; Serada, S.; Fujimoto, M.; Hiramatsu, K.; Ohkawara, T.; Tanaka, K.; Miyazaki, Y.; Makino, T.; Kurokawa, Y.; et al. SOCS1 Gene Therapy Improves Radiosensitivity and Enhances Irradiation-Induced DNA Damage in Esophageal Squamous Cell Carcinoma. *Cancer Res.* **2017**, *77*, 6975-6986, doi:10.1158/0008-5472.CAN-17-1525.
- (166) Sugase, T.; Takahashi, T.; Serada, S.; Fujimoto, M.; Ohkawara, T.; Hiramatsu, K.; Nishida, T.; Hirota, S.; Saito, Y.; Tanaka, K.; et al. SOCS1 gene therapy has antitumor effects in imatinib-resistant gastrointestinal stromal tumor cells through FAK/PI3 K signaling. *Gastric Cancer* **2018**, *21*, 968-976, doi:10.1007/s10120-018-0822-1.
- (167) Yoneda, T.; Kunimura, N.; Kitagawa, K.; Fukui, Y.; Saito, H.; Narikiyo, K.; Ishiko, M.; Otsuki, N.; Nibu, K.I.; Fujisawa, M.; et al. Overexpression of SOCS3 mediated by adenovirus vector in mouse and human castration-resistant prostate cancer cells increases the sensitivity to NK cells in vitro and in vivo. *Cancer Gene Ther.* **2019**, doi:10.1038/s41417-018-0075-5.

- (168) de la Iglesia, N.; Konopka, G.; Puram, S.V.; Chan, J.A.; Bachoo, R.M.; You, M.J.; Levy, D.E.; Depinho, R.A.; Bonni, A. Identification of a PTEN-regulated STAT3 brain tumor suppressor pathway. *Genes Dev.* **2008**, *22*, 449-462, doi:10.1101/gad.1606508.
- (169) Sherry, M.M.; Reeves, A.; Wu, J.K.; Cochran, B.H. STAT3 is required for proliferation and maintenance of multipotency in glioblastoma stem cells. *Stem Cells* **2009**, *27*, 2383-2392, doi:10.1002/stem.185.
- (170) Pencik, J.; Schlederer, M.; Gruber, W.; Unger, C.; Walker, S.M.; Chalaris, A.; Marie, I.J.; Hassler, M.R.; Javaheri, T.; Aksoy, O.; et al. STAT3 regulated ARF expression suppresses prostate cancer metastasis. *Nat. Commun.* **2015**, *6*, 7736, doi:10.1038/ncomms8736.
- (171) Lessard, F.; Morin, F.; Ivanchuk, S.; Langlois, F.; Stefanovsky, V.; Rutka, J.; Moss, T. The ARF tumor suppressor controls ribosome biogenesis by regulating the RNA polymerase I transcription factor TTF-I. *Mol. Cell* **2010**, *38*, 539-550, doi:10.1016/j.molcel.2010.03.015.
- (172) Sherr, C.J. The INK4a/ARF network in tumour suppression. *Nat. Rev. Mol. Cell Biol.* **2001**, *2*, 731-737, doi:10.1038/35096061.
- (173) Ko, A.; Han, S.Y.; Song, J. Regulatory Network of ARF in Cancer Development. *Mol. Cell* **2018**, *41*, 381-389, doi:10.14348/molcells.2018.0100.
- (174) Ferbeyre, G.; de Stanchina, E.; Lin, A.W.; Querido, E.; McCurrach, M.E.; Hannon, G.J.; Lowe, S.W. Oncogenic ras and p53 cooperate to induce cellular senescence. *Mol. Cell Biol.* **2002**, *22*, 3497-3508.
- (175) Pencik, J.; Wiebringhaus, R.; Susani, M.; Culig, Z.; Kenner, L. IL-6/STAT3/ARF: The guardians of senescence, cancer progression and metastasis in prostate cancer. *Swiss Med. Wkly.* **2015**, *145*, w14215, doi:10.4414/smw.2015.14215.
- (176) Chin, Y.E.; Kitagawa, M.; Su, W.C.; You, Z.H.; Iwamoto, Y.; Fu, X.Y. Cell growth arrest and induction of cyclin-dependent kinase inhibitor p21 WAF1/CIP1 mediated by STAT1. *Science* **1996**, *272*, 719-722.
- (177) Bellido, T.; O'Brien, C.A.; Roberson, P.K.; Manolagas, S.C. Transcriptional activation of the p21(WAF1,CIP1,SDI1) gene by interleukin-6 type cytokines. A prerequisite for their pro-differentiating and anti-apoptotic effects on human osteoblastic cells. *J. Biol. Chem.* **1998**, *273*, 21137-21144, doi:10.1074/jbc.273.33.21137.
- (178) Grabner, B.; Schramek, D.; Mueller, K.M.; Moll, H.P.; Svinka, J.; Hoffmann, T.; Bauer, E.; Blaas, L.; Hruschka, N.; Zboray, K.; et al. Disruption of STAT3 signalling promotes KRAS-induced lung tumorigenesis. *Nat. Commun.* **2015**, *6*, 6285, doi:10.1038/ncomms7285.

- (179) Musteanu, M.; Blaas, L.; Mair, M.; Schlederer, M.; Bilban, M.; Tauber, S.; Esterbauer, H.; Mueller, M.; Casanova, E.; Kenner, L.; et al. Stat3 is a negative regulator of intestinal tumor progression in Apc(Min) mice. *Gastroenterology* **2010**, *138*, 1003-1011, doi:10.1053/j.gastro.2009.11.049.
- (180) Lee, J.; Kim, J.C.; Lee, S.E.; Quinley, C.; Kim, H.; Herdman, S.; Corr, M.; Raz, E. Signal transducer and activator of transcription 3 (STAT3) protein suppresses adenoma-to-carcinoma transition in Apcmin/+ mice via regulation of Snail-1 (SNAI) protein stability. *J. Biol. Chem.* **2012**, *287*, 18182-18189, doi:10.1074/jbc.M111.328831.
- (181) Couto, J.P.; Daly, L.; Almeida, A.; Knauf, J.A.; Fagin, J.A.; Sobrinho-Simoes, M.; Lima, J.; Maximo, V.; Soares, P.; Lyden, D.; et al. STAT3 negatively regulates thyroid tumorigenesis. *Proc. Natl. Acad. Sci. USA* **2012**, *109*, E2361-E2370, doi:10.1073/pnas.1201232109.
- (182) Wang, H.; Lafdil, F.; Wang, L.; Park, O.; Yin, S.; Niu, J.; Miller, A.M.; Sun, Z.; Gao, B. Hepatoprotective versus oncogenic functions of STAT3 in liver tumorigenesis. *Am. J. Pathol.* **2011**, *179*, 714-724, doi:10.1016/j.ajpath.2011.05.005.
- (183) Schneller, D.; Machat, G.; Sousek, A.; Proell, V.; van Zijl, F.; Zulehner, G.; Huber, H.; Mair, M.; Muellner, M.K.; Nijman, S.M.; et al. p19(ARF)/p14(ARF) controls oncogenic functions of signal transducer and activator of transcription 3 in hepatocellular carcinoma. *Hepatology* **2011**, *54*, 164-172, doi:10.1002/hep.24329.
- (184) Zhang, H.F.; Chen, Y.; Wu, C.; Wu, Z.Y.; Twardy, D.J.; Alshareef, A.; Liao, L.D.; Xue, Y.J.; Wu, J.Y.; Chen, B.; et al. The Opposing Function of STAT3 as an Oncoprotein and Tumor Suppressor Is Dictated by the Expression Status of STAT3beta in Esophageal Squamous Cell Carcinoma. *Clin. Cancer Res.* **2016**, *22*, 691-703, doi:10.1158/1078-0432.CCR-15-1253.
- (185) Pectasides, E.; Egloff, A.M.; Sasaki, C.; Kountourakis, P.; Burtness, B.; Fountzilias, G.; Dafni, U.; Zaramboukas, T.; Rampias, T.; Rimm, D.; et al. Nuclear localization of signal transducer and activator of transcription 3 in head and neck squamous cell carcinoma is associated with a better prognosis. *Clin. Cancer Res.* **2010**, *16*, 2427-2434, doi:10.1158/1078-0432.CCR-09-2658.
- (186) Gordziel, C.; Bratsch, J.; Moriggl, R.; Knosel, T.; Friedrich, K. Both STAT1 and STAT3 are favourable prognostic determinants in colorectal carcinoma. *Br. J. Cancer* **2013**, *109*, 138-146, doi:10.1038/bjc.2013.274.
- (187) Ettl, T.; Stiegler, C.; Zeitler, K.; Agaimy, A.; Zenk, J.; Reichert, T.E.; Gosau, M.; Kuhnel, T.; Brockhoff, G.; Schwarz, S. EGFR, HER2, survivin, and loss of pSTAT3 characterize high-grade malignancy in salivary gland cancer with impact on prognosis. *Hum. Pathol.* **2012**, *43*, 921-931, doi:10.1016/j.humpath.2011.08.006.

- (188) Sato, T.; Neilson, L.M.; Peck, A.R.; Liu, C.; Tran, T.H.; Witkiewicz, A.; Hyslop, T.; Nevalainen, M.T.; Sauter, G.; Rui, H. Signal transducer and activator of transcription-3 and breast cancer prognosis. *Am. J. Cancer Res.* **2011**, *1*, 347-355.

# Chapter 3

---

## Discussion

### 3.1. General

Cellular transformation is a complex process opposed by tumor suppressor mechanisms such as cellular senescence. Here we show new molecular markers of senescence and features of senescent cells that enforce the senescence response as well as bypass the senescence response. We have demonstrated alterations in ribosome biogenesis and metabolism of NAD as main contributors to the induction of cellular senescence. Key findings of our research include ribosome biogenesis alterations in senescent cells leading to the accumulation of rRNA precursors and likewise the accumulation of RPL29 and RPS14. We showed RPL29 accumulation could be used as a biomarker to detect senescent cells *in vitro* and *in vivo*. Furthermore, we have identified RPS14 as novel cyclin dependant kinase inhibitors (CDKi). RPS14 is able to bind CDK4, cyclin D1, and the CDK4-cyclin D1 complex to inhibit cell cycle progression. Finally, we have shown that the increased degradation of rRNA processing factor RSL1D1 and DDX21 led to an accumulation of unprocessed rRNA. These accumulated rRNA precursors reinforce the senescence response.

Regarding the metabolic alterations in senescent cells, our key findings include the observation that NADH accumulation induces senescence. Mechanistically, increased NADH levels can stabilize p53 and maintain the senescence response. Moreover, we identified a new metabolic complex composed of a cytosolic fraction of PC, ME1, and MDH1 that transfers reducing equivalents from NADH to NADP while regenerating NAD<sup>+</sup> and producing NADPH. Concerted action of this complex allowed for bypass of cellular senescence and transformation of primary cells.

All in all, we demonstrated two key alterations in senescent cells, and we provided evidence towards cellular pathways that enforce cellular senescence as well as abolish the senescence response. In the following, the results will be discussed in greater detail.

## 3.2. Ribosome biogenesis alterations in senescence

Cellular senescence is a tumor suppressor mechanism that is activated in cells to avoid transformation [104]. Here we report that cellular senescence is accompanied by defects in ribosome biogenesis and alterations in the nucleolar organization. The nucleolus is a highly organized membrane-less structure in the nucleus and the area where ribosome biogenesis takes place. In normal and transformed cells, several nucleoli per cell can be observed and a feature typically observed in highly proliferative cells is an increase in nucleoli size to accommodate for higher ribosome biogenesis [498]. Interestingly, senescent cells display a single big nucleolus in contrast to several big ones in cancer cells [498]. The single nucleolus was previously reported in senescent cells; however, the authors did not link this big nucleolus with any biological feature of senescent cells [499].

Remarkably, because they do not divide, senescent cells do not need to amplify their ribosomes but still display the big nucleolus normally associated with high ribosome biogenesis. Surprisingly, we could not observe an increase in rRNA synthesis, generally associated with the increased nucleolar size in cancer cells [498] but rather a decrease of rRNA synthesis in several senescence models. In an attempt to explain the increased nucleolar size, we used fluorescence *in situ* hybridization (FISH) for specific rRNA processing sites. We were able to show that processing intermediates of rRNA were increased in senescent cells, likely driving the increased nucleolar size. Furthermore, site-specific northern blots of rRNA processing revealed accumulation of 47S RNA in OIS as well as replicative senescence. Increased 47S rRNA was previously observed in cases where nucleolar RNAs U3 and U8 were decreased, and this was linked to nucleolar fusion into one prominent nucleolus [500]. Those results allowed us to conclude that senescence is accompanied by reduced *de novo* RNA synthesis, as well as ribosome processing alterations. Concordantly, those alterations likely promote the stability of the senescence response.

Interestingly, the decreased ribosome biogenesis does not lead to a decrease of translation [239] nor an increase in ribosomal translation errors. In fact, it was shown that senescent cells have higher translation termination fidelity than dividing fibroblasts or cancer cells [29]. However, whether other translation alterations such as increased missense, nonsense errors, preferential use of uORF, premature termination do increase with senescence is yet unknown [501]. The observation that senescent cells do have decreased ribosome biogenesis, nevertheless still have functional ribosomes allows speculating that there are specialized ribosomes in senescent cells [241, 502]. Specialized ribosomes are characterized by, for example, differential methylation or 2'-O-methylation, helping them to acquire new features. Those new features could allow for higher fidelity, increased stability, increased translation of non-cap dependent mRNAs or translation of

distinct sub-pools of mRNA, and further changes [502, 503]. In addition, specialized ribosomes in senescent cells could have modifications rendering them less prone to degradation or also less prone to errors. In light of this, a recent meeting report showed that senescent dermal fibroblasts have alterations in specific methylation sites in the ribosome [504].

### 3.2.1. RPL29, a new marker of cellular senescence

The ribosomal biogenesis alterations not only led to alterations in the ribosome but also in the organization of nucleolus. The fact that senescent cells have a single big nucleolus can be used as a marker of senescence. We were able to show that ribosomal protein large subunit 29 also known as eL29 (RPL29) a protein which was previously linked to accumulate in nucleoli following defects in ribosome biogenesis, can be used as a senescent marker *in vitro* as well as *in vivo*. Identifications of new senescent specific markers are the most pressing subject in the senescence field as no senescent specific marker is available [131]. We have not tested whether RPL29 accumulation is a universal marker of senescence, but we could show *in vitro* in models of TIS, OIS, MSIS, tumor suppressor activation that RPL29 accumulates in the nucleolus. Moreover, we were able to show in two of the most classic *in vivo* models of senescence, BPH [133] and nevi [33], that RPL29 does accumulate in comparison to normal tissues. Proper identification of senescent cells is highly relevant for evaluation of senolytic treatments. As mentioned before, it was shown that many age-related diseases are at least partially caused by an accumulation of senescent cells, and removal of those senescent cells alleviates those effects [151, 505]. Having a good marker of senescence allows identifying the efficiency of senescent cell removal.

### 3.2.2. Impact of accumulation of other ribosomal proteins

Cellular senescence is mediated by the combined actions of tumor suppressors p53 and RB [124]. It was demonstrated that UV irradiation of the nucleolus could lead to the accumulation of ribosomal proteins (RPs) such as ribosomal protein large subunit 11 also known as uL5 (RPL11) and ribosomal protein large subunit 5 also known as uL18 (RPL5). Accumulation of those proteins were shown to stabilize p53 by inhibiting the function of p53 E3 ligase MDM2 [238, 506–508]. Further large and small subunit RPs regulating p53 and senescence include RPL3, RPL6, RPL22, RPL23, RPL26, RPS3, RPS7, RPS9, and RPS13 [5, 128, 509]. All those discoveries led to the idea that impaired ribosomal biogenesis leads to p53 activation. In contrast to p53 activation, we were able to show that impaired ribosome biogenesis can also activate the RB pathway. We have identified ribosomal protein small subunit 14 also known as uS11 (RPS14) as an inhibitory protein of CDK4 kinase activity. CDK4 can phosphorylate RB, and this phosphorylation releases



E2F proteins, which promote transition into the S phase of the cell cycle [5]. RPS14, as RPL29, does accumulate in a ribosomal-free fraction in senescent cells following ribosome biogenesis alterations. We used knockdown of RSL1D1 as well as NS, EBP2, and DDX21 to alter ribosome processing and knockdown of all proteins resulted in the accumulation of ribosome-free RPs and induction of senescence.

Similar to RPS14, we found that RPL22 is a regulator of the cell cycle, too [8]. RPS14 and RPL22 can inhibit the CDK4-cyclin D1 complex. Interestingly, RPS14 does accumulate in the nucleoplasm, whereas RPL22 does instead accumulate in the nucleolus and only partially in the nucleoplasm. Furthermore, we did determine for RPL22 and RPS14 that they can bind to CDK4 as well as to cyclin D1 and the complex between them, suggesting that the mechanism of RPS14 induced CDK4 inhibition could be both as the CIP type (inhibiting the complex) or as the INK type (inhibiting the CDK association to cyclins). There is also the possibility that ribosomal protein inhibiting CDKs (RPIC) has a specific mode of action by binding the cyclins. The mechanism of action of RPIC has various implications for cancer drug development. Specific inhibitors of CDK activity, like palbociclib, are already available. In case the mode of action of RPIC is inhibition of the cyclins, combinations of CDK4 inhibition and RPS14 could evolve into a two-punch strategy. This could be achieved with inhibition of CDK4 by palbociclib and a drug that mimics the action of RPS14 or RPL22. Combination therapies are more prone to success as two inactivating mutations in the CDK4 cyclin complex have to occur in order to overcome this treatment [510].

An aspect that we have not covered in our paper is how ribosomal free RPs accumulate in senescence. It is possible that the cross-talk between Pol I/III, for ribosomal RNA transcription, and Pol II, for mRNA of ribosomal proteins, is altered in senescence leading to the accumulation of RPs without proper processed ribosomal RNA. This possibility would allow for an interesting sensing pathway of cellular stress, which is yet to be uncovered. Single-cell expression data on ribosomal RNA and RPs over the time of the induction of senescence would allow for the proper identification of such a process. Other possibilities of ribosomal free RPs accumulation are that ribosomes would lose some proteins or be modified in case of cellular stress, thus leading to the release of RPs. Ribosomes that could sense exterior stresses would be an interesting aspect from an evolutionary standpoint as ribosomes are one of the first complex biomolecules. In line with this, it is known that ribosome biogenesis can decrease with cellular stress; however, it is unknown how ribosomal stress can induce a response program. Release of RPs could be the molecular trigger of this response.

Another interesting aspect here is that we were able to show that RPS14 can inhibit the cell cycle in a p53 independent manner. About 50% of cancer have a mutation in p53, and the remaining have alterations in p53 response, highlighting the importance of treatments that do not require

functional p53 [79]. RPS14 was shown to reduce proliferation in p53 null or mutant cell lines. An interesting aspect of the discovery of RPS14 as a cell cycle regulator is that RPS14 was identified as a haploinsufficient tumor suppressor in the myeloproliferative 5q-syndrome [511]. 5q syndrome is a hematological disorder driven by a deletion of part of the large arm of chromosome 5 [512]. Interestingly, the only suggested tumor suppressor identified in the deleted region is RPS14 [511], and we were able to mechanistically confirm that RPS14 seems likely to be the tumor suppressor lost in 5q syndrome. Furthermore, we showed that expression of RPS14 in cells isolated from 5q syndrome patients could reduce p-RB levels resulting in a reduction of the proliferation of those cells. These results highlight the importance of the RPS14 protein as a tumor suppressor. These results are particularly interesting because no further amplification of cell cycle regulators was found in 5q syndrome, suggesting that RPS14 is a major regulator of cell cycle progression.

Drugs targeting ribosome biogenesis have been recently developed, for example, CX5461 [513]. It was shown that CX5461 could induce senescence even in the absence of p53 in solid tumors [514], suggesting that the actions of RPS14 and maybe other ribosome-free RPs are major tumor suppressors. Here we identified RPS14, and subsequent studies identified RPL22 as CDK4 cyclin D1 inhibitors, but it is tempting to speculate that each CDK can have its own ribosomal protein. In fact, analysis of deletions and alterations of RPs in cancer showed that about 40% (4620 out of 10,744 tumors) have a heterozygous inactivating mutation [515], suggesting that not only RPS14 can be a tumor suppressor but several other RPs. In an OncoPrint analysis of down and upregulated RPs it was identified that RPS15 (uS19), and RPS12 (eS12) in the small subunit and RPL3 (uL3), RPL26 (uL24), RPL15 (eL15), and RPL37 (eL37) in the large subunit are more often downregulated in cancer than upregulated. The results confirm the idea that those RPs can indeed be tumor suppressors [128].

Apart from the identification that RPs are frequently heterozygously mutated in cancer, it seems also advantageous from an evolutionary standpoint for a cell to use RPs for other cellular functions. In fact, the cell cycle in yeast is inhibited by one protein p40<sup>Sic1</sup> and mutants in this gene show increased cell cycle speed and reduced G1 arrest [516]. Furthermore, in yeast, it was shown that ribosomal stress leads to cell cycle arrest [517] and the release of ribosomal protein could be major drivers of this cell cycle arrest.

All in all, the identification of ribosome biogenesis alterations in senescence seems to become an established marker of senescence, and further research will uncover further molecular roles of ribosome biogenesis in maintaining the senescence response. Further research will most likely uncover further roles than cell cycle regulation of ribosomal free RPL and RPS.

### 3.3. STAT3 in aging and cancer

In the review article and the publication in *Molecular Cell*, we showed that STAT3 alterations could drive aging and cancer. An important aspect of STAT3 signaling in aging and cancer is its import into the mitochondria. Even though it is known that STAT3 is present in the mitochondria, the exact mechanisms of how STAT3 can enter into the mitochondria and its roles are still a matter of debate. In our results, we have confirmed STAT localization in the mitochondria in two ways using PLA of STAT3 and ATPase family AAA domain containing 3A protein (ATAD3A) and purification techniques of mitochondria. Nevertheless, STAT3 does not have a classic mitochondrial import signal, and it was suggested that STAT3 could interact with gene associated with retinoic and interferon-induced mortality 19 protein (GRIM19) and GRIM19 helps to transfer STAT3 to the mitochondria [518]. Furthermore, it was shown that TOMM20, an integral part of the TIMM/TOMM mitochondrial import complex, and STAT3 could interact together [519], suggesting that STAT3 import into mitochondria is a regulated process.

An interesting observation on STAT3 is that neither STAT3-GFP nor STAT3-FLAG was imported into mitochondria regardless of localization of the tag [520]. In our hands' similar results were observed (data not shown in the papers), suggesting that the introns, 3' or 5' UTR play a crucial role in STAT3 mitochondrial import. The suggestion is based on the fact that the overexpression of STAT3 with retroviral or transfected vectors does not contain introns nor 3' or 5' UTR. In fact, it has been shown in yeast that some mRNA of mitochondrial proteins are localized to mitochondrion-bound polysomes [521] and this was dependent on a nucleotide sequence in the 3' UTR of the mRNA [522]. Similar processes were suggested for mammalian cells, and evidence starts to accumulate that, indeed, about 30% of mitochondrial proteins are imported into mitochondria in a co-translational fashion [523]. Further studies will reveal if the mRNA of STAT3 contains a mitochondrion import RNA ZIP Code.

Regardless of how endogenous STAT3 is imported into the mitochondria, we confirmed the presence of STAT3 in the mitochondria and forced import of STAT3, a fusion of STAT3 mRNA with a mitochondrial import sequence, into mitochondria resulted in normalization of phenotypes observed in STAT3 low cells. The fission rate of mitochondria was reduced, and cells did not enter into senescence. Moreover, the NAD<sup>+</sup>/NADH ratio was normalized after forced mitochondrial STAT3 expression. Thus, these results suggest that mitochondrial STAT3 is the main trigger of the induction of senescence in STAT3 low cells. We did not formally address the possibility of a contribution of nuclear or cytosolic STAT3 protein for senescence induction, but the fact that the expression of MitoSTAT3 was sufficient to abolish senescence phenotypes in STAT3 low cells suggest a major mitochondrial STAT3 contribution. It is still possible that mitochondrial-targeted

STAT3 can be exported out of the mitochondria, but no report of STAT3 export from mitochondria is available.

There were several roles for STAT3 in the mitochondria, and we were able to confirm that loss of STAT3 results in lower mt-ND1 and mt-ND4 levels suggesting that STAT3 regulates mitochondrial gene transcription [299]. Our results that cristae are disrupted following the loss of STAT3 give rise to the possibility that on top of the transcriptional regulation of mt-ND1 and mt-ND4, STAT3 can also regulate mitochondrial structure organization. As described above, it was suggested that assembly of mitochondrial super-complex requires STAT3 entry in the mitochondria. Whether the lack of super-complex formation can explain all the ultrastructural alterations observed in STAT3 low cells is unclear; however, it is possible that further interacting partners of STAT3 can organize the cristae structure. For example, we confirmed by PLA the interaction of STAT3 with the mitochondrial structural organization ATPase family AAA domain containing 3A protein (ATAD3A) [299]. It was shown that loss of ATAD3A function leads to mitochondrial dysfunction and alteration in mitochondrial fusion and fission [524, 525]. Even though the functions of ATAD3A are known, the potential interaction partners of ATAD3A are yet to be uncovered. This allows for the possibility that the interaction of STAT3 with ATAD3A helps the function of ATAD3A, and loss of STAT3, as observed in senescence, will result in lower ATAD3A activity. Hence, the loss of STAT3-ATAD3A interaction could explain the increased mitochondrial fission and puncta structure of the mitochondria in senescence.

In light of aging and age-related diseases, decreased levels of MitoSTAT3 in the brain, in cardiac cells, and  $\beta$ -cells were shown [295, 301, 526]. Moreover, loss of global STAT3 levels in aging have been shown in aged bone [527]. The roles of MitoSTAT3 are most described in cardiac functions, and it was shown that increased STAT3 has protective effects in several cardio-related diseases. First of all, a decrease of mitochondrial STAT3 results in mitochondrial dysfunction in cardiac cells [528]. It was shown that high STAT3 levels protect from apoptotic cells death in ischemic reperfusion injury by maintaining mitochondrial respiration, delaying MPTP opening, and alterations in releasing  $\text{Ca}^{2+}$  [529, 530]. Interestingly, in aged mice and STAT3 knockout mice, protective effects of STAT3 were abolished, suggesting that there is an age-dependent degradation of STAT3 in cardiac cells [531]. Regardless of those demonstrations, it is still a matter of debate how STAT3 can be cardioprotective. One mechanism which can be suggested based on our observation is that STAT3 can regulate NAD<sup>+</sup> levels via the increased complex I activity. Therefore, increased complex I activity would increase NAD<sup>+</sup> levels. Higher NAD<sup>+</sup> levels were suggested to be required to protect cardiac myoblasts from re-oxygenation injury [532].

Interestingly, normal STAT3 functions in cardiac fibroblast include the regulation of ECM proteins and production of collagen [301], suggesting that high STAT3 can contribute to increased

fibrosis. Furthermore, increased collagen production by fibroblasts is linked to fibrosis, a major age-related problem, in which fibroblasts increase the amount of secreted collagen leading to scarring of the tissue and finally loss of tissue function [533]. Intriguingly, knockout of STAT3 in cardiomyocytes, however, led to increased fibrosis and premature cardiac-related death [534].

Given the fact that STAT3 levels decrease with aging and the cardioprotective roles of STAT3, it seems interesting to evaluate the roles of STAT3 after senescent cells removal in cardiac tissues in order to understand whether the loss of STAT3 would rather be beneficial or detrimental highlighting in the same time a crucial role for fibrosis and senescent cell interaction. The role of senescent cells in fibrosis in general and in cardiac fibrosis, in particular, is still a matter of debate as reports suggest that the accumulation of senescent cells around the heart would increase fibrosis and age-related cardiac diseases [301, 535]. Interestingly, those effects can be alleviated by senescent cell removal [536, 537]. On the other hand, other reports have shown that senescent cells do limit fibrosis in cardiac tissue [538] and the removal of senescent cells would lead to increased fibrosis. Those results again highlight the duality of STAT3, and further research will elucidate the beneficial and detrimental roles of STAT3 in cardiac disease, fibrosis and, other age-related diseases.

In contrast, there were also reports of increased STAT3 signaling inducing senescence or aging phenotypes, but those reports mostly showed roles of increased STAT3 in inflammation and Inflammaging, thus, highlighting the pleiotropic effects of STAT3 [539]. Thus, it seems that nuclear STAT3 functions promote aging, and the non-canonical functions in the mitochondria prevent aging [283, 299, 539, 540]. Intriguingly, in stem cells, a state opposite to senescence increased mitochondrial STAT3 levels were shown to be important to maintain pluripotency [299].

### **3.3.1. Are alterations in STAT3 levels oncogenic?**

In our study, we have confirmed STAT3 decrease in senescent cells and senescence opposes transformation thus, confirming the oncogenic roles for STAT3 in transformation.

Oncogenic roles of STAT3 are various, and increased STAT3 activity can be found in up to 70% of cancers as well as in many cancer-driving settings [540]. For example, STAT3 can increase chronic inflammation in an IL6 dependent way resulting in increased tumor initiation [540]. Interestingly, STAT3 is a major regulator of oncogenic SASP components, and loss of STAT3 in several contexts has shown a less oncogenic SASP [541]. Concordantly, in senescent bone marrow stem cells, decreased activity of STAT3 resulted in a decrease of IL1 $\alpha$ , IL1 $\beta$ , IL6, CXCL1 and 15 as well as MMP3 and 12 expression levels [542]. All those proteins were associated with the oncogenic functions of the SASP [543]. Other than the regulation of inflammation, high STAT3 level can increase cell cycle, promote resistance to apoptosis, promote angiogenesis, epithelial-mesenchymal

transition (EMT), increase glycolysis and mitochondrial function, all of which are associated with increased cancer progression [540, 544]. In light of metabolism, the functions of STAT3 seem to depend on its activity as a nuclear and mitochondrial gene transcription factor [284, 545] although other functions can not be excluded. Especially the regulation of mitochondrial homeostasis and activity of the ETC by MitoSTAT3 is most likely not by a 1:1 protein-protein interaction as levels of MitoSTAT3 are low in comparison to mitochondrial proteins [546].

Regarding metabolic regulation by nuclear STAT3, it was shown that constant STAT3 could induce a Warburg-like phenotype in primary MEF cells. These effects were mediated via a STAT3 dependent HIF1 $\alpha$  expression [547, 548]. Increased HIF1 $\alpha$  results in increased expression of GLUT1 and ENO1, two key enzymes of glycolysis, and increased lactate secretion. Moreover, it was shown that those cells become addicted to glucose as a fuel, and in contrast to other reports, they showed decreased activity of the ETC and reduced PDH activity [547]. Furthermore, they showed a reduced generation of ROS in cells expressing constitutionally active STAT3 compared to WT STAT3. However, it is not clear whether this is due to decreased ETC activity or increased expression of ROS defense genes, as it was also shown that STAT3 could regulate the gamma-glutamyl cycle, a cycle to generate the antioxidant glutathione (GSH) [549].

In concordance with our observation that loss of STAT3 in the mitochondria is tumor suppressive, it was shown that increased MitoSTAT3 could drive cancer formation in Barrett's epithelial cells [550], as well as MitoSTAT3 levels, were shown to increase in pancreas cancer [551], breast cancer [552] and myeloproliferative neoplasms [553]. Furthermore, it was suggested that increased MitoSTAT3 levels could drive the formation of cancer initiation cells or stem-like cancer cells as well as tissue stem cells [554–556]. Even though evidence supports the idea that STAT3, in many cases, can be an oncogene, its exact oncogenic functions, mitochondrial gene transcription, nuclear transcription, protein-protein interactions, ETC regulation, and their contribution to the transformation process remain elusive.

Some reports have suggested that STAT3 can have tumor-suppressive roles, which was mainly associated with increased STAT3 $\beta$ , a shorter STAT3 isoform. STAT3 $\beta$  was shown to have tumor-suppressive roles in acute myeloid leukemia [557], esophageal cancer [558], lung cancer, and melanoma [559]. Mechanistically, STAT3 $\beta$  was suggested to be a dominant-negative regulator of STAT3 $\alpha$  as higher STAT3 $\beta$  resulted in decreased cyclin D1 level [540]. However, in recent times distinct roles of STAT3 $\beta$  were shown. These include expression of TNF-related apoptosis-inducing ligand (TRAIL), the TRAIL receptor, STAT1 $\beta$ , and lens epithelium-derived growth factor (LEDGF). Interestingly, the expression of phosphorodiamidate morpholino oligomer (morpholinos) to manipulate an enhancer for the splicing of STAT3 in favor of STAT3 $\beta$  resulted in

tumor regression in breast cancer xenograft, again highlighting the tumor-suppressive roles of STAT3 $\beta$  [560].

However, not only STAT3 $\beta$  was shown to have tumor-suppressive roles also full-length STAT3 was shown to be able to suppress tumor growth, especially in the context of low PTEN levels in the brain as well as in prostate cancer [90, 561, 562]. It was shown by Pencik *et al.*, that prostate epithelial knockout of *Pten* in combination with *Stat3* knockout resulted in faster prostate tumor development and more aggressive tumors [562]. We used this particular mouse model to demonstrate that HTC levels can be increased in prostate cancer. We demonstrated that levels of HTC enzymes were higher in the double knockout than in the WT mouse prostate. Interestingly, HTC was increased in the knockout of *Pten*, a condition normally associated with cellular senescence. At the time of analysis, 19 weeks of age, we could show that the senescence response was already abolished in several areas of the *Pten* knockout prostate. These senescent devoided regions had high Ki67 staining, and those areas had higher HTC levels than the surrounding tissue. However, we could still identify areas with low Ki67 in *Pten* knockout prostate tissue; thus, cells were still senescent, and concordantly, HTC levels were low. Histopathologic analysis of *Pten* knockout, at 19 weeks revealed that in about 50% of the *Pten* knockout mice a invasive regions, precursor of prostate cancer, had developed. Interestingly, although SA- $\beta$ -GAL was not detected in prostate epithelial in *Stat3* knockout, histopathology from *Stat3* knockout tissues revealed that those prostates had the development of prostatic intraepithelial neoplasia (PIN), the precursor of prostate carcinoma. However, even at 52 weeks, no invasion or adenocarcinoma in *Stat3* knockout was detected, highlighting the double role of STAT3 again, as knockout alone is tumor-suppressive, but knockout in combination with loss of PTEN is tumor-promoting.

Similar to the pleiotropic roles of STAT3, the role of PTEN knockout in prostate cancer development and cellular senescence is still controversial. Different prostate cancer mouse models showed that PTEN loss-induced senescence is unstable, but the timing of tumor initiation and bypass of senescence is different for each mouse model [110, 562, 563]. Moreover, it was shown that PTEN could regulate p53 stability and p53 transcriptional targets; thus, loss of PTEN reduces tumor-suppressive capacity by p53 [564].

It is tempting to suggest that loss of STAT3 in the prostate leads to mitochondrial dysfunction, as observed *in vitro* and a concordant NAD<sup>+</sup>/NADH ratio decreases and a slight increase in glycolysis to maintain viability. However, in case STAT3 and PTEN are lost, STAT3 will still induce mitochondrial dysfunction, and the loss of PTEN will activate AKT, which can drive expression of NADK as well as metabolic enzymes including PC and MDH1 resulting in the normalization of the NAD<sup>+</sup>/NADH ratio [337]. Moreover, a loss of PTEN was shown to alter the transcriptional p53 targets, so that p53 in the absence of PTEN may no longer repress the HTC enzymes.

The contributions of HTC enzymes and STAT3 in prostate tumors are still under investigation, but it seems likely that subtypes of tumors require high HTC expression for sufficient transformation. Our results in PC-3 cells that knockdown of any component of the HTC complex is sufficient to reduce growth and altered the NAD<sup>+</sup>/NADH as well as the NADP<sup>+</sup>/NADPH ratio suggest that at least in the context of loss of STAT3 loss of PTEN and loss of p53 as found in PC-3 cells, HTC is a major contributor to maintain cellular proliferation and anchorage-independent growth. Further studies will reveal if HTC activity inhibition is an interesting avenue *in vivo* to slow the growth of prostate cancer or other cancer types.

The choice of prostate cancer as a model to study the function of HTC was mostly based on the availability to us of a prostate cancer mouse model as well as the availability of human prostate cancer samples. In the future, other tumor types should be characterized, and interestingly, analysis of expression data of HTC components in breast cancer revealed decreased survival in ME1, MDH1, and PC high expression cancers. Similarly, analysis of normal tissue with cancerous tissue revealed that expression of HTC components is significantly higher in small squamous lung cancer. The mechanistic insights into those observations remain elusive but highlight that HTC might not only be important for prostate cancer but a more general mechanism hijacked by cancer cells.

### **3.4. Implication of metabolic changes in senescent cells**

One of the key aspects that we have confirmed are the alterations in metabolic activity in senescent cells. Our tracing data showed higher citrate generation in senescent cells, although the metabolic reason for this remains elusive. Even though supplementation with aspartate did not rescue the senescent phenotype, we could confirm that aspartate levels decreased in senescent cells. Decreases in aspartate levels have various consequences in senescent cells. Our data support the idea that nucleotide biosynthesis decreases due to low aspartate levels, but we could not show that increasing nucleotide synthesis by aspartate supplementation alone was sufficient to bypass the senescence response. These data are in contrast to reports where it was shown that the lack of nucleotides was a sole driver of senescence response [228]. Intriguingly, we could observe decreased DNA damage foci in senescent cells treated with aspartate, adding to the growing evidence that DNA damage is not a requirement nor a sole driver for the induction of OIS or MSIS [124]. Our data rather supports the idea that the senescence response acts on two different areas. The first area would be the nucleotide synthesis, which can be corrected by aspartate supplementation but senescence also have lower dNTP levels which did not increase in cells supplemented with aspartate. Concordantly, RNR, the enzyme that makes dNTPs, is an E2F target gene repressed by p53, and



those results highlight that not only lack of aspartate drives the changes in dNTP levels but also the repression of RNR by RB and p53. Induction of high p53 levels in senescent cells is normally associated with phosphorylation on S15 due to DNA damage, but p53 can also be stabilized by acetylation [565] or high levels of NADH [494, 566].

Steady-state analysis of amino acid content in shSTAT3 senescent cells also confirmed studies that showed that cysteine does increase in senescent models. The roles of cysteine increase are still under debate, but it could be suggested that this could explain alteration in the ferroptosis response as well as alterations in the glutathione cycle [439, 446]. Herein, we could show that  $\gamma$ -l-glutamyl-l-cysteine, the precursor of glutathione, is decreased in senescent cells, highlighting higher GSH requirements in senescent cells. Moreover, we could observe alterations in levels of oxidized glutathione in senescent cells as well as a normalization of those levels in cells that express HTC. The normalization of the GSH/GSSG ratio is most likely due to the increased NADPH generation in HTC expressing cells, highlighting the role of NADPH for the senescence response.

Apart from the glutathione cycle, it is interesting to notice that the levels of S-Adenosyl-L-homocysteine (SAH) and SAM decrease in the induction of senescence. This is because SAH and SAM are important metabolites of the methionine cycle, and SAM is used as a methyl donor for methylation reactions [567].

Alterations in methylation reactions have a prominent impact on epigenetic regulation, and increasing evidence suggests that alterations in the methylation of DNA or Histones can drive aging and cellular senescence [568, 569]. It was shown that hypomethylation of the DNA is observed in the elderly [570, 571] and researchers could demonstrate the methylation state was a better predictor of human age than telomere length or proteomic changes [572]. However, subsequent research has determined that it is not a general hypomethylation but rather hypomethylation at constitutive-heterochromatin repeat regions, whereas other areas such as promoter CpGs increase in methylation with age [573, 574]. Altogether, these data underpin the highly complex regulation of methylation in the aging phenotype, and further research will elucidate the contributions of methylation to human aging. Another interesting aspect of methylation in aging is the observed reactivation of retroposons in aging. It was supposed that the increased mobility of retrotransposon elements could be a marker of hypomethylation of certain DNA regions as well as a driver of senescence [575].

Regardless of the exact role of methylation in aging, the increased requirement of glutathione can route away cysteine and methionine from the methionine cycle, thus reducing SAH and SAM levels in senescent cells, which in turn result in an alteration of methylation of DNA and Histones. Of note, serine, another precursor for GSH synthesis, is also decreased in senescent cells [446] confirming the higher requirements for GSH synthesis. Moreover, the increased NADPH need for

GSSG reduction reduces the availability of NADPH for the methionine and folate cycle. Those alterations have been suggested as major drivers of the senescence response, especially in light of the profound changes of hetero- and eu-chromatin in senescent cells [214].

In contrast, in cells with forced HTC expression, we see increased NADPH levels. The increase in NADPH levels results in increased methionine and SAM cycle, as NADPH is one of the limiting factors of the folate and methionine cycle [492]. Although we have not formally tested the levels of SAM and SAH after senescence bypass by HTC expression, the fact that the HTC expression in combination with oncogenic Ras can transform the cells suggests that the methylation state of the cells is altered. Therefore, it would be interesting to look at the methylation state of cells that have bypassed the senescence response, and those cells may display a methylation pattern of cancerous cells. Another interesting link can be drawn with the altered methylation state, metabolism, and ribosome biogenesis. It was shown that a decrease in ribosome biogenesis is often concomitant with alteration in the methylation of ribosomal DNA promoter regions in such decreased of SAM levels could be a consequence of increased rDNA methylation [576]. Increased rDNA methylation is followed by decreased ribosomal RNA expression resulting in a feed-forward positive cycle to maintain the senescence response. It remains to be determined whether decreased SAM levels in senescent cells are due to increased methylation or increased demands for glutathione.

Altogether, the results suggest that the decreases of certain metabolites, namely aspartate, serine, SAM, and SAH, are characteristics of a tumor-suppressive metabolism in senescent cells as they limit nucleotide biosynthesis and also drive age-dependent changes in methylation.

### **3.4.1. Implication of PC outside of mitochondria**

One important result of the discovery of HTC is the presence of pyruvate carboxylase outside of the mitochondria. In mammalian cells, PC is was described as a mitochondrial only enzyme, but previous reports have already shown that in certain contexts, two-cell embryo and after viral infection, PC can be outside the mitochondria [577, 578]. Interestingly, PC is a cytosolic enzyme in yeast and filamentous fungi, such as *Aspergillus nidulans*, *A. terreus*, and *R. oryzae* [579]. Moreover, in *Xenopus* and *C.elegans*, there are isoforms of pyruvate carboxylase in the cytosol. In contrast, PC is in the mitochondria in *Drosophila* and higher mammals such as pigs or cows. Those observations suggest that PC became a mitochondrial enzyme somewhere in the development of insects and higher mammals. It is tempting to suggest that the change in localization of PC could be a tumor suppressor mechanism. Those results call for a detailed analysis of PC localization over the time of evolution from yeast towards mammalian cells. Those analyses are mainly limited right now as most of the localization of proteins in an organism is based on predicted structure

homology or function homology. However, the gold standard to infirm or confirm PC localization in the mitochondria would be electron microscopic images with immunolabelled PC.

Furthermore, we have shown in cancerous cells that there are shorter PC isoforms. Using bioinformatics tools that predict the likelihood of a protein being imported into the mitochondria, we identified two predicted isoforms X11 and X10, with a low prediction score for mitochondrial import. The regulation of those isoforms is yet unknown but is it possible that those isoforms increase expression during the transformation process or in cancerous cells. As mentioned before, we have identified the minimal interaction region of ME1, MDH1, and PC; as such, we can not exclude the possibility that shorter isoforms of PC can be present in the HTC complex. For example, the isoforms x11 and x10 could be present in HTC, as both contain the identified minimal residues of PC to interact with ME1 and MDH1. Nevertheless, we were not able to show that those isoforms are metabolically active. Another possible way PC can be outside of the mitochondria is through N-terminal protein degradation or N-terminal protein trimming, leading to PC isoforms that are not imported into mitochondria. In fact, PC expression with a c terminal tag from retroviral vector, no 3' or 5' nor any introns, revealed similar isoforms then observed endogenously in cancer cells. N terminal proteolysis is normally linked to the N-end rule pathway of protein degradation, but it is also possible that removal of N-terminal residues changes localization or function of a protein resulting in an increased proteome diversity [580]. Increased protein diversity was recently linked to cancer development [581].

All in all, the discovery of a cytosolic fraction of PC seems just the tip of the iceberg, and further studies will most likely uncover more proteins that can hide in the mitochondria as a tumor suppressor mechanism. Furthermore, we will focus on the identification of the exact composition of the HTC complex.

### **3.5. Different roles of HTC**

An interesting aspect of our studies is the identification of the HTC and its ability to bypass the senescence response. HTC is composed of a cytosolic fraction of PC, ME1, and MDH1, and its action is to transfer the hydride ion from NADH into NADPH, thus the name hydride transfer complex. Our analysis showed that the HTC could be hijacked by cancer cells to improve their NAD<sup>+</sup> levels as well as improve their NADPH levels. Both metabolites are crucial metabolites for metabolic rewiring, which takes place during the transformation process [22, 582, 583]. However, HTC is not only important in transformation and cancer cells but has been shown to have implications in hypoxia and other physiological contexts.

Although we are the first to show the roles of the HTC in cellular transformation, the idea that the combined action of PC, ME1, and MDH1 can be beneficial for cells is not new. Intriguingly, researchers have filled out a patent of a yeast strain that expresses *mae* (the *S. pombe* homolog of ME1), *mdh2* (the yeast homolog of human MDH1), and *pyc1* (the yeast homologs of human PC). The patent showed that the concerted action of those three proteins could increase biomass production by yeast. A recent preprint publication showed that concerted actions of *smae*, an engineered *mae*, that can not go to the mitochondria, *mdh2*, and *pyc1*, can increase fatty alcohol production in yeast. Normally *mae* can be a cytosolic and mitochondrial enzyme in yeast. The fact that the *mae* which did not go to mitochondria further increased fatty alcohol production highlights the requirements of physical interaction of the HTC complex. Altogether, these results further confirmed the idea that the interaction of metabolic enzymes increases reaction speed [584].

A similar idea of a hydride transfer cycle was proposed in some gram-negative bacteria, among others, *Pseudomonas fluorescens*. In case those bacteria are challenged by oxidative stress, the concerted actions of PC, ME1, and MDH1 allow for regeneration of NADPH for redox defense [585]. Likewise, in *Candida tropicalis*, a yeast strain that is used to produce xylitol (a sugar-free sweetener) at industry scale, it was shown that expression of pyruvate carboxylase, malic enzymes, and malate dehydrogenase resulted in higher resistance to oxidative stress and increased xylitol secretion [586]. Interestingly, this cycle was particularly upregulated in case the yeast was grown in a hypoxic environment [586].

Altogether, those results suggest that the actions of HTC are context-dependent but can be observed in less developed organisms. The possibility that HTC has beneficial roles in yeast and some bacteria proposes that this cycle could be conserved through evolution, and further studies might reveal other organisms with HTC activities. The observation that this hydride transfer cycle is particularly active in hypoxic yeast cells is in concordance with our results that show that HTC can form in cells in a hypoxic environment, as we have demonstrated that HTC formation allows cancer cells to cope with hypoxia.

### **3.5.1. Role of HTC in Cancer**

Rewiring and plasticity of metabolism is a common trait of cancer [22, 587]. Our identification of the presence of HTC adds to the growing evidence that one of the key aspects of cancer metabolism is the generation of sufficient NAD<sup>+</sup> and NADPH to fuel key metabolic reactions needed to produce ATP and biomass [387, 583]. Furthermore, our results that show that inhibition of HTC in PC-3 cancer cells allows for growth reduction even though p53 and PTEN, two major tumor suppressors, are inactive. These results allow for the suggestion that NAD<sup>+</sup> and NADPH-driven cell cycle arrest can act downstream of p53 and PTEN. Concordantly, a decrease of redox power

in cancer cells has been shown to dampen neoplastic growth in all aspects of tumor development [473].

Firstly, it was shown that increased NAD<sup>+</sup> levels in the primary tumor allow for increased glycolytic flux [387, 588]. For instance, it was demonstrated that malate dehydrogenase 1 (MDH1), the enzyme that catalyzes the reaction from OAA to malate with NADH to NAD<sup>+</sup> conversion, could be in proximity with GADPH. Thereby, the use of NAD<sup>+</sup> by GADPH increased, resulting in faster glycolysis [588]. Furthermore, it was demonstrated that an increase in NADPH in the primary tumor resulted in better resistance to metabolic insults such as hypoxia and an increase in ROS [490].

An interesting aspect that we have not covered yet is metastasis and the roles of NAD<sup>+</sup> and NADPH therein. It was shown that cancer cells that express high levels of NAMPT, to increase NAD pools, have higher metastatic rates than cells with low NAMPT expression [589, 590]. These results suggest that an increase in NAD<sup>+</sup> levels, as observed in HTC expressing cells, might increase cancer cells' metastasis. Likewise, it was shown that the dissociation process of cells from the primary tumor results in increased ROS levels in the cells [490]. Thus, higher NADPH levels, as generated by HTC, help to cope with higher ROS levels, suggesting again that HTC expression could drive a higher metastasis rate. Finally, changes in NAD<sup>+</sup> availability increased colonization of tumors at the distant metastatic site [591].

Altogether, those results suggest that HTC expression could fuel various aspects of neoplastic growth, and future work will elucidate the contribution of HTC towards malignant growth.

### **3.5.2. Role of HTC in physiological contexts**

Our data not only supports the idea that HTC is important in prolonging lifespan and can lead to transformation, but we were able to identify one physiological role of the HTC complex. We have shown that cells cultured in hypoxia can upregulate the HTC complex, and this upregulation might help to cope with the hypoxic stress. Cells in hypoxia can not use the ETC to generate ATP, as oxygen is required as an electron acceptor, nor can they use complex I to regenerate NAD<sup>+</sup>. It was shown that supplementation with NAD or NAD precursors alleviates hypoxia-induced damage in cardiac kidney and brain tissues [532, 592, 593]. It was previously shown that Ras-induced senescence can be bypassed if cells are cultured under hypoxic conditions; nevertheless, mechanistically, it was not clear how the senescence bypass occurred. We have shown that the expression of HTC components abolished the senescence response in Ras-senescent cells cultured in hypoxia. The observations suggest that NAD regeneration allows for senescence bypass, at least in hypoxic cells.

Another interesting role of MDH1/2, ME1, and PC was shown in  $\beta$ -cells. In this case, PC was in the mitochondria, so no physical complex was formed; however, the concerted actions of PC, MDH1/2, and ME1 were important for insulin secretion. So, in this case, it should rather be called a hydride transfer cycle or pyruvate/malate cycle.

Insulin secretion from the  $\beta$ -cells can be achieved by the triggering pathway where glucose can enter the  $\beta$ -cell followed by glycolysis, leading to an increased ATP/ADP ratio, calcium influx, and secretion of insulin [594]. In recent times, however, it was suggested that other pathways might be involved, and those pathways were controlled by NADP, NAD, and intermediates of the TCA cycle [595]. Interestingly, PC is highly expressed in the  $\beta$ -cells, although no apparent physiological need for high PC activity was found in the  $\beta$ -cells suggesting PC-mediated anaplerosis of the TCA cycle could be used as a signaling function. It was shown that mitochondria isolated from  $\beta$ -cells stimulated by labeled 1-C<sub>14</sub> pyruvate secrete large amounts of labeled malate [596]. In order to retain the label, the pyruvate has to enter the TCA via PC as the label would be lost in the PDH reaction. (See Figure 1 or 4 of Molecular Cell paper). Oxaloacetate generated by PC can then be converted into malate and be exported or converted by ME1 into pyruvate. This cycle would allow for NADPH generation, and this cycle with the increased NADPH was shown to increase insulin secretion [597, 598]. Moreover, alterations in other metabolites have been suggested to be implicated in insulin secretion, and this cycle can be even more complex and involves citrate export of mitochondria and conversion of cytosolic citrate into malate and oxaloacetate [595, 599, 600]. Furthermore, this conversion can also implicate isocitrate and  $\alpha$ -KG adding a further layer of complexity. For an overview, see figure [3.1].

Furthermore, a recent report has shown an alternative way for increase insulin secretion that did not involve NADPH production. They suggested that alterations in glycerolipids and glycolytic intermediate DHAP would drive insulin secretion [602]. The concerted actions of ME1, MDH1/2, ACLY, GOT1/2, and PC on insulin secretion and NADPH generation are still a matter of debate, and further experiments will allow for more detailed conclusions [400, 601, 602].

An interesting link that can be drawn here is a link to Metformin. Metformin is one of the most common drugs used in Diabetes type II. The suggested actions of Metformin are the following; increased insulin secretion and a reduction of glucose production in the liver. However, molecular and mechanistic proves for Metformin actions are not fully understood [603]. We and others have reported that Metformin can increase NADH levels via its capacity to inhibit the ETC [554, 604, 605] and its inhibition of glycerol-3-phosphate dehydrogenase (GPDH) [603, 606]. Increased NADH level can have several effects, among other increased glycolysis triggering more calcium influx and more insulin secretion. Furthermore, it is also possible that the increased NADH levels are converted into NADPH by either NADK or the concerted actions of MDH1/2, PC, and ME1, as

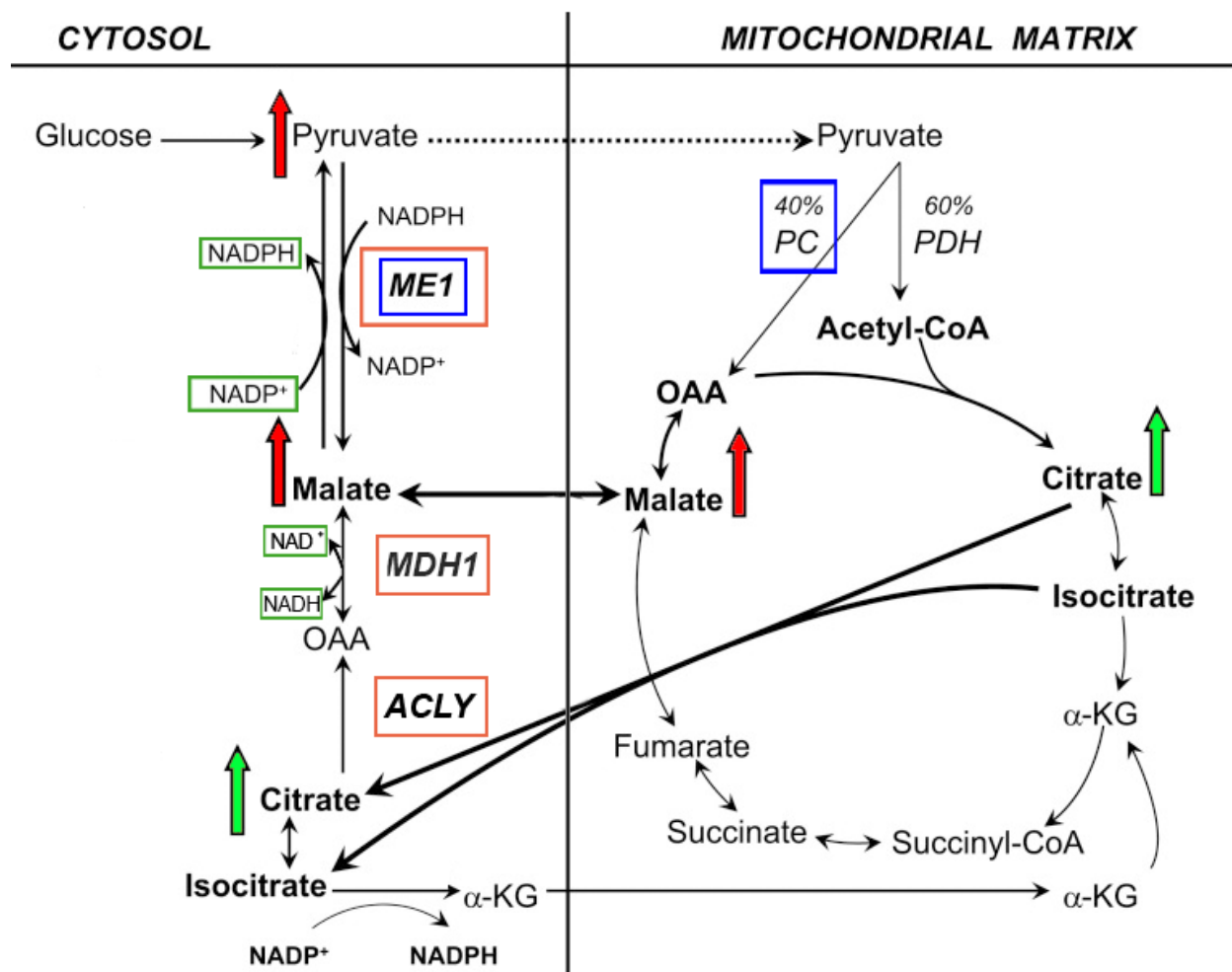


**Figure 3.1. Pyruvate cycling pathways in insulin secretion**

Increased levels of malate or pyruvate can stimulate pyruvate cycling to trigger insulin release. Important pathways are highlighted in orange for citrate-based OAA generation. For malate-based pyruvate generation blue. Important redox metabolites are highlighted in dark green. Important metabolites are highlighted in red or green. Figure adapted from [601]. Abbreviations: MDH1: Malate dehydrogenase 1, ACLY: ATP-citrate lyase, ME1: Malic enzyme 1, PC: Pyruvate carboxylase, PDH: Pyruvate dehydrogenase, OAA: Oxaloacetate,  $\alpha$ -KG:  $\alpha$ -Ketoglutarate.

described above. First hints that actions of NADH and senescence in the  $\beta$  cells are connected was obtained as insulin secretion in senescent  $\beta$ -cells increased [607]; however, these effects do not last as more and more senescent cells accumulate with age [608]. Thus, these observations suggest repression of NADH conversion into NADPH in senescent cells. Further research will allow us to elucidate if the expression of hydride cycle proteins can alleviate diabetes phenotypes.

### 3.5.3. The roles of HTC on aging T-cells

The roles of NAD<sup>+</sup> and NADPH have not only implications in cancer development but are relevant for several other biological functions. One interesting observation is the fact that T and B cells require a high amount of NAD<sup>+</sup> for their functions [609–611]. It is known that during the rapid expansion phase of T-cells, the metabolism is rewired towards higher glycolysis and glutaminolysis [609, 612]. One observation is the increased secretion of lactate of rapid proliferation T-cells, and it was suggested that the secretion of lactate helps to maintain the proper NAD<sup>+</sup>/NADH ratio to sustain the high glycolytic rate [609]. Interestingly, exhausted T-cells have dysfunctional mitochondria and a decreased NAD<sup>+</sup>/NADH ratio. It was proposed that normalization of this ratio might retard T-cell exhaustion [613, 614]. Furthermore, it was demonstrated that NAD supplementation potentiates the anti-tumor response of tumor infiltrated T-cells [614, 615]. Likewise, expression of mitochondrial biogenesis factors resulting in higher complex I activity improved T-cell function [616], and inhibition of CD38, a NADase, also resulted in higher T-cell killing activity [611]. Right now T-cell exhaustion is limiting the use of personalized chimeric antigen receptors T-cells (CAR-T) cells in the clinic. CAR-T-cells are engineered to specifically recognize antigen present on the surface of tumor cells [190]. Once those cells are generated, they are subjected to a rapid expansion protocol. One limit here is that *in vitro* CAR-T-cells become exhausted once their mitochondria become dysfunctional or the NAD<sup>+</sup>/NADH ratio decreases resulting in an induction of cellular senescence. Given the roles of expression of HTC in senescence and NAD regeneration, it can be suggested that expression of HTC in those engineered CAR-T-cells would allow for a normalization of NAD<sup>+</sup>/NADH ratio and potentially allow for a longer proliferation phase of those cells and higher efficiency of tumor-killing once inside the body.

### 3.5.4. HTC in the mitochondria

An interesting aspect of the discovery of HTC is that it seems that HTC is localized to the cytosol. We used several techniques, immunofluorescence, immunogold labeling, and mitochondria purification, to prove that a fraction of PC can be outside the mitochondria; nevertheless, there is still a fraction of PC inside the mitochondria. We have not formally addressed the possibility of whether ME2 and MDH2 can interact with mitochondrial PC in order to form an HTC complex in the mitochondria. However, co-precipitation assays of purified proteins showed that PC and MDH2, as well as PC and ME2, can weakly co-precipitate [617] suggesting a possible HTC complex in the mitochondria. Our rationale for focusing on the cytosolic HTC formation was based on our results using cytosolic LBNOX and duroquinone, which indicated that cytosolic NAD<sup>+</sup> regeneration is more important in senescent cells than mitochondrial NAD<sup>+</sup> regeneration. A point



apart from this is that a recent report also shows that NAD pools of cytosol and mitochondria can actually communicate as researchers identified a transporter that can transport NAD from each compartment into the other, highlighting the possibility that also mitochondrial NAD<sup>+</sup> regeneration can normalize cytosolic NAD<sup>+</sup> levels [618]. The existence of a mitochondrial HTC at this point can not be excluded, and further research will allow validation of this cycle.

### 3.5.5. The core complex HTC

As pointed out in the limitations of our studies, we were not able to identify the exact stoichiometry of the HTC complex, nor were we able to exclude that other proteins take part in the HTC complex. We assembled the HTC complex with ME1, MDH1, and PC, suggesting those three can form the core of the HTC complex, but we can not exclude further interaction partners. In fact, we were able to show colocalization with LDH in case we cultured PC-3 cells on lactate. In this case, the lactate is taken up by the cell and converted into pyruvate, generating NADH. In the presence of HTC, this NADH can be converted into NAD<sup>+</sup> via MDH1 reaction. Thus, we were able to show that at least components of the HTC complex are in close proximity to the LDH, which would allow for a rapid NAD<sup>+</sup> regeneration in those cells. Furthermore, our blue native gel analysis revealed a complex of a size bigger than 1MDa, allowing for the possibility of several HTC subunits or interaction with other proteins upon *in vivo* assembly of HTC. In a similar idea, it was shown that GADPH, NAD<sup>+</sup> requiring enzyme of the glycolysis, can interact with MDH1, and this interaction would allow for a rapid NAD<sup>+</sup> regeneration by MDH1 and faster glycolysis speed [619]. It is quite possible that other dehydrogenases or hydrogenases can interact closely with MDH1, PC, or ME1, in order to allow for a faster reaction speed of NAD regeneration. In fact, we tried to identify by biotin ligation assay followed by mass spectrometry further interaction partner of the HTC complex and could identify several dehydrogenases being present in our BIO ID. Further experiments will likely confirm the presence of those partners. Interacting of HTC with other partners will allow for a rapid response in case of different stresses to the cell, and one idea that seems tempting to suggest is the idea of increased metabolic flexibility in cells that express HTC. The concept of metabolic flexibility was suggested, especially in cancer metabolism, following the identification of fast rewiring of metabolism in case of nutrients deficiency. One example of this rapid rewiring of metabolism in cancer cells is the observation that PC-3 cells can grow on lactate; however, removal of HTC impeded the growth of PC-3 cells.

As discussed before, glutamine removal by inhibition of glutamine importer in PDAC cells resulted in a rapid increase of micropinocytosis and autophagy to maintain high intracellular glutamine levels. Other instances of this metabolic flexibility were described in various cancer, and

high metabolic flexibility was suggested as one of the main drivers of aggressiveness and potential metastasis of the tumor [620].

All in all, the results on the different roles of HTC highlight two major components. First, it seems important that HTC expression can regulate key metabolic pathways so that cells can meet their bioenergetic and biosynthetic needs rapidly and adapt to stressors arising from their environment. Furthermore, HTC can drive metabolic flexibility in normal and cancer cells by supplying NAD<sup>+</sup> and NADPH. Supply of NAD<sup>+</sup> and NADPH are definitively key metabolites in various metabolic pathways.

### **3.6. Transformation with NAD without loss of p53 or RB**

One interesting aspect of our studies is the observation that cells can get transformed by the action of HTC in combination with oncogenic RAS. Normally, the expression of oncogenic RAS would result in induction of cellular senescence [52], but co-expression with HTC was sufficient to bypass the senescence response and transform those cells. Intriguingly, the cell maintained an intact p53 pathway suggesting that normalization of NAD and NADPH metabolism following oncogenic activation is sufficient to transform cells. To our knowledge, this is the first report to show a combined action of metabolic enzymes with the oncogene RAS would be sufficient to transform cells. A recent report suggested that in immortalized fibroblasts the expression of G6PD, the key limiting enzyme of the PPP, would be sufficient to transform cells. As those cells were previously immortalized by using expression of large T-antigen, thus disabling p53 and RB and all key features of cellular senescence those results have limited translation effect. Nonobstant the fact that senescence was bypassed by large T-antigen, it required eight weeks for the G6PD BJ cell line to start forming tumors whereas the oncogene RAS in BJ with large T-antigen expression can form palpable tumors within three weeks [457]. The requirements of NAD and NADPH generation for cellular transformation are interesting aspects and open the question of the key functions of each metabolite for transformation.

Apart from the transformation process, HTC can also have implications in tumor metastasis, as it was recently shown that tumor cells do require an increased amount of NADPH during the migration process as the detachment from the primary tumor, the amount of ROS in the cells increases. A higher level of NADPH allows for better ROS detoxification via glutathione metabolism. The high NAD<sup>+</sup> level are likely required during the migration process as it was shown that metabolism at the distant site of metastasis could require different NAD status than the primary tumor [621]. For instance, it was shown that serine is not required for primary breast tumor, but the metastasis in the lung requires high serine synthesis [621] and high serine synthesis requires high NAD<sup>+</sup> levels

[433]. Furthermore, serine biosynthesis from glucose requires high NAD<sup>+</sup> levels since converting glyceraldehyde-3-phosphate into 1,3 bisphosphoglycerate in glycolysis requires NAD. Likewise, converting glycolysis intermediate 3-phosphoglycerate into 3-phospho-hydroxypyruvate, the first step of serine biosynthesis, does require NAD<sup>+</sup>.

### 3.7. Impact of other metabolons or metabolic cycles

The discovery of the metabolon HTC is not the only metabolon that was recently proposed to be increased in cancer cells. The idea of metabolons was proposed by P. A. Srere and A. Kuzin in the 70ies and 80ies as a concept to increase the reaction speed of metabolic enzymes in case those enzymes could go into close proximity [622–624]. The close proximity would allow for increased reaction speed as metabolites and cofactors do not have to travel through the space between the enzymes. Metabolons have been suggested and partially confirmed for many metabolic pathway including TCA cycle [622, 625], glycolysis [626], nucleotide biosynthesis [627], fatty acids oxidation [617], lipid biosynthesis [617], and other metabolic pathways in mammalian cells as well as bacteria and plants [617, 623, 626].

Our study identified HTC as a novel metabolon to generate NAD<sup>+</sup> and NADPH, two key factors maintaining high metabolic flexibility in cancer cells. Another metabolic cycle that was recently described is the GOT1, MDH1, ME1 cycle that maintains high cytosolic NADPH levels in PDAC cancer [628]. In those reports, it was shown that aspartate generated by glutaminolysis could be exported into the cytosol and then converted into OAA by GOT1. Thus, OAA can supply MDH1 reaction followed by ME1 reaction.

In comparison with our results, the supply route for OAA is different, but the final consequences are the same in HCT expressing cells as well as in cells that use the GOT1, MDH1, ME1 cycle. In both cases, the cycles result in increased NADPH and NAD<sup>+</sup> levels. In our hands, we have excluded GOT1, MDH1, ME1 being active in senescence for two reasons.

First, the supplementation with aspartate did not reverse the alterations in NAD<sup>+</sup>/NADH ratio, nor did it convincingly bypass the senescence response. Secondly, it was suggested that the malate aspartate shuttle requires a functional ETC and might be down-regulated in a stress-dependent manner [629].

Altogether, these observations do not exclude the coexistence of both cycles being relevant in cancer, but it seems that HTC can bypass cellular senescence on top of being important in cancer cells. Maybe forced expression of GOT1, MDH1 and ME1 could bypass cellular senescence; however, there are no reports showing that GOT1 is repressed in senescent cells. Interestingly,

although the authors of the GOT1, MDH1, and ME1 cycle did not show physical interaction of those proteins, it was shown that loss of MDH1 dimer formation could stop this cycle [630].

Another interesting metabolic cycle involving ME1 was recently shown [631]. In their report, the authors could show that in tumors with low glucose supply, lactate and glutamine can be used to generate NADPH in a ME1/IDH1 dependent manner. First, lactate can be imported into the cell converted into pyruvate, and then pyruvate can be imported into the TCA cycle to generate citrate. This citrate can be exported or continue the TCA cycle. If the TCA cycle continues, eventually, there is malate generation, and this malate can be exported and ME1 and generate pyruvate and NADPH. In case citrate is exported, it is converted into isocitrate, and IDH1 can generate  $\alpha$ -KG and NADPH. In the latter, glutaminolysis allows for TCA cycle anaplerosis [631].

Furthermore, a recent report mentioned that decrease of PC and ME1 in PDAC cells results in reduced growth of those cells. Interestingly, the double knockout of PC and ME1 result in even higher growth inhibition [632]. Unfortunately, the authors did not explain why the combination of ME1 and PC knockout results in higher growth inhibition, but it is quite possible that this would be a consequence of HTC disruption.

In summary, the relevance of metabolic cycles to fuel neoplastic growth and allow metabolic plasticity is rapidly increasing in the past years. The roles of HTC integrate well into known evidence of metabolic cycles being relevant for NAD<sup>+</sup> and NADPH production. An interesting aspect in further research will be to uncover the integration of those metabolic cycles with each other and their respective relevance in sub-cancer types. Although not all metabolic cycle displays physical interaction between the enzymes, it seems likely that further research will allow uncovering other interactions and metabolic cycles that allow cancers to meet their bioenergetic and biosynthetic needs and adapt to stressors emanating from their microenvironment.

### **3.8. NAD regulation in senescence, aging, and stem cells**

One of the main observations is the alterations in the NAD<sup>+</sup>/NADH ratio during the induction of senescence. First of all, there is consensus that replicative senescence as well as mitochondrial dysfunction induced senescence, and some therapy-induced senescence display alterations in the NAD<sup>+</sup>/NADH ratio [127, 459, 460] similar to our observations. In contrast to our observation, however, groups have shown in oncogene-induced senescence that there are no difference or increase in NAD<sup>+</sup>/NADH [127, 633]. These discrepancies might be explained by differences in experimental design. For instance, the presence of pyruvate in the media can normalize the NAD<sup>+</sup>/NADH ratio via the LDH reaction. Furthermore, the amounts of oxygen present were shown to influence the NAD<sup>+</sup>/NADH ratio. Regardless of whether oncogene-induced senescence

does or does not alter the NAD<sup>+</sup>/NADH ratio, supplementation with precursors of NAD such as NR or NMN resulted in increased NAD levels and a pro-inflammatory SASP. Furthermore, NAD supplementation resulted in an increased speed of cancer development [633] highlighting that increased NAD metabolism is a pro-oncogenic event.

*In vivo* observation of the NAD<sup>+</sup>/NADH ratio is still limited, and further research on NAD<sup>+</sup>/NADH ratio in senescent *in vivo* lesions will elucidate the contribution of NAD<sup>+</sup>/NADH ratio in oncogene-induced senescence.

### **3.9. Roles of NAD and ribosomes biogenesis alterations on tissue aging**

The major points of this thesis are, how cellular senescence is maintained in cells, and what are the biological consequences of those senescent cells? The description of ribosome biogenesis alterations and mitochondrial ultrastructure alteration in senescent cells demonstrate two contributors of cellular senescence, which drive the aging phenotype in the human body. In fact, ribosome biogenesis decrease was previously linked to several neurodegenerative diseases [634]. For example, it was shown in Parkinson's disease (PD) that there is a decreased ribosome biogenesis and an alteration of nucleolar structure in dopaminergic neurons, the cells that are affected in PD [635]. Furthermore, it was demonstrated that those alterations in the nucleolar structure were most likely due to decreasing nucleolin (NCL) levels in PD patients [636]. Of note, NCL is an important regulator of nucleolus organization and rRNA processing [268]. Furthermore, we have previously identified NCL as a target of SAPD, and it was shown that knockdown of NCL in glioma cells induces senescence [637]. Moreover, alterations in ribosome biogenesis were observed in Alzheimer's disease [634, 638]. Interestingly, it was shown that removal of senescent cells in both PD and Alzheimer's disease mouse models opposed the development of symptoms of those neurodegenerative diseases [141, 639]. Those observations confirm that altered ribosome biogenesis can be a major driver of the senescence response, and accumulation of those senescent cells can lead to human age-related diseases. The role of reduced ribosome biogenesis in aging is not as black and white as described above, as it has also been shown in caloric restriction (CR) that there is a decreased ribosome biogenesis but an increase in longevity [634]. Furthermore, in a mouse model of high ribosome biogenesis, it was shown that lifespan is reduced [634]. In light of those observations, the contribution of reduced ribosome biogenesis to the aging phenotype is not yet completely understood.

In contrast to this, the contribution of mitochondrial dysfunction and alterations in the mitochondria structural organization seems more clear. The idea that dysfunctional mitochondria are

a major driver of aging was suggested in the 50/60ies with the idea of the increased amount of ROS generated by dysfunctional mitochondria in aged tissues [640, 641] and over the past years, more and more molecular details on how ROS and dysfunctional mitochondria could drive aging we shown [184].

An interesting aspect of mitochondrial dysfunction-induced senescence is the observation of RPL29 accumulation in this senescent type. An increase of nucleolar size suggests that there is a communication of mitochondria with ribosome biogenesis. We did not directly address how mitochondrial dysfunction results in ribosome biogenesis alterations, but several ways can be suggested. First, ribosome biogenesis requires a large amount of ATP, and cells with dysfunctional mitochondria have been shown to have lower ATP levels [127]. Thus, lower ATP levels would result in alterations in ribosome biogenesis. Furthermore, the increased amount of ROS can result in DNA damage in ribosomal DNA, resulting in nucleolar caps [642]. Nucleolar caps are transcriptionally inactive repeats of the rDNA adjacent to the nucleolus to allow for DNA repair [643, 644]. Persistent nucleolar caps or rDNA instability has been shown to drive premature aging in yeast as well as in humans [645, 646]. Interestingly, it was shown that the tumor suppressor PML could associate with nucleolar caps and persistent nucleolar caps (pNC). PML-pNC complex persisted over time and maintained a constant DDR response, a feature of senescent cells. Furthermore persistent PML foci can induce senescence [118]. We have seen increased PML nuclear bodies and DNA damage foci in cells with ribosome biogenesis defects as well as in cells with mitochondrial dysfunction. However, we have not analyzed the proportion of cells with PML DNA damage foci at nucleolar caps, leaving the possibility of a simple coincidence or an actual causal link between mitochondrial dysfunction-induced rDNA damage and ribosomal biogenesis alterations.

Finally, a link between mitochondrial dysfunction, ribosome biogenesis alterations, and rDNA instability could be alterations in the NAD<sup>+</sup> availability and sirtuin activity. The roles of sirtuins and ribosome biogenesis were mainly proven in yeast, but recent reports have suggested similar action in human cells [474]. As mentioned before, in senescence, NAD<sup>+</sup> levels are reduced, and sirtuins require high NAD<sup>+</sup> levels to function. Consequently, it was shown that sirtuin 7 (SIRT7) could regulate the association of rDNA with SWI/SNF-related matrix-associated actin-dependent regulator of chromatin subfamily A member 5 (SMARCA5), a component of the nucleolar heterochromatin-silencing complex. In the presence of rDNA damage, par exemple induced by increased ROS reduced activity of SIRT7 resulted in an increased fraction of non repaired rDNA transcription and replication stress. In fact, replication stress on rDNA was shown to be a major driver for hematopoietic stem cells exhaustion and aging [25].

Further research will demonstrate whether the feed-forward cycle between mitochondrial dysfunction and alterations of ribosome biogenesis in senescence exist or whether both are independent inducers of senescence. Recent reports also suggest that alterations liquid-liquid phase-separation (llps) could be a driving force of nucleolar alterations, and this was shown to be especially true in cells with altered metabolism [647].

### **3.10. Implications of liquid-liquid phase separation in HTC formation and nucleolus**

Another interesting observation is the formation of the HTC complex by llps. Phase separation is a process where a well-mixed solution of macromolecules separate into two phases allowing for concentration of the macromolecule in the dense phase resulting in membrane-less compartments [648]. Phase separation was shown to have implications in almost all biological functions allowing for fine-tuning the spatiotemporal protein function. For example, aberrant llps were found to be a driver of neurological diseases and aging phenotypes; however, beneficial roles of llps include the formation of PML nuclear bodies and DNA repair condensates via 53BP1 and PARP1 [648]. In light of metabolic regulation by phase separation, most of the studies were done in yeast, but evidence suggests that most of those results can be applied to mammalian cells, too [649]. Interestingly, one trigger for phase separation of metabolic enzymes is hypoxia, a condition in which we identified assembly of HTC [649].

Apart from HTC, there are reports demonstrating the glutamine metabolism in cancer cells can be regulated by llps [649]. It was shown that under glutamine starvation, the mRNA of GLS1, the first enzyme of glutaminolysis, can go into stress granules via llps. These stress granules allow for mRNA to be stored until the stress is over and faster recovery once glutamine becomes available again. Interestingly, the formation of stress granules also allowed longer survival under glutamine deprivation [650].

Another pathway that was recently shown to be regulated by llps is glycolysis. It was shown that phosphofructokinase 1 (PFK1) could go into liquid-like membrane-less compartments in response to hypoxia. This assembly allowed for increased glycolysis and prolonged survival of neurons and muscle cells in hypoxia [651].

Trugunly, also the assembly and structure of the nucleolus is considered to be mediated by llps [652]. It was shown that many nucleolar proteins have intrinsically disordered regions (IDRs) a requisite for llps. Furthermore, it was shown that local increases in rRNA could drive assembly of the nucleolus allowing for controlled assembly at the active transcription of rRNA [653]. Nucleoli formation then allows for the recruitment of proteins and processing factors to modulate ribosome

biogenesis. In our study on alterations in ribosome biogenesis in senescence, we did not look at the potential impact of ltps, but it seems that ltps could drive the formation of one big nucleolus in senescent cells. Consequently, it can be suggested that alterations in ltps could drive aging phenotypes.

Given that ltps mediate both the nucleolus and the formation of local metabolic areas, it seems tempting to suggest that alterations in ltps might drive aging phenotypes. Recent reports have suggested some evidence for this theory. For instance, it was shown that small decreases in ATP levels as they can be observed in senescent cells led to increased viscosity of the nucleolus resulting in protein aggregation and liquid to solid transition [654, 655]. Once the nucleolus is in a solid phase, it is hard to dissolve the aggregates again, and those amyloid-like aggregates can drive aging. Alteration in ATP levels can not only drive nucleolus alterations but also have been shown to be implicated in many neurodegenerative diseases. One characteristic of neurodegenerative diseases like, ALS or frontotemporal dementia (FTD), is, the accumulation of aggregates formed by ltps and liquid to solid transitions [647]. Even though most evidence is available that neurodegenerative aging is mediated by ltps, it has also been shown that tumor suppressors such as p53 can undergo ltps resulting in loss of function and increased cancer incidence [656].

Altogether, liquid-liquid phase separation seems a novel avenue to explain aging along with senescence phenotypes, and further research will allow identifying key contributions of this interesting bio-physical phenomenon.

### **3.11. Does cellular transformation require cellular senescence bypass**

One of the main topics of this thesis is cellular senescence and the roles of cellular senescence in tumor suppression and malignant transformation. In the results presented in the articles, it is clear that cellular senescence can be a tumor suppressor mechanism. However, we only provided correlative evidence that cellular senescence needs to be bypassed to get transformation. Our results that show that RPS14 can regulate the cell cycle even in the absence of p53 and p16, the main mediators of senescence, point to the fact that senescence is implicated in malignant transformation. However, the results are not a proof that the bypass of the senescence response is a prerequisite to malignant transformation. Furthermore, the growth arrest by RPS14 is not permanent in p16 and p53 mutated cells, suggesting that senescence is not the sole tumor suppressor mechanism bypassed in cancer cells.

Our results that forced expression of HTC in already senescent cells allow for cell cycle re-entry strongly suggest that at least in some contexts, senescence bypass is a pre-requirement of malignant



transformation. However, we did not mark the senescent cells and then micro-injected the HTC into one senescent cell. We rather used the population, allowing for the rare possibility that the cells that grow again have never been senescent. Cell tracing experiments with a good senescent marker would provide formal proof of the requirements of senescence bypass for malignant transformation.

Furthermore, our results were obtained *in vitro*, and it might be completely different *in vivo*. Taken together, it seems that there is some evidence that senescence bypass is a requirement at least *in vitro* to malignant transformation, but further research will allow demonstrating the role of cellular senescence bypass for malignant transformation *in vivo*. One argument against the theory that senescence bypass is a requirement for malignant transformation is the fact that people can live with nevi or benign prostatic hyperplasia (BPH) without getting cancer. In fact, it was rather suggested that in the prostate, it is not the senescent cells that get transformed but rather the surrounding cells [657]. However, the appearance of PanIN the senescent lesion of the pancreases, almost always, results in pancreatic cancer [38]. Altogether, those results highlight the variety of the strength of the senescence response *in vivo* and the crucial need for further analysis of senescence bypass preferentially with single-cell tracing experiments to uncover the roles of senescence bypass in malignant transformation *in vivo*.

### 3.12. Conclusion

The results in this thesis allow for the following conclusions. First of all, we have confirmed the role of cellular senescence as a tumor suppressor mechanism. Likewise, we have added to the growing evidence of senescent cell biomarkers and molecular phenotypes observed in senescent cells. We have shown with RPS14 a novel way to regulate the cell cycle and maintain cells in the senescent state. Furthermore, we have identified a novel senescent cell biomarker with RPL29. Both of these discoveries can be integrated into the goal of the thesis as a phenotype that maintains the senescence response. See figure 3.2. Likewise, the identification of the HTC complex is a novel way to bypass cellular senescence, as such highlighting the requirements of cells for malignant transformation. See also 3.2.

Most of this work was initiated from the observation that specific proteins are degraded in senescent cells, and this senescence-specific protein degradation was a major contributor to maintaining a stable senescence response in cells following oncogenic events. We have provided molecular details on how ribosome biogenesis alterations and mitochondrial dysfunction can be drivers of cellular senescence. Furthermore, we have shown implications on how cancer cells lose tumor suppressor mechanisms and enter the transformation process.

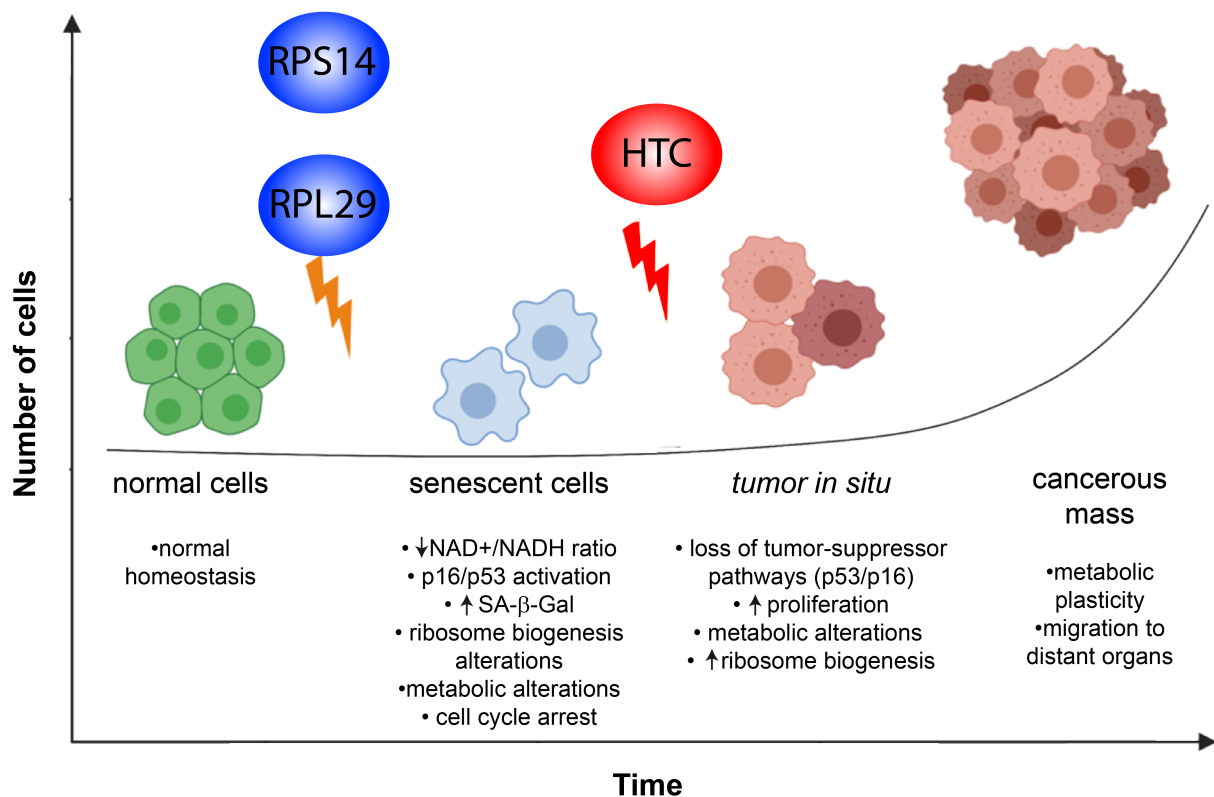


**Figure 3.2. Contributions of RPS14, RPL29, and the HTC complex in cellular senescence**  
RPS14 and RPL29 contribute to the senescence response/ RPS14 is a novel CDKi thus reducing the cell cycle and maintaining cells in the senescent state. Likewise, RPL29 can be used as a biomarker to identify senescent cells, thus allowing for even *in vivo* tracking of senescent cells. The HTC complex is the first complex that allowed, by metabolic rewiring, the bypass of senescence and malignant transformation

In the case of ribosomal free ribo-proteins, we have just started to demonstrate the implications of those proteins in cell cycle regulation and other biological pathways. Many remaining questions are still open in this field, and future work will elucidate to which extent ribosomal free ribo-proteins are major contributors to regulating cellular processes. An interesting suggestion combining the two main topics of this thesis would be ribosomal free proteins in regulating metabolism. However, this remains pure speculation.

Regarding the mitochondrial and metabolic alteration in senescent cells and their impact on cellular aging and age-related diseases, it can be concluded that even though the phenotypes have been described for quite some time now, their individual contributions towards senescence remained elusive. In particular, it will be interesting to see the implication of NAD metabolism in

aging. Even though our results confirm low NAD<sup>+</sup> levels in aged cells, it is still far from warranted to boost NAD<sup>+</sup> to fight aging phenotypes. Our results rather suggest that NAD supplementation might increase cancer incidence, and human trials with NAD supplementation should pay particular attention to the cancer incidences. As a reminder, in the 90ies and early 2000, several human trials for antioxidants, which were suggested to be the new cure for aging, had to be stopped because people developed more cancer than people in the control group.

Furthermore, in light of our description of the HTC complex, many key research questions remain open, and it will be particularly interesting to see whether the physiological roles in hypoxia, the oncogenic roles of HTC, or the roles of HTC in NAD regeneration for aging will be the predominant driver on further research questions.

Finally, the identifications of new inducers of senescence in NADH alterations and ribosome biogenesis pave the way to new anticancer therapies by targeting the metabolic fitness of neoplasia with the long-term goal to identify clinically exploitable metabolic vulnerabilities of cancer.

## Bibliography

---

- [1] **Avis de publication - Statistiques canadiennes sur le cancer 2019.** 2019.
- [2] E. Bianconi et al. **An estimation of the number of cells in the human body.** *Ann. Hum. Biol.* (2013).
- [3] K. Vermeulen, D. R. Van Bockstaele, and Z. N. Berneman. **The cell cycle: A review of regulation, deregulation and therapeutic targets in cancer.** *Cell Prolif.* 36.3 (2003), pp. 131–149.
- [4] B. Alberts et al. *Molecular Biology of the Cell 5th edition.* 2007.
- [5] M. Bury et al. **New Insights into CDK Regulators: Novel Opportunities for Cancer Therapy.** *Trends Cell Biol.* 31.5 (2021), pp. 331–344.
- [6] J. C. Saldivar et al. **An intrinsic S/G2 checkpoint enforced by ATR.** *Science* 361.6404 (2018), pp. 806–810.
- [7] F. Lessard et al. **Senescence-associated ribosome biogenesis defects contributes to cell cycle arrest through the Rb pathway.** *Nat. Cell Biol.* 20.7 (2018), pp. 789–799.
- [8] N. Del Toro et al. **Ribosomal protein RPL22/eL22 regulates the cell cycle by acting as an inhibitor of the CDK4-cyclin D complex.** *Cell Cycle* 18.6-7 (2019), pp. 759–770.
- [9] R. A. Weinberg. *The Biology of Cancer.* 2006.
- [10] D. Hanahan and R. A. Weinberg. **The hallmarks of cancer.** *Cell* 100.1 (2000), pp. 57–70.
- [11] B. N. Ames and L. S. Gold. **Endogenous mutagens and the causes of aging and cancer.** *Mutat. Res. - Fundam. Mol. Mech. Mutagen.* (1991).
- [12] A. A. Morley and D. R. Turner. **The contribution of exogenous and endogenous mutagens to in vivo mutations.** *Mutat. Res. - Fundam. Mol. Mech. Mutagen.* (1999).
- [13] J. H. Hoeijmakers. **DNA Damage, Aging, and Cancer.** *N. Engl. J. Med.* (2009).
- [14] A. Tubbs and A. Nussenzweig. **Endogenous DNA Damage as a Source of Genomic Instability in Cancer.** *Cell* (2017).
- [15] C. Tomasetti, L. Li, and B. Vogelstein. **Stem cell divisions, somatic mutations, cancer etiology, and cancer prevention.** *Science* (2017).
- [16] G. G. Luo and J. h. J. Ou. **Oncogenic viruses and cancer.** *Viol. Sin.* (2015).
- [17] R. J. LOFFIELD et al. **Helicobacter pylori and gastric carcinoma.** *Histopathology* 17.6 (1990), pp. 537–541.

- [18] M. Watson, D. M. Holman, and M. Maguire-Eisen. **Ultraviolet Radiation Exposure and Its Impact on Skin Cancer Risk.** *Semin. Oncol. Nurs.* (2016).
- [19] A. King, M. A. Selak, and E. Gottlieb. **Succinate dehydrogenase and fumarate hydratase: Linking mitochondrial dysfunction and cancer.** *Oncogene* (2006).
- [20] H. Yan et al. **IDH1 and IDH2 Mutations in Gliomas.** *N. Engl. J. Med.* (2009).
- [21] C. B. Thompson. **Metabolic Enzymes as Oncogenes or Tumor Suppressors.** *N. Engl. J. Med.* (2009).
- [22] D. Hanahan and R. A. Weinberg. **Hallmarks of Cancer: The Next Generation.** *Cell* 144.5 (2011), pp. 646–674.
- [23] J. V. Lee, S. A. Shah, and K. E. Wellen. **Obesity, cancer and acetyl-CoA metabolism.** *Drug Discov. Today Dis. Mech.* (2013).
- [24] A. Chiarugi et al. **The NAD metabolome - A key determinant of cancer cell biology.** *Nat. Rev. Cancer* (2012).
- [25] T. G. Demarest et al. **NAD<sup>+</sup> metabolism in aging and cancer.** *Annu. Rev. Cancer Biol.* (2019).
- [26] T. Gutschner and S. Diederichs. **The hallmarks of cancer: A long non-coding RNA point of view.** *RNA Biol.* 9.6 (2012), pp. 703–719.
- [27] E. Rheinbay and J. Zamora. **Analyses of non-coding somatic drivers in 2,658 cancer whole genomes.** *Nature* (2020).
- [28] N. N. Vellichirammal et al. **Pan-Cancer Analysis Reveals the Diverse Landscape of Novel Sense and Antisense Fusion Transcripts.** *Mol. Ther. - Nucleic Acids* (2020).
- [29] N. del Toro et al. **The retinoblastoma tumor suppressor limits ribosomal readthrough during oncogene induced senescence.** *bioRxiv* (2019).
- [30] P. Nenclares and K. J. Harrington. **The biology of cancer.** *Med. (United Kingdom)* 48.2 (2020), pp. 67–72.
- [31] P. Nowell. **The clonal evolution of tumor cell populations.** *Science* (80 194.4260 (1976), pp. 23–28.
- [32] M. Greaves and C. C. Maley. **Clonal evolution in cancer.** *Nature* 481.7381 (2012), pp. 306–313.
- [33] C. Michaloglou et al. **BRAFE600-associated senescence-like cell cycle arrest of human naevi.** *Nature* 436.7051 (2005), pp. 720–724.
- [34] M. E. Caldwell et al. **Cellular features of senescence during the evolution of human and murine ductal pancreatic cancer.** *Oncogene* 31.12 (2012), pp. 1599–1608.

- [35] V. Krizhanovsky et al. **Implications of Cellular Senescence in Tissue Damage Response, Tumor Suppression, and Stem Cell Biology.** *Cold Spring Harb. Symp. Quant. Biol.* 73 (2008), pp. 513–522.
- [36] P. Castro et al. **Cellular senescence in the pathogenesis of benign prostatic hyperplasia.** *Prostate* 55.1 (2003), pp. 30–38.
- [37] M. Collado et al. **Senescence in premalignant tumours.** *Nature* 436.7051 (2005), pp. 642–642.
- [38] R. H. Hruban et al. **Progression model for pancreatic cancer.** *Clin. Cancer Res.* 6.8 (2000), pp. 2969–2972.
- [39] J. P. Morris, S. C. Wang, and M. Hebrok. **KRAS, Hedgehog, Wnt and the twisted developmental biology of pancreatic ductal adenocarcinoma.** *Nat. Rev. Cancer* 10.10 (2010), pp. 683–695.
- [40] A. Alkhazraji et al. **All cancer hallmarks lead to diversity.** *Int J Clin Exp Med* 12.1 (2019), pp. 132–157.
- [41] M. J. Bissell and D. Radisky. **Putting tumours in context.** *Nat. Rev. Cancer* 1.1 (2001), pp. 46–54.
- [42] T. Boveri. **Concerning the Origin of Malignant Tumours by Theodor Boveri. Translated and annotated by Henry Harris.** *J. Cell Sci.* 121.Supplement\_1 (2008), pp. 1–84.
- [43] T. Boveri. *Zur Frage der Entstehung Maligner Tumoren.* Gustav Fischer, 1914, pp. 1–64.
- [44] G. S. Martin. **TIMELINE The hunting of the Src.** *Nat Rev Mol Cell Biol* 2.6 (2001), pp. 467–75.
- [45] P. H. Duesberg and P. K. Vogt. **Differences between the Ribonucleic Acids of Transforming and Nontransforming Avian Tumor Viruses.** *Proc. Natl. Acad. Sci.* 67.4 (1970), pp. 1673–1680.
- [46] A. P. Czernilofsky et al. **Nucleotide sequence of an avian sarcoma virus oncogene (src) and proposed amino acid sequence for gene product.** *Nature* 287.5779 (1980), pp. 198–203.
- [47] D. Stehelin et al. **DNA related to the transforming gene(s) of avian sarcoma viruses is present in normal avian DNA.** *Nature* 260.5547 (1976), pp. 170–173.
- [48] S. Pulciani et al. **Transforming genes in human tumors.** *J. Cell. Biochem.* 20.1 (1982), pp. 51–61.
- [49] H. J. Burstein and R. S. Schwartz. **Molecular Origins of Cancer.** *N. Engl. J. Med.* 358.5 (2008), pp. 527–527.
- [50] P. J. Campbell and J. Zhang. **Pan-cancer analysis of whole genomes.** *Nature* (2020).

- [51] R. F. Newbold and R. W. Overell. **Fibroblast immortality is a prerequisite for transformation by EJ c-Ha-ras oncogene.** *Nature* 304.5927 (1983), pp. 648–651.
- [52] M. Serrano et al. **Oncogenic ras provokes premature cell senescence associated with accumulation of p53 and p16INK4a.** *Cell* 88.5 (1997), pp. 593–602.
- [53] G. Ferbeyre and S. W. Lowe. **The price of tumour suppression?** *Nature* 415.6867 (2002), pp. 26–27.
- [54] L. Hayflick. **The limited in vitro lifetime of human diploid cell strains.** *Exp Cell Res* 37 (1965), pp. 614–636.
- [55] L. Hayflick and P. Moorhead. **The serial cultivation of human diploid cell strains.** *Exp. Cell Res.* 25.3 (1961), pp. 585–621.
- [56] C. J. Sherr. **Principles of Tumor Suppression.** *Cell* (2004).
- [57] S. W. Lowe, E. Cepero, and G. Evan. **Intrinsic tumour suppression.** *Nature* 432.7015 (2004), pp. 307–315.
- [58] N. Rivlin et al. **Mutations in the p53 Tumor Suppressor Gene: Important Milestones at the Various Steps of Tumorigenesis.** *Genes Cancer* 2.4 (2011), pp. 466–474.
- [59] K. T. Bieging, S. S. Mello, and L. D. Attardi. **Unravelling mechanisms of p53-mediated tumour suppression.** *Nat. Rev. Cancer* 14.5 (2014), pp. 359–370.
- [60] M. Lacroix et al. **Metabolic functions of the tumor suppressor p53: Implications in normal physiology, metabolic disorders, and cancer.** *Mol. Metab.* 33 (2020), pp. 2–22.
- [61] A. G. Knudson. **Two genetic hits (more or less) to cancer.** *Nat. Rev. Cancer* 1.2 (2001), pp. 157–162.
- [62] A. G. Knudson. **Mutation and cancer: statistical study of retinoblastoma.** *Proc. Natl. Acad. Sci. U. S. A.* (1971).
- [63] S. Venkatachalam et al. **Retention of wild-type p53 in tumors from p53 heterozygous mice: Reduction of p53 dosage can promote cancer formation.** *EMBO J.* (1998).
- [64] M. Wu, M. R. Wallace, and D. Muir. **Nf1 haploinsufficiency augments angiogenesis.** *Oncogene* 25.16 (2006), pp. 2297–2303.
- [65] J. Dong et al. **Identification of PATCHED mutations in medulloblastomas by direct sequencing.** *Hum. Mutat.* 16.1 (2000), pp. 89–90.
- [66] M. L. Fero et al. **The murine gene p27(Kip 1) is haplo-insufficient for tumour suppression.** *Nature* (1998).
- [67] D. H. Gutmann et al. **Haploinsufficiency for the neurofibromatosis 1 (NF1) tumor suppressor results in increased astrocyte proliferation.** *Oncogene* (1999).
- [68] K. Inoue and E. A. Fry. **Haploinsufficient tumor suppressor genes.** *Adv. Med. Biol.* 118 (2017), pp. 84–122.

- [69] K. W. Kinzler and B. Vogelstein. **Gatekeepers and caretakers.** *Nature* 386.6627 (1997), pp. 761–763.
- [70] F. Michor, Y. Iwasa, and M. A. Nowak. **Dynamics of cancer progression.** *Nat. Rev. Cancer* 4.3 (2004), pp. 197–205.
- [71] A. M. Oliveira, J. S. Ross, and J. A. Fletcher. **Tumor Suppressor Genes in Breast Cancer.** *Pathol. Patterns Rev.* 124.suppl\_1 (2005), S16–S28.
- [72] K. Macleod. **Tumor suppressor genes.** *Curr. Opin. Genet. Dev.* 10.1 (2000), pp. 81–93.
- [73] H. Semb and G. Christofori. **The Tumor-Suppressor Function of E-Cadherin.** *Am. J. Hum. Genet.* 63.6 (1998), pp. 1588–1593.
- [74] M. D. Wellenstein and K. E. de Visser. **Cancer-Cell-Intrinsic Mechanisms Shaping the Tumor Immune Landscape.** *Immunity* 48.3 (2018), pp. 399–416.
- [75] D. Xiong, Y. Wang, and M. You. **Tumor intrinsic immunity related proteins may be novel tumor suppressors in some types of cancer.** *Sci. Rep.* (2019).
- [76] Q. Cheng and J. Chen. **Mechanism of p53 stabilization by ATM after DNA damage.** *Cell Cycle* 9.3 (2010), pp. 472–478.
- [77] H. F. Horn and K. H. Vousden. **Coping with stress: multiple ways to activate p53.** *Oncogene* 26.9 (2007), pp. 1306–1316.
- [78] M. Fischer. **Census and evaluation of p53 target genes.** *Oncogene* 36.28 (2017), pp. 3943–3956.
- [79] A. M. Boutelle and L. D. Attardi. **p53 and Tumor Suppression: It Takes a Network.** *Trends Cell Biol.* 31.4 (2021), pp. 298–310.
- [80] R. G. Jones and C. B. Thompson. **Tumor suppressors and cell metabolism: a recipe for cancer growth.** *Genes Dev.* 23.5 (2009), pp. 537–548.
- [81] A. King, M. A. Selak, and E. Gottlieb. **Succinate dehydrogenase and fumarate hydratase: linking mitochondrial dysfunction and cancer.** *Oncogene* 25.34 (2006), pp. 4675–4682.
- [82] K. Bensaad et al. **TIGAR, a p53-Inducible Regulator of Glycolysis and Apoptosis.** *Cell* 126.1 (2006), pp. 107–120.
- [83] B. E. Baysal. **Mutations in SDHD, a Mitochondrial Complex II Gene, in Hereditary Paraganglioma.** *Science* 287.5454 (2000), pp. 848–851.
- [84] K. E. Yen et al. **Cancer-associated IDH mutations: biomarker and therapeutic opportunities.** *Oncogene* 29.49 (2010), pp. 6409–6417.
- [85] J. H. MARXSEN et al. **Hypoxia-inducible factor-1 (HIF-1) promotes its degradation by induction of HIF- $\alpha$ -prolyl-4-hydroxylases.** *Biochem. J.* 381.3 (2004), pp. 761–767.



- [86] D. A. Tennant and E. Gottlieb. **HIF prolyl hydroxylase-3 mediates alpha-ketoglutarate-induced apoptosis and tumor suppression.** *J. Mol. Med.* 88.8 (2010), pp. 839–849.
- [87] K. G. de la Cruz-López et al. **Lactate in the Regulation of Tumor Microenvironment and Therapeutic Approaches.** *Front. Oncol.* 9 (2019).
- [88] D. Zagzag et al. **Expression of hypoxia-inducible factor 1? in brain tumors.** *Cancer* 88.11 (2000), pp. 2606–2618.
- [89] W. Xu et al. **Oncometabolite 2-Hydroxyglutarate Is a Competitive Inhibitor of  $\alpha$ -Ketoglutarate-Dependent Dioxygenases.** *Cancer Cell* 19.1 (2011), pp. 17–30.
- [90] S. Igelmann, H. A. Neubauer, and G. Ferbeyre. **STAT3 and STAT5 activation in solid cancers.** 2019.
- [91] T. Wartewig and J. Ruland. **PD-1 Tumor Suppressor Signaling in T Cell Lymphomas.** *Trends Immunol.* 40.5 (2019), pp. 403–414.
- [92] J. J. Manfredi. **The Mdm2-p53 relationship evolves: Mdm2 swings both ways as an oncogene and a tumor suppressor.** *Genes Dev.* 24.15 (2010), pp. 1580–1589.
- [93] X. Deschênes-Simard et al. **Tumor suppressor activity of the ERK/MAPK pathway by promoting selective protein degradation.** *Genes Dev.* 27.8 (2013), pp. 900–15.
- [94] X. Deschênes-Simard et al. **ERKs in Cancer: Friends or Foes?** *Cancer Res.* 74.2 (2014), pp. 412–419.
- [95] J. Martín-Caballero et al. **Tumor susceptibility of p21(Waf1/Cip1)-deficient mice.** *Cancer Res.* 61.16 (2001), pp. 6234–8.
- [96] A. Besson et al. **Discovery of an oncogenic activity in p27Kip1 that causes stem cell expansion and a multiple tumor phenotype.** *Genes Dev.* 21.14 (2007), pp. 1731–46.
- [97] S. M. Brouxhon et al. **Soluble E-cadherin: a critical oncogene modulating receptor tyrosine kinases, MAPK and PI3K/Akt/mTOR signaling.** *Oncogene* 33.2 (2014), pp. 225–235.
- [98] H. L. Klein. **The consequences of Rad51 overexpression for normal and tumor cells.** *DNA Repair (Amst).* 7.5 (2008), pp. 686–693.
- [99] X. Wang and S. Li. **Protein mislocalization: Mechanisms, functions and clinical applications in cancer.** *Biochim. Biophys. Acta - Rev. Cancer* 1846.1 (2014), pp. 13–25.
- [100] J. W. Szostak and E. H. Blackburn. **Cloning yeast telomeres on linear plasmid vectors.** *Cell* 29.1 (1982), pp. 245–255.
- [101] C. W. Greider and E. H. Blackburn. **Identification of a specific telomere terminal transferase activity in tetrahymena extracts.** *Cell* 43.2 (1985), pp. 405–413.
- [102] G. B. Morin. **The human telomere terminal transferase enzyme is a ribonucleoprotein that synthesizes TTAGGG repeats.** *Cell* 59.3 (1989), pp. 521–529.

- [103] J. W. Shay and W. E. Wright. **Hayflick, his limit, and cellular ageing.** *Nat. Rev. Mol. Cell Biol.* 1.1 (2000), pp. 72–76.
- [104] V. Gorgoulis et al. **Cellular Senescence: Defining a Path Forward.** *Cell* 179.4 (2019), pp. 813–827.
- [105] J. Zhu et al. **Senescence of human fibroblasts induced by oncogenic Raf.** *Genes Dev.* 12.19 (1998), pp. 2997–3007.
- [106] C. A. Schmitt. **Senescence, apoptosis and therapy — cutting the lifelines of cancer.** *Nat. Rev. Cancer* 3.4 (2003), pp. 286–295.
- [107] H. Miyauchi et al. **Akt negatively regulates the in vitro lifespan of human endothelial cells via a p53/p21-dependent pathway.** *EMBO J.* 23.1 (2004), pp. 212–220.
- [108] F. A. Mallette, M.-F. Gaumont-Leclerc, and G. Ferbeyre. **The DNA damage signaling pathway is a critical mediator of oncogene-induced senescence.** *Genes Dev.* 21.1 (2007), pp. 43–48.
- [109] N. Wajapeyee et al. **Senescence induction in human fibroblasts and hematopoietic progenitors by leukemogenic fusion proteins.** *Blood* 115.24 (2010), pp. 5057–5060.
- [110] Z. Chen et al. **Crucial role of p53-dependent cellular senescence in suppression of Pten-deficient tumorigenesis.** *Nature* 436.7051 (2005), pp. 725–730.
- [111] S. Courtois-Cox et al. **A negative feedback signaling network underlies oncogene-induced senescence.** *Cancer Cell* 10.6 (2006), pp. 459–472.
- [112] B. D. Chang et al. **A senescence-like phenotype distinguishes tumor cells that undergo terminal proliferation arrest after exposure to anticancer agents.** *Cancer Res.* 59.15 (1999), pp. 3761–7.
- [113] J. A. Ewald et al. **Therapy-Induced Senescence in Cancer.** *JNCI J. Natl. Cancer Inst.* 102.20 (2010), pp. 1536–1546.
- [114] M. Acevedo et al. **A CDK4/6-Dependent Epigenetic Mechanism Protects Cancer Cells from PML-induced Senescence.** *Cancer Res.* 76.11 (2016), pp. 3252–3264.
- [115] H. Fleury et al. **Exploiting interconnected synthetic lethal interactions between PARP inhibition and cancer cell reversible senescence.** *Nat. Commun.* 10.1 (2019), p. 2556.
- [116] G. H. Stein et al. **Differential Roles for Cyclin-Dependent Kinase Inhibitors p21 and p16 in the Mechanisms of Senescence and Differentiation in Human Fibroblasts.** *Mol. Cell. Biol.* 19.3 (1999), pp. 2109–2117.
- [117] W. Xue et al. **Senescence and tumour clearance is triggered by p53 restoration in murine liver carcinomas.** *Nature* 445.7128 (2007), pp. 656–660.
- [118] G. Ferbeyre et al. **PML is induced by oncogenic ras and promotes premature senescence.** *Genes Dev.* 14.16 (2000), pp. 2015–27.

- [119] V. Calabrese et al. **SOCS1 Links Cytokine Signaling to p53 and Senescence.** *Mol. Cell* 36.5 (2009), pp. 754–767.
- [120] M. Storer et al. **Senescence Is a Developmental Mechanism that Contributes to Embryonic Growth and Patterning.** *Cell* 155.5 (2013), pp. 1119–1130.
- [121] D. Muñoz-Espín et al. **Programmed Cell Senescence during Mammalian Embryonic Development.** *Cell* 155.5 (2013), pp. 1104–1118.
- [122] M. Demaria et al. **An Essential Role for Senescent Cells in Optimal Wound Healing through Secretion of PDGF-AA.** *Dev. Cell* 31.6 (2014), pp. 722–733.
- [123] F. d’Adda di Fagagna et al. **A DNA damage checkpoint response in telomere-initiated senescence.** *Nature* 426.6963 (2003), pp. 194–198.
- [124] R. Salama et al. **Cellular senescence and its effector programs.** *Genes Dev.* 28.2 (2014), pp. 99–114.
- [125] O. Moiseeva et al. **Mitochondrial Dysfunction Contributes to Oncogene-Induced Senescence.** *Mol. Cell. Biol.* 29.16 (2009), pp. 4495–4507.
- [126] I. G. Zubova et al. **Induction of premature senescence program by an inhibitor of histone deacetylase sodium butyrate in normal and transformed rat fibroblasts.** *Tsitologiia* 47.12 (2005), pp. 1055–62.
- [127] C. D. Wiley et al. **Mitochondrial Dysfunction Induces Senescence with a Distinct Secretory Phenotype.** *Cell Metab.* 23.2 (2016), pp. 303–314.
- [128] F. Lessard, L. Brakier-Gingras, and G. Ferbeyre. **Ribosomal Proteins Control Tumor Suppressor Pathways in Response to Nucleolar Stress.** *BioEssays* 41.3 (2019), p. 1800183.
- [129] T. Kuilman et al. **Oncogene-Induced Senescence Relayed by an Interleukin-Dependent Inflammatory Network.** *Cell* 133.6 (2008), pp. 1019–1031.
- [130] J.-L. Ren et al. **Inflammatory signaling and cellular senescence.** *Cell. Signal.* 21.3 (2009), pp. 378–383.
- [131] N. E. Sharpless and C. J. Sherr. **Forging a signature of in vivo senescence.** *Nat. Rev. Cancer* 15.7 (2015), pp. 397–408.
- [132] A. S. Wang and O. Dreesen. **Biomarkers of Cellular Senescence and Skin Aging.** *Front. Genet.* 9 (2018).
- [133] M. Vernier et al. **Regulation of E2Fs and senescence by PML nuclear bodies.** *Genes Dev.* 25.1 (2011), pp. 41–50.
- [134] M. Narita and S. W. Lowe. **Senescence comes of age.** *Nat. Med.* 11.9 (2005), pp. 920–922.
- [135] D. J. Baker et al. **Clearance of p16Ink4a-positive senescent cells delays ageing-associated disorders.** *Nature* 479.7372 (2011), pp. 232–236.

- [136] H. Rayess, M. B. Wang, and E. S. Srivatsan. **Cellular senescence and tumor suppressor gene p16.** *Int. J. Cancer* 130.8 (2012), pp. 1715–1725.
- [137] Y. Guo et al. **CENP-E–dependent BubR1 autophosphorylation enhances chromosome alignment and the mitotic checkpoint.** *J. Cell Biol.* 198.2 (2012), pp. 205–217.
- [138] D. J. Baker et al. **Naturally occurring p16Ink4a-positive cells shorten healthy lifespan.** *Nature* 530.7589 (2016), pp. 184–189.
- [139] B. G. Childs et al. **Senescent intimal foam cells are deleterious at all stages of atherosclerosis.** *Science (80-. )*. 354.6311 (2016), pp. 472–477.
- [140] J. N. Farr et al. **Targeting cellular senescence prevents age-related bone loss in mice.** *Nat. Med.* 23.9 (2017), pp. 1072–1079.
- [141] T. J. Bussian et al. **Clearance of senescent glial cells prevents tau-dependent pathology and cognitive decline.** *Nature* 562.7728 (2018), pp. 578–582.
- [142] B. G. Childs et al. **Senescent cells: an emerging target for diseases of ageing.** *Nat. Rev. Drug Discov.* 16.10 (2017), pp. 718–735.
- [143] M. J. Schafer et al. **Cellular senescence mediates fibrotic pulmonary disease.** *Nat. Commun.* 8.1 (2017), p. 14532.
- [144] O. H. Jeon et al. **Local clearance of senescent cells attenuates the development of post-traumatic osteoarthritis and creates a pro-regenerative environment.** *Nat. Med.* 23.6 (2017), pp. 775–781.
- [145] S. Crespo-Garcia et al. **Pathological angiogenesis in retinopathy engages cellular senescence and is amenable to therapeutic elimination via BCL-xL inhibition.** *Cell Metab.* 33.4 (2021), 818–832.e7.
- [146] B. G. Childs et al. **Senescence and apoptosis: dueling or complementary cell fates?** *EMBO Rep.* 15.11 (2014), pp. 1139–1153.
- [147] R. Yosef et al. **Directed elimination of senescent cells by inhibition of BCL-W and BCL-XL.** *Nat. Commun.* 7.1 (2016), p. 11190.
- [148] J. Chang et al. **Clearance of senescent cells by ABT263 rejuvenates aged hematopoietic stem cells in mice.** *Nat. Med.* 22.1 (2016), pp. 78–83.
- [149] Y. Zhu et al. **Identification of a novel senolytic agent, navitoclax, targeting the Bcl-2 family of anti-apoptotic factors.** *Aging Cell* 15.3 (2016), pp. 428–435.
- [150] Y. Zhu et al. **The Achilles’ heel of senescent cells: from transcriptome to senolytic drugs.** *Aging Cell* 14.4 (2015), pp. 644–658.
- [151] J. L. Kirkland and T. Tchkonina. **Senolytic drugs: from discovery to translation.** *J. Intern. Med.* 288.5 (2020), pp. 518–536.

- [152] X. Chu, J. Wen, and R. P. Raju. **Rapid senescence-like response after acute injury.** *Aging Cell* 19.9 (2020).
- [153] L. Grosse et al. **Defined p16<sup>High</sup> Senescent Cell Types Are Indispensable for Mouse Healthspan.** *Cell Metab.* 32.1 (2020), 87–99.e6.
- [154] S. Omori et al. **Generation of a p16 Reporter Mouse and Its Use to Characterize and Target p16<sup>high</sup> Cells In Vivo.** *Cell Metab.* 32.5 (2020), 814–828.e6.
- [155] C. von Kobbe. **Targeting senescent cells: approaches, opportunities, challenges.** *Aging (Albany, NY)*. 11.24 (2019), pp. 12844–12861.
- [156] J.-I. Jun and L. F. Lau. **The matricellular protein CCN1 induces fibroblast senescence and restricts fibrosis in cutaneous wound healing.** *Nat. Cell Biol.* 12.7 (2010), pp. 676–685.
- [157] V. Krizhanovsky et al. **Senescence of Activated Stellate Cells Limits Liver Fibrosis.** *Cell* 134.4 (2008), pp. 657–667.
- [158] M. J. Schafer et al. **Cellular senescence mediates fibrotic pulmonary disease.** *Nat. Commun.* 8.1 (2017), p. 14532.
- [159] F. Zhu et al. **Senescent Cardiac Fibroblast Is Critical for Cardiac Fibrosis after Myocardial Infarction.** *PLoS One* 8.9 (2013). Ed. by D. Kletsas, e74535.
- [160] M. Lehmann et al. **Senolytic drugs target alveolar epithelial cell function and attenuate experimental lung fibrosis ex vivo.** *Eur. Respir. J.* 50.2 (2017), p. 1602367.
- [161] A. Banito and S. W. Lowe. **A New Development in Senescence.** *Cell* 155.5 (2013), pp. 977–978.
- [162] É. Villiard et al. **Senescence gives insights into the morphogenetic evolution of anamniotes.** *Biol. Open* (2017).
- [163] H. Davaapil, J. P. Brockes, and M. H. Yun. **Conserved and novel functions of programmed cellular senescence during vertebrate development.** *Development* (2016).
- [164] M. Rhinn, B. Ritschka, and W. M. Keyes. **Cellular senescence in development, regeneration and disease.** *Development* 146.20 (2019).
- [165] X. Deschênes-Simard et al. **Cellular senescence and protein degradation.** *Cell Cycle* 13.12 (2014), pp. 1840–1858.
- [166] F. Rodier and J. Campisi. **Four faces of cellular senescence.** *J. Cell Biol.* 192.4 (2011), pp. 547–556.
- [167] G. P. Dimri et al. **A biomarker that identifies senescent human cells in culture and in aging skin in vivo.** *Proc. Natl. Acad. Sci.* 92.20 (1995), pp. 9363–9367.
- [168] J. C. Acosta et al. **Chemokine Signaling via the CXCR2 Receptor Reinforces Senescence.** *Cell* 133.6 (2008), pp. 1006–1018.

- [169] J.-P. Coppé et al. **The Senescence-Associated Secretory Phenotype: The Dark Side of Tumor Suppression.** *Annu. Rev. Pathol. Mech. Dis.* 5.1 (2010), pp. 99–118.
- [170] T. Kuilman and D. S. Peeper. **Senescence-messaging secretome: SMS-ing cellular stress.** *Nat. Rev. Cancer* 9.2 (2009), pp. 81–94.
- [171] S. Lopes-Paciencia et al. **The senescence-associated secretory phenotype and its regulation.** *Cytokine* 117 (2019), pp. 15–22.
- [172] A. Hernandez-Segura et al. **Unmasking Transcriptional Heterogeneity in Senescent Cells.** *Curr. Biol.* 27.17 (2017), 2652–2660.e4.
- [173] N. Basisty et al. **A proteomic atlas of senescence-associated secretomes for aging biomarker development.** *PLOS Biol.* 18.1 (2020). Ed. by M. Serrano, e3000599.
- [174] J. C. Acosta et al. **A complex secretory program orchestrated by the inflammasome controls paracrine senescence.** *Nat. Cell Biol.* 15.8 (2013), pp. 978–990.
- [175] A. Sagiv et al. **NKG2D ligands mediate immunosurveillance of senescent cells.** *Aging (Albany, NY).* 8.2 (2016), pp. 328–344.
- [176] D. Mevorach et al. **What do we mean when we write “senescence,” “apoptosis,” “necrosis,” or “clearance of dying cells”?** *Ann. N. Y. Acad. Sci.* 1209.1 (2010), pp. 1–9.
- [177] T.-W. Kang et al. **Senescence surveillance of pre-malignant hepatocytes limits liver cancer development.** *Nature* 479.7374 (2011), pp. 547–551.
- [178] L. G. L. Prata et al. **Senescent cell clearance by the immune system: Emerging therapeutic opportunities.** *Semin. Immunol.* 40 (2018), p. 101275.
- [179] A. Kale et al. **Role of immune cells in the removal of deleterious senescent cells.** *Immun. Ageing* 17.1 (2020), p. 16.
- [180] B. I. Pereira et al. **Senescent cells evade immune clearance via HLA-E-mediated NK and CD8+ T cell inhibition.** *Nat. Commun.* 10.1 (2019), p. 2387.
- [181] J.-P. Coppé et al. **The Senescence-Associated Secretory Phenotype: The Dark Side of Tumor Suppression.** *Annu. Rev. Pathol. Mech. Dis.* 5.1 (2010), pp. 99–118.
- [182] J. Campisi. **Aging, Cellular Senescence, and Cancer.** *Annu. Rev. Physiol.* 75.1 (2013), pp. 685–705.
- [183] C. Franceschi and J. Campisi. **Chronic Inflammation (Inflammaging) and Its Potential Contribution to Age-Associated Diseases.** *Journals Gerontol. Ser. A Biol. Sci. Med. Sci.* 69.Suppl 1 (2014), S4–S9.
- [184] C. López-Otín et al. **The Hallmarks of Aging.** *Cell* 153.6 (2013), pp. 1194–1217.
- [185] C. Guerra et al. **Pancreatitis-Induced Inflammation Contributes to Pancreatic Cancer by Inhibiting Oncogene-Induced Senescence.** *Cancer Cell* 19.6 (2011), pp. 728–739.

- [186] G. Casella et al. **Transcriptome signature of cellular senescence.** *Nucleic Acids Res.* 47.14 (2019), pp. 7294–7305.
- [187] B. Uyar et al. **Single-cell analyses of aging, inflammation and senescence.** *Ageing Res. Rev.* 64 (2020), p. 101156.
- [188] W. Chen et al. **Single-Cell Transcriptome Analysis Reveals Six Subpopulations Reflecting Distinct Cellular Fates in Senescent Mouse Embryonic Fibroblasts.** *Front. Genet.* 11 (2020).
- [189] Y. Sun, N. Sheshadri, and W.-X. Zong. **SERPINB3 and B4: From biochemistry to biology.** *Semin. Cell Dev. Biol.* 62 (2017), pp. 170–177.
- [190] C. Amor et al. **Senolytic CAR T cells reverse senescence-associated pathologies.** *Nature* 583.7814 (2020), pp. 127–132.
- [191] J. M. van Deursen. **The role of senescent cells in ageing.** *Nature* 509.7501 (2014), pp. 439–446.
- [192] Y. Ohno-Iwashita et al. **Plasma membrane microdomains in aging and disease.** *Geriatr. Gerontol. Int.* 10 (2010), S41–S52.
- [193] D. Y. Lizardo et al. **Regulation of lipids is central to replicative senescence.** *Mol. Biosyst.* 13.3 (2017), pp. 498–509.
- [194] A. C. Flor et al. **A signature of enhanced lipid metabolism, lipid peroxidation and aldehyde stress in therapy-induced senescence.** *Cell Death Discov.* 3.1 (2017), p. 17075.
- [195] A. Millner, D. Y. Lizardo, and G. E. Atilla-Gokcumen. **Untargeted Lipidomics Highlight the Depletion of Deoxyceramides during Therapy-Induced Senescence.** *Proteomics* 20.10 (2020), p. 2000013.
- [196] M. E. Venable and X. Yin. **Ceramide induces endothelial cell senescence.** *Cell Biochem. Funct.* 27.8 (2009), pp. 547–551.
- [197] A. Millner and G. E. Atilla-Gokcumen. **Lipid Players of Cellular Senescence.** *Metabolites* 10.9 (2020), p. 339.
- [198] P. Arivazhagan et al. **Cardiolipin induces premature senescence in normal human fibroblasts.** *Biochem. Biophys. Res. Commun.* 323.3 (2004), pp. 739–742.
- [199] J. Chapman, E. Fielder, and J. F. Passos. **Mitochondrial dysfunction and cell senescence: deciphering a complex relationship.** *FEBS Lett.* 593.13 (2019), pp. 1566–1579.
- [200] J. S. Roh and D. H. Sohn. **Damage-Associated Molecular Patterns in Inflammatory Diseases.** *Immune Netw.* 18.4 (2018).
- [201] K. Chen et al. **Age-dependent decline in stress response capacity revealed by proteins dynamics analysis.** *Sci. Rep.* 10.1 (2020), p. 15211.

- [202] A. Orbach et al. **Biophysical and Biochemical Markers of Red Blood Cell Fragility.** *Transfus. Med. Hemotherapy* 44.3 (2017), pp. 183–187.
- [203] X. Mu et al. **Cytoskeleton stiffness regulates cellular senescence and innate immune response in Hutchinson–Gilford Progeria Syndrome.** *Aging Cell* 19.8 (2020).
- [204] V. J. D. Krouwer et al. **Endothelial cell senescence is associated with disrupted cell-cell junctions and increased monolayer permeability.** *Vasc. Cell* 4.1 (2012), p. 12.
- [205] J. Janikiewicz et al. **Mitochondria-associated membranes in aging and senescence: structure, function, and dynamics.** *Cell Death Dis.* 9.3 (2018), p. 332.
- [206] F. Martins et al. **Nuclear envelope dysfunction and its contribution to the aging process.** *Aging Cell* 19.5 (2020).
- [207] O. S. Ademowo et al. **Lipid (per) oxidation in mitochondria: an emerging target in the ageing process?** *Biogerontology* 18.6 (2017), pp. 859–879.
- [208] A. Freund et al. **Lamin B1 loss is a senescence-associated biomarker.** *Mol. Biol. Cell* 23.11 (2012). Ed. by T. M. Magin, pp. 2066–2075.
- [209] A. Ivanov et al. **Lysosome-mediated processing of chromatin in senescence.** *J. Cell Biol.* 202.1 (2013), pp. 129–143.
- [210] Z. Dou et al. **Autophagy mediates degradation of nuclear lamina.** *Nature* 527.7576 (2015), pp. 105–109.
- [211] Z. Dou et al. **Cytoplasmic chromatin triggers inflammation in senescence and cancer.** *Nature* 550.7676 (2017), pp. 402–406.
- [212] K. Chen, J. Liu, and X. Cao. **cGAS-STING pathway in senescence-related inflammation.** *Natl. Sci. Rev.* 5.3 (2018), pp. 308–310.
- [213] T. Chandra and M. Narita. **High-order chromatin structure and the epigenome in SAHFs.** *Nucleus* 4.1 (2013), pp. 23–28.
- [214] M. Narita et al. **Rb-Mediated Heterochromatin Formation and Silencing of E2F Target Genes during Cellular Senescence.** *Cell* 113.6 (2003), pp. 703–716.
- [215] X. Ye et al. **Downregulation of Wnt Signaling Is a Trigger for Formation of Facultative Heterochromatin and Onset of Cell Senescence in Primary Human Cells.** *Mol. Cell* 27.2 (2007), pp. 183–196.
- [216] R. Zhang et al. **Formation of MacroH2A-Containing Senescence-Associated Heterochromatin Foci and Senescence Driven by ASF1a and HIRA.** *Dev. Cell* 8.1 (2005), pp. 19–30.
- [217] M. Narita et al. **A Novel Role for High-Mobility Group A Proteins in Cellular Senescence and Heterochromatin Formation.** *Cell* 126.3 (2006), pp. 503–514.



- [218] K. M. Aird et al. **HMGB2 orchestrates the chromatin landscape of senescence-associated secretory phenotype gene loci.** *J. Cell Biol.* 215.3 (2016), pp. 325–334.
- [219] C. Zhang et al. **ATF3 drives senescence by reconstructing accessible chromatin profiles.** *Aging Cell* 20.3 (2021).
- [220] F. A. Mallette, M.-F. Gaumont-Leclerc, and G. Ferbeyre. **The DNA damage signaling pathway is a critical mediator of oncogene-induced senescence.** *Genes Dev.* 21.1 (2007), pp. 43–48.
- [221] R. Di Micco et al. **Oncogene-induced senescence is a DNA damage response triggered by DNA hyper-replication.** *Nature* 444.7119 (2006), pp. 638–642.
- [222] J. Bartkova et al. **Oncogene-induced senescence is part of the tumorigenesis barrier imposed by DNA damage checkpoints.** *Nature* 444.7119 (2006), pp. 633–637.
- [223] M. Ogrunc et al. **Oncogene-induced reactive oxygen species fuel hyperproliferation and DNA damage response activation.** *Cell Death Differ.* 21.6 (2014), pp. 998–1012.
- [224] Y. Liu, S. I. Bloom, and A. J. Donato. **The role of senescence, telomere dysfunction and shelterin in vascular aging.** *Microcirculation* 26.2 (2019), e12487.
- [225] R. G. Morgan et al. **Age-related telomere uncapping is associated with cellular senescence and inflammation independent of telomere shortening in human arteries.** *Am. J. Physiol. Circ. Physiol.* 305.2 (2013), H251–H258.
- [226] T. Ahmad et al. **Shelterin Telomere Protection Protein 1 Reduction Causes Telomere Attrition and Cellular Senescence via Sirtuin 1 Deacetylase in Chronic Obstructive Pulmonary Disease.** *Am. J. Respir. Cell Mol. Biol.* 56.1 (2017), pp. 38–49.
- [227] M. Fumagalli et al. **Telomeric DNA damage is irreparable and causes persistent DNA-damage-response activation.** *Nat. Cell Biol.* 14.4 (2012), pp. 355–365.
- [228] K. M. Aird et al. **Suppression of Nucleotide Metabolism Underlies the Establishment and Maintenance of Oncogene-Induced Senescence.** *Cell Rep.* 3.4 (2013), pp. 1252–1265.
- [229] L. Ivanschitz, H. De Thé, and M. Le Bras. **PML, SUMOylation, and Senescence.** *Front. Oncol.* 3 (2013).
- [230] F. P. McManus et al. **Quantitative SUMO proteomics reveals the modulation of several PML nuclear body associated proteins and an anti-senescence function of UBC9.** *Sci. Rep.* 8.1 (2018), p. 7754.
- [231] A. Hernandez-Segura, J. Nehme, and M. Demaria. **Hallmarks of Cellular Senescence.** *Trends Cell Biol.* 28.6 (2018), pp. 436–453.

- [232] D. Kurz et al. **Senescence-associated (beta)-galactosidase reflects an increase in lysosomal mass during replicative ageing of human endothelial cells.** *J. Cell Sci.* 113.20 (2000), pp. 3613–3622.
- [233] A. R. Young et al. **Autophagy mediates the mitotic senescence transition.** *Genes Dev.* 23.7 (2009), pp. 798–803.
- [234] N. Mizushima and M. Komatsu. **Autophagy: Renovation of Cells and Tissues.** *Cell* 147.4 (2011), pp. 728–741.
- [235] S. Yang et al. **Pancreatic cancers require autophagy for tumor growth.** *Genes Dev.* 25.7 (2011), pp. 717–729.
- [236] J. Deng et al. **Activation of GCN2 in UV-Irradiated Cells Inhibits Translation.** *Curr. Biol.* 12.15 (2002), pp. 1279–1286.
- [237] K. Rajesh et al. **eIF2 $\alpha$  phosphorylation bypasses premature senescence caused by oxidative stress and pro-oxidant antitumor therapies.** *Aging (Albany, NY).* 5.12 (2013), pp. 884–901.
- [238] M. J. Payea et al. **Translational Control during Cellular Senescence.** *Mol. Cell. Biol.* 41.2 (2021).
- [239] M. Narita et al. **Spatial Coupling of mTOR and Autophagy Augments Secretory Phenotypes.** *Science* 332.6032 (2011), pp. 966–970.
- [240] Z. N. Demidenko et al. **Rapamycin decelerates cellular senescence.** *Cell Cycle* 8.12 (2009), pp. 1888–1895.
- [241] Y. Gonskikh and N. Polacek. **Alterations of the translation apparatus during aging and stress response.** *Mech. Ageing Dev.* 168 (2017), pp. 30–36.
- [242] T. Weichhart. **mTOR as Regulator of Lifespan, Aging, and Cellular Senescence: A Mini-Review.** *Gerontology* 64.2 (2018), pp. 127–134.
- [243] S. K. Young and R. C. Wek. **Upstream Open Reading Frames Differentially Regulate Gene-specific Translation in the Integrated Stress Response.** *J. Biol. Chem.* 291.33 (2016), pp. 16927–16935.
- [244] S. Chakradeo, L. W. Elmore, and D. A. Gewirtz. **Is Senescence Reversible?** *Curr. Drug Targets* 17.4 (2016), pp. 460–466.
- [245] M. Schosserer, J. Grillari, and M. Breitenbach. **The Dual Role of Cellular Senescence in Developing Tumors and Their Response to Cancer Therapy.** *Front. Oncol.* 7 (2017).
- [246] G. Ferbeyre. **Aberrant signaling and senescence associated protein degradation.** *Exp. Gerontol.* 107 (2018), pp. 50–54.
- [247] R. Eferl and E. F. Wagner. **AP-1: a double-edged sword in tumorigenesis.** *Nat. Rev. Cancer* 3.11 (2003), pp. 859–868.

- [248] C. V. Dang. **MYC on the Path to Cancer**. *Cell* 149.1 (2012), pp. 22–35.
- [249] K. Labib. **Uninterrupted MCM2-7 Function Required for DNA Replication Fork Progression**. *Science* 288.5471 (2000), pp. 1643–1647.
- [250] H. Takai, A. Smogorzewska, and T. de Lange. **DNA Damage Foci at Dysfunctional Telomeres**. *Curr. Biol.* 13.17 (2003), pp. 1549–1556.
- [251] M. Fumagalli et al. **Telomeric DNA damage is irreparable and causes persistent DNA-damage-response activation**. *Nat. Cell Biol.* 14.4 (2012), pp. 355–365.
- [252] G. Hewitt et al. **Telomeres are favoured targets of a persistent DNA damage response in ageing and stress-induced senescence**. *Nat. Commun.* 3.1 (2012), p. 708.
- [253] A. Suram et al. **Oncogene-induced telomere dysfunction enforces cellular senescence in human cancer precursor lesions**. *EMBO J.* 31.13 (2012), pp. 2839–2851.
- [254] J. L. Woolford and S. J. Baserga. **Ribosome Biogenesis in the Yeast *Saccharomyces cerevisiae***. *Genetics* 195.3 (2013), pp. 643–681.
- [255] S. Nait Slimane et al. **Ribosome Biogenesis Alterations in Colorectal Cancer**. *Cells* 9.11 (2020), p. 2361.
- [256] N. Ban et al. **A new system for naming ribosomal proteins**. *Curr. Opin. Struct. Biol.* 24 (2014), pp. 165–169.
- [257] M. Chaker-Margot and S. Klinge. **Assembly and early maturation of large subunit precursors**. *RNA* 25.4 (2019), pp. 465–471.
- [258] Z. A. Sanghai et al. **Modular assembly of the nucleolar pre-60S ribosomal subunit**. *Nature* 556.7699 (2018), pp. 126–129.
- [259] J. Barandun et al. **The complete structure of the small-subunit processome**. *Nat. Struct. Mol. Biol.* 24.11 (2017), pp. 944–953.
- [260] M. Chaker-Margot et al. **Architecture of the yeast small subunit processome**. *Science* 355.6321 (2017), eaal1880.
- [261] S. Klinge and J. L. Woolford. **Ribosome assembly coming into focus**. *Nat. Rev. Mol. Cell Biol.* 20.2 (2019), pp. 116–131.
- [262] L. Srivastava et al. **Mammalian DEAD Box Protein Ddx51 Acts in 3' End Maturation of 28S rRNA by Promoting the Release of U8 snoRNA**. *Mol. Cell. Biol.* 30.12 (2010), pp. 2947–2956.
- [263] E. Calo et al. **RNA helicase DDX21 coordinates transcription and ribosomal RNA processing**. *Nature* 518.7538 (2015), pp. 249–253.
- [264] L. Meng, H. Yasumoto, and R. Y. L. Tsai. **Multiple controls regulate nucleostemin partitioning between nucleolus and nucleoplasm**. *J. Cell Sci.* 119.24 (2006), pp. 5124–5136.

- [265] L. Ma et al. **CSIG Inhibits PTEN Translation in Replicative Senescence.** *Mol. Cell. Biol.* 28.20 (2008), pp. 6290–6301.
- [266] B. Utama et al. **Isolation and characterization of a new nucleolar protein, Nrap, that is conserved from yeast to humans.** *Genes to Cells* 7.2 (2002), pp. 115–132.
- [267] J. Wu et al. **Transcriptional Repressor NIR Functions in the Ribosome RNA Processing of Both 40S and 60S Subunits.** *PLoS One* 7.2 (2012). Ed. by Z.-M. Yuan, e31692.
- [268] K. Abdelmohsen and M. Gorospe. **RNA-binding protein nucleolin in disease.** *RNA Biol.* 9.6 (2012), pp. 799–808.
- [269] A. Artero-Castro et al. **Rplp1 bypasses replicative senescence and contributes to transformation.** *Exp. Cell Res.* 315.8 (2009), pp. 1372–1383.
- [270] T. Moss. **At the crossroads of growth control; making ribosomal RNA.** *Curr. Opin. Genet. Dev.* 14.2 (2004), pp. 210–217.
- [271] K. Itahana et al. **Tumor Suppressor ARF Degrades B23, a Nucleolar Protein Involved in Ribosome Biogenesis and Cell Proliferation.** *Mol. Cell* 12.5 (2003), pp. 1151–1164.
- [272] K. Tago, S. Chiocca, and C. J. Sherr. **Sumoylation induced by the Arf tumor suppressor: A p53-independent function.** *Proc. Natl. Acad. Sci.* 102.21 (2005), pp. 7689–7694.
- [273] J. K. Box et al. **Nucleophosmin: from structure and function to disease development.** *BMC Mol. Biol.* 17.1 (2016), p. 19.
- [274] A. B. Meriin et al. **Hsp70–Bag3 complex is a hub for proteotoxicity-induced signaling that controls protein aggregation.** *Proc. Natl. Acad. Sci.* 115.30 (2018), E7043–E7052.
- [275] E. Stürner and C. Behl. **The Role of the Multifunctional BAG3 Protein in Cellular Protein Quality Control and in Disease.** *Front. Mol. Neurosci.* 10 (2017).
- [276] T. Komiyama. **Binding of mitochondrial precursor proteins to the cytoplasmic domains of the import receptors Tom70 and Tom20 is determined by cytoplasmic chaperones.** *EMBO J.* 16.14 (1997), pp. 4267–4275.
- [277] N. V. Bobkova et al. **Exogenous Hsp70 delays senescence and improves cognitive function in aging mice.** *Proc. Natl. Acad. Sci.* 112.52 (2015), pp. 16006–16011.
- [278] H. Yamamoto et al. **Roles of Tom70 in Import of Presequence-containing Mitochondrial Proteins.** *J. Biol. Chem.* 284.46 (2009), pp. 31635–31646.
- [279] S. Kreimendahl and J. Rassow. **The Mitochondrial Outer Membrane Protein Tom70-Mediator in Protein Traffic, Membrane Contact Sites and Innate Immunity.** *Int. J. Mol. Sci.* 21.19 (2020), p. 7262.
- [280] E. Trias et al. **Emergence of Microglia Bearing Senescence Markers During Paralysis Progression in a Rat Model of Inherited ALS.** *Front. Aging Neurosci.* 11 (2019).

- [281] B. C. Lin et al. **ALS/FTD mutations in UBQLN2 are linked to mitochondrial dysfunction through loss-of-function in mitochondrial protein import.** *Hum. Mol. Genet.* 30.13 (2021), pp. 1230–1246.
- [282] N. C. Reich. **STAT3 Revs Up the Powerhouse.** *Sci. Signal.* 2.90 (2009), pe61–pe61.
- [283] M. Rincon and F. Pereira. **A New Perspective: Mitochondrial Stat3 as a Regulator for Lymphocyte Function.** *Int. J. Mol. Sci.* 19.6 (2018), p. 1656.
- [284] M. Demaria, A. Camporeale, and V. Poli. **STAT3 and metabolism: How many ways to use a single molecule?** *Int. J. Cancer* 135.9 (2014), pp. 1997–2003.
- [285] D. J. Garama et al. **Mitochondrial STAT3: Powering up a potent factor.** *Cytokine* 87 (2016), pp. 20–25.
- [286] L. You et al. **The role of STAT3 in autophagy.** *Autophagy* 11.5 (2015), pp. 729–739.
- [287] S. Shen et al. **Cytoplasmic STAT3 Represses Autophagy by Inhibiting PKR Activity.** *Mol. Cell* 48.5 (2012), pp. 667–680.
- [288] A. Camporeale et al. **STAT3 Activities and Energy Metabolism: Dangerous Liaisons.** *Cancers (Basel).* 6.3 (2014), pp. 1579–1596.
- [289] L. Avalle and V. Poli. **Nucleus, Mitochondrion, or Reticulum? STAT3 à La Carte.** *Int. J. Mol. Sci.* 19.9 (2018), p. 2820.
- [290] L. Avalle et al. **STAT3 in cancer: A double edged sword.** *Cytokine* 98 (2017), pp. 42–50.
- [291] K.-S. Chun, J.-H. Jang, and D.-H. Kim. **Perspectives Regarding the Intersections between STAT3 and Oxidative Metabolism in Cancer.** *Cells* 9.10 (2020), p. 2202.
- [292] J. Wegrzyn et al. **Function of Mitochondrial Stat3 in Cellular Respiration.** *Science (80-. )*. 323.5915 (2009), pp. 793–797.
- [293] D. J. Gough et al. **Mitochondrial STAT3 Supports Ras-Dependent Oncogenic Transformation.** *Science* 324.5935 (2009), pp. 1713–1716.
- [294] C. Mantel et al. **Mouse hematopoietic cell-targeted STAT3 deletion: stem/progenitor cell defects, mitochondrial dysfunction, ROS overproduction, and a rapid aging-like phenotype.** *Blood* 120.13 (2012), pp. 2589–2599.
- [295] E. A. Mohamed and W. M. Sayed. **Implication of JAK1/STAT3/SOCS3 Pathway in Aging of Cerebellum of Male Rat: Histological and Molecular study.** *Sci. Rep.* 10.1 (2020), p. 8840.
- [296] M. Tkach et al. **Targeting Stat3 Induces Senescence in Tumor Cells and Elicits Prophylactic and Therapeutic Immune Responses against Breast Cancer Growth Mediated by NK Cells and CD4 + T Cells.** *J. Immunol.* 189.3 (2012), pp. 1162–1172.

- [297] T. Lahiri et al. **Mitochondrial STAT3 regulates antioxidant gene expression through complex I-derived NAD in triple negative breast cancer.** *Mol. Oncol.* 15.5 (2021), pp. 1432–1449.
- [298] Y. S. Xu et al. **STAT3 Undergoes Acetylation-dependent Mitochondrial Translocation to Regulate Pyruvate Metabolism.** *Sci. Rep.* 6.1 (2016), p. 39517.
- [299] E. Carbognin et al. **Stat3 promotes mitochondrial transcription and oxidative respiration during maintenance and induction of naive pluripotency.** *EMBO J.* 35.6 (2016), pp. 618–634.
- [300] E. Macias et al. **Stat3 binds to mtDNA and regulates mitochondrial gene expression in keratinocytes.** *J. Invest. Dermatol.* 134.7 (2014), pp. 1971–80.
- [301] Z. Harhous et al. **An Update on the Multifaceted Roles of STAT3 in the Heart.** *Front. Cardiovasc. Med.* 6 (2019).
- [302] K. Szczepanek et al. **Mitochondrial-targeted Signal Transducer and Activator of Transcription 3 (STAT3) Protects against Ischemia-induced Changes in the Electron Transport Chain and the Generation of Reactive Oxygen Species.** *J. Biol. Chem.* 286.34 (2011), pp. 29610–29620.
- [303] R. Yang et al. **Mitochondrial Ca<sup>2+</sup> and membrane potential, an alternative pathway for Interleukin 6 to regulate CD4 cell effector function.** *Elife* 4 (2015).
- [304] P. Vasileiou et al. **Mitochondrial Homeostasis and Cellular Senescence.** *Cells* 8.7 (2019), p. 686.
- [305] K. Khrapko et al. **Cell-by-cell scanning of whole mitochondrial genomes in aged human heart reveals a significant fraction of myocytes with clonally expanded deletions.** *Nucleic Acids Res.* 27.11 (1999), pp. 2434–2441.
- [306] A. Ameer et al. **Ultra-Deep Sequencing of Mouse Mitochondrial DNA: Mutational Patterns and Their Origins.** *PLoS Genet.* 7.3 (2011). Ed. by G. S. Barsh, e1002028.
- [307] B. A. I. Payne et al. **Mitochondrial aging is accelerated by anti-retroviral therapy through the clonal expansion of mtDNA mutations.** *Nat. Genet.* 43.8 (2011), pp. 806–810.
- [308] G. Saretzki, M. P. Murphy, and T. von Zglinicki. **MitoQ counteracts telomere shortening and elongates lifespan of fibroblasts under mild oxidative stress.** *Aging Cell* 2.2 (2003), pp. 141–143.
- [309] J. F. Passos et al. **Mitochondrial Dysfunction Accounts for the Stochastic Heterogeneity in Telomere-Dependent Senescence.** *PLoS Biol.* 5.5 (2007). Ed. by T. De Lange, e110.

- [310] M. Caron et al. **Contribution of mitochondrial dysfunction and oxidative stress to cellular premature senescence induced by antiretroviral thymidine analogues.** *Antivir. Ther.* 13.1 (2008), pp. 27–38.
- [311] S. Mai et al. **Decreased expression of Drp1 and Fis1 mediates mitochondrial elongation in senescent cells and enhances resistance to oxidative stress through PINK1.** *J. Cell Sci.* 123.6 (2010), pp. 917–926.
- [312] J. F. Passos et al. **Feedback between p21 and reactive oxygen production is necessary for cell senescence.** *Mol. Syst. Biol.* 6.1 (2010), p. 347.
- [313] J. Kaplon et al. **A key role for mitochondrial gatekeeper pyruvate dehydrogenase in oncogene-induced senescence.** *Nature* 498.7452 (2013), pp. 109–12.
- [314] X. R. Bao et al. **Mitochondrial dysfunction remodels one-carbon metabolism in human cells.** *Elife* 5 (2016).
- [315] C. Correia-Melo et al. **Mitochondria are required for pro-ageing features of the senescent phenotype.** *EMBO J.* 35.7 (2016), pp. 724–742.
- [316] C. Correia-Melo and J. F. Passos. **Mitochondria: Are they causal players in cellular senescence?** *Biochim. Biophys. Acta - Bioenerg.* 1847.11 (2015), pp. 1373–1379.
- [317] V. I. Korolchuk et al. **Mitochondria in Cell Senescence: Is Mitophagy the Weakest Link?** *EBioMedicine* 21 (2017), pp. 7–13.
- [318] A. A. Cluntun et al. **Glutamine Metabolism in Cancer: Understanding the Heterogeneity.** *Trends in Cancer* 3.3 (2017), pp. 169–180.
- [319] M. Watford. **Glutamine and glutamate: Nonessential or essential amino acids?** *Anim. Nutr.* 1.3 (2015), pp. 119–122.
- [320] Y. Johmura et al. **Senolysis by glutaminolysis inhibition ameliorates various age-associated disorders.** *Science* 371.6526 (2021), pp. 265–270.
- [321] L. Yang, S. Venneti, and D. Negrath. **Glutaminolysis: A Hallmark of Cancer Metabolism.** *Annu. Rev. Biomed. Eng.* 19.1 (2017), pp. 163–194.
- [322] J. M. Phang. **Proline Metabolism in Cell Regulation and Cancer Biology: Recent Advances and Hypotheses.** *Antioxid. Redox Signal.* 30.4 (2019), pp. 635–649.
- [323] W. Liu et al. **Proline biosynthesis augments tumor cell growth and aerobic glycolysis: involvement of pyridine nucleotides.** *Sci. Rep.* 5.1 (2015), p. 17206.
- [324] C. D’Aniello et al. **Proline Metabolism in Tumor Growth and Metastatic Progression.** *Front. Oncol.* 10 (2020).
- [325] I. Elia et al. **Proline metabolism supports metastasis formation and could be inhibited to selectively target metastasizing cancer cells.** *Nat. Commun.* 8.1 (2017), p. 15267.

- [326] C. H. Hagedorn and J. M. Phang. **Transfer of reducing equivalents into mitochondria by the interconversions of proline and  $\Delta$ 1-pyrroline-5-carboxylate.** *Arch. Biochem. Biophys.* 225.1 (1983), pp. 95–101.
- [327] C. H. Hagedorn and J. M. Phang. **Catalytic transfer of hydride ions from NADPH to oxygen by the interconversions of proline and  $\Delta$ 1-pyrroline-5-carboxylate.** *Arch. Biochem. Biophys.* 248.1 (1986), pp. 166–174.
- [328] L. Burke et al. **The Janus-like role of proline metabolism in cancer.** *Cell Death Discov.* 6.1 (2020), p. 104.
- [329] V. L. Albaugh, C. Pinzon-Guzman, and A. Barbul. **Arginine-Dual roles as an onconutrient and immunonutrient.** *J. Surg. Oncol.* 115.3 (2017), pp. 273–280.
- [330] K. A. Tran, C. M. Dillingham, and R. Sridharan. **The role of  $\alpha$ -ketoglutarate-dependent proteins in pluripotency acquisition and maintenance.** *J. Biol. Chem.* 294.14 (2019), pp. 5408–5419.
- [331] J. P. Morris et al.  **$\alpha$ -Ketoglutarate links p53 to cell fate during tumour suppression.** *Nature* 573.7775 (2019), pp. 595–599.
- [332] P. T. Schumacker. **Reactive oxygen species in cancer cells: Live by the sword, die by the sword.** *Cancer Cell* 10.3 (2006), pp. 175–176.
- [333] S. Yang et al. **Mitochondrial glutamine metabolism via GOT2 supports pancreatic cancer growth through senescence inhibition.** *Cell Death Dis.* 9.2 (2018), p. 55.
- [334] T. Cheng et al. **Pyruvate carboxylase is required for glutamine-independent growth of tumor cells.** *Proc. Natl. Acad. Sci.* 108.21 (2011), pp. 8674–8679.
- [335] K. Sellers et al. **Pyruvate carboxylase is critical for non-small-cell lung cancer proliferation.** *J. Clin. Invest.* 125.2 (2015), pp. 687–698.
- [336] D. C. Singleton et al. **Pyruvate anaplerosis is a mechanism of resistance to pharmacological glutaminase inhibition in triple-receptor negative breast cancer.** *BMC Cancer* 20.1 (2020), p. 470.
- [337] V. A. Kiesel et al. **Pyruvate carboxylase and cancer progression.** *Cancer Metab.* 9.1 (2021), p. 20.
- [338] Z. Wang et al. **Targeting Glutaminolysis: New Perspectives to Understand Cancer Development and Novel Strategies for Potential Target Therapies.** *Front. Oncol.* 10 (2020).
- [339] J.-W. Seo et al. **Autophagy is required for PDAC glutamine metabolism.** *Sci. Rep.* 6.1 (2016), p. 37594.
- [340] C. M. Metallo et al. **Reductive glutamine metabolism by IDH1 mediates lipogenesis under hypoxia.** *Nature* 481.7381 (2012), pp. 380–384.



- [341] P. A. Gameiro et al. **In Vivo HIF-Mediated Reductive Carboxylation Is Regulated by Citrate Levels and Sensitizes VHL-Deficient Cells to Glutamine Deprivation.** *Cell Metab.* 17.3 (2013), pp. 372–385.
- [342] A. R. Mullen et al. **Reductive carboxylation supports growth in tumour cells with defective mitochondria.** *Nature* 481.7381 (2012), pp. 385–388.
- [343] S.-M. Fendt et al. **Reductive glutamine metabolism is a function of the  $\alpha$ -ketoglutarate to citrate ratio in cells.** *Nat. Commun.* 4.1 (2013), p. 2236.
- [344] J. Du et al. **Reductive carboxylation is a major metabolic pathway in the retinal pigment epithelium.** *Proc. Natl. Acad. Sci.* 113.51 (2016), pp. 14710–14715.
- [345] N. Koundouros and G. Poulogiannis. **Reprogramming of fatty acid metabolism in cancer.** *Br. J. Cancer* 122.1 (2020), pp. 4–22.
- [346] L. P. Fernández, M. Gómez de Cedrón, and A. Ramírez de Molina. **Alterations of Lipid Metabolism in Cancer: Implications in Prognosis and Treatment.** *Front. Oncol.* 10 (2020).
- [347] R. Munir et al. **Lipid metabolism in cancer cells under metabolic stress.** *Br. J. Cancer* 120.12 (2019), pp. 1090–1098.
- [348] P. Icard et al. **Understanding the Central Role of Citrate in the Metabolism of Cancer Cells and Tumors: An Update.** *Int. J. Mol. Sci.* 22.12 (2021), p. 6587.
- [349] Y. Wang, Y. Chen, and J. Fang. **Post-Transcriptional and Post-translational Regulation of Central Carbon Metabolic Enzymes in Cancer.** *Anticancer. Agents Med. Chem.* 17.11 (2017).
- [350] Z.-J. Han et al. **The post-translational modification, SUMOylation, and cancer (Review).** *Int. J. Oncol.* (2018).
- [351] M. Rodríguez-Paredes and F. Lyko. **The importance of non-histone protein methylation in cancer therapy.** *Nat. Rev. Mol. Cell Biol.* 20.10 (2019), pp. 569–570.
- [352] L. ESPINOZA, M. SMULSON, and Z. CHEN. **Prolonged poly(ADP-ribose) polymerase-1 activity regulates JP-8-induced sustained cytokine expression in alveolar macrophages.** *Free Radic. Biol. Med.* 42.9 (2007), pp. 1430–1440.
- [353] P. Chang, M. K. Jacobson, and T. J. Mitchison. **Poly(ADP-ribose) is required for spindle assembly and structure.** *Nature* 432.7017 (2004), pp. 645–649.
- [354] M. J. Gamble and R. P. Fisher. **SET and PARP1 remove DEK from chromatin to permit access by the transcription machinery.** *Nat. Struct. Mol. Biol.* 14.6 (2007), pp. 548–555.
- [355] P. Bai and C. Cantó. **The Role of PARP-1 and PARP-2 Enzymes in Metabolic Regulation and Disease.** *Cell Metab.* 16.3 (2012), pp. 290–295.

- [356] A. N. Weaver and E. S. Yang. **Beyond DNA Repair: Additional Functions of PARP-1 in Cancer.** *Front. Oncol.* 3 (2013).
- [357] X. Luo and W. L. Kraus. **On PAR with PARP: cellular stress signaling through poly(ADP-ribose) and PARP-1.** *Genes Dev.* 26.5 (2012), pp. 417–432.
- [358] S. C. Larsen et al. **Systems-wide Analysis of Serine ADP-Ribosylation Reveals Widespread Occurrence and Site-Specific Overlap with Phosphorylation.** *Cell Rep.* 24.9 (2018), 2493–2505.e4.
- [359] K. Grube and A. Burkle. **Poly(ADP-ribose) polymerase activity in mononuclear leukocytes of 13 mammalian species correlates with species-specific life span.** *Proc. Natl. Acad. Sci.* 89.24 (1992), pp. 11759–11763.
- [360] A. Ghorai et al. **Sustained inhibition of PARP-1 activity delays glioblastoma recurrence by enhancing radiation-induced senescence.** *Cancer Lett.* 490 (2020), pp. 44–53.
- [361] K. J. Menzies et al. **Protein acetylation in metabolism — metabolites and cofactors.** *Nat. Rev. Endocrinol.* 12.1 (2016), pp. 43–60.
- [362] M. W. Van Dyke. **Lysine Deacetylase (KDAC) Regulatory Pathways: an Alternative Approach to Selective Modulation.** *ChemMedChem* 9.3 (2014), pp. 511–522.
- [363] A. J. de RUIJTER et al. **Histone deacetylases (HDACs): characterization of the classical HDAC family.** *Biochem. J.* 370.3 (2003), pp. 737–749.
- [364] L. Bosch-Presegue and A. Vaquero. **The Dual Role of Sirtuins in Cancer.** *Genes Cancer* 2.6 (2011), pp. 648–662.
- [365] S. Monteiro-Reis et al. **Sirtuins' Deregulation in Bladder Cancer: SIRT7 Is Implicated in Tumor Progression through Epithelial to Mesenchymal Transition Promotion.** *Cancers (Basel).* 12.5 (2020), p. 1066.
- [366] I. Ali et al. **Lysine Acetylation Goes Global: From Epigenetics to Metabolism and Therapeutics.** *Chem. Rev.* 118.3 (2018), pp. 1216–1252.
- [367] S. Rokudai et al. **MOZ increases p53 acetylation and premature senescence through its complex formation with PML.** *Proc. Natl. Acad. Sci.* 110.10 (2013), pp. 3895–3900.
- [368] C. Choudhary et al. **Lysine Acetylation Targets Protein Complexes and Co-Regulates Major Cellular Functions.** *Science (80-. ).* 325.5942 (2009), pp. 834–840.
- [369] L. Lv et al. **Acetylation Targets the M2 Isoform of Pyruvate Kinase for Degradation through Chaperone-Mediated Autophagy and Promotes Tumor Growth.** *Mol. Cell* 42.6 (2011), pp. 719–730.
- [370] O. Warburg, K. Posener, and E. Nägelein. **Über den Stoffwechsel der Carcinomzelle\_Warburg\_1924-1.pdf.** 1924.

- [371] W. Wadsak and M. Mitterhauser. **Basics and principles of radiopharmaceuticals for PET/CT.** *Eur. J. Radiol.* 73.3 (2010), pp. 461–469.
- [372] R. J. DeBerardinis and N. S. Chandel. **We need to talk about the Warburg effect.** *Nat. Metab.* 2.2 (2020), pp. 127–129.
- [373] M. V. Liberti and J. W. Locasale. **The Warburg Effect: How Does it Benefit Cancer Cells?** *Trends Biochem. Sci.* 41.3 (2016), pp. 211–218.
- [374] J. D. Rabinowitz and H. A. Collier. **Partners in the Warburg effect.** *Elife* 5 (2016).
- [375] S. Pavlides et al. **The reverse Warburg effect: Aerobic glycolysis in cancer associated fibroblasts and the tumor stroma.** *Cell Cycle* 8.23 (2009), pp. 3984–4001.
- [376] H. Zhao et al. **Tumor microenvironment derived exosomes pleiotropically modulate cancer cell metabolism.** *Elife* 5 (2016).
- [377] R. Iurlaro, C. L. León-Annicchiarico, and C. Muñoz-Pinedo. **Regulation of Cancer Metabolism by Oncogenes and Tumor Suppressors.** 2014, pp. 59–80.
- [378] P. Ruiz-Lozano et al. **p53 is a transcriptional activator of the muscle-specific phosphoglycerate mutase gene and contributes in vivo to the control of its cardiac expression.** *Cell Growth Differ.* 10.5 (1999), pp. 295–306.
- [379] F. Schwartzenberg-Bar-Yoseph, M. Armoni, and E. Karnieli. **The Tumor Suppressor p53 Down-Regulates Glucose Transporters GLUT1 and GLUT4 Gene Expression.** *Cancer Res.* 64.7 (2004), pp. 2627–2633.
- [380] K. Fischer et al. **Inhibitory effect of tumor cell-derived lactic acid on human T cells.** *Blood* 109.9 (2007), pp. 3812–3819.
- [381] O. R. Colegio et al. **Functional polarization of tumour-associated macrophages by tumour-derived lactic acid.** *Nature* 513.7519 (2014), pp. 559–563.
- [382] A. Brand et al. **LDHA-Associated Lactic Acid Production Blunts Tumor Immunosurveillance by T and NK Cells.** *Cell Metab.* 24.5 (2016), pp. 657–671.
- [383] K. G. de la Cruz-López et al. **Lactate in the Regulation of Tumor Microenvironment and Therapeutic Approaches.** *Front. Oncol.* 9 (2019).
- [384] S. Pilon-Thomas et al. **Neutralization of Tumor Acidity Improves Antitumor Responses to Immunotherapy.** *Cancer Res.* 76.6 (2016), pp. 1381–1390.
- [385] D. Anastasiou et al. **Inhibition of Pyruvate Kinase M2 by Reactive Oxygen Species Contributes to Cellular Antioxidant Responses.** *Science* 6060 (2011), pp. 1278–1283.
- [386] T. L. Dayton et al. **Germline loss of PKM2 promotes metabolic distress and hepatocellular carcinoma.** *Genes Dev.* 30.9 (2016), pp. 1020–1033.
- [387] A. Luengo et al. **Increased demand for NAD<sup>+</sup> relative to ATP drives aerobic glycolysis.** *Mol. Cell* 81.4 (2021), 691–707.e6.

- [388] R. G. Jones et al. **AMP-Activated Protein Kinase Induces a p53-Dependent Metabolic Checkpoint.** *Mol. Cell* 18.3 (2005), pp. 283–293.
- [389] Z. Feng et al. **The coordinate regulation of the p53 and mTOR pathways in cells.** *Proc. Natl. Acad. Sci.* 102.23 (2005), pp. 8204–8209.
- [390] D. Crighton et al. **DRAM, a p53-Induced Modulator of Autophagy, Is Critical for Apoptosis.** *Cell* 126.1 (2006), pp. 121–134.
- [391] H. Kondoh et al. **Glycolytic enzymes can modulate cellular life span.** *Cancer Res.* 65.1 (2005), pp. 177–85.
- [392] S. Matoba. **p53 Regulates Mitochondrial Respiration.** *Science* 312.5780 (2006), pp. 1650–1653.
- [393] A. Lahalle et al. **The p53 Pathway and Metabolism: The Tree That Hides the Forest.** *Cancers (Basel)*. 13.1 (2021), p. 133.
- [394] S.-H. Moon et al. **p53 Represses the Mevalonate Pathway to Mediate Tumor Suppression.** *Cell* 176.3 (2019), 564–580.e19.
- [395] R. Beckerman and C. Prives. **Transcriptional Regulation by P53.** *Cold Spring Harb. Perspect. Biol.* 2.8 (2010), a000935–a000935.
- [396] M. A. Sammons et al. **Tumor suppressor p53: from engaging DNA to target gene regulation.** *Nucleic Acids Res.* 48.16 (2020), pp. 8848–8869.
- [397] K. D. Sullivan et al. **Mechanisms of transcriptional regulation by p53.** *Cell Death Differ.* 25.1 (2018), pp. 133–143.
- [398] K. Engeland. **Cell cycle arrest through indirect transcriptional repression by p53: I have a DREAM.** *Cell Death Differ.* 25.1 (2018), pp. 114–132.
- [399] S. Sadasivam and J. A. DeCaprio. **The DREAM complex: master coordinator of cell cycle-dependent gene expression.** *Nat. Rev. Cancer* 13.8 (2013), pp. 585–595.
- [400] X. Li et al. **The MDM2–p53–pyruvate carboxylase signalling axis couples mitochondrial metabolism to glucose-stimulated insulin secretion in pancreatic  $\beta$ -cells.** *Nat. Commun.* 7.1 (2016), p. 11740.
- [401] S. M. Davidson et al. **Environment Impacts the Metabolic Dependencies of Ras-Driven Non-Small Cell Lung Cancer.** *Cell Metab.* 23.3 (2016), pp. 517–528.
- [402] P. Phannasil et al. **Pyruvate Carboxylase Is Up-Regulated in Breast Cancer and Essential to Support Growth and Invasion of MDA-MB-231 Cells.** *PLoS One* 10.6 (2015). Ed. by P. K. Singh, e0129848.
- [403] M.-z. Ma et al. **Long Noncoding RNA GCASPC , a Target of miR-17-3p, Negatively Regulates Pyruvate Carboxylase-Dependent Cell Proliferation in Gallbladder Cancer.** *Cancer Res.* 76.18 (2016), pp. 5361–5371.

- [404] E. E. Battin and J. L. Brumaghim. **Antioxidant Activity of Sulfur and Selenium: A Review of Reactive Oxygen Species Scavenging, Glutathione Peroxidase, and Metal-Binding Antioxidant Mechanisms.** *Cell Biochem. Biophys.* 55.1 (2009), pp. 1–23.
- [405] P. Jiang et al. **Reciprocal regulation of p53 and malic enzymes modulates metabolism and senescence.** *Nature* 493.7434 (2013), pp. 689–93.
- [406] L. Li et al. **p53 regulation of ammonia metabolism through urea cycle controls polyamine biosynthesis.** *Nature* 567.7747 (2019), pp. 253–256.
- [407] R. Boidot et al. **Regulation of Monocarboxylate Transporter MCT1 Expression by p53 Mediates Inward and Outward Lactate Fluxes in Tumors.** *Cancer Res.* 72.4 (2012), pp. 939–948.
- [408] D. A. Franklin et al. **p53 coordinates DNA repair with nucleotide synthesis by suppressing PFKFB3 expression and promoting the pentose phosphate pathway.** *Sci. Rep.* 6.1 (2016), p. 38067.
- [409] C. Quijano et al. **Oncogene-induced senescence results in marked metabolic and bioenergetic alterations.** *Cell Cycle* 11.7 (2012), pp. 1383–1392.
- [410] J. Fafián-Labora et al. **FASN activity is important for the initial stages of the induction of senescence.** *Cell Death Dis.* 10.4 (2019), p. 318.
- [411] N. Yahagi et al. **p53 Activation in Adipocytes of Obese Mice.** *J. Biol. Chem.* 278.28 (2003), pp. 25395–25400.
- [412] P. Jiang et al. **p53 regulates biosynthesis through direct inactivation of glucose-6-phosphate dehydrogenase.** *Nat. Cell Biol.* 13.3 (2011), pp. 310–316.
- [413] M. Trayssac, Y. A. Hannun, and L. M. Obeid. **Role of sphingolipids in senescence: implication in aging and age-related diseases.** *J. Clin. Invest.* 128.7 (2018), pp. 2702–2712.
- [414] M. E. Venable et al. **Role of Ceramide in Cellular Senescence.** *J. Biol. Chem.* 270.51 (1995), pp. 30701–30708.
- [415] E. L. James et al. **Replicatively senescent human fibroblasts reveal a distinct intracellular metabolic profile with alterations in NAD<sup>+</sup> and nicotinamide metabolism.** *Sci. Rep.* 6.1 (2016), p. 38489.
- [416] C. D. Wiley et al. **Oxylipin biosynthesis reinforces cellular senescence and allows detection of senolysis.** *Cell Metab.* 33.6 (2021), 1124–1136.e5.
- [417] J. P. Chou et al. **Prostaglandin E2 Promotes Features of Replicative Senescence in Chronically Activated Human CD8<sup>+</sup> T Cells.** *PLoS One* 9.6 (2014). Ed. by D. Unutmaz, e99432.
- [418] A. Lorenzini et al. **Is increased arachidonic acid release a cause or a consequence of replicative senescence?** *Exp. Gerontol.* 36.1 (2001), pp. 65–78.

- [419] A. Hernandez-Segura, J. Nehme, and M. Demaria. **Hallmarks of Cellular Senescence.** *Trends Cell Biol.* 28.6 (2018), pp. 436–453.
- [420] E. L. James et al. **Senescent Human Fibroblasts Show Increased Glycolysis and Redox Homeostasis with Extracellular Metabolomes That Overlap with Those of Irreparable DNA Damage, Aging, and Disease.** *J. Proteome Res.* 14.4 (2015), pp. 1854–1871.
- [421] J.-H. Lee et al. **ATP-citrate lyase regulates cellular senescence via an AMPK- and p53-dependent pathway.** *FEBS J.* 282.2 (2015), pp. 361–371.
- [422] K. M. Aird and R. Zhang. **Metabolic alterations accompanying oncogene-induced senescence.** *Mol. Cell. Oncol.* 1.3 (2014).
- [423] K. M. Aird et al. **Suppression of Nucleotide Metabolism Underlies the Establishment and Maintenance of Oncogene-Induced Senescence.** *Cell Rep.* 3.4 (2013), pp. 1252–1265.
- [424] A. Delfarah et al. **Inhibition of nucleotide synthesis promotes replicative senescence of human mammary epithelial cells.** *J. Biol. Chem.* 294.27 (2019), pp. 10564–10578.
- [425] S. Hubackova et al. **Replication and ribosomal stress induced by targeting pyrimidine synthesis and cellular checkpoints suppress p53-deficient tumors.** *Cell Death Dis.* 11.2 (2020), p. 110.
- [426] C. S. Ahn and C. M. Metallo. **Mitochondria as biosynthetic factories for cancer proliferation.** *Cancer Metab.* 3.1 (2015), p. 1.
- [427] K. Birsoy et al. **An Essential Role of the Mitochondrial Electron Transport Chain in Cell Proliferation Is to Enable Aspartate Synthesis.** *Cell* 162.3 (2015), pp. 540–551.
- [428] L. B. Sullivan et al. **Supporting Aspartate Biosynthesis Is an Essential Function of Respiration in Proliferating Cells.** *Cell* 162.3 (2015), pp. 552–563.
- [429] S. Cardaci et al. **Pyruvate carboxylation enables growth of SDH-deficient cells by supporting aspartate biosynthesis.** *Nat. Cell Biol.* 17.10 (2015), pp. 1317–1326.
- [430] J. Garcia-Bermudez et al. **Aspartate is a limiting metabolite for cancer cell proliferation under hypoxia and in tumours.** *Nat. Cell Biol.* 20.7 (2018), pp. 775–781.
- [431] C. N. Nagineni et al. **Radiation-Induced Senescence Reprograms Secretory and Metabolic Pathways in Colon Cancer HCT-116 Cells.** *Int. J. Mol. Sci.* 22.9 (2021), p. 4835.
- [432] R. S. Banh et al. **Neurons Release Serine to Support mRNA Translation in Pancreatic Cancer.** *Cell* 183.5 (2020), 1202–1218.e25.
- [433] F. F. Diehl et al. **Cellular redox state constrains serine synthesis and nucleotide production to impact cell proliferation.** *Nat. Metab.* 1.9 (2019), pp. 861–867.
- [434] L. Yang et al. **Serine Catabolism Feeds NADH when Respiration Is Impaired.** *Cell Metab.* 31.4 (2020), 809–821.e6.

- [435] S. Suzuki et al. **Phosphate-activated glutaminase (GLS2), a p53-inducible regulator of glutamine metabolism and reactive oxygen species.** *Proc. Natl. Acad. Sci.* 107.16 (2010), pp. 7461–7466.
- [436] W. Hu et al. **Glutaminase 2, a novel p53 target gene regulating energy metabolism and antioxidant function.** *Proc. Natl. Acad. Sci.* 107.16 (2010), pp. 7455–7460.
- [437] L. Li et al. **p53 regulation of ammonia metabolism through urea cycle controls polyamine biosynthesis.** *Nature* 567.7747 (2019), pp. 253–256.
- [438] D. P. Jones et al. **Redox analysis of human plasma allows separation of pro-oxidant events of aging from decline in antioxidant defenses.** *Free Radic. Biol. Med.* 33.9 (2002), pp. 1290–1300.
- [439] E. Saint-Germain et al. **SOCS1 regulates senescence and ferroptosis by modulating the expression of p53 target genes.** *Aging (Albany. NY).* 9.10 (2017), pp. 2137–2162.
- [440] S. Masaldan et al. **Iron accumulation in senescent cells is coupled with impaired ferritinophagy and inhibition of ferroptosis.** *Redox Biol.* 14 (2018), pp. 100–115.
- [441] G. Wu et al. **Glutathione Metabolism and Its Implications for Health.** *J. Nutr.* 134.3 (2004), pp. 489–492.
- [442] Y. Chen et al. **Early onset senescence occurs when fibroblasts lack the glutamate–cysteine ligase modifier subunit.** *Free Radic. Biol. Med.* 47.4 (2009), pp. 410–418.
- [443] K. Taniguchi et al. **Depletion of gamma-glutamylcyclotransferase in cancer cells induces autophagy followed by cellular senescence.** *Am. J. Cancer Res.* 8.4 (2018), pp. 650–661.
- [444] J. Sabbatinelli et al. **Where Metabolism Meets Senescence: Focus on Endothelial Cells.** *Front. Physiol.* 10 (2019).
- [445] M. Nakano et al. **Branched-Chain Amino Acids Enhance Premature Senescence through Mammalian Target of Rapamycin Complex I-Mediated Upregulation of p21 Protein.** *PLoS One* 8.11 (2013). Ed. by G. M. Das, e80411.
- [446] C.-A. Canfield and P. C. Bradshaw. **Amino acids in the regulation of aging and aging-related diseases.** *Transl. Med. Aging* 3 (2019), pp. 70–89.
- [447] C. Edwards et al. **Mechanisms of amino acid-mediated lifespan extension in *Caenorhabditis elegans*.** *BMC Genet.* 16.1 (2015), p. 8.
- [448] P. P. Jung et al. **Natural variation of chronological aging in the *Saccharomyces cerevisiae* species reveals diet-dependent mechanisms of life span control.** *npj Aging Mech. Dis.* 4.1 (2018), p. 3.

- [449] B. F. Darst et al. **Longitudinal plasma metabolomics of aging and sex.** *Aging (Albany, NY)*. 11.4 (2019), pp. 1262–1282.
- [450] R. H. Houtkooper et al. **The metabolic footprint of aging in mice.** *Sci. Rep.* 1.1 (2011), p. 134.
- [451] A. S. Krall et al. **Asparagine couples mitochondrial respiration to ATF4 activity and tumor growth.** *Cell Metab.* 33.5 (2021), 1013–1026.e6.
- [452] L. Hulea et al. **Translational and HIF-1 $\alpha$ -Dependent Metabolic Reprogramming Underpin Metabolic Plasticity and Responses to Kinase Inhibitors and Biguanides.** *Cell Metab.* 28.6 (2018), 817–832.e8.
- [453] J. S. Thompson et al. **Intestinal glucose uptake is increased in aged mice.** *Mech. Ageing Dev.* 46.1-3 (1988), pp. 135–143.
- [454] M. Oka et al. **Increasing neuronal glucose uptake attenuates brain aging and promotes life span under dietary restriction in Drosophila.** *iScience* 24.1 (2021), p. 101979.
- [455] J. R. Dörr et al. **Synthetic lethal metabolic targeting of cellular senescence in cancer therapy.** *Nature* 501.7467 (2013), pp. 421–425.
- [456] S. Nóbrega-Pereira et al. **G6PD protects from oxidative damage and improves healthspan in mice.** *Nat. Commun.* 7.1 (2016), p. 10894.
- [457] Y. Zhang et al. **Upregulation of Antioxidant Capacity and Nucleotide Precursor Availability Suffices for Oncogenic Transformation.** *Cell Metab.* 33.1 (2021), 94–109.e8.
- [458] J. Yoshino, J. A. Baur, and S.-i. Imai. **NAD<sup>+</sup> Intermediates: The Biology and Therapeutic Potential of NMN and NR.** *Cell Metab.* 27.3 (2018), pp. 513–528.
- [459] E. Verdin. **NAD<sup>+</sup> in aging, metabolism, and neurodegeneration.** *Science* 350.6265 (2015), pp. 1208–1213.
- [460] A. J. Covarrubias et al. **NAD<sup>+</sup> metabolism and its roles in cellular processes during ageing.** *Nat. Rev. Mol. Cell Biol.* 22.2 (2021), pp. 119–141.
- [461] L. E. Navas and A. Carnero. **NAD<sup>+</sup> metabolism, stemness, the immune response, and cancer.** *Signal Transduct. Target. Ther.* 6.1 (2021), p. 2.
- [462] S. Lautrup et al. **NAD<sup>+</sup> in Brain Aging and Neurodegenerative Disorders.** *Cell Metab.* 30.4 (2019), pp. 630–655.
- [463] E. F. Fang et al. **NAD<sup>+</sup> Replenishment Improves Lifespan and Healthspan in Ataxia Telangiectasia Models via Mitophagy and DNA Repair.** *Cell Metab.* 24.4 (2016), pp. 566–581.
- [464] A. P. Gomes et al. **Declining NAD<sup>+</sup> Induces a Pseudohypoxic State Disrupting Nuclear-Mitochondrial Communication during Aging.** *Cell* 155.7 (2013), pp. 1624–1638.



- [465] J. Yoshino et al. **Nicotinamide Mononucleotide, a Key NAD<sup>+</sup> Intermediate, Treats the Pathophysiology of Diet- and Age-Induced Diabetes in Mice.** *Cell Metab.* 14.4 (2011), pp. 528–536.
- [466] L. Mouchiroud et al. **The NAD<sup>+</sup>/Sirtuin Pathway Modulates Longevity through Activation of Mitochondrial UPR and FOXO Signaling.** *Cell* 154.2 (2013), pp. 430–441.
- [467] D. C. Schöndorf et al. **The NAD<sup>+</sup> Precursor Nicotinamide Riboside Rescues Mitochondrial Defects and Neuronal Loss in iPSC and Fly Models of Parkinson’s Disease.** *Cell Rep.* 23.10 (2018), pp. 2976–2988.
- [468] K. F. Mills et al. **Long-Term Administration of Nicotinamide Mononucleotide Mitigates Age-Associated Physiological Decline in Mice.** *Cell Metab.* 24.6 (2016), pp. 795–806.
- [469] Z. Yao et al. **Nicotinamide mononucleotide inhibits JNK activation to reverse Alzheimer disease.** *Neurosci. Lett.* 647 (2017), pp. 133–140.
- [470] M. Yoshino et al. **Nicotinamide mononucleotide increases muscle insulin sensitivity in prediabetic women.** *Science* (80 372.6547 (2021), pp. 1224–1229.
- [471] U. Harjes. **Context determines which pathway to use for NAD synthesis.** *Nat. Rev. Cancer* 19.7 (2019), pp. 365–365.
- [472] S. Chowdhry et al. **NAD metabolic dependency in cancer is shaped by gene amplification and enhancer remodelling.** *Nature* 569.7757 (2019), pp. 570–575.
- [473] A. A. Pramono et al. **NAD- and NADPH-Contributing Enzymes as Therapeutic Targets in Cancer: An Overview.** *Biomolecules* 10.3 (2020), p. 358.
- [474] N. Xie et al. **NAD<sup>+</sup> metabolism: pathophysiologic mechanisms and therapeutic potential.** *Signal Transduct. Target. Ther.* 5.1 (2020), p. 227.
- [475] J. W. Kincaid and N. A. Berger. **NAD metabolism in aging and cancer.** *Exp. Biol. Med.* 245.17 (2020), pp. 1594–1614.
- [476] E. Ansó et al. **The mitochondrial respiratory chain is essential for haematopoietic stem cell function.** *Nat. Cell Biol.* 19.6 (2017), pp. 614–625.
- [477] M. J. Son et al. **Nicotinamide Overcomes Pluripotency Deficits and Reprogramming Barriers.** *Stem Cells* 31.6 (2013), pp. 1121–1135.
- [478] R. N. Jadeja et al. **Loss of NAMPT in aging retinal pigment epithelium reduces NAD<sup>+</sup> availability and promotes cellular senescence.** *Aging (Albany. NY).* 10.6 (2018), pp. 1306–1323.
- [479] D. M. P. H. J. Boesten et al. **Accelerated Aging during Chronic Oxidative Stress: A Role for PARP-1.** *Oxid. Med. Cell. Longev.* 2013 (2013), pp. 1–10.

- [480] Z. Wang et al. **Olaparib induced senescence under P16 or P53 dependent manner in ovarian cancer.** *J. Gynecol. Oncol.* 30.2 (2019).
- [481] A. J. Covarrubias et al. **Senescent cells promote tissue NAD<sup>+</sup> decline during ageing via the activation of CD38<sup>+</sup> macrophages.** *Nat. Metab.* 2.11 (2020), pp. 1265–1283.
- [482] G. Hoxhaj et al. **Direct stimulation of NADP<sup>+</sup> synthesis through Akt-mediated phosphorylation of NAD kinase.** *Science* 363.6431 (2019), pp. 1088–1092.
- [483] K. Ohashi, S. Kawai, and K. Murata. **Identification and characterization of a human mitochondrial NAD kinase.** *Nat. Commun.* 3.1 (2012), p. 1248.
- [484] P. A. Gameiro et al. **Cofactor Balance by Nicotinamide Nucleotide Transhydrogenase (NNT) Coordinates Reductive Carboxylation and Glucose Catabolism in the Tricarboxylic Acid (TCA) Cycle.** *J. Biol. Chem.* 288.18 (2013), pp. 12967–12977.
- [485] F. Ciccarese and V. Ciminale. **Escaping Death: Mitochondrial Redox Homeostasis in Cancer Cells.** *Front. Oncol.* 7 (2017).
- [486] N. P. Ward et al. **Nicotinamide nucleotide transhydrogenase regulates mitochondrial metabolism in NSCLC through maintenance of Fe-S protein function.** *J. Exp. Med.* 217.6 (2020).
- [487] H.-Y. Ho et al. **Nicotinamide nucleotide transhydrogenase (NNT) deficiency dysregulates mitochondrial retrograde signaling and impedes proliferation.** *Redox Biol.* 12 (2017), pp. 916–928.
- [488] M. J. Son et al. **Restoration of Mitochondrial NAD<sup>+</sup> Levels Delays Stem Cell Senescence and Facilitates Reprogramming of Aged Somatic Cells.** *Stem Cells* 34.12 (2016), pp. 2840–2851.
- [489] A. G. Nickel et al. **Reversal of Mitochondrial Transhydrogenase Causes Oxidative Stress in Heart Failure.** *Cell Metab.* 22.3 (2015), pp. 472–484.
- [490] H.-Q. Ju et al. **NADPH homeostasis in cancer: functions, mechanisms and therapeutic implications.** *Signal Transduct. Target. Ther.* 5.1 (2020), p. 231.
- [491] J. B. Hoek and J. Rydström. **Physiological roles of nicotinamide nucleotide transhydrogenase.** *Biochem. J.* 254.1 (1988), pp. 1–10.
- [492] L. Chen et al. **NADPH production by the oxidative pentose-phosphate pathway supports folate metabolism.** *Nat. Metab.* 1 (2019), pp. 404–415.
- [493] G. Asher. **A mechanism of ubiquitin-independent proteasomal degradation of the tumor suppressors p53 and p73.** *Genes Dev.* 19.3 (2005), pp. 316–321.
- [494] G. Asher et al. **NQO1 stabilizes p53 through a distinct pathway.** *Proc. Natl. Acad. Sci.* 99.5 (2002), pp. 3099–3104.

- [495] C. N. Birts et al. **p53 is regulated by aerobic glycolysis in cancer cells by the CtBP family of NADH-dependent transcriptional regulators.** *Sci. Signal.* 13.630 (2020), eaau9529.
- [496] O. Aksoy et al. **The atypical E2F family member E2F7 couples the p53 and RB pathways during cellular senescence.** *Genes Dev.* 26.14 (2012), pp. 1546–1557.
- [497] S. Igelmann et al. **A hydride transfer complex reprograms NAD metabolism and bypasses senescence.** *Mol. Cell* 81.18 (2021), 3848–3865.e19.
- [498] M. Bhat et al. **Targeting the translation machinery in cancer.** *Nat. Rev. Drug Discov.* 14.4 (2015), pp. 261–278.
- [499] M. Narita et al. **Rb-Mediated Heterochromatin Formation and Silencing of E2F Target Genes during Cellular Senescence.** *Cell* 113.6 (2003), pp. 703–716.
- [500] J.-L. Langhendries et al. **The human box C/D snoRNAs U3 and U8 are required for pre-rRNA processing and tumorigenesis.** *Oncotarget* 7.37 (2016), pp. 59519–59534.
- [501] D. Shcherbakov et al. **Ribosomal mistranslation leads to silencing of the unfolded protein response and increased mitochondrial biogenesis.** *Commun. Biol.* 2.1 (2019), p. 381.
- [502] H. Guo. **Specialized ribosomes and the control of translation.** *Biochem. Soc. Trans.* 46.4 (2018), pp. 855–869.
- [503] Z. Shi et al. **Heterogeneous Ribosomes Preferentially Translate Distinct Subpools of mRNAs Genome-wide.** *Mol. Cell* 67.1 (2017), 71–83.e7.
- [504] M. Schosserer et al. **Specialized ribosomes in human dermal fibroblast senescence.** *49th Annu. ESDR Meet.* 49th Annual ESDR Meeting, 2019.
- [505] B. G. Childs et al. **Senescent cells: An emerging target for diseases of ageing.** 2017.
- [506] M. A. Lohrum et al. **Regulation of HDM2 activity by the ribosomal protein L11.** *Cancer Cell* 3.6 (2003), pp. 577–587.
- [507] Y. Zhang et al. **Ribosomal Protein L11 Negatively Regulates Oncoprotein MDM2 and Mediates a p53-Dependent Ribosomal-Stress Checkpoint Pathway.** *Mol. Cell. Biol.* 23.23 (2003), pp. 8902–8912.
- [508] M.-S. Dai and H. Lu. **Inhibition of MDM2-mediated p53 Ubiquitination and Degradation by Ribosomal Protein L5.** *J. Biol. Chem.* 279.43 (2004), pp. 44475–44482.
- [509] X. Zhou et al. **Ribosomal proteins: functions beyond the ribosome.** *J. Mol. Cell Biol.* 7.2 (2015), pp. 92–104.
- [510] K. Pandey et al. **Molecular mechanisms of resistance to CDK4/6 inhibitors in breast cancer: A review.** *Int. J. Cancer* 145.5 (2019), pp. 1179–1188.
- [511] B. L. Ebert et al. **Identification of RPS14 as a 5q- syndrome gene by RNA interference screen.** *Nature* 451.7176 (2008), pp. 335–339.

- [512] A. Giagounidis et al. **Hematological Malignancies**. *Hematology* 9.4 (2004), pp. 271–277.
- [513] M. Haddach et al. **Discovery of CX-5461, the First Direct and Selective Inhibitor of RNA Polymerase I, for Cancer Therapeutics**. *ACS Med. Chem. Lett.* 3.7 (2012), pp. 602–606.
- [514] A. Khot et al. **First-in-Human RNA Polymerase I Transcription Inhibitor CX-5461 in Patients with Advanced Hematologic Cancers: Results of a Phase I Dose-Escalation Study**. *Cancer Discov.* 9.8 (2019), pp. 1036–1049.
- [515] R. Ajore et al. **Deletion of ribosomal protein genes is a common vulnerability in human cancer, especially in concert with TP 53 mutations**. *EMBO Mol. Med.* 9.4 (2017), pp. 498–507.
- [516] A. D. Clercq and D. Inzé. **Cyclin-Dependent Kinase Inhibitors in Yeast, Animals, and Plants: A Functional Comparison**. *Crit. Rev. Biochem. Mol. Biol.* 41.5 (2006), pp. 293–313.
- [517] M. Shamsuzzaman et al. **Analysis of cell cycle parameters during the transition from unhindered growth to ribosomal and translational stress conditions**. *PLoS One* 12.10 (2017). Ed. by M. Polymenis, e0186494.
- [518] P. Tammineni et al. **The Import of the Transcription Factor STAT3 into Mitochondria Depends on GRIM-19, a Component of the Electron Transport Chain**. *J. Biol. Chem.* 288.7 (2013), pp. 4723–4732.
- [519] K. Boengler et al. **Inhibition of permeability transition pore opening by mitochondrial STAT3 and its role in myocardial ischemia/reperfusion**. *Basic Res. Cardiol.* 105.6 (2010), pp. 771–785.
- [520] R. Khan et al. **Live-Cell Imaging of the Association of STAT6-GFP with Mitochondria**. *PLoS One* 8.1 (2013). Ed. by V. Saks, e55426.
- [521] P. Marc et al. **Genome-wide analysis of mRNAs targeted to yeast mitochondria**. *EMBO Rep.* 3.2 (2002), pp. 159–164.
- [522] J. M. Liu and D. R. Liu. **Discovery of a mRNA mitochondrial localization element in *Saccharomyces cerevisiae* by nonhomologous random recombination and in vivo selection**. *Nucleic Acids Res.* 35.20 (2007), pp. 6750–6761.
- [523] K. A. Lashkevich and S. E. Dmitriev. **mRNA Targeting, Transport and Local Translation in Eukaryotic Cells: From the Classical View to a Diversity of New Concepts**. *Mol. Biol.* 55.4 (2021), pp. 507–537.
- [524] H. M. Cooper et al. **ATPase-deficient mitochondrial inner membrane protein ATAD3A disturbs mitochondrial dynamics in dominant hereditary spastic paraplegia**. *Hum. Mol. Genet.* 26.8 (2017), pp. 1432–1443.

- [525] N. Dorison et al. **Mitochondrial dysfunction caused by novel ATAD3A mutations.** *Mol. Genet. Metab.* 131.1-2 (2020), pp. 107–113.
- [526] A. Schaschkow et al. **STAT3 Regulates Mitochondrial Gene Expression in Pancreatic  $\beta$ -Cells and Its Deficiency Induces Glucose Intolerance in Obesity.** *Diabetes* (2021), db201222.
- [527] R. K. Davidson et al. **The loss of STAT3 in mature osteoclasts has detrimental effects on bone structure.** *PLoS One* 15.7 (2020). Ed. by S. V. Reddy, e0236891.
- [528] M. Elschami et al. **Reduction of STAT3 expression induces mitochondrial dysfunction and autophagy in cardiac HL-1 cells.** *Eur. J. Cell Biol.* 92.1 (2013), pp. 21–29.
- [529] K. Szczepanek et al. **Cytoprotection by the modulation of mitochondrial electron transport chain: The emerging role of mitochondrial STAT3.** *Mitochondrion* 12.2 (2012), pp. 180–189.
- [530] K. Boengler et al. **Cardioprotection by Ischemic Postconditioning Is Lost in Aged and STAT3-Deficient Mice.** *Circ. Res.* 102.1 (2008), pp. 131–135.
- [531] K. Boengler et al. **Inhibition of permeability transition pore opening by mitochondrial STAT3 and its role in myocardial ischemia/reperfusion.** *Basic Res. Cardiol.* 105.6 (2010), pp. 771–785.
- [532] L. Liu et al. **Exogenous NAD<sup>+</sup> supplementation protects H9c2 cardiac myoblasts against hypoxia/reoxygenation injury via Sirt1-p53 pathway.** *Fundam. Clin. Pharmacol.* 28.2 (2014), pp. 180–189.
- [533] S. Hinderer and K. Schenke-Layland. **Cardiac fibrosis – A short review of causes and therapeutic strategies.** *Adv. Drug Deliv. Rev.* 146 (2019), pp. 77–82.
- [534] J. J. Jacoby et al. **Cardiomyocyte-restricted knockout of STAT3 results in higher sensitivity to inflammation, cardiac fibrosis, and heart failure with advanced age.** *Proc. Natl. Acad. Sci.* 100.22 (2003), pp. 12929–12934.
- [535] X. Meng et al. **The potential role of senescence in limiting fibrosis caused by aging.** *J. Cell. Physiol.* 235.5 (2020), pp. 4046–4059.
- [536] A. Walaszczyk et al. **Pharmacological clearance of senescent cells improves survival and recovery in aged mice following acute myocardial infarction.** *Aging Cell* 18.3 (2019), e12945.
- [537] P. Song, Q. Zhao, and M.-H. Zou. **Targeting senescent cells to attenuate cardiovascular disease progression.** *Ageing Res. Rev.* 60 (2020), p. 101072.
- [538] F. Zhu et al. **Senescent Cardiac Fibroblast Is Critical for Cardiac Fibrosis after Myocardial Infarction.** *PLoS One* 8.9 (2013). Ed. by D. Kletsas, e74535.

- [539] D. Piber et al. **Inflammaging: Age and Systemic, Cellular, and Nuclear Inflammatory Biology in Older Adults.** *Journals Gerontol. Ser. A* 74.11 (2019), pp. 1716–1724.
- [540] M. Tolomeo and A. Cascio. **The Multifaced Role of STAT3 in Cancer and Its Implication for Anticancer Therapy.** *Int. J. Mol. Sci.* 22.2 (2021), p. 603.
- [541] H. Kojima et al. **IL-6-STAT3 signaling and premature senescence.** *JAK-STAT* 2.4 (2013), e25763.
- [542] W. Wu et al. **JAK2/STAT3 regulates estrogen-related senescence of bone marrow stem cells.** *J. Endocrinol.* 245.1 (2020), pp. 141–153.
- [543] D. V. Faget, Q. Ren, and S. A. Stewart. **Unmasking senescence: context-dependent effects of SASP in cancer.** *Nat. Rev. Cancer* 19.8 (2019), pp. 439–453.
- [544] B. Wang, J. Kohli, and M. Demaria. **Senescent Cells in Cancer Therapy: Friends or Foes?** *Trends in Cancer* 6.10 (2020), pp. 838–857.
- [545] D. J. Garama et al. **Mitochondrial STAT3: Powering up a potent factor.** *Cytokine* 87 (2016), pp. 20–25.
- [546] D. Phillips et al. **Stoichiometry of STAT3 and Mitochondrial Proteins.** *J. Biol. Chem.* 285.31 (2010), pp. 23532–23536.
- [547] M. Demaria et al. **{A} {STAT}3-mediated metabolic switch is involved in tumour transformation and {STAT}3 addiction.** *Aging (Albany NY)* 2.11 (2010), pp. 823–842.
- [548] M. Demaria and V. Poli. **PKM2, STAT3 and HIF-1 $\alpha$ .** *JAK-STAT* 1.3 (2012), pp. 194–196.
- [549] D. J. Garama et al. **A Synthetic Lethal Interaction between Glutathione Synthesis and Mitochondrial Reactive Oxygen Species Provides a Tumor-Specific Vulnerability Dependent on STAT3.** *Mol. Cell. Biol.* 35.21 (2015), pp. 3646–3656.
- [550] C. Yu et al. **Mitochondrial STAT3 contributes to transformation of Barrett’s epithelial cells that express oncogenic Ras in a p53-independent fashion.** *Am. J. Physiol. Liver Physiol.* 309.3 (2015), G146–G161.
- [551] D. J. Garama et al. **Mitochondrial STAT3: Powering up a potent factor.** *Cytokine* 87 (2016), pp. 20–25.
- [552] Q. Zhang et al. **Mitochondrial Localized Stat3 Promotes Breast Cancer Growth via Phosphorylation of Serine 727.** *J. Biol. Chem.* 288.43 (2013), pp. 31280–31288.
- [553] D. J. Gough et al. **STAT3 supports experimental K-RasG12D-induced murine myeloproliferative neoplasms dependent on serine phosphorylation.** *Blood* 124.14 (2014), pp. 2252–2261.
- [554] X. Deschênes-Simard et al. **Circumventing senescence is associated with stem cell properties and metformin sensitivity.** *Aging Cell* 18.2 (2019), e12889.

- [555] M. Galoczova, P. Coates, and B. Vojtesek. **STAT3, stem cells, cancer stem cells and p63.** *Cell. Mol. Biol. Lett.* 23.1 (2018), p. 12.
- [556] M. Peron et al. **Y705 and S727 are required for mitochondrial import and transcriptional activities of STAT3 and regulate proliferation of embryonic and tissue stem cells.** *bioRxiv* (2021), p. 20200717208264.
- [557] P. Aigner et al. **STAT3 $\beta$  is a tumor suppressor in acute myeloid leukemia.** *Blood Adv.* 3.13 (2019), pp. 1989–2002.
- [558] H.-F. Zhang et al. **The Opposing Function of STAT3 as an Oncoprotein and Tumor Suppressor Is Dictated by the Expression Status of STAT3 $\beta$  in Esophageal Squamous Cell Carcinoma.** *Clin. Cancer Res.* 22.3 (2016), pp. 691–703.
- [559] P. Aigner, V. Just, and D. Stoiber. **STAT3 isoforms: Alternative fates in cancer?** *Cytokine* 118 (2019), pp. 27–34.
- [560] F. Zammarchi et al. **Antitumorigenic potential of STAT3 alternative splicing modulation.** *Proc. Natl. Acad. Sci.* 108.43 (2011), pp. 17779–17784.
- [561] N. de la Iglesia et al. **Identification of a PTEN-regulated STAT3 brain tumor suppressor pathway.** *Genes Dev.* 22.4 (2008), pp. 449–462.
- [562] J. Pencik et al. **STAT3 regulated ARF expression suppresses prostate cancer metastasis.** *Nat. Commun.* 6.1 (2015), p. 7736.
- [563] M. Parisotto et al. **PTEN deletion in luminal cells of mature prostate induces replication stress and senescence in vivo.** *J. Exp. Med.* 215.6 (2018), pp. 1749–1763.
- [564] D. J. Freeman et al. **PTEN tumor suppressor regulates p53 protein levels and activity through phosphatase-dependent and -independent mechanisms.** *Cancer Cell* 3.2 (2003), pp. 117–130.
- [565] C. Prives and J. L. Manley. **Why Is p53 Acetylated?** *Cell* 107.7 (2001), pp. 815–818.
- [566] C. N. Birts et al. **p53 is regulated by aerobic glycolysis in cancer cells by the CtBP family of NADH-dependent transcriptional regulators.** *Sci. Signal.* 13.630 (2020), eaau9529.
- [567] S. M. Sanderson et al. **Methionine metabolism in health and cancer: a nexus of diet and precision medicine.** *Nat. Rev. Cancer* 19.11 (2019), pp. 625–637.
- [568] X. Zhu et al. **Inflammation, epigenetics, and metabolism converge to cell senescence and ageing: the regulation and intervention.** *Signal Transduct. Target. Ther.* 6.1 (2021), p. 245.
- [569] A. E. Field et al. **DNA Methylation Clocks in Aging: Categories, Causes, and Consequences.** *Mol. Cell* 71.6 (2018), pp. 882–895.

- [570] M. J. Jones, S. J. Goodman, and M. S. Kobor. **DNA methylation and healthy human aging.** *Aging Cell* 14.6 (2015), pp. 924–932.
- [571] H. Heyn et al. **Distinct DNA methylomes of newborns and centenarians.** *Proc. Natl. Acad. Sci.* 109.26 (2012), pp. 10522–10527.
- [572] S. Horvath and K. Raj. **DNA methylation-based biomarkers and the epigenetic clock theory of ageing.** *Nat. Rev. Genet.* 19.6 (2018), pp. 371–384.
- [573] E. M. Michalak et al. **The roles of DNA, RNA and histone methylation in ageing and cancer.** *Nat. Rev. Mol. Cell Biol.* 20.10 (2019), pp. 573–589.
- [574] A. Unnikrishnan et al. **Revisiting the genomic hypomethylation hypothesis of aging.** *Ann. N. Y. Acad. Sci.* 1418.1 (2018), pp. 69–79.
- [575] M. De Cecco et al. **L1 drives IFN in senescent cells and promotes age-associated inflammation.** *Nature* 566.7742 (2019), pp. 73–78.
- [576] M. Wang and B. Lemos. **Ribosomal DNA harbors an evolutionarily conserved clock of biological aging.** *Genome Res.* 3 (2019), pp. 325–333.
- [577] Z. Cao et al. **Pyruvate Carboxylase Activates the RIG-I-like Receptor-Mediated Antiviral Immune Response by Targeting the MAVS signalosome.** *Sci. Rep.* 6.1 (2016), p. 22002.
- [578] R. Nagaraj et al. **Nuclear Localization of Mitochondrial TCA Cycle Enzymes as a Critical Step in Mammalian Zygotic Genome Activation.** *Cell* 168.1-2 (2017), 210–223.e11.
- [579] S. Jitrapakdee et al. **Structure, mechanism and regulation of pyruvate carboxylase.** *Biochem. J.* 413.3 (2008), pp. 369–387.
- [580] K. T. Nguyen et al. **Control of protein degradation by N-terminal acetylation and the N-end rule pathway.** *Exp. Mol. Med.* 50.7 (2018), pp. 1–8.
- [581] R. F. Ramalho and D. M. Carraro. **Increasing evidence for the presence of alternative proteins in human tissues and cell lines.** *Appl. Cancer Res.* 37.1 (2017), p. 10.
- [582] R. J. DeBerardinis and N. S. Chandel. **Fundamentals of cancer metabolism.** *Sci. Adv.* 2.5 (2016), e1600200.
- [583] B. Faubert, A. Solmonson, and R. J. DeBerardinis. **Metabolic reprogramming and cancer progression.** *Science (80-. )*. 368.6487 (2020), eaaw5473.
- [584] B. A. McNeil et al. **Evaluating the effects of synthetic POM cycles and NAD kinase expression on fatty alcohol production in *Saccharomyces cerevisiae*.** *Res. Sq.* (2020).
- [585] R. Singh et al. **A Novel Strategy Involved Anti-Oxidative Defense: The Conversion of NADH into NADPH by a Metabolic Network.** *PLoS One* 3.7 (2008). Ed. by E. Abraham, e2682.



- [586] T. GRANSTROM. **Metabolic Flux Analysis of *Candida tropicalis* Growing on Xylose in an Oxygen-Limited Chemostat.** *Metab. Eng.* 3 (2002), pp. 248–256.
- [587] M. G. Vander Heiden and R. J. DeBerardinis. **Understanding the Intersections between Metabolism and Cancer Biology.** *Cell* 168.4 (2017), pp. 657–669.
- [588] E. A. Hanse et al. **Cytosolic malate dehydrogenase activity helps support glycolysis in actively proliferating cells and cancer.** *Oncogene* 36.27 (2017), pp. 3915–3924.
- [589] M. Jiménez-García, E. Verdugo-Sivianes, and A. Lucena-Cacace. **Nicotinamide adenine dinucleotide + metabolism biomarkers in malignant gliomas.** *Cancer Transl. Med.* 2.6 (2016), p. 189.
- [590] A. Lucena-Cacace et al. **NAMPT overexpression induces cancer stemness and defines a novel tumor signature for glioma prognosis.** *Oncotarget* 8.59 (2017), pp. 99514–99530.
- [591] T. Schild et al. **Unique Metabolic Adaptations Dictate Distal Organ-Specific Metastatic Colonization.** *Cancer Cell* 33.3 (2018), pp. 347–354.
- [592] P. K. Shetty, F. Galeffi, and D. A. Turner. **Nicotinamide pre-treatment ameliorates NAD(H) hyperoxidation and improves neuronal function after severe hypoxia.** *Neurobiol. Dis.* 62 (2014), pp. 469–478.
- [593] R. Zapata-Pérez et al. **Reduced nicotinamide mononucleotide is a new and potent NAD + precursor in mammalian cells and mice.** *FASEB J.* 35.4 (2021).
- [594] J. C. Henquin. **Triggering and amplifying pathways of regulation of insulin secretion by glucose.** *Diabetes* 49.11 (2000), pp. 1751–1760.
- [595] M. V. Jensen et al. **Metabolic cycling in control of glucose-stimulated insulin secretion.** *Am. J. Physiol. Metab.* 295.6 (2008), E1287–E1297.
- [596] M. J. MacDonald. **Feasibility of a mitochondrial pyruvate malate shuttle in pancreatic islets. Further implication of cytosolic NADPH in insulin secretion.** *J. Biol. Chem.* 271.9 (1995), 5287a.
- [597] D. Lu et al. **<sup>13</sup>C NMR isotopomer analysis reveals a connection between pyruvate cycling and glucose-stimulated insulin secretion (GSIS).** *Proc. Natl. Acad. Sci.* 99.5 (2002), pp. 2708–2713.
- [598] R. Ivarsson et al. **Redox Control of Exocytosis: Regulatory Role of NADPH, Thioredoxin, and Glutaredoxin.** *Diabetes* 54.7 (2005), pp. 2132–2142.
- [599] C. Guay et al. **A Role for ATP-Citrate Lyase, Malic Enzyme, and Pyruvate/Citrate Cycling in Glucose-induced Insulin Secretion.** *J. Biol. Chem.* 282.49 (2007), pp. 35657–35665.
- [600] F. Schuit et al. **Metabolic Fate of Glucose in Purified Islet Cells.** *J. Biol. Chem.* 272.30 (1997), pp. 18572–18579.

- [601] E. Heart et al. **Role for malic enzyme, pyruvate carboxylation, and mitochondrial malate import in glucose-stimulated insulin secretion.** *Am. J. Physiol. Metab.* 296.6 (2009), E1354–E1362.
- [602] J. Lamontagne et al. **Identification of the signals for glucose-induced insulin secretion in INS1 (832/13)  $\beta$ -cells using metformin-induced metabolic deceleration as a model.** *J. Biol. Chem.* 292.47 (2017), pp. 19458–19468.
- [603] M. Foretz et al. **Metformin: From Mechanisms of Action to Therapies.** *Cell Metab.* 20.6 (2014), pp. 953–966.
- [604] K. Birsoy et al. **Metabolic determinants of cancer cell sensitivity to glucose limitation and biguanides.** *Nature* 508.7494 (2014), pp. 108–112.
- [605] O. Moiseeva et al. **Metformin, aging and cancer.** *Aging (Albany, NY).* 5.5 (2013), pp. 330–331.
- [606] A. K. Madiraju et al. **Metformin suppresses gluconeogenesis by inhibiting mitochondrial glycerophosphate dehydrogenase.** *Nature* 510.7506 (2014), pp. 542–546.
- [607] A. Helman et al. **p16Ink4a-induced senescence of pancreatic beta cells enhances insulin secretion.** *Nat. Med.* 22.4 (2016), pp. 412–420.
- [608] C. Aguayo-Mazzucato. **Functional changes in beta cells during ageing and senescence.** *Diabetologia* 63.10 (2020), pp. 2022–2029.
- [609] B. A. Olenchock, J. C. Rathmell, and M. G. Vander Heiden. **Biochemical Underpinnings of Immune Cell Metabolic Phenotypes.** *Immunity* 46.5 (2017), pp. 703–713.
- [610] L. R. Waters et al. **Initial B Cell Activation Induces Metabolic Reprogramming and Mitochondrial Remodeling.** *iScience* 5 (2018), pp. 99–109.
- [611] F. Morandi, A. L. Horenstein, and F. Malavasi. **The Key Role of NAD<sup>+</sup> in Anti-Tumor Immune Response: An Update.** *Front. Immunol.* 12 (2021).
- [612] M. Slack, T. Wang, and R. Wang. **T cell metabolic reprogramming and plasticity.** *Mol. Immunol.* 68.2 (2015), pp. 507–512.
- [613] G. Soto-Herederó, G. Desdín-Micó, and M. Mittelbrunn. **Mitochondrial dysfunction defines T cell exhaustion.** *Cell Metab.* 33.3 (2021), pp. 470–472.
- [614] Y.-R. Yu et al. **Disturbed mitochondrial dynamics in CD8<sup>+</sup> TILs reinforce T cell exhaustion.** *Nat. Immunol.* 21.12 (2020), pp. 1540–1551.
- [615] Y. Wang et al. **Potentiating the anti-tumor response of tumor infiltrated T cells by NAD<sup>+</sup> supplementation.** *bioRxiv* (2020).
- [616] G. Desdín-Micó et al. **T cells with dysfunctional mitochondria induce multimorbidity and premature senescence.** *Science* 368.6497 (2020), pp. 1371–1376.

- [617] P. A. Srere. **COMPLEXES OF SEQUENTIAL METABOLIC ENZYMES.** *Annual Review of Biochemistry* 56.1 (1987), pp. 89–124.
- [618] T. S. Luongo et al. **SLC25A51 is a mammalian mitochondrial NAD<sup>+</sup> transporter.** *Nature* 588.7836 (2020), pp. 174–179.
- [619] E. Gaude et al. **NADH Shuttling Couples Cytosolic Reductive Carboxylation of Glutamine with Glycolysis in Cells with Mitochondrial Dysfunction.** *Mol. Cell* 69.4 (2018), 581–593.e7.
- [620] P. Kreuzaler et al. **Adapt and conquer: Metabolic flexibility in cancer growth, invasion and evasion.** *Mol. Metab.* 33 (2020), pp. 83–101.
- [621] G. Rinaldi et al. **In Vivo Evidence for Serine Biosynthesis-Defined Sensitivity of Lung Metastasis, but Not of Primary Breast Tumors, to mTORC1 Inhibition.** *Mol. Cell* 81.2 (2021), 386–397.e7.
- [622] P. A. Srere. **IS THERE AN ORGANIZATION OF KREBS CYCLE ENZYMES IN THE MITOCHONDRIAL MATRIX?** *Energy Metab. Regul. Metab. Process. Mitochondria.* Elsevier, 1972, pp. 79–91.
- [623] Y. Zhang and A. R. Fernie. **Metabolons, enzyme–enzyme assemblies that mediate substrate channeling, and their roles in plant metabolism.** *Plant Commun.* 2.1 (2021), p. 100081.
- [624] Y. Zhang and A. R. Fernie. **Stable and Temporary Enzyme Complexes and Metabolons Involved in Energy and Redox Metabolism.** *Antioxid. Redox Signal.* (2020), ars.2019.7981.
- [625] F. Wu and S. Minter. **Krebs Cycle Metabolon: Structural Evidence of Substrate Channeling Revealed by Cross-Linking and Mass Spectrometry.** *Angew. Chemie Int. Ed.* 54.6 (2015), pp. 1851–1854.
- [626] Y. Zhang and A. R. Fernie. **Stable and Temporary Enzyme Complexes and Metabolons Involved in Energy and Redox Metabolism.** *Antioxid. Redox Signal.* (2020), ars.2019.7981.
- [627] V. Pareek et al. **Metabolomics and mass spectrometry imaging reveal channeled de novo purine synthesis in cells.** *Science (80-. ).* 368.6488 (2020), pp. 283–290.
- [628] J. Son et al. **Glutamine supports pancreatic cancer growth through a KRAS-regulated metabolic pathway.** *Nature* 496.7443 (2013), pp. 101–105.
- [629] P. Borst. **The malate–aspartate shuttle (Borst cycle): How it started and developed into a major metabolic pathway.** *IUBMB Life* 11 (2020), pp. 2241–2259.
- [630] Y.-P. Wang et al. **Arginine Methylation of MDH1 by CARM1 Inhibits Glutamine Metabolism and Suppresses Pancreatic Cancer.** *Mol. Cell* 64.4 (2016), pp. 673–687.

- [631] M. Ying et al. **Lactate and glutamine support NADPH generation in cancer cells under glucose deprived conditions.** *Redox Biol.* 46 (2021), p. 102065.
- [632] A. N. Lau et al. **Dissecting cell-type-specific metabolism in pancreatic ductal adenocarcinoma.** *Elife* (2020).
- [633] T. Nacarelli et al. **NAD<sup>+</sup> metabolism governs the proinflammatory senescence-associated secretome.** *Nat. Cell Biol.* 21.3 (2019), pp. 397–407.
- [634] Z. Turi et al. **Impaired ribosome biogenesis: mechanisms and relevance to cancer and aging.** *Aging (Albany, NY).* 11.8 (2019), pp. 2512–2540.
- [635] M. Healy-Stoffel et al. **Altered nucleolar morphology in substantia nigra dopamine neurons following 6-hydroxydopamine lesion in rats.** *Neurosci. Lett.* 546 (2013), pp. 26–30.
- [636] W. M. Caudle et al. **A role for a novel protein, nucleolin, in Parkinson’s disease.** *Neurosci. Lett.* 459.1 (2009), pp. 11–15.
- [637] Z. Xu et al. **Knocking down nucleolin expression in gliomas inhibits tumor growth and induces cell cycle arrest.** *J. Neurooncol.* 108.1 (2012), pp. 59–67.
- [638] E. Bou Samra et al. **A role for Tau protein in maintaining ribosomal DNA stability and cytidine deaminase-deficient cell survival.** *Nat. Commun.* 8.1 (2017), p. 693.
- [639] S. J. Chinta et al. **Cellular Senescence Is Induced by the Environmental Neurotoxin Paraquat and Contributes to Neuropathology Linked to Parkinson’s Disease.** *Cell Rep.* 22.4 (2018), pp. 930–940.
- [640] H. Cui, Y. Kong, and H. Zhang. **Oxidative Stress, Mitochondrial Dysfunction, and Aging.** *J. Signal Transduct.* 2012 (2012), pp. 1–13.
- [641] D. Harman. **Aging: A Theory Based on Free Radical and Radiation Chemistry.** *J. Gerontol.* 11.3 (1956), pp. 298–300.
- [642] L. M. Ogawa and S. J. Baserga. **Crosstalk between the nucleolus and the DNA damage response.** *Mol. Biosyst.* 13.3 (2017), pp. 443–455.
- [643] D. H. Larsen and M. Stucki. **Nucleolar responses to DNA double-strand breaks.** *Nucleic Acids Res.* 44.2 (2016), pp. 538–544.
- [644] Y. Shav-Tal et al. **Dynamic Sorting of Nuclear Components into Distinct Nucleolar Caps during Transcriptional Inhibition.** *Mol. Biol. Cell* 16.5 (2005), pp. 2395–2413.
- [645] L. M. Korsholm et al. **Recent advances in the nucleolar responses to DNA double-strand breaks.** *Nucleic Acids Res.* 48.17 (2020), pp. 9449–9461.
- [646] J. Chen and L. A. Stark. **Insights into the Relationship between Nucleolar Stress and the NF- $\kappa$ B Pathway.** *Trends Genet.* 35.10 (2019), pp. 768–780.

- [647] S. Alberti and A. A. Hyman. **Are aberrant phase transitions a driver of cellular aging?** *BioEssays* 38.10 (2016), pp. 959–968.
- [648] S. Jiang et al. **Protein phase separation and its role in tumorigenesis.** *Elife* 9 (2020).
- [649] M. Prouteau and R. Loewith. **Regulation of Cellular Metabolism through Phase Separation of Enzymes.** *Biomolecules* 8.4 (2018), p. 160.
- [650] R. Wang et al. **LncRNA GIRGL drives CAPRIN1-mediated phase separation to suppress glutaminase-1 translation under glutamine deprivation.** *Sci. Adv.* 7.13 (2021), eabe5708.
- [651] S. Jang et al. **The Glycolytic Protein Phosphofructokinase Dynamically Relocalizes into Subcellular Compartments with Liquid-like Properties in vivo.** *bioRxiv* (2019).
- [652] D. L. J. Lafontaine et al. **The nucleolus as a multiphase liquid condensate.** *Nat. Rev. Mol. Cell Biol.* 22.3 (2021), pp. 165–182.
- [653] J. A. Riback et al. *Nature* 581.7807 (2020).
- [654] C. P. Brangwynne, T. J. Mitchison, and A. A. Hyman. **Active liquid-like behavior of nucleoli determines their size and shape in *Xenopus laevis* oocytes.** *Proc. Natl. Acad. Sci.* 108.11 (2011), pp. 4334–4339.
- [655] K. J. Abraham et al. **Nucleolar RNA polymerase II drives ribosome biogenesis.** *Nature* 585.7824 (2020), pp. 298–302.
- [656] G. Wang and A. R. Fersht. **Propagation of aggregated p53: Cross-reaction and coaggregation vs. seeding.** *Proc. Natl. Acad. Sci.* 112.8 (2015), pp. 2443–2448.
- [657] X. Dai et al. **Benign Prostatic Hyperplasia and the Risk of Prostate Cancer and Bladder Cancer.** *Medicine (Baltimore).* 95.18 (2016), e3493.

# Chapter A

---

## Appendix

**A.1. Supplementary files from the article "Senescence-associated ribosome biogenesis defects contribute to cell cycle arrest through the Rb pathway"**

In the format provided by the authors and unedited.

## Senescence-associated ribosome biogenesis defects contributes to cell cycle arrest through the Rb pathway

Frédéric Lessard<sup>1</sup>, Sebastian Igelmann<sup>1</sup>, Christian Trahan<sup>2</sup>, Geneviève Huot<sup>1</sup>, Emmanuelle Saint-Germain<sup>1</sup>, Lian Mignacca<sup>1</sup>, Neylen Del Toro<sup>1</sup>, Stéphane Lopes-Paciencia<sup>1</sup>, Benjamin Le Calvé<sup>5</sup>, Marinieve Montero<sup>1</sup>, Xavier Deschênes-Simard<sup>4</sup>, Marina Bury<sup>6</sup>, Olga Moiseeva<sup>7</sup>, Marie-Camille Rowell<sup>1</sup>, Cornelia E. Zorca<sup>1</sup>, Daniel Zenklusen <sup>1</sup>, Léa Brakier-Gingras<sup>1</sup>, Véronique Bourdeau<sup>1</sup>, Marlene Oeffinger<sup>1,2,3</sup> and Gerardo Ferbeyre <sup>1\*</sup>

<sup>1</sup>Department of Biochemistry and Molecular Medicine, Université de Montréal, Montreal, Quebec, Canada. <sup>2</sup>Institut de Recherches Cliniques de Montréal, Montreal, Quebec, Canada. <sup>3</sup>Faculty of Medicine, Division of Experimental Medicine, McGill University, Montreal, Quebec, Canada. <sup>4</sup>Faculty of Medicine, Department of Medicine, McGill University, Montreal, Quebec, Canada. <sup>5</sup>URBC-NARILIS, University of Namur, Namur, Belgium. <sup>6</sup>Lady Davis Institute for Medical Research, McGill University, Montreal, Quebec, Canada. <sup>7</sup>Generium 601125 Vladimirskaia obl, Petushinsky, Russia. \*e-mail: [g.ferbeyre@umontreal.ca](mailto:g.ferbeyre@umontreal.ca)

## Methods

**Reagents.** CX-5461 was purchased from Selleckchem (Cedarlane, Burlington, ON). Staurosporine, camptothecin and palbociclib (PD0332991) were purchased from Sigma-Aldrich (Oakville, ON). Interferon  $\beta$ -1a ( $\beta$ -IFN) (Avonex, Biogen Idec) was a gift from D. P. Baker (Biogen Idec, Cambridge, MA).

**Plasmids.** Retroviruses pLPC, pLPC-3xFLAG, pBABE, pBABE-H-RasV12, pWZL, pWZL-H-RasV12 and pWZL-PML-IV were described previously<sup>1</sup>. pLXSN, pLXSN-E6, pLXSN-E7, pLXSN-E6/E7, pBABE-p16(WT), pBABE-CDK4(WT), pBABE-CDK6(WT) and pMPLP-shp21 were a gift from S. W. Lowe (Memorial Sloan-Kettering Cancer Center, New York, NY). ShRb, shp16 and shNTC were subcloned in BglII/AgeI restriction sites to create retroviral vectors pMSCV-shRb, pMSCV-shp16, pMSCV-shNTC and pMLPX-shNTC (pMLPX is pMLP without GFP reporter). pLXSN-E7( $\Delta$ 6-10), pLXSN-E7( $\Delta$ 21-24) and pLXSN-E7( $\Delta$ 79-83) were a gift from D. A. Galloway (Fred Hutchinson Cancer Center, Seattle, WA).

RSL1D1(WT) was PCR amplified and subcloned in BamHI/EcoRI restriction sites to create pBABE-RSL1D1(WT). pcDNA3.1-3xFLAG-RSL1D1 was made first by subcloning the PCR amplified 3xFLAG tag into EcoRV/EcoRI restriction sites of the vector pcDNA3.1(-) (Life Technologies, Invitrogen, Burlington, ON) to create pcDNA3.1-3xFLAG. Then RSL1D1(WT) was PCR amplified and subcloned in EcoRI/BamHI restriction sites to create pcDNA3.1-3xFLAG-RSL1D1(WT). CDK4(WT) and CDK4(K35M) were PCR amplified with primer containing the 3xFLAG tag and subcloned in BamHI/EcoRI restriction sites to create pBABE-3xFLAG-CDK4(WT) and pBABE-3xFLAG-CDK4(K35M). RPS14(WT)-Myc was PCR amplified from the vector pCMV6-RPS14-Myc-FLAG tagged (RC223055, Origene, Atlanta, GA) and subcloned in BamHI/Sall restriction sites to create pBABE-RPS14(WT)-Myc. RPS14(WT)-Myc was subcloned in BamHI/XhoI restriction sites to create retroviral vectors pMSCV-RPS14(WT)-Myc. RPS14(WT), RPS14(2-88) and RPS14(89-151) were PCR amplified and subcloned in BamHI/EcoRI restriction sites to create pcDNA3-FLAG-RPS14(WT), pcDNA3-FLAG-RPS14(2-88) and pcDNA3-FLAG-RPS14(89-151). Cyclin D1 was PCR amplified and subcloned in BamHI/EcoRI restriction sites to create pcDNA3-Myc-Cyclin D1(WT). For PCR primers used for cloning see Supplementary Table S4.

Lentiviruses pLKO expressing shRSL1D1 (shR-A, shR-B), shNS (shNS-A, shNS-B), shDDX21 (shD-A, shD-B), shEBP2 (shE-A, shE-B), shRPS14 (shRPS14-A, shRPS14-B) and shCTR were from Sigma-Aldrich (nos. 159162, 159486, 293679, 293681, 51198, 51199, 310234, 72461, 8643, 8644 and SHC002). Finally, pCMV-VSV-G (Addgene no. 8454) and pCMV-dR.91 (Delta8.9) were from R. Weinberg's laboratory (Whitehead Institute, Cambridge, MA). ShRNA target sequences are presented in Supplementary Table 3.

**Cells and viral gene transfer.** Phoenix amphi packaging cells were a gift from S. W. Lowe. Human embryonic kidney HEK-293T cells, U2OS, PC3, H1299 were obtained from American Type Culture Collection (ATCC, Manassas, VA), normal human diploid fibroblasts IMR90 were obtained from the American Type Culture Collection or from Coriell Institute for Medical Research (Camden, NJ) and MUTZ-8 cells were obtained from the Leibniz Institute DSMZ-German Collection of Microorganisms and Cell Cultures (DSMZ no. ACC 689). PC3 cells were cultured in RPMI medium (Wisent, Montreal, QC) supplemented with 10% fetal bovine serum (FBS; Wisent), 1% penicillin/streptomycin (Wisent) and 2 mM L-glutamine (Wisent). MUTZ-8 cells were cultured in  $\alpha$ -MEM (Invitrogen; cat. no. 12571063) supplemented with 20% fetal bovine serum (FBS; Wisent), 1% penicillin/streptomycin sulfate (Wisent) and 10 ng ml<sup>-1</sup> of human recombinant GM-CSF (Peprotech; cat. no. 300-03-100ug). All other cell lines were cultured in Dulbecco's modified Eagle medium (DMEM; Wisent) supplemented with 10% FBS (Wisent) and 1% penicillin/streptomycin sulfate (Wisent).

Retroviral-mediated gene transfer was done as described<sup>1</sup>. For lentiviral transduction,  $5 \times 10^6$  HEK-293 cells were seeded in 10 cm cell culture dishes and grown for 24 hours. Then, cells were transiently transfected using 2-3  $\mu$ g of a lentiviral expression vector, 1  $\mu$ g of the pCMV-VSV-G envelope protein expression plasmid and 2  $\mu$ g of the pCMV-dR.91 (Delta8.9) plasmid containing gag, pol and rev genes in 900  $\mu$ l of 1  $\times$  Opti-MEM (Gibco Life Technologies, Burlington, ON). Then, 16  $\mu$ l of X-tremeGENE 9 DNA Transfection reagent (Roche, Laval, QC) was added. Tubes were inverted 4-5 times and after 10 min at room temperature, the mix was added to the cells. The medium was changed after 24 hours incubation. Supernatants from the transfected plates were collected 48 to 72 hours after transfection. The viral soups were filtered through a 0.45  $\mu$ m filter, supplemented with 4  $\mu$ g ml<sup>-1</sup> polybrene (Sigma) and added on target cells. Twelve hours after the last infection, infected cell populations were selected using 2.5  $\mu$ g ml<sup>-1</sup> puromycin (Wisent) and/or 75  $\mu$ g ml<sup>-1</sup> hygromycin (Wisent) and/or 400  $\mu$ g ml<sup>-1</sup> G418 (Wisent).

**Cell fractionation and immunoblotting.** Cell fractions<sup>41</sup> and immunoblotting<sup>23</sup> were performed as previously described. For antibodies see Supplementary Table 6.

**Cells proliferation and senescence analysis.** Proliferation was assessed from estimations of cell number according to a crystal violet retention assay<sup>3</sup>. Senescence-associated- $\beta$ -galactosidase (SA- $\beta$ -gal) activity was assayed as described previously<sup>7</sup>. Source data for growth curves are presented in Supplementary Table 5.

**Immunohistochemistry.** Paraffin-embedded tissue samples were heated at 55 °C for 1 hour prior to deparaffinization and rehydration by sequential incubation in xylene (2  $\times$  6 min), 100% ethanol (1  $\times$  5 min), 95% ethanol (1  $\times$  3 min), 75% ethanol (1  $\times$  3 min) and 40% ethanol (1  $\times$  3 min). Samples were washed in 1  $\times$  TBS/0.3% Triton X-100 for 5 min and then in dH<sub>2</sub>O for 3 min. Skin TMAs SK803 were bleached with the delicate melanin bleach kit for special stains and IHC (catalogue no. 24909-1, Polysciences, Warrington, PA). Antigen retrieval was performed by heating for 15 min at 95 °C in 10 mM citrate buffer (pH 6.0). Samples were cooled for at least 1 hour and washed 3 times for 3 min with 1  $\times$  TBS/0.3% Triton X-100. Endogenous peroxidases were inactivated by incubation for 5 min at room temperature in a solution of 3% H<sub>2</sub>O<sub>2</sub>. Samples were washed 3 times for 3 min in 1  $\times$  TBS/0.3% Triton X-100 and tissues were delimited using a hydrophobic barrier pen. Tissues were blocked 1 hour at room temperature with a protein-blocking serum-free ready-to-use reagent (DAKO, cat. no. X0909, Carpinteria, CA), and incubated overnight at 4 °C with primary antibodies diluted in 5% goat serum in 1  $\times$  TBS/0.3% Triton X-100. Antibodies were: anti-INK4a (p16, p16INK4a) rabbit monoclonal (1:250, EPR1473, ab108349, lot: GR155011-2, Abcam, Toronto, ON) and anti-RPL29 rabbit polyclonal (1:250, GTX101833, lot: 40681, Gene Tex, Irvine, CA). Tissues were washed 3 times for 3 min in 1  $\times$  TBS/0.3% Triton X-100 followed by primary antibody detection using the LSAB2 System-HRP (DAKO, cat. no. K0675, Carpinteria, CA), for 30 min using the secondary biotinylated antibody (DAKO, cat. no. K0675, Carpinteria, CA) then, tissues were washed 2 times for 5 min in 1  $\times$  TBS/0.3% Triton X-100 and then incubated for 30 min with streptavidin-HRP (DAKO, cat. no. K0675, Carpinteria, CA). Tissues were washed 3 times for 3 min with 1  $\times$  TBS/0.3% Triton X-100. Finally, the specimens were stained for peroxidase with Di-amine-benzidine (DAB) substrate kit (SK-4100, Vector Labs., Burlington, ON). The reaction was stopped by washing with water when the staining was sufficient; the same incubation time was applied to all samples. Tissues were counterstained with hematoxylin (HHS16, Sigma-Aldrich) and dehydrated by sequential incubation in 40% ethanol (1  $\times$  1 min), 75% ethanol (1  $\times$  1 min), 95% ethanol (1  $\times$  1 min), 100% ethanol (1  $\times$  1 min) and xylene (2  $\times$  5 min). Finally, slides were mounted with Cytoseal 60 (8310-4, Thermo Scientific, Burlington, ON) and scanned with a NanoZoomer 2.0-HT scanner (Hamamatsu). Images were processed with NDP.view 2.6.8 (NanoZoomer Digital Pathology.view 2.6.8)(Hamamatsu).

We purchased TMAs from US Biomax (catalogue no. PR807a and SK803, Rockville, MD). SK803 is a skin basal cell carcinoma tissue microarray with 30 cases of skin basal cell carcinoma, 18 benign naevi and 3 normal skins (all in duplicate). PR807a is a prostatic adenocarcinoma, hyperplasia and normal tissue microarray with 50 prostate adenocarcinomas, 20 benign prostatic hyperplasia and 3 cases of normal prostate (single core per case). TMAs from US Biomax were reviewed by two board certified pathologists.

**Immunofluorescence.** Immunofluorescence images were performed as described<sup>1</sup>. For antibodies see Supplementary Table 6. Images were acquired with a FV300 Olympus confocal microscope with a PMT first generation and Fluoview V4.2 or a Zeiss Axio Imager Z2 upright microscope with a CoolSNAP FX camera (Photometrics) and/or AxioCam camera and ZEN 2 Imager (2.0.14283.302). Images were processed with ImageJ (2.0.0-rc-49/1.51.g).

For superresolution structured illumination microscopy, images were acquired with Super Resolution microscope Axio Observer Z1 ZEISS Elyra PS.1, from Zeiss. Raw data were captured using EMCCD Du885K ISO VP461 camera. Images were acquired at 5 rotations and final image was generated using the structured illumination algorithm of ZEN 2.1 (V11.0.0.190).

**Fluorescence in situ hybridization (FISH).** For FISH,  $3 \times 10^5$  IMR90 cells were seeded onto 18 mm round glass coverslips overnight. Cells were washed once with 1  $\times$  PBS at room temperature and fixed by 4% paraformaldehyde/1  $\times$  PBS at room temperature for 10 min. Cells were washed twice with 1  $\times$  PBS at room temperature for 5 min followed by a wash with 1.5 ml of 70% ethanol per well. To dehydrate, cells were sequentially incubated at room temperature in 70% ethanol (1  $\times$  2 min), 85% ethanol (1  $\times$  2 min), 100% ethanol (1  $\times$  2 min), air dry at room temperature. To rehydrate, cells were incubated in 10% formamide/2 $\times$  SSC at room temperature for 10 min. Cells were then washed in fresh prehybridization solution (10% formamide/2 $\times$  SSC pH 7.2) for 10 min at room temperature. Antisense probe (5'-ACTCCGAGAGGGGTCGGAA-3') and sense probe (5'-TTCCGACCCCTCTCCGGAGTC-3') were purchased already labelled with a fluorophore Alexa fluor 594 (Invitrogen). For each hybridization, 25 ng of the antisense probe was used or 50 ng of the sense probe. Probes were mixed with 20  $\mu$ g of yeast tRNA:ssDNA, dried in a SpeedVac and dissolved in 40  $\mu$ l of 1  $\times$  hybridization solution (10% deionized formamide (Sigma)/10% dextran sulfate/2 $\times$ SSC/2 mM VRC (RNase inhibitor)/1% BSA New England Biolabs, Whitby, ON) and heated for 3 min at 95 °C. Reconstituted probe were centrifuged for 3 min at 17,500  $\times$ g, to eliminate any air from the sample. Probe hybridization mix was added to the cells, sealed with parafilm paper and incubated overnight in a humid chamber at 37 °C. Coverslips were transferred to a 12-well plate containing 10% formamide/2 $\times$ SSC for 30 min at 37 °C protected from light. Then, cells were washed twice with 2 $\times$ SSC for 30 min at room temperature. Cells were also washed with 1  $\times$  PBS and mounted with ProLong Gold with DAPI (Molecular



Probe, Logan, UT). Images were acquired with a Zeiss Z2 upright microscope and processed with ImageJ. Statistics source data for FISH are presented in Supplementary Table 5.

**Ribosome purification by sedimentation.** To separate ribosomal RPS14 from non-ribosomal RPS14 we modified a previously used protocol to purify these fractions<sup>42</sup>. Cells were washed once with 10 ml of ice-cold 1× PBS on ice. After thorough removal of the 1× PBS, 400 µl of ice-cold lysis Polysome buffer: 20 mM Tris-HCl pH 7.4, 150 mM NaCl, 5 mM MgCl<sub>2</sub>, 1 mM DTT, 1% Triton X-100 [BioShop], 25 U ml<sup>-1</sup> of DNase I-RNase free [Thermo Scientific] were added onto cells with a special attention to cover the entire surface of the dish. Cells were recovered by scrapping and clumps were dispersed by pipetting several times. Lysates were then transferred in a microfuge tube and incubated 10 min on ice. Then, lysates were centrifuged at 9,600×g for 10 min at 4°C to eliminate debris. To pellet ribosomes, 200 µl of supernatant were transferred to a 11 mm×34 mm polycarbonate ultracentrifuge tube (Beckman Coulter, no. 343778) and 600 µl of 1 M sucrose cushion (Polysome buffer, 1 M sucrose) were carefully added at the very bottom of the tube before centrifugation in a S150-AT rotor at 195,944×g for 4 hours at 4°C. Proteins from the supernatant were precipitated with methanol/chloroform. For 200 µl of supernatant, 800 µl of methanol were added and well vortexed. Then, 200 µl of chloroform were added and well vortexed. Then, 600 µl of ddH<sub>2</sub>O was added and well vortexed. After a 5 min centrifugation at 17,000×g, the top aqueous layer was discarded. Then, 800 µl of methanol were added, well vortexed, centrifuged 5 min at 17,000×g. The latter protein pellets as well as the ribosomal pellets were resuspended in 2× Laemmli sample buffer (4% SDS, 20% glycerol, 120 mM Tris-HCl pH 6.8.) for immunoblotting analysis. Total RNA from 200 µl of supernatant was extracted with 800 µl of TRIzol (Invitrogen) while RNA from ribosomal pellets was extracted with 1 ml of TRIzol and resolved with a formaldehyde agarose gel.

**RNA analysis, electrophoresis and northern blotting.** Pulse labelling of rRNA synthesis was performed as previously described<sup>41</sup>. Northern blots were performed as previously described<sup>41</sup>. Briefly, total RNA extracts were prepared in TRIzol (Invitrogen) according to the manufacturer's instructions. Seven µg of total RNA from IMR90 cells were resolved on 1% agarose-formaldehyde gels in Tricine-Triethanolamine and transferred on nylon membrane in 10× SSC by capillary. Probes were fluorescently labelled with DyLight 800 NHS Ester. The following probes were used: 5' of ITS1 (position 5520) (<sup>3</sup>H,N-5'-cctcgccctccggctcctgtaagatc-3'-NH<sub>2</sub>'), 3' of ITS1 (position 6512) (<sup>3</sup>H,N-5'-cgcccaagaggagaggggggttcctcag-3'-NH<sub>2</sub>'), and ITS2 (position 7564) (<sup>3</sup>H,N-5'-gctgcacggggcagcagcaccgctc-3'-NH<sub>2</sub>'). Bands were acquired with an Infrared Imaging System (model: Odyssey, model no: 9120, LI-COR, Biosciences) and quantified using Adobe Photoshop. 18S and 28S rRNA levels were used as loading controls and detected with methylene blue staining. Statistics source data for northern blots are presented in Supplementary Table 5.

**Immunoprecipitation.** 5×10<sup>6</sup> or 1.5×10<sup>6</sup> HEK-293T cells were seeded in 10 or 6 cm cell culture dishes respectively and grown for 24 hours. Then, cells were transiently transfected using the calcium phosphate method with 15 µg (10 cm) or 5 µg (6 cm) of pcDNA3.1(C1)-3xFLAG or pcDNA3.1(C1)-3xFLAG-RSL1D1 and cells were scraped 24 hours later. Three 10 cm cell culture dishes for each condition were used for mass spectrometry and one 6 cm cell culture dish for each condition was used for confirmation experiments. IMR90 cells were co-infected with retroviruses containing pBabe-3xFLAG-CDK4(K35M) or pLPC-3xFLAG and lentiviruses expressing shRSL1D1 (shR-A) and were scraped at day 10 post-infection. Forty 10 cm cell culture dishes for each condition were used for the mass spectrometry experiment. Co-immunoprecipitation and interaction domains mapping between CDK4 or Myc-cyclin D1 with FLAG-RPS14(WT) or FLAG-RPS14(2-88) or FLAG-RPS14(89-151) was confirmed in HEK-293 cells. Cells were transiently transfected using the calcium phosphate method with 15 µg (10 cm) of pcDNA3.1(C1)-3xFLAG, pcDNA3-FLAG-RPS14(WT), pcDNA3-FLAG-RPS14(2-88) or pcDNA3-RPS14(89-151) with pBabe-CDK4(WT) or pcDNA3-Myc-cyclin D1 in presence of 20 µM of MG132 (Sigma-Aldrich) for 12 hours and cells were scraped 24 hours post transfection. Co-immunoprecipitation between endogenous CDK4 and endogenous RPS14 was performed using two 10 cm cell culture dishes of PC3 cells or H1299 cells at 80% confluence for each condition.

Cells were scraped in IP buffer (50 mM Tris-HCl, pH 7.9, 1 mM EDTA, 0.1 mM EGTA, 12.5 mM MgCl<sub>2</sub>, 400 mM NaCl, 20% glycerol, 1% Triton X-100 (BioShop), 0.1% SDS and 1× complete-EDTA free protease inhibitor cocktail (Roche Applied Science)). Cell lysates were kept on ice for 15 min and then sonicated for 40 seconds at the lowest intensity. Cell lysates were cleared by centrifugation at 16,300×g for 1 min and immunoprecipitations were performed with anti-FLAG M2 Affinity Gel (no. A2220-5ML, lot: SLBT8835, Sigma-Aldrich, St Louis, MO) for 30 min at 4°C. For endogenous interaction between CDK4 and RPS14, immunoprecipitations were performed with anti-RPS14 rabbit polyclonal (5 µg per condition, A304-031A, lot: A304-031A-1, Bethyl Laboratories) or rabbit pre-immune serum for 90 min at 4°C. Then, immunoprecipitates were recovered with a 1:1 mix of protein-A and -G sepharose (Sigma-Aldrich). Protein-A/Protein-G sepharose mix and anti-FLAG M2 Affinity Gel were blocked for 1 hour at 4°C in IP

buffer containing 2.5% BSA, 0.16 µg µl<sup>-1</sup> salmon sperm DNA (Sigma-Aldrich) and 0.16 µg µl<sup>-1</sup> *E. coli* tRNA (Sigma-Aldrich) and then washed twice with IP buffer before immunoprecipitation. Immunoprecipitates were recovered after 30 min (45 min for endogenous IP) of incubation at 4°C and washed three times for 30 min in IP buffer. Proteins of immunoprecipitates and total cell lysates were separated by SDS-PAGE and transferred to nitrocellulose membranes and analysed by Western Blotting with the antibodies described in the section Immunoblotting. For mass spectrometry analysis, proteins from immunoprecipitates were separated by SDS-PAGE, stained with Coomassie and gels from each condition were cut in four pieces for analysis by LC-MS/MS.

**Liquid chromatography and mass spectrometry (LC-MS/MS).** Bands were shrunk in 50% acetonitrile (ACN) and reconstituted in 50 mM ammonium bicarbonate with 10 mM TCEP and vortexed for 1 hour at 37°C. Chloroacetamide was added for alkylation to a final concentration of 55 mM. Samples were vortexed for another hour at 37°C prior to addition of 1 µg of trypsin and the digestion was left for 8 hours at 37°C. Peptide extraction was conducted with 90% ACN. Extracted peptide samples were dried down and solubilized in 5% ACN/0.2% formic acid (FA). Samples were loaded on a homemade C18 precolumn (0.3 mm i.d. x 5 mm) connected directly to the switching valve and separated on a homemade reversed-phase column (150 µm i.d. x 150 mm) with a 56-min gradient from 10–30% acetonitrile (0.2% FA) and a 600 nl min<sup>-1</sup> flow rate on a NanoLC-2D system (Eksigent, Dublin, CA) connected to an Q-Exactive Plus (Thermo Fisher Scientific). Each full MS spectrum acquired with a 60,000 resolution was followed by 12 MS/MS spectra, where the 12 most abundant multiply charged ions were selected for MS/MS sequencing. Tandem MS experiments were performed using HCD. The data were processed using PEAKS 7.0 (Bio-informatics Solutions, Waterloo, ON) and the Uniprot database. Tolerances on precursors and fragments were 15 ppm and 0.01 Da, respectively. Variable selected post-translational modifications were carbamidomethyl (C), oxidation (M), deamidation (NQ) and phosphorylation (STY).

**Bioinformatic analysis of data from LC-MS/MS.** After the protein identification described above, the full list of all proteins was analysed using the FatiGO analysis tool<sup>44</sup> on the Babelomics 4.3 and 5.0 platforms. In order to identify overrepresented groups, the identified proteins were compared to the whole genome protein list provided by the Babelomics platform (<http://babelomics.bioinfo.cipf.es/>). The databases used were GO biological process, GO molecular function and GO cellular component. Significance was determined using a two-tailed Fisher exact test. The GO terms and their associated proteins were then grouped in general categories based on knowledge and literature.

**In vitro protein phosphorylation.** Recombinant RPS14-Myc-FLAG was produced in HEK-293 cells transiently transfected using the calcium phosphate method with 15 µg (10 cm) of pCMV6-RPS14-Myc-FLAG and then immunoprecipitated with anti-FLAG M2 Affinity Gel as previously described, washed three times for 5 min in 1×TBS, eluted for 1 hour at 4°C with 250 ng µl<sup>-1</sup> of FLAG peptide (Sigma-Aldrich) in 1×TBS and protein concentration was evaluated using a NanoDrop2000c spectrophotometer (A280).

Human active CDK4/cyclin D1 (cat. no. C0620, lot: SLBK7657V, Sigma-Aldrich, St. Louis, MO) or human active CDK1/cyclin B1 (cat. no. C22-10G, lot: E094-1, SignalChem, Richmond, BC) were incubated alone or with human recombinant GST-Rb (773-928) (cat. no. R05-55G, lot M166-3, SignalChem) in presence or absence of pabociclib (1 µM) or staurosporine (1 µM) or with a gradient of human recombinant RPS14-Myc-FLAG in kinase assay buffer 1 (cat. no. K01-09, SignalChem): 25 mM MOPS, pH 7.2, 12.5 mM β-glycerol-phosphate, 25 mM MgCl<sub>2</sub>, 5 mM EGTA, 2 mM EDTA, 0.25 mM dithiothreitol (DTT), 40 µM ATP with or not 1 µCi (γ-<sup>32</sup>P)ATP at 30°C for 30 min. Then Laemmli buffer was added to stop the reaction, samples were boiled at 98°C for 5 min and the reaction products were separated by SDS-PAGE, transferred to nitrocellulose membranes and <sup>32</sup>P incorporation was analysed by autoradiography and quantified with Adobe Photoshop. Total proteins were visualized with Ponceau. IC<sub>50</sub> of RPS14 on 0.5 µg of CDK4/cyclin D1 was determined by quantifying <sup>32</sup>P incorporation in function of RPS14 amount from three independent experiments.

**In vitro protein interaction (GST pulldown assay).** Human recombinant RPS14-Myc-FLAG was produced as previously described (see 'In vitro protein phosphorylation'). GST (50 ng) (cat. no. SRP5348, lot: F664-2, Sigma-Aldrich, St Louis, MO) or GST tagged human active CDK4/cyclin D1 (50 ng) (cat. no. C0620, lot: SLBK7657V, Sigma-Aldrich) or GST tagged human CDK4 (50 ng) (cat. no. C31-14G, lot: K127-1, Signal Chem, Richmond, BC) or GST tagged human cyclin D1 (50 ng) (cat. no. 009-001-153S, lot: 37136, Rockland Antibodies & Assays, Limerick, PA) were incubated with human recombinant RPS14-Myc-FLAG (200 ng) in 300 µl of PB buffer (20 mM Hepes, pH 7.5, 130 mM KCl, 5 mM MgCl<sub>2</sub>, 1 mM DTT, 0.5 mM EDTA, 0.05% NP40) and mixed using a rotating machine at 30°C for 2 hours. Proper amounts of glutathione-Sepharose beads (cat. no. 17-0756-01, GE Healthcare, Sweden) were washed three times with PB buffer. Then, 10 µl of glutathione beads and 5 µl of BSA (25% stock solution) were added to proteins mix and incubation continued at room temperature for

30 min with rotation. The beads were then washed three times for 15 minutes with PB buffer at room temperature with rotation. Then, the appropriated quantity of 6× loading buffer (0.5 M Tris-HCl pH6.8, 30% glycerol, 10% SDS, 1% bromophenol blue and 15% β-mercaptoethanol) was added. The samples were boiled for 5 min and separated by SDS-PAGE for western blotting.

**Real-time PCR.** Total RNA extracts were prepared in TRIzol (Invitrogen) according to the manufacturer's instructions. Total RNA was reverse transcribed and gene expression level was determined with a LightCycler 480 (software release 1.5.1.62 SP2) and/or a LightCycler 96 (software version 1.1) Real-Time PCR System (Roche Applied Science), using SYBR Green technologies as described before<sup>7</sup>. qPCR primers are presented in Supplementary Table 4. Source data for qPCR are presented in Supplementary Table 5.

**Statistics and reproducibility.** Statistical analysis (two-tailed Student's *t*-test) was performed using Excel and (Mann-Whitney U test) was performed using Statistica software (StatSoft, Tulsa, OK). A value of  $P < 0.05$  was considered statistically significant. Experiments were repeated at least three times, except for those in Figs. 1g–h, 2d, 5c and 6j–m and Supplementary Figs. 2a–c, 3e–g,i–j, 4a,f, 5b (CDK6), 5c–m, 6a–e,i, 7a (PML), 7b–c and 8a–h, which were repeated twice, and Supplementary Figs. 3b–d, 4b–e,g–j, 5a (CDK6) and Supplementary Tables 1 and 2, which were performed once. Experiments that were only performed once or twice include three technical replicates except Fig. 5c where immunoblots were performed using two independent shRNAs and Fig. 6k where immunoblots were performed twice. Also in many instances of 1 or 2 independent experiments data were collected from replicates of two independent shRNAs or in different models of senescence adding robustness to the results. For SA-β-Gal, data were quantified from many fields within one experiment to properly represent the entire petri

dish and subsequently confirmed as described in figure captions. For IF, data were quantified from three technical counts within one experiment and subsequently confirmed as described in figure captions.

**Reporting Summary.** Further information on experimental design is available in the Nature Research Reporting Summary linked to this article.

**Data availability.** Mass spectrometry data have been deposited in ProteomeXchange with the primary accession code [PASS01176](#). Source data for Figs. 1e–f, 4h, 5a–b, 6a,c,e,g,i,l–m and 7d and Supplementary Figs. 1b–d, 2d–e, 3b–g,i–j, 4b–j, 5b–h,j–m, 6a–e,i and 8a,c,e,g can be found in Supplementary Table 5. All other data that support the findings of this study are available from the corresponding author upon reasonable request.

## References

1. Lessard, F. et al. The ARF tumor suppressor controls ribosome biogenesis by regulating the RNA polymerase I transcription factor TTF-I. *Mol. Cell* **38**, 539–550 (2010).
2. Ingolia, N. T., Brar, G. A., Rouskin, S., McGeachy, A. M. & Weissman, J. S. The ribosome profiling strategy for monitoring translation in vivo by deep sequencing of ribosome-protected mRNA fragments. *Nat. Protoc.* **7**, 1534–1550 (2012).
3. Scott, D. D. et al. Npl12 is a multifunctional RNA binding protein at the nexus of RNA and DNA metabolism. *Nucleic Acids Res.* **45**, 12509–12528 (2017).
4. Al-Shahrour, F., Diaz-Uriarte, R. & Dopazo, J. FatiGO: a web tool for finding significant associations of Gene Ontology terms with groups of genes. *Bioinformatics* **20**, 578–580 (2004).

## Reporting Summary

Nature Research wishes to improve the reproducibility of the work that we publish. This form provides structure for consistency and transparency in reporting. For further information on Nature Research policies, see [Authors & Referees](#) and the [Editorial Policy Checklist](#).

### Statistical parameters

When statistical analyses are reported, confirm that the following items are present in the relevant location (e.g. figure legend, table legend, main text, or Methods section).

n/a Confirmed

- The **exact sample size** ( $n$ ) for each experimental group/condition, given as a discrete number and unit of measurement
- An indication of whether measurements were taken from distinct samples or whether the same sample was measured repeatedly
- The statistical test(s) used AND whether they are one- or two-sided  
*Only common tests should be described solely by name; describe more complex techniques in the Methods section.*
- A description of all covariates tested
- A description of any assumptions or corrections, such as tests of normality and adjustment for multiple comparisons
- A full description of the statistics including **central tendency** (e.g. means) or other basic estimates (e.g. regression coefficient) AND **variation** (e.g. standard deviation) or associated **estimates of uncertainty** (e.g. confidence intervals)
- For null hypothesis testing, the test statistic (e.g.  $F$ ,  $t$ ,  $r$ ) with confidence intervals, effect sizes, degrees of freedom and  $P$  value noted  
*Give  $P$  values as exact values whenever suitable.*
- For Bayesian analysis, information on the choice of priors and Markov chain Monte Carlo settings
- For hierarchical and complex designs, identification of the appropriate level for tests and full reporting of outcomes
- Estimates of effect sizes (e.g. Cohen's  $d$ , Pearson's  $r$ ), indicating how they were calculated
- Clearly defined error bars  
*State explicitly what error bars represent (e.g. SD, SE, CI)*

*Our web collection on [statistics for biologists](#) may be useful.*

### Software and code

Policy information about [availability of computer code](#)

Data collection

Immunofluorescence and Fluorescence In Situ Hybridization : Image acquisition with ZEN 2 Imager (2.0.14283.302) (Zeiss).  
Superresolution microscopy : Final image was generated using the structured illumination algorithm of ZEN 2.1 (V11.0.0.190) (Zeiss).  
Real-time PCR: Data collection with a LightCycler 480 (software release 1.5.1.62 SP2) and/or a LightCycler 96 (software version 1.1).

Data analysis

Immunohistochemistry: Images were processed with NDP.view 2.6.8 (Hamamatsu Photonics).  
Immunofluorescence and Fluorescence In Situ Hybridization: Images were processed with Image J (2.0.0-rc-49/1.51g).  
Liquid Chromatography and mass spectrometry (LC-MS/MS): The data were processed using PEAKS 7.0 (Bio-informatics Solutions).  
Bioinformatic of LC-MS/MS : With Fatigo analysis tool on the Babelomics 4.3 and 5.0 platforms (<http://babelomics.bioinfo.cipf.es/>).  
Real-time PCR: With a LightCycler 480 (software release 1.5.1.62 SP2) and/or a LightCycler 96 (software version 1.1).

For manuscripts utilizing custom algorithms or software that are central to the research but not yet described in published literature, software must be made available to editors/reviewers upon request. We strongly encourage code deposition in a community repository (e.g. GitHub). See the Nature Research [guidelines for submitting code & software](#) for further information.

### Data

Policy information about [availability of data](#)

All manuscripts must include a [data availability statement](#). This statement should provide the following information, where applicable:

- Accession codes, unique identifiers, or web links for publicly available datasets
- A list of figures that have associated raw data
- A description of any restrictions on data availability

The datasets that support the findings of this study are available upon reasonable request from the first and the corresponding author.

## Field-specific reporting

Please select the best fit for your research. If you are not sure, read the appropriate sections before making your selection.

Life sciences  Behavioural & social sciences

For a reference copy of the document with all sections, see [nature.com/authors/policies/ReportingSummary-flat.pdf](https://nature.com/authors/policies/ReportingSummary-flat.pdf)

## Life sciences

### Study design

All studies must disclose on these points even when the disclosure is negative.

Sample size	No sample size calculations were performed. Sample size was determined after discussions with team members and from our experience on calculating statistical significance. For SA-beta-gal, data were quantified from many fields to properly represent the entire petri dish. For IF, data were quantified from 100 cell counts in triplicate to properly represent the entire petri dish. For QPCR, data were derived from technical triplicates. For northern blots, data were derived from biological triplicates. For growth-curves, data were derived from 3 different petri dishes. For nucleolar area and mean intensity, data were quantified from more than 90 nucleolus to properly represent variability between cells and conditions. For superresolution microscopy, the number of cells taken is related to time and space for data. For more precision, see figure legends and methods.
Data exclusions	We did not take in consideration the 7 samples of cancer adjacent normal prostate tissue from the prostate tissue microarray. Our objective was to compare normal tissue, cancer tissue and benign prostatic hyperplasia. Those excluded samples have a genetic background leading to tumorigenesis and we wanted to take in consideration only real normal tissue.
Replication	All n are identified in figure legends. Experiments are reproducible and unreproducible experiments are not presented in this paper. Mass spectrometry experiments have been done once but interaction important for this article were replicated.
Randomization	Allocation was not random. Covariates were controlled: By using control empty vectors, control shRNA and independent shRNA. By doing time courses. By comparing different models of senescence. By studying senescence phenotypes with different markers and with different technics. By using different cell lines. By showing protein interactions with different technics as mass spectrometry, overexpression, mapping, at the endogenous level, in vitro interaction and with kinase assay.
Blinding	Blinding was not relevant to our study considering that for all cellular experiments different extracts were analysed by different persons. See authors' contributions for a description of how people reproduced data from other people.

### Materials & experimental systems

Policy information about [availability of materials](#)

n/a	Involved in the study
<input type="checkbox"/>	<input checked="" type="checkbox"/> Unique materials
<input type="checkbox"/>	<input checked="" type="checkbox"/> Antibodies
<input type="checkbox"/>	<input checked="" type="checkbox"/> Eukaryotic cell lines
<input checked="" type="checkbox"/>	<input type="checkbox"/> Research animals
<input checked="" type="checkbox"/>	<input type="checkbox"/> Human research participants

#### Unique materials

Obtaining unique materials	<p>anti-UBF(#8) rabbit polyclonal (1 :1000, clone #8) was raised against mouse UBF (aa 2-404) and kindly provided by Dr. Tom Moss (Centre de recherche sur le cancer, Université Laval, QC). -The amount of the antibody is limited, but Dr. Tom Moss regularly provide aliquots.</p> <p>Interferon beta-1a (β-IFN) (Avonex, Biogen Idec) was a gift from Dr. Darren P. Baker (Biogen Idec, Cambridge, MA). -This protein is commercially available.</p>
----------------------------	--

## Antibodies

### Antibodies used

Antibodies identification (see Supplementary Table 6).

#### For IHC:

anti-INK4a rabbit monoclonal (1:250, EPR1473, lot : GR155011-2 , ab108349, Abcam, Toronto, ON).  
anti-RPL29 rabbit polyclonal (1:250, GTX101833, lot : 40681, Gene Tex, Irvine, CA).

#### For IF:

anti-FBL rabbit monoclonal (1:350, clone C13C3, #2639, lot : 2, Cell Signaling Technology, Pickering, ON).  
anti-RPL29 mouse polyclonal (1:125, #H00006159-B01P, lot : 10230, Novus Biologicals, Oakville, ON).  
anti-RPS14 rabbit polyclonal (1:80, clone H-130, sc-68873, lot : C1914, Santa Cruz Biotechnology, Santa Cruz, CA).  
anti-53BP1 rabbit polyclonal (1:200, Ab-1, Cat# PC712, lot : D00137736, Calbiochem, EMD Biosciences, San Diego, CA).  
anti-phospho-gammaH2A.XS139 mouse monoclonal (1:100, JBW-301, Cat# 05-636-l, lot : 2552645, Millipore, Billerica, MA).  
anti-cyclin D1 mouse monoclonal (1:60, clone HD11, sc-246, lot : D2108 , Santa Cruz Biotechnology, Santa Cruz, CA).  
anti-PML rabbit polyclonal (1:200, A301-167A, lot : A301-167A-2, Bethyl Laboratories).  
goat anti-rabbit IgG (H+L) conjugated to Alexa Fluor 488 (1:1000, #A11008, lot: 1166843, Molecular Probes, Invitrogen, Eugene, OR).  
goat anti-mouse IgG (H+L) conjugated to Alexa Fluor 488 (1:1000, #A11029, lot: 1423008, Life Technologies, Eugene, OR).  
goat anti-rabbit IgG (H+L) conjugated to Alexa Fluor 568 (1:1000, #A11036, lot: 1504529, Life Technologies, Eugene, OR).  
goat anti-mouse IgG (H+L) conjugated to Alexa Fluor 568 (1:1000, #A11031, lot: 1398018, Life Technologies, Eugene, OR).

#### For IP:

anti-RPS14 rabbit polyclonal (5 µg per condition, A304-031A, lot : A304-031A-1, Bethyl Laboratories, Montgomery TX).  
anti-FLAG mouse monoclonal Affinity Gel (#A2220-5ML, lot: SLBT8835, Sigma-Aldrich, St. Louis, MO).

#### For WB:

anti-H-RAS mouse monoclonal (1:250, clone F235, Sc-29, lot : C0608, Santa Cruz Biotechnology, Santa Cruz, CA).  
anti-PML rabbit polyclonal (1:1000, A301-167A, lot : A301-167A-2, Bethyl Laboratories, Montgomery, TX).  
anti-phospho-H3S10 rabbit polyclonal (1:1000, #06-570, lot : 2517793, Millipore, Billerica, MA).  
anti-RSL1D1 goat polyclonal (1:1000, GTX88161, lot : 821500642, GeneTex, San Antonio, TX).  
anti-RSL1D1 rabbit polyclonal (1:4000, HPA043483, lot : R40297, Sigma-Aldrich).  
anti-NS rabbit polyclonal (1:1000, clone H-270, Sc-67012, lot : G1009, Santa Cruz Biotechnology, Santa Cruz, CA).  
anti-DDX21 rabbit polyclonal (1:1000, GTX115199, lot : 40618, GeneTex).  
anti-EBP2 goat polyclonal (1:500, clone N-13, sc-46316, lot : H1611, Santa Cruz Biotechnology, Santa Cruz, CA).  
anti-MCM6 rabbit polyclonal (1:1000, A300-194A, lot : A300-194A-2, Bethyl Laboratories).  
anti-p53 mouse monoclonal (1:1000, clone DO-1, Sc-126, lot : C1413, Santa Cruz Biotechnology, Santa Cruz, CA).  
anti-phospho-p53S15 rabbit polyclonal (1:500, #9284, lot : 9, Cell Signaling).  
anti-FLAG mouse monoclonal (1:1000, F1804, M2, lot : SLBK1346V, Sigma-Aldrich).  
anti-c-Myc rabbit polyclonal (1:1000, clone A-14, sc-789, lot : K0215, Santa Cruz Biotechnology, Santa Cruz, CA).  
anti-Myc tag mouse monoclonal (1:2000, 9E10, lot : 114K4821, Sigma, Saint Louis, Missouri).  
anti-phospho-RBS795 rabbit polyclonal (1:500, #9301, lot : 13, Cell Signaling).  
anti-RB mouse monoclonal (1:1000, clone G3-245, #554136, lot : 71957, BD Pharmingen).  
anti-RPL29 rabbit polyclonal (1:1000, GTX101833, lot : 40681, GeneTex, Irvine, CA).  
anti-RPS14 rabbit polyclonal (1:1000, clone H-130, sc-68873, lot : C1914, Santa Cruz Biotechnology, Santa Cruz, CA).  
anti-RPS14 rabbit polyclonal (1:4000, A304-031A, lot : A304-031A-1, Bethyl Laboratories, Montgomery TX).  
anti-RPS3 mouse monoclonal (1:1000, clone C-7, sc-376008, lot : D2116, Santa Cruz Biotechnology, Santa Cruz, CA).  
anti-CDK4 rabbit polyclonal (1:2000, A304-225A, lot : A304-225A-1, Bethyl Laboratories).  
anti-α-Tubulin mouse monoclonal (1:20000, clone B-5-1-2, T6074, lot : 023M4813, Sigma-Aldrich).  
anti-GST mouse monoclonal (1:2000, clone GST-2, G1160, lot : 012M4814, Sigma-Aldrich).  
anti-H3 rabbit polyclonal (1:2000, clone ab1791, lot : GR206453-1, Abcam).  
anti-CDK4(HRP) rabbit monoclonal (1:2000, clone ab193968, lot : GR205710-1, Abcam).  
anti-UBF(#8) rabbit polyclonal (1 :1000, clone #8) was raised against mouse UBF (aa 2-404) and kindly provided by Dr. Tom Moss (Centre de recherche sur le cancer, Université Laval, QC).  
goat anti-rabbit IgG (H-L) conjugated to HRP (1:3000, #170-6515, lot: 64126042, Bio-Rad, Mississauga, ON).  
goat anti-mouse IgG (H-L) conjugated to HRP (1:3000, #170-6516, lot: 64132955, Bio-Rad, Mississauga, ON).  
donkey anti-goat IgG conjugated to HRP (1:3000, Sc-2020, lot: E2313, Santa Cruz Biotechnology, Santa Cruz, CA).

### Validation

Antibodies identification (see Supplementary Table 6).

#### For IHC:

anti-INK4a rabbit monoclonal (1:250, EPR1473, lot : GR155011-2 , ab108349, Abcam, Toronto, ON). Tested by western blot (WB) after overexpression of human INK4a and by IHC on human samples. Cited 24 times on company website (Many for WB and IHC in human).

anti-RPL29 rabbit polyclonal (1:250, GTX101833, lot : 40681, Gene Tex, Irvine, CA). Tested by western blot on IMR90 cells and by IHC on human samples. Tested by company for IHC and WB on human cell lines.

#### For IF:

anti-FBL rabbit monoclonal (1:350, clone C13C3, #2639, lot : 2, Cell Signaling Technology, Pickering, ON). Tested by WB on IMR90 cells. Cited 17 times on company website. Tested by company for IF and WB on human cells.

anti-RPL29 mouse polyclonal (1:125, #H00006159-B01P, lot : 10230, Novus Biologicals, Oakville, ON). We used and tested this antibody only for IF. Tested by company for IHC, IF and WB of human cells.

anti-RPS14 rabbit polyclonal (1:80, clone H-130, sc-68873, lot : C1914, Santa Cruz Biotechnology, Santa Cruz, CA). Tested by WB after depletion of RPS14 with two different shRNA in many human cell lines and by IF on IMR90 cells. Cited 3 times on company website. Tested by company or reviewer for WB, IF and IHC on human cells.

anti-53BP1 rabbit polyclonal (1:200, Ab-1, Cat# PC712, lot : D00137736, Calbiochem, EMD Biosciences, San Diego, CA). We routinely use this antibody for IF. On company website : Key applications are IF, WB and IP. Works for human and mouse.

anti-phospho-gammaH2A.XS139 mouse monoclonal (1:100, JBW-301, Cat# 05-636-1, lot : 2552645, Millipore, Billerica, MA). We routinely use this antibody for IF. On company website : Well published antibody validated in ChIP, ICC, IF and WB. Works for human, mouse and rat.

anti-cyclin D1 mouse monoclonal (1:60, clone HD11, sc-246, lot : D2108 , Santa Cruz Biotechnology). Cited 189 times on company website. We used and tested this antibody only for IF. Tested by company or reviewer for WB, IF and IHC on human cells.

anti-PML rabbit polyclonal (1:200, A301-167A, lot : A301-167A-2, Bethyl Laboratories). Cited 37 times on company website. We used and tested this antibody for WB and IF on human IMR90 cells. Tested by company for WB, IP, IHC and IF on human cells.

goat anti-rabbit IgG (H+L) conjugated to Alexa Fluor 488 (1:1000, #A11008, lot: 1166843, Molecular Probes, Invitrogen, Eugene, OR). We routinely use this antibody for IF. On company website : More than 50 000 published references, applications and experimental tips.

goat anti-mouse IgG (H+L) conjugated to Alexa Fluor 488 (1:1000, #A11029, lot: 1423008, Life Technologies, Eugene, OR). We routinely use this antibody for IF. On company website : More than 50 000 published references, applications and experimental tips.

goat anti-rabbit IgG (H+L) conjugated to Alexa Fluor 568 (1:1000, #A11036, lot: 1504529, Life Technologies, Eugene, OR). We routinely use this antibody for IF. On company website : More than 50 000 published references, applications and experimental tips.

goat anti-mouse IgG (H+L) conjugated to Alexa Fluor 568 (1:1000, #A11031, lot: 1398018, Life Technologies, Eugene, OR). We routinely use this antibody for IF. On company website : More than 50 000 published references, applications and experimental tips.

For IP:

anti-RPS14 rabbit polyclonal (5 µg per condition, A304-031A, lot : A304-031A-1, Bethyl Laboratories, Montgomery TX). Tested by IP (PC3 and NCI-H1299) and WB on many human cell lines. Tested by company for IP and WB on human cells.

anti-FLAG mouse monoclonal Affinity Gel (#A2220-5ML, lot: SLBT8835, Sigma-Aldrich, St. Louis, MO). Cited 300 times on company website. Tested for IP after overexpression of different Flag-tagged-proteins.

For WB:

anti-H-RAS mouse monoclonal (1:250, clone F235, Sc-29, lot : C0608, Santa Cruz Biotechnology, Santa Cruz, CA). Cited 64 times on company website. Tested by WB after overexpression of H-RASv12 in IMR90 cells. Tested by company or reviewer for WB and IHC on human cells.

anti-PML rabbit polyclonal (1:1000, A301-167A, lot : A301-167A-2, Bethyl Laboratories, Montgomery, TX). Cited 37 times on company website. We used and tested this antibody for WB and IF on human IMR90 cells. Tested by company for WB, IP, IHC, IF and PLA (proximity ligation assay) on human cells.

anti-phospho-H3S10 rabbit polyclonal (1:1000, #06-570, lot : 2517793, Millipore, Billerica, MA). Tested by WB after different induction of cell cycle arrest. On company website : This highly published antibody has been validated in ICC, IP and WB. Works for human and mouse.

anti-RSL1D1 goat polyclonal (1:1000, GTX88161, lot : 821500642, GeneTex, San Antonio, TX). Tested by WB after depletion of RSL1D1 with two different shRNA in human IMR90 cells. Tested by company for WB on human cells.

anti-RSL1D1 rabbit polyclonal (1:4000, HPA043483, lot : R40297, Sigma-Aldrich). Tested by WB and IHC on human cells. On company website : (Human Protein Atlas) This antibody has been used for staining of 44 normal human tissue samples as well as human cancer samples covering the 20 most common cancer types and up to 12 patients for each cancer type.

anti-NS rabbit polyclonal (1:1000, clone H-270, Sc-67012, lot : G1009, Santa Cruz Biotechnology). Tested by WB after depletion of NS with two different shRNA in human IMR90 cells. Tested by company for WB and IF on human cells.

anti-DDX21 rabbit polyclonal (1:1000, GTX115199, lot : 40618, GeneTex). Tested by WB after depletion of DDX21 with two different shRNA in human IMR90 cells. Tested by company for WB and IF on human cells.

anti-EBP2 goat polyclonal (1:500, clone N-13, sc-46316, lot : H1611, Santa Cruz Biotechnology). Tested by WB after depletion of EBP2 with two different shRNA in human IMR90 cells. Tested by company for WB and IF on human cells.

anti-MCM6 rabbit polyclonal (1:1000, A300-194A, lot : A300-194A-2, Bethyl Laboratories). Cited 6 times on company website. We routinely use this antibody for WB and tested by WB after different induction of cell cycle arrest. Tested by company for WB

and IHC on human cells.

anti-p53 mouse monoclonal (1:1000, clone DO-1, Sc-126, lot : C1413, Santa Cruz Biotechnology). Cited 1668 times on company website. Tested by WB and IF. Tested by company for WB, IF and IHC.

anti-phospho-p53S15 rabbit polyclonal (1:500, #9284, lot : 9, Cell Signaling). Cited 506 times on company website. Used for WB after nucleolar stress or induction of senescence.

anti-FLAG mouse monoclonal (1:1000, F1804, M2, lot : SLBK1346V, Sigma-Aldrich). Cited 387 times on company website. Tested for WB and IP after overexpression of different Flag-tagged-proteins.

anti-c-Myc rabbit polyclonal (1:1000, clone A-14, sc-789, lot : K0215, Santa Cruz Biotechnology). Cited 429 times on company website. Tested for WB after overexpression of Myc-tagged-proteins. Tested by company for WB and IF after overexpression of Myc-tagged-proteins.

anti-Myc tag mouse monoclonal (1:2000, 9E10, lot : 114K4821, Sigma, Saint Louis, Missouri). Cited 1036 times on company website. Tested for WB after overexpression of Myc-tagged-proteins. Tested by company for WB and IF after overexpression of Myc-tagged-proteins.

anti-phospho-RBS795 rabbit polyclonal (1:500, #9301, lot : 13, Cell Signaling). Cited 74 times on company website. We routinely use this antibody for WB and tested by WB after different induction of cell cycle arrest. Tested by company for WB on human cells.

anti-RB mouse monoclonal (1:1000, clone G3-245, #554136, lot : 71957, BD Pharmingen). 9 references on company website. Tested by WB on human cells. Tested by company for WB and IF on human cell lines.

anti-RPL29 rabbit polyclonal (1:1000, GTX101833, lot : 40681, GeneTex, Irvine, CA). Tested by western blot on IMR90 cells and by IHC on human samples. Tested by company for IHC and WB on human cell lines.

anti-RPS14 rabbit polyclonal (1:1000, clone H-130, sc-68873, lot : C1914, Santa Cruz Biotechnology, Santa Cruz, CA). Tested by WB after depletion of RPS14 with two different shRNA in many human cell lines and by IF on IMR90 cells. Cited 3 times on company website. Tested by company or reviewer for WB, IF and IHC on human cells.

anti-RPS14 rabbit polyclonal (1:4000, A304-031A, lot : A304-031A-1, Bethyl Laboratories, Montgomery TX). Tested by IP and WB on human cell lines. Tested by company for IP and WB on human cells.

anti-RPS3 mouse monoclonal (1:1000, clone C-7, sc-376008, lot : D2116, Santa Cruz Biotechnology). Tested for WB on different human cell lines. Tested by company or reviewer for WB and IHC on human cells.

anti-CDK4 rabbit polyclonal (1:2000, A304-225A, lot : A304-225A-1, Bethyl Laboratories). Tested for WB and IP on human cells. Tested by company for WB, IP and IHC on human cells.

anti- $\alpha$ -Tubulin mouse monoclonal (1:20000, clone B-5-1-2, T6074, lot : 023M4813, Sigma-Aldrich). Cited 449 times on company website. Tested for WB on human cells. Tested by company for WB, and IF on human cells.

anti-GST mouse monoclonal (1:2000, clone GST-2, G1160, lot : 012M4814, Sigma-Aldrich). Cited 57 times on company website. Tested on many purchased GST-tagged recombinant proteins. Tested by company on GST purified protein by WB.

anti-H3 rabbit polyclonal (1:2000, clone ab1791, lot : GR206453-1, Abcam). Cited 1477 times on company website. Tested for WB on IMR90 cells. Tested by company for WB, IP, IF, IHC and ChIP on human cell lines.

anti-CDK4(HRP) rabbit monoclonal (1:2000, clone ab193968, lot : GR205710-1, Abcam). Tested for WB on PC3 and NCI-H1299 human cell lines. Tested by company for WB and IHC on human cells.

anti-UBF(#8) rabbit polyclonal (1 :1000, clone #8) was raised against mouse UBF (aa 2-404) and kindly provided by Dr. Tom Moss (Centre de recherche sur le cancer, Université Laval, QC). Tested by WB and IF on IMR90 cells. This antibody is also working by WB and IF on mouse cells.

See :

1-Hamdane, N. et al. (2014). Conditional Inactivation of Upstream Binding Factor Reveals Its Epigenetic Functions and the Existence of a Somatic Nucleolar Precursor Body. *PLoS Genet* 10(8): e1004505. <https://doi.org/10.1371/journal.pgen.1004505>  
2-Lessard, F. et al. (2010). The ARF tumor suppressor controls ribosome biogenesis by regulating the RNA polymerase I transcription factor TTF-I. *Mol Cell* 38, 539-550.

goat anti-rabbit IgG (H-L) conjugated to HRP (1:3000, #170-6515, lot: 64126042, Bio-Rad, Mississauga, ON). We routinely use this antibody for WB. Cited 125 times on company website.

goat anti-mouse IgG (H-L) conjugated to HRP (1:3000, #170-6516, lot: 64132955, Bio-Rad, Mississauga, ON). We routinely use this antibody for WB. Cited 104 times on company website.

donkey anti-goat IgG conjugated to HRP (1:3000, Sc-2020, lot: E2313, Santa Cruz Biotechnology). We routinely use this antibody for WB. Cited 677 times on company website.

## Eukaryotic cell lines

Policy information about [cell lines](#)

Cell line source(s)	Phoenix amphi packaging cells were a gift from S. W. Lowe. (HEK)-293T, U2OS, PC3 and H1299 cells were obtained from American Type Culture Collection (ATCC, Manassas, VA). IMR90 cells were obtained from the American Type Culture Collection (ATCC, Manassas, VA) and/or from Coriell Institute for Medical Research (Camden, NJ). MUTZ-8 cells were obtained from the Leibniz Institute DSMZ-German Collection of Microorganisms and Cell Cultures
Authentication	Certificate of authentication was provided for normal human fibroblasts IMR90 cells from Coriell. MUTZ-8 cells underwent a careful identity control in the Leibniz Institute : <a href="https://www.dsmz.de/catalogues/catalogue-human-and-animal-cell-lines/quality-assurance/identity-control.html">https://www.dsmz.de/catalogues/catalogue-human-and-animal-cell-lines/quality-assurance/identity-control.html</a> . All other cell lines comes from ATCC and we confirmed their key molecular characteristics relevant for our study: H1299 and PC3 are p53 negative, U2OS are p53 wild type. Also their morphology is the same as published in many other papers with these cell lines. Phoenix amphi packaging cells were not authenticated and were used only for retrovirus production.
Mycoplasma contamination	All cell lines tested negative for mycoplasma contamination.
Commonly misidentified lines (See <a href="#">ICLAC</a> register)	(HEK) 293T cells : We use them for retroviral and lentiviral production, coimmunoprecipitation after overexpression of recombinant proteins and purification of recombinant proteins.

## Method-specific reporting

n/a	Involvement in the study
<input checked="" type="checkbox"/>	<input type="checkbox"/> ChIP-seq
<input checked="" type="checkbox"/>	<input type="checkbox"/> Flow cytometry
<input checked="" type="checkbox"/>	<input type="checkbox"/> Magnetic resonance imaging



## Antibodies

	Host	Dilution	Clone	Lot	Catalogue #	Company
IHC						
anti-INK4a	rabbit monoclonal	1/250	EPR1473	GR155011-2	ab108349	Abcam
anti-RPL29	rabbit polyclonal	1/250		40681	GTX101833	Gene Tex
IF						
anti-FBL	rabbit monoclonal	1/350	C13C3	2	2639	Cell Signaling Technology
anti-RPL29	mouse polyclonal	1/125		10230	H00006159-B01P	Novus Biologicals
anti-RPS14	rabbit polyclonal	1/80	H-130	C1914	sc-68873	Santa Cruz Biotechnology
anti-53BP1	rabbit polyclonal	1/200	Ab-1	D00137736	PC712	Calbiochem
anti-phospho-gammaH2A.XS139	mouse monoclonal	1/100	JBW-301	2552645	05-636-I	Millipore
anti-cyclin D1	mouse monoclonal	1/60	HD11	D2108	sc-246	Santa Cruz Biotechnology
anti-PML	rabbit polyclonal	1/200		A301-167A-2	A301-167A	Bethyl Laboratories
goat anti-rabbit IgG (H+L) conjugated to Alexa Fluor 488		1/1000		1166843	A11008	Molecular Probes
goat anti-mouse IgG (H+L) conjugated to Alexa Fluor 488		1/1000		1423008	A11029	Life Technologies
goat anti-rabbit IgG (H+L) conjugated to Alexa Fluor 568		1/1000		1504529	A11036	Life Technologies
goat anti-mouse IgG (H+L) conjugated to Alexa Fluor 568		1/1000		1398018	A11031	Life Technologies
IP						
anti-RPS14	rabbit polyclonal	5 µg per condition		A304-031A-1	A304-031A	Bethyl Laboratories
anti-FLAG mouse monoclonal Affinity Gel	mouse monoclonal			SLBT8835	A2220-5ML	Sigma-Aldrich
WB						
anti-H-RAS	mouse monoclonal	1/250	F235	C0608	Sc-29	Santa Cruz Biotechnology
anti-PML	rabbit polyclonal	1/1000		A301-167A-2	A301-167A	Bethyl Laboratories

anti-phospho-H3S10	rabbit polyclonal	1/1000		2517793	06-570	Millipore
anti-RSL1D1	goat polyclonal	1/1000		821500642	GTX88161	GeneTex
anti-RSL1D1	rabbit polyclonal	1/4000		R40297	HPA043483	Sigma-Aldrich
anti-NS	rabbit polyclonal	1/1000	H-270	G1009	Sc-67012	Santa Cruz Biotechnology
anti-DDX21	rabbit polyclonal	1/1000		40618	GTX115199	GeneTex
anti-EBP2	goat polyclonal	1/500	N-13	H1611	sc-46316	Santa Cruz Biotechnology
anti-MCM6	rabbit polyclonal	1/1000		A300-194A-2	A300-194A	Bethyl Laboratories
anti-p53	mouse monoclonal	1/1000	DO-1	C1413	Sc-126	Santa Cruz Biotechnology
anti-phospho-p53S15	rabbit polyclonal	1/500		9	9284	Cell Signaling
anti-FLAG	mouse monoclonal	1/1000	M2	SLBK1346V	F1804	Sigma-Aldrich
anti-c-Myc	rabbit polyclonal	1/1000	A-14	K0215	sc-789	Santa Cruz Biotechnology
anti-Myc tag	mouse monoclonal	1/2000	# 9E10	114K4821	# 9E10	Sigma
anti-phospho-RBS795	rabbit polyclonal	1/500		13	9301	Cell Signaling
anti-RB	mouse monoclonal	1/1000	G3-245	71957	554136	BD Pharmingen
anti-RPL29	rabbit polyclonal	1/1000		40681	GTX101833	GeneTex
anti-RPS14	rabbit polyclonal	1/1000	H-130	C1914	sc-68873	Santa Cruz Biotechnology
anti-RPS14	rabbit polyclonal	1/4000		A304-031A-1	A304-031A	Bethyl Laboratories
anti-RPS3	mouse monoclonal	1/1000	C-7	D2116	sc-376008	Santa Cruz Biotechnology
anti-CDK4	rabbit polyclonal	1/2000		A304-225A-1	A304-225A	Bethyl Laboratories
anti- $\alpha$ -Tubulin	mouse monoclonal	1/20000	B-5-1-2	023M4813	T6074	Sigma-Aldrich
anti-GST	mouse monoclonal	1/2000	GST-2	012M4814	G1160	Sigma-Aldrich
anti-H3	rabbit polyclonal	1/2000	ab1791	GR206453-1	ab1791	Abcam
anti-CDK4(HRP)	rabbit monoclonal	1/2000	ab193968	GR205710-1	ab193968	Abcam

anti-UBF(#8)	rabbit polyclonal	1/1000	#8			mouse UBF (aa 2-404) and kindly provided by Dr. Tom Moss.
goat anti-rabbit IgG (H-L) conjugated to HRP		1/3000		64126042	170-6515	Bio-Rad
goat anti-mouse IgG (H-L) conjugated to HRP		1/3000		64132955	170-6516	Bio-Rad
donkey anti-goat IgG conjugated to HRP		1/3000		E2313	Sc-2020	Santa Cruz Biotechnology

Real-time PCR primers		
Name	5' forward primer (5'-3')	3' reverse primer (5'-3')
CDK6	TGAACTAGGCAAAGACCTACTTCTGA	GGGAATCCAGGTTTTCTTTGCAC
CDK4	CAGTGCAGTCGGTGGTACCTGA	GGCAGAGATTCGCTTGTGTGG
CDKN2A	GCTGAGGAGCTGGGCCATCG	CTGGTTCTTTCAATCGGGGATG
CDKN1A/p21	ACCCTTGTGCCTCGCTCAGG	GCGTTTGGAGTGGTAGAAATCTGT
CENPA	AATGGATTCTGCGATGCTGTCTGG	TTTTCAGGCCTTTGGAACGGTGT
DDX21	GCTTTGATGTACCTACCGCATCA	CTGCCAGCGTCGTGAATCAT
EBP2	GGACCAGAAAGCTGTTGATCCAG	CGGGGTAAGACTGCAAGCACTG
FANCD2	CCTTAGTAGCCGACTGAAACAGG	TGCAAGTAATGGACGCTCTG
GADD45A	TTGCAATATGACTTTGGAGGAA	CATCCCCACCTTATCCAT
HMBS	GGCAATGCGGCTGCAA	GGGTACCCACGCGAATCAC
IL6	CCAGGAGCCCAGCTATGAACTC	AAGGCAGCAGGCAACACCAG
IL8	GGCACAACTTTCAGAGACAGCA	GGCAAACTGCACCTTCACACA
KI67	AGAAGACAGTACCGCAGATGA	CGGCTCACTAATTTAACGCTGG
MCM6	ATCCCTCTTGCCAAGGATT	GAAAAGTCCGCTCACAAGC
NS	TGTATCCATGGGGCTTACAAGG	TGCTGGACTTCGCAGAGCAAG
p16	CCCAACGCACCGAATAGTTACG	GCTGCCCATCATCATGACCT
RSL1D1	TCCCACAGCTGGTACCAATAGGA	TCCTGTGGCATGTTTTTGAATCTC
TBP	GCTGGCCCATAGTGATCTTTGC	CTTCACACGCCAAGAAACAGTGA

## shRNA sequences

Name	Vector	Sequence (sense strand 5'-3')
shNTC	pLKO	CAACAAGATGAAGAGCACCAA
shRSL1D1-A (shR-A)	pLKO	GCCTTTGTAACCTTCTCTAAA
shRSL1D1-B (shR-B)	pLKO	CAAGAGAGATCAATGACTGTA
shGNL3-A (shNS-A)	pLKO	ATTTGGAGAGCTGGCTAAATT
shGNL3-B (shNS-B)	pLKO	GTGCCTCATTAGCTTACTATT
shDDX21-A (shD-A)	pLKO	GCGGAGTTTCAGTAAAGCATT
shDDX21-B (shD-B)	pLKO	CCCATATCTGAAGAAACTATT
shEBNA1BP2-A (shE-A)	pLKO	GGAGTCGGAATCCGATGAATC
shEBNA1BP2-B (shE-B)	pLKO	GCCCATATGATGAATGCTATT
shRPS14-A	pLKO	CCTTGCCCGCTCGGGTATGAA
shRPS14-B	pLKO	CCATATCTTTGCATCCTTCAA
shNTC	MSCV	AATTGATGTGTTTAGTCGCTAG
shp16	MSCV	ACCGTAACTATTCGGTGC GTTGGG CA
shRB	MSCV	GCAGTTCGATATCTACTGAAATA
shNTC	MLPX	AATTGATGTGTTTAGTCGCTAG
shp21	MLP	GCCTCTGGCATTAGAATTATTTA

**A.2. Supplementary files from the article "A Hydride transfer complex reprograms NAD metabolism and bypasses senescence"**



## STAR★METHODS

## KEY RESOURCES TABLE

REAGENT or RESOURCE	SOURCE	IDENTIFIER
<b>Antibodies</b>		
anti-PC mouse monoclonal	Santa Cruz Biotechnology	Cat# sc 365673; RRID:AB_10842023
anti-ME1 rabbit polyclonal	GeneTex	Cat# GTX104122; RRID:AB_1950905
anti p53 mouse monoclonal	Santa Cruz Biotechnology	Cat# sc98; RRID:AB_628085
anti-Ki67 rabbit monoclonal	Thermo Fisher Scientific	Cat# RM9106; RRID:AB_2335745
anti-53BP1 rabbit polyclonal	Calbiochem	Cat# PC712; RRID:AB_564982
anti-phospho- $\gamma$ -H2A.X <sup>S139</sup> mouse monoclonal	Millipore	Cat# 05-636-I; RRID:AB_2755003
anti-PML rabbit polyclonal	Bethyl Laboratories	Cat# A301-167A; RRID:AB_873108
anti-TOMM20 rabbit polyclonal	Santa Cruz Biotechnology	Cat# FL-145; RRID:AB_2207533
anti-FLAG rabbit monoclonal	Cell Signaling	Cat# 14793; RRID:AB_2572291
anti-MYC tag mouse monoclonal	Sigma-Aldrich	Cat# M4439; RRID:AB_439694
donkey anti-mouse IgG (H+L) conjugated to Alexa Fluor 405	Abcam	Cat# ab175658; RRID:AB_2687445
donkey anti-rabbit IgG (H+L) conjugated to Alexa Fluor 488	Life Technologies/ Molecular Probes/ Invitrogen/Thermo Fisher Scientific	Cat# A21206; RRID:AB_2535792
donkey anti mouse IgG (H+L) conjugated to Alexa Fluor 488	Life Technologies/ Molecular Probes/ Invitrogen/Thermo Fisher Scientific	Cat# A21202; RRID:AB_141607
goat anti-mouse IgG (H+L) conjugated to Alexa Fluor 488	Life Technologies/ Molecular Probes/ Invitrogen/Thermo Fisher Scientific	Cat# A11029; RRID:AB_138404
donkey anti-goat IgG (H+L) conjugated to Alexa Fluor 488	Life Technologies/ Molecular Probes/ Invitrogen/Thermo Fisher Scientific	Cat# A11055; RRID:AB_2534102
goat anti-rabbit IgG (H+L) conjugated to Alexa Fluor 488	Life Technologies/ Molecular Probes/ Invitrogen/Thermo Fisher Scientific	Cat# A11008; RRID:AB_143165
goat anti-rabbit IgG (H+L) conjugated to Alexa Fluor 568	Life Technologies/ Molecular Probes/ Invitrogen/Thermo Fisher Scientific	Cat# A11036; RRID:AB_10563566
goat anti-mouse IgG (H+L) conjugated to Alexa Fluor 568	Life Technologies/ Molecular Probes/ Invitrogen/Thermo Fisher Scientific	Cat# A11031; RRID:AB_144696
donkey anti-rabbit IgG (H+L) conjugated to Alexa Fluor 568	Life Technologies/ Molecular Probes/ Invitrogen/Thermo Fisher Scientific	Cat# A10042; RRID:AB_2534017
donkey anti-goat IgG (H+L) conjugated to Alexa Fluor 647	Life Technologies/ Molecular Probes/ Invitrogen/Thermo Fisher Scientific	Cat# A21447; RRID:AB_141844
donkey anti-mouse IgG (H+L) conjugated to Alexa Fluor 647	Life Technologies/ Molecular Probes/ Invitrogen/Thermo Fisher Scientific	Cat# A31571; RRID:AB_162542
donkey anti-rabbit IgG (H+L) conjugated to Alexa Fluor 647	Life Technologies/ Molecular Probes/ Invitrogen/Thermo Fisher Scientific	Cat# A31573; RRID:AB_2536183
normal rabbit IgG	Cell Signaling	Cat# 2729S; RRID:AB_1031062
anti-HA mouse monoclonal magnetic beads	Pierce /ThermoFisher	Cat# 88836; RRID:AB_2749815
anti-FLAG mouse monoclonal Affinity Gel	Sigma-Aldrich	Cat# A2220-5ML; RRID:AB_10063035
Dynabeads® Protein G	Invitrogen/ThermoFisher Scientific	Cat# 100.04D; RRID:SCR_008452
Dynabeads® Protein A	Invitrogen/ThermoFisher Scientific	Cat# 10002D; RRID:SCR_008452
anti-H-RAS mouse monoclonal	Santa Cruz Biotechnology	Cat# Sc-29; RRID:AB_627750
anti-p21 mouse monoclonal	BD PharMingen	Cat# 556431; RRID:AB_396415
anti-phospho-H3S10 rabbit polyclonal	Millipore	Cat# 06-570; RRID:AB_310177
anti-PC goat polyclonal	Santa Cruz Biotechnology	Cat# sc46228; RRID:AB_653879
anti-mt-nd1 rabbit polyclonal	Elabscience	Cat# E-AB-32173

(Continued on next page)

<b>Continued</b>		
REAGENT or RESOURCE	SOURCE	IDENTIFIER
anti-mt-nd4 rabbit polyclonal	Novus Biologicals	Cat# NBP2-47365
anti-MCM6 rabbit polyclonal	Bethyl Laboratories	Cat# A300-194A; RRID:AB_162727
anti-p53 mouse monoclonal	Santa Cruz Biotechnology	Cat# Sc-126; RRID:AB_628082
anti-phospho-p53 <sup>S15</sup> rabbit polyclonal	Cell Signaling	Cat# 9284; RRID:AB_331464
anti-FLAG mouse monoclonal	Sigma-Aldrich	Cat# F1804; RRID:AB_262044
anti-MYC tag rabbit polyclonal	Santa Cruz Biotechnology	Cat# sc-789; RRID:AB_631274
anti-H3 rabbit polyclonal	Abcam	Cat# ab1791; RRID:AB_302613
anti-RNR mouse monoclonal	Santa Cruz Biotechnology	Cat# sc-398294
anti- $\alpha$ -Tubulin mouse monoclonal	Sigma-Aldrich	Cat# T6074; RRID:AB_477582
anti-phospho-RBS <sup>795</sup> rabbit polyclonal	Cell Signaling	Cat# 9301; RRID:AB_330013
anti-RB mouse monoclonal	BD PharMingen	Cat# 554136; RRID:AB_395259
anti-HA tag goat polyclonal	Abcam	Cat# ab9134; RRID:AB_307035
anti-HA tag rabbit polyclonal	Cell Signaling	Cat# 3724 RRID:AB_1549585
anti-HA tag 12CA5 mouse monoclonal	University of Montreal Department of Biochemistry	n/a
anti-MDH1 mouse monoclonal	Santa Cruz Biotechnology	Cat# sc 166880; RRID:AB_10609512
Protein A- Gold 10 nm	Cell Microscopy Core, Department of Cell Biology University Medical Center Utrecht	Cat# PAG 10 nm
goat anti-rabbit IgG (H-L) conjugated to HRP	Bio-Rad	Cat# 170-6515 RRID:AB_11125142
goat anti-mouse IgG (H-L) conjugated to HRP	Bio-Rad	Cat# 170-6516 RRID:AB_11125547
mouse anti-goat IgG HRP	Santa Cruz Biotechnology	Cat# sc-2354; RRID:AB_628490
donkey anti-goat IgG HRP	Santa Cruz Biotechnology	Cat# sc 2020; RRID:AB_631728
mouse anti-rabbit IgG conformation specific HRP L27A9	Cell Signaling	Cat# #3678; RRID:AB_1549606
Rat mAB to Ms IgG HRP confirmation specific	Abcam	Cat# ab131368
anti-KI67 mouse monoclonal	DAKO	RRID:AB_2631211
anti-LDH mouse monoclonal	Santa Cruz Biotechnology	Cat# sc-133123; RRID:AB_2134964
anti-ATAD3A rabbit polyclonal	Novus Biologicals	Cat# NBP1-76586; RRID:AB_11025339
anti-PC rabbit polyclonal	Novus Biologicals	Cat# NBP1-49536; RRID:AB_10011589
anti-MDH1 rabbit polyclonal	Novus Biologicals	Cat# NBP1-89515; RRID:AB_11036600
<b>Biological samples</b>		
Tissue Micro Array (TMA) of prostate cancer samples	US Biomax Rockville, MD	Cat# PR807c
<b>Chemicals, peptides, and recombinant proteins</b>		
MDH1 recombinant protein	This study	N/A
PC 486-1178 recombinant protein	This study	N/A
PC 21 –1178 recombinant protein	This study	N/A
ME1 recombinant protein	This study	N/A
Crystal Violet	Bioshop	Cat # CRY 422.100
X-Gal	Wisent Bioproducts	Cat # 800-145-UG
Sodium pyruvate	Sigma-Aldrich	Cat # P8574
DAPI (4',6-Diamidino-2-Phenylindole, Dihydrochloride)	Invitrogen/ Thermo Fisher Scientific	Cat # D1306
Duroquinone	Sigma-Aldrich	Cat # D223204
L-Aspartic acid	Sigma-Aldrich	Cat # A6683
Methanol for LC-MS	Sigma-Aldrich	Cat # 34885-1L

(Continued on next page)



**Continued**

REAGENT or RESOURCE	SOURCE	IDENTIFIER
1,6-Hexanediol	Sigma-Aldrich	Cat # 240117
NAD free acid	Roche	Cat # 10127965001
NADH disodium salt	Roche	Cat # 10128023001
NADP disodium salt	Roche	Cat # 10128058001
NADPH	Roche	Cat # 10107824001
Adenosine 5'-triphosphate disodium salt hydrate(ATP)	Sigma-Aldrich	Cat # 3377
MG132 (Z-Leu-Leu-al)	Sigma-Aldrich	Cat # C2211
Piericidin A	Santa Cruz Biotechnology	Cat # sc-202287
Potassium hexacyanoferrate(II) trihydrate	Sigma-Aldrich	Cat # P3289
Potassium ferricyanide(III)	Sigma-Aldrich	Cat # 702587
Poly(ethylene glycol)	Sigma-Aldrich	Cat # 81310
PhosStop	Roche	Cat # 04906837001
cOmplete protease inhibitor	Roche	Cat # 37378900
Sodium L-lactate	Sigma-Aldrich	Cat # 71718
Unstained Protein Standard	Thermo Fisher Scientific	Cat # LC0725
Dimethylmalate	Sigma-Aldrich	Cat # 374318
DMEM without pyruvate	Wisent Bioproducts	Cat # 319-015
RPMI	Wisent Bioproducts	Cat# 350-000
RPMI without glucose	Wisent Bioproducts	Cat# 350-060
JumpStart™ Tag DNA Polymerase	Sigma-Aldrich	Cat # D9307
TRIZOL™ Reagent	Thermo Fisher Scientific	Cat #15596026
Hygromycin B	Wisent Bioproducts	Cat # 450-141-XL
G418 sulfate	Wisent Bioproducts	Cat# 400-130-UG
Puromycin	Wisent Bioproducts	Cat # 400-160-EM
Blaticidin S. Hydrochloride	Wisent Bioproducts	Cat # 400-190-EM
Paraformaldehyde	BioShop	Cat # PAR070
Osmium tetroxide solution	Sigma-Aldrich	Cat # 75632
Sodium (meta)periodate	Sigma-Aldrich	Cat # S1878
LR White Resin	London Resin Company	Cat # AGR1281
L-Lysine monohydrochloride	Sigma-Aldrich	Cat # L5626
Nutragen® Bovine Type I Collagen mix	Advanced BioMatrix	Cat # 5010
X-treme Gene 9	Roche	Cat # 6365787001
<i>E. coli</i> tRNA	Sigma-Aldrich	Cat #10109541001
Deoxyribonucleic acid, low molecularweight from salmonperm	Sigma-Aldrich	Cat # 31149
hexamethrine bromide (Polybrene)	Sigma-Aldrich	Cat # 107689
Slide-A-Lyzer	Thermo Fisher Scientific	Cat # 66203
Pierce™ Monomeric Avidin Agarose	Thermo Fisher Scientific	Cat # 20228
Glucose Solution	Wisent Bioproducts	Cat # 609-036-EL
D- Glucose (3,4- <sup>13</sup> C <sub>2</sub> )	Cambridge Isotope Laboratories	CLM-6750-PK
D-Glucose(3- <sup>13</sup> C)	Cambridge Isotope Laboratories	CLM-1393
D-Glucose( <sup>13</sup> C <sub>6</sub> )	Sigma-Aldrich	Cat # 389374
Sodium butyrate	Sigma-Aldrich	Cat # 303410
DMEM with L-glutamine & phenol red,without D-glucose	Wisent Bioproducts	Cat # 319-061-CL
Biotin	Oakwood Chemicals	Cat # M02926
BioVision 10 kDa Spin Column	BioVision	Cat # 1997

(Continued on next page)

**Continued**

REAGENT or RESOURCE	SOURCE	IDENTIFIER
Ammonium formate	Sigma-Aldrich	Cat # 78314
Dithiothreitol (DTT)	Inalco	Cat #1758-9030
Isopropyl- $\beta$ -D-thiogalactopyranoside (IPTG)	Inalco	Cat#1758-1400
Tobacco Etch Virus (TEV) protease	<a href="#">Cappadocia et al., 2015a</a> , <a href="#">Cappadocia et al., 2015b</a>	N/A
Glutathione Sepharose 4B	GE Healthcare	Cat # 17-0756-05
Chelating Sepharose Fast Flow	GE Healthcare	Cat # 17-0575-01
Imidazole	Sigma-Aldrich	Cat # I202
N-tert-Butyldimethylsilyl-N-methyltrifluoroacetamide	Sigma Aldrich	Cat # 394882
Tris(2-carboxyethyl)phosphine (TCEP)	Cayman chemicals	Cat # 14329
4-20% native Polyacrylamide Gel	Bio-Rad	Cat # 4568094
Amicon® Ultra-15 Centrifugal Filter Units with 10KDa cutoff	Millipore	Cat # UFC901024
Amicon® Ultra-4 Centrifugal Filter Units with 10KDa cutoff	Millipore	Cat # UFC801024
Amicon Ultra-0.5 mL	Millipore	Cat # UFC500396
Bovine Serum Albumin	BioShop	Cat # ALB001
ABT-263 (Navitoclax)	APEXBIO	Cat # AA3007
Acrylamide/Bisacrylamide, 30% Solution, 37.5:1	Bioshop	Cat # ACR010.502
<b>Critical commercial assays</b>		
NAD <sup>+</sup> /NADH Kit	BioVision	Cat # K337
NADP <sup>+</sup> /NADPH Kit	BioVision	Cat # K347
GSH/GSSG Ratio Detection Assay Kit	Abcam	Cat # ab138881
Mitochondria Isolation Kit for Cultured Cells	Abcam	Cat # ab110170
MitoTracker™ Deep Red FM	Invitrogen/Thermo Fisher Scientific	Cat # M22426
H <sub>2</sub> DCFDA	Invitrogen/Thermo Fisher Scientific	Cat # D399
MitoSOX™ Red Mitochondrial Superoxide Indicator, for live-cell imaging	Invitrogen/Thermo Fisher Scientific	Cat # M36008
Seahorse MitoStress Kit	Aligent	Cat # 103015-100
RNAlater®	Sigma-Aldrich	Cat # R0901
5x All in One RT Master Mix	ABM	Cat # G490
Duolink® PLA Multicolor Probemarker Kit Red	Sigma-Aldrich	Cat # DUO96910
Duolink® PLA Multicolor Probemarker Kit Green	Sigma-Aldrich	Cat # DUO96920
Duolink® PLA Multicolor Reagent Pack	Sigma-Aldrich	Cat # DUO96000
Duolink® <i>In Situ</i> Green Starter Kit Mouse/Rabbit	Sigma-Aldrich	Cat # DUO92014
Duolink® <i>In Situ</i> Wash Buffers, Fluorescence	Sigma-Aldrich	Cat # DUO82049
MicroBCA Pprotein Assay Kit	Thermo Fisher Scientific	Cat # 23235
BCA Protein Assay Kit	Thermo Fisher Scientific	Cat # 23237
Bio-Rad protein assay	Bio Rad	Cat # 5000006
LSAB2 System-HRP	DAKO	Cat # K0675
Di-amine-benzidine (DAB) substrate kit	Vector Labs	Cat # SK-4100
<b>Deposited Data</b>		
Cancer Cell Line Encyclopedia (CCLE)	<a href="#">(Ghandi et al., 2019)</a>	RRID:SCR_013836

(Continued on next page)

**Continued**

REAGENT or RESOURCE	SOURCE	IDENTIFIER
For p53 ChIP seq depth and SISSR peaks dataset	(Nguyen et al., 2018)	N/A
Additional p53 and E2F binding sequences were obtained in ChIP Atlas and positions extracted from UCSC genome Browser using Transcription factor ChIP-Seq Clusters (161 factors) from ENCODE	(Consortium, 2012; Davis et al., 2018) Atlas (Oki et al., 2018)	RRID:SCR_006793
<b>Experimental models: Cell lines</b>		
IMR90 (normal human diploid fibroblasts)	American Type Culture Collection (ATCC, Manassas, VA)	ATCC Cat # CCL-186; RRID:CVCL_0347
IMR90 (normal human diploid fibroblasts)	Coriell Institute for Medical Research (Camden, NJ)	Coriell Cat # I90-83; RRID:CVCL_0347
PC-3 (prostate cancer)	American Type Culture Collection (ATCC, Manassas, VA)	ATCC Cat # CRL-7934; RRID:CVCL_0035
HEK293T (embryonic kidney)	American Type Culture Collection (ATCC, Manassas, VA)	ATCC Cat # CRL-3216, RRID:CVCL_0063
HuH-7 (liver cancer)		RRID:CVCL_0336
Primary MEFs	S. Meloche (IRIC, Université de Montréal)	N/A
Phoenix Ampho packaging cells	S. W Lowe (MSKCC, New York)	RRID:CVCL_H716
MEF p53 <sup>-/-</sup>	S. W Lowe (MSKCC, New York)	N/A
BJ, Human normal foreskin fibroblasts	ATCC	CCRL-2522
<b>Experimental models: Organisms/strains</b>		
Transgenic male mice with prostate-specific deletions of <i>Stat3</i> , <i>Pten</i> and double <i>Stat3</i> and <i>Pten</i> deletion	(Pencik et al., 2015)	N/A
mouse for allograftmale NOD.Cg-Rag1 <sup>tm1Mom</sup> Il2rg <sup>tm1WJ</sup> /SzJ (also called NRG)	CRCHUM mouse colony. F.Rodier	RRID:IMSR_JAX:007799
BL21 Star (DE3): F ompT hsdSB(rB <sup>-</sup> mB <sup>-</sup> ) gal dcm rne131 (DE3)	Department of Biochemistry, University of Montreal	N/A
<b>Oligonucleotides</b>		
Table S1 for qPCR primer		N/A
Table S1 for shRNA target sequences		N/A
Table S1 for cloning primer		N/A
<b>Recombinant DNA</b>		
pLPC-puromycin –3xFLAG	Ferbeyre Laboratory or are also available on addgene	<a href="#">Acevedo et al. Cancer Res. 2016 Addgene</a>
pBABE with selection marker puromycin, hygromycin or neomycin	Ferbeyre Laboratory or are also available on addgene	described in (Lessard et al., 2018) also available from Addgene
pBABE-puromycin-H-RASV12	Ferbeyre Laboratory or are also available on addgene	described in (Lessard et al., 2018) also available from Addgene
pWZL-hygromycin	Ferbeyre Laboratory or are also available on addgene	described in (Lessard et al., 2018) also available from Addgene
pWZL-hygromycin-H-RASV12	Ferbeyre Laboratory or are also available on addgene	described in (Lessard et al., 2018) also available from Addgene
pCMV-VSV-G	Addgene 8454	(Stewart et al., 2003); Addgene 8454
pCMV-dR.8.2dvpr	Addgene 8455	(Stewart et al., 2003); Addgene 8455
pLPC-puromycin-binary	S. W Lowe (MSKCC, New York)	N/A
pMLP-shp21 puromycin	S. W Lowe (MSKCC, New York)	N/A
pMLP-shp53 puromycin	Ferbeyre laboratory	<a href="#">Moiseeva et al., 2011</a>
pMLP-shp53-neomycin	Ferbeyre laboratory	<a href="#">Moiseeva et al., 2011</a>

(Continued on next page)

REAGENT or RESOURCE	SOURCE	IDENTIFIER
<i>pMLPX-shNTC-puromycin</i>	Addgene 65232	Described in (Lessard et al., 2018); Addgene 65232
<i>pMLPX-shNTC-neomycin</i>	Addgene 65233	Described in (Lessard et al., 2018); Addgene 65233
Vector expressing <i>NDI 1</i>	N. Chandel (Northwestern University, Chicago, IL).	N/A
<i>pBABE-puromycin-NDI-1-FLAG</i>	this study	N/A
<i>pMSCV-puromycin-mCherry</i>	this study	N/A
<i>pMSCV-puromycin-mCherry-NDI-1</i>	this study	N/A
<i>pRetroSuper-shp53-hygromycin</i>	R Agami Division of Tumor Biology, the Netherlands Cancer Institute,	Voorhoeve and Agami, 2003
<i>pRetroSuper-shGFP-hygromycin</i>	R Agami Division of Tumor Biology, the Netherlands Cancer Institute,	Voorhoeve and Agami, 2003
<i>pBABE-puromycin-MDH1</i>	this study	N/A
<i>pLPC-puromycin-binary-MDH1</i>	this study	N/A
<i>pLPC-puromycinbinary-MDH1-3xFLAG</i>	this study	N/A
<i>pcDNA3-MDH1-3xFLAG</i>	this study	N/A
<i>pcDNA3</i>	(Life Technologies, Burlington, ON)	N/A
<i>pBABE-puromycin-ME1</i>	Addgene # 49163	(Jiang et al., 2013) Addgene # 49163
<i>pcDNA3-ME1-HA</i>	this study	N/A
<i>pLPC-puromycin-binary-MDH1-3xFLAG-ME1-HA</i>	this study	N/A
<i>pBABE-puromycin-ME1-HA</i>	this study	N/A
<i>pBABE-neomycin-PC-MYC</i>	this study	N/A
<i>pcDNA3-PC-MYC</i>	this study	N/A
<i>pcDNA3-3xFLAG</i>	this study	N/A
<i>pcDNA3-MYC-tag</i>	this study	N/A
<i>pcDNA3-HA-tag</i>	this study	N/A
<i>pCDNA3-ME1(1-191)-HA</i>	this study	N/A
<i>pCDNA3-ME1(356-572)-HA</i>	this study	N/A
<i>pcDNA3-MDH1(1-90)-3x-FLAG</i>	this study	N/A
<i>pcDNA3-MDH1(1-141)-3x-FLAG</i>	this study	N/A
<i>pcDNA3-MDH1(105-334)-3x-FLAG</i>	this study	N/A
<i>pcDNA3-MDH1(1-90)-3x-FLAG</i>	this study	N/A
<i>pcDNA3-MDH1(142-334)-3x-FLAG</i>	this study	N/A
<i>pcDNA3-PC(1-956)-MYC</i>	this study	N/A
<i>pcDNA3-PC(1-534)-MYC</i>	this study	N/A
<i>pcDNA3-PC(430-1178)-MYC</i>	this study	N/A
<i>pLPC-puromycin-mito-iSTAT3-3xFLAG</i>	this study	N/A
<i>pLKO-shSTAT3 -A- puromycin</i>	Sigma-Aldrich	TRCN0000020840
<i>pLKO-shSTAT3 -B- puromycin</i>	Sigma-Aldrich	TRCN0000329887
<i>pLKO-shMDH1 -A- puromycin</i>	Sigma-Aldrich	TRCN0000028484
<i>pLKO-shMDH1 -B- puromycin</i>	Sigma-Aldrich	TRCN0000275198
<i>pLKO-shME1 -A- puromycin</i>	Sigma-Aldrich	TRCN0000064728
<i>pLKO-shME1 -B- puromycin</i>	Sigma-Aldrich	TRCN0000064731
<i>pLKO shPC-A-puromycin</i>	Sigma-Aldrich	TRCN0000078453
<i>pLKO-shPC-B-puromycin</i>	Sigma-Aldrich	TRCN0000413496
<i>pMXs-3XHA-EGFP-OMP25</i>	Addgene plasmid # 83356	Addgene plasmid # 83356
<i>pET-28-ME1</i>	Addgene plasmid # 38857	Addgene plasmid # 38857

(Continued on next page)

**Continued**

REAGENT or RESOURCE	SOURCE	IDENTIFIER
BirA ( <i>E. coli</i> Biotin Protein Ligase),	L. Tong (Columbia Univ., NY).	N/A
SCBPL ( <i>Saccharomyces cerevisiae</i> Biotin Protein Ligase)	L. Tong (Columbia Univ., NY).	N/A
PC-full	L. Tong (Columbia Univ., NY).	N/A
<i>pHIS-MDH1-HIS</i>	this study	N/A
<i>pHIS-PC-HIS</i>	this study	N/A
<i>pHIS-PC 486-1178-HIS</i>	this study	N/A
<i>pHIS</i>		<a href="#">Mascle et al., 2020</a>
<i>pTEV-ME1-GST</i>	this study	N/A
<i>pTEV-GST</i>		<a href="#">Mascle et al., 2020</a>
<i>pBABE-puromycin-mcherry-PC</i>	this study	N/A
<i>pBABE-hygromycin-PC ΔInterm-MYC(PC 21-1178)</i>	this study	N/A
<i>pMSCV with selection marker puromycin, hygromycin or neomycin</i>	Ferbeyre Laboratory or are also available on addgene	<a href="#">Lessard et al., 2018</a>
<i>pLPC-puromycin</i>	Ferbeyre Laboratory or is also available on addgene	<a href="#">Lessard et al., 2018</a>
<i>pLKO-shNTC-puromycin</i>	Sigma-Aldrich	<a href="#">Lessard et al., 2018</a>
<i>pLKO-shNTC-hygromycin</i>	this study	N/A
<i>pLKO-shNTC-neomycin</i>	this study	N/A
<i>pLKO-shNTC-blasticidin</i>	this study	N/A
<i>pLKO-shSTAT3-A -hygromycin</i>	this study	N/A
<i>pLKO-shSTAT3 -A- neomycin</i>	this study	N/A
<i>pLKO-shSTAT3 -B- hygromycin</i>	this study	N/A
<i>pLKO-shSTAT3 -B- neomycin</i>	this study	N/A
<i>pLKO-shSTAT3 -A- blasticidin</i>	this study	N/A
<i>pLKO-shSTAT3 -B- blasticidin</i>	this study	N/A
<i>pBabe-hygromycin-MDH1-3-X-FLAG</i>	this study	N/A
<i>pLV-EV1-RFP</i>	N. Chandel (Northwestern University)	Vectorbuilder VB 160708-1059xrd
<i>pLV-EV1-RFP-cyto-LBNOX -3-x-FLAG</i>	N. Chandel (Northwestern University)	Vectorbuilder VB 160708-1059xrd ; Original research paper generating LBNOX PMID 27124460 Addgene # 75285
<i>pUltra</i>	Addgene 24129	RRID: Addgene_24129
<i>pUltra-MDH1-ME1</i>	this study	N/A
<i>pUltra-hot</i>	Addgene 24130	RRID: Addgene_24130
<i>pUltra-hot-PC</i>	this study	N/A
<b>Software and algorithms</b>		
Prism 6-9	<a href="https://www.graphpad.com/">https://www.graphpad.com/</a>	RRID: SCR_002798
Imaris	<a href="https://imaris.oxinst.com/packages">https://imaris.oxinst.com/packages</a>	RRID: SCR_007370
Adobe Illustrator	<a href="https://www.adobe.com/products/illustrator.html">https://www.adobe.com/products/illustrator.html</a>	RRID: SCR_010279
Agilent Masshunter Quantitative Analysis software	<a href="http://www.agilent.com/en-us/products/software-informatics/masshunter-suite/masshunter/masshunter-software">http://www.agilent.com/en-us/products/software-informatics/masshunter-suite/masshunter/masshunter-software</a>	RRID: SCR_015040
Seahorse Wave	<a href="http://www.agilent.com/en-us/products/cell-analysis-(seahorse)/software-download-for-wave-desktop">http://www.agilent.com/en-us/products/cell-analysis-(seahorse)/software-download-for-wave-desktop</a>	RRID:SCR_014526
Astra	<a href="https://www.wyatt.com/products/software/astra.html">https://www.wyatt.com/products/software/astra.html</a>	RRID:SCR_01625

(Continued on next page)

<b>Continued</b>		
REAGENT or RESOURCE	SOURCE	IDENTIFIER
ZEN Digital Imaging for Light Microscopy	<a href="http://www.zeiss.com/microscopy/en_us/products/microscope-software/zen.html#introduction">http://www.zeiss.com/microscopy/en_us/products/microscope-software/zen.html#introduction</a>	RRID:SCR_013672
Olympus Fluoview FV10-ASW	<a href="http://www.photonics.com/Product.aspx?PRID=47380">http://www.photonics.com/Product.aspx?PRID=47380</a>	RRID:SCR_014215
Fiji	<a href="https://fiji.sc/">https://fiji.sc/</a>	RRID: SCR_002285
Image Lab	<a href="https://www.bio-rad.com/en-us/sku/1709690-image-lab-software">https://www.bio-rad.com/en-us/sku/1709690-image-lab-software</a>	RRID: SCR_014210
FlowJo	<a href="https://www.flowjo.com/solutions/flowjo">https://www.flowjo.com/solutions/flowjo</a>	(RRID:SCR_008520)
BD FACSDiva Software	<a href="http://www.bdbiosciences.com/instruments/software/facsdiva/index.jsp">http://www.bdbiosciences.com/instruments/software/facsdiva/index.jsp</a>	(RRID:SCR_001456)
LightCycler Software	<a href="http://www.roche-applied-science.com/shop/products/absolute-quantification-with-the-lightcycler-carousel-based-system">http://www.roche-applied-science.com/shop/products/absolute-quantification-with-the-lightcycler-carousel-based-system</a>	(RRID:SCR_012155)
NDP.view 2.6.8 (NanoZoomer Digital Pathology.view 2.6.8)	Hamamatsu	N/A
OlyVIA 2.9 Virtual Slide Scanner	Olympus	N/A
<b>Additional information</b>		
Mendeley data		<a href="http://doi.org/10.17632/xsxwjjfhz8f.1">http://doi.org/10.17632/xsxwjjfhz8f.1</a>
Immunogold staining protocol	<a href="http://www.me-udem.com">www.me-udem.com</a>	<a href="http://www.me-udem.com">www.me-udem.com</a>
IHC staining protocol	<a href="https://www.chumontreal.qc.ca/en/crchum/facilities-and-services">https://www.chumontreal.qc.ca/en/crchum/facilities-and-services</a>	<a href="https://www.chumontreal.qc.ca/en/crchum/facilities-and-services">https://www.chumontreal.qc.ca/en/crchum/facilities-and-services</a>
Metabolic tracing analysis	<a href="https://www.mcgill.ca/gci/facilities/metabolomics-innovation-resource-mir">https://www.mcgill.ca/gci/facilities/metabolomics-innovation-resource-mir</a>	<a href="https://www.mcgill.ca/gci/facilities/metabolomics-innovation-resource-mir">https://www.mcgill.ca/gci/facilities/metabolomics-innovation-resource-mir</a>

## RESOURCE AVAILABILITY

### Lead contact

All reasonable requests for material generated for this study should be addressed to G. Ferbeyre ([g.ferbeyre@umontreal.ca](mailto:g.ferbeyre@umontreal.ca)).

### Materials availability

Materials generated in this study are available from the lead contact.

There are restrictions to the availability of TMA of prostate tissue since its discontinued but similar TMA are available from US Bio-max. There are restrictions to the availability of HA antibody but its available from commercial distributor.

There are restrictions to the availability of tissue samples from allograft as only a limited number of tumor were generated. Request for *Stat3<sup>-/-</sup> Pten<sup>-/-</sup>* knockout tissue should be addressed to Richard Morigg or Lukas Kenner

There are restrictions to the availability of tissue samples from *Stat3<sup>-/-</sup> Pten<sup>-/-</sup>* as only a limited number of paraffin embedded slides were generated

There are restrictions to the availability of frozen proteins MDH1, ME1, and PC as limited amount of purified proteins were generated.

### Data and code availability

- Quantification data of Immunofluorescence, quantification of SA-β-Gal, ROS analysis, NAD analysis, oxygen consumption, analyzed metabolomics data, unprocessed mitochondrial ultrastructure images, unprocessed allograft images, PLA images and unprocessed SA-β-Gal images were deposited to Mendeley Data and DOI is listed in the key resources table. Link to Mendeley <http://doi.org/10.17632/xsxwjjfhz8f.1>. This paper analyses existing, publicly available data. These accession numbers for the datasets are listed in the key resources table. All source data not on Mendeley Data and all supporting information are either included in the figures or will be made available upon request to the lead author or the first author.
- This paper does not report original code.
- Any additional information required to reanalyse the data reported in this paper is available from the lead contact upon reasonable request.

## EXPERIMENTAL MODEL AND SUBJECT DETAILS

### Mouse Model

All animal experiments were reviewed and approved by the Austrian ministry authorities (BMWF-66.009/0281-I/3b/2012) and the CIPA (Comité Institutionnel d'expérimentation animale du CHUM), protocol C18046GFs. Transgenic male mice with prostate-specific deletions of *Stat3*, *Pten* and double *Stat3* and *Pten* deletion (Pencik et al., 2015) were used to show levels of HTC enzymes in genetic model of prostate cancer development.

Allografts were performed using 7 weeks old male NOD.Cg-Rag1<sup>tm1Mom</sup> Il2rg<sup>tm1Wjl</sup>/SzJ (also called NRG) mice.

### Cell culture model

IMR90 and BJ normal human diploid fibroblasts, PC-3 (prostate cancer), HEK293T (embryonic kidney) and HuH-7 (liver cancer) cells were purchased from American Type Culture Collection (ATCC, Manassas, VA) and Coriell Institute for Medical Research (Camden, NJ). Primary MEFs were supplied by S. Meloche (IRIC, Université de Montréal). Phoenix Amphi packaging cells were a gift from S. W. Lowe (MSK, New York). MEF p53<sup>-/-</sup> were provided by S. Lowe. IMR90, MEF and BJ were cultured in Dulbecco's Modified Eagle Medium (DMEM, Wisent Montreal, QC) without pyruvate, supplemented with 10% high grade fetal bovine serum (FBS, Wisent) and 1% penicillin/streptomycin (Wisent). HEK293T, Huh-7 and Phoenix Amphi packaging cells were cultured in Dulbecco's modified Eagle medium (DMEM, Wisent Montreal, QC) without pyruvate, supplemented with 10% fetal bovine serum (FBS, Wisent), 2 mM L-glutamine (Wisent) and 1% penicillin/streptomycin (Wisent). PC-3 cells were cultured in RPMI medium (Wisent) supplemented with 10% fetal bovine serum 1% penicillin/streptomycin (Wisent) and 2 mM L-glutamine.

## METHODS DETAILS

### Reagents

Pyruvate, aspartate, lactate, MG132, NADH, NADPH, ATP, NAD<sup>+</sup>, NADP<sup>+</sup>, duroquinone and dimethylmalate were purchased from Sigma-Aldrich (Oakville, ON) and piericidin A from Santa Cruz Biotechnology (Dallas, TX). ABT-263 was purchased from APEXBio (Boston, MA).

### Plasmids

Retroviruses, , *pBABE*, *pBABE-H-RASV12*, *pWZL* and *pWZL-H-RASV12* are available today on Addgene, but we obtained them from S. W. Lowe (Memorial Sloan Kettering Cancer Center, New York, NY). *pBABE* (Addgene number #1764), *pBABE-H-RASV12* (Addgene number #1768), *H-RASV12* was cloned with *Bam*HI and *Sall* restriction enzymes into *pBABE* vector. *pBABE-puromycin* selection marker can be removed by digestion with *Hind*III and *Clal* and new selection marker can be inserted using compatible restriction enzymes. For this study we used *pBABE-puromycin*, *pBABE-hygromycin* and *pBABE* neomycin. *pWZL* hygromycin (Addgene number 18750) and *pWZL-hygro-mycinH-RASV12* (Addgene number 18749). *pWZL-hygromycin-H-RASV12* was generated by cloning *H-RASV12* into *Bam*HI / *Sall* restriction sites of *pWZL-hygromycin* vector. *pLPC* and *pMSCV* were originally generated by Clontech. *pLPC3XFLAG* has Addgene number 73560 and was generated by cloning *3xFLAG* sequence into *Bam*HI/*Xho*I restriction site. *pMSCV* was modified by the Ferbeyre lab to generate *pMSCV* with multiple cloning site by inserting in *Bgl*II / *Hpa*I of *MSCV* the following linker gatctggatcccagtggtggtacgtacgatccatccactggcggccgactcgcagcaatgcatggtt (Lessard et al., 2018). From modified *pMSCV-puromycin*, the selection marker can be removed by *Hind*III/*Clal* digestion and replaced by neomycin or hygromycin with compatible restriction enzymes (Lessard et al., 2018).

*pCMV-VSV-G* (Addgene no. 8454) and *pCMV-dR8.2 dvpr* (Addgene no. 8455) were from R. Weinberg's laboratory (Whitehead Institute, Cambridge, MA) (Stewart et al., 2003). *pLPC binary* and *pMLP-shp21* were a gift from S. W. Lowe (Memorial Sloan Kettering Cancer Center, New York, NY). *pRetroSuper-shp53* and *pRetroSuper-shGFP* were described in (Voorhoeve and Agami, 2003). The sequence of *shp53* from *pRetroSuper* was also subcloned into *mir30* context of *MLP-puromycin* and *neomycin* (Moiseeva et al., 2011). *ShNTC* with *mir30* context was subcloned in *Bgl*II/*Age*I restriction sites to create retroviral vectors *pMSCV-shNTC* and *pMLPX-shNTC* (*pMLPX* is *pMLP* without GFP reporter). *NDI1* and *LBNOX-3xFLAG* vectors were a gift from N. Chandel (Northwestern University, Chicago, IL). The *LBNOX* construct was from Addgene 75285 (Titov et al., 2016). *pBABE-NDI-1-FLAG* was generated by PCR amplification with primers containing *3xFLAG* sequence and digested with *Eco*RI/*Sall*. *NDI1-Cherry* was generated by PCR amplification with *Eco*RI/*Eco*RV overhangs and cloned into *pMSCV-Cherry* with *Eco*RI/*Hpa*I sites. *MDH1* was PCR amplified and subcloned in *Bam*HI/*Eco*RI restriction sites to create *pBABE-MDH1* (WT) and *pLPCbinary MDH1*. To create *pLPC binary MDH1-3xFLAG* and *pcDNA3-MDH1-3xFLAG*, *MDH1* was PCR amplified with one primer containing the *3xFLAG* tag and subcloned in *Bam*HI/*Eco*RI restriction sites to create *pcDNA3-3xFLAG-MDH1* and *pLPC-binary MDH1-3XFLAG*. *pcDNA3* was from (Life Technologies, Burlington, ON). *ME1* was purchased from Addgene (Addgene # 49163) (Jiang et al., 2013). To generate *pcDNA3 ME1-HA* and *pLPC binary MDH1-3xFLAG-ME1-HA*, *ME1* was PCR amplified with one primer containing the HA tag and subcloned into *Bam*HI/*Xho*I sites of *pcDNA 3* or *pLPC binary* using compatible overlapping ends generated by digestion of *Bgl*II/*Sall*. *PC* was purchased from OriGene (Rockville, MD 20850, USA). *pBABE-PC-MYC* and *pcDNA3-PC-MYC* were generated by PCR amplification of *PC*, one of the primers containing the *MYC* tag and subcloned into *Bam*HI/*Eco*RI sites. To generate *pcDNA3-MDH1-MYC* *MDH1* was PCR amplified with one primer containing the *MYC* tag and subcloned in *Bam*HI/*Eco*RI restriction

sites to create *pcDNA3-MYC-MDH1*. To generate *pcDNA3-PC-3xFLAG* PC was PCR amplified with one primer containing the 3xFLAG tag and subcloned in BamHI/EcoRI restriction sites to create *pcDNA3-PC-3xFLAG*. *pcDNA3-3xFLAG*, *pcDNA3-MYC-tag* and *pcDNA3-HA-tag* were generated by cloning double-stranded oligonucleotides coding for the mentioned tags. All variants of *ME1* used for mapping were PCR amplified and then cloned into BamHI/XhoI sites of *pcDNA3*. For *MDH1* and *PC* variants all fragments were PCR amplified with 3xFLAG tag or *MYC* tag and cloned BamHI/EcoRI into *pcDNA3*. To construct *mito-iSTAT3* resistant to shSTAT3A we first introduced seven mismatches in the sequence targeted by the shRNA keeping the same protein sequence. The new sequence is: "atG **TTA ACT AAT AAC CCT AAA Aat**"; while the WT sequence is: "atG CTG ACC AAC AAT CCC AAG Aat," (modified nucleotides are shown in bold and the capital letters indicate the target sequence of the shRNA). We then added the mitochondrial pre-sequence of Cytochrome c oxidase subunit IV from yeast to the N terminus of the mutated STAT3 and a FLAG tag to the C terminus using PCR. The PCR product was subcloned into the HindIII and XhoI sites of *pLPC*. Lentiviral vectors expressing HTC enzymes were generated from *pULTRA* and *pULTRA-hot* from Malcolm Moore (Addgene plasmids # 24129 and # 24130). PC was cloned in *pULTRA-hot* as a PCR XbaI/BamHI fragment. MDH1 and ME1 were cloned into *pULTRA* as a fusion protein separated by an intein cleavage site as follows. First, we generated *pUltra-ME1* from a PCR fragment obtained from *pBabe-ME1* and digested with NheI/SalI. Then the MDH1 ORF without stop codon was PCR amplified adding restriction sites XbaI/BamHI for cloning into *pUltra-ME1*.

All PCR primers used for cloning in this study are in Table S1. Lentiviruses *pLKO* expressing *shSTAT3* (*sh3-A*, *sh3-B*), *shMDH1* (*shMDH1-A*, *shMDH1-B*), *shPC* (*shPC-A*, *shPC-B*), *shME1* (*shME1-A*, *shME1-B*), and *shNTC* were from Sigma-Aldrich. To generate *shSTAT3* expression vectors with *hygromycin*, *neomycin* and *blastidicin* resistance, each resistance gene was PCR amplified with primers containing BamHI and KpnI restriction sites and subcloned into *pLKO-puroMYCIN* to replace the puro resistance gene. *shRNA* target sequences are described in Table S1.

For protein expression in bacteria, *H. sapiens* ME1 expression vector was a gift from N. Burgess-Brown (Addgene plasmid # 38857). BirA (*E. coli* Biotin Protein Ligase), SCBPL (*Saccharomyces cerevisiae* Biotin Protein Ligase), and PC full length were a gift from L. Tong (Columbia Univ., NY). *MDH1-His* and *PC*-full length and *PC 486-1176* were amplified by PCR and cloned via BamHI/EcoRI sites into *pHis* that enables the expression of N-terminal 6xHIS fusion proteins or into *pTEV* that enables the expression of N-terminal glutathione-S-transferase (GST) that can be cleaved by the TEV protease (Masclé et al., 2020). *pMXs-3XHA-EGFP-OMP25* for mitochondrial purification was purchased from Addgene (Addgene plasmid # 83356).

#### Proliferation analysis and Senescence associated $\beta$ -galactosidase staining (SA- $\beta$ -Gal).

Growth curves for IMR90 and PC-3 cells were measured using 0.1% crystal violet in PBS (Gillies et al., 1986). Briefly, IMR90 were counted using a hemocytometer and 10,000 cells were plated in a 12-well plate in technical triplicates and a minimum of 4 different plates. Cells were incubated for indicated times and fixed for 10 min using 1% glutaraldehyde solution in PBS. Media was replaced with fresh media every 3 days. Fixed cells were washed twice with PBS and then conserved in PBS with 0.1% NaN<sub>3</sub> until all time points were recovered. Then they were washed twice with PBS followed by staining with 0.1% crystal violet in PBS for 30 min at RT. After staining, cells were washed in tap water until no crystal violet dissolved any longer in water. Colored cells were dried for a minimum of 24 h at RT. To measure growth, crystal violet was extracted with 10% acetic acid in water for 15 min with moderate shaking and OD at 590 nm was measured using photometer. The amount of crystal violet correlates well with cell numbers as we verified experimentally.

For all experiments, the number of biological replicates (n) is indicated and within each biological replicate the mean of three technical replicates was taken. For the experiment done in IMR90 expressing RAS and two of the three HTC enzymes each biological replicate only included technical duplicates. For colony assays with MEFs, 10,000 cells were plated in triplicate into 6 cm plates and incubated for 12 days. Cells were fixed with 1% glutaraldehyde in PBS and then colored with 0.1% crystal violet in PBS. Pictures were taken with a Bio-Rad bio imager.

SA- $\beta$ -Gal staining was performed as described (Deschênes-Simard et al., 2013). Briefly, cells were plated and fixed 24 h after in 0.5% glutaraldehyde in PBS for 10 min at RT. Then they were washed once with PBS for 5 min and twice for 10 min with PBS pH 6.0 containing 1 mM MgCl<sub>2</sub>. Staining solution was added to cells and incubated for 1-6 h away from light at 37°C. SA- $\beta$ -Gal staining solution consisted of PBS pH 6.0, 1 mM MgCl<sub>2</sub>, 2.5  $\mu$ M X-Gal, 5  $\mu$ M potassium ferricyanide and 5  $\mu$ M potassium ferrocyanide. Solution was filtered using 0.45  $\mu$ m filter and heated to 37°C. For MEFs, PBS 1 mM MgCl<sub>2</sub> was at pH 5.5 and for PC-3 cells pH = 5.75 and cells were incubated overnight. For quantification, a minimum of 50 cells per biological replicate were scored under the light microscope.

Clonogenic assay with PC-3 cells was performed in 48-wells plates (Corning, NY) pre-coated with Nutragen® Bovine Type I Collagen mix, (Advanced BioMatrix, San Diego, CA) diluted at 2 mg/mL in ice-cold growth medium, then warmed at 37°C for 30 min to form the gel. PC-3 cells were trypsinized to generate a single-cell suspension and 2,500 cells were prepared in Nutragen®/media mix and deposited in each well to form the second layer. Plates were incubated at 37°C for 45 min to allow the second layer to jelly. Finally, fresh media was added on top of each well and changed every 3 days. Colony formation was scored 1 week after.

#### Retroviral and Lentiviral infections

For lentiviral infections, 5x10<sup>6</sup> HEK293T cells were seeded in 10 cm plates and grown for 16 h. Then, cells were transiently transfected using 3  $\mu$ g of a lentiviral expression vector, 2  $\mu$ g of the *pCMV-dR8.2 dvpr* plasmid and 1  $\mu$ g of the *pCMV-VSV-G* envelope



protein expression plasmid in 900  $\mu$ L of 1  $\times$  Opti-MEM (GIBCO Life Technologies, Burlington, ON). Mixture of DNA with 1  $\times$  Opti-MEM was vortexed for 10 s followed by adding 16  $\mu$ L of X-tremeGENE 9 DNA Transfection reagent (Roche, Laval, QC) at the bottom of the Eppendorf tube. Tubes were inverted 6 times and incubated for 15 min at room temperature and then the mix was added to the cells. After 16 h, 10 mM sodium butyrate (Sigma-Aldrich) was added for a minimum of 6 h, and then the medium was changed. Supernatants from the transfected plates were collected 36 to 60 h after transfection. The viral soups were filtered through a 0.45  $\mu$ m filter, supplemented with 4  $\mu$ g/mL polybrene (Sigma) as well as 10% high grade serum and added on target cells. In preliminary test the viral titer produced by one 10 cm dish was sufficient to infect two 10 cm of target cells (Lessard et al., 2018). For shSTAT3 and shNTC in IMR90 2.5 mL of a 10 mL the lentiviral soup was used to infect cells (depletion of STAT3 with high viral titer induces apoptosis in IMR90 cells). For all other IMR90 and PC-3 cells lentiviral infections, 5 mL of a 10 mL lentiviral soup was used. For IMR90 lentiviral soup was incubated for a minimum of 8 h. For all other cell lines 24 h.

For retroviral infections  $5 \times 10^6$  Phoenix-Ampho packaging cells were plated into a 10 cm plates and transfected with 20  $\mu$ g of retroviral plasmid and 10  $\mu$ g of 4070A amphotropic envelope protein expression plasmid *pAMPHO* by using calcium phosphate method as described (Ferbeyre et al., 2000). Following transfection, the viral soup from one 10 cm plate was used to infect one 10 cm dish of target cells and incubated for a minimum of 8 h. Fresh media was added to the packaging cells and the targets cells were reinfected 8 h after. To prepare target cells for infection cells were seeded so that on day of infection target cells were 70–80 percent confluent. After a minimum of 12 h post last infection, target cell population was selected using 2.0  $\mu$ g/mL puromycin (Wisent) and/or 50  $\mu$ g/mL hygromycin (Wisent) and/or 400  $\mu$ g/mL G418 and/or 2.5  $\mu$ g/mL Blasticidin S (Wisent). In case two or more selection agents were used at the same time doses were 1.0  $\mu$ g/mL puromycin (Wisent) and/or 25  $\mu$ g/mL hygromycin (Wisent) and/or 300  $\mu$ g/mL G418 and/or 2.5  $\mu$ g/mL Blasticidin S. If three or more selection were required selection was done sequentially starting by puromycin and G418 followed by hygromycin and G418. For PC-3 cells selection was maintained for the length of the experiments (Ferbeyre et al., 2000).

For spinfection of senescent BJ cells with HTC expression vectors, BJ cells were plated into 6-well plates so that on day of infection they were 90% confluent. Production of pseudo viral particles was done as described above with the modification that 1/10 of a 10 cm produced viral soup was used per well. For infection, viral soup was added with 4  $\mu$ g/mL polybrene and 10% high grade serum to BJ cells and cells were spun at 3200 RPM for 3 h at 32°C.

For LBNOX expression, IMR90 cells were infected with either control empty vector with RFP selection or its derivative expressing *LBNOX-3-xFLAG*. After infection, cells were incubated for 7 days then selected by RFP positive cells using BD FACSAria cell sorter at IRIC flow cytometry core platform.

#### Pyruvate/Aspartate/Duroquinone/ Dimethylmalate/ and $\text{CoCl}_2$ supplementation

Pyruvate and aspartate were dissolved in DMEM growth media and replaced every 48 h. For vehicle normal DMEM growth media was used. As pyruvate and aspartate were dissolved in the same vehicle only one vehicle condition for both supplementations was run, resulting in same value for three replicates for control conditions (shNTC+ Veh, shS3[A]+ Veh, shS3[B]+ Veh) for growth curve, SA- $\beta$ -Gal, NAD<sup>+</sup>/NADH ratio and immunofluorescence. As growth curve of aspartate showed big variation two more independent *n* were performed. Supplementation started on the day the cells were infected. For duroquinone and dimethylmalate both were dissolved in high-grade DMSO (Sigma) and replaced every 48 h. For  $\text{CoCl}_2$  treatment, IMR90 cells expressing PC-cherry were plated on coverslips and treated for 48 h with the  $\text{CoCl}_2$  (Bioshop). Cells were washed and fixed by 4%PFA and standard immunofluorescent protocol. Images were acquired with LSM 800 confocal microscope and Elyra hyper resolution microscope. For quantification, the filter set 77 of Zeiss was used as such the colocalization appears as yellow color where no colocalization is seen as red or green in the oculars. Areas with no colocalization (Red signal from PC cherry) were counted per cell.

#### Cell culture with hypoxia

Experiments with 1% oxygen were done as described in (Kilic Eren and Tabor, 2014) IMR90 fibroblast were infected with RAS oncogene and control shRNA (shNTC) or RAS oncogene and shRNA targeting a component of the HTC complex and on day 3 post-infection cells were split into two different plates, one was maintained in 21% oxygen and the other one was transferred into a Xvivo System glove box (BioSperix, Parish NY) hypoxia chamber connected to  $\text{N}_2$ ,  $\text{CO}_2$  and  $\text{O}_2$  gas. The chamber was set to 37°C, 5%  $\text{CO}_2$ , and relative humidity of 60%. Oxygen level was adjusted to 5% and monitored using the system's own pre-calibrated oxygen sensors. After 24 h at 5% oxygen the chamber oxygen levels were decreased to 1% for the rest of the experiment. Media of the cells was changed every 48 h and replaced with fresh DMEM media. To avoid residual oxygen in the media trypsin or PBS, the solutions were preincubated for a minimum of 24 h in 1% oxygen prior to use. For immunofluorescence to visualize HTC foci, 150,000 cells were plated on coverslips and incubated for another 24 h, Slides were then processed as described in immunofluorescence.

#### MitoTracker staining

In order to visualize mitochondria, MitoTracker Deep Red (M22426 Thermofisher) was used according to manufactures instructions. To stain cells 250 nM of freshly dissolved MitoTracker Deep Red was added for 20 min to cells. Cells were washed twice with PBS and processed for immunofluorescence as described below. All steps after staining were carried out avoiding exposure to light.

### Hexanediol treatment

For 1,6-hexanediol treatment cells were plated for immunofluorescence on coverslips. Media was replaced with media containing 1% hexanediol (Sigma) and then placed for 10 min in the incubator at 37°C. Media was removed and cells were washed twice with PBS and processed for immunofluorescence as described below.

### Immunoblots and Immunoprecipitation

Immunoblots and immunoprecipitation were performed as described previously (Lessard et al., 2018). Cells were washed twice with ice cold PBS followed by aspiration of residual PBS. Cells were lysed in 500  $\mu$ L to 2 mL of modified Laemmli Buffer (4% SDS, 20% glycerol, 0.125 M Tris-HCl pH 6.8) and recovered using a clean cell scraper. Samples were transferred into tubes and sonicated at lowest intensity for 20 s followed by heating for 5 min at 97.5°C. Samples were cooled to RT and protein were quantified using Nano-drop absorbance at A280. Samples were diluted to 2 mg/mL using modified Laemmli Buffer and 10% 2-mercapthoethanol, 0.1% bromophenol blue was added. Samples were kept at  $-20^{\circ}$ C until use.

Multilayered SDS-Gels were poured as follows. For all gels, we used 0.1% SDS, APS and TEMED. For resolving gels, 375 mM Tris HCl, pH = 8.8 was used. A first layer of higher concentration of Acrylamide-BisAcrylamide(37.5:1) (15% or 12%) was poured, then isopropanol was added on top. Isopropanol was removed after the gel was solidified and a second layer of Acrylamide-BisAcrylamide(37.5:1) (12% or 10%) was dispensed and again layered with isopropanol. Isopropanol was again removed and a third layer of Acrylamide-BisAcrylamide(37.5:1) (10% or 8% or 7%) was poured and covered by isopropanol. Finally, after removing the isopropanol, the gel was topped with Acrylamide-BisAcrylamide(37.5:1) (4%, with 0.125 M Tris HCl-pH = 6.8) and wells were made using a comb. Once all gels were solidified, samples were heated to 95°C for 2 min and spun down for 30 s at 16,000 g. 20 to 40  $\mu$ g of protein was loaded per sample. Gels were run in SDS-PAGE Mini (BioRad) machines with Tris-Glycine SDS buffer according to manufacturer's instruction. SDS-PAGE was transferred onto nitrocellulose (BioRad) or PVDF (Millipore) membrane with Tris-Glycine MeOH buffer according to manufacturer's instructions. Membranes were blocked for 1 h in 5% skim milk diluted in TBS (Tris-buffered saline) and incubated overnight at 4°C or 30 min at RT with primary antibodies (see supplementary table S2 for antibody dilutions). After primary antibody incubation, membranes were washed with 3 times 5 min with TBST (Tris-buffered saline with 0.05% Tween-20). Secondary antibody coupled to HRP were diluted 1:3000 in milk TBS and incubated for 1 h at RT. Membranes were rinsed 3 times followed by 3 washes of 10 min each with TBST. To reveal signal, ECL substrate was added (Perkin Elmer (Western Lightning Plus-ECL, Enhanced Chemiluminescence) or Amersham(Amersham ECL Detection Reagents)) and images were acquired using autoradiography.

For estimation of protein molecular weight FroggBio BLUelf Prestained Protein ladder was run on each SDS-PAGE. In immunoblots, a minimum of one size mark is shown. Of note membranes were cut into pieces to incubate with different antibodies. In case of experiments were performed on several membranes' representative tubulin blot as loading control is shown. Primary antibodies dilutions are listed in Table S2.

Immunoprecipitation protocol was performed as in the great protocol described here (Lessard et al., 2018). Briefly, to reveal endogenous interactions of the HTC enzymes we grew HuH-7 cells in a 15 cm cell culture dish, washed them twice with ice-cold PBS and scrapped them with 1 mL of IP buffer (50 mM Tris-HCl, pH 7.9, 1 mM EDTA, 0.1 mM EGTA, 12.5 mM MgCl<sub>2</sub>, 400 mM NaCl, 20% glycerol, 1% Triton X-100, 0.1% SDS and 1x cOmplete-EDTA free protease inhibitor cocktail from Roche Applied Science). Cell lysates were sonicated at lowest intensity for 30 s and then cleared at 16,300 g for 30 s. Immunoprecipitation was done using either 5  $\mu$ g of anti-ME1 rabbit polyclonal or rabbit pre-immune serum overnight at 4°C. Recovery of immunoprecipitated proteins was performed using a 1:1 mix of Protein-A and -G dynabeads (Invitrogen). Prior to use, Protein A/ Protein G mix was blocked for 30 min in IP Buffer containing 2.5% BSA, 0.16  $\mu$ g/ $\mu$ L *E. coli* tRNA (Sigma-Aldrich) and 0.16  $\mu$ g/ $\mu$ L salmon sperm DNA (Sigma-Aldrich). Dynabeads were added to cleared lysates and incubated for 2 h at 4°C. Finally, the mixture was washed 2x 10 min at 4°C in IP Buffer followed by 3x 1 h wash in IP Buffer at 4°C. Total cell lysates and immunoprecipitates were separated by SDS-PAGE and analyzed by western blot.

Immunoprecipitations with FLAG-M2 Sepharose beads (Sigma) or HA magnetic beads (Pierce/Invitrogen) were done as described above, with the following modifications. For immunoprecipitations with FLAG-M2 Sepharose beads, 20  $\mu$ L of beads per immunoprecipitation were used. For HA immunoprecipitations, 10  $\mu$ L of magnetic beads were used for each immunoprecipitation. The amount of plasmid transfected for each experiment is detailed in Table S3. HEK293T cells were transfected with calcium phosphate method as described above incubated for a minimum of 16 h and then washed with 1xHEPES and incubated for another 6 h in cell incubator. Finally, cells were washed with ice cold PBS twice and then lysed in IP buffer (50 mM Tris-HCl, pH 7.9, 1 mM EDTA, 0.1 mM EGTA, 12.5 mM MgCl<sub>2</sub>, 400 mM NaCl, 20% glycerol, 1% Triton X-100, 0.1% SDS and 1x cOmplete-EDTA free protease inhibitor cocktail from Roche Applied Science). Lysates were sonicated at lowest intensity for 30 s and then cleared at 16,300 g for 30 s. Cleared lysates were incubated for 1 h at 4°C on a rocking platform with corresponding beads. Mixture of beads and immunoprecipitate were washed 2x with IP buffer and then washed 3x for 10 min at 4°C on a rocking platform. For FLAG immunoprecipitations, beads were spun down another time and washed again 2x with IP buffer. Total cell lysates and immunoprecipitates were separated by SDS-PAGE and analyzed by western blot.

For Mapping of the interaction sites of ME1, MDH1 and PC, gene fragments for each of the three proteins were generated by PCR as described above. The amount of plasmid transfected for each experiment can be found in Table S3. For ME1 fragments HEK293T cells were treated for 6 h with 20  $\mu$ M of MG132 in order to stabilize unstable ME1 fragments.



### Protein purification

All proteins were purified in three steps; first by metal affinity chromatography followed by ion-exchange chromatography (IEX) and then size-exclusion chromatography as adapted from (Tao et al., 2003) and references therein. For the purification of ME1, the bacterial expression vector was transformed into the *E. coli* BL21 Star expression strain and bacteria were grown at 37°C to an OD<sub>600nm</sub> of 0.8. Expression of ME1-HIS was induced for 6 h at 30°C with 1 mM isopropyl β-D-1-thiogalactopyranoside (IPTG). Bacterial pellets were resuspended and lysed in Lysis Buffer (30 mM imidazole, 30 mM Tris-HCl pH 8.0, 500 mM NaCl) supplemented with 1x cOmplete protease inhibitor cocktail (Roche) and passed through a French Press. Bacterial lysates were centrifugated at 35,000 rpm in a Beckman 55Ti rotor for 45 min at 4°C. The cleared lysates were loaded on a column of chelating Sepharose Fast Flow immobilized metal affinity chromatography resin (GE Healthcare) charged with nickel and washed with 15 column volumes (CV) of 30 mM imidazole, 30 mM Tris-HCl pH 8.0, 500 mM NaCl and 1x cOmplete protease inhibitor followed by a second wash with 2 CV of 60 mM imidazole, 30 mM Tris-HCl pH 8.0, 500 mM NaCl, and 1x cOmplete protease inhibitor. Proteins were eluted with 5 CV of 250 mM imidazole, 500 mM NaCl, 30 mM Tris-HCl pH 8.0, 10% Glycerol and dialysed with 125 mM NaCl, 30 mM Tris-HCl pH 8.0, 5 mM DTT overnight at 4°C, then loaded into a Q Sepharose FF column (GE Healthcare). After loading, the column was washed with 0.5 CV of Buffer A (30 mM Tris-HCl pH 8.0, 75 mM NaCl, 5 mM DTT) or until UV absorbance returned to baseline. The column was then washed with 2 CV of Mix buffer A and buffer B (30 mM Tris-HCl, 1M NaCl, 5 mM DTT) at conductivity of 20 mS/cm. Gradient of B was set to 50 percent for 60 min.

We used the same protocol to purify MDH1 with the following modifications. For MDH1, expression was induced with IPTG at 30°C, eluted from the nickel column with 300 mM imidazole, 500 mM NaCl, 30 mM Tris-HCl pH 8.0, and the purified protein was dialysed into 25 mM NaCl, 30 mM Tris-HCl pH 8.0, 5 mM DTT overnight at 4°C. IEX on the Q-Sepharose column was then performed with Buffer A (30 mM Tris-HCl pH 8.0, 25 mM NaCl, 5 mM DTT) and Buffer B (30 mM Tris-HCl pH 8.0, 500 mM NaCl, 5 mM DTT). ME1 and MDH1 were then concentrated using Amicon centrifugal tubes with a MW cut-off of 10 kDa (Millipore). Samples were frozen at -80°C in 10% glycerol, 200 mM NaCl, 5 mM DTT until used.

For PC full-length, BL21 Star bacteria bearing PC- and BPSCL-expressing plasmids were grown until an OD<sub>600</sub> of 0.9. Then, 25 mg/L of Biotin and 0.1 mM of MnCl<sub>2</sub> were added and incubated for another 45 min. Expression was induced for 16 h with 1 mM IPTG at 18°C. For metal affinity chromatography, cleared lysates were loaded on the nickel column washed with 15 CV of 30 mM imidazole, 30 mM Tris-HCl pH 8.0, 500 mM NaCl and 1x protease inhibitor cocktail, followed by washes with 2 CV of 40 mM imidazole and 1 CV of 60 mM imidazole. Proteins were first eluted with 200 mM imidazole, 30 mM Tris-HCl pH 8.0, 500 mM NaCl and then concentrated using slow dialysis by supplying a saturated solution of 35K PEG (Sigma). Dialysis solution 15% glycerol, 200 mM NaCl, 30 mM Tris-HCl pH 8.0 with saturated PEG 35K. Proteins were then frozen at -80°C until used.

For the PC (486-1178) fragment, BL21 Star bacteria bearing PC- and BirA-expressing plasmids were grown until an OD<sub>600</sub> of 0.9. Then, 25 mg/L of Biotin and 0.1 mM of MnCl<sub>2</sub> were added and incubated for another 45 min. Expression was induced for 16 h with 1 mM IPTG at 18°C. For metal affinity chromatography, cleared lysates were loaded on the nickel column washed with 15 CV of 30 mM imidazole, 30 mM Tris-HCl pH 8.0, 500 mM NaCl, protease inhibitor cocktail followed by washes of 2 CV of 40 mM imidazole and 1 CV of 60 mM imidazole. Proteins were eluted with 200 mM imidazole, 30 mM Tris-HCl pH 8.0, 500 mM NaCl and dialysed with 75 mM NaCl, 30 mM Tris-HCl pH 8.0, 10% glycerol, 1 mM (tris(2-carboxyethyl)phosphine) (TCEP), 2 mM MnCl<sub>2</sub> overnight at 4°C. IEX on the Q-Sepharose column was then performed with Buffer A (75 mM NaCl, 30 mM Tris-HCl pH 8.0, 10% glycerol, 0.2 mM TCEP, 2 mM MnCl<sub>2</sub>) and Buffer B (500 mM NaCl, 30 mM Tris-HCl pH 8.0, 10% glycerol, 0.2 mM TCEP, 2 mM MnCl<sub>2</sub>).

For SEC, all frozen proteins were thawed and dialysed into 10% glycerol, 50 mM NaCl, 20 mM MgCl<sub>2</sub>, 0.2 mM EDTA, 2 mM MnCl<sub>2</sub>, 30 mM Tris-HCl, pH 7.55. SEC was performed on either a Superdex 200, a Superdex 200 Increase or Superose 6 columns. In all cases, the running buffer was 10% glycerol, 50 mM NaCl, 20 mM MgCl<sub>2</sub>, 0.2 mM EDTA, 2 mM MnCl<sub>2</sub>, 30 mM Tris-HCl pH 7.55 supplemented with 1 mM ATP, 1 mM NADH, 1 mM NADPH and 0.2 mM TCEP.

### Native separation of multi-protein complexes

The procedure was previously described (Camacho-Carvajal et al., 2004). In brief, a 10 cm Petri dish of HuH-7 at ~85% confluence was washed twice with ice-cold PBS. Then, cells were scraped in PBS on ice and centrifuged for 10 min at 1500 rpm (Napco, 2028R) at 4°C. Cells were lysed in 250 μL of cold CSH buffer (50 mM Tris-HCl pH 7.5, 25 mM NaCl, 1 mM EDTA, 0.1% Triton X-100) supplemented with 1x PhosSTOP and 1x cOmplete EDTA-free protease inhibitors (Roche), and incubated for 30 min on ice. Lysates were spun down for 20 min at 15 000 g at 4°C and the supernatant was loaded on a BioVision 10 kDa Spin column with 375 μL of cold BN buffer (500 mM 6-aminocaproic acid, 20 mM Bis-Tris pH 7.0, 2 mM EDTA, 12 mM NaCl, 10% glycerol, 0.1% Triton X-100, complete EDTA-free protease inhibitor). The column was centrifuged for 45 min at 15 000 g at 4°C. The flow-through was discarded and 350 μL of cold BN buffer was added to the column. This procedure was repeated, then the column was centrifuged for an additional 90 min or until the column content was concentrated to ~150 μL. 50 μL per well of this product was separated on a 4%–20% native gel (4568094, Bio-Rad) overnight at 16 mA in a cold-room with the anode buffer (50 mM Bis-Tris pH 7.0) and cathode buffer (50 mM Tricine, 15 mM Bis-Tris pH 7.0, 0.02% Coomassie G-250) and using 7 μL of the ladder Native Mark (ThermoFisher). The following day, half of the gel containing the sample and the ladder was stained with Coomassie R-250 to assess the migration of the blue native gel, and a replicate lane containing the sample was cut in 9 equivalent pieces from top (piece 1) to bottom (piece 9). Each gel piece was denatured for 1 h in 1 mL of 2x Laemmli Buffer (4% SDS, 20% glycerol, 120 mM Tris-Cl pH 6.8, 10% β-mercaptoethanol). Then, each piece was inserted in a well of a second 10-well 4%–20% gradient gel with fresh 2x Laemmli Buffer to avoid bubbles, and the gel

was migrated in a SDS-PAGE running buffer (192 mM Glycine, 25 mM Tris base, 0.1% SDS) with the BlueEye Protein ladder (Froggabi) at 90V until the ladder was well separated.

#### Avidin pull down

To perform Avidin pull-down experiments, either PC or PC(468-1178) was mixed with a 5-molar excess of purified MDH1-HIS and ME1. MDH1, PC and PC(468-1178) were purified as described above. For ME1, the protein was obtained by expressing an ME1-GST fusion protein in *E. coli* BL21 cells that were grown at 37°C to an O.D.<sub>600nm</sub> of 0.01. Expression of ME1-GST was induced for 16 h at 20°C with 20 μM isopropyl β-D-1-thiogalactopyranoside (IPTG). Bacterial pellets were resuspended and lysed in Lysis Buffer (30 mM Tris-HCl pH 8.0, 500 mM NaCl, 5% DTT) and passed through a French Press. Lysed cells were centrifuged at 35,000 rpm in a Beckman 55Ti rotor for 45 min at 4°C. The supernatant was incubated 1 h, at 4°C with Glutathione Sepharose 4B (GSH; GE Healthcare) resin. After this, the resin was spun down washed three times with lysis buffer to remove non-specifically bound molecules followed by three washes with TEV buffer (20 mM Tris-HCl = pH 7.4, 125 mM NaCl, 5 mM DTT) and incubated twice for 18 h at 4°C with 100 units of TEV protease. After the first 18 h, resin was spun down and supernatant was collected and reserved. New TEV was added and incubated again for 18 h. Both fractions were combined filtered and extensively dialyzed into 20 mM Tris-HCl = pH 7.4, 250 mM NaCl, 5% Glycerol.

For control of non-specific binding to Avidin beads, PC or PC (486-1178) was not added to mixture. All of the following steps were performed for both PC, MDH1, ME or MDH1, ME1 alone. A mixture of PC, ME1 and MDH1 was dialyzed for 4 h into 50 mM Tris-HCl, pH 7.9, 1 mM EDTA, 0.1 mM EGTA, 12.5 mM MgCl<sub>2</sub>, 150 mM NaCl, 20% glycerol, 1% Triton X-100, 0.1% SDS at 4°C with rotation. Samples were recovered, and 1% of the mixture was reserved as input. The remaining portion of the mixture was transferred into an Eppendorf tube containing a 30 μL of slurry of Avidin beads (Pierce/ThermoFisher) prepared as described by the manufacturer. The protein mixture was incubated with the avidin beads for 1 h on a rocking platform at 4°C. The beads were washed three times with wash buffer (50 mM Tris-HCl, pH 7.9, 1 mM EDTA, 0.1 mM EGTA, 12.5 mM MgCl<sub>2</sub>, 300 mM NaCl, 20% glycerol, 1% Triton X-100, 0.1% SDS). To elute proteins from the beads, 50 μL of 6x SDS-loading buffer (0.5 M Tris-HCl pH 6.8, 30% glycerol, 10% SDS, 1% bromophenol blue and 15% β-mercaptoethanol) was added to the mixture and boiled 3x for 10 min, then loaded on an SDS-PAGE gel and transferred onto nitrocellulose membrane for western blot analysis.

#### Assembly of ternary complex

For assembly of the ternary complex, equimolar quantities of purified PC, MDH1 and ME1 were incubated together in assembly buffer (10% glycerol, 50 mM NaCl, 20 mM MgCl<sub>2</sub>, 0.2 mM EDTA, 2 mM MnCl<sub>2</sub>, 30 mM Tris-HCl, pH 7.55) supplemented with 5 mM ATP, 5 mM NADH, 5 mM NADPH and 0.2 mM TCEP on a rocking platform for 1 h at room temperature. SEC as described above was performed and the proteins eluted between 8 and 12 mL were taken for analysis. The sample was then concentrated using centricon mini tubes with a cut-off of 3 kDa.

#### SEC-MALS

SEC-MALS was performed using a microAкта (GE Healthcare) in-line with a Dawn HELEOS II (Wyatt Technology) and OptiLab T-rEX (Wyatt Technology). For data acquisition, ASTRA 6.1.6.5 (Wyatt Technology) software was used. Freshly prepared BSA (Sigma) and Aldolase (Sigma) were used as standards to normalize the detectors and align the signals at 280 nm absorbance. A Superdex 200 Increase column was used for the SEC portion of all experiments. The column flow rate was set to 300 μL/min and SEC buffer was as described above for protein purification. The flow from the column was collected in 0.5 mL fractions and protein content verified afterward on an SDS-PAGE gel with Coomassie staining. In addition, experiments containing MDH1 or assembled complexes were monitored for absorbance at both 280 nm and 340 nm. Before each experiment, the column and detector were equilibrated with running buffer overnight. The calibration constant for the Dawn Heleos II was determined for these experiments with  $3.8200 \times 10^{-5} \text{ 1/(V cm)}$ . For the analysis, the data acquired from experiments with proteins of interest were aligned and band broadening and normalization was applied. For Aldolase, the dynamic radius was set to 4.8 nm and for monomeric BSA to 3.3 nm. After normalization, despiking of data was set to heavy and baselines as well as peaks were defined. Peaks were defined as half heights of peaks. For multiple peaks, peaks were manually adjusted. Detectors with low signal, high angle and low angle were disabled until fitting line of  $K^*c/R(\theta)$  to  $\sin^2(\theta/2)$  was diagonal. Molecular mass was determined using Zimm modeling. The dynamic radius was obtained by Rh from QLES in Astra with analysis standard parameters. Analysis was verified with the results fitting tool and by moving through the peak and molar mass.

#### Immunofluorescence

A minimum of 50,000 cells were seeded on 1.5 mm thickness coverslips and incubated for at least 48 h. Cells were washed twice with ice cool PBS and then fixed for 15 min with 4%PFA at RT. Then cells were washed three times for 5 min with 0.1 M glycine in PBS to inactivate PFA and stored in PBS 0.2%NaN<sub>3</sub> at 4°C until use. Cells were washed twice 5 min at RT with PBS to remove azide and then permeabilized with 0.1M glycine and 0.4% Triton X-100 in PBS for 5 min at 4°C. Then, they were incubated 3 times for 15 min with 3% BSA in PBS. Primary antibody was diluted in 3%BSA in PBS and 2% Donkey or 2% Goat serum. For dilutions of primary antibody see supplementary table S2. Primary antibody was added to coverslip and incubated in humidified chamber at 4°C overnight. Next day, the cells were washed 3 times with PBS 3%BSA for 10 min. Secondary antibody was diluted 1:1500 in 3%BSA in PBS and 2% Donkey or 2% Goat serum and incubated for 1 h at RT. Cells were then washed three times with PBS, excess PBS was removed and mounted on glass coverslips in Vectashield with DAPI. Edges were sealed off with nail polish and mounted cells were kept

for a minimum of 24 h at 4°C. On day of confocal imaging coverslips were removed from the fridge at least 1 h prior to imaging and put in microscope box to warm up to RT of the microscope. Images were taken randomly in at least 5 different regions of the coverslip to ensure representation of sample using the Zeiss Axio Imager Z2 upright microscope equipped with a CoolSNAP FX camera (Photometrics) and/or Axiocam camera and ZEN 2 blue and black edition software. Images were analyzed using ImageJ and Fiji. For quantification of DNA damage foci, PML nuclear bodies and mitochondrial fragmentation a minimum of 50 cells was counted and scored on microscope. For co-localization, we used an FV300 Olympus confocal microscope (Richmond Hill, ON) with a PMT first generation and Fluoview V4.2 Software. For super-resolution structured illumination microscopy (SR-SIM), images were taken with Super-Resolution microscope Axio Observer Z1 ZEISS Elyra PS.1, from Zeiss (Carl Zeiss, Oberkochen, Germany). All raw data were acquired with EMCCD Du885K ISO VP461 camera. Images were taken with 5 rotations. To obtain the final image the structured illumination algorithm of ZEN 2.1 was used. For further confocal microscope imaging the Zeiss LSM 800 with spectral analysis detector was used. All images were acquired sequentially. The data was acquired with a maximal airy unit of 1. For colocalization, secondary antibodies were incubated sequentially to avoid cross-reactivity between the antibodies. To quantify the colocalization between HTC enzymes, foci containing signals for the three enzymes were counted in different cells. The background was subtracted, and brightness adjusted to the same level for all images. Pseudocolor was added and an overly image was generated using the merge color function of ImageJ. For this function double co-localization is shown in yellow and triple co-localization is shown in white. Colocalization was expressed as the number of foci with visible white signal. Colocalization was also measured using the Plot profile function of ImageJ. The fluorescent intensity for each pixel was determined across a line drawn as shown in Figure 2.

#### Immunohistochemistry

For TMA of prostate tissue sequential TMA slides were heated at 55 °C for 1 h followed by steps of sequential incubation in xylene (2 × 6 min), 100% ethanol (1 × 5 min), 95% ethanol (1 × 3 min), 75% ethanol (1 × 3 min) and 40% ethanol (1 × 3 min). Finally, samples were washed in dH<sub>2</sub>O for 3 min.

Heat antigen retrieval was performed by using a steamer with the following settings, 45 min in 10 mM citrate buffer (pH 6.0). The steamer was started at RT and reached 95 °C in 15-20 min. Slides were then incubated for another 25-30 min. Slides were cooled and washed with PBS containing 0.3% Triton X-100 3 times for 3 min with 1 × TBS/0.3% Triton X-100. To inactivate endogenous peroxidases slides were incubated for 5 min at room temperature in a solution of 3% H<sub>2</sub>O<sub>2</sub> followed by 3 washes for 3 min in 1 × TBS/0.3% Triton X-100. To delimit tissues a hydrophobic barrier pen (DAKO) was used. Tissues were blocked 1 h at RT with a protein-blocking serum-free ready-to-use reagent (DAKO, cat. no. X0909, Carpinteria, CA). Excess of blocking was tapped off and tissues were incubated overnight at 4°C with primary antibodies diluted in 5% goat serum in 1 × TBS/0.3% Triton X-100. Antibodies used were: anti-MDH1 (1:2000, Santa Cruz), anti-PC (1:500, Santa Cruz) and anti-ME1 (1:500, Genetex). After overnight incubation samples were washed 3 times for 3 min in 1 × TBS/0.3% Triton X-100 followed by primary antibody detection using the LSAB2 System-HRP (DAKO, cat. no. K0675, Carpinteria, CA). Secondary biotinylated antibody (DAKO) was incubated for 30 min followed by washes as above. Finally, samples were incubated for another 30 min with streptavidin-HRP (DAKO) and washed as above. To reveal staining peroxidase with Di-amine-benzidine (DAB) substrate kit (SK-4100, Vector Labs., Burlington, ON) was used. To stop the reaction, slides were washed in tap water when the staining was sufficient; the same incubation time was applied to all samples.

For visualization, counterstaining with hematoxylin (HHS16, Sigma-Aldrich) was used and tissues were rapidly dehydrated by sequential incubation in 40% ethanol (1 × 1 min), 75% ethanol (1 × 1 min), 95% ethanol (1 × 1 min), 100% ethanol (1 × 1 min) and xylene (2 × 5 min). Slides were mounted in Cytoseal (8310-4, Thermo Fisher) mounting media and scanned with NanoZoomer 2.0-HT scanner (Hamamatsu). Images were processed with NDP.view 2.6.8 (NanoZoomer Digital Pathology.view 2.6.8) (Hamamatsu) and ImageJ.

Tissue Micro Arrays were purchased from US Biomax (catalog no. PR807c, Rockville, MD). TMAs from US Biomax were reviewed by two board-certified pathologists. Quantification was done by two independent persons and combined. In case of disagreement, the mean of both intensities was taken. There was no occurrence of disagreement by more than 1 score point. Mouse samples IHC were performed at the Molecular Pathology platform of CR-CHUM following the platform protocol <https://www.chumontreal.qc.ca/en/crchum/facilities-and-services>. For quantification, three sections were selected blindly by one person based on histology for prostate epithelial tissue. For Pten<sup>-/-</sup>, six sections were selected to better represent diversity of the tissue. It is important to notice that Pten<sup>-/-</sup> knockout is only present in the prostate epithelial cells and all other cells in the prostate still contain Pten. For one Pten<sup>-/-</sup> sample, only two sections were selected as there was little prostate epithelial cell regions identified. All selected sections were then scored by two independent persons for Ki67, MDH1, ME1 and PCX staining intensity according to a scoring key and scoring was combined. In case of disagreement, the mean of both intensities was taken. There was no occurrence of disagreement by more than 1 score point.

#### STAT3-ATAD3A Proximity ligation assay (PLA)

PLA was done using Duolink® *In Situ* Green Starter Kit Mouse/Rabbit according to manufacture instructions. To prepare wash buffer A 1 pouch of wash buffer A powder was solubilized in 1L of MilliQ Water. To prepare wash buffer B 1 pouch of wash buffer B was solubilized in 1L of MilliQ Water. Wash buffers were kept at 4°C for no longer than 1 month. Prior to use, wash buffers were warmed to RT.

To prepare cells for PLA, IMR90 fibroblasts were plated on coverslips and incubated for 48 h at 37°C. Cells were fixed using 4% PFA in PBS for 10 min. This followed by a two 5-min wash with PBS 0.1M Glycine. Cells were permeabilized with PBS 0.1M Glycine and 0.4% Triton-X100 for 5 min at 4°C. Cells were then blocked using Duolink blocking buffer for 1 h at 37°C. Primary antibodies were diluted with Duolink antibody dilution and incubated in humidified chamber overnight at 4°C. The cells were washed 3x5 min in 1x Wash Buffer A at room temperature. PLUS and MINUS PLA probes were diluted to 1x in the Duolink® Antibody Diluent and incubated on cells in a humidified chamber for 1 h at 37°C. The cells were washed 3x 5 min in 1x Wash Buffer A at room temperature. Ligase solution was prepared by diluting Duolink® Ligation buffer to 1 x and 1 μL of ligase was added for each 40 μL of 1x ligation buffer. Ligation mixture was added on cells in a pre-heated humidity chamber for 30 min at 37°C followed by 3 washes in 1x Wash Buffer A at room temperature. Amplification solution was prepared by diluting Duolink® Amplification buffer to 1 x and 1 μL of Polymerase was added for each 80 μL of 1x Amplification buffer. Polymerase was incubated for 2 h at 37°C in a pre-heated humidity chamber followed by washes of 3x 10 min in 1x Wash Buffer B at room temperature and a final wash of 0.01x Wash Buffer B for 1 min. Cells on the coverslips were mounted using Vectorshield with DAPI and analyzed no later than 48 after the experiment using the confocal microscope LSM800 as described before. To analyze PLA staining in ImageJ, Circle ROI with a diameter of 5 μm was defined. The background was subtracted and the threshold was set. A binary image was created and analyzed using Analyze Particle with the following settings: Max size of particle 2 μm<sup>2</sup> and circularity of 0.5-1.

#### PC-MDH1 and PC-ME1 Proximity ligation assay (PLA)

PLA was done using Duolink Multicolor Kit with red and green conjugation kits. Conjugation of primary antibodies to green and red oligos was done according to manufacturer's instructions and conjugated antibodies were stored at 4°C. PLA on cells was performed according to manufacturer's protocol with the following modifications. The conjugated antibodies were further diluted using antibody diluent for PC-MDH1 1/75 and for PC-ME1 1/50 and incubated overnight at 4°C. For ligation the multicolor ligase was diluted 1/20 and incubated for 30 min at 37°C. The amplification step was carried out for 120 min at 37°C and the detection step for 45 min at 37°C.

For PLA on tissue, the following modification to the manufacturer's protocol was done. Preparation of tissue slides was done as described in immunohistochemistry. Briefly, paraffin-embedded tissue samples were heated at 55 °C for 20 min followed by incubation in xylene (3 × 5 min), 100% ethanol (2 × 5 min), 95% ethanol (1 × 5 min), 75% ethanol (1 × 5 min) and 40% ethanol (1 × 3 min). Followed by two wash in ddH<sub>2</sub>O. Antigen retrieval was performed by heating in a steamer for 45 min in 10 mM citrate buffer (pH 6.0) with 0.3% Tween 20. The steamer was started at RT and reached 95 °C in 15-20 min. Slides were then incubated for another 25-30 min. Slides were cooled and cells were permeabilized with PBS containing 0.4% Triton X-100 and 0.1M Glycine for 10 min. Slides were washed two times in PBS followed by blocking. For blocking the Duolink block buffer was used and washing times were increased to 10 min and performed 4 times with wash buffer A. Image acquisition was done as described above. For quantification of colocalization of PLA signal (Figure 2 G) the filter set 77 of Zeiss was used as such the colocalization appears as yellow color where no colocalization is seen as red or green in the oculars. For intensity scoring of PLA colocalization signal (Figure 2H) signal intensity of green and red for a given foci is the square root of multiplication of green and red fluorescent intensity. For analysis 15 random foci per condition were chosen.

#### Electron microscopy and colloidal gold immunocytochemistry

Electron microscopy and colloidal gold immunocytochemistry were performed according to (Fouillen et al., 2017). 1x10<sup>7</sup> cells were recovered using Trypsin, washed twice with 0.1M Phosphate Buffer (PB) pH 7.3 (Sambrook Cold Spring Laboratory protocols) and fixed for 30 min at 4°C on a rocking platform using freshly prepared PLP (Periodate L/Lysine paraformaldehyde) fixative consisting of 4% PFA, 0.01 M NaIO<sub>4</sub> and 0.028125 M L-lysine monochloride (Sigma) in 0.1 M PB, then filtered with 0.45 μM filter to remove residual impurities. After fixation cells were washed 3x with PB pH 7.3. Cells were post-fixed for 1 h with 1% potassium ferrocyanide-reduced osmium tetroxide, dehydrated with graded ethanol and then processed for embedding in LR white resin (London Resin Company; Berkshire, UK) as previously reported (Fouillen et al., 2017). Ultrathin 80–100 nm sections were prepared using a diamond knife and transferred onto Formvar®-coated (polyvinyl formate) 200-mesh nickel grids.

For ultrastructural analysis of mitochondria, some ultrathin sections were stained with uranyl acetate and lead citrate and examined either in a FEI Tecnai 12 (Eindhoven, the Netherlands) transmission electron microscope operating at 120 kV or in a Hitachi Regulus 8220 (Tokyo, Japan) scanning electron microscope operating at 30 kV in Bright STEM mode.

For post-embedding colloidal gold immunocytochemistry, some ultrathin sections were incubated with an aqueous solution of 5% sodium metaperiodate for 45 min and washed with distilled water. The nickel grids were then floated on a drop of blocking solution consisting of 1% Ovalbumin in 0.01 M PB for 15 min to avoid non-specific binding, then transferred onto a drop of primary antibody (anti-PC 1:200) and incubated overnight at 4°C. Grids were then rinsed with PB and placed in blocking solution for 15 min. Antibody-antigen complexes were then revealed by floating the grids on a drop of protein A-10 nm colloidal gold complex for 30 min. Negative controls consisted of incubations with protein A-gold alone. Sections were then stained with uranyl acetate and lead citrate, and examined in a FEI Tecnai 12 (Eindhoven, the Netherlands) transmission electron microscope operating at 120 kV.

#### NAD<sup>+</sup>/NADH, NADP<sup>+</sup>/NADPH and glutathione measurements

For NAD<sup>+</sup>/NADH measurements, approx. 50,000 cells were plated for technical triplicates in 6 cm plates and incubated for 48 h and processed by a kit from BioVision. Briefly, cells were sonicated 2x for 15 s and lysates were diluted 5 to 20 times to remain in the linear

range of the kit. For NADP<sup>+</sup>/NADPH measurements, approx. 1,000,000 cells were seeded in triplicate and incubated for at least 48 h. Cells were lysed by sonication twice for 15 s, spun at 13000 rpm in a 10 kDa Spin column to remove endogenous proteins and lysates were assayed using a NADP<sup>+</sup>/NADPH quantification kit (BioVision) according to manufacturer's instructions. For glutathione measurements approx. 5,000,000 cells were plated in technical triplicates, grown for 48 h, harvested in PBS pH 6.0 and 0.1% NP40, lysed by sonication on ice twice for 10 s, spun with a 10k Da Spin column to remove endogenous protein and then analyzed using Abcam Glutathione kit according to manufacturer's instructions. For all three assays, protein content was determined using a Bradford assay kit (Bio-Rad) according to manufacturer's instructions. All assays were carried out in biological triplicates (cells generated from different infections). For NAD and NADP quantification in Figure 4 and Figure S6 same extracts were used to further compare samples.

#### qPCR

To analyze mRNA expression, cells were collected in Trizol (#15596018, Invitrogen) and RNA extraction was performed according to the manufacturer's instructions. For cDNA preparation, 2  $\mu$ g or total RNA were reverse transcribed in a 20  $\mu$ L reaction using the 5X All-In-One RT kit (G590, ABM, Richmond, BC, Canada) as per the manufacturer protocol. Reverse transcription products were diluted 10 times with pure water prior to real-time quantitative PCR. Reactions for qPCR were performed in technical triplicate using 1  $\mu$ L of diluted cDNA samples per 10  $\mu$ L reaction volume also containing: 0.25  $\mu$ M of each primer (synthesized by Biocorp), 0.2 mM dNTP (DD0056, BioBasic), 0.33X Syber Green I (S7563, Invitrogen), 0.25U Jump Start Taq DNA polymerase (D9307, MilliporeSigma) in 1x reaction buffer (provided with the enzyme) enrich with 2.5 mM more of MgCl<sub>2</sub> (M1028, Sigma). The LightCycler 96 Real-Time PCR System (Roche Applied Science) was used to detect the amplification level and was programmed to an initial step of six minutes at 95°C, followed by 50 cycles of 20 s at 95°C, 20 s at 58°C and 20 s at 72°C. A high resolution melting from 60°C to 98°C followed the amplifications. All reactions were run in triplicate and the average values were used for relative quantification of target genes using the  $\Delta\Delta$ CT method. Outlier of triplicates were excluded if the value was 1 Cq different than average.

Prior to use, primers' efficiency was determined by a minimum of 4 serial dilutions and efficiency of amplification between 1.95 and 2.05 was accepted. Primers were validated to show just one amplification product either by running product on agarose gel after PCR or unique peak in melting curves. Primers were designed to be intron spanning where possible. To test for DNA contamination and other contaminants in qPCR a control with no RT was used and a Cq higher than 35 was considered negative for DNA contamination. For normalization TBP and HMBS were used in IMR90 as both mRNA were previously validated to be good housekeeping genes in this cell line (Lessard et al., 2018). For MEFs TBP, HMBS and  $\beta$ -actin were used as housekeeping genes (Deschênes-Simard et al., 2013). Variation of less than 1 Cq in housekeeping genes between conditions was considered acceptable. qPCR primers are presented in Table S1.

#### MitoSox and DCFDA measurements

ROS measurements were done as described previously (Moiseeva et al., 2009) at the FACS CORE Facility of IRIC Research Center at the University of Montreal, Canada. Briefly, cells were incubated at 37°C for 30 min with either MitoSox (Molecular Probes, Eugene, OR) or H<sub>2</sub>DCFDA (Molecular Probes). Cells were collected using Trypsin and washed twice with PBS. Cells were resuspended in 500  $\mu$ L of HBSS for sorting in the BD FACSCanto II system ran with DiVa analysis software. Acquired data were further analyzed using FlowJO software.

#### Mitochondrial purification

For PC localization studies, mitochondria were purified using Mitochondria Isolation Kit for Cultured Cells (Abcam) according to manufacturer's instructions. For mitochondrial STAT3 levels in senescent cells mitochondria were purified by immunoprecipitation according to (Chen et al., 2017). For each experiment, an anti-HA immunoprecipitation was performed on IMR90 cells expressing 3XHA-EGFP-OMP25 and RASV12 or an empty vector. At day 12 post-infection, five 10 cm plates of cells were washed twice with PBS and then scraped into 1 mL chilled KPBS buffer (136 mM KCl, 10 mM KH<sub>2</sub>PO<sub>4</sub>, pH 7.25). The following steps for mitochondrial isolation and metabolite extraction were performed as described in (Chen et al., 2017), except for the incubation with magnetic beads, in which the supernatants were incubated with 30  $\mu$ L of prewashed anti-HA magnetic beads (88837; ThermoFisher Scientific) on a vertical-rotating mixer for 20 min. Proteins were eluted by adding 100  $\mu$ L 6x SDS loading buffer (0.5 M Tris-HCl pH 6.8, 30% glycerol, 10% SDS, 1% bromophenol blue and 15%  $\beta$ -mercaptoethanol) and then analyzed by SDS-PAGE. Immunoprecipitates were run on SDS-PAGE and transferred onto nitrocellulose membrane for western blot analysis. The efficiency of mitochondrial purification was assessed with anti-TOMM20 antibodies and the efficiency of immunoprecipitation was assessed using an immunoblot against HA.

#### Animals

Transgenic male mice with prostate-specific deletions of Stat3, Pten and double Stat3 and Pten deletion (Pencik et al., 2015) were sacrificed at 19-weeks old and their prostate were collected and frozen in OCT for cryosections or in RNAlater (Invitrogen) for RNA and protein extraction. For further information on the mouse model please refer to (Pencik et al., 2015). For immunohistochemistry, a piece of tissue treated with RNAlater was washed with PBS, incubated for 8 h in 15% sucrose in PBS and then 16 h in 30% sucrose in

PBS at 4°C and then fixed in 10% formalin for 24 h at 4°C. After fixation and embedding into paraffin, 4 μm serial sections were cut to perform immunohistochemistry according to CR-CHUM histology core platform. For antibodies see Table S2.

Allografts were performed as described (Deschênes-Simard et al., 2013) using 7 weeks old male NOD.Cg-Rag1<sup>tm1Mom</sup>Il2rg<sup>tm1Wjl</sup>/SzJ (also called NRG) mice injected subcutaneously in both flanks with 100 μL of a premixed solution 1:1 of Matrigel (BD Biosciences) and PBS-resuspended cells at 4°C, containing 1x10<sup>6</sup> MEFs cells expressing the different vectors. Tumor formation was evaluated over a period of 40 days. Tumors volumes were assessed with a caliper every two days as soon as the tumors were palpable, and mice were euthanized before 40 days if tumor volume reached 1.5 cm<sup>3</sup>. At endpoint, half of each tumor collected was flash-frozen for RNA and protein purification and the other half was fixed in 10% neutral buffered formalin (Sigma) for at least 72 h before paraffin embedding.

Serial sections of 4 μm of each tumor were then cut at the Molecular Pathology platform of CR-CHUM and immunohistochemistry was performed, as described above. For histopathology analysis, H&E staining was done at the CR-CHUM Molecular Pathology facility and evaluated by the histopathology laboratory of Dr. Trudel. For RNA and protein extractions, tumor pieces were transferred into Eppendorf tubes and immediately flash-frozen in liquid nitrogen and then kept at -80°C until further use. For RNA isolation, Trizol was added to frozen tumor samples and then tumors were homogenized using a POLYTRON® PT 1200 E (Kinematica). For protein extraction, frozen tumor samples were also homogenized, but only in Laemmli 2x buffer (4% SDS, 20% glycerol, 120 mM Tris-HCl pH 6.8) instead. Extracted proteins were quantified using Micro BCA Protein Assay Kit (Pierce) and equal amount of proteins were run in SDS-PAGE. All mice work was approved by the ethics committee of the CR-CHUM. The following formula was used to determine tumor volume considered as an ellipsoid after measuring the diameter in x, y and z axis.

$$V = \frac{4\pi \frac{h}{2} \frac{w}{2} \frac{l}{2}}{3} = \frac{4\pi \frac{hwl}{8}}{3} = \frac{\pi hwl}{6}$$

where, h: height, w: width, l: length. Each measured dimension is divided by two to get the radius of tumors.

#### Stable Isotope Tracer Analysis

8x10<sup>5</sup> cells were seeded in 10-cm dishes to obtain cells at 80% confluency. The media was removed and replaced with fresh DMEM containing 25 mM glucose without pyruvate to equilibrate the cells for 2 h for experiment with fully labeled glucose. For tracer analysis with 3-<sup>13</sup>C-glucose or 3-4 <sup>13</sup>C<sub>2</sub>-glucose equilibration media contained 10 mM of Glucose. The equilibration media was replaced with DMEM containing either 25 mM <sup>13</sup>C<sub>6</sub>-glucose (389374, Sigma Aldrich, Oakville, ON)-labeled media or 10 mM 3-<sup>13</sup>C-glucose (CLM-1393, Cambridge Isotope Laboratories, Cambridge, MA)- or 10 mM 3-4 <sup>13</sup>C<sub>2</sub>-glucose (CLM-6750-PK Cambridge Isotope Laboratories) for 2 min, 10 min, 1 h or 4 h.

The media was discarded and cells were washed 3x with 4°C isotonic saline solution on ice and quenched with 600 μL of 80% methanol at < -20°C on dry ice. Cells were scraped from the plates and transferred to prechilled tubes. Cell suspensions were lysed using a sonicator at 4°C for 10 min in cycles of 30 s on, 30 s off, at high setting with Diagenode Bioruptor. Sonication was repeated to ensure complete recovery of metabolites. Cell debris were removed by centrifugation (14000 rpm, 4°C) and supernatants were transferred to prechilled tubes and dried in a cold trap overnight at 4°C. Dried pellets were dissolved in 30 μL of pyridine containing methoxyamine-HCl (10 mg/mL) using a sonicator and vortex. Samples were spun down at 14000 rpm, incubated for 30 min at 70°C and then transferred to GC-MS injection vials containing 70 μL of N-tert-Butyldimethylsilyl-N-methyltrifluoroacetamide (Sigma). The sample mixtures were further incubated at 70°C for 1 h. One μL of each sample was injected for GC-MS analysis. GC-MS instrumentation and software were all from Agilent. GC-MS methods and mass isotopomer distribution analyses are as previously described (Gravel et al., 2016). Briefly, GC/MS analysis was conducted on an Agilent 5975C series GC-MSD with triple-axis HED/EM detector, equipped with DB-5MS + DG capillary column (30 m length, 10 m Duraguard deactivated fused silica tubing, 0.25 mm internal diameter, 0.25 μm film thickness) (Agilent, USA) and a 7890A gas chromatograph, with a 7693 autosampler.

1 μL sample was injected in the GC in splitless mode with inlet temperature at 280°C with helium gas as the carrier at a flow rate at 1.552 mL/min. The quadrupole was set at 150°C and the GC/MS interface at 285°C. The oven program for all metabolite analyses started at 60°C held at 1 min and increased at a rate of 10°C/min up to 320°C. Bake-out was at 320°C for 9 min. All data was collected by electron impact set at 70eV. Sample data were acquired both in scan (1-600 m/z) and selected ion monitoring (SIM) modes.

Metabolites were identified by matching mass spectra and retention times using authentic standards from Sigma. Measurements of metabolite concentrations are taken from the metabolite quantifier integration divided by the internal standard quantifier integration (myristic acid-D<sub>27</sub>) and normalized to cell count. For stable isotope tracer analysis, the integration values for quantifier (m+0) and all possible isotopomers (m+1, m+2, etc...) are summed up to obtain the total amount of metabolite. The mass isotopomer distribution (MID) vector is obtained by dividing the m+0 and all isotopomer by the total amount of metabolite. The corrected MID is obtained by removing the contribution of naturally occurring stable isotopes (McGuirk et al., 2013). The resulting isotopomers are expressed as fractions of the total metabolite pool. To determine the relative ion abundance, the corrected MID is multiplied by the relative metabolite amount at steady state.

Data analysis was performed using the Agilent Chemstation and MassHunter software (Agilent, Santa Clara, USA). For labeling experiment leading to Figure 1, Figure 4 and Figure S6 experiments control cells (shNTC) and senescent cells (shS3[A]) are the same as all 4 conditions (shNTC, shS3[A], shS3[A]+ shp53, and shS3A+HTC) were done together. Biological replicates were performed on independent infections.



### Bioenergetic Analyses

Cellular respiration in the Seahorse Analyzer was measured as described previously (Audet-Walsh et al., 2016). Briefly, IMR90 cells (7,500 growing or 5000 senescent) were seeded in 250  $\mu$ L of culture media in a XFe24 cell culture plate and incubated for 24 h at 37°C. Cells were washed twice and incubated in 525  $\mu$ L of XF media for 1 h at 37°C in a CO<sub>2</sub>-free incubator. Measurements were normalized to  $\mu$ g protein.

### Nucleotide and nucleoside analysis

5x10<sup>6</sup> cells were washed twice with 150 mM ammonium formate and collected in 80% methanol (LC-MS grade, Sigma) chilled to –80°C. Every step was performed on dry ice. The methanol:cell mixture was transferred into pre-chilled 2 mL Eppendorf tubes containing 1.4 mm ceramic beads, then beaten on bead beater for 2 min at 30 Hz. After this, we added an equal volume of ice-cold dichloromethane and half the volume of ice-cold H<sub>2</sub>O. The mixture was vortexed for 1 min at maximum speed and left for 10 min on ice. Samples were spun at 4000 rpm at 1°C and the aqueous phase was transferred into a new pre-chilled Eppendorf tube. Samples were dried overnight in a cold trap (Labconco). Samples were suspended and prepared for LC-MS/MS as described above. Data acquisition was performed on Agilent 6430 Triple Quadrupole LC/MS system.

### Bioinformatic analysis

Expression of HTC enzymes to find cell lines with high expression was analyzed from the Cancer Cell Line Encyclopedia (CCLE) (Ghandi et al., 2019).

To generate representation of genes shown in Figure S4 we used UCSC genome Browser with different tools. For p53 ChIP seq depth and SISR peaks dataset (data are shown in green) the tool p53 ChIP seq depth and SISR peaks dataset was used. This dataset comes from 41 ChIP-seq data analyzed with a common pipeline. In order to get representation the sequence must be found in at least two independent studies. For further information on the pipeline and analysis parameters see Nguyen et al. (Nguyen et al., 2018). Additional p53 and E2F binding sequences were obtained in ChIP Atlas and positions extracted from UCSC genome Browser using Transcription factor ChIP-Seq Clusters (161 factors) from ENCODE. For further information see ENCODE integrative analysis (Consortium, 2012; Davis et al., 2018) and for CHIP Atlas (Oki et al., 2018). Information on H3K27Ac marks on 7 cell lines (Often Found Near Regulatory Elements shown in red) was extracted from ENCODE (Consortium, 2012; Davis et al., 2018). Promoter regions (shown in pink) were extracted from EPDnewNC human version 001 and GeneCards genes TSS v4.14 (Fishilevich et al., 2017; Stelzer et al., 2016). Data for known or predicted gene enhancer regions were extracted using Interactions between GeneHancer regulatory elements and genes tool (double elite) v4.14 (Fishilevich et al., 2017; Stelzer et al., 2016).

### QUANTIFICATION AND STATISTICAL ANALYSIS

For Statistical analysis unpaired two-tailed Student's t test or ANOVA with compensation of multiple comparison with Dunnett, Tukey or Sidák based on Prism 9 recommendations for experimental design was performed unless stated otherwise in the figure legend using Graph Pad Prism 6-9 and Excel. A value of  $p < 0.05$  was considered significant. For statistical analysis technical replicates were averaged prior to statistical analysis. In figures, data is shown unless stated otherwise as mean  $\pm$  SD of data from independent experiments and the  $p$  value was indicated with three digits after decimal or  $p \leq 0.05$  equal to \*,  $p \leq 0.01$  equal to \*\*,  $p \leq 0.001$  equal to \*\*\* and  $p \leq 0.0001$  equal to \*\*\*\*. For analysis of immunohistochemistry we used Mann-Whitney non-parametric test, two tailed using Graph Pad Prism 6-9. Details of statistical test were deposited with data on Mendeley: <http://doi.org/10.17632/xsxwjfhz8f.1>

### ADDITIONAL RESOURCES

Further details senescence bypass experiments can be found in additional resources on Mendeley Data

For additional information on immunogold staining [www.me-udem.com](http://www.me-udem.com)

For additional information on immunohistochemistry performed by the CR-CHUM core facility

<https://www.chumontreal.qc.ca/en/crchum/facilities-and-services>

For additional information of metabolic tracing analysis <https://www.mcgill.ca/gci/facilities/metabolomics-innovation-resource-mir>

**Supplementary table 3. Transfection quantities of DNA for protein-protein interaction mapping, Related to STAR Methods.**

Full length and CTL	ME1-HA	PC-MYC	MDH-1 FLAG	3xFLAG	HA
ME1-HA, PC-MYC, 3xFLAG	7.5µg	5µg		5µg	
ME1-HA, PC-MYC, MDH1 3xFLAG	7.5µg	5µg	5µg		
HA, PC-MYC, MDH1 3xFLAG		5µg	5µg		5µg

For MDH1 variants	ME1-HA	PC-MYC	MDH1 3xFLAG variant	3xFLAG	HA
ME1-HA, PC-MYC, MDH1 1-90	7.5µg	5µg	5µg	5µg	
ME1-HA, PC-MYC, MDH1 1-142	7.5µg	5µg	10µg		
ME1-HA, PC-MYC, MDH1 1-192	7.5µg	5µg	7.5µg	2.5µg	
ME1-HA, PC-MYC, MDH1 105-334	7.5µg	5µg	10µg		
ME1-HA, PC-MYC, MDH1 141-334	7.5µg	5µg	10µg		

For PC variants	ME1-HA	PC-MYC variant	MDH1 3xFLAG	3xFLAG	HA
ME1-HA, PC-MYC 430-1178, MDH1 3xFLAG	7.5µg	10µg	5µg	5µg	
ME1-HA, PC-MYC 1-956, MDH1 3xFLAG	7.5µg	15µg	5µg		
ME1-HA, PC-MYC 1-534, MDH1 3xFLAG	7.5µg	15µg	5µg		

For ME1 variants	ME1-HA variant	PC-MYC	MDH1 3xFLAG	3xFLAG	HA
ME1-HA 1-191, PC-MYC, MDH1 3xFLAG	10µg	5µg	5µg		11.5µg
ME1-HA 356-572, PC-MYC, MDH1 3xFLAG	21.5µg	5µg	5µg		

### **A.3. Article contributions**

During the time of my PhD is contributed to the following articles in chronological order. I listed here the abstracts as well as my contributions.

### A.3.1. Metformin inhibits the senescence-associated secretory phenotype by interfering with IKK/NF- $\kappa$ B activation

> *Aging Cell*. 2013 Jun;12(3):489-98. doi: 10.1111/accel.12075. Epub 2013 Apr 23.

#### Metformin inhibits the senescence-associated secretory phenotype by interfering with IKK/NF- $\kappa$ B activation

Olga Moiseeva <sup>1</sup>, Xavier Deschênes-Simard, Emmanuelle St-Germain, Sebastian Igelmann, Geneviève Huot, Alexandra E Cadar, Véronique Bourdeau, Michael N Pollak, Gerardo Ferbeyre

Affiliations + expand

PMID: 23521863 DOI: 10.1111/accel.12075

[Free article](#)

#### Abstract

We show that the antidiabetic drug metformin inhibits the expression of genes coding for multiple inflammatory cytokines seen during cellular senescence. Conditioned medium (CM) from senescent cells stimulates the growth of prostate cancer cells but treatment of senescent cells with metformin inhibited this effect. Bioinformatic analysis of genes downregulated by metformin suggests that the drug blocks the activity of the transcription factor NF- $\kappa$ B. In agreement, metformin prevented the translocation of NF- $\kappa$ B to the nucleus and inhibited the phosphorylation of I $\kappa$ B and IKK $\alpha/\beta$ , events required for activation of the NF- $\kappa$ B pathway. These effects were not dependent on AMPK activation or on the context of cellular senescence, as metformin inhibited the NF- $\kappa$ B pathway stimulated by lipopolysaccharide (LPS) in ampk null fibroblasts and in macrophages. Taken together, our results provide a novel mechanism for the antiaging and antineoplastic effects of metformin reported in animal models and in diabetic patients taking this drug.

#### Summary and contributions

In this article we demonstrated that the senescence-associated secretory phenotype (SASP) in oncogene induced senescence can be decreased by metformin treatment. I contributed to the immunofluorescence shown in figure 3E and F as well as figure 5A and to the Western Blot shown in figure 5C

### A.3.2. Tumor suppressor activity of the ERK/MAPK pathway by promoting selective protein degradation

> *Genes Dev.* 2013 Apr 15;27(8):900-15. doi: 10.1101/gad.203984.112. Epub 2013 Apr 18.

#### Tumor suppressor activity of the ERK/MAPK pathway by promoting selective protein degradation

Xavier Deschênes-Simard <sup>1</sup>, Marie-France Gaumont-Leclerc, Véronique Bourdeau, Frédéric Lessard, Olga Moiseeva, Valérie Forest, Sebastian Igelmann, Frédéric A Mallette, Marc K Saba-El-Leil, Sylvain Meloche, Fred Saad, Anne-Marie Mes-Masson, Gerardo Ferbeyre

Affiliations + expand

PMID: 23599344 PMCID: PMC3650227 DOI: 10.1101/gad.203984.112

[Free PMC article](#)

#### Abstract

Constitutive activation of growth factor signaling pathways paradoxically triggers a cell cycle arrest known as cellular senescence. In primary cells expressing oncogenic ras, this mechanism effectively prevents cell transformation. Surprisingly, attenuation of ERK/MAP kinase signaling by genetic inactivation of Erk2, RNAi-mediated knockdown of ERK1 or ERK2, or MEK inhibitors prevented the activation of the senescence mechanism, allowing oncogenic ras to transform primary cells. Mechanistically, ERK-mediated senescence involved the proteasome-dependent degradation of proteins required for cell cycle progression, mitochondrial functions, cell migration, RNA metabolism, and cell signaling. This senescence-associated protein degradation (SAPD) was observed not only in cells expressing ectopic ras, but also in cells that senesced due to short telomeres. Individual RNAi-mediated inactivation of SAPD targets was sufficient to restore senescence in cells transformed by oncogenic ras or trigger senescence in normal cells. Conversely, the anti-senescence viral oncoproteins E1A, E6, and E7 prevented SAPD. In human prostate neoplasms, high levels of phosphorylated ERK were found in benign lesions, correlating with other senescence markers and low levels of STAT3, one of the SAPD targets. We thus identified a mechanism that links aberrant activation of growth signaling pathways and short telomeres to protein degradation and cellular senescence.

#### Summary and contributions

In this article, we demonstrated that the induction of senescence is accompanied by a specific protein degradation called SAPD. Moreover, we were able to show a tumor-suppressive role of ERK as inactivation of ERK in OIS was sufficient to bypass RAS-induced senescence. Finally, we were able to show that the specific degradation of proteins helps to maintain the senescence state of cells as cells that have bypassed the senescence response do not display any more site senescence-specific degradation. The results of this paper are the basis of my thesis, and my contributions

to this paper are the following. I help to generate cell extract for Figure 4B-D and prepared one replicate for figure 4E and 6I. I helped and prepared one biological replicate for Figures S8A, S8J, and S9A.

### A.3.3. Ribosomal protein RPL22/eL22 regulates the cell cycle by acting as an inhibitor of the CDK4-cyclin D complex

> *Cell Cycle*. Mar-Apr 2019;18(6-7):759-770. doi: 10.1080/15384101.2019.1593708. Epub 2019 Mar 28.

#### Ribosomal protein RPL22/eL22 regulates the cell cycle by acting as an inhibitor of the CDK4-cyclin D complex

Neylen Del Toro <sup>1</sup>, Ana Fernandez-Ruiz <sup>1 2</sup>, Lian Mignacca <sup>1</sup>, Paloma Kalegari <sup>1 2</sup>, Marie-Camille Rowell <sup>1 2</sup>, Sebastian Igelmann <sup>1</sup>, Emmanuelle Saint-Germain <sup>1</sup>, Mehdi Benfdil <sup>1</sup>, Stéphane Lopes-Paciencia <sup>1 2</sup>, Léa Brakier-Gingras <sup>1</sup>, Véronique Bourdeau <sup>1</sup>, Gerardo Ferbeyre <sup>1 2</sup>, Frédéric Lessard <sup>1</sup>

Affiliations + expand

PMID: 30874462 PMCID: PMC6464582 DOI: 10.1080/15384101.2019.1593708

[Free PMC article](#)

#### Abstract

Senescence is a tumor suppressor program characterized by a stable growth arrest while maintaining cell viability. Senescence-associated ribogenesis defects (SARD) have been shown to regulate senescence through the ability of the ribosomal protein S14 (RPS14 or uS11) to bind and inhibit the cyclin-dependent kinase 4 (CDK4). Here we report another ribosomal protein that binds and inhibits CDK4 in senescent cells: L22 (RPL22 or eL22). Enforcing the expression of RPL22/eL22 is sufficient to induce an RB and p53-dependent cellular senescent phenotype in human fibroblasts. Mechanistically, RPL22/eL22 can interact with and inhibit CDK4-Cyclin D1 to decrease RB phosphorylation both in vitro and in cells. Briefly, we show that ribosome-free RPL22/eL22 causes a cell cycle arrest which could be relevant during situations of nucleolar stress such as cellular senescence or the response to cancer chemotherapy.

#### Summary and contributions

In this article we provided evidence that not only RPS14 but also RPL22 can act as a CDKi. My contributions are the following. I performed the immunofluorescence in Figure 1(e) and bioinformatics analysis of the mass-spectrometry .

### A.3.4. Circumventing senescence is associated with stem cell properties and metformin sensitivity

> [Aging Cell](#). 2019 Apr;18(2):e12889. doi: 10.1111/accel.12889. Epub 2019 Jan 6.

## Circumventing senescence is associated with stem cell properties and metformin sensitivity

Xavier Deschênes-Simard <sup>1</sup>, Maxime Parisotto <sup>1</sup>, Marie-Camille Rowell <sup>1</sup>, Benjamin Le Calvé <sup>1, 2</sup>, Sebastian Igelmann <sup>1</sup>, Karine Moineau-Vallée <sup>1</sup>, Emmanuelle Saint-Germain <sup>1</sup>, Paloma Kalegari <sup>1</sup>, Véronique Bourdeau <sup>1</sup>, Filippos Kottakis <sup>3</sup>, Nabeel Bardeesy <sup>3</sup>, Gerardo Ferbeyre <sup>1</sup>

Affiliations + expand

PMID: 30614183 PMCID: PMC6413657 DOI: 10.1111/accel.12889

[Free PMC article](#)

### Abstract

Most cancers arise in old individuals, which also accumulate senescent cells. Cellular senescence can be experimentally induced by expression of oncogenes or telomere shortening during serial passage in culture. In vivo, precursor lesions of several cancer types accumulate senescent cells, which are thought to represent a barrier to malignant progression and a response to the aberrant activation of growth signaling pathways by oncogenes (oncogene toxicity). Here, we sought to define gene expression changes associated with cells that bypass senescence induced by oncogenic RAS. In the context of pancreatic ductal adenocarcinoma (PDAC), oncogenic KRAS induces benign pancreatic intraepithelial neoplasias (PanINs), which exhibit features of oncogene-induced senescence. We found that the bypass of senescence in PanINs leads to malignant PDAC cells characterized by gene signatures of epithelial-mesenchymal transition, stem cells, and mitochondria. Stem cell properties were similarly acquired in PanIN cells treated with LPS, and in primary fibroblasts and mammary epithelial cells that bypassed Ras-induced senescence after reduction of ERK signaling. Intriguingly, maintenance of cells that circumvented senescence and acquired stem cell properties was blocked by metformin, an inhibitor of complex I of the electron transport chain or depletion of STAT3, a protein required for mitochondrial functions and stemness. Thus, our studies link bypass of senescence in premalignant lesions to loss of differentiation, acquisition of stemness features, and increased reliance on mitochondrial functions.

### Summary and contributions

My contributions are the following. I performed immunofluorescence leading to Figure 1 i and j.